

Lecture Notes in Civil Engineering

Ashim Kanti Dey  
Jagat Jyoti Mandal  
Bappaditya Manna *Editors*

# Proceedings of the 7th Indian Young Geotechnical Engineers Conference

7IYGEC—2019

 Springer

# Lecture Notes in Civil Engineering

Volume 195

## Series Editors

Marco di Prisco, Politecnico di Milano, Milano, Italy

Sheng-Hong Chen, School of Water Resources and Hydropower Engineering,  
Wuhan University, Wuhan, China

Ioannis Vayas, Institute of Steel Structures, National Technical University of  
Athens, Athens, Greece

Sanjay Kumar Shukla, School of Engineering, Edith Cowan University, Joondalup,  
WA, Australia

Anuj Sharma, Iowa State University, Ames, IA, USA

Nagesh Kumar, Department of Civil Engineering, Indian Institute of Science  
Bangalore, Bengaluru, Karnataka, India

Chien Ming Wang, School of Civil Engineering, The University of Queensland,  
Brisbane, QLD, Australia

**Lecture Notes in Civil Engineering (LNCE)** publishes the latest developments in Civil Engineering - quickly, informally and in top quality. Though original research reported in proceedings and post-proceedings represents the core of LNCE, edited volumes of exceptionally high quality and interest may also be considered for publication. Volumes published in LNCE embrace all aspects and subfields of, as well as new challenges in, Civil Engineering. Topics in the series include:

- Construction and Structural Mechanics
- Building Materials
- Concrete, Steel and Timber Structures
- Geotechnical Engineering
- Earthquake Engineering
- Coastal Engineering
- Ocean and Offshore Engineering; Ships and Floating Structures
- Hydraulics, Hydrology and Water Resources Engineering
- Environmental Engineering and Sustainability
- Structural Health and Monitoring
- Surveying and Geographical Information Systems
- Indoor Environments
- Transportation and Traffic
- Risk Analysis
- Safety and Security

To submit a proposal or request further information, please contact the appropriate Springer Editor:

- Pierpaolo Riva at [pierpaolo.riva@springer.com](mailto:pierpaolo.riva@springer.com) (Europe and Americas);
- Swati Meherishi at [swati.meherishi@springer.com](mailto:swati.meherishi@springer.com) (Asia - except China, and Australia, New Zealand);
- Wayne Hu at [wayne.hu@springer.com](mailto:wayne.hu@springer.com) (China).

**All books in the series now indexed by Scopus and EI Compendex database!**

More information about this series at <https://link.springer.com/bookseries/15087>

Ashim Kanti Dey · Jagat Jyoti Mandal ·  
Bappaditya Manna  
Editors

# Proceedings of the 7th Indian Young Geotechnical Engineers Conference

7IYGEC—2019

 Springer



*Editors*

Ashim Kanti Dey  
Department of Civil Engineering  
National Institute of Technology Silchar  
Silchar, Assam, India

Jagat Jyoti Mandal  
Department of Civil Engineering  
National Institute of Technical Teachers'  
Training and Research  
Kolkata, India

Bappaditya Manna  
Department of Civil Engineering  
Indian Institute of Technology Delhi  
New Delhi, India

ISSN 2366-2557

ISSN 2366-2565 (electronic)

Lecture Notes in Civil Engineering

ISBN 978-981-16-6455-7

ISBN 978-981-16-6456-4 (eBook)

<https://doi.org/10.1007/978-981-16-6456-4>

© Springer Nature Singapore Pte Ltd. 2022

This work is subject to copyright. All rights are reserved by the Publisher, whether the whole or part of the material is concerned, specifically the rights of translation, reprinting, reuse of illustrations, recitation, broadcasting, reproduction on microfilms or in any other physical way, and transmission or information storage and retrieval, electronic adaptation, computer software, or by similar or dissimilar methodology now known or hereafter developed.

The use of general descriptive names, registered names, trademarks, service marks, etc. in this publication does not imply, even in the absence of a specific statement, that such names are exempt from the relevant protective laws and regulations and therefore free for general use.

The publisher, the authors and the editors are safe to assume that the advice and information in this book are believed to be true and accurate at the date of publication. Neither the publisher nor the authors or the editors give a warranty, expressed or implied, with respect to the material contained herein or for any errors or omissions that may have been made. The publisher remains neutral with regard to jurisdictional claims in published maps and institutional affiliations.

This Springer imprint is published by the registered company Springer Nature Singapore Pte Ltd.

The registered company address is: 152 Beach Road, #21-01/04 Gateway East, Singapore 189721, Singapore

## **Foreword from the Honorary Secretary, IGS**

It gives me an immense pleasure to see that the conference volume of 7th Indian Young Geotechnical Engineers Conference (7IYGEC-19) is being published by Springer. The volume covers a good number of technical papers, some being highly innovative and thought provoking, which were presented in the conference by young geotechnical engineers of less than 35 years of age. The contributions are timely and address contemporary issues and challenges in geotechnical engineering. I hope that the proceeding will give a better understanding of ongoing research in geotechnical engineering to the budding engineers.

I congratulate the organizers and the contributors for bringing out this proceeding.

New Delhi, India

Prof. J. T. Shahu  
Honorary Secretary  
Indian Geotechnical Society

# Foreword from the IGS President

The conference volume on the 7th Indian Young Geotechnical Engineers Conference (7IYGEC-19) is an outcome of the technical papers submitted to the conference held on 15 and 16 March 2019 at NIT Silchar, Assam. The compilation has excellent contributions in the area of shallow and deep foundations, rock mechanics, ground improvement techniques, geo-environmental engineering, slope stability and landslides, soil dynamics and earthquake engineering, site investigations and case studies, computational geomechanics, engineering properties and characteristics of soil and remote sensing and GIS in geotechnical engineering. The subthemes have covered the potential areas in current research topics in geotechnical engineering. I am happy to see a good number of participations from different reputed institutions and renowned geotechnical consultancy firms in India.

The conference has given an exposure to young geotechnical engineers to disseminate their knowledge and research output with fellow researchers from different parts of India. It also gave an opportunity to the young research scholars and practitioners to have an exposure to the beauty of the North East. I wholeheartedly congratulate all the authors of the technical papers and editors of the volume for their commendable efforts in preparing this fruitful contribution towards helping geotechnical engineers, academicians and researchers.

Bangalore, India

Prof. G. L. Siva Kumar Babu  
President  
India Geotechnical Society

# Preface

In order to cater the need of geotechnical knowledge to solve diversified soil problems in India, the Indian Geotechnical Society is relentlessly working through academicians, researchers, field engineers and laboratory technicians. The dissemination of knowledge is done through international and national conferences and seminars, short-term training programmes, site visits, expert meetings, etc. To encourage the students for exploring their young brain and tireless efforts, student chapters are being set up under the umbrella of different local chapters of the society. In addition to it, the society organizes National Conferences on Young Geotechnical Engineers biennially to promote research activities and to share the research outcomes among the young engineers with age less than 35 years. The 7th conference named as “7th Indian Young Geotechnical Engineers Conference (7IYGEC-19)” was held on 15 and 16 March 2019 at NIT Silchar under the auspices of IGS Silchar Chapter.

Considering the trend of research in India and the need of solutions to specific geotechnical problems in the North East, ten subthemes as mentioned below were chosen:

1. Shallow and Deep Foundations
2. Rock Mechanics and Rock Engineering
3. Ground Improvement Techniques
4. Geo-environmental Engineering
5. Slope Stability and Landslides
6. Soil Dynamics and Earthquake Engineering
7. Site Investigations and Case Studies
8. Computational Geomechanics
9. Engineering Properties and Characteristics of Soil
10. Remote Sensing and GIS in Geotechnical Engineering

Each subtheme was well represented by the participants. Around 150 abstracts were received and reviewed by experts from IISc, IITs, NITs and other technical institutes of high repute. Finally, 103 abstracts were selected for presentation in the conference. The full-length papers were received from different corners of India. Some of the papers contain minute details of fundamental research and were highly appreciated.

In addition to conference papers, there were two invited lectures and six key note lectures delivered by well-known experts in the geotechnical field.

The organizers are grateful to the authors and technical contributors for their contributions and hard work. Special thanks are extended to the reviewers who promptly reviewed the abstracts and full-length papers in spite of their busy schedule. It is believed that the knowledge shared through this conference volume will enhance the understanding in the field of geotechnical engineering. The exposure of the young engineers in this conference will enable them to tackle future challenges and to promote fundamental research on geotechnical engineering. Very special thanks to Springer publications to accept our request for publishing the conference volume.

Silchar, India  
Kolkata, India  
New Delhi, India

Prof. Ashim Kanti Dey  
Prof. Jagat Jyoti Mandal  
Prof. Bappaditya Manna

# Chairman Message



**Prof. Ashim Kanti Dey**  
Conference Chairman, 7IYGEC  
Professor, Civil Engineering Department  
National Institute of Technology Silchar  
Silchar, Assam

I feel proud to be associated with the Geotechnical Engineering Division of the Institute which is organising the 7th Indian Young Geotechnical Engineers Conference (7IYGEC) in association with the IGS Silchar Chapter. I am thankful to Prof. G. L. Siva Kumar Babu, President, Indian Geotechnical Society, who gave us an opportunity to arrange such a mega event in the North East part of India in spite of many geographical and communication constraints of this region. We have invited eminent persons as our guests and keynote speakers. Our team comprising of academicians, consultants, field engineers, students and non-technical persons is working very hard to make an all-out success of the conference. In case there is any loop hole, it is my ignorance and negligence.

I am grateful to our Director, NIT Silchar, for his kind support and all sorts of help to organize the conference. I am also grateful to our TEQIP III coordinator who has recommended for a major financial support.

I take this opportunity to thank our sponsors for their benevolent financial support to arrange such a mega event.

I take this opportunity to record deep appreciation and gratitude for the remarkable contributions by all the members of the organizing committee. M/S Sungraphics have done a great job in printing all the materials including the proceeding at the last moment.

Looking forward to welcome you all.

# Director Message



**Prof. Sivaji Bandyopadhyay**  
Chief Patron, 7IYGEC  
Director, National Institute of Technology Silchar  
Silchar, Assam

It gives me immense pleasure to share that the Indian Geotechnical Society Silchar Chapter and Civil Engineering Department, NIT Silchar, are organizing the 7th Indian Young Geotechnical Engineers Conference (7IYGEC-19) at NIT Silchar. It is my belief that the conference will be a hub for a plethora of academic activities and will be a dynamic venue where brilliant minds from all over the country will converge and share their vast reserves of knowledge and experience. In addition, I am confident that the lectures delivered by experts from reputed institutes and organizations in India will usher fresh insights into various fields of geotechnical engineering.

I convey my greetings and felicitations to the organizers and all the participants of 7IYGEC and my best wishes for a grand success of the event.



## HOD Message



**Prof. Parthasarathi Choudhury**  
Patron, 7IYGEC  
Head, Civil Engineering Department  
National Institute of Technology Silchar  
Silchar, Assam

I am very happy to know that Geotechnical Engineering Division along with IGS Silchar Chapter is organising a National Level Young Geotechnical Engineers Conference (7IYGEC) on 15 and 16 March 2019 at NIT Silchar. The Civil Engineering Department is the most vibrant department in the institute and is involved in several academic, consultancy and social activities throughout the year. I feel very proud to be associated with 7IYGEC which will amalgamate young brains in development of new research areas in the field of geotechnical engineering.

I expect that this conference would cultivate state-of-the-art ideas among the participants towards solution to several problems in soil structure, foundations, landslides, soil erosion, etc. I strongly believe the conference will be a highly successful one.

# Message from the Organizing Secretaries, 7IYGEC



Dr. Debjit Bhowmik  
Organizing Secretary, 7IYGEC



Dr. Amit Kumar Das  
Organizing Secretary, 7IYGEC

It is our pleasure to have the opportunity to organize 7th Indian Young Geotechnical Engineers Conference (7IYGEC) on 15 and 16 March 2019 as part of IGS Silchar Chapter and National Institute of Technology Silchar under TEQIP-III. Geotechnical engineering is a core division of civil engineering, and this field of civil engineering is enriched by research and innovation. The young minds of our country are the best to address and deliver in this regard if appropriate platform is provided. 7IYGEC is such a platform, where experts and young Indian engineers meet to explore the new advancements in the field of geotechnical engineering. It is our belief that this conference will serve rightly to fulfil its purpose.

We wish all the success of the conference.

# Contents

## Shallow and Deep Foundation

<b>Parametric Influence on the Behavior of Skirted Foundation</b> .....	3
Arghadeep Biswas, Anish Banerjee, and Rishab Das	
<b>Dynamic Analysis of Cantilever Sheet Pile Walls in Liquefiable Soil Using FLAC2D</b> .....	9
Akshay Pratap Singh and Kaustav Chatterjee	
<b>Bearing Capacity of Strip Footing Over Rectangular Tunnel in Soft Clay</b> .....	17
Puja Dutta, Penke Sriharsha, and Paramita Bhattacharya	
<b>Combined Effect of Vertical and Horizontal Loads on the Behavior of Pile Foundations in Layered Soils</b> .....	27
Manne Manoj Kumar and A. Murali Krishna	
<b>Behavior of Laterally Loaded Piles Using Finite Difference Method</b> ....	37
B. K. Huchegowda, Teja Munaga, and Gonavaram Kalyan Kumar	
<b>Bearing Capacity of Strip Footing Placed on Reinforced Cohesionless Soil Slope Using Conic Programming</b> .....	45
Koushik Halder and Debarghya Chakraborty	
<b>Optimizing the Bearing Capacity of Pile Foundation in Clay</b> .....	55
Mantu Majumder and Debarghya Chakraborty	
<b>Numerical Analysis of Soft Soil Reinforced with Geogrid Encased Stone Column</b> .....	65
B. K. Pandey, S. Rajesh, and S. Chandra	
<b>Ground Improvement Technique</b>	
<b>Behaviour of Multi-layered Geocell-Reinforced Soil Embankment</b> .....	75
Haradhan Sarkar and Arghadeep Biswas	

<b>Parametric Effect on Granular Columns: A Brief Review</b> .....	81
Samrat Ghose, Arghadeep Biswas, and Utpal Mandal	
<b>Challenges and Strategies in Treatment of Terrace Material Encountered in Place of Rock at Foundation of Spillway</b> .....	91
Vinod Kumar Mauriya	
<b>Effect of Sand Content and Plasticity on Swell and Hydraulic Behaviour of Expansive Soils</b> .....	101
Sabari Ramesh and T. Thyagaraj	
<b>Effect of Lime Treatment on Expansive Soils at High Initial Water Content</b> .....	111
T. Ashok Kumar, T. Thyagaraj, and R. G. Robinson	
<b>Sulfate Effects on Lime and Sulfate-Resistant Cement-Stabilized Expansive Soil</b> .....	119
P. Sriram Karthick Raja and T. Thyagaraj	
<b>Cementation of Sand by Microbial Induced Calcite Precipitation</b> .....	127
Vineeth Reddy Karnati, M. Sudhakar, Kalyan Kumar Gonavaram, and Amitava Bandhu	
<b>Strength and Deformation Aspects of Glass Fibre-Reinforced Clayey Soil</b> .....	137
Suchit Kumar Patel and Baleshwar Singh	
<b>Behavior of Geosynthetic Encased Stone Column</b> .....	145
Mrinal Bhaumik, Suresh Prasad Singh, and Preetynanda Nanda	
<b>Evaluating the Utility of Pond Ash as an Alternative Foundation Material Partially Replacing Sand for Foundation Layers</b> .....	157
Aditya Shankar Ghosh and Tapash Kumar Roy	
<b>pH and Electrical Conductivity of Cement-Treated Peat</b> .....	167
Abhinaba Paul and Monowar Hussain	
<b>Bearing Capacity of Circular Footing on Geonatural and Geosynthetic Reinforced Sand</b> .....	175
B. Venkatesh and T. Thyagaraj	
<b>Geo-environmental Engineering</b>	
<b>Mechanical Characterization of a Bio-enzyme Treated Granular Lateritic Soil for Application in Low Volume Roads</b> .....	185
Vishal Khanna, Brundaban Beriha, and Umesh Chandra Sahoo	
<b>Study of Municipal Solid Waste in Road Embankment</b> .....	195
Parul Rawat and Supriya Mohanty	

**Hydraulic Conductivity of Steel Slag and Potential Influence of Leaching on Groundwater Alkalinity** ..... 209  
 Rituraj Devrani, Anant Aishwarya Dubey, K. Ravi, and Clint Thankachan

**Evaluation of Geotechnical Properties of Mineral Oil-Contaminated Clay Soil** ..... 217  
 Atriya Chowdhury

**Plasticity Characteristics of Geopolymer Stabilized Expansive Soil** ..... 225  
 Manaswini Mishra, Soumyaprakash Sahoo, and Suresh Prasad Singh

**Slope Stability and Landslides**

**Effect of Joint Orientation and Weathering on Static Stability of Rock Slope Having Transmission Tower** ..... 237  
 Mohammad Zaid and Md. Rehan Sadique

**Stability of Slope During Rainfall: A Finite Element Approach** ..... 251  
 J. Sharailin Gidon and Smurtirekha Sahoo

**Landslide Early Warning System in Kalimpong, West Bengal** ..... 261  
 Abhirup Dikshit and Neelima Satyam

**Investigating the Influence of Groundwater Level Variation on Performance of Soil Nailed Slopes** ..... 269  
 Meletetsega Gashaw and A. Murali Krishna

**Effect of Vertical Seismic Coefficient in Slope Stability Analysis** ..... 281  
 Sukanta Das and B. K. Maheshwari

**Prediction of Stability of Hill Slope Through Electrical Resistivity Tomography** ..... 289  
 Arindam Saha, Ashim Kanti Dey, Bedanta Kalita, Surya Pratap Vishwakarma, and Nayan Ahmed

**Soil Dynamics and Earthquake Engineering**

**Effect of Excavation Depths on Soil Pressure Acting on Embedded Cantilever Retaining Walls Under Dynamic Loadings** ..... 301  
 Sanku Konai

**Earthquake Response Analysis of Sites Using DEEPSOIL** ..... 309  
 D. Nishanth Kiran, Mohammad Muzzaffar Khan, M. Madhu Sudhan Reddy, and Gonavaram Kalyan Kumar

**Evaluation of Dynamics Properties and Liquefaction Potential of Kasai River Sand by Cyclic Triaxial Test** ..... 317  
 Satya Prakash Vikal and Paramita Bhattacharya

<b>Determination of Geometric Attenuation Parameters of Surface Amplitude in Soil Medium Due to Installation of Impact Pile Casing</b> . . .	327
B. Vinoth	
<b>Numerical Analysis of Layered Soil-Ash-Foundation System</b> . . . . .	339
Amit Kumar Ram and Supriya Mohanty	
<b>Comparative Study on Static and Seismic Performance of Ash-Foundation System</b> . . . . .	353
M. V. Ravi Kishore Reddy, Supriya Mohanty, and Shaik Rehana	
<b>Influence of Bedrock on Site Response</b> . . . . .	363
Bhavesh Pandey, Ravi S. Jakka, and Ashok Kumar	
<b>Comparative Seismic Fragility Study of Railway Concrete Bridge Piers Without and with the Effect of Soil-Structure Interaction</b> . . . . .	377
Saranika Das and Arjun Sil	
<b>Site Investigation and Case Studies</b>	
<b>Stabilization of Railway Tracks Using Geosynthetics—A Review</b> . . . . .	387
Rajashekar Mallikarjun Hubballi	
<b>Micro-Piles as Foundation for G+10 Building at Chhattisgarh—A Case Study</b> . . . . .	397
Rutuj Chheda, Chhaya Kandpal, Harshita Anjana, Atharva Pisolkar, Aditya Soni, and Jigisha Vashi	
<b>Phosphogypsum Dumping Yards—A Review</b> . . . . .	405
K. Tulasi and C. N. V. Satyanarayana Reddy	
<b>Long-Term Deformations of Soft Clays: A Case Study</b> . . . . .	413
Atriya Chowdhury	
<b>Effect of Interface Connection on Performance of Narrow Shored Reinforced Earth Wall</b> . . . . .	425
Charmy Joshi, Sweta Dave, Shalini Singh, and Manish Shah	
<b>Analytical Methods for Predicting Load Carrying Capacity of Granular Piles—A Review</b> . . . . .	437
Murtaza Hasan and N. K. Samadhiya	
<b>A Season-Wise Geotechnical and Morphological Study of Alteration in Coastal Profile Along the Shores of Puducherry, India</b> . . . . .	445
Nazeel Sabah, Arjun Sil, and G. Vijayakumar	

**Computational Geomechanics**

**Numerical Analysis of Hybrid Back-To-Back MSE Wall with Select and Marginal Backfill** ..... 457

Gopika Rajagopal and T. K. Sudheesh

**Numerical Modeling by Finite Elements for a Pile Foundation Under Tension Load** ..... 467

B. K. Huchegowda, Chethan Bagoor, and G. Kalyan Kumar

**Prediction of Settlement of Shallow Foundation on Cohesionless Soil Using Artificial Neural Network** ..... 477

Sinjan Debnath and Parbin Sultana

**Finite Element Modelling of Piled Raft in Sand Under Earthquake Load** ..... 487

Prasun Halder and Bappaditya Manna

**Engineering Properties and Characteristics of Soil**

**Effect of Salt Solution on Engineering Behaviour of Soil** ..... 497

Swagatika Senapati, Subhadeep Banerjee, and T. Thyagaraj

**Application of X-Ray Computed Tomography for Capturing the Desiccation Cracks of Soils** ..... 505

M. Julina and T. Thyagaraj

**A Study on the Improvement of Engineering Properties of Locally Available Soil of Kokrajhar by Using Burnt Brick Dust** ..... 515

Shafi Kamal Rahman, Mantu Kumar Das, and Joutish Deka

**Geotechnical Properties of Sand-Bentonite Liner Material Permeated with Calcium Chloride Solution** ..... 521

Debtanu Seth, Suryaleen Rout, and Suresh Prasad Singh

## About the Editors

**Dr. Ashim Kanti Dey** is currently a professor at the Department of Civil Engineering, National Institute of Technology Silchar, Assam. He obtained his B.E. from REC Silchar under Gauhati University, M.C.E. from Jadavpur University and Ph.D. from Indian Institute of Technology Madras, Chennai. His research interests include soil characterization, ground improvement techniques, geo-environmental engineering and geotechnical earthquake engineering. He has published 25 papers in respected national and international journals and more than 60 papers in national and international conferences. Dr. Dey is a recipient of Gold Medal in Bachelor of Engineering. He has received IGS-Geotechnical Biennial Award for the Best Paper on “Innovations in Field Exploration” in 2000, IGS-Shri. M. S. Jain Biennial Award 2015 for the best paper on “Innovations in Piling and Other Foundation Construction Techniques” in 2015, IRC—Maharashtra PWD Award 2015 for the best paper on “Construction” in 2015.

**Dr. Jagat Jyoti Mandal** is at the Department of Civil Engineering of National Institute of Technical Teachers’ Training and Research (NITTTR), Kolkata, as a faculty member since 2008. After graduating with Honours in Civil Engineering from IIT Kharagpur, he obtained his M.Tech. in Civil Engineering (with Specialization in Soil Mechanics and Foundation Engineering) and Ph.D. in Civil Engineering from IIT Kharagpur. He has taught various subjects of Civil Engineering at Graduate and Post-Graduate level at various institutes for the past 30 years. He has published more than 20 articles in international and national journals and conference proceedings. His research interests include numerical geo-technique, soil and structural dynamics and their applications in earthquake engineering, ground improvement techniques. He has conducted short-term training programmes on various topics including Geotechnical Investigation and Testing, Analysis and Design of Foundations, Ground Improvement Techniques, Testing of Civil Engineering Materials, Introductory Courses on Applications of FEM in Civil Engineering, introductory courses on Soil and Structural dynamics, Design of Reinforced Concrete structural Elements etc.



**Dr. Bappaditya Manna** is currently an Associate Professor at the Department of Civil Engineering, Indian Institute of Technology Delhi, New Delhi. He obtained his B.E. from Bengal Engineering College (Deemed University), Shibpur; M.Tech. from Indian Institute of Technology Kanpur; and Ph.D. from the Indian Institute of Technology Kharagpur. His major areas of research interests include pile foundations under machine induced vibrations, block foundation, stability of unreinforced and reinforced slopes, and analysis of dam foundation on jointed rock mass. He has published 25 papers in respected international journals and more than 50 papers in national and international conferences. Dr. Manna received the IGS-Guwahati Chapter Young Geotechnical Engineer (YGE) Award 2014, IEI Young Engineers Award 2012–2013, ISTE-SGSITS National Award 2012–2013, DAAD Fellowship 2012, DAE Research Award for Young Scientists 2012, DST Young Scientist Award 2011, Outstanding Young Faculty Fellow in the Area of Engineering for the Year 2011, Endeavour Research Fellowship—2010. He already guided 5 Ph.D. students and 25 M.Tech. students. Dr. Manna is also a reviewer of more than 10 international journals.

# **Shallow and Deep Foundation**

# Parametric Influence on the Behavior of Skirted Foundation



Arghadeep Biswas , Anish Banerjee, and Rishab Das

**Abstract** The study reports a numerical analysis on the behavior of skirted foundation under different parametric condition and configuration. The skirts are in the form of interconnected casing, as well as, plates (not-interconnected) of different lengths. In the study, footing was rested on soil surface, and, a uniform incremental load is applied. Analysis is performed in standard explicit ABAQUS, a commercially available finite element software. The simulation responses are monitored with respect to load-deformation behavior of the soil within and around the skirting. Responses of the model test indicated significant influence of skirting on the performance of foundation in terms of deformation and bearing capacity. It is observed that introduction of skirting increases the bearing capacity and reduces the surface deformation around the footing. A soil-column penetration is observed at the bottom of skirted soil which was depended on the depth of skirts extended. The penetration showed a parabolic nature depending of skirting type, i.e., casing and/or not-interconnected plates.

**Keywords** Skirted foundation · Numerical modeling · Parametric influence · Ground improvement

## 1 Introduction

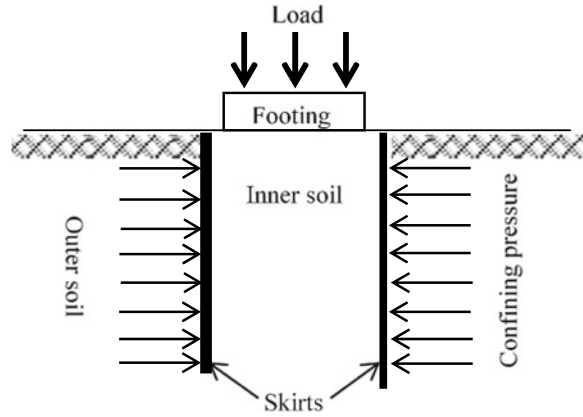
Various ground modification techniques are implemented for improving the properties of soft soil depending on type of applications and practicality. Skirted foundation is one of such effective ground improvement technique for enhancing the load-bearing capacity and reducing the vulnerability to excessive settlements of the soft clay. The skirts serve as an effective alternative to pile foundation by confining the soil within (Fig. 1) and develop a better distribution system which transmits the load to greater depths more effectively [1–6]. The laterally restraint encased soil leads to improved shear strength through enhanced density with footing settlement. Hence, it

---

A. Biswas (✉) · A. Banerjee · R. Das  
Department of Civil Engineering, Jalpaiguri Government Engineering College, Jalpaiguri 735102, India

© Springer Nature Singapore Pte Ltd. 2022  
A. K. Dey et al. (eds.), *Proceedings of the 7th Indian Young Geotechnical Engineers Conference*, Lecture Notes in Civil Engineering 195,  
[https://doi.org/10.1007/978-981-16-6456-4\\_1](https://doi.org/10.1007/978-981-16-6456-4_1)

**Fig. 1** Schematic of skirted foundation



prevents shear failure of the soil at shallow depths and increases the overall bearing capacity of the concern geo-structure. The present study is a numerical modeling of a skirted foundation using the finite element analysis software ABAQUS CAE and thereby investigates the influence of skirting type, skirting depth, shapes, and aspect ratio of footing on the degree of confinement of the soft soil and deformation behavior.

## 2 Modeling

### 2.1 Material Modeling

The present study considered ABAQUS CAE to simulate the behavior of skirted foundation. In modeling phase, a 3D model of a soil block (outer soil) is prepared assuming elastic and isotropic material properties. Another soil block, having similar material properties, is prepared to represent the soil under the rigid footing (inner soil), while the rigid footing is constructed with a block having elastic properties only. The two types of skirt considered (casing and plate type) are given the elastic properties (representing a steel plates of 25 mm thick). Henceforth, these parts are assembled with suitable interfacial properties to represent a confined model, either having non-interconnecting plates as skirts or a monolithic encasement representing the skirt. The dimensional values of these parts are later varied in order to determine the different behavioral characteristics of soil under varying conditions. The analysis is carried out using incremental static load with varying time period. An initial pressure of  $100 \text{ kN/m}^2$  is applied on the top surface of the footing. The procedure for analysis is kept in static mode; however, in general, the time period for each models generated was varied. Boundary conditions are used to specify the constraints and displacements for a particular surface of the assembly. The base of the whole soil

**Table 1** Dimensions of unreinforced models

Footing type	Geometric parameters	
	Constants	Variables
Square	Length and width = 1, 1.5 m	Thickness = 0.25, 0.50, 0.75 m
Rectangular	Length = 2.0, 2.5 m Width = 1.5, 2.0 m	Thickness = 0.25, 0.50, 0.75 m

**Table 2** Dimensions of skirted models

Footing type	Geometric parameters		Skirt depth
	Constants	Variables	
Square	Length and width = 1, 1.5 m	Thickness = 0.25, 0.50, 0.75 m	1.5, 3.0, 4.5, 6.0 m
Rectangular	Length = 2.0, 2.5 m Width = 1.5, 2.0 m	Thickness = 0.25, 0.50, 0.75 m	

block is provided with an encastre condition; the base of the soil block within the confinement was having a  $z$ -symmetric condition. For the casing-type model stimulation, the confining reinforcement was having a  $z$ -symmetric condition; however, in case of plates, each of the plate was provided with either  $x$ -symmetry or  $y$ -symmetry condition depending on their direction of plane of the surface considered. Finally with the completion of the basic definitions, the parts of the model are assembled and meshed in tetrahedral elements of varying size to get better and more accurate results.

## 2.2 Model Geometry

To indicate the effect of skirting, a set of analysis is performed on unreinforced soil. Two types of footings are considered; square and rectangle with different aspect (length to width) ratios. Tables 1 and 2 are the model dimensions considered for the analysis.

## 3 Analysis and Results

Similar skirting depth are prepared for both plate- and case-type skirtings for models having varied footing shapes and dimensions. Comparisons have been made in between reinforced and their respective unreinforced models. A typical unreinforced foundation and its deformed shape is presented in Fig. 2. In unreinforced cases, the nature of failure remains same for all. Figure 3a represents a sectional view of a

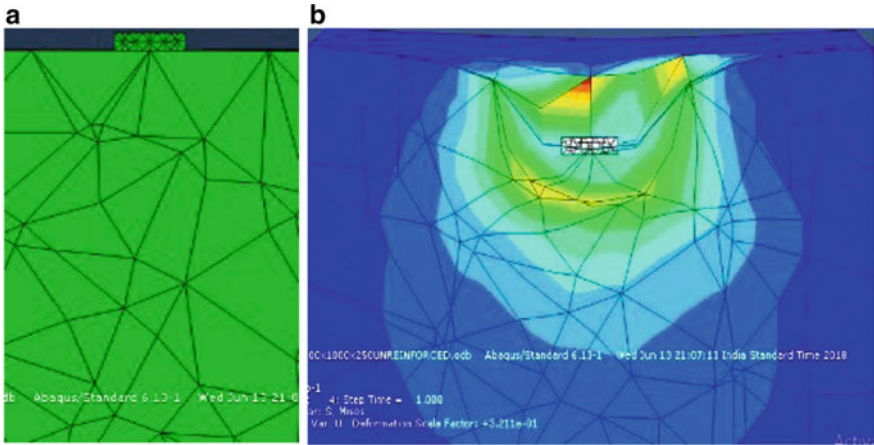


**Fig. 2** Typical unreinforced model: **a** undeformed; **b** deformed model

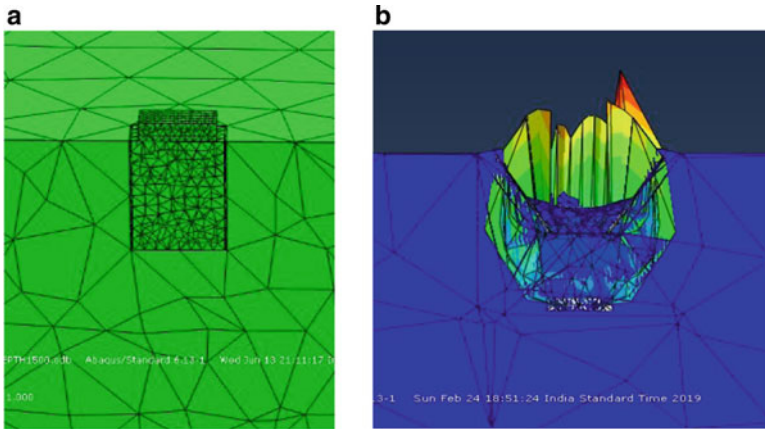


**Fig. 3** Plate-type skirted model: **a** sectional view; **b** deformed shape

typical cased-type skirted model of 1.5 m depth under a footing of plan area (1.5 m  $\times$  1.5 m) and 0.25 m thickness. In plate-type reinforced skirt models, the failure surface formation was non-uniform (Fig. 3b). Here, the non-interconnected plates failed to withstand the hoop stress generated and undergoes tilting and differential settlements. In case-type reinforced models, the failure surface at bottom of the skirted soil was parabolic in nature (Fig. 4). As shown in Fig. 2b the failure surface for the unreinforced models lie just under the rigid footing base, while in cased-type skirt (Fig. 4) causes the failure surface which forms at the tip of case-end. In Fig. 4a and b, the effect of footing dimension is indicated. It shows that, at same skirting depth of 1.5 m, the peak strain magnitude decreases irrespective of the shape of footings, while the footing dimension is increased. However, as can be seen in Fig. 4c,

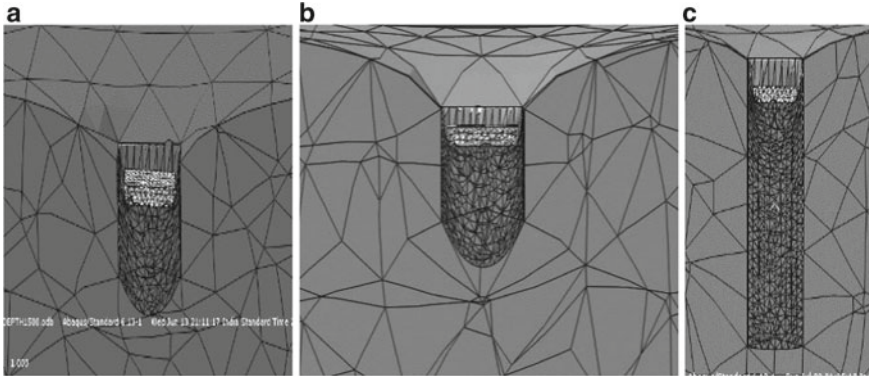


**Fig. 4** Typical deformation of skirted foundation (from left to right) **a** 1 m × 1 m footing, **b** 1.5 m × 1.5 m footing, and **c** effect of skirting depth

the failure surface stops forming the bulging up to the bottom of the open-casing for skirting depth greater than 3 m.

The load settlement behavior has demonstrated that the introduction of skirt reduces the magnitude of settlement under fixed loading. In the analysis, load intensity of 100 kN/m<sup>2</sup> is maintained across all the models, while the rate of load increment varies depending on model characteristics. It is seen that under constant load intensity skirting depth further reduces the magnitude of settlement. Such behavior is also observed irrespective of footing shapes. It is noticed that as foundation dimensions and depth increases the volume of load propagation increases and load dispersion becomes more efficient. However, at the same time, it implies the increased self-weight of soil within the casing which plays an important role on the magnitude of settlement observed.

## 4 Conclusions

The present study reports the behavior of skirted foundation of square and rectangular shapes. Different types of skirt configuration is considered including a plate-type non-interconnected and an encasement-type skirting of varying lengths. It is found that introduction of skirt of any type improves the foundation system; however, encased type performed better than the plate type. The casing-type skirt causes the failure surface to form at the tip of case end, at a greater depth, while the plate-type skirt, under loading, opens up and fail to serve the purpose. It is further noticed that by keeping the skirting depth same if the footing dimension is increased peak strain magnitude decreases making flat parabolic soil surfaces at bottom. Soil under the foundation base settles according to the improved load distribution and increased self-weight if the footing dimensions are increased.

## References

1. Al-Aghbari MY (2002) Settlement of shallow square foundation with structural skirts resting on sand. In: Proceedings of the second international conference on geotechnical and geoenvironmental engineering in arid land. Riyadh, Saudi Arabia, pp. 189–193
2. Al-Aghbari MY, Dutta RK (2008) Performance of square footing with structural skirt resting on sand. *Geomech Geoeng* 3(4):271–277
3. Al-Aghbari MY, Mohamedzein YEA (2004) Bearing capacity of strip foundations with structural skirts. *Geotech Geol Eng* 22(1):43–57
4. Bransby MF, Randolph MF (1998) Combined loading of skirted foundations. *Geotechnique* 48(5):637–655
5. Gourvenec S, Randolph MF (2010) Consolidation beneath skirted foundations. *Int J Geomech* 10(1):22–29
6. Hu Y, Randolph MF, Watson PG (1999) Bearing response of skirted foundation on nonhomogeneous soil. *Int J Geotech Geoenviron Eng* 125(11):924–934



# Dynamic Analysis of Cantilever Sheet Pile Walls in Liquefiable Soil Using FLAC2D



Akshay Pratap Singh and Kaustav Chatterjee

**Abstract** Retaining walls are generally used to support backfill soil. However, collapse of retaining walls due to earthquake forces has been observed in the past decades. In the present study, numerical modeling of a cantilever sheet pile wall passing through both liquefiable and non-liquefiable soil is carried out using finite difference-based computer program FLAC2D. The numerical analysis has been executed in cohesionless soil under both liquefiable and non-liquefiable soil conditions. The acceleration-time history of 1940 El Centro and 1989 Loma Prieta earthquakes is considered as the input dynamic loadings. From the results obtained, it is observed that both displacement and bending moment of sheet pile wall are increased in liquefiable soil as compared to non-liquefiable soil due to significant reduction in shear strength and stiffness of the soil. The present results can be used for design of cantilever sheet pile wall passing through liquefiable soil in earthquake prone areas.

**Keywords** Dynamic analysis · FLAC2D · Cantilever sheet pile walls · Liquefiable soil

## 1 Introduction

Failure of retaining walls due to sliding, overturning, or bearing capacity has been observed during various past earthquakes. Although failure mechanisms of rigid retaining walls have been analyzed significantly [4, 6]; however, due to complex nature of dynamic soil–structure interaction, an accurate study on flexible cantilever sheet pile wall is still lacking in literature. Flexible cantilever sheet pile walls are used to support moderate height of excavation in both cohesive and cohesionless

---

A. P. Singh (✉) · K. Chatterjee  
Indian Institute of Technology Roorkee, Roorkee 247667, India  
e-mail: [asingh4@ce.iitr.ac.in](mailto:asingh4@ce.iitr.ac.in)

K. Chatterjee  
e-mail: [kchatfce@iitr.ac.in](mailto:kchatfce@iitr.ac.in)

soil as a temporary or permanent structure. It derives its stability from the passive resistance of soil near its toe.

The simplest approach in the seismic design of retaining structure is pseudo static approach in which the seismic forces are assumed constant over a time and space by equivalent acceleration expected at the ground surface assuming a collapse mechanism. Although it is convenient to use but, its assumptions make it incapable for a real-time damage of structure. Further, in a seismically active zone, a cantilever sheet pile passing through a saturated loose, cohesionless soil may be subjected to liquefaction induced by earthquake forces, causing it to fail. Therefore, considering the need of present scenario, this paper investigates the dynamic analysis of cantilever sheet pile wall in liquefiable as well as non-liquefiable soils using finite difference-based computer program FLAC2D [5].

## 2 Numerical Modeling of Sheet Pile

The numerical modeling of a cantilever sheet pile wall passing through both liquefiable and non-liquefiable soil is carried out using an explicit finite difference-based computer program FLAC2D (Fast Lagrangian Analysis of Continua) assuming a two-dimensional and plane strain problem. The finite difference method is a well-established approach that can be used for analysis of any problem in geotechnical engineering. The analysis is done in two phases; namely excavation phase and dynamic phase. In excavation phase, Mohr–Coulomb elastic perfectly plastic soil model is used for establishing in-situ stress, and excavation with wall installation is done assuming shear modulus of soil as 0.3 times the original shear modulus of soil [3]. The boundary conditions of the model are standard boundary conditions. Fixed boundary conditions are provided at the base of the soil model in both  $x$ - and  $y$ -directions under static conditions, while for lateral boundaries, the  $x$ -direction was fixed and  $y$ -direction was kept free. In dynamic phase, the seismic motion is applied at the base of soil model. Free field and quiet boundary conditions are applied in the model for preventing reflections at the boundary.

An elastic-perfectly plastic Mohr–Coulomb model with non-associated flow rule is used for modeling the non-liquefiable soil (properties given in Table 1), and Finn-Byrne model is used to simulate liquefiable soil. For present study, the model assumed is shown as in Fig. 1 with excavation height  $h = 3$  m and embedded depth  $d = 5$  m. The sheet pile used is of type SKZ 20 [8] with properties given in Table 2. The dimensions of grid are chosen carefully to avoid filtering of high frequencies and must be less than one-tenth of the wavelength associated. The sheet pile is represented by beam elements.

In seismic analysis, material damping developed due to viscous properties of soil are also applied using the numerical fits to Seed and Idriss [7] data for sand as given in FLAC2D. The S-shaped curve of secant shear modulus versus logarithm of cyclic strain is used in default hysteresis model. The secant modulus  $M_s$  is expressed as:

**Table 1** Soil properties considered in present study [adopted from Chatterjee et al. [2] and Bowles [1]]

Properties	Values
Density (kg/m <sup>3</sup> )	1400
Young's modulus (MPa)	36
Shear modulus (MPa)	13
Poisson's ratio	0.38
Friction angle (°)	30
Bulk modulus (MPa)	50
Soil-wall interface angle (°)	20

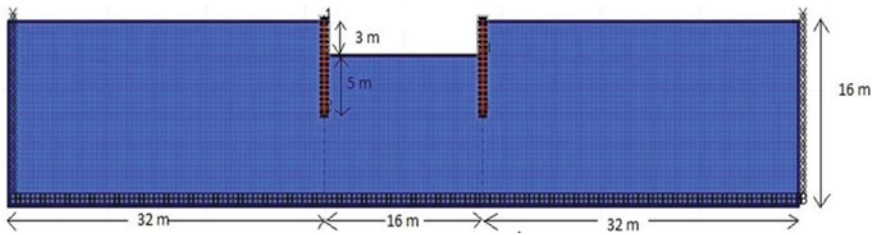


**Fig. 1** Sheet pile model considered in the present numerical study

**Table 2** Properties of sheet pile adopted from Skyline steel [8]

Type	Cross section area (cm <sup>2</sup> /m)	Section modulus (cm <sup>3</sup> /m)	Moment of inertia (cm <sup>4</sup> /m)
SKZ 20	127	1704	34,618

$$M_s = s^2(3 - 2s) \tag{1}$$

where  $s = (L2 - L)/(L2 - L1)$  and  $L$  is logarithmic strain. The parameters  $L1$  and  $L2$  are two extreme values of logarithmic strain and having values of  $-3$  and  $1$ , respectively, in the present study. For liquefaction analysis, Finn-Byrne liquefaction model is used which is given in FLAC2D with water table corresponding to dredge level in model. The water is modeled with a density of  $1000 \text{ kg/m}^3$  and bulk modulus of  $2 \text{ GPa}$ .

### 2.1 Input Seismic Motions

Two different acceleration-time histories are applied at the base of model in this present analysis, i.e., 1940 El Centro and 1989 Loma Prieta input motions. The properties of these two ground motions such as maximum ground acceleration, Arias intensity, response spectrum, and others are given in Table 3.

**Table 3** Strong motion parameters of earthquake motion in present study

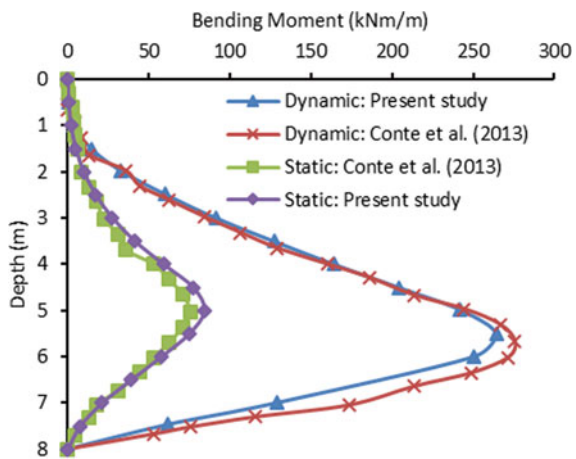
Earthquake strong motion parameters	1989 Loma Prieta Earthquake	1940 El Centro Earthquake
Date of occurrence	18 October 1989	19 May 1940
Moment magnitude (Mw)	7	6.9
Bedrock level acceleration (g)	0.33	0.2
Arias intensity (m/s)	1.108	1.126
Response spectrum (m/s <sup>2</sup> )	12.26	0.639
Peak ground displacement (m)	0.1226	6.32

### 2.2 Validation of Present Study

In order to validate the present numerical model, the results of this model in dry sand were compared with the results of Conti et al. [3]. In the numerical analysis, Conti et al. [3] used an elastic perfect plastic Mohr–Coulomb model for the dry soil with soil friction angle  $\phi = 35^\circ$ , cohesion  $c = 0$ , and density = 2.04 Mg/m<sup>3</sup>. The retaining walls were modeled having a diameter of 0.6 and 0.7 m spacing bored piles with bending stiffness =  $2.7 \times 10^5$  kNm<sup>2</sup>/m and soil–wall interface angle 20°. The total length of retaining wall was 8 m with excavated depth  $H = 4$  m. 1976 Friuli earthquake, which occurred in Tolmezzo, having peak ground acceleration 0.35 g is used for comparing the present results with that of Conti et al. [3].

It is observed from Fig. 2, that the bending moment obtained in the present study shows a similar trend and matches reasonably well with the bending moment magnitudes of Conti et al. [3] under both static as well as dynamic condition. The slight

**Fig. 2** Comparison of bending moment obtained in the present study with previous results for both static and dynamic conditions



variation in results may be attributed to the grid size difference of two models. In present study, a uniform grid size of 0.5 m is maintained in the model, while in Conti et al. [3] a grid size of 0.33 m was considered near the embedded wall consisting of total 4838 elements.

### 3 Results and Discussion

After validating the present numerical model with the results of Conti et al. [3], a parametric study of sheet pile wall passing through liquefiable soil and subjected to two different earthquake motions is carried out using FLAC2D computer program. The dimensions of the model are kept constant (excavated height  $h = 3$  m and embedded depth  $D = 5$  m) when subjected to both the ground motions, and bending moment, lateral displacement and net pressure data are analyzed for static as well as seismic condition.

In static conditions, the maximum bending moment observed is 34.1 kNm/m which increased significantly under dynamic conditions. When 1940 El Centro ground motion having bedrock level acceleration 0.2 g is applied at the base of the soil model, the bending moment increased to 88 kNm/m in non-liquefiable soil, and for liquefiable soil conditions, the bending moment increased to 128 kNm/m as shown in Fig. 3a. The increase was about 2.5 and 3.75 times in non-liquefiable and

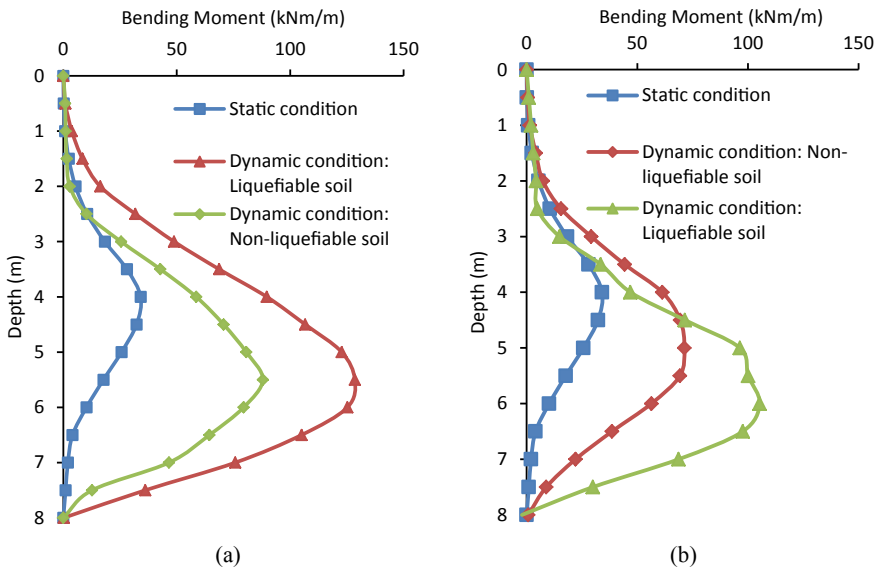


**Fig. 3** Comparison of bending moment for **a** 1940 El Centro earthquake and **b** 1989 Loma Prieta earthquake

liquefiable soil, respectively, as compared to static conditions. Similarly, when 1989 Loma Prieta ground motion is applied, the maximum bending moment increased to 71.3 kNm/m and 105.3 kNm/m in non-liquefiable and liquefiable soil, respectively, as shown in Fig. 3b. On comparing the bending moment due to both ground motions, it is observed that maximum bending moment occurred due to 1940 El Centro ground motion with bedrock level acceleration 0.2 g than 1989 Loma Prieta ground motion having bedrock level acceleration of 0.33 g. This may be due to the large bracketed duration of former seismic motion. It is also observed that the depth of sheet pile at which the maximum bending moment occurs becomes more in dynamic condition than static condition. Further, the maximum bending moment occurred at the instants after the time of peak ground acceleration. At the time of maximum acceleration, the backfill soil remains at active limit condition, and after that, the horizontal stresses are greater than the corresponding active values on retained side [3].

The displacement of the sheet pile is also influenced by the input seismic motions. In static condition, the wall displacement measured 8.55 mm which drastically increased to 412.3 and 1000 mm in non-liquefiable soil and liquefiable soil, respectively, for 1940 El Centro ground motion as shown in Fig. 4a. The lateral wall displacement observed in 1989 Loma Prieta earthquake, as shown in Fig. 4b, are 81 and 691 mm in non-liquefiable soil and liquefiable soil, respectively, which are less than 1940 El Centro ground motion. From net pressure diagrams as shown in Fig. 5, it is observed that the active pressure on backfill side is higher in dynamic condition than static condition. The increase in dynamic active earth pressure in backfill soil

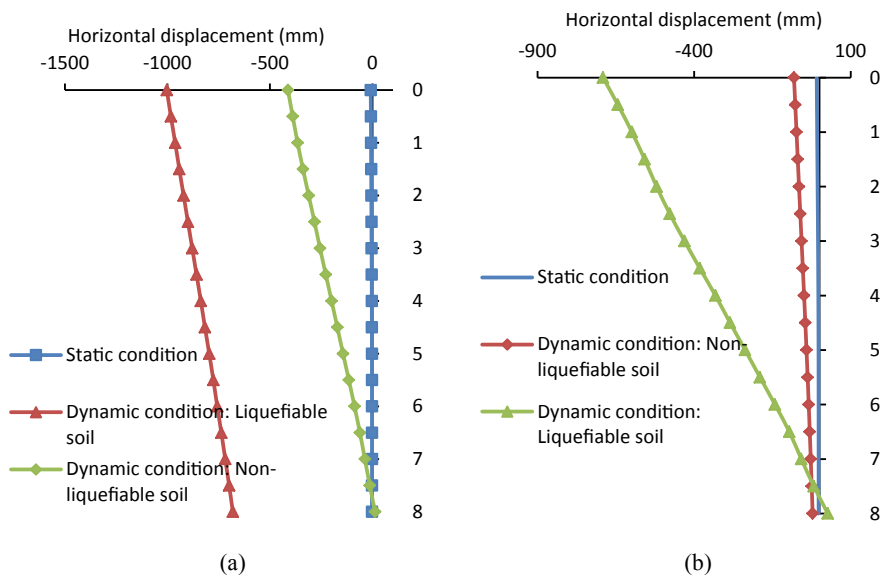


**Fig. 4** Comparison of lateral wall displacement for **a** 1940 El Centro earthquake and **b** 1989 Loma Prieta earthquake

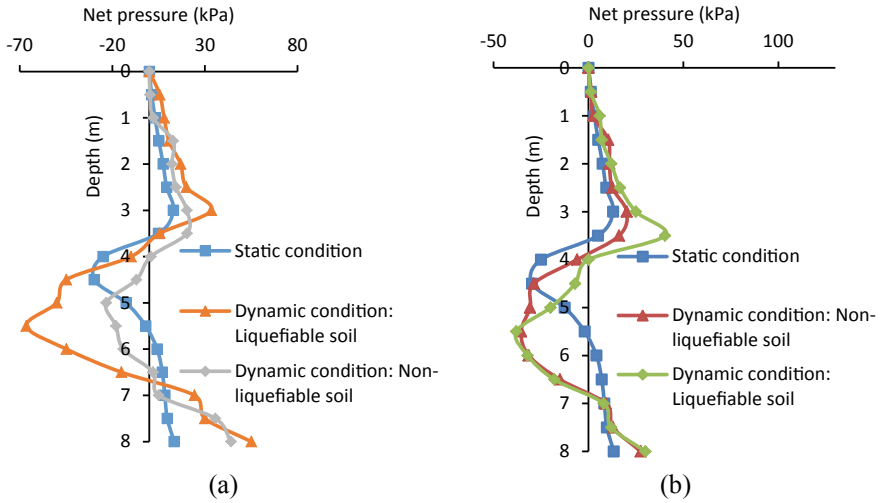


**Fig. 5** Comparison of net pressure for **a** 1940 El Centro earthquake and **b** 1989 Loma Prieta earthquake

**Table 4** Maximum bending moment and horizontal displacement values at different conditions

Parameters	Static condition	Dynamic condition			
		1940 El centro earthquake		1989 Loma Prieta earthquake	
		Non-liquefiable soil	Liquefiable soil	Non-liquefiable soil	Liquefiable soil
Maximum bending moment (kNm/m)	34.1	88	128	71.3	105.3
Horizontal displacement (mm)	8.55	412.3	1000	81	691

contributes to the mobilization of net passive earth pressure below the dredge level. The maximum bending moment and horizontal displacement in the sheet pile for static and dynamic conditions are tabulated in Table 4.

## 4 Conclusion

The present study analyzes the influence of two earthquake motions on a cantilever sheet pile wall in both liquefiable and non-liquefiable soil through numerical analysis using FLAC2D computer program. The results obtained from the present numerical

study are compared with available solutions in literature and good agreement between the results are observed. The major conclusions drawn from the present study are:

- The maximum bending moment under dynamic conditions are greater than the static conditions.
- The bending moment observed in the sheet piles are more in liquefiable soil when compared to non-liquefiable soil under dynamic conditions. This is due to the reduction in shear strength and stiffness of the saturated soil.
- The maximum bending moment occurred after the time instants of peak ground acceleration as the horizontal stresses increased after limit conditions at time of peak ground acceleration is attained.
- The bending moment occurred and horizontal displacement was observed to be higher for 1940 El Centro earthquake having a bedrock level acceleration of 0.2 g than 1989 Loma Prieta earthquake having bedrock level acceleration of 0.33 g, due to large bracketed duration of the former motion.
- Hence, the present results using FLAC2D can be used for design of cantilever sheet pile wall passing through liquefiable soil in earthquake prone areas.

## References

1. Bowles JE (1997) Foundation analysis and design, 5th edn. McGraw-Hill, New York
2. Chatterjee K, Choudhury D, Poulos HG (2015) Seismic analysis of laterally loaded pile under influence of vertical loading using finite element method. *Comput Geotech* 67:172–186
3. Conti R, Viggiani GMB, Burali D'Arezzo F (2013) Some remarks on the seismic behaviour of embedded cantilevered retaining walls. *Géotechnique* 64(1):40–50
4. Fang YS, Yang YC, Chen TJ (2003) Retaining walls damaged in the Chi-Chi earthquake. *Can Geotech J* 40(6):1142–1153
5. FLAC2D (2016) Fast Lagrangian analysis of continua. Version 8.0, Itasca Consulting Group, Minneapolis, Minnesota, USA
6. Koseki J, Koda M, Matsuo S, Takasaki H, Fujiwara T (2012) Damage to railway earth structures and foundations caused by the 2011 off the Pacific Coast of Tohoku Earthquake. *Soils Found* 52(5):872–889
7. Seed HB, Idriss IM (1970) Soil moduli and damping factors for dynamic response analysis. Report No. UCB/EERC-70/10. Earthquake Engineering Research Center, University of California, Berkeley
8. Skyline Steel (2017) Technical product manual. New Jersey, USA



# Bearing Capacity of Strip Footing Over Rectangular Tunnel in Soft Clay



Puja Dutta, Penke Sriharsha, and Paramita Bhattacharya

**Abstract** This research work examines the bearing capacity of strip footing over rectangular tunnel in soft clay. The bearing capacity under undrained condition is being obtained for a various conjunctions of  $B/D$ ,  $H/D$ ,  $c_{uo}/\gamma D$  and  $m$  where  $D$ ,  $B$  and  $H$  are height, width and soil cover depth of the tunnel, respectively,  $c_{uo}$  is the undrained shear strength of the soil at the ground surface,  $\gamma$  is the unit weight of the soil and  $m$  is a dimensionless parameter which depicts the linear variation of undrained shear strength of soil with depth. The analysis is being performed using lower bound limit analysis, finite elements and nonlinear programming. The present results indicate that normalized bearing pressure decreases with a decrease in normalized vertical distance between tunnel and footing and it becomes constant at a critical normalized distance or say critical cover depth of the tunnel. The values of the critical depth depends upon the size of underlying tunnel and  $m$ . In case the tunnel is placed above this critical depth, the bearing capacity of footing varies with size and cover depth of tunnel and also on non-homogeneity of undrained clay.

**Keywords** Footing · Bearing capacity · Tunnel · Limit analysis · Nonlinear programming

## 1 Introduction

The usage of underground space through tunnelling has been proved to be one of the best solutions for rapid urbanization. The presence of tunnel under any foundation might create risk of failure; hence it becomes an important task to study the stability of foundation above an underground opening. There has been quite a few literatures reported. Baus and Wang [2] carried out studies regarding the bearing capacity of strip footing on clay for singular continuous voids of circular and rectangular shape embedded. Wang and Badie [9] studied the effects on the capacity of strip and square footings of different size and embedment depths due to void location, size and shape

---

P. Dutta (✉) · P. Sriharsha · P. Bhattacharya  
Indian Institute of Technology Kharagpur, Kharagpur 721302, India  
e-mail: PUJADUTTA@iitkgp.ac.in

© Springer Nature Singapore Pte Ltd. 2022  
A. K. Dey et al. (eds.), *Proceedings of the 7th Indian Young Geotechnical Engineers Conference*, Lecture Notes in Civil Engineering 195,  
[https://doi.org/10.1007/978-981-16-6456-4\\_3](https://doi.org/10.1007/978-981-16-6456-4_3)

(circular and cubical). Wang and Hsieh [10] suggested failure mechanisms for strip footing above circular void in cohesive-frictional soil. Azam et al. [1] performed the finite element analysis to estimate the bearing capacity of strip footing placed on a homogeneous soil and stratified deposit consist of different soil layers with and without an inclusion of void of rectangular/square/circular shape. Singh and Basudhar [8] studied the lower bound bearing capacity of smooth strip footing over a rectangular opening in cohesive-frictional soil. Kiyosumi et al. [5] studied the effects on the yield pressure of strip footing resting on calcareous soil due to multiple voids embedded below. Kiyosumi et al. [6] executed model tests of strip footing on stiff ground with square voids embedded under it. Lee et al. [7] studied stability of surface strip footing above rectangular voids by finite element analysis. Chakraborty and Sawant [3] determined the bearing capacity of strip above a circular void in presence of seismic forces. In this analysis they assumed a weightless soil condition.

From the literature review, it is understood that no research work is available to determine the lower bound of the bearing pressure of strip footing in homogeneous and non-homogeneous clay soil under undrained condition with  $\phi_u = 0^\circ$  in the presence of rectangular and square openings placed centrally below the footing. The goal of this study is to determine the effect on bearing capacity of strip footing due to the presence of rectangular and square openings in undrained clay.

## 2 Problem Definition

The problem definition consist of a strip footing located over an existing rectangular tunnel of height ( $D$ ) and width ( $B$ ) present at a cover depth ( $H$ ). In the present analysis, the width of footing has been taken equal to the height of the rectangular tunnel. The tunnel is located in soft clay with  $\gamma$  as unit weight of the soil and  $c_{u0}$  as undrained soil cohesion at ground surface;  $m$  is the normalized rate which implies a linear variation of increase in shear strength of soil with depth. The soil mass follows Mohr–Coulomb yield criteria and an associative flow rule. The soil cohesion ( $c_u$ ) at any depth  $h_v$  from ground surface is defined by Eq. 1:

$$C_u = C_{u0}[1 + mh_v/d] \quad (1)$$

The normalized bearing capacity  $p/c_{u0}$  has been determined for various  $H/D$ ,  $B/D$ ,  $c_{u0}/\gamma D$  and  $m$ .

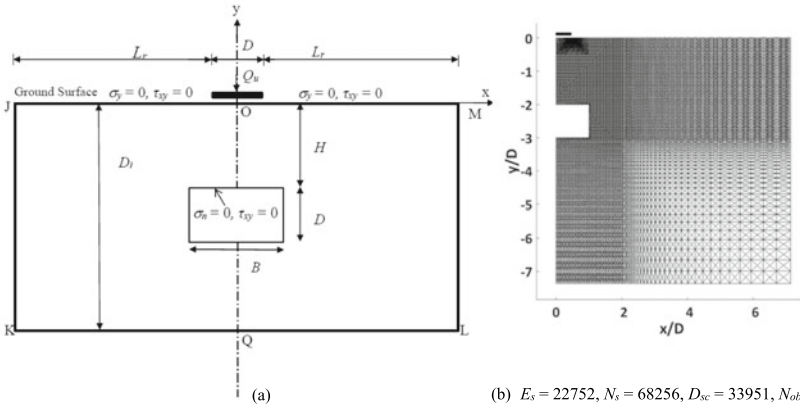


**Fig. 1** **a** Schematic diagram of strip footing over rectangular tunnel, **b** finite element mesh for  $B/D = 2$  and  $H/D = 2$

### 3 Finite Element Mesh, Domain and Stress Boundary Conditions

A strip footing of width  $D$  has been kept resting on the surface of a soil domain JKLM, as mentioned in Fig. 1a, where a tunnel with height  $D$  and width  $B$  is at a depth  $H$ . The problem definition is similar along the  $y$ -axis about the centre of the footing. Hence, only half of the domain, i.e. OQLM has been used for the analysis. The extent in the horizontal direction ( $L_r$ ) varies from  $4D$  to  $10D$  and in the vertical direction ( $D_i$ ) from  $5D$  to  $11D$  for  $H/D = 1$  and  $H/D = 5$ , respectively. The stress boundary conditions are mentioned in Fig. 1a. The problem domain size is selected such that the yielded elements are well inside the boundaries and there is no change in the collapse load with further increase in domain size. Finite element mesh used for  $B/D = 2$  and  $H/D = 2$  is shown in Fig. 1b where the notations  $E_s$ ,  $N_s$ ,  $D_{sc}$  and  $N_{ob}$  expresses the total number of elements, nodes, discontinuities and objective nodes, respectively.

### 4 Analysis

The analysis is being carried out in plane strain condition using lower bound limit analysis with finite elements and second order conic programming technique. The domain is discretized into 3-noded triangular elements. The stress is varied linearly throughout each element and the nodal stresses  $\sigma_x$ ,  $\sigma_y$  and  $\tau_{xy}$  are the unknown basic variables. The equilibrium conditions along with stress discontinuities are satisfied

throughout the problem domain. The stress conditions are enforced along the nodes of the boundary and tunnel periphery. Mohr–Coulomb yield criteria under plane strain condition is given as:

$$\sqrt{(\sigma_x - \sigma_y)^2 + (2\tau_{xy})^2} \leq 2c \cos \phi - 0.5(\sigma_x + \sigma_y) \sin \phi \quad (2)$$

The above criteria can be exhibited as a 3-dimensional second order cone for each node  $i$ , which leads as  $x^i_{SOCP} = \{s_{xx}, s_{xy}, s_{aux}\}^T$  where the relation between basic stress variables and conic variables are as follows:

$$s_{xx} = 0.5(\sigma_x - \sigma_y); s_{xy} = \tau_{xy} \text{ and } s_{aux} = c \cos \phi - 0.5(\sigma_x + \sigma_y) \sin \phi \quad (3)$$

The inequality constraint given in Eq. (2) will be represented according to second order constraint,

$$\sqrt{s_{xx}^2 + s_{xy}^2} \leq s_{aux} \quad (4)$$

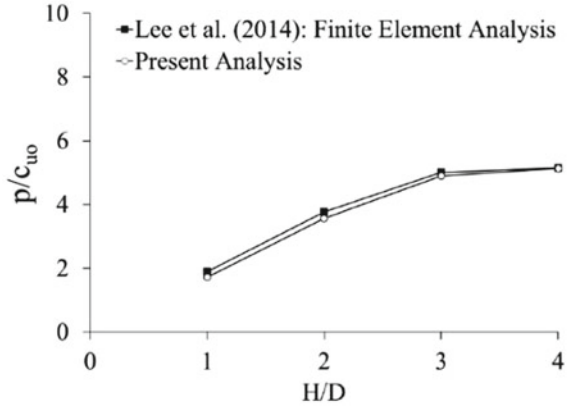
The value of  $p/c_{uo}$  is obtained by maximizing the compressive stress around the footing surface subjected to element equilibrium, discontinuity condition, stress boundary condition and second order inequality constraint satisfying Mohr–Coulomb yield criteria at all nodes. The bearing pressure ( $p$ ) is calculated as:  $p = (Q_u/(D \times L_x))$ , where  $Q_u$  is collapse load,  $L_x$  is the out of plane length of the footing. For plane strain problem,  $L_x = 1$  unit.

## 5 Comparison and Results

### 5.1 Comparison

The present analysis has been compared with solutions of the elasto-plastic finite element analysis reported by Lee et al. [7] for square tunnel under strip footing in homogenous soil for  $c_{uo}/\gamma D = 3$  with size of the footing being equal to height of the tunnel and the comparison is presented in Fig. 2. The measure of  $p/c_{uo}$  of the present analysis is smaller than that obtained by Lee et al. [7]. The difference tends to reduce with an increase in  $H/D$  and becomes negligible at  $H/D = 4$  for square tunnel and homogenous soil condition. Lower bound theorem always provides a safer collapse load which is lower or equal to the actual ultimate collapse load; hence the solution obtained from present analysis is lower than solution reported by Lee et al. [7].

**Fig. 2** Comparison of present analysis with Lee et al. [7] for  $c_{uo}/\gamma D = 3$ ,  $m = 0$  and  $B/D = 1$



### 5.2 Results

The plane strain analysis is being carried out for rectangular tunnel in soft clay under strip footing of width  $D$  for various values of (i)  $B/D = 1-3$  with an interval gap of 1, (ii)  $c_{uo}/\gamma D$  equal to 1, 2, 3 and 4 and (iii)  $m = 0, 0.25, 0.5, 0.75$  and 1. The results of analysis for (i)  $B/D = 1, 2$  and 3, (ii)  $m = 0, 0.5$  and 1 and (iii)  $c_{uo}/\gamma D = 1, 2, 3$ , and 4 are plotted in terms of variation of  $p/c_{uo}$  with  $H/D$  as shown in Figs. 3 and 4. It has been observed from the numerical analysis that for  $m = 0$  and  $c_{uo}/\gamma D = 1$  and 2 the value of  $p/c_{uo}$  decreases with increase in cover depth ratio for every  $B/D$ . This suggests that in these cases the existence of tunnel under strip footing reduces its capacity substantially. Apart from the above mentioned cases, the value of normalized bearing pressure ( $p/c_{uo}$ ) has been found to decrease with decrease in depth of tunnel for all combinations of  $m$ ,  $c_{uo}/\gamma D$  and  $B/D$ . The increase in  $p/c_{uo}$  continues till it reaches to a maximum value which is equal to the value of  $p/c_{uo}$  obtained without underground opening and thereafter becomes constant. The charts also show the effect of  $B/D$  on the value of  $p/c_{uo}$ . Wider rectangular tunnel tends to decrease the capacity of the footing.

### 5.3 Proximity of Stress State at a Point to Failure

The stress state at a point with respect to the available shear strength of soil is determined by a ratio  $a/d$  where:

$$a = (\sigma_x - \sigma_y)^2 + (2\tau_{xy})^2 \text{ and } d = (2c \cos \phi - (\sigma_x + \sigma_y) \sin \phi)^2.$$

The ratio of  $a/d$  remains smaller than 1 for non-yielding points and becomes unity where shear failure has occurred. The failure plots are shown in Fig. 5a-c for  $c_{uo}/\gamma D = 1$  and  $m = 0.5$ . Figure 5a, b illustrates the failure plot for  $H/D = 2$  and

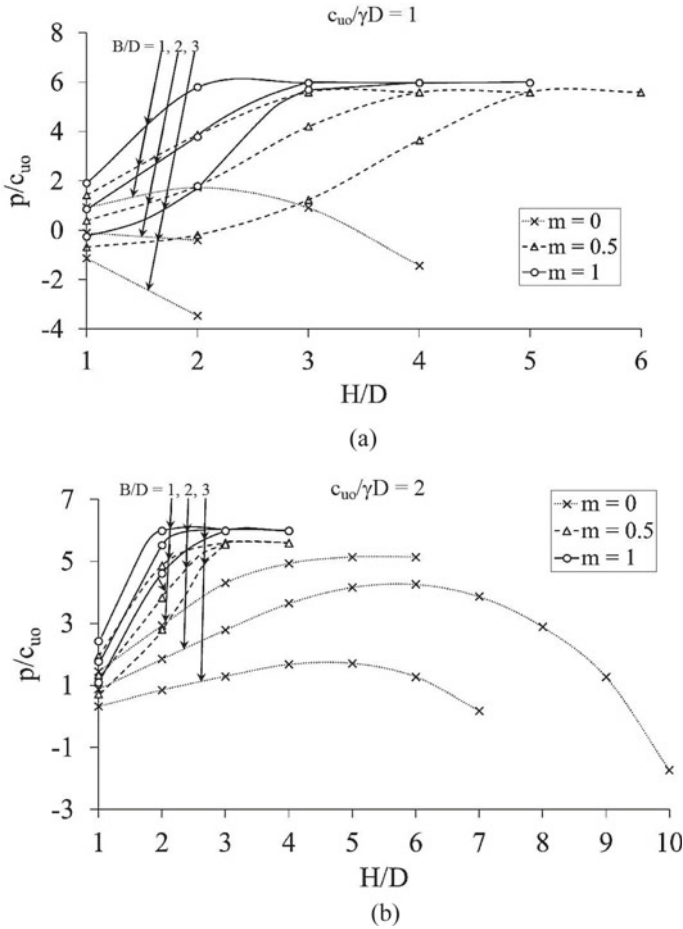


**Fig. 3** Charts showing variation of  $p/c_{u0}$  with  $H/D$  for **a**  $c_{u0}/\gamma D = 1$  and **b**  $c_{u0}/\gamma D = 2$

4, respectively with  $B/D = 1.5$  and Fig. 5c shows the failure plot for  $H/D = 2$  with  $B/D = 3$ . It can be noted from the plots that the failure surface extends towards the tunnel until it reaches the critical normalized depth and thereafter the existence of tunnel does not pose any hindrance to the workability of the footing. It has also been found that the size of failure surface increases when there is an increase in size of the underlying tunnel (Table 1).

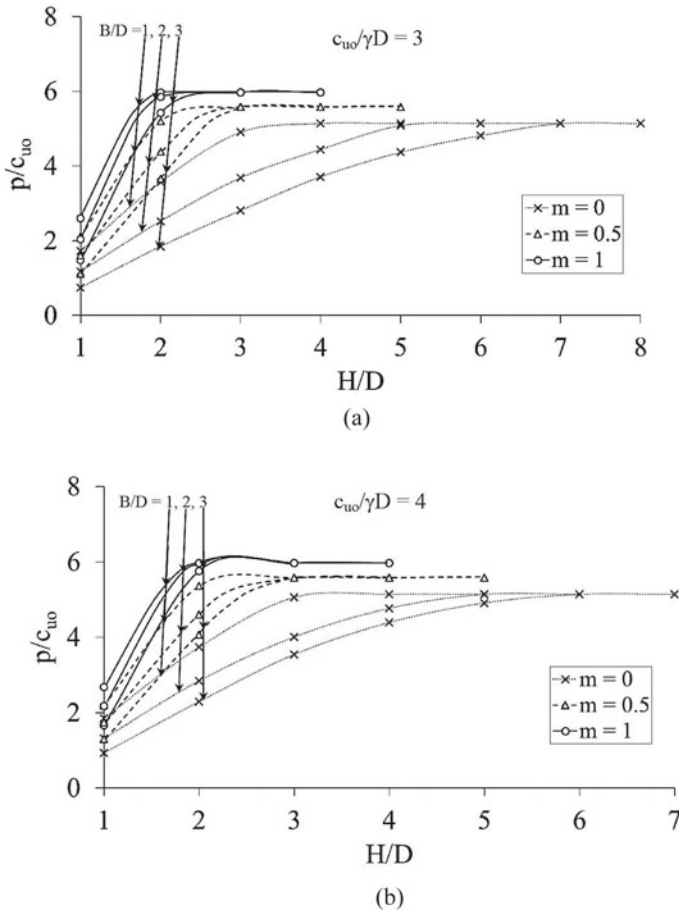
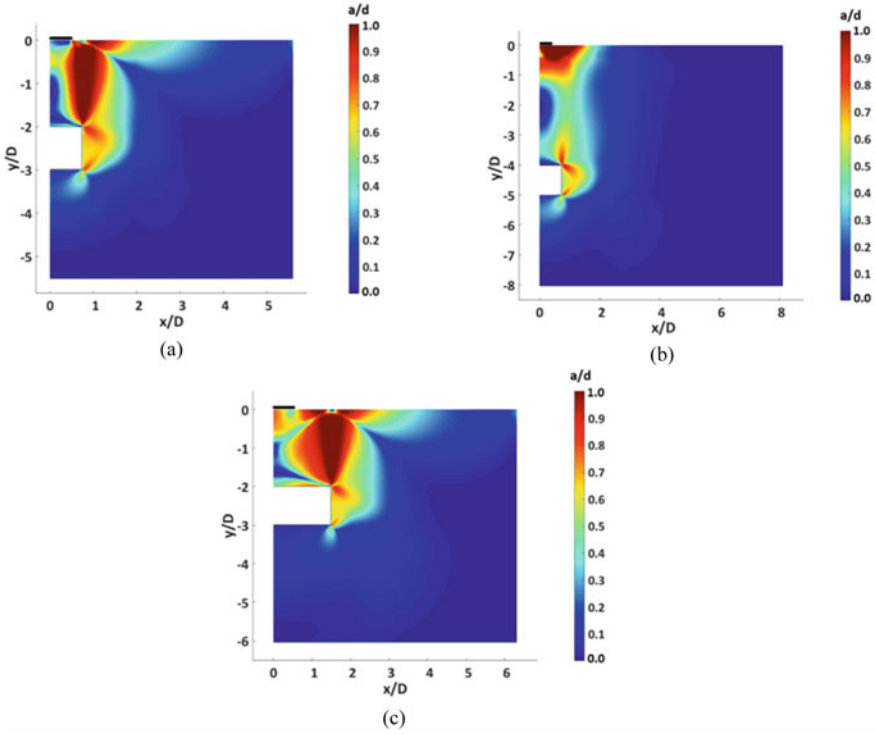


Fig. 4 Charts showing variation of  $p/c_{u0}$  with  $H/D$  for a  $c_{u0}/\gamma D = 3$  and b  $c_{u0}/\gamma D = 4$

## 6 Conclusion

By implementing the use of lower bound limit analysis, finite elements and SOCP technique, the normalized bearing capacity of strip footing above a rectangular tunnel has been evaluated. It has been found that in most cases except a few, the value of normalized bearing pressure increases with increase in normalized depth of tunnel till it reaches critical normalized depth and thereafter becomes constant attaining the maximum normalized bearing pressure. As the strength of soil increases with increase in non-homogeneity, the value of maximum normalized bearing pressure also increases. The value of  $(H/D)_{cr}$  for non-homogenous soil condition has been observed to decrease with increase in strength of the soil. The influence of aspect ratio of the tunnel has also been observed to affect the capacity of the footing.



**Fig. 5** Stress contour plots for  $m = 0.5$ ; **a**  $H/D = 2, B/D = 1.5$ , **b**  $H/D = 4, B/D = 1.5$  and **c**  $H/D = 2, B/D = 3$

Constructing the tunnel at depths higher than the critical depth will prevent the interference of tunnel with the footing, thus preventing the reduction of bearing capacity. The present work provides a few charts on variation of  $p/c_{u0}$  with  $H/D$  for various values of (i)  $B/D$ , (ii)  $c_{u0}/\gamma D$  and (iii)  $m$  which are expected to be useful in evaluating the performance of a strip footing over a rectangular tunnel.



**Table 1** Critical normalized cover depth  $(H/D)_{cr}$

$m$	$c_{uo}/\gamma D$	$(B/D)$					$(p/c_{uo})$ at $(H/D)_{cr}$
		1	1.5	2	2.5	3	
0	1						5.14 (5.14)*
	2	5	8				
	3	4	5	6	6	7	
	4	4	4	5	6	6	
0.25	1	4	5	6	7	8	5.37 (5.4)*
	2	3	4	4	4	5	
	3	3	3	4	4	4	
	4	3	3	3	4	4	
0.5	1	3	4	4	5	5	5.59 (5.58)*
	2	3	3	3	3	4	
	3	3	3	3	3	3	
	4	3	3	3	3	3	
0.75	1	3	3	4	4	4	5.79 (5.79)
	2	2	3	3	3	3	
	3	2	3	3	3	3	
	4	2	3	3	3	3	
1	1	3	3	3	3	4	5.97 (5.96)*
	2	2	3	3	3	3	
	3	2	2	3	3	3	
	4	2	2	3	3	3	

\* Bearing capacity factors given by Davis and Booker [4]

## References

1. Azam G, Hsieh CW, Wang MC (1991) Performance of strip footing on stratified soil deposit with void. *J Geotech Geoenviron Eng* 117(5):753–772
2. Baus RL, Wang MC (1983) Bearing capacity of strip footings above void. *J Geotech Eng* 109(1):1–14
3. Chakraborty D, Sawant AS (2016) Seismic bearing capacity of strip footing above an unsupported circular tunnel in undrained clay. *Int J Geotech Eng* 11(1):97–105
4. Davis EH, Booker JR (1973) The effect of increasing strength with depth on the bearing capacity of clays. *Geotechnique* 23(4):551–563
5. Kiyosumi M, Kusakabe O, Ohuchi M, Peng FL (2007) Yielding pressure of spread footing above multiple voids. *J Geotech Geoenviron Eng* 133:1522–1531
6. Kiyosumi M, Kusakabe O, Ohuchi M (2011) Model tests and analyses of bearing capacity of strip footing on stiff ground with voids. *J Geotech Geoenviron Eng* 137:363–375
7. Lee JK, Jeong S, Ko J (2014) Undrained stability of surface strip footings above voids. *Comput Geotech* 62:128–135
8. Singh DN, Basudhar PK (1995) Lower bound bearing capacity of a strip footing over underground openings. PACAM IV, University of Salvador, Argentina

9. Wang MC, Badie A (1986) Effect of underground void on foundation stability. *J Geotech Eng* 111:1008–1019
10. Wang MC, Hsieh CW (1987) Collapse load of strip footing above circular void. *J Geotech Eng* 113:511–515

# Combined Effect of Vertical and Horizontal Loads on the Behavior of Pile Foundations in Layered Soils



Manne Manoj Kumar and A. Murali Krishna

**Abstract** Piles are generally used to carry both vertical and horizontal loads. For small lateral loads, the piles response is evaluated separately without considering their possible interaction of both lateral and vertical loads. In the construction of several offshore structures, the lateral loads are comparatively high where the combined effect of both vertical and lateral loads should be taken into account. As in practical conditions the natural soils are stratified and for the construction of high-rise buildings, pile foundations are to be used which emphasizes to analyze the behavior of piles in layered soils considering the combined effect of vertical and horizontal loads. In this study, numerical analysis was carried out considering the soil continuum behavior and non-linearity using the finite element geotechnical software Plaxis 3D. Single pile behavior subjected to combined lateral and vertical loads in case of layered soils has been discussed. It can be noted that by considering the effects of both these loads, it would lead to a more safe and cost-effective pile foundation design.

**Keywords** Lateral loads · Plaxis 3D · Lateral pressure · Pile foundation

## 1 Introduction

Pile foundations generally support different structure types built on weak soils, where the soil bearing capacity is low and also in places where shallow foundations would not support the loads coming on to them. Piles are slender columns generally used to resist vertical loads coming on to them. But as the loads are not always vertical, the piles should be able to resist any type of load coming on to it. In general, when analysis of piles is carried out it is first analyzed for a normal load to find the bearing capacity and its corresponding settlement, and then it is analyzed for the horizontal

---

M. M. Kumar (✉) · A. Murali Krishna  
Department of Civil Engineering, Indian Institute of Technology Guwahati, Guwahati, Assam,  
India  
e-mail: [manoj174104095@iitg.ac.in](mailto:manoj174104095@iitg.ac.in)

A. Murali Krishna  
e-mail: [amurali@iitg.ac.in](mailto:amurali@iitg.ac.in)

© Springer Nature Singapore Pte Ltd. 2022  
A. K. Dey et al. (eds.), *Proceedings of the 7th Indian Young Geotechnical Engineers Conference*, Lecture Notes in Civil Engineering 195,  
[https://doi.org/10.1007/978-981-16-6456-4\\_4](https://doi.org/10.1007/978-981-16-6456-4_4)

load for obtaining the flexural behavior. However, this type of analysis is normally valid for very less horizontal loads. In case of offshore structures, the lateral loads are large as compared to vertical loads. So, in that case it is necessary to study the combined effect of vertical and lateral loads considering their possible interaction between them.

Several researchers [7, 8] have observed the behavior of piles under pure vertical and pure lateral loads and some generalized solutions were provided. However, there is less effort made to understand the lateral response of piles due to the influence of vertical load in case of stratified medium and the literature available was sparse on this study. Anagnostopoulos and Georgiadis [1] studied through model lab testing of a pile that the combined effect of loads cannot be used for in general by the conventional methods of analysis with the help of using two-dimensional (2D) finite element analysis. Therefore, the researchers suggested to use non-linear three-dimensional (3D) numerical analysis techniques for analyzing this condition. With advanced computer technology, the non-linearity effects and elasto-plastic nature of soil medium etc., can be analyzed. Karthigeyan et al. [4, 5] have observed that the lateral response of piles significantly increases the capacity in sandy soils and marginally decreases the capacity in clayey soils respectively due to the influence of vertical loads. Trochanis et al. [10] analyzed the combined effect of loads through Abaqus software. Generally, piles are not designed to resist only horizontal loads, the response of piles under combination of loads is more critical and becomes more interesting for the design engineers.

In this study, the behavior of piles subjected to pure lateral loads and also combination of both loads embedded in layered soil medium was analyzed using finite-element (FE) analysis Plaxis 3D. The developed numerical model details, the validation of that model against the field load test data and the results obtained from the parametric study were discussed.

## 2 Numerical Model

A geotechnical finite element (FE) program Plaxis 3D was used for analyzing the soil-pile behavior. Plaxis 3D is a FE program extensively used for various types of geotechnical applications for conducting deformation and stability analysis.

## 2.1 Validation

The developed numerical model has been validated by back predicting the field pile load test data for different cases and the complete details corresponding to the both considered cases were described below.

### Case study-I

Karasev et al. [3] conducted field load tests to determine the influence of different load combinations considered. The same pile was modeled in Plaxis 3D. Model dimensions used in Plaxis 3D are  $6 \times 6 \times 13$  m (number of trials were done such that there is no boundary effect and dimensions were fixed) and the diameter and length of the test pile made of concrete was 0.6 m and 3 m, respectively. The pile was installed in a sandy clay for more than 7 m thickness overlain by 6 m thick very stiff sandy loam. The cohesion and friction angle for the top soil layer was 18 kPa and  $18^\circ$  and that of the bottom layer was 24 kPa and  $14^\circ$  respectively. The Young's modulus ( $E$ ) and the Poisson's ratio ( $\mu$ ) was calculated based on empirical correlations [2] and the values obtained were 25,000 kPa and 0.35 for top soil and that of bottom soil was 20,000 kPa and 0.40 respectively. For the soils considered, zero dilation angle was assumed. The load application sequence was same as done in field testing that was followed in the current FE analysis i.e., the load is applied vertically first and then by keeping the vertical load constant the horizontal loads were applied. Mohr–Coulomb constitutive model was used to model the elasto-plastic soil behavior.

After the application of the loading the results obtained were compared with the field load test results which were reasonably comparable and also have been compared with Karthigeyan et al. [5] as shown in Fig. 1.

### Case Study-II

For the construction of a Cosmetic Factory Plant at Pacharia, Dadara, North Guwahati, Guwahati, field vertical and lateral pile load test were conducted for the determination of pile ultimate capacity and the corresponding deformations. For obtaining the validity of our numerical model, the field lateral pile load test data was back predicted with the help of Plaxis 3D finite element program. The soil model adopted was  $24 \times 24 \times 40$  m (trials were done to adopt the model dimensions such that there are no boundary effects) as shown in Fig. 2; a very fine mesh was adopted to analyze the model. The subsoil details were obtained from rigorous subsoil investigation analysis and the details were tabulated in Table 1. Ground water table is available at 1.5 m depth from the surface level.  $E$  and  $\mu$  used in the model were determined by same procedure as explained in case study-I for layers of soil considered.

A load of 120 kN is applied as per the field load test. The length of the pile adopted is of 26 m length and 600 mm diameter made of M25 grade of concrete. The results obtained from the numerical analysis were plotted and compared with field lateral load test results as shown in Fig. 2.

In both the cases described above, the results were closely matching with the field case results which signify that the numerical model using Plaxis 3D has been well predicted and can be used for further analysis.

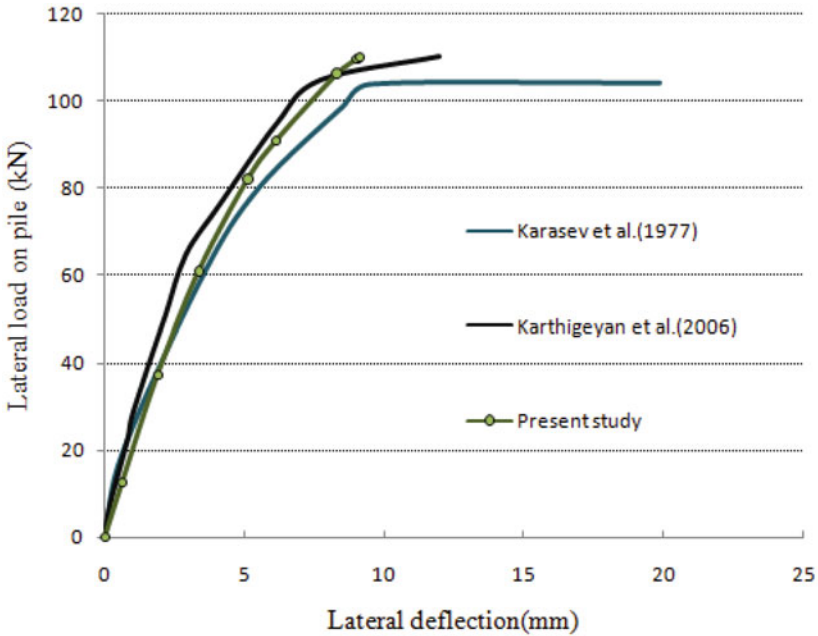


Fig. 1 Load-deformation curve

### 3 Analysis of Piles Subjected to Combined Loads

For analyzing the single pile behavior in case of layered soils, the soil profile, pile cross section and material details were also same as described in case-II. For obtaining the effect of combined loading different combinations of vertical and horizontal loads used are 0.25, 0.5, 0.75 Vult, Vult (ultimate bearing capacity of the pile = 1832 kN obtained from field load test and validation also) and 120 kN, 360 kN respectively.

#### 3.1 Lateral Response Due to Influence of Vertical Load

Analysis of pile embedded in a layered stratum was considered. Pile is modeled as an embedded beam with linear-elastic behavior, while the surrounding soil's behavior was simulated using Mohr–Coulomb shear strength criteria with appropriate engineering properties (Table 1). The Soil-Structure-Interaction (SSI) has been modeled using the interface properties available in the FE program. An inter-face stiffness value ( $R_{int}$ ) of 0.67 has been set to account for any gapping/slip that may have occurred during the loading phases. Geometrical extent of the model has been decided based on the literature suggested ranges. A lateral extent of  $\pm 20D$  (12 m) in both the lateral directions (X and Y) was chosen while an extent of 1.5L along the depth

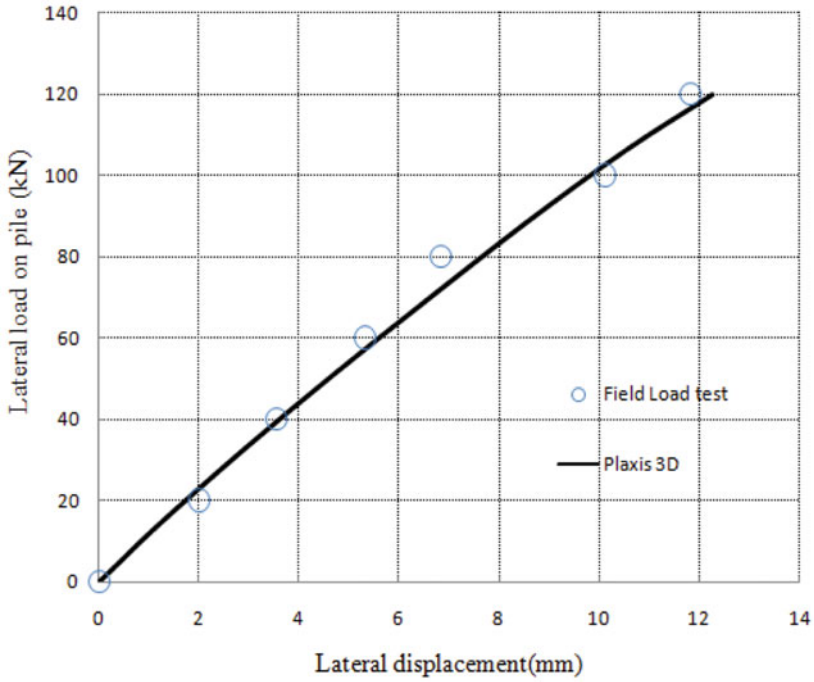
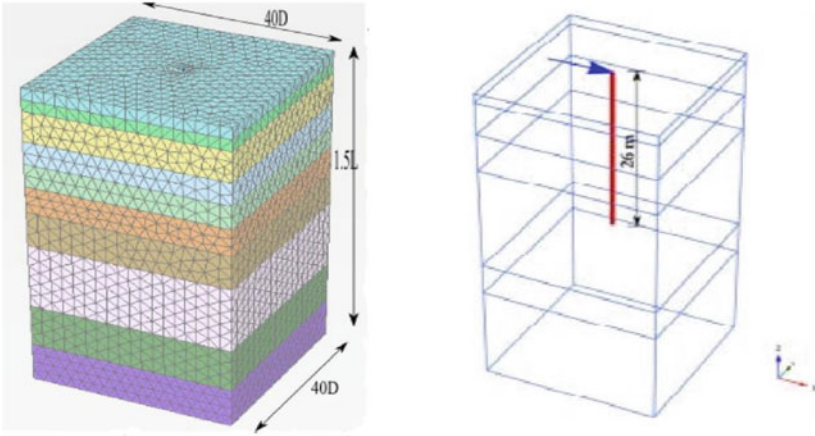


Fig. 2 Comparison of lateral response of pile with field test results

Table 1 Soil stratigraphy at the site

Depth (m)	Soil classification (USCS)	Unit weight (kN/m <sup>3</sup> )	Cohesion (kN/m <sup>3</sup> )	Friction angle (°)	SPT N-value
0–1.5	OL	16	0	0	3
1.5–3	CL	19.5	27	2	7
3–7	CL	19.6	33	2	7
7–10	CL/SM	19.7	43	2	10
10–13	CL/SM	19.8	48	2	15
13–16.5	SP	19	0	31	25
16.5–21	SP	19.5	0	33	33
21–29.5	SP	21	0	37	42
29.5–35	CL	19.9	53	2	30
35–40	SP	22	0	38	47



**Fig. 3** Three-dimensional soil-pile model

(Z direction) was considered. These boundary extents would satisfy no-stress effect due to the finite boundary conditions prevailing [6] (Fig. 3).

Vertical roller boundary conditions have been applied at the sides of the model restricting the lateral deformations and pinned boundaries (full fixities) were applied at the model base. A very fine mesh was used for the enhanced accuracy of the results. The calculations have been performed in multiple stages-(1) only soil with equilibrium conditions achieved (2) pile construction and application of loading phase.

The application of loads is done in two steps (i) first vertical load was applied and (ii) next, keeping the vertical loads constant, lateral loads were applied which is similar as in several practical cases such as overhead tanks, transmission line towers and pile jetties.

For the considered soil profile, the variation of lateral displacement due to the application of vertical loading (and for  $H = 120 \text{ kN}$ ,  $360 \text{ kN}$ ) is tabulated in Table 2. It can be seen that with increase in vertical load, there is a marginal decrease in lateral displacement as shown in Fig. 4.

**Table 2** Variation of displacement with different combinations of loading

Vertical load Applied(kN)	Lateral displacement (mm)	
	Horizontal load = 120 kN	Horizontal load = 360 kN
0	11.09	59.03
0.25 Vult	10.87	58.7
0.5 Vult	10.83	58.35
0.75 Vult	10.79	58.18
Vult	10.77	58.14



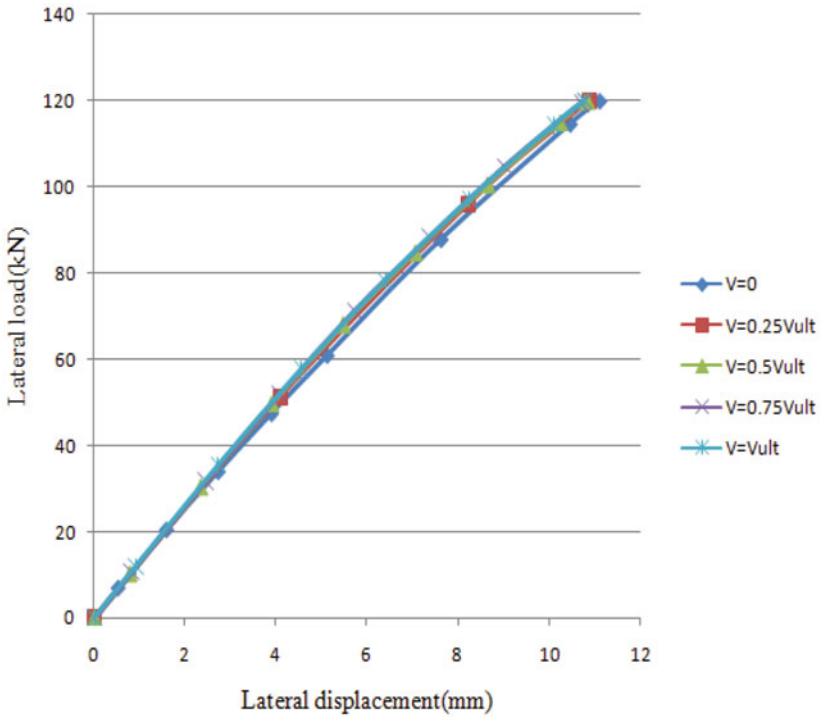


Fig. 4 Influence of vertical load on lateral displacement

### 3.2 Variation of Deflection and Bending Moment (BM)

For the considered soil profile, the variation of the lateral displacement and bending moment along the pile depth for different combination of loads has been shown in Fig. 5. It was observed that the variation of deflection and BM is more in the top few meters of the soil depth. There is not much change in deflection and bending moment due to the application of vertical load for the considered soil characteristics.

But this might not be the case for all the layered soil profiles, there will be a change in the deflection and BM due to the application of combined vertical and lateral loading which needs to be considered in the analysis and design of pile foundations.

## 4 Summary and Conclusions

- In this study, analysis was carried out for a pile subjected to pure horizontal load and a combination of horizontal and vertical loads. The numerical model

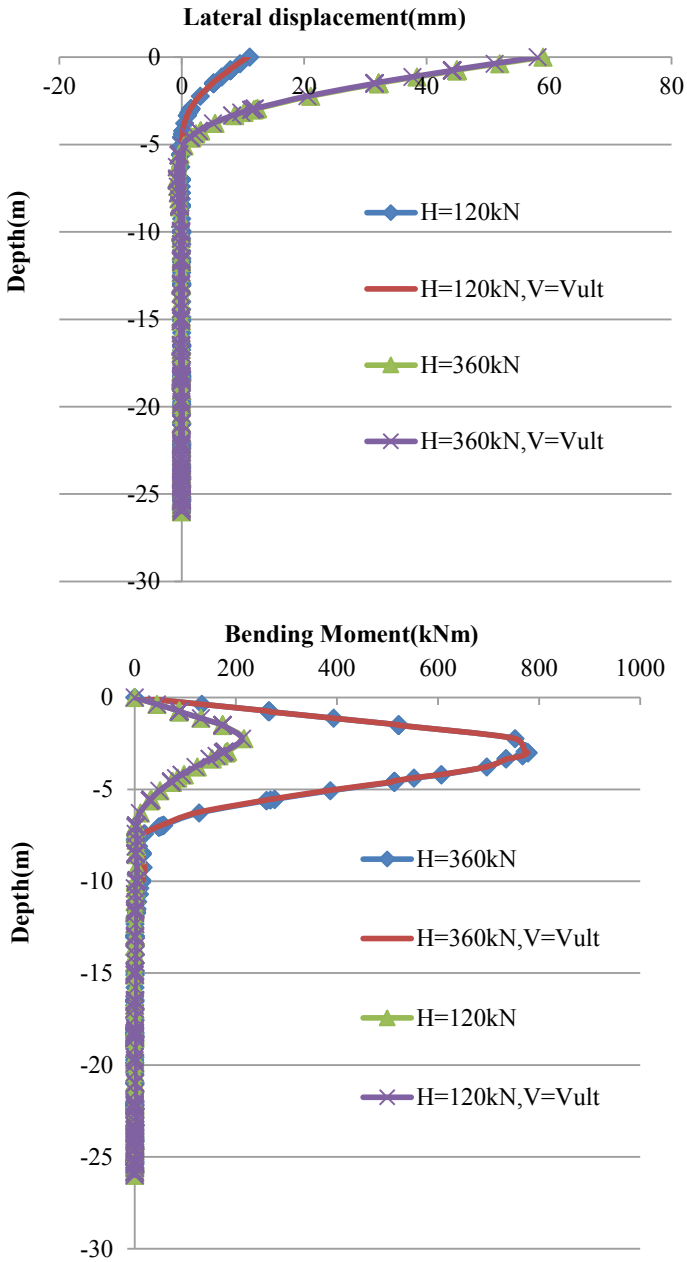


Fig. 5 Variation of lateral displacement and bending moment

was validated against the field pile load test results, in which the adopted finite element analysis well predicted with the measured results.

- For the soil profile characteristics and the pile considered, it was observed that the pile is safe for a lateral load of 120 kN as the deflection obtained is between 2 and 4% of the pile diameter which can be considered allowable for serviceability limit state [9].
- Due to the presence of vertical load, there was a marginal decrease in the deflection when compared to the case of a pure lateral load for the considered layered soil profile which is not always possible.
- It was observed that the lateral deflection and bending moment did not appear to vary considerably with and without the application of vertical load for the considered soil profile.
- However, it is most important to consider the presence of a vertical load for determining the pile lateral capacity, and it is unsafe and uneconomical to assume that there is no interaction between vertical and lateral loads for designing the piles.

## References

1. Anagnostopoulos C, Georgiadis M (1993) Interaction of axial and lateral pile responses. *J Geotech Eng* 119(4):793–798
2. Bowles JE (1988) *Foundation analysis and design*, 4th edn. McGraw Hill Company, New York, USA
3. Karasev OV, Talanov GP, Benda SF (1977) Investigation of the work of single situ-cast piles under different load combinations. *Soil Mech Found Eng* 14(3):173–177
4. Karthigeyan S, Ramakrishna VVGST, Rajagopal K (2006) Influence of vertical load on the lateral response of piles in sand. *Comput Geotech* 33(2):121–131
5. Karthigeyan S, Ramakrishna VVGST, Rajagopal K (2007) Numerical investigation of the effect of vertical load on the lateral response of piles. *J Geotech Geoenviron Eng* 133(5):512–521
6. Kumar A, Choudhury D, Katzenbach R (2016) Effect of earthquake on combined pile–raft foundation. *Int J Geomech* 16(5):04016013
7. Matlock H, Reese LC (1960) Generalized solutions for laterally loaded piles. *J Soil Mech Found Div ASCE* 86(5):63–91
8. Poulos HG (1971) Behaviour of laterally loaded piles: II. Group of piles. *J Soil Mech Found Eng* 97:733–751
9. Shirato M, Kohnno T, Nakatani S (2009) Geotechnical criteria for serviceability limit state of horizontally loaded deep foundations. In: *Proceedings of the second international symposium on geotechnical risk and safety*, pp 119–126
10. Trochanis AM, Bielak J, Paul Christiano P (1991) Three-dimensional nonlinear study of piles. *J Geotech Eng* 117:429–447

# Behavior of Laterally Loaded Piles Using Finite Difference Method



B. K. Huchegowda, Teja Munaga, and Gonavaram Kalyan Kumar

**Abstract** Structures resting on piles, i.e., high-rise buildings, bridge abutments, piers, earth-retaining structures, and offshore structures, are frequently subjected to horizontal forces owing to wind, wave, traffic, and seismic events. The response of the pile to lateral load can be analyzed by measuring the deformation along the length of the pile. However, the deformation of the pile along the length is difficult to be measured in a field test. Finite difference method (FDM) offers a solution to analyze the behavior based on modulus of subgrade reaction. Modulus of subgrade reaction is calculated by using elastic properties of soil and pile. The validity of the presented FDM solution was verified against the field data obtained from lateral load tests. In this study, a parametric analysis is conducted on piles of different length/diameter ( $L/D$ ) ratio embedded in sand and soil. Further, the deformation of the pile, bending moment, shear force, and soil reaction were calculated using FDM and compared for different criteria. It is observed that the response of pile to lateral load is mainly affected by properties of the pile and soil (up to a depth of 2–4 times the pile diameter).

**Keywords** Laterally loaded piles · Modulus of subgrade reaction · Finite difference method

## 1 Introduction

Since the very early days of soil mechanics, it was recognized that geotechnical material varied from one location to another. The main objective of pile design is to ensure proper performance in the environment it is built for, and to find the best possible solution [1–5]. The governing criteria in designing pile foundations subjected to lateral loading is maximum deflection rather than ultimate capacity [6]. Several analytical

---

B. K. Huchegowda  
IIT Hyderabad, Hyderabad, Telangana, India

T. Munaga · G. Kalyan Kumar (✉)  
NIT Warangal, Warangal, Telangana, India  
e-mail: [kalyan@nitw.ac.in](mailto:kalyan@nitw.ac.in)

and numerical methods are available to obtain the maximum deflection of a pile [7–9]. The current pile design practice involves the consideration of allowable stress and load factor design [10]. This practice often leads to inconsistency and non-uniform pile safety. In order to attain consistency and uniformity of safety margin, proper solution is required for layered soils. An attempt have been made for determining the lateral loaded pile in uniform and stratified soil using finite difference method. The deformation of the wedge in clay is less than that of sand due to resistance offered by clays in form of sliding reaction and self-weight. Soft clays provide least resistance to lateral load due to less shear strength and forms a small wedge at the top surface.

### 1.1 Finite Difference Method

Finite difference method (FDM) can be advantageously employed for problems involving complexity in loading, boundary configurations, mathematical expressions, load distribution, and sectional properties [11–13]. FDM is applicable for statically determinate structures, indeterminate structures, vibration problems, and beams of elastic foundations. Partial differential equations are invariably employed in solving problems of two-dimensional structural elements. This method is used for determination of moments, shear forces, deflections, and buckling of columns [14–16]. The equations used for formulating the laterally loaded piles are given below.

The beam equation for actively loaded piles is given as:

$$(EI)p(\partial^4 y/\partial z^4) + d.k.y = \dots \quad (1)$$

FD formulation for a laterally loaded pile for active loading can be written as:

$$(EI)p/\Delta z^4 [y_{(i-2)} - 4y_{(i-1)} + 6y_i - 4y_{(i+1)} + y_{(i+2)}]kdy_i = \dots \quad (2)$$

where  $E$  = Modulus of elasticity of pile material.

$I$  = Moment of inertia of pile.

$y$  = Deflection at specific node (as per notation in FDM).

$i$  = Node number (as per notation in FDM).

$K$  = Modulus of subgrade reaction.

$\Delta z$  = Distance between nodes (as per notation in FDM).

## 2 Methodology

The validation of finite difference method was done using data obtained from filed tests. This is achieved by comparing the field test results of Alizadeh and Davisson

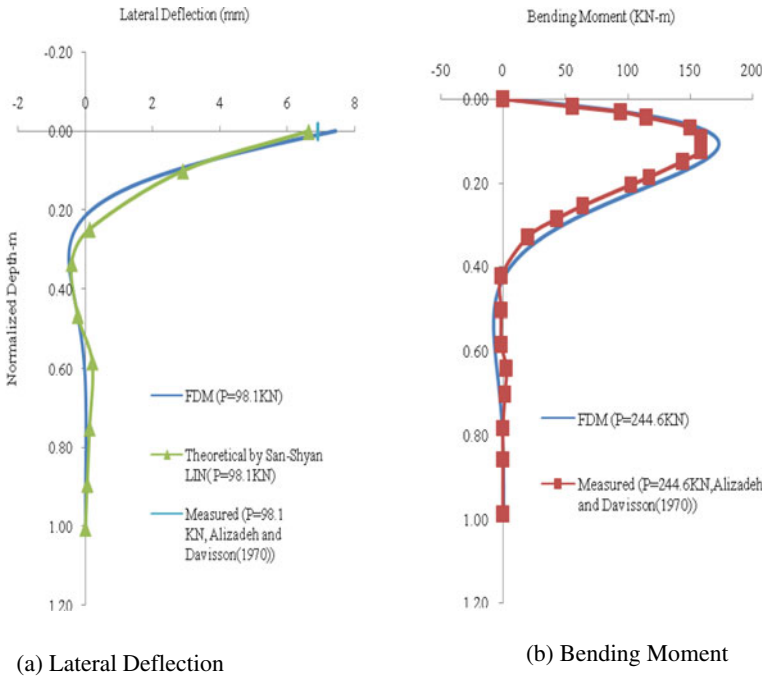


**Fig. 1** Comparison of the FDM solution with field and theoretical solution

[1] with the analysis performed using FDM. Similarly, Lin [10] derived theoretical solutions for the same and calculated the deformation over depth of the pile. The deformation, shear force, and bending moment obtained from all the three methods are compared in Fig. 1a, b, and c, respectively. The figures clearly indicate that results obtained from the current solution are in reasonably good agreement with the measured data and theoretical solution.

A parametrical study is carried out to study the lateral response of pile under various conditions. The detailed parametric study is divided into three cases as discussed in Table 1.

Case I: The behavior pile is studied in uniform sand. The response of pile is analyzed for different load applied at ground level ( $h = 0$ ) and 0.6 m ( $2D$ ) above the ground level, where  $D$  is diameter of the pile.

Case II: The behavior pile is studied in uniform clay. The response of pile is analyzed for varying stiffness of clay for same load applied at different depth.

Case III: The deformation and bending moment experienced by the pile are evaluated by replacing top layer of clay with dense sand of relative density 70%, angle of internal friction,  $\phi = 38^\circ$ , unit weight,  $\gamma = 18 \text{ KN/m}^3$ , modulus of subgrade reaction, and  $K = 50,000 \text{ KN/m}^3$ .

**Table 1** Properties of soil and pile for three cases

Case I	$h = 0, P = 20 \text{ KN}$	Case II	Soft clay $h = 0, K = 12,000 \text{ KN/m}^3$
Sand	$h = 0, P = 50 \text{ KN}$	Clay	Medium clay $h = 0, K = 35,500 \text{ KN/m}^3$
$K = 40,000 \text{ KN/m}^3$	$h = 0, P = 100 \text{ KN}$	$P = 50 \text{ KN}$	Soft clay $h = 0.6 \text{ m}, K = 12,000 \text{ KN/m}^3$
	$h = 0.6 \text{ m}, P = 20 \text{ KN}$		M clay $h = 0.6 \text{ m}, K = 35,500 \text{ KN/m}^3$
	$h = 0.6 \text{ m}, P = 50 \text{ KN}$		
	$h = 0.6 \text{ m}, P = 100 \text{ KN}$		
Case III	Sand:Clay	Pile	$D = 0.3 \text{ m}$
$P = 100 \text{ KN}$	0D:20D		$L/D = 20$
$K_c = 12,000 \text{ KN/m}^3$	1D:19D		$E_p = 2.5 \times 10^7 \text{ kPa}$
$K_s = 50,000 \text{ KN/m}^3$	2D:18D		Free head concrete pile

### 3 Results and Discussion

The response of the pile to lateral load is evaluated in terms of deflection and bending moment along the length of the pile. The deflection and bending moment are calculated according to finite difference equations discussed in Sect. 1.1.

#### 3.1 Case I

The variation of deformation and bending moment with depth is shown in Figs. 2a, b and 3a, b for cases I and II, respectively. The peak deformation of pile head for a load of 20 KN applied at ground level is 2.48 mm as shown in Fig. 2a. Maximum bending moment of 8.71 KN-m occurred at 1.08 m below the GL as shown in Fig. 3a. The pile deflection shifted from positive to negative at a depth of 2.16 m. With an increase in load, deformation and maximum bending moment increased, but the depth of occurrence of maximum bending moment remained same.

When load of 20 KN is applied 0.6 m above the ground level, maximum deformation at pile head is found to be 3.58 mm and maximum bending moment of 17.73 KN-m occurred at a depth of 0.66 m below the ground level. Hence, it can be inferred that for same stiffness of soil, if same load applied above the GL, deformation and maximum bending moment increase, while the depth of occurrence of maximum bending moment shifted toward ground level.

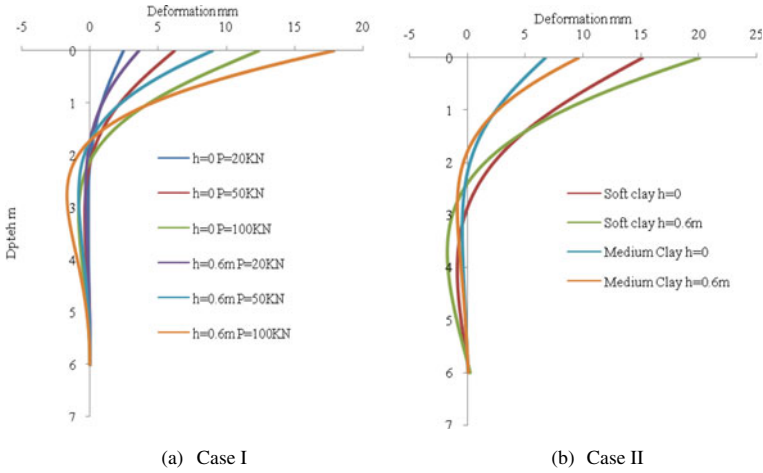


Fig. 2 Variation of deflection over depth

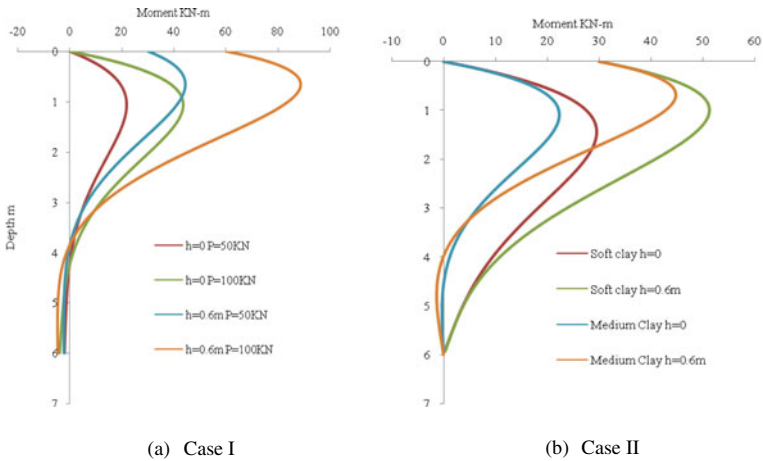


Fig. 3 Variation of bending moment over depth

### 3.2 Case II

The variation of deformation and bending moment with depth is shown in Fig. 2a, b and 3a, b for cases I and II, respectively. When the load is applied at ground level on a pile embedded in soft clay, pile head deformation is found to be 15.09 mm as shown in Fig. 2b, while a maximum bending moment of 29.47 KN-m occurred at a depth of 2.88 m shown in Fig. 3b. When same load is applied by increasing the stiffness of soil, maximum deformation and bending moment decrease, while the depth of occurrence of maximum bending moment shifted upward.



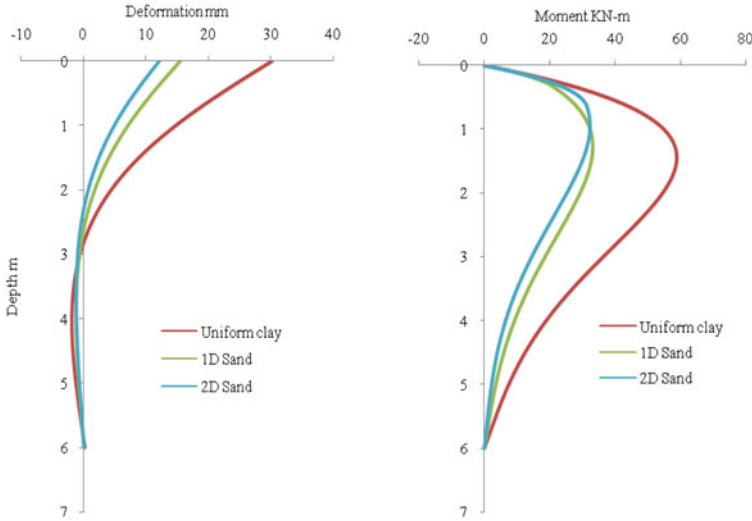


Fig. 4 Variation of deformation and bending moment for case III

When the load is applied at 0.6 m above ground level, the pile head deflection is found to be 20.09 mm and a maximum bending moment of 51.28 KN-m occurred at a depth of 1.02 m. Hence, it can be inferred that when the load is applied above the ground level, pile head deflection, and bending moment increases, while the depth of occurrence of maximum bending moment shifted upward.

### 3.3 Case III

The variation of deformation and bending moment along the length of the pile for case III is shown in Fig. 4a and b, respectively. The pile head deflection is found to be 30.19 mm for uniform soft clay, while it reduced to 15.48 and 12.20 mm for replacing top layer of clay with sand for a depth of 1D and 2D, respectively. A maximum bending moment of 58.94 KN-m occurred at a depth of 1.44 m for uniform clay, while maximum bending moment experienced by the pile decreased by replacing top layer of clay with sand. Also, the depth of occurrence of maximum bending moment shifted upward.

## 4 Conclusions

This paper focuses on evaluating the behavior of laterally loaded piles using finite difference method. Firstly, finite difference method was validated using field results

and theoretical results. Then, a parametric analysis was conducted to study the response of laterally loaded pile with change in point of application of load and soil strata. The main findings and conclusions from this study are as follows:

1. With an increase in lateral load, maximum deformation and bending moment increase. With shift in position of application of load to 0.6 m above ground level, pile head deflection increased by 44% and maximum bending moment increased by 100%.
2. With an increase in the stiffness of clay, pile head deflection and maximum bending moment experienced by the pile decrease. With shift in position of application of load to 0.6 m above ground level, pile head deflection increased by 33% in soft clay and 43% in medium clay.
3. The replacement of top soft clay layer of thickness 1D and 2D with sand of relative density 70% resulted in reduction of pile head deflection by 48% and 60%, respectively.
4. The replacement of top soft clay layer of thickness 1D and 2D with sand of relative density 70% resulted in reduction of maximum bending moment experienced by the pile by 43% and 45%, respectively. Also, the depth of occurrence of maximum bending moment shifted upward.

## References

1. Alizadeh M, Davisson MT (1970) Lateral load tests on piles-Arkansas River project. *J Soil Mech Found Div*
2. Beena KS, Kavitha PE, Narayanan KP (2018) Model studies on laterally loaded piles in sloping clay bed. *Indian Geotech J* 48(1):114–124
3. Broms BB (1964) Lateral resistance of piles in cohesive soils. *J Soil Mech Found Div* 90(2):27–64
4. Broms BB (1964) Lateral resistance of piles in cohesionless soils. *J Soil Mech Found Div* 90(3):123–158
5. Caliendo JA, Anderson LR (1996) Lateral load testing of model piles: phase 1. No. MPC Rpt No. 96-60. Utah State University, Department of Civil and Environmental Engineering
6. Chandrasekaran SS, Boominathan A, Dodagoudar GR (2009) Group interaction effects on laterally loaded piles in clay. *J Geotech Geoenviron Eng* 136(4):573–582
7. Davisson MT, Gill HL (1963) Laterally loaded piles in a layered soil system. *J Soil Mech Found Div* 89(3):63–94
8. Kanakeswararao T, Ganesh B (2017) Analysis of pile foundation subjected to lateral and vertical loads. *Int J Eng Trends Technol (IJETT)* 46(2)
9. Kok ST, Bujang BK, Huat (2008) Numerical modeling of laterally loaded piles. *Am J Appl Sci* 5(10):1403–1408
10. Lin S-S, Chang W-K (2002) Buckling of piles in a layered elastic medium. *J Chin Inst Eng* 25(2):157–169
11. Madhusudan Reddy K, Ayothiraman R (2015) Experimental studies on behavior of single pile under combined uplift and lateral loading. *J Geotech Geoenviron Eng* 141(7):04015030
12. Matlock H, Reese LC (1960) Generalized solutions for laterally loaded piles. *J Soil Mech Found Div* 86(5):63–94
13. Reese LC, Cox WR, Koop FD (1974) Analysis of laterally loaded piles in sand. In: *Offshore technology in civil engineering hall of fame papers from the early years*, pp 95–105

14. Rollins KM, Peterson KT, Weaver TJ (1998) Lateral load behavior of full-scale pile group in clay. *J Geotech Geoenviron Eng* 124(6):468–478
15. Yang Z, Jeremić B (2002) Numerical analysis of pile behaviour under lateral loads in layered elastic–plastic soils. *Int J Numer Anal Methods Geomech* 26(14):1385–1406
16. Zhang L, Zhao M, Zou X (2013) Behavior of laterally loaded piles in multilayered soils. *Int J Geomech* 15(2):06014017

# Bearing Capacity of Strip Footing Placed on Reinforced Cohesionless Soil Slope Using Conic Programming



Koushik Halder and Debarghya Chakraborty

**Abstract** By using lower bound finite element limit analysis technique with the combination of conic programming, the present study computes the bearing capacity of strip footing placed on the edge of a reinforced cohesionless soil slope and also subjected to a surcharge load. The bearing capacity factors (i)  $N_q$  associated with overburden pressure and (ii)  $N_\gamma$  associated with soil unit weight are computed by varying footing setback distance ( $b$ ), soil friction angle ( $\phi$ ), and placement depth of reinforcement layer ( $d$ ). The bearing capacity factors of the strip footing placed on the reinforced slope are found to be higher than that obtained for a strip footing situated on the unreinforced slope. The efficacy of the reinforcement layer is expressed in terms of dimensionless factors,  $\eta_q$  and  $\eta_\gamma$  which are the ratio of  $N_q$  and  $N_\gamma$  values obtained for the reinforced slope to the unreinforced slope. However, the maximum effectiveness of the reinforcement layer ( $\eta_{q-max}$  and  $\eta_{\gamma-max}$ ) is achieved when it is placed at an optimum distance ( $d_{cr}$ ) from the footing base. The magnitude of the efficiency factors increases if the reinforcement layer is embedded in a soil having higher soil friction angle and it is also found that the increment is more in case of  $\eta_{\gamma-max}$ . In contrast, the effectiveness of reinforcement is found to be maximum when footing is placed at the slope edge. The use of conic programming is found to be effective as the computational time reduces in comparison to linear programming during the computation of  $N_q$  and  $N_\gamma$ .

**Keywords** Strip footing · Reinforced slope · Lower bound limit analysis · Conic programming

---

K. Halder (✉) · D. Chakraborty  
Indian Institute of Technology Kharagpur, Kharagpur 721302, India  
e-mail: [koushikhalder@iitkgp.ac.in](mailto:koushikhalder@iitkgp.ac.in)

D. Chakraborty  
e-mail: [debarghya@civil.iitkgp.ac.in](mailto:debarghya@civil.iitkgp.ac.in)

## 1 Introduction

Safe design of foundations for various structures such as buildings, bridge abutments, electrical transmission towers etc. situated on foothills and sloping grounds is a challenging task. The reduction in the load-bearing capacity and increasing chances of slope instability make these structures more vulnerable than the structures situated on the level ground [1–3]. With the advancement of reinforced earth technology, a number of laboratory-based model tests [4–6] as well as numerical studies [5, 7–10] were carried out to investigate the effect of reinforcement on the performance of both footing and slope. The laboratory-based experimental studies have shortcomings regarding the generalization point of view; they were very much case specific. On the other hand, Latha and Rajagopal [7] used finite element method; Alamshahi and Hataf [5] used finite element software Plaxis; Halder and Chakraborty [8, 9] used lower bound limit analysis method with linear programming. It is to be mentioned that the lower bound limit analysis technique is found to be advantageous than other methods on the following points: (1) the shape of the failure surface is not required to be presumed before the analysis, (ii) only shear strength parameters of soil (cohesion and friction angle) are required to be considered. The authors [8, 9] have used linear programming in their earlier works where failure surface was linearized by a polygon according to the formulation of Bottero et al. [11]. However, the linearization of yield surface generates a large number of inequality constraints which in turn increase the computational time. A non-linear programming technique can overcome the deficiencies raised by the implementation of linear programming. Among the available non-linear programming techniques, the second-order cone programming (SOCP), formulated by Makrodimopoulos and Martin [12] is advantageous as in case of SOCP formulation, the yield function is not required to be non-differentiable at some points, and thus there is no need of smoothening of yield surface either on the corners of the hexagon or at its apex [13]. Various researchers [13–15] used SOCP with lower bound limit analysis in solving various geotechnical problems in recent years. In addition to that according to the authors knowledge, no research studies were conducted till now for the computation of the bearing capacity factor ( $N_q$ ) of a strip footing placed on the reinforced soil slope and subjected to surcharge loading.

Therefore, the present study computes the bearing capacity factors ( $N_q$  and  $N_\gamma$ ) of a strip footing placed on the top of the reinforced cohesionless soil slope by using the lower bound finite element limit analysis technique with the non-linear programming. Reinforcement is modeled as per the formulation of Chakraborty and Kumar [16]. The influence of soil friction angle ( $\phi$ ), footing setback distance ( $b$ ), and placement depth of reinforcement layer ( $d$ ) on the computed values of  $N_q$  and  $N_\gamma$  are studied.

## 2 Problem Domain and Mesh Details

The two-dimensional plane strain problem domain used in the present study is illustrated by Fig. 1. The surface strip footing of width  $B$  is situated at a distance of  $b$  from the slope edge. The footing is subjected to a non-inclined and non-eccentric compressive load  $Q_u$ . A uniform surcharge of  $q$  is also acted over the horizontal line AB of the problem domain. The slope is inclined at an angle of  $25^\circ$ . A single layer of reinforcement is laid at a distance of  $d$  from the footing base. The frictional soil fill of the slope is assumed to follow Mohr–Coulomb constitutive model and associative flow rule. Similar to Chakraborty and Kumar [16], the effect of reinforcement in the analysis is considered by modifying stress discontinuities along the reinforcement-soil interface layer. Figure 1 shows that the domain is extended up to  $12.80B$  in the horizontal direction and from  $12.04B$  in the downward direction. While choosing the size of the problem domain it is ensured that (i) failure stresses should not reach to the domain boundary, and (ii) magnitude of collapse load should not change abruptly with the change in the size of the problem domain. The normal and shear stresses applied along the horizontal ground surface (GH and IJ) and slope face (JK) are equal to  $q$  and zero, respectively. Roughness between footing and soil interface along HI line is implemented with the help of equation  $|\tau_{xy}| \leq (c - \sigma_y \tan \varphi)$ .

Three noded triangular elements are used to discretize the problem domain. A relatively denser mesh is chosen near the singularity point below the two corners of the footing edge while a coarser mesh is created near the boundary region. According to the plane strain formulation of Sloan [17], each node consists of three unknown stresses; (i) two normal stresses in  $x$  ( $\sigma_x$ ) and  $y$  ( $\sigma_y$ ) direction, and (ii) shear stress

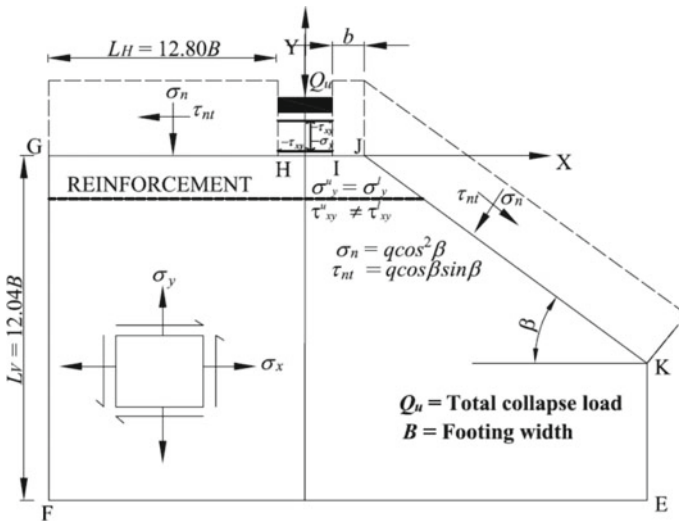
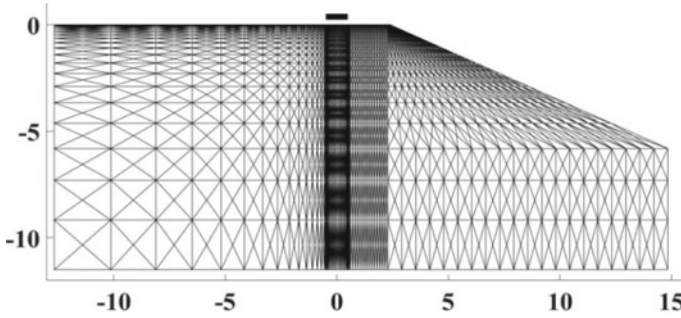


Fig. 1 Problem domain



**Fig. 2** FE mesh used in the analysis

( $\tau_{xy}$ ). A typical mesh discretization of the slope having  $\beta = 25^\circ$ ,  $\phi = 30^\circ$ , and  $b/B = 2$  is shown in Fig. 2 where  $N$ ,  $E$ ,  $D_c$ , and  $N_i$  represent the total number of (i) nodes, (ii) elements, (iii) discontinuities, and (iv) nodes along footing-soil interface, respectively.

### 3 Methodology

The lower bound value of the collapse load of footing is obtained in the present study by employing the plane strain lower bound formulation of Sloan [17]. According to Sloan [17], the admissible stress field would furnish the lower bound solution after the satisfaction of (i) element equilibrium condition throughout the problem domain, (ii) stress boundary conditions at the boundary edges, (iii) stress discontinuity conditions along the line of stress discontinuity formed by two adjacent triangles, and (iv) yield criterion at all the nodes of the elements. No external element is used to model the reinforcement layer. The reinforcement modeling is done by following the formulation of Chakraborty and Kumar [16]. Chakraborty and Kumar [16] modified the stress discontinuities along the reinforcement-soil interface layer. Shear stresses were set aside discontinuous along the reinforcement-soil interface layer, but normal stresses were permitted. Whereas, in all other places, both the normal and shear stresses were kept continuous along the edges of discontinuity. Due to the implementation of element equilibrium, stress boundary, and stress discontinuity conditions, equality constraints are generated. As mentioned earlier, a non-linear programming technique, SOCP is used in the present study instead of linear programming as suggested by Sloan [17]. According to the SOCP formulation, the Mohr–Coulomb yield surface is used in the form of a conic quadratic constraints with the use of auxiliary variables. A set of inequality constraints are thus generated. After the generation of equality and inequality constraints, the objective function (collapse load) is then maximized. The expression of the objective function is obtained with the numerical integration of normal stresses along the nodes representing footing. One can follow the work of

Sloan [17] for the detailed formulation of lower bound finite element limit analysis and the work of Tang et al. [13] for the SOCP formulation. Here, only the final form of the optimization scheme is presented in Eqs. 1 and 2.

Maximize

$$\{g\}^T \{\sigma\} \quad (1)$$

subjected to

$$[A]\{\sigma\} = \{B\} \quad (2)$$

whereas,

$$\begin{bmatrix} A_{EQ} & 0 \\ A_{SB} & 0 \\ A_{DS} & 0 \\ A_{SC} & I \end{bmatrix} \{b\} = \begin{Bmatrix} b_{EQ} \\ b_{SB} \\ b_{DS} \\ b_{SC} \end{Bmatrix} \quad (3)$$

In the above expressions,  $\{g^T\}$  is the vector consists of the coefficients obtained from the objective function;  $\{\sigma\}$  is the global stress vector;  $[A_{EQ}]$ ,  $[A_{SB}]$ , and  $[A_{DS}]$  are the matrices comprised of right-hand side coefficients from constraints obtained after the employment of equilibrium, stress boundary, and stress discontinuity conditions.  $[I]$  is the identity matrix. Whereas,  $\{b_{EQ}\}$ ,  $\{b_{SB}\}$ , and  $\{b_{DS}\}$  are the vectors composed of left-hand side coefficients of the constraints generated due to the fulfillment of equilibrium, stress boundary, and stress discontinuity conditions. A code is written in MATLAB [18] to carry out the lower bound limit analysis. An optimization toolbox MOSEK [19] is used for carrying out non-linear programming.

## 4 Results

Figure 3 shows the variation between the efficiency factors ( $\eta_q$  and  $\eta_\gamma$ ) and placement depth of reinforcement for various combinations of  $\phi$  and  $b/B$ . Two values of friction angle ( $\phi = 30^\circ$  and  $40^\circ$ ) of the cohesionless soil fill are considered. The strip footing is placed at three setback distances ( $b/B$ ) of 0, 2, and 4. The magnitudes of the efficiency factors ( $\eta_q$  and  $\eta_\gamma$ ) increase rapidly after a certain value of  $d/B$ , after that it reduces drastically. The placement depth of reinforcement where efficiency factors attain the maximum value ( $\eta_{q-max}$  or  $\eta_{\gamma-max}$ ) is known as optimum depth of placement of the reinforcement ( $d_{cr}/B$ ). The magnitude of the  $\eta_{q-max}$  and  $\eta_{\gamma-max}$  increases if the reinforcement layer is embedded in a soil having higher soil friction angle. As an example for a slope having  $\beta = 25^\circ$ ,  $b/B = 0$ , the magnitude of  $\eta_{q-max}$  increases from 1.56 to 1.71 and the value of  $\eta_{\gamma-max}$  enhances from 1.68 to 1.79 with the change in  $\phi$  value from  $30^\circ$  to  $40^\circ$ . Figure 3 shows that the optimum depth of placement required



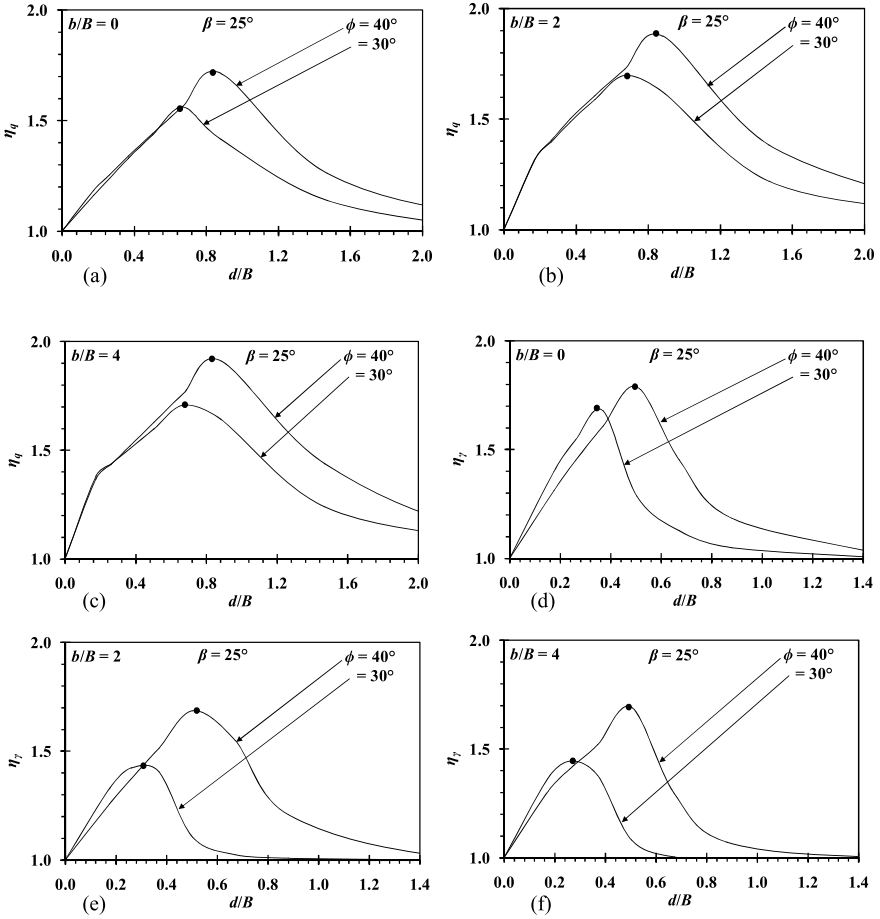


**Fig. 3** Variation of  $\eta_q$  with  $d/B$  of a reinforced slope having  $\beta = 25^\circ$ ,  $\phi = 30^\circ, 40^\circ$  and **a**  $b/B = 0$ ; **b**  $b/B = 2$ ; **c**  $b/B = 4$ ; variation of  $\eta_\gamma$  with  $d/B$  of a reinforced slope having  $\beta = 25^\circ$ ,  $\phi = 30^\circ, 40^\circ$  and **d**  $b/B = 0$ ; **e**  $b/B = 2$ ; **f**  $b/B = 4$

to obtain the value of  $\eta_{\gamma\text{-max}}$  is found to be higher than that required to obtain the value of  $\eta_{q\text{-max}}$ . The value of  $\eta_\gamma$  is found to be maximum when footing is placed on the edge of the slope rather than at a distance from the slope edge. As an instance for a slope having  $\beta = 25^\circ$  and  $\phi = 30^\circ$ , the magnitude of  $\eta_{\gamma\text{-max}}$  reduces from 1.68 to 1.42 with the increment in the value of  $b/B$  from 0 to 4.

**Table 1** Comparison between the values of  $\eta_{\gamma\text{-max}}$  and  $d_{\text{cr}}/B$  obtained from present study and Halder and Chakraborty [8]

$\beta = 25^\circ, \phi = 30^\circ$				
$b/B$	Present Study		Halder and Chakraborty [8]	
	$\eta_{\gamma\text{-max}}$	$d_{\text{cr}}/B$	$\eta_{\gamma\text{-max}}$	$d_{\text{cr}}/B$
0	1.68	0.37	1.70	0.31
2	1.44	0.26	1.49	0.31
4	1.42	0.26	1.46	0.31

## 4.1 Comparison

The magnitude of  $\eta_{\gamma\text{-max}}$  and  $d_{\text{cr}}/B$  obtained from the present study is compared with the obtained results from Halder and Chakraborty [8] for a slope configuration of  $\beta = 25^\circ, \phi = 30^\circ$ , and  $b/B = 0, 2$ , and  $4$  (refer Table 1). Halder and Chakraborty [8] used lower bound finite element limit analysis technique with linear programming. It is found that in all of the cases present value matches well with the reported results of Halder and Chakraborty [8]. However, the present value is lower than the reported value.

## 5 Failure Patterns

Failure mechanisms of both unreinforced and reinforced slopes are shown in Figs. 3a–f after plotting the state of stresses of any point after failure in two-dimensional object space. In the Fig. 3,  $alf$  equal to one denotes the state of shear failure. By contrast, for all those non-yielding points, the value of  $alf$  is less than one. The value of  $a$  and  $f$  is obtained from following equations:

$$a = (\sigma_x - \sigma_y)^2 + (2\tau_{xy})^2, \text{ and } f = [-(\sigma_x + \sigma_y) \sin \varphi]^2 \quad (4)$$

Figure 4a–c show failure mechanisms of both unreinforced and reinforced slopes when footing is positioned at the slope edge. For both unreinforced and reinforced slopes (refer Fig. 4a–b), failure zone in the LHS of the footing is visibly truncated and the failure zone in the RHS of the footing easily reaches to the slope face.

However, with the inclusion of a reinforcement layer, the plastic zone of the failure surface propagates more in the downward direction, which in turn increases the bearing capacity of the footing. Figure 4c shows that when reinforcement is placed at a deeper depth, failure surface propagates over the reinforcement layer. Figure 4d–f illustrate that when footing is placed at a setback distance of 4, plastic zone develops on both sides of the footing, irrespective of unreinforced or reinforced slope. It is quite similar to the failure patterns obtained for the footing placed on the level ground.

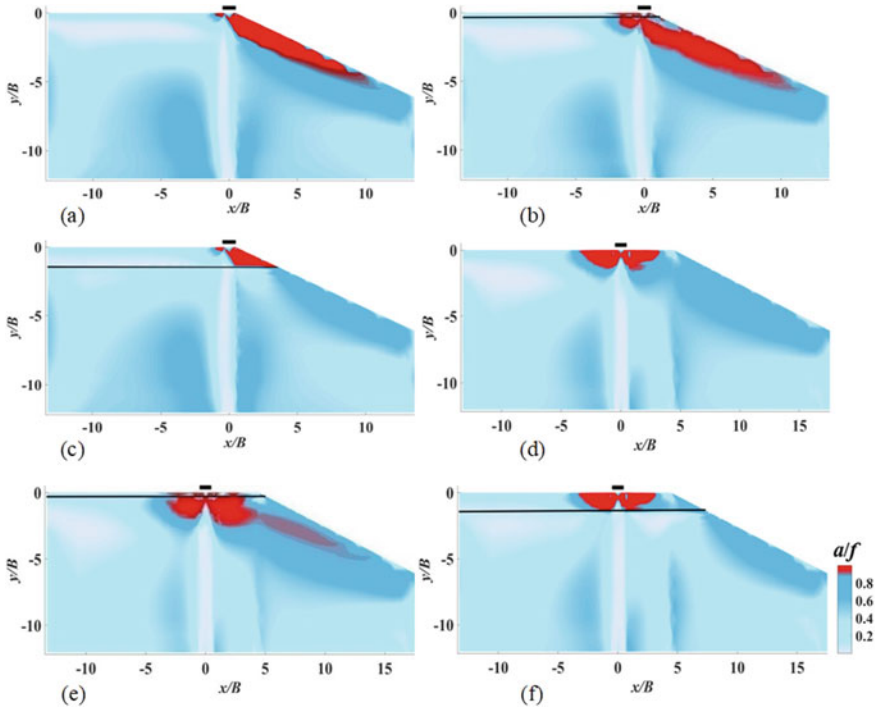


**Fig. 4** Failure patterns obtained for a slope of  $\beta = 25^\circ$ ,  $\phi = 30^\circ$  with **a** unreinforced,  $b/B = 0$ ; **b** reinforcement at optimum depth,  $b/B = 0$ ; **c** reinforcement at higher depth,  $b/B = 0$ ; **d** unreinforced,  $b/B = 4$ ; **e** reinforcement at optimum depth,  $b/B = 4$ ; **f** reinforcement at higher depth,  $b/B = 4$

## 6 Conclusions

By using the lower bound finite element limit analysis technique with conic programming, the bearing capacity factors ( $N_q$  and  $N_\gamma$ ) are obtained for a strip footing placed on the top of the reinforced cohesionless soil slopes. The inclusion of a single layer of reinforcement is found to be very effective as both the values of  $N_q$  and  $N_\gamma$  increase by a significant amount. This increment is observed to be highest when footing is placed on the slope edge. The magnitude of  $N_q$  and  $N_\gamma$  for strip footing situated on the edge of a reinforced slope of  $\beta = 25^\circ$  and  $\phi = 30^\circ$  increases by 1.56 and 1.68 times than that obtained for strip footing placed on the unreinforced slope.

## References

1. Meyerhof GG (1963) Some recent research on the bearing capacity of foundations. *Can Geotech J* 1(1):16–26
2. Kumar J, Chakraborty D (2013) Seismic bearing capacity of foundations on cohesionless slopes. *J Geotech Geoenviron Eng* 139(11):1986–1993
3. Halder K, Chakraborty D, Dash SK (2019) Bearing capacity of a strip footing situated on soil slope using a non-associated flow rule in lower bound limit analysis. *Int J Geotech Eng* 13(2):103–111
4. Selvadurai A, Gnanendran C (1989) An experimental study of a footing located on a sloped fill: influence of a soil reinforcement layer. *Can Geotech J* 26(3):467–473
5. Alamshahi S, Hataf N (2009) Bearing capacity of strip footings on sand slopes reinforced with geogrid and grid-anchor. *Geotext Geomembr* 27(3):217–226
6. Mehrjardi GT, Ghanbari A, Mehdizadeh H (2016) Experimental study on the behaviour of geogrid-reinforced slopes with respect to aggregate size. *Geotext Geomembr* 44(6):862–871
7. Latha GM, Rajagopal K (2007) Parametric finite element analyses of geocell-supported embankments. *Can Geotech J* 44(8):917–927
8. Halder K, Chakraborty D (2018) Bearing capacity of strip footing placed on the reinforced soil slope. *Int J Geomech* 18(11):06018025
9. Halder K, Chakraborty D (2019) Effect of interface friction angle between soil and reinforcement on the bearing capacity of strip footing placed on the reinforced slope. *Int J Geomech* 19(5):06019008
10. Halder K, Chakraborty D (2018) Probabilistic stability analyses of reinforced slope subjected to strip loading. *Geotech Eng J SEAGS AGSSEA* 49(4):92–99
11. Bottero A, Negre R, Pastor J, Turgeman S (1980) Finite element method and limit analysis theory for soil mechanics problems. *Comput Methods Appl Mech Eng* 22(1):131–149
12. Makrodimitropoulos A, Martin CM (2006) Lower bound limit analysis of cohesive-frictional materials using second-order cone programming. *Int J Numer Meth Eng* 66(4):604–634
13. Tang C, Phoon KK, Toh KC (2014) Lower-bound limit analysis of seismic passive earth pressure on rigid walls. *Int J Geomech* 14(5):04014022
14. Sahoo JP, Khuntia S (2018) Lower bound solutions for uplift capacity of strip anchors adjacent to sloping ground in clay. *Mar Georesour Geotechnol* 36(4):405–416
15. Kumar J, Rahaman O (2019) Vertical uplift resistance of horizontal plate anchors for eccentric and inclined loads. *Can Geotech J* 56(2):290–299
16. Chakraborty D, Kumar J (2014) Bearing capacity of strip foundations in reinforced soils. *Int J Geomech* 14(1):45–58
17. Sloan SW (1988) Lower bound limit analysis using finite elements and linear programming. *Int J Numer Anal Meth Geomech* 12(1):61–77
18. Matlab 8.5 [Computer software]. Natick, MA, MathWorks
19. MOSEK ApS version 8.0 [Computer software]. MOSEK, Copenhagen, Denmark

# Optimizing the Bearing Capacity of Pile Foundation in Clay



Mantu Majumder and Debarghya Chakraborty

**Abstract** The ultimate collapse load (bearing capacity) of constant cross-section pile, tapered pile, and under-reamed pile in clay is estimated with the help of lower bound finite element limit analysis. Four different types of piles are considered: constant cross-section pile of smaller diameter, constant cross-section pile of larger diameter, tapered pile, and under-reamed pile. A comparison of the ultimate collapse load of four different piles is made by considering variables such as pile length, shaft diameter, taper angle, and bulb to shaft diameter ratio. For a given pile length and volume, the ultimate collapse load of the under-reamed pile is significantly higher than constant cross-section pile and tapered pile. The percent increase in the ultimate collapse load of the under-reamed pile is significant for a smaller length of the pile. For piles of a given length, the ultimate collapse load of under-reamed pile increases significantly compared to constant cross-section pile and tapered pile, for an increase in the bulb to shaft diameter ratio. From this study, it is concluded that among constant cross-section, tapered, and under-reamed pile, under-reamed pile gives the highest bearing capacity.

**Keywords** Pile foundation · Clay · Bearing capacity · Limit analysis · Plasticity

## 1 Introduction

Pile foundations are often constructed in clay to carry the axial compressive load. The load carrying capacity of a pile foundation in clay is governed by soil cohesion, pile geometry, and pile-soil interface adhesion. For a given value of cohesion and pile-soil adhesion, the bearing capacity of a pile foundation is significantly affected by the pile geometry. Based on the variation of cross-section pile foundation can be three types namely constant cross-section pile, tapered pile, and under-reamed pile. Constant cross-section piles have a constant cross-section throughout its length. The cross-section of a tapered pile varies along the length. Under reamed piles have

---

M. Majumder (✉) · D. Chakraborty  
Department of Civil Engineering, Indian Institute of Technology, Kharagpur 721302, India  
e-mail: [mantu.majumder@iitkgp.ac.in](mailto:mantu.majumder@iitkgp.ac.in)

© Springer Nature Singapore Pte Ltd. 2022  
A. K. Dey et al. (eds.), *Proceedings of the 7th Indian Young Geotechnical Engineers Conference*, Lecture Notes in Civil Engineering 195,  
[https://doi.org/10.1007/978-981-16-6456-4\\_7](https://doi.org/10.1007/978-981-16-6456-4_7)

one or more enlarged cross-sections, called bulbs or under-reams. Bearing capacity of constant cross-section pile in clay is studied by many researchers [5, 8–10, 12, 13, 15]. The bearing capacity of tapered piles in clay is studied by Majumder and Chakraborty [7]. The bearing capacity of the under-reamed pile in clay (undrained clay) is studied by Cooke and Whitaker [2], IS 2911-Part III [4], and Shrivastava and Bhatia [11]. However, the comparison of the bearing capacity of constant cross-section pile, tapered pile, and under-reamed pile is studied by very few researchers. Vali et al. [14] estimated the bearing capacity and settlement of tapered and under-reamed piles by considering various pile and soil parameters. In this study, a cohesive frictional soil was considered. It was observed that both tapered and under-reamed piles were effective in terms of bearing capacity in certain soil conditions. Kong et al. [6] compared the performance of constant cross-section circular pile, tapered pile, belled pile, and belled wedge pile. The pile shaft was embedded in soft clay whereas the pile tip was placed on a sand layer. The bearing capacity of the belled wedge pile was found to be significantly higher than constant cross-section pile and tapered pile but close to the belled pile. As per the author's knowledge, no studies have reported on the comparison of the bearing capacity of constant cross-section, tapered and under-reamed piles in undrained clay. Therefore, in the current study, bearing capacity of constant cross-section pile, tapered pile, and under-reamed pile in clay is estimated with the help of lower bound finite element limit analysis.

## 2 Problem Considered

Four different types of piles, constant cross-section pile with a smaller diameter (UCS1), constant cross-section pile with a larger diameter (UCS2), tapered pile (T1), and under-reamed pile (UR1) are considered in the analysis, as shown in Fig. 1. The volume of the piles UCS2, T1, and UR1 are kept equal, and greater than the volume of pile UCS1. The length of the pile to shaft diameter ratio ( $L/D_1$ ) is considered in the range of 10–20. The dimensions of different piles are shown in Table 1. A purely cohesive (angle of internal friction,  $\phi = 0$ ) homogeneous soil is considered. The un-drained cohesion and pile-soil adhesion factor are considered as 10.34 kPa and 0.53, respectively [2]. The soil is considered as perfectly plastic and an associated flow rule is assumed to be applicable. The soil is assumed to be weightless [3, 5]. The Mohr–Coulomb failure criteria is applicable to the soil mass. The lower bound estimate of the ultimate collapse load of different piles is needed to be calculated.

## 3 Method of Analysis

Axi-symmetric lower bound finite element limit analysis along with linear optimization is used to obtain the ultimate collapse load of different piles. The formulation provided by Khatri and Kumar [5] is used in the present analysis. The soil domain in

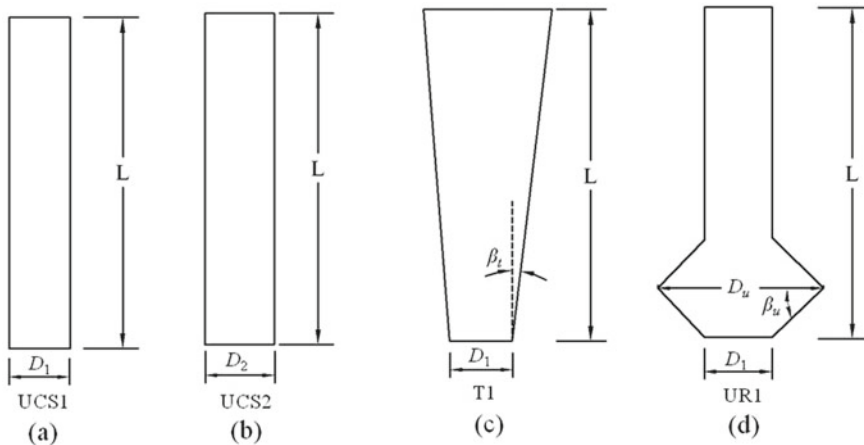


**Fig. 1** Details of different piles **a** Constant cross-section pile of smaller diameter, **b** constant cross-section pile of larger diameter, **c** tapered pile, and **d** under-reamed pile

the  $r-z$  plane is discretized by triangular elements with three nodes at vertices. The variables at each node are stresses  $\sigma_r, \sigma_z, \tau_{rz}$ , and  $\sigma_\theta$ . The objective function for each pile is obtained by integrating stresses throughout the pile-soil interface. The objective function is maximized such that a number of linear equality and linear inequality constraints are satisfied. Linear equality constraints arise from stress equilibrium of elements, stress discontinuity along the common boundary of adjacent elements, stress boundary condition along the axis of symmetry and along the ground surface. Linear inequality constraints arise from the limits of shear stress throughout the pile-soil interface and satisfaction of yield condition at each node. The constraints are assembled over the entire domain to obtain the global constraint matrices and vectors. The mathematical form of the optimization problem can be represented by the following equations.

Maximize the objective function:

$$\{g\}^T \{\sigma\} \tag{1}$$

Subjected to:

$$[A_{\text{leq}}]\{\sigma\} = \{B_{\text{leq}}\} \tag{2}$$

$$[A_{\text{lineq}}]\{\sigma\} \leq \{B_{\text{lineq}}\} \tag{3}$$

where  $\{g\}$  is a vector comprises of coefficients of the objective function,  $\{\sigma\}$  is the vector of all nodal stresses,  $[A_{\text{leq}}]$  and  $\{B_{\text{leq}}\}$  are matrix and vector, respectively, in the global linear equality constraint in Eq. (2),  $[A_{\text{lineq}}]$  and  $\{B_{\text{lineq}}\}$  are matrix and vector, respectively, in the global linear inequality constraint in Eq. (3).





Computer programs are developed in MATLAB for the generation of the mesh and constructing linear equality and inequality constraint matrices and vectors. LINPROG, an inbuilt library function in MATLAB for solving a linear programming problem, is used for the optimization.

## 4 Results and Discussions

The variation of the ultimate collapse load of different piles with pile length for different bulb diameter to shaft diameter ratio is shown in Fig. 2. The collapse load of pile increases in the order of UCS1, T1, UCS2, and UR1, irrespective of the pile length. For an equal pile length and volume, the collapse load of UR1 is significantly higher than the collapse load of UCS2 and T1. The ultimate collapse load of UCS2 is slightly greater than the collapse load of T1. For a given  $D_u/D_1$ , the percent increase in the ultimate collapse load of the under-reamed pile (UR1) with respect to constant cross-section pile (UCS1) increases with the decrease in pile length. For  $D_u/D_1 = 2.5$ , the ultimate collapse load of the under-reamed pile (UR1) increases from 63.47 to 108.77% when pile length decreases from 4 to 2 m. For a given pile length, the percent increase in the ultimate collapse load of the under-reamed pile (UR1) increases significantly with an increase in  $D_u/D_1$ . For the length of the pile of 4 m, the ultimate collapse load of under-reamed pile (UR1) increases from 34.24 to 102.37% when the ratio  $D_u/D_1$  increases from 2 to 3. Therefore, for the same pile length and volume, the maximum bearing capacity in clay is obtained by providing an under-reamed pile. Also, the ultimate collapse load of the under-reamed pile is increased with an increase in the bulb to shaft diameter ratio. The bulb of the under-reamed pile provides additional bearing and shearing resistance under compressive loads. The reason behind the maximum collapse load of the under-reamed pile is the larger bearing area (including pile base and bottom of the bulb) compared to other piles and also the position of the bulb is at the base.

## 5 Comparisons

The ultimate collapse load from the present analysis is compared with the previous studies. Table 2 shows the comparison of the ultimate collapse load with Meyerhof [8], IS 2911-Part III [4], Chakraborty and Kumar [1], and Majumder and Chakraborty [7]. It is to be mentioned here that the analysis of Meyerhof [8] is based on limit equilibrium, analysis of Chakraborty and Kumar [1] and Majumder and Chakraborty [7] is based on lower bound finite element limit analysis. The recommendations of IS 2911-Part III [4] are derived from the general principles of pile foundations and from field experience. The ultimate collapse load of constant cross-section pile (UCS1) is very close to Chakraborty and Kumar [1] but significantly less than Meyerhof [8] irrespective of the length of the pile. The ultimate collapse load of the tapered pile

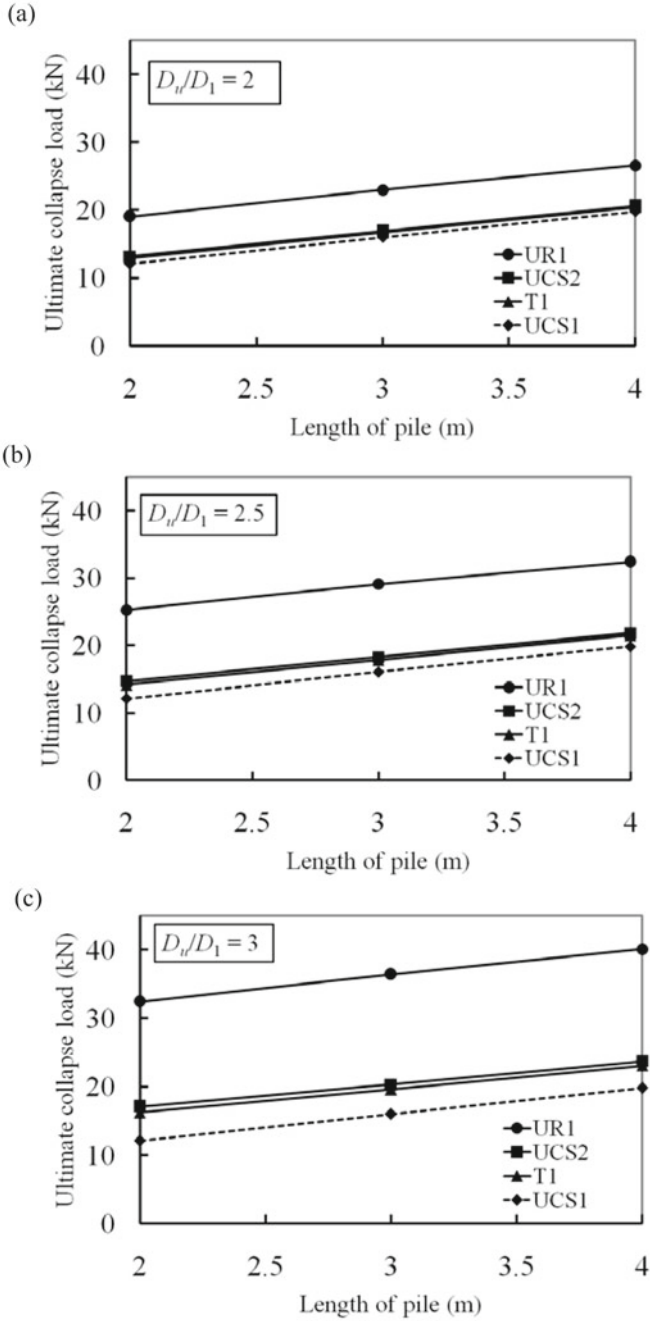


**Fig. 2** Variation of ultimate collapse load with length of pile for **a**  $D_u/D_1 = 2$ , **b**  $D_u/D_1 = 2.5$ , **c**  $D_u/D_1 = 3$

**Table 2** Comparison of the ultimate collapse load of different piles for  $D_u/D_1 = 2.5$

Length of pile (m)	Ultimate collapse load (kN)						
	UCS1			T1		UR1	
	Present analysis	Chakraborty and Kumar [1]	Meyerhof [8]	Present analysis	Majumder and Chakraborty [7]	Present analysis	IS 2911 - Part III [4]
2	12.09	11.75	12.90	14.14	16.24	25.24	22.24
3	15.99	15.77	18.34	17.77	–	29.07	25.68
4	19.79	19.55	23.79	21.44	25.34	32.35	29.12

(T1) from the present analysis is less than Majumder and Chakraborty [7] irrespective of the length of the pile. The difference may be due to the different pile-soil adhesion factor ( $\alpha_s = 0.67$  and  $\alpha_b = 1$ ) used by Majumder and Chakraborty [7]. The ultimate collapse load of the under-reamed pile (UR1) is higher than IS 2911-Part III [4] irrespective of the length of the pile. In the present study, resistance from both the top and bottom surface of the bulb is considered whereas in IS 2911-Part III [4] only the resistance from the bottom surface of the bulb is considered. It is also noted that the IS code considered the factor  $N_c$  as 9 irrespective of the embedment length of the pile. However, a previous study by Chakraborty and Kumar [1] has found that  $N_c$  is higher than 9 at greater depth.

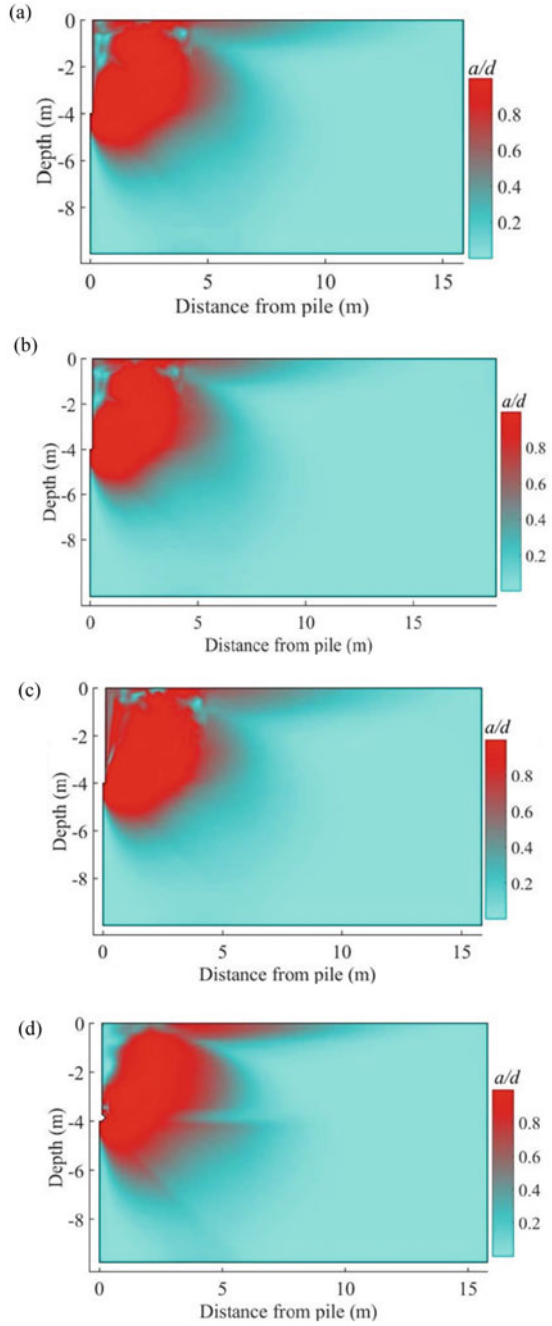
## 6 Failure Patterns

The state of plastic shear failure is obtained in a plot of depth, distance from the pile, and the ratio  $a/d$ . Here,  $a$  and  $d$  are two components of the Mohr–Coulomb failure criteria, where  $a = (\sigma_r - \sigma_z)^2 + (2\tau_{rz})^2$  and  $d = 4c^2$ . The ratio  $a/d$  varies from 0 to 1. If  $a/d$  equals to one it means the point in the soil is in a state of plastic shear failure. If  $a/d$  less than one the point in the soil is in the elastic state. The failure pattern of UCS1, UCS2, T1 and UR1 for the case of  $L = 4$  m and  $D_u/D_1 = 2.5$  is shown in Fig. 3. The dark shaded area represents the region of the plastic shear failure. In all four types of piles, the zone of plastic shear failure starts below the pile base and extends laterally and vertically, reaches up to ground surface. The shape and extent of the failure zone vary for each pile.

## 7 Conclusions

In this study, the ultimate collapse load of constant cross-section pile, tapered pile, and the under-reamed pile is computed with the help of lower bound finite element limit

**Fig. 3** Failure patterns for  $L = 4$  m and  $D_u/D_1 = 2.5$  **a** UCS1, **b** UCS2, **c** T1, and **d** UR1



analysis. The ultimate collapse load of constant cross-section pile, tapered pile, and under-reamed pile increase with the increase in pile length. For an equal increase in pile volume, the bearing capacity of under-reamed pile increases significantly compared to constant cross-section pile and tapered pile. The percent increase in the ultimate collapse load of the under-reamed pile is significant compared to other piles for a smaller length of the pile. For a given length of pile, the ultimate collapse load of under-reamed pile increases significantly with the increase in bulb diameter. Therefore, it can be concluded that for the improvement of the ultimate load carrying capacity of the pile in clay, under-reamed pile is more economical than providing a larger diameter constant cross-section pile or a tapered pile.

## References

1. Chakraborty D, Kumar J (2013) Bearing capacity of piles in soft clay underlain by cohesive-frictional soil. *Int J Geomech* 13(3):311–317
2. Cooke RW, Whitaker T (1961) Experiments on model piles with enlarged bases. *Geotechnique* 11(1):1–13
3. Houlsby GT, Martin CM (2003) Undrained bearing capacity factors for conical footings on clay. *Geotechnique* 53(5):513–520
4. IS 2911 - Part III (1980) Indian standard code of practice for design and construction of pile foundations (Part-III): under-reamed piles (first revision). Bureau of Indian Standards, Manak Bhavan, New Delhi, India
5. Khatri VN, Kumar J (2009) Bearing capacity factor  $N_c$  under  $\phi = 0$  condition for piles in clays. *Int J Numer Anal Meth Geomech* 33(9):1203–1225
6. Kong GQ, Yang Q, Liu HL, Liang RY (2013) Numerical study of a new belled wedge pile type under different loading modes. *Eur J Environ Civ Eng* 17(sup1):65–82
7. Majumder M, Chakraborty D (2018) Bearing capacity of tapered piles in clay under un-drained condition. *Int J Geotech Eng* 1–7
8. Meyerhof GG (1963) Some recent research on the bearing capacity of foundations. *Can Geotech J* 1(1):16–26
9. Poulos HG (1982) The influence of shaft length on pile load capacity in clays. *Geotechnique* 32(2):145–148
10. Randolph MF, Murphy BS (1985) Shaft capacity of driven piles in clay. In: *Proceedings of offshore technology conference*, vol 1. Houston, pp 371–378
11. Shrivastava N, Bhatia N (2008) Ultimate bearing capacity of under-reamed pile-finite element approach. In: *12th International conference of international association for computer methods and advances in geomechanics (IACMAG)*. Goa, India, pp 3490–3497
12. Skempton AW (1959) Cast in-situ bored piles in London clay. *Geotechnique* 9(4):153–173
13. Tomlinson MJ (1957) The adhesion of piles driven in clay soils. In: *Proceedings of 4th International conference on soil mechanics and foundation engineering*, vol 2. London, England, pp 66–71
14. Vali R, Mehrinejad Khotbehsara E, Saberian M, Li J, Mehrinejad M, Jahandari S (2017) A three-dimensional numerical comparison of bearing capacity and settlement of tapered and under-reamed piles. *Int J Geotech Eng* 1–13
15. Vijayvergiya VA, Focht JA Jr (1972) A new way to predict capacity of piles in clays. In: *Proceedings of 4th offshore technology conference*. Houston, pp 865–874

# Numerical Analysis of Soft Soil Reinforced with Geogrid Encased Stone Column



B. K. Pandey, S. Rajesh, and S. Chandra

**Abstract** The use of geosynthetic encased stone columns for improving very soft soil has been widely recognized both regarding economy and performance. The stone columns are encased to offer lateral confinement against bulging which causes excessive settlement. In this study, the analysis of the embankment, resting on very soft soil reinforced with stone column encased from geogrid is carried out to understand its behavior. In this study a comprehensive numerical analysis is executed to study the consequence of encasement parameters like its length and stiffness on the on time-dependent behavior of the system. The result of the study shows significant improvement regarding settlement reduction and lesser lateral bulging of the column. Moreover, it also shows that encasing the column fully perform better as compared to the partially encased column. Similarly, using stiffness of geogrid beyond 5000 kN/m does not show substantial improvement.

**Keywords** Stone column · Soil improvement · Geogrid

## 1 Introduction

The use of stone columns has proven efficacious both regarding economy and performance. Moreover, it is very successful because of its advantages. It helps in slope stability improvement, increasing bearing capacity and the time rate of settlement, reduction in both differential and total settlement, reducing liquefaction potential [1, 2]. The application of a stone column serves its purpose if the undrained shear strength ( $C_u$ ) of soil lies between 15 and 50 kPa. However, if the undrained shear strength of the soil is  $< 15$  kPa, then the confinement provided to the stone column by the surrounding soil is inadequate, and hence it fails in excessive settlement due to bulging. Therefore, reinforcing the stone column either by encasement or by placing the horizontal strip of geosynthetic along the length of the column, these two approaches provides the extra resistance against radial bulging of the column as

---

B. K. Pandey (✉) · S. Rajesh · S. Chandra  
Department of Civil Engineering, IIT Kanpur, Kanpur, Uttar Pradesh 208016, India  
e-mail: [balbir@iitk.ac.in](mailto:balbir@iitk.ac.in)

© Springer Nature Singapore Pte Ltd. 2022  
A. K. Dey et al. (eds.), *Proceedings of the 7th Indian Young Geotechnical Engineers Conference*, Lecture Notes in Civil Engineering 195,  
[https://doi.org/10.1007/978-981-16-6456-4\\_8](https://doi.org/10.1007/978-981-16-6456-4_8)

stated by Alexiew et al. [3] and Ali et al. [4]. In last two decades various projects for the railroad and road embankment, bridge ramp, flood protection dike were accomplished using encased stone columns in Germany, Netherland, Sweden, and India [5, 6].

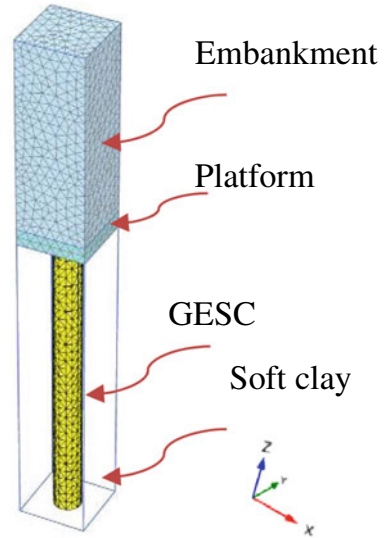
The idea of encasing the column in full or part is studied experimentally by numerous researchers like Rathiel et al. [6] and Murugesan and Rajagopal [7] under undrained condition. In discovering the performance of geogrid encased stone columns (GESCs), numerical modeling has also been extensively used. Yoo and Kim [8] adopted a unit cell (both 3D and axisymmetric) and full 3D model to compare the different modeling approach. Yoo [9] reported the effects of various parameters by modeling quarter of column and full 3D model. Majority of the studies focus on unit cell approach (either 3D or axisymmetric or quarter column) by loading the column only or entire unit cell ([10, 11] and others) or unit cell with embankment loading [12–15]. However, an only limited study has been conducted in details considering the encasement parameter's (length and stiffness) on time-dependent responses under embankment loading. Therefore, there is a need for a comprehensive study to understand the modeling details as well as the behavior of GESC under the embankment loading.

This study focuses on understanding the consequence of encasement length, encasement on the performance of geogrid encased stone column under embankment loading through 3D unit cell model. The impact of the parameters mentioned above is evaluated regarding settlement reduction and lateral deformation of the column along its length.

## 2 Geometry and Model Description

A finite element package Plaxis 3D [16] is used in the numerical analysis, where a hypothetical case study is formulated. The soil layer consists of 9.5 m of soft clay underlying a 0.5 m of the sand platform. The sand platform is laid before the construction of the embankment, and it serves as the drainage blanket. The ground water table lies at 0.5 m below the ground. The dimension of the unit is 2 m  $\times$  2 m  $\times$  10 m (L  $\times$  B  $\times$  H) with column installed at the center of the unit cell. The dimension of the unit cell is chosen based on a square pattern of installation having a spacing of 2 m between the columns. The diameter ( $d$ ) of column adopted in the study is 0.8 m which is equivalent to the area replacement ratio of 12.5% as reported in Balbir et al. (2018). Figure 1 displays the details of the mesh connectivity plot of GESC reinforced soft ground. In the present study, the length of GESC ( $L_{\text{GESC}}$ ) is varied between 5 and 10 m, and the axial stiffness of encasement is varied between 500 and 6000 kN/m [7, 17]. The embankment is constructed in three stages; having a height of 2 m in each stage similar to Yoo [9]. The duration of each stage consists of two parts. First part is a construction period of 20 days succeeded by a 30 days of rest period.

**Fig. 1** Generated mesh connectivity plot and details for 3D unit cell



The hydraulic and deformation boundary conditions for the model are chosen based on the symmetry. Therefore, considering symmetry into account no displacement in the perpendicular direction of the symmetry plane and to the base is allowed [9]. Congruently, at the symmetry plane, no flow at the boundary will take place. Therefore, the symmetry plane has been kept as a closed consolidation boundary. Moreover, the bottom boundary is also held closed consolidation boundary considering the impervious layer below the soft clay [10]. The soft soil constitutive material model has been used for modeling the soft soil. However, for the embankment, stone column, and sand platform the Mohr–Coulomb material model is used. Table 1 summarizes the constitutive model and related parameters used in the analysis. The geogrid is used in the study and is modeled as an elastic material having orthotropic behavior. The soft soil, sand platform, and embankment were modeled using twelve node tetrahedral elements. The geogrid was modeled using six node triangular surface element. For modeling soil-geogrid interaction, joint elements (interfaces) were added to geogrid and surrounding soil. The interfaces comprise of twelve node interface elements with zero thickness. The  $R_{inter}$  adopted in the present study for soft soil, sand platform, embankment, and stone column are one as reported by Aljanabi et al. [18], whereas for geogrid soil interface it is 0.7 as reported by Chen et al. [19] and Pandey et al. [20]. These are slender structures that can sustain only tensile force and no compression. The present study is validated with the study conducted by Rajesh [10] in which the surface load is applied to the top of an axisymmetric problem.

However, in the present study, 3D unit cell having a square cross-sectional area of dimension  $2.25 \times 2.25$  m is used as reported by Rajesh [10]. All the material properties and the dimensions were kept intact, except properties of the plate. A steel plate of thickness ( $t_p$ ) 30 mm, unit weight of steel ( $\gamma_{steel}$ ) =  $78.5 \text{ kN/m}^3$  and  $E =$



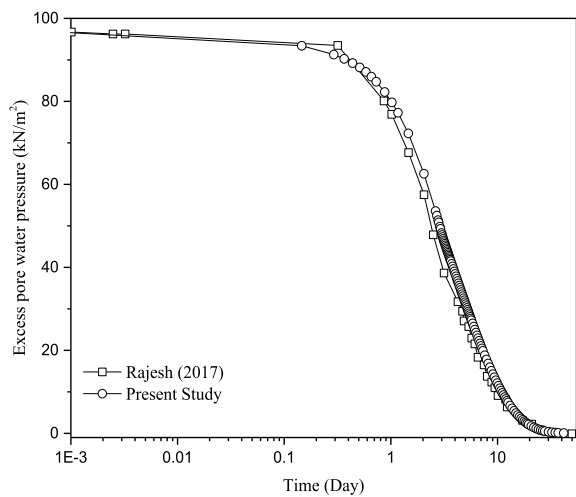
**Table 1** Summary of the constitutive model and related parameter

	Column (Mohr–Coulomb)	Soft clay (soft soil)	Platform (Mohr–Coulomb)	Embankment (Mohr–Coulomb)
Properties	Chen et al. [19]	Hosseinpour et al. [14]	Huang et al. [21]	Aljanabi et al. [18]
$\gamma$ (kN/m <sup>2</sup> )	22	14.50	20	20
$E$ (kPa)	40,000	750	20,000	20,000
$\nu$	0.30	0.28	0.33	0.30
$c'$ (kPa)	0.50	4	5	5
$\varphi'$ (0°)	38	27.50	32	30
$\Psi$ (0°)	10	–	–	–
$C_c$	–	1.26	–	–
$C_s$	–	0.097	–	–
kh (m/day)	10.368	$7.50 \times 10^{-5}$	1	1
kv (m/day)	10.368	$8.40 \times 10^{-5}$	1	1

Note  $E$  = Tangential elastic modulus;  $\nu$  = Poisson’s ratio;  $\gamma$  = Soil unit weight;  $c'$  = Cohesion of Soil;  $\varphi'$  = Soil friction angle;  $\psi$  = Dilation angle;  $C_c$  = Compressibility index;  $C_s$  = Swelling Index;  $k$  = Permeability (Subscript  $h$  and  $v$  corresponds to Horizontal and vertical respectively); – = Data not given

$4.44 \times 10^6$  kN/m<sup>2</sup> is used for the loading. The linear isotropic constitutive model has been adopted for steel plate. The details of the constitutive model and related parameters for other materials can be found in the referred paper. Figure 2 shows the result of the 3D unit cell compared with the axisymmetric model of Rajesh [10] for soft soil reinforced with ordinary stone column (OSC). The results show that the model is in good agreement with the referred study.

**Fig. 2** Validation with Rajesh [10] for OSC (very fine mesh)



### 3 Outcomes and Discussion

The primary emphasis in the present paper is to understand the consequence of encasement parameters like its stiffness and length on the performance of the geogrid reinforced stone column.

#### 3.1 Effect of Length of Encasement

The impact of length of encasement on the behavior of GESG is analyzed by varying encasement length ( $\zeta$ ) between zero and one. The reference encasement stiffness used for this parametric study is 2000 kN/m. In Fig. 3, settlement reduction factor ( $\beta$ ) is plotted against embankment resting on GESG improved ground having varying encasement length. From this figure, it can be observed that column encased fully results in a significant diminution in the settlement ( $> 61\%$ ) as compared to the column without encasement. Moreover, the variance in the settlement reduction ( $\beta$ ) for  $\zeta = 0.75$  and  $\zeta = 0.85$  w.r.t,  $\zeta = 1$  is approximately 21% and 16%, respectively. Seeing this variation, one can state that the column encased fully contributes a significant decrease in the settlement when compared to partially encase. Additionally, the column bulging laterally is dominant at the location where encasement terminates at the bottom as can be noticed from Fig. 4. In this figure, lateral deformation is plotted against column depth of GESG for various length of encasement as stated above. However, the deformation in the case of the column encased fully is almost twice as equated to the column without encasement (i.e., OSC) at the point of termination of the encasement (example let us say at 5 m from the top for  $\zeta = 0.50$ ).

**Fig. 3** Settlement reduction factor for embankment resting on GESG having varying length of GESG

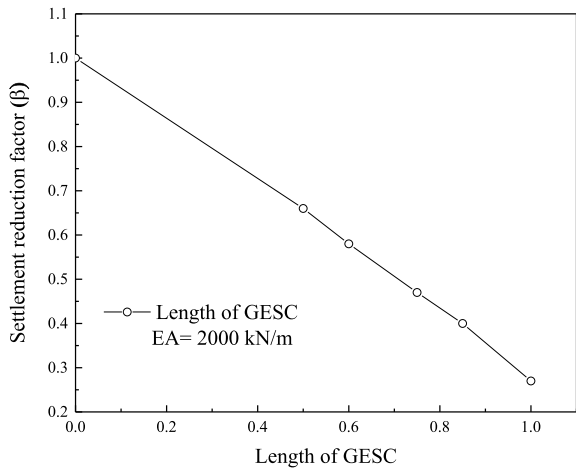
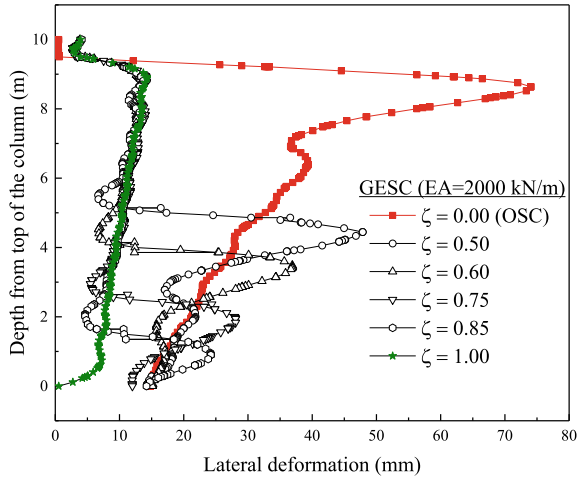


**Fig. 4** Lateral deformation of GESC having different encasement length

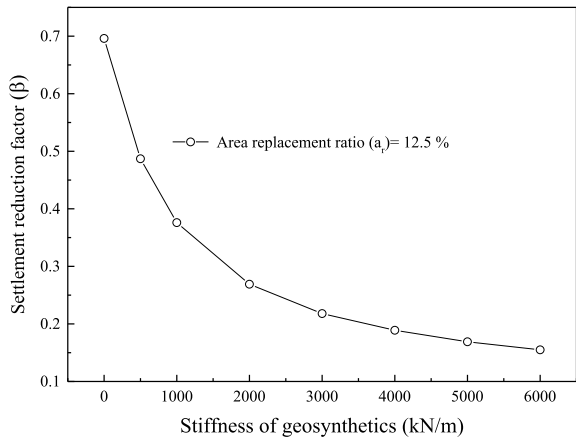


### 3.2 Effect of Encasement Stiffness

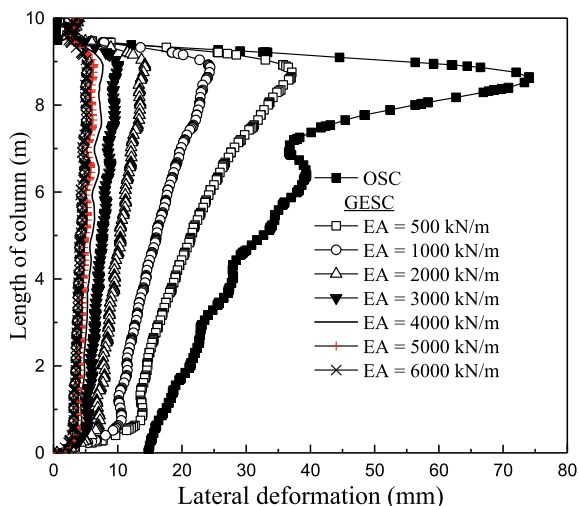
To weigh the impact of geogrid stiffness, its axial stiffness is varied between 500 and 6000 kN/m. In Fig. 5, settlement reduction factor ( $\beta$ ) is plotted against GESC improved ground having different encasement stiffness. However, from this figure we can, clearly, see that the difference in the settlement reduction by using GESC with encasement having stiffness 6000 kN/m is inconsequential (approx. 8%) as compared to encasement having 5000 kN/m stiffness. Therefore, we can state that using encasement stiffness above 5000 kN/m has no determinantal effect.

Figure 6 illustrates the lateral deformation of the OSC and GESC having the different stiffness of the encasement. As expected the lateral deformation in the case of OSC is 14.43 times higher as compared to GESC with the stiffness of 6000 kN/m.

**Fig. 5** Settlement reduction factor for GESC improved ground having different encasement stiffness



**Fig. 6** Lateral deformation of the column of OSC and GESC for different encasement stiffness



However, it is 1.18 times for the encasement stiffness 5000 kN/m as compared to 6000 kN/m. From the previous studies [2, 8] the maximum lateral deformation occurs at the depth varying between 2 and 3\*D from the top of the column. This maximum deformation depth is dependent on the loading area as well as the strength of the surrounding soil. In the current study as can be seen from Fig. 6, this depth is nearly 1.7\*D.

## 4 Conclusion

The paper presents an organized numerical analysis of embankment resting on a stone column encased with geogrid. The area replacement ratio study is kept constant at 12.5% during the analysis. From the study, the following points are concluded.

1. The fully encased stone column shows better performance as compared to a partially encased column regarding both settlement reduction and in prevention of radial bulging of the column.
2. It is observed that when the column is partially encased, maximum bulging occurs at the location where encasement terminates.

## References


1. Abhishek SV, Rajyalakshmi K, Madhav MR (2016) Int J Geotech Eng 10(4):337–357
2. Barksdale RD, Bachus RC (1983) Design and construction of stone column, vol 1. U.S Department of Transportation, Report No-FHA FHWA/RD-83

3. Alexiew D, Raithel M, Kuster V, Detert O (2012) 15 years of experience with geotextile encased granular columns as foundation system. In: ISSMGE-TC 211 International symposium on ground improvement. IS-GI, Brussels
4. Ali K, Shahu JT, Sharma KG (2012) Model tests on geosynthetic-reinforced stone columns: a comparative study. *Geosynth Int* 19(4):292–305
5. Mahajan R, Korulla M, Rimoldi P (2016) Geotextile encased columns design and installation. In: Proceedings of the 6th Asian regional conference on geosynthetics—geosynthetics for infrastructure development. New Delhi, India:188–194 (2016).
6. Raithel M, Kirchner A, Schade C, Leusink E (2005) Foundation of construction on very soft soil with geotextile encased column-state of the art. In: Proceedings of Geo-frontiers 2005. Austin, Texas, United States, pp 1–11
7. Murugesan S, Rajagopal K (2006) Geosynthetic-encased stone columns: Numerical evaluation. *Geotext Geomembr* 24:349–358
8. Yoo C, Kim S-B (2009) Numerical modeling of geosynthetic-encased stone column-reinforced ground. *Geosynthetic Int* 16:116–126
9. Yoo C (2010) Performance of geosynthetic-encased stone columns in embankment construction: numerical investigation. *J Geotech Geoenviron Eng* 136:1148–1160
10. Rajesh S (2017) Time-dependent behaviour of fully and partially penetrated geosynthetic encased stone columns. *Geosynthetic Int* 24:60–71
11. Rajesh S, Jain P (2015) Influence of permeability of soft clay on the efficiency of stone columns and geosynthetic encased stone columns—a numerical study. *Int J Geotech Eng* 9(5):483–493
12. Almeida MSS, Riccio M, Hosseinpour I (2013) Performance of a geosynthetic-encased column (GEC) in soft ground: numerical and analytical studies. *Geosynthetic Int* 20:252–262
13. Elsayw MBD (2013) Behavior of soft ground improved by conventional and geogrid-encased stone columns, based on FEM study. *Geosynthetic Int* 20:276–285
14. Hosseinpour I, Riccio M, Almeida MSS (2014) Numerical evaluation of a granular column reinforced by geosynthetics using encasement and laminated disks. *Geotext Geomembr* 42:363–373
15. Zhang L, Zhao M (2015) Deformation analysis of geotextile-encased stone columns. *Int J Geomech* 15:1–10
16. Brinkgreve RBJ, Engin E, Swolf WM (2013) *Plaxis 3D 2013 Manual*. Plaxis Bv. The Netherland
17. Khabbazian M, Kaliakin VN, Meehan CL (2010) Numerical study of the effect of geosynthetic encasement on the behaviour of granular columns. *Geosynthetic Int* 17:132–143
18. Aljanabi QA, Chik Z, Kasa A (2013) Construction of a new highway embankment on the soft clay soil treatment by stone columns in Malaysia. *J Eng Sci Technol* 8:448–456
19. Chen J-F, Li LY, Xue J-F, Feng S-Z (2015) Failure mechanism of geosynthetic-encased stone columns in soft soils under embankment. *Geotext Geomembr* 43:424–431
20. Pandey BK, Rajesh S, Chandra S (2018) 3-D finite element study of embankment resisting on soft soil reinforced with encased stone column. In: Proceedings of Indian geotechnical conference. Bangalore, pp 1–8
21. Huang J, Han J, Oztoprak S (2009) Coupled mechanical and hydraulic modeling of geosynthetic-reinforced column-supported embankments. *J Geotech Geoenviron Eng* 135(8):1011–1021

# **Ground Improvement Technique**

# Behaviour of Multi-layered Geocell-Reinforced Soil Embankment



Haradhan Sarkar and Arghadeep Biswas 

**Abstract** Geocells are interconnected honeycombing geosynthetics used for strengthening the weak soil, pavement base/subgrade, embankment, etc. Considerable numbers of researches are performed; however, till date, an exact behaviour of geocell-reinforced soil is complex enough to predict. Modelling of geocell-reinforced soil, through numerical methods, is a difficult task because of its geometry and soil-reinforcement interaction; however, the modern FEM software are capable to provide considerably good estimate. This study, numerically, compares the behaviour of single and multi-layered geocell-reinforced embankment system with reference to study reported by Krishnaswamy et al. (in *Geotech Test J* 23:45–54, 2000) and Latha and Rajagopal (in *Can Geotech J* 44:917–927, 2007). It is observed a splitted (multi-layered) geocell system demonstrates improved performance compared to a single-layer geocell-soil composite of same thickness. In this study, a preliminary verification the concept is performed using PLAXIS<sup>2D</sup> simulating the work reported by Krishnaswamy et al. (in *Geotech Test J* 23:45–54, 2000). After satisfactory matching, it is further extended for multi-layer geocell system which is very encouraging for the concept envisaged.

**Keywords** Multi-layer-geocell · Numerical simulation · Embankment · Weak soil · Bearing capacity

## 1 Introduction

Embankments play major role in providing competent foundation for roadways, railways, earthen dams, etc. In many cases, reinforcing the embankment becomes necessary due to weak nature of the native soil. In practice (and, as a topic of research for

---

H. Sarkar

Department of Civil Engineering, Ghani Khan Choudhury Institute of Engineering and Technology, Malda, West Bengal 732141, India

A. Biswas (✉)

Department of Civil Engineering, Jalpaiguri Government Engineering College, Jalpaiguri, West Bengal 735102, India

© Springer Nature Singapore Pte Ltd. 2022

A. K. Dey et al. (eds.), *Proceedings of the 7th Indian Young Geotechnical Engineers Conference*, Lecture Notes in Civil Engineering 195, [https://doi.org/10.1007/978-981-16-6456-4\\_9](https://doi.org/10.1007/978-981-16-6456-4_9)

decades), strengthening the embankments with different types of geosynthetics (with geocells in many instances) has become a trend. In most of the cases, it is observed that it is fruitful to combine geocell reinforcement [1] with other ground improvement techniques (such as wick drain [3]) is an effective measure for an embankment constructed over soft ground. Cowland and Wang [2] have confirmed that the geocell application is cost-effective over traditional ground improvement methods for construction over soft foundation soil. Inspiring from such field successes, several detailed in-house parametric investigations are performed to improve the application and performance of geocell-reinforced systems in different conditions and configurations. Krishnaswamy et al. [5] studied the behaviour of geocell-reinforced embankments constructed over a soft subgrade through a series of laboratory model tests. The results depicted provision of geocells, at the base, improves the load bearing capacity and deformation behaviour of the embankment. In this study, influence of stiffness of geocell-making geogrid was also verified and found that higher the stiffness, greater was the improvement. However, the performance was independent of the pattern of geocell formation (i.e. chevron and diamond). It was also noticed that the geocell layer can be truncated at the toe of the embankment without any significant reduction in the bearing capacity. Later, Latha and Rajagopal [6] re-investigated the model considered by Krishnaswamy et al. [5] through finite element analyses for rigorous parametric influences. Recently, Khalaj et al. [4] and Tafreshi et al. [4, 7, 8] have conducted series of model plate load tests on multi-layered geocell-reinforced systems. It is concluded that multiple geocell layers, each of a relatively low thickness, are more beneficial than a single-layer geocell.

This paper presents an initial investigation of the behaviour of multi-layered geocell embankment. For the purpose, a validation is made for the model study on the embankment behavior reported by Krishnaswamy et al. [5] through Plaxis<sup>2D</sup> (a commercially available finite element software package). Henceforth, an embankment is modelled with single layer of geocell [6] and compared that with multi-layered systems.

## 2 Modelling and Validation

### 2.1 Simulation of Composite Geocell-Soil Layer

The finite element analysis reported in this paper is performed using the PLAXIS<sup>2D</sup>. In PLAXIS, soils are modelled using nonlinear elastic–plastic constitutive model following Mohr–Coulomb yield criteria and non-associated flow rule (for a simplified fast analysis with negligible deviation, as per Wulandari and Tjandra [8]). Geocell layers are modelled as an equivalent composite layer as proposed by Latha and Rajagopal [6]. In the method, the geocell-soil layer is simulated as a soil with higher cohesion but unaltered internal friction angle; where, the geocell-induced cohesion is termed as apparent cohesion ( $c_r$ ). With the modified shear parameters, the equivalent



stiffness of geocell ( $E_g$ ) layer is calculated using Eq. 1–3, where  $\Delta\sigma_3$  is the additional confining pressure due to membrane stress;  $\varepsilon_a$  is the axial strain at failure;  $D_0$  is the initial diameter;  $M$  is the secant modulus of membrane;  $K_p$  is the coefficient of passive earth pressure, and  $K_u$  is the dimensionless modulus parameter for the unreinforced sand.

$$C_r = \frac{\Delta\sigma_3}{2} \sqrt{K_p} \tag{1}$$

$$\Delta\sigma_3 = \frac{2M}{D_0} \left( \frac{1 - \sqrt{1 - \varepsilon_a}}{1 - \varepsilon_a} \right) \tag{2}$$

$$E_g = 4(\sigma_3)0.7(K_u + 200M^{0.16}) \tag{3}$$

### 2.2 Validation

Study reported by Krishnaswamy et al. [5] (Fig. 1a) is validated using PLAXIS<sup>2D</sup> with the method described above. The load-settlement and deformation behaviour (Fig. 1b) depicted good predictability of the numerical model with the experimental observations reported. Hence, the method is accepted and further extended for the multiple-layer geocell-reinforced embankment system. The geometry of modelled single and multi-layered embankments are presented in Fig. 2.

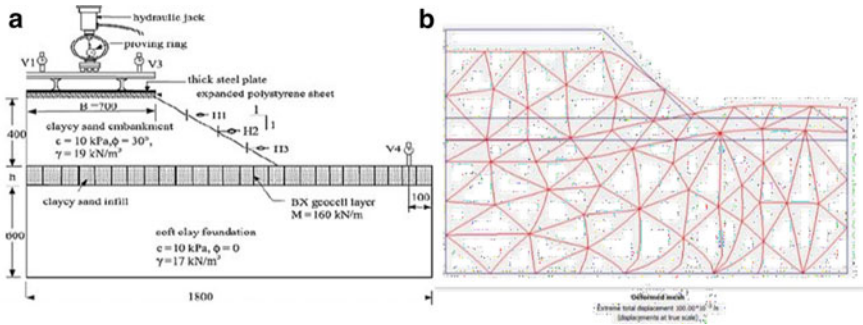


**Fig. 1** **a** Test setup considered by Krishnaswamy et al. [5] and **b** Deformed mesh from PLAXIS<sup>2D</sup> analysis

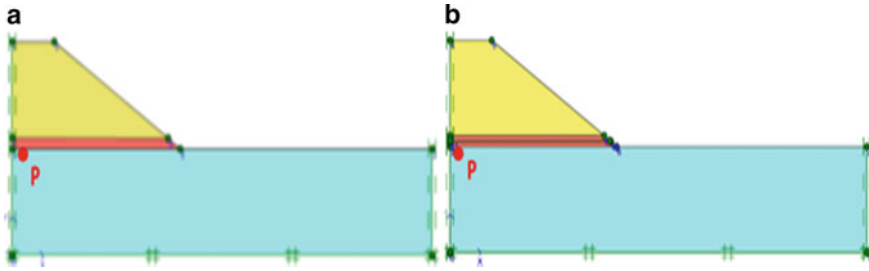


Fig. 2 PLAXIS<sup>2D</sup> model a Single and b Multi-layered geocell-reinforced embankment

### 3 Results and Analysis

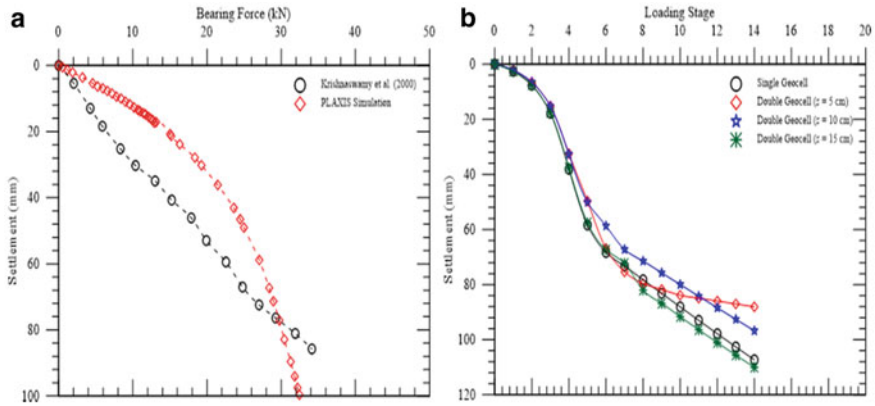
In the analysis, an embankment of 10 m height above a soft clay of 10 m thick is reinforced with geocell. To verify the advantages of multi-layer geocell, a model with single-layer geocell of thickness 1 m and three models with two layers of geocells are considered. The multi-layer systems are designed in such a way that the total reinforced-soil thickness, including the vertical spacing ( $z$ ) in between two geocell layers, should be the same. Hence, the height of geocells are as 47.5, 45 and 42.5 cm, with the vertical spacing in between as 5 cm, 10 cm and 15 cm, respectively, are considered.

The models are simulated in PLAXIS<sup>2D</sup> adopting the soil parameters mentioned by Latha and Rajagopal [6]. Geocell layer was considered as equivalent composite soil as described earlier. The required parameters for geocells for the equivalence are calculated through Eqs. 1–3 [6]. Table 1 presents a brief of the material properties. Plane strain, 15 node element, and drained conditions are selected for the analysis which provided an acceptable matching as shown in Fig. 3a. Plastic calculation is considered to investigate the influence of multi-layer geocells with respect to deflection and stress at the point ‘P’ (Fig. 2). The method is adopted for elastic–plastic deformation analysis in which it is not necessary to take the decay of excess pore pressure with time.

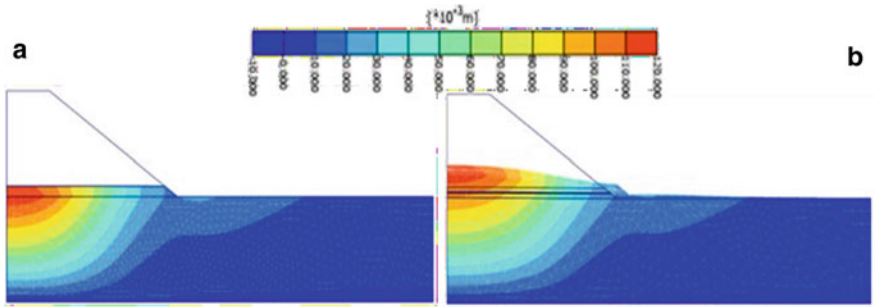
From the analysis, it is observed that multi-layer geocell system gives better result in terms of reduced ‘deformation’ (Fig. 3b) and ‘stress’ at point ‘P’ (Fig. 4). It can be attributed to stress distribution which reduces the stress intensity at the point ‘P’ to increase the overall load bearing capacity of the foundation. Overall, it is found that the multi-layer geocell system is better compared to single-layer geocell system. The

Table 1 Parameter used for analysis (after Latha and Rajagopal [6])

Soil layers	$c_u$ (kPa)	$\varphi$ (°)	$E$ (kN/m <sup>2</sup> )	$\gamma$ (kN/m <sup>3</sup> )	$\nu$
Foundation soil	10	0	3000	17	0.45
Embankment soil	10	45	50,000	19	0.30
Geocell-reinforced sand layer	13	45	93,618	19	0.30



**Fig. 3** a Comparison of results: PLAXIS simulation and test result of Krishnaswamy et al. [5]; and b Variation of settlement for point ‘P’ at different loading stage for single and multi-layer geocell-reinforced systems



**Fig. 4** Deformation behaviour: a Single and b Double layer ( $z = 10$  cm) geocell-reinforced system

study found multi-layer geocell system performed better with a vertical spacing of 10 cm with respect to deflection criteria (Fig. 4); whereas, geocell layers with 5 cm vertical spacing gave better performance in terms of effective Cartesian stress ( $\sigma_{yy}$ ) (Table 2) (Fig. 5).

**Table 2** Performance comparison of single and multi-layer geocell-reinforced systems

Reinforcement condition		Displacement (mm)	$\sigma_{yy}$ (kN/m <sup>2</sup> )
Single-layer geocell system		118.50	188.46
Double-layer geocell system	$z = 5$ cm	119.77	187.60
	$z = 10$ cm	116.87	188.12
	$z = 15$ cm	117.16	189.51

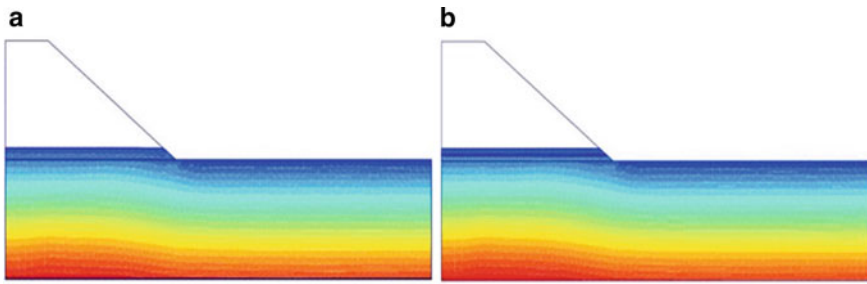


**Fig. 5** Variation of effective stress ( $\sigma_{yy}$ ) with loading stages: **a** Single and **b** Double-layer ( $z = 5$  cm) geocell-reinforced embankment

## 4 Conclusions

Present study has investigated the benefits of multi-layered geocell-reinforced embankment system and compared the performance with a single-layer geocell system of same thickness. From the result analysis, it may be concluded that multi-layered system performs better in terms of decreasing the deformation and reducing the effective stress beneath the geocell layers. Hence, the stability and load carrying capacity of the embankment system increases. Besides, it can also be inferred from the geometry considered that adopting multi-layer geocells can optimise the cost with respect to reduction in material (geocell) used.

## References

1. Bush DI, Jenner CG, Bassett RH (1990) The design and construction of geocell foundation mattresses supporting embankments over soft ground. *Geotext Geomembr* 9:83–98
2. Cowland JW, Wong SCK (1993) Performance of a road embankment on soft clay supported on a geocell mattress foundation. *Geotext Geomembr* 12:687–705
3. Humphrey DN, Holtz RD (1986) Reinforced embankments—a review of case histories. *Geotext Geomembr* 4:129–144
4. Khalaj O, Tafreshi SNM, Masek B, Dowson AR (2015) Improvement of pavement foundation response with multilayers of geocell reinforcement: cyclic plate load test. *Geomech Eng* 9(3):373–395
5. Krishnaswamy NR, Rajagopal K, Latha GM (2000) Model studies on geocell supported embankments constructed over a soft clay foundation. *Geotech Test J* 23(1):45–54
6. Latha GM, Rajagopal K (2007) Parametric finite element analyses of geocell supported embankments. *Can Geotech J* 44:917–927
7. Tafreshi SNM, Khalaj O, Dowson AR (2013) Pilot scale load tests of a combined multilayered geocell and rubber-reinforced foundation. *Geosynthetic Int* 20(3):143–161
8. Wulandari PS, Tjandra D (2015) Analysis of geotextile reinforced road embankment using PLAXIS 2D. *Procedia Eng* 358–362

# Parametric Effect on Granular Columns: A Brief Review



Samrat Ghose, Arghadeep Biswas , and Utpal Mandal

**Abstract** Granular columns are quite common in soft soils, mostly in clays, for improving pressure-settlement behavior of concern foundation. Load transmission in granular column mechanized by grain-to-grain contact and/or deriving resistance through interfacial interaction. Performance of such columns are highly depended on native soil condition which imparts passive pressure against the possible bulging in different configurations. Parameters, such as geometry (length and diameter), quality of in-filled aggregates, drainage condition, application of reinforcements etc., are responsible for the variations in performances. Phenomenon such as squeezing of soft clay into the aggregates and vice-versa reduces the functionality of granular column. Reinforcing the granular column with anchors, horizontal and 3-dimensional encapsulation has been very effective in enhancing the performance and/or reducing the detrimental effects. Studies have indicated the benefits and/or restrictions using granular columns under various parametric alterations. This paper presents a brief review on such parametric effects on granular columns under varying configurations and conditions.

**Keywords** Granular columns · Reinforcement · Parametric effects · Soft soil

## 1 Introduction

The granular inclusion in soft soil (as column) has been very effective in improving load bearing capacity and reducing excessive settlement of concern geo-structure. It is constructed by filling and compacting the granules, such as sand/gravel/coarse aggregates, by replacement (in a pre-bored column) or displacement (using vibration) technique. The granules, being stiffer, attracts majority of the imposed load and transfer deeper through contacts. Besides, being permeable, it allows faster pore water

---

S. Ghose · A. Biswas (✉)

Jalpaiguri Government Engineering College, Jalpaiguri, West Bengal 735102, India

U. Mandal

Ramkrishna Mahato Government Engineering College, Purulia, West Bengal 723103, India

© Springer Nature Singapore Pte Ltd. 2022

A. K. Dey et al. (eds.), *Proceedings of the 7th Indian Young Geotechnical Engineers Conference*, Lecture Notes in Civil Engineering 195,

[https://doi.org/10.1007/978-981-16-6456-4\\_10](https://doi.org/10.1007/978-981-16-6456-4_10)

dissipation (acting as vertical drain) and speed-up the soil-consolidation; whereas, the surrounding soil provides lateral confinement (passive resistance) to reduce the bulging [1, 2]. In present days, artificially, additional confinement is provided by encasing the column with a suitable reinforcement, mostly with geosynthetics [3–6]. In such cases, the lateral restraint is applied in the form of hoop stress, generated through the encasement, during the bulge formation [7–10]. A number of study has investigated various parametric influences, such as geometry, in-fill density, encasement type etc., on the performance of granular columns. This article presents a brief review on such parametric dependencies of granular columns which would be useful for researchers and practicing engineers.

## 2 Parametric Studies

### 2.1 *Physical Model Investigations*

Physical model tests in varying configurations, with respect to geometry, type of loading, confining conditions and soil types etc., are performed to understand the behavior of granular columns. The effect of column-geometry (length, diameter etc.) was studied by Rao et al. [11]. The study indicated column length should be between 5 and 8 times the diameters of the column. Hughes and Withers [2], Hughes et al. [12] observed higher bearing capacity of granular column as compared to theoretical estimation. It was attributed to larger peripheral deformation (radial bulging) in field. Accordingly, different pattern of distortions (both vertical and lateral) of granular columns were also postulated under varying conditions. In connection to the above, Wood et al. [13] justified different modes of failure depending on arrangement of columns (in groups) and indicated that critical column length varies proportionally with the area ratio. Ambily and Gandhi [14] observed that the granular column performs better when subjected to a surcharge loading (i.e., load is shared by the surrounding soil) as compared to column loaded alone (Fig. 1a). It was found that the bulge formation is less in case of surcharge loading which is attributed to improved composite stiffness when soil was loaded simultaneously. At present, encasing the granular column (which provides an additional lateral resistance through hoop stress) has become very effective and popular in improving load bearing capacity and to limit the bulging. Malarvizhi and Ilamparuthi [7] have considered encased granular column and confirmed that bearing capacity improvement is proportional to the stiffness of the encasing material. However, the benefit has varied oppositely with increased column diameter. Such behavior was recognized as insufficient strain mobilization for required hoop stress generation. Ayadat and Hanna [4], Murugesan and Rajagopal [5], Ghazavi and Nazari [9] have also reported similar observations (as reduced vertical compression at the column-top) with stiffer encasement.

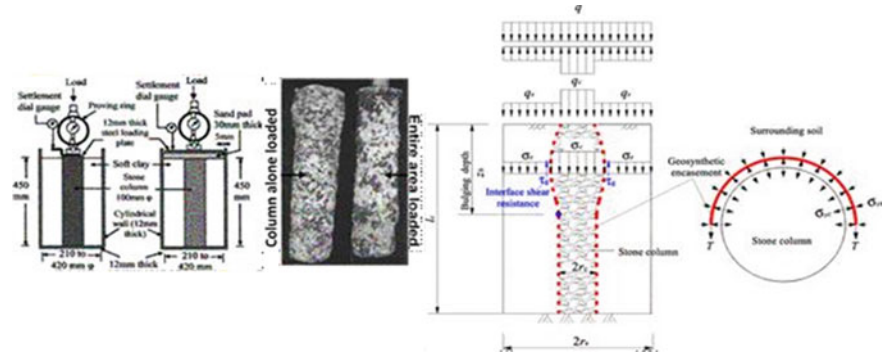


**Fig. 1** a Influence of loading type [14]; b typical encasement mechanism [17]

### 2.2 Theoretical Analysis

Theoretical analysis is the contemporary of physical tests. In most of the cases, analytical and/or numerical solutions overcomes the difficulties/drawbacks of physical modeling (which involves several unavoidable uncertainties) and predicts an ideal behavior under varying configurations. Hughes and Withers [2] proposed an expression for ultimate stress generation on granular column. It is concluded that the bearing capacity of the column is notable up to a critical “length to diameter ratio”. Continuing the study-type, Ambily and Gandhi [14] verified their physical test outcomes through Finite Element analysis and a design methodology is proposed considering “load sharing” between columns and the surrounding clay. Presently, software based simulative analysis of reinforced (encased) granular column is very popular. Murugesan and Rajagopal [8] studied the effective length (depth of maximum bulge formation) of encasement and concluded it as twice the column diameter. Added to the above, it is also mentioned that the stress intensity on the granular column increases with stiffer geosynthetics. However, Yoo and Kim [15], Yoo [16] observed no encasement-benefit beyond a critical stiffness which is independent of the area replacement ratio.

### 3 Mechanism of Granular Column

Primarily, installation of granular columns (as sand and/or stone column) are intended to carry the structural load. The load carrying capacity is developed through grain-to-grain stress propagation and mobilizing passive resistance by the surrounding clay. During loading, the aggregate dilates causing a lateral bulging. The bulging, to some extent, benefiting the granular system as anchor-column. In present practice, additional confinement is imposed through an encasement. It develops hoop stress and produces lateral support which can be increased with tensile-modulus of the

encasing material. The “encasement” confines aggregates within and restricts the spreading. Thus, it creates “integrity” within the discrete aggregates and a better load transmission throughout the column length is established. In absence of encasement, the column material disperse into the surrounding clay (loss in aggregates) and vice-versa, creates problem in drainage and transferring the load. Regarding the loading pattern, a surcharge load on surrounding soil enhances the passive resistance which improves the stability of the column. The stress localization (which creates bulging) also gets reduced and improves the functionality of the column. Figure 1a depicts bulging of a stone column under different types of loading and the mechanism of encasement is presented in Fig. 1b.

### 4 Effecting Parameters

Studies have revealed various parameters effecting the performance of granular column. The following section briefly discusses the influencing parameters and their effect on the behavior of granular columns.

#### 4.1 Undrained Shear Strength of Clay ( $c_u$ )

Undrained shear strength ( $c_u$ ) of surrounding clay has significant contribution on the performance of granular column. It provides the initial lateral confinement to the granular column when encasement is not provided. However, in case of very low  $c_u$ , the clay and column-aggregates squeezed into each other causing disturbance in drainage and load carrying mechanism. Ambily and Gandhi [14] observed that the limiting axial stress on granular column is independent of  $c_u$  (Fig. 2a). The ground stiffness improves with surcharge loading which is independent of clay strength, however, depends on spacing between the columns (Fig. 2b). Najjar et al.

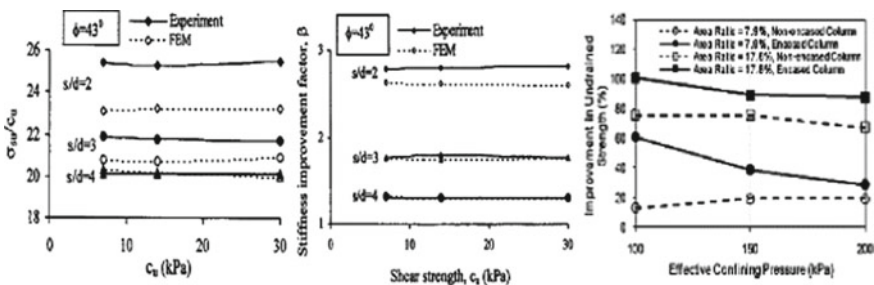


Fig. 2 Confinement effect of surrounding soil on a limiting axial stress of granular column, b stiffness [14], and c undrained shear strength of treated ground [18]



[18] observed the ‘variation in shear strength with depth’ is independent of the embedment depth of the sand column. However, for geotextile-encased column, the improvement in  $c_u$  decreased with the depth of confinement (Fig. 2c).

### 4.2 Internal Friction Angle of Aggregates ( $\phi$ )

In general, the stiffness (thus the bearing capacity) of stone column increases with internal friction angle ( $\phi$ ) which depends on angularity, interface characteristics and packing of aggregates [19]. It was concluded that the gravel is the most efficient column material having high friction angle and requires lowest compactive effort for the desired degree of packing. Malarvizhi and Illamparuthi [7] observed that the influence of “ $\phi$ ” in “settlement reduction ratio” is more for unreinforced case (Fig. 3). This is due to stiffness of encasing material which provides additional confinement to loosely packed column material. Keykhosropur et al. [20] concluded that reduction in settlement and lateral bulging (due to greater friction angles in encased column) results in higher stability for the granular column (Fig. 4).

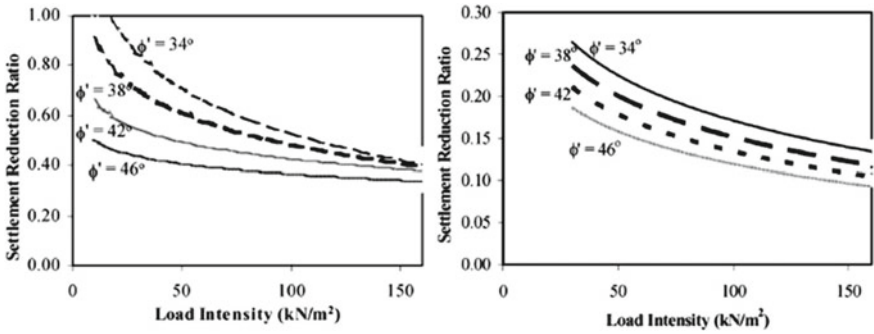


Fig. 3 Variation in settlement reduction ratio for a unreinforced and b encased column [7]

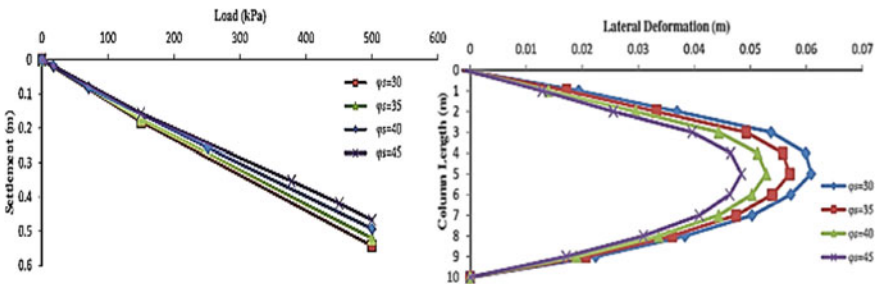
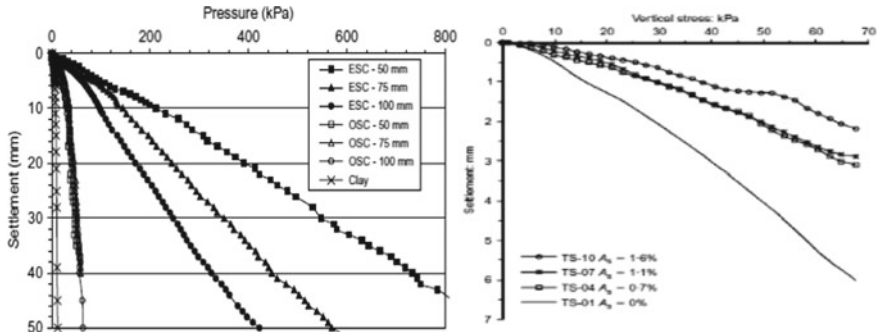


Fig. 4 Effect of  $\phi$  values of encased granular column on a load-settlement response, b lateral deformation [20]



**Fig. 5** a Load-settlement response of unreinforced and encased granular column for different diameters [21] and b effect of area ratio [25]

### 4.3 Diameter of Granular Column ( $D$ )

Method of installation and the stiffness of surrounding soil influences the most to the diameter of granular column. In practice, during installation/compaction, the diameter of granular column becomes larger depending on soil stiffness. This increase in diameter enhances the estimated bearing capacity and drainage function. Hughes et al. [12] obtained about 30% higher bearing capacity (in the field) as compared to the predicted values reported earlier [2]. Similar observation was also reported by Murugesan and Rajagopal [21]; in addition, they noticed a reduced rate of improvement for encased column due to limited hoop stress (Fig. 5).

### 4.4 Critical Length of Granular Column ( $l_{crit}$ )

Performance of granular column depends on the critical length,  $l_{crit}$  (i.e., the length beyond which the granular column does not contribute). As per model tests the critical length to diameter ratio lies between 5 and 8 [2, 11, 13]. McKelvey et al. [22], Sivakumar et al. [23], Black et al. [24] reported that longer columns are useful for settlement control (due to adequate bulge formation); while, a punching failure can be expected for end-bearing shorter columns. Black et al. [24] observed larger deviator stress and lesser pore pressure generation at failure for a fully penetrating column triggering the aggregate-dilation during bulging. Ali et al. [6] noticed that end-bearing column performs better in load sharing irrespective of reinforcement condition.

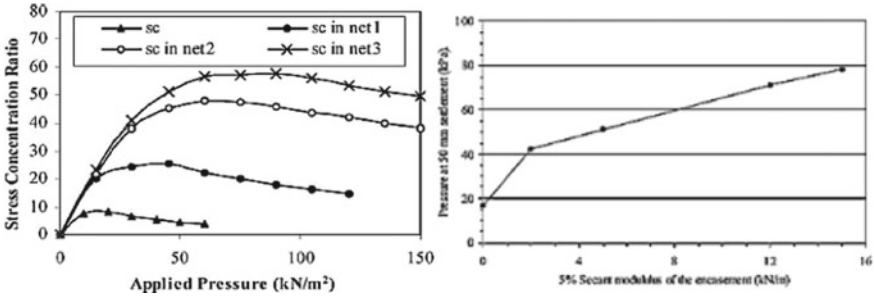


**Fig. 6** **a** Stress concentration ratio of encased column [7] and **b** effect of modulus of encasement on the encased column [21]

### 4.5 Modulus of Encasement ( $E_s$ )

The stiffness of column is enhanced with stiffer encasement (Fig. 6) [7, 8, 15, 16]. Malarvizhi and Ilamparuthi [7] reported improvement in stress concentration ratio (SCR = Ratio of stress on column to that on adjacent soil) with stiffer encasement.

### 4.6 Length of Encasement ( $l_{esc}$ )

The prime objective of encasement is to subdue the lateral deformation and provide confinement for imparting stiffness to the granular column. Murugesan and Rajagopal [21], Yoo and Lee [26] concluded the effective length of the encasement as 2–3  $D$  from the top of the column. Ali et al. [6] recommended for the full length encasement, irrespective of end bearing or floating columns. However, Dash and Bora [27] observed that partially encased (60% of column length) floating column performs better which was attributed to “deep seated bulge formation” at the bottom.

## 5 Conclusions

This article present a brief review on the behavior of granular column under different parametric variations. Following conclusions may be drawn based on the discussions:

- The granular column can be floating or end bearing type.
- For short floating column, the failure occurs due to punching; while long column fails by bulging.
- Depth of maximum radial deformation (bulging) of a granular column is about of 2–3 times the column diameter from the top.

- The critical length to diameter ratio lies within 5–8, beyond which improvement is marginal.
- Performance increases with higher angle of internal friction of the aggregates.
- The stiffer is the encasement, higher will be the improvement (due to greater confinement generated with larger hoop stress mobilized).
- The effect of confinement decreases as the diameter of the encased granular column increases.

**Acknowledgements** The authors sincerely acknowledge the support received from DHESTBT, Govt. of West Bengal, India [Memo No. 183(Sanc.)/ST/P/S&T/6G-33/2017 dated 16/03/2018].

## References

1. Greenwood DA (1970) Mechanical improvement of soils below ground surface. *Ground Eng* 11–22
2. Hughes JMO, Withers NJ (1974) Reinforcing of soft cohesive soils with stone columns. *Ground Eng* 7(3):42–49
3. Raithel M, Kempfert HG (2000) Calculation models for dam foundations with geotextile coated sand columns. In: Proceedings of international conference on geotechnical and geological engineering, GeoEngg-2000. Melbourne
4. Ayadat T, Hanna AM (2005) Encapsulated stone columns as a soil improvement technique for collapsible soil. *Ground Improv* 9(4):137–147
5. Murugesan S, Rajagopal K (2010) Studies on the behaviour of single and group geosynthetic encased stone columns. *J Geotech Geoenviron Eng* 136(1):129–139
6. Ali K, Shahu JT, Sharma KG (2012) Model test on geosynthetics-reinforced stone columns: a comparative study. *Geosynth Int* 19(4):292–305
7. Malarvizhi SN, Ilamparuthi K (2007) Comparative study on behaviour of encased stone column and conventional stone column. *Soil Found* 47(5):873–885
8. Murugesan S, Rajagopal K (2006) Geosynthetic-encased stone columns: numerical evaluation. *Geotext Geomembr* 24(6):349–358
9. Ghazavi M, Nazari AJ (2013) Bearing capacity of geosynthetic encased stone column. *Geotext Geomembr* 27(3):167–175
10. Gu M, Zhao M, Zhang L, Han J (2016) Effects of geogrid encasement on lateral and vertical deformations of stone columns in model tests. *Geosynth Int* 23(2):100–112
11. Rao NS, Prasad YVS, Rao HV (1992) Use of stone columns in soft marine clays. In: Proceedings of 45th Canadian geotechnical conference. Toronto, Ontario, pp. 9/1–9/7
12. Hughes JMO, Withers NJ, Greenwood DA (1975) A field trial of the reinforcing effect of a stone column in soil. *Geotechnique* 25(1):31–44
13. Wood MD, Hu W, Nash DFT (2000) Group effects in stone column foundations: model tests. *Geotechnique* 50(6):689–698
14. Ambily AP, Gandhi SR (2007) Behaviour of stone columns based on experimental and FEM analysis. *J Geotech Geoenviron Eng* 133(4):405–415
15. Yoo C, Kim SB (2009) Numerical modeling of geosynthetic-encased granular column-reinforced ground. *Geosynth Int* 16(3):116–126
16. Yoo C (2010) Performance of geosynthetic-encased granular columns in embankment construction: numerical investigation. *J Geotech Geoenviron Eng* 136(8):1148–1160
17. Zhang L, Zhao M (2014) Deformation analysis of geotextile encased stone column. *Int J Geomech* 5:1–10

18. Najjar SS, Sadek S, Maakaroun T (2010) Effect of sand columns on the undrained load response of soft clays. *J Geotech Geoenviron Eng* 136(9):1263–1277
19. Bergado DT, Lam FL (1987) Full scale load test of granular piles with different densities and different proportions of gravel and sand in the soft Bangkok clay. *Soils Found* 27(1):86–93
20. Murugesan S, Rajagopal K (2007) Model tests on geosynthetic encased stone columns. *Geosynth Int* 24(6):349–358
21. Mckelvey D, Sivakumar V, Bell A, Graham J (2004) Modeling of vibrated stone columns in soft clay. *Geotech Eng* 157(3):137–149
22. Keykhosropur L, Soroush A, Imam R (2012) 3D numerical analyses of geosynthetic encased stone columns. *Geotext Geomembr* 35:61–68
23. Sivakumar V, McKelvey D, Graham J, Hughes D (2004) Triaxial tests on model sand columns in clay. *Can Geotech J* 41:299–312
24. Black JV, Sivakumar V, Mckinley JD (2007) Performance of clay samples reinforced with vertical granular columns. *Can Geotech J* 44:89–95
25. Black JV, Sivakumar V, Bell A (2011) The settlement performance of stone column foundations. *Geotechnique* 61(11):909–922
26. Yoo C, Lee D (2012) Performance of geogrid-encased stone columns in soft ground: full scale load tests. *Geosynth Int* 19(4):480–490
27. Dash SK, Bora MC (2013) Influence of geosynthetic encasement on the performance of stone columns floating in soft clays. *Can Geotech J* 41:754–765

# Challenges and Strategies in Treatment of Terrace Material Encountered in Place of Rock at Foundation of Spillway



Vinod Kumar Mauriya

**Abstract** The Koldam HPP( $4 \times 200$  MW) located on river Satluj in Bilaspur district of Himachal Pradesh, utilizes a drop of about 140 m by constructing a 167 m high rock and gravel fill Dam. The spillway of Koldam Project has 6 bays, each of 17.1 m width with crest at El 625 m, separated by 6 m wide piers. Based on the initial investigations carried out by various agencies during design, the arrangement of spillway was finalized on the left flank considering rock foundation. However, during excavation of spillway foundations in chute area, terrace material was encountered. This was not suitable for founding the Spillway Chute slab. Mid-course correction was necessitated to ensure the structure meets its intended purpose for the designed life. The present paper deliberates the challenges faced and strategies adopted in treatment of terrace material encountered in place of rock at foundation of Spillway. The alternatives were explored for treating above area as either to remove the terrace material and backfill with concrete or to do the grouting of the whole terrace area below spillway chute. NTPC decided to found the spillway chute on the grouted terrace material with design modification required for the terrace material portion. In spite of the various challenges encountered during execution of the Spillway, spillway chute was cast successfully on the treated area with additional measures like grouting of terrace material and structure has efficiently performed during operation.

**Keywords** Koldam · Spillway · Excavation · Terrace material · Grouting

## 1 Introduction

Spillways are of great importance, which act as a safety valve provided in the dam to dispose surplus floodwater from the reservoir. Besides sufficient capacity, the spillway must be hydraulically adequate and structurally safe and must be located in such a way that the out-falling discharges back into the river do not erode or undermine the downstream toe of the dam. The surface of the spillway should be

---

V. K. Mauriya (✉)  
NTPC Ltd, EOC Noida, Gautambudhnagar, UP 201301, India  
e-mail: [vkmauriya@ntpc.co.in](mailto:vkmauriya@ntpc.co.in)

© Springer Nature Singapore Pte Ltd. 2022  
A. K. Dey et al. (eds.), *Proceedings of the 7th Indian Young Geotechnical Engineers Conference*, Lecture Notes in Civil Engineering 195,  
[https://doi.org/10.1007/978-981-16-6456-4\\_11](https://doi.org/10.1007/978-981-16-6456-4_11)

such that it is able to withstand erosion or scouring due to the very high velocities generated during the passage of a flood through the spillway. The floodwater discharging through the spillway has to flow down from a higher elevation at the reservoir surface level to a lower elevation at the natural river level on the downstream through a passage, which is also considered a part of the spillway. At the bottom of the channel, where the water rushes out to meet the natural river, is usually provided with an energy dissipation arrangement that kills most of the energy of the flowing water to prevent the river surface from getting dangerously scoured by the impact of the out-falling water.

## 2 Spillway

The Koldam spillway is of Chute type with length of 420m and varying width from 132 m (top) to 70 m (bottom) along the chute [1]. The Spillway has the capacity for flood discharge of 16,500 m<sup>3</sup>/s (Probable Maximum Flood). The crest of Spillway is at El 625 m with a length of 102.6 m and it has been divided in 6 modules for radial gates with each bay of 17.1 m wide. Six Radial gates have been provided in spillway for safely releasing the water from reservoir during flood and excess inflow in the river. Spilled water passing through spillway path would pass through ogee and subsequently 1% slope, 15% slope and 30% slope of chute slabs, then fall in energy dissipation arrangement comprising flip bucket and plunge pool and lastly would be discharged back into Satluj river at downstream. Under chute slab, an elaborate system of under drainage has been provided with drained water led to drainage gallery provided below the raft of right guide wall. Main components of Spillway structure are Weir and Pier, Chute, Left and Right Guide Wall and Flip Bucket. In continuation of the flip bucket, Plunge Pool is provided to dissipate the energy of water flowing with high speeds.

## 3 Challenges in Treatment of Terrace Material

### 3.1 Original Provisions

The rock excavation carried out upstream of the spillway directs the stream flow lines in the optimum direction for hydraulic efficiency. The approach speed in the reservoir during passing of the Probable Maximum Flood 16,500 m<sup>3</sup>/s is approximately 6 m/s, which is relatively high. Flow in the chute is characterized by speeds between 20 m/s and 40 m/s. These speeds require specifying of a concrete formulation that will resist abrasion, the phenomenon of abrasion being aggravated by the fact that the water passing through the chute may be filled with suspended material.

The spillway chute is having a length of 420 m, a variable width of 108.5 m upstream to 70 m downstream, and the energy dissipation is through a flip bucket. Based on the initial investigations carried out by various agencies during design, the arrangement of spillway was finalized on the left bank considering rock foundation.

### 3.2 Terrace Material at Foundation of Chute

The natural surface level in spillway area was El + 690m requiring huge excavation. Loose soil excavation was carried out by digging with excavator and excavation in compacted conglomerates and rock was carried out by conventional drill and blast method. In excavation, benches have been provided at regular interval of 10m. The excavated slopes were stabilized using cement grouted rock bolts (32 mm/25 mm diameter and 6–9 m deep) and 100 mm thick shotcrete with wire mesh [2]. The choice of grout materials for alluvial soil is given in IS 14343:1996 [3].

The chute structure of Spillway was originally designed to be founded on rock. However, during actual excavation in this area, it was observed that in a portion of foundation of chute structure (approx. 150 m length) terrace material is encountered where rock was anticipated. Design consultant suggested that the whole terrace material needs to be removed and backfilled with concrete. The typical Spillway model and actual strata during excavation is shown in Figs. 1 and 2.

The location of terrace material encountered and a typical view of the actual excavation in spillway area is presented in following Figs. 3 and 4 respectively.

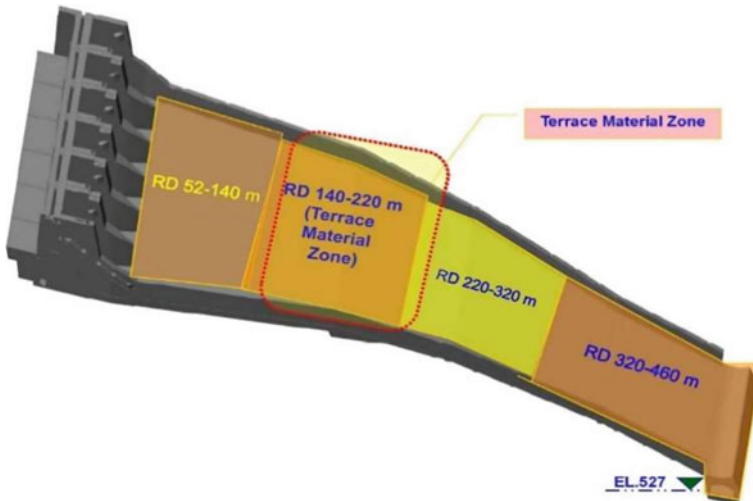


Fig. 1 Typical Spillway model





Fig. 2 Actual strata at Spillway during excavation

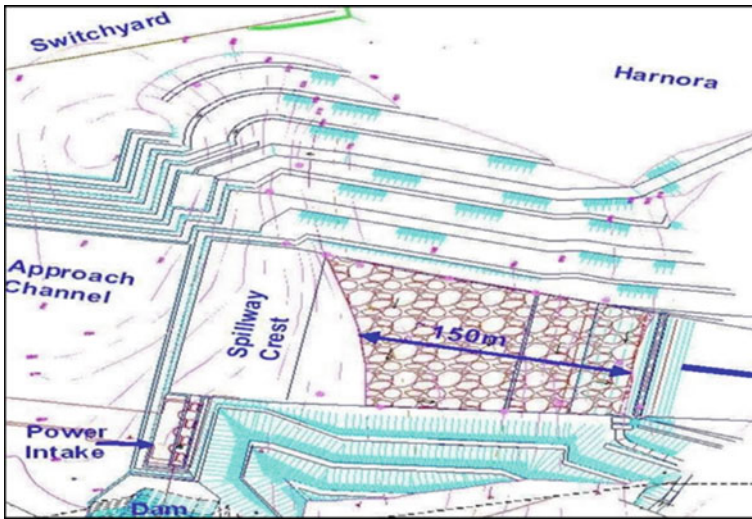


Fig. 3 Location of terrace material: plan

### 3.3 Geological Conditions

The details of relevant drill holes, drifts and seismic profiling done during different stages of investigation at the location of spillway and its vicinity can be seen in following Fig. 5. Two drill holes (DH 84-5 and DH 84 -7) were drilled near the

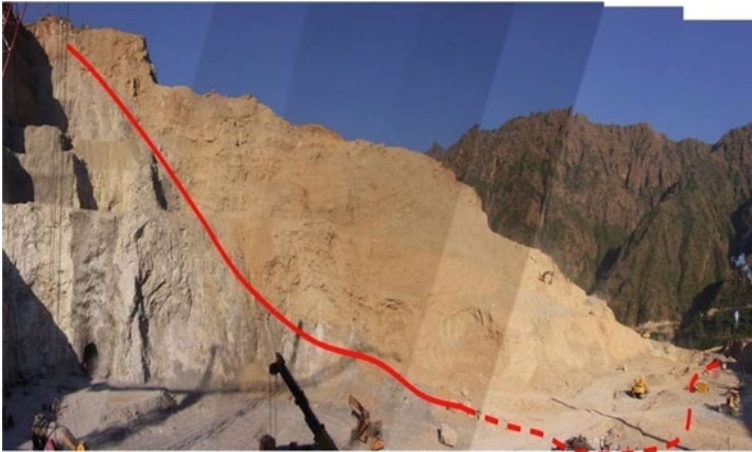


Fig. 4 View of the actual excavation in spillway area

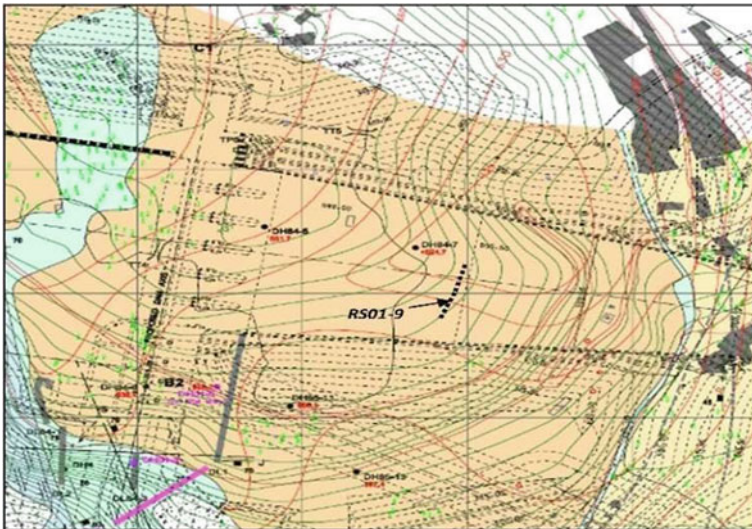


Fig. 5 Investigations in Spillway area

centerline of spillway and four boreholes (DH 84-6, DH 01-5, DH 85- 11, DH 85-13) were drilled between the right bank of spillway and dam. In all the boreholes rock was encountered except in DH 84-7, which was terminated at El  $\pm$  624 m. Rock contour had been developed based on the information obtained from these boreholes. Further, refraction profiling was also done in the middle of the chute about 200 m downstream of the dam axis showed P-wave velocity of 3200m/sec at about El  $\pm$  670 m, which is shown in Fig. 6. Such high P-wave velocity is generally anticipated in

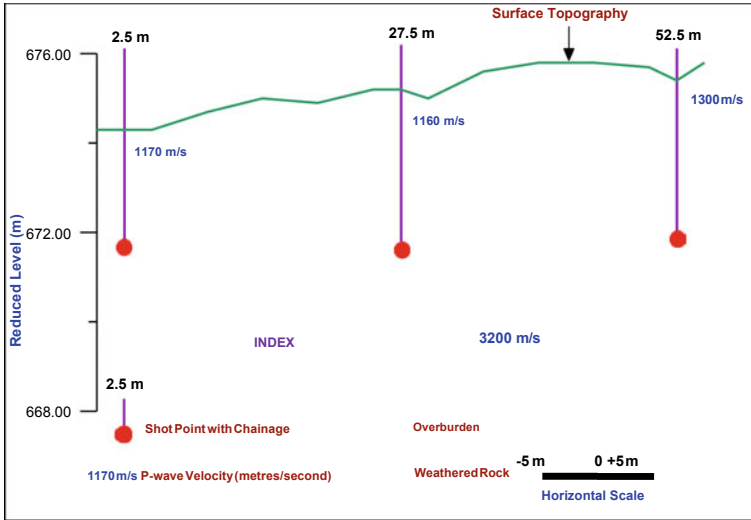


Fig. 6 Depth Section along Profile 9 (Spillway Chute area)

weathered rock. In one of the drift (DL-1) which is located near the spillway and was extended till the left guide wall location, failed to encounter rock despite excavation of a pit at its end up to El 641m. However, this drift is at higher elevation and does not give the information about the depth of terrace deposit.

### 3.4 Additional Geotechnical Investigation at Spillway Foundation

During the progress of excavation work, as rock was not encountered at the anticipated level, some additional geotechnical investigations were carried out to ascertain the actual rock levels. The investigations indicated the presence of well-consolidated terrace deposit consisting of boulders/gravel/pebbles and cementations below chute for a stretch of about 150m length with depth varying from 0 m to 20 m. The presence of these deposits at these depths was not envisaged earlier. It was found that rock profile in that area is highly undulating. The geological cross-section along the spillway axis is as shown in Fig. 7. The anticipated and actual rock profile in Spillway chute area is presented in Fig. 8.

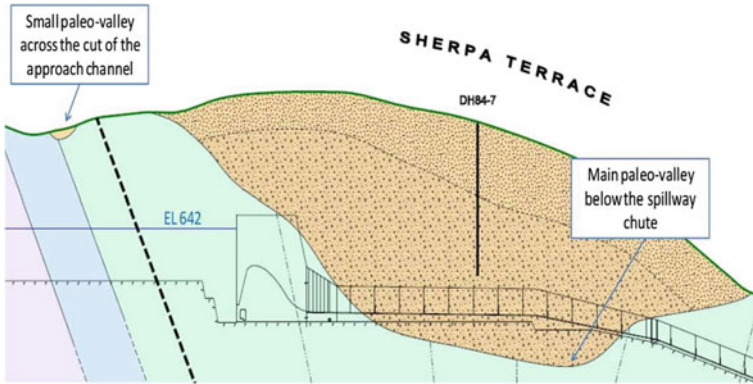


Fig. 7 Geological cross-section along the spillway axis

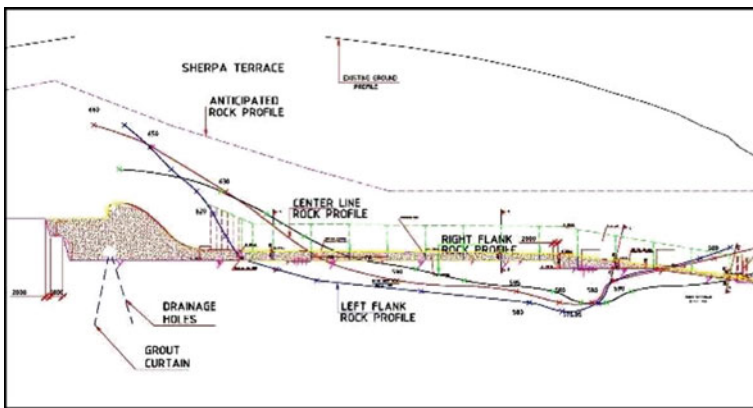


Fig. 8 Anticipated and actual rock profile in chute area

## 4 Strategy Adopted in Treatment of Terrace Material

### 4.1 Design Evaluation and Strategy Adopted

The encountered terrace material in place of rock-foundation was not suitable for founding the Spillway Chute slab. Mid-course correction was necessitated to ensure the structure meets its intended purpose for the designed life. Design consultant advised that the level of the underside of the spillway and chute reinforced concrete structure to be maintained as per original design. For the zone where the buried river channel crosses the foundation of the chute structure a concrete backfill will be required to avoid founding the structure on overburden. This would also necessitate

adjustment of slopes below El 625 temporarily in order to perform the concrete back-filling works and the spillway structure before backfilling to achieve 1(V):1.35(H) design slopes.

The removal of the terrace material and replacing it with concrete up to rock level was estimated to be INR 50 crore and would require 18 months to complete the same. However, grouting the terrace material by drilling up to 1 m in rock was costing INR 7.5 crore and the activity can be completed in 5 months saving 13 months over the other alternative.

Further, after detailed deliberations, it was decided to found the spillway chute on the grouted overburden material with modification required for the terrace material portion by providing shear keys along longitudinal and transverse joints of the concrete slabs to minimize possibility of differential movement of chute slab due to uplift during heavy flow of water on chute in line with IS: 5186 [4] and accordingly modification in location of drain pipes for transverse joints.

## 4.2 Methodology

The area between left and right guide walls to be confined by providing grout curtains and the whole mass between confined area be grouted. Curtain grouting through drilled boreholes @ 1.5 m center-to-center spacing was done under pressure to confine the terrace material area. Subsequently, consolidation/ area grouting through drilled boreholes @ 3 m center to center spacing was done in the terrace material area to consolidate the area for foundation of spillway structure. Total drilling and grouting (up to 1 m in rock) was worked to be 25,000 m. Following was sequence for carrying out the grouting activities in terrace material area:

- i. Drilling in terrace material
- ii. In-situ permeability tests in borehole
- iii. Performance grouting with cement, bentonite and super plasticizer (sodium silicate gel).

The marked grouted area is shown in following Figs. 9 and 10.

## 5 Conclusion

The unforeseen geological occurrence at Spillway Chute foundation necessitated additional geotechnical investigations and required separate methodology of execution due to varying rock profile. It was learned that the adequate geotechnical investigations shall be carried out covering all the prominent component structures to observe geological changes at advanced stage and incorporate necessary changes at early stage to avoid cost overrun due to delays and contractual disputes during





**Fig. 9** Location of consolidation/area grouting and curtain grouting in terrace material portion



**Fig. 10** Location of consolidation/ area grouting and curtain grouting in terrace material portion

execution stage. However, in the present case of the posed challenges and surprises encountered during execution of the Spillway Chute foundation, the treatment of terrace material is successfully carried out and constructed spillway structure has efficiently performed during operation.

## References

1. Project Completion Report (Part A, B & C) (2017) Koldam hydro power project (4x200MW). Himachal Pradesh, India
2. IS 4999(1991) Indian standard for Recommendations for grouting of pervious soils, Bureau of Indian Standards, New Delhi
3. IS 14343 (1996) Indian standard for Choice of grouting material for alluvial grouting- Guide lines, Bureau of Indian Standards, New Delhi
4. IS 5186 (1994) Indian standard for Design of Chute and Side Channel Spillways-Criteria, Bureau of Indian Standards, New Delhi.

# Effect of Sand Content and Plasticity on Swell and Hydraulic Behaviour of Expansive Soils



Sabari Ramesh and T. Thyagaraj

**Abstract** Swelling and shrinkage of expansive soils raise concern over their performance for various geotechnical and geoenvironmental engineering applications such as top and bottom liners of landfills. Swelling results in heaving of expansive soil, whereas the shrinkage results in the formation of desiccation cracks. To overcome these volume changes in the expansive soils, they can be modified by adding sand which can reduce the swell potential and the formation of desiccation cracks. Plasticity, compaction, swelling and permeability characteristics of expansive soils get altered upon the addition of sand. In the present study, these characteristics of an expansive natural soil amended with sand and their interdependency with each other were examined through the experimental laboratory studies. Clay-sand mixtures passing through 2 mm sieve were prepared by thoroughly mixing the sand with expansive soil in three different proportions, namely low, medium and high sand content. Swell potential and hydraulic conductivity of different specimens under a surcharge load of 12.5 kN/m<sup>2</sup> were obtained from one-dimensional swell tests and rigid wall permeability tests, respectively. Although there was a considerable variation in the sand proportion added, the consistency limit tests showed only smaller reduction in liquid limit and plasticity index because of a lesser percentage of fine sand in the total sand added. In spite of the small changes in the consistency limits, a reduction of more than 50% in swell potential and increased hydraulic conductivity was observed, indicating the more significant influence of coarser non-swelling fraction on the swell and hydraulic behaviour of clay-sand mixtures.

**Keywords** Expansive soil · Plasticity · Swell potential · Hydraulic conductivity

---

S. Ramesh (✉) · T. Thyagaraj  
Department of Civil Engineering, Indian Institute of Technology Madras, Chennai 600036, India

© Springer Nature Singapore Pte Ltd. 2022  
A. K. Dey et al. (eds.), *Proceedings of the 7th Indian Young Geotechnical Engineers Conference*, Lecture Notes in Civil Engineering 195,  
[https://doi.org/10.1007/978-981-16-6456-4\\_12](https://doi.org/10.1007/978-981-16-6456-4_12)

101



## 1 Introduction

The volume change behaviour of soils is governed by the type and amount of clay minerals, structure, initial soil conditions, physico-chemical aspects and environmental factors. In soils, any process which changes their effective stress can induce volume change in them. The effective stress in soil can be altered due to the variations in total stress or pore water pressure. When the soil is dry, it tries to imbibe more water resulting in an increased pore water pressure. The increased pore water pressure decreases the effective stress and leads to swelling due to double layer expansion. On the other hand, during drying of wet soil, moisture loss from the soil resulted in increased matric suction and effective stress, thereby causing shrinkage of soils [9]. Swelling results in heaving of expansive soil, whereas the shrinkage results in the formation of desiccation cracks. The desiccation behaviour exhibited by expansive soils has to be controlled for increasing its applications in various fields of geotechnical and geoenvironmental engineering. Compacted clayey soils restrict the flow of leachate and thereby preventing contamination of the surrounding soil and groundwater when used as base liners in landfills.

Studies pertaining to hydraulic conductivity as well as swell-shrink behaviour of compacted expansive soils was carried out exhaustively by many researchers [3, 4, 6, 7, 15]. Compacted clay soils used as liners in landfills should have a very low hydraulic conductivity ( $\leq 1 \times 10^{-9}$  m/s) and should exhibit minimal volume changes [4, 6, 16, 17]. Expansive soils generally exhibit low hydraulic conductivity values but undergo a large amount of volume change. Addition of an optimum percentage of sand to expansive soil can reduce the volume change and also restrict the hydraulic conductivity within the allowable values.

In clayey soils, the amount of clay and type of clay mineral are the major factors controlling the liquid limit. In the case of sand-bentonite mixtures, liquid limit values do not vary linearly with the amount of clay, indicating an interaction between different soil types in mixtures which in turn affect the liquid limit of mixtures. The liquid limit of clay-sand mixtures depends on the size of sand particles, whereas it is independent of the shape of sand particles [12, 14]. A soil containing sufficient amount of sand with enough clay and silt to seal the voids between sand particles would be a perfect choice as a liner regarding crack resistance and hydraulic conductivity [8]. For clay-sand mixtures to fulfil the minimum criteria requirements as landfill liners, a proper equilibrium has to be maintained between the particle sizes of clay and sand. A soil with an optimum amount of sand and clay providing both improved rigidity and reduced permeability, respectively, would satisfy the requirements for a liner [10].

According to Shaker and Elkady [11], for mixtures with less than 30% clay content, clay component did not fill the pores of sand and flow would be dominated by macropores, whereas for clay content more than 30%, flow would be through micropores within the clay and thereby resulting in significant reduction of hydraulic conductivity in clay-sand mixtures. For sand-bentonite mixtures composed of lower

percentage of bentonite, the size of coarser fractions governed the hydraulic conductivity of the mixture whereas when percentage of bentonite was higher enough to fill all the voids between coarser fractions, hydraulic conductivity was governed by clay content alone [13]. Cui et al. [5] performed experiments on clay-sand mixtures considering both constant volume and free swell conditions. When the volume of mixtures during experiment was kept constant, swelling of clay aggregates resulted in a reduction of macropore volume and thus decreasing the hydraulic conductivity. On the other hand, during free swell condition, swelling of aggregate resulted in increased macropore volume, thereby increasing the hydraulic conductivity.

From the studies mentioned above, it is clearly understood that when expansive soil is amended with sand, it modifies their plasticity, compaction, swelling and permeability characteristics. The influence of sand content present in clay-sand mixtures on the above characteristics and their interdependency with each other has not been investigated in detail. Therefore, in this paper, the role of sand content and plasticity on the swell and hydraulic behaviour of expansive soils is investigated by conducting laboratory experiments.

## 2 Materials and Methods

### 2.1 Soil Properties and Characterization

Expansive soil for the present study was obtained from Kishkinta, Chennai, Tamil Nadu and was air-dried, crushed and sieved using 2 mm sieve (No. 10 sieve) before the start of the experimental programme. The sand used was river sand which was also air-dried, cleaned and sieved using 2 mm sieve. Different clay-sand mixtures were prepared by spreading the required amount of expansive soil and sand on a glass plate and then thoroughly mixed using spatulas. Table 1 presents the proportions of sand added and designations of clay-sand mixtures. The basic characteristics of prepared clay-sand mixtures were found out from standard laboratory experiments. The plasticity characteristics were determined for clay-sand mixtures as per ASTM

**Table 1** Designations and mix proportions adopted for clay-sand mixtures in the present study

Soil	Specimen designation	Sand (%)	Expansive soil (%)
Natural expansive soil	C100	0	100
Sand amended soil 1	C68-S32	32	68
Sand amended soil 2	C50-S50	50	50
Sand amended soil 3	C32-S68	68	32

D4318 [1], and compaction tests were conducted as per ASTM D698[2]. Figures 1 and 2 show the particle size distribution curves and standard Proctor compaction curves for all clay-sand mixtures, respectively. Table 2 shows the basic properties obtained for expansive soil and clay-sand mixtures.

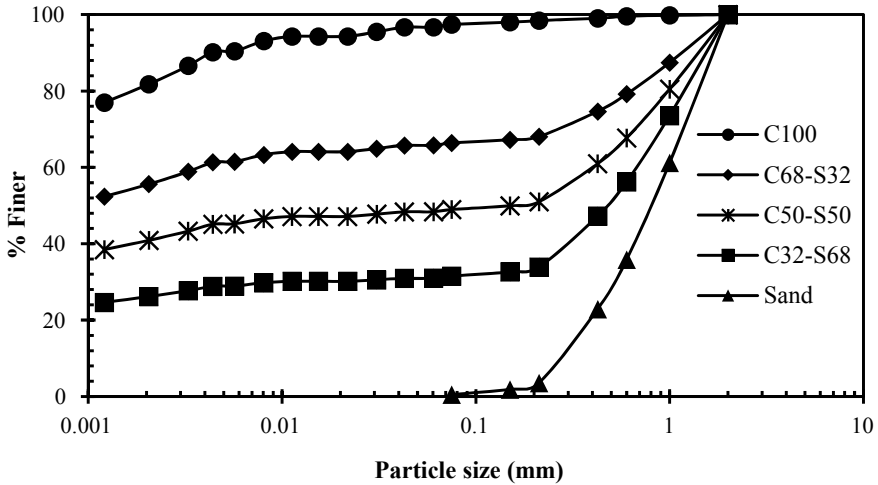


Fig. 1 Gradation curves obtained for clay, sand and clay-sand mixtures

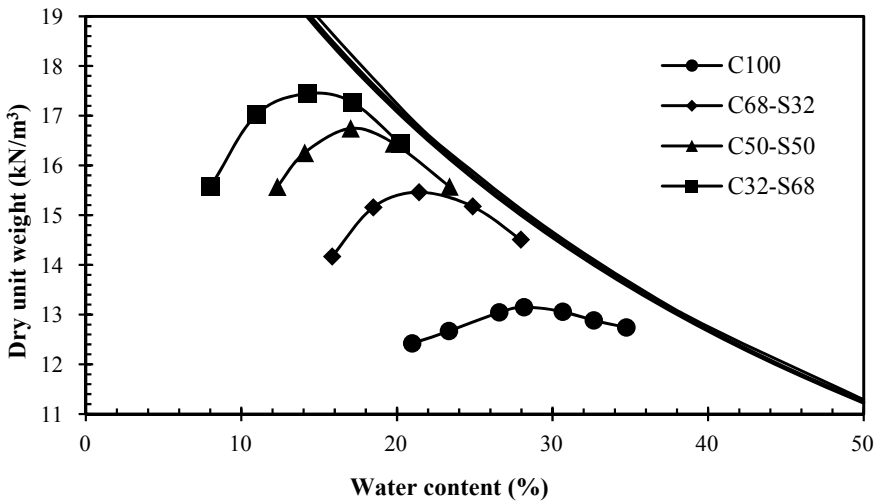


Fig. 2 Standard proctor compaction curves

**Table 2** Basic characteristics of expansive soil and clay-sand mixtures

Property	C100	C68-S32	C50-S50	C32-S68
Liquid limit (%)	87	81	67	63
Plastic limit (%)	32	31	26	18
Plasticity index (%)	55	50	41	45
Specific gravity	2.71	2.69	2.68	2.67
Optimum moisture content (%)	28	24	17	15
Maximum dry unit weight (kN/m <sup>3</sup> )	13.1	15.3	16.8	17.5

## 2.2 Experimental Programme

**One-dimensional swell potential tests.** All the compacted specimens necessary for this study were prepared at a dry unit weight and moisture content as given in Table 2. To start with, the soil was mixed thoroughly using spatulas with distilled water as remoulding fluid and placed in airtight ziplock covers for two days to attain moisture equilibration. Test specimens were obtained by statically compacting the soil in steel oedometer rings of diameter  $7.5 \times 10^{-2}$  m and height  $3 \times 10^{-2}$  m. Specimen height of  $2 \times 10^{-2}$  m was achieved by using a spacer disc of height  $1 \times 10^{-2}$  m. Specimens were placed between two porous stones and filter papers at top and bottom, and they were placed in the swelling assembly under a vertical pressure of  $12.5 \text{ kN/m}^2$ . The swelling assembly was attached with a dial gauge of least count  $2 \times 10^{-6}$  m to record the vertical deformations. The inundating fluid added was distilled water and corresponding swollen heights of the specimen for different time intervals were recorded continuously until the readings became constant for two consecutive days. After the swell tests, specimens were taken out cautiously from the assembly and their weight and height were noted down. The swell potential for all the soil specimens was calculated using the equation

$$\% \text{Swell} = \frac{\Delta H}{H_i} \times 100. \quad (1)$$

where  $\Delta H$  is the increase in height at a vertical stress of  $12.5 \text{ kN/m}^2$  and  $H_i$  is the initial height for compacted specimens.

**Hydraulic conductivity tests.** Falling head rigid wall hydraulic conductivity experiments were carried out on the swollen specimens obtained after swell tests. Oedometer ring with soil specimen was removed from swelling apparatus and kept in permeability mould for measuring hydraulic conductivity. In the permeability moulds, porous stones and filter papers were kept both above and below the specimens and water was allowed to enter the specimens from the bottom. Tests were conducted under a hydraulic gradient of 20 and a surcharge pressure of  $12.5 \text{ kN/m}^2$ . By measuring the drop in head of water at different time, the hydraulic conductivity was obtained using the following equation

$$k = 2.303 \times \frac{a \times L}{A \times t} \times \log \frac{h_1}{h_2} \quad (2)$$

where  $k$  is the hydraulic conductivity,  $a$  and  $A$  are cross-section areas of the pipe and the specimen, respectively,  $L$  is the length of the specimen,  $t$  is time, and  $h_1$  and  $h_2$  are heads of water at different time intervals.

### 3 Results and Discussion

#### 3.1 Plasticity and Compaction Characteristics

Atterberg limit tests were carried out on all the four soils, and the obtained values are shown in Table 2. By adding sand to expansive soil, a reduction in the liquid limit and plastic limit values was observed as a result of replacement of plastic clay soil with non-plastic sand fraction. Plasticity index also reduced but showed an increased value for C32-S68 specimen due to a substantial reduction in the plastic limit with increase in sand content from 50 to 68%. Figure 3 a, b show the change in Atterberg limits with the addition of sand passing No. 10 and No. 40 sieves, respectively.

The added sand passing through No. 10 sieve adopted for the study contains 77% of medium sand and 23% of fine sand. The changes in consistency limits with reference to the added sand percentages were marginal, and their variation is not linear. The marginal reduction in consistency limits is attributed to the lower percentage of fine sand in the added sand. To bring out the effect of the size of added sand, separate tests were conducted on the clay-sand mixtures obtained by mixing expansive soil with sand passing through No. 40 sieve. In this case considerable variation of consistency limits is observed as shown in Fig. 3b. The soil passing through No. 40 sieve is adopted for Atterberg limit tests, but if the tested soil has a higher percentage of particles coarser than No. 40 sieve, the values obtained from this test have less significance. Figure 2 clearly shows that by adding sand, the maximum dry unit weight increased and optimum moisture content reduced owing to the denser packing of clay-sand mixtures and reduction in clay content.

#### 3.2 Swell Potential and Hydraulic Conductivity

Swell potential results obtained for different clay-sand mixtures are shown in Fig. 4a. Upon the addition of sand, the swell potential reduced due to the replacement of clay with non-swelling sand fractions and swelling of clay in the voids of sand. In spite of a smaller variation in Atterberg limits and increased dry density, the swelling capacity of soil minimized drastically with the addition of sand. A swell potential

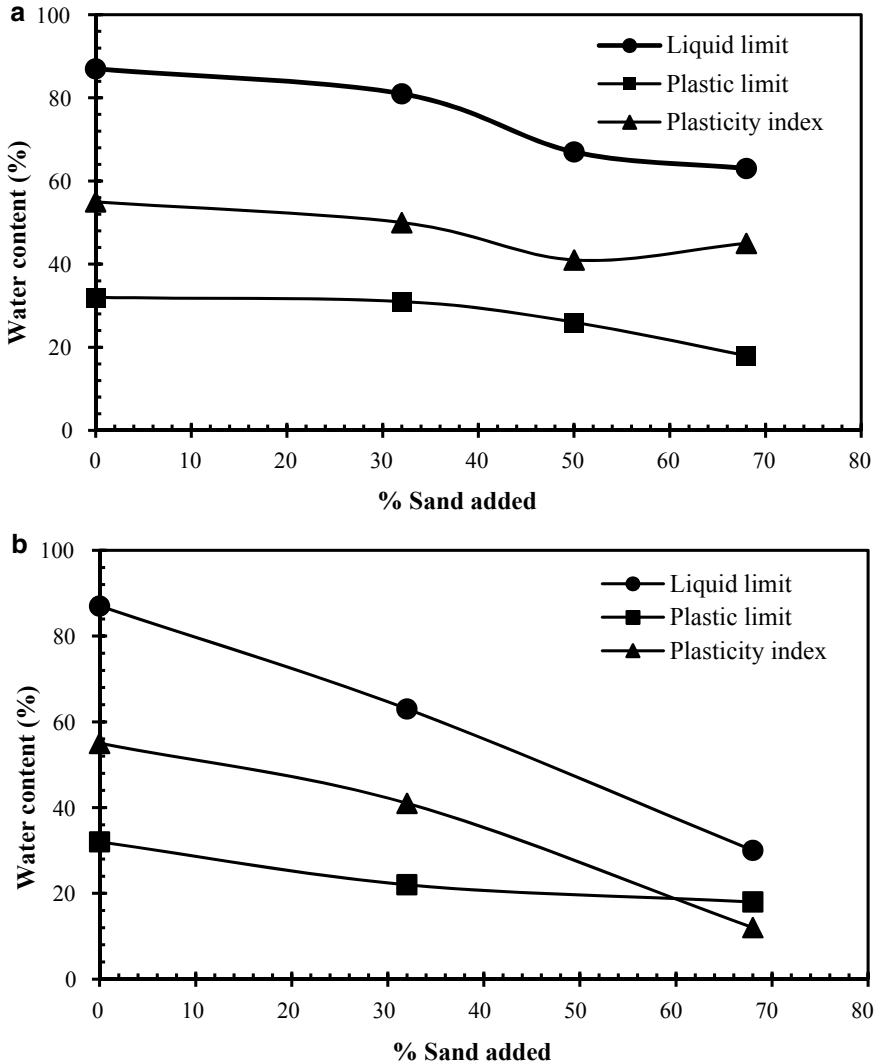


**Fig. 3** a. Change in Atterberg limits for sand content finer than No. 10 sieve. b Change in Atterberg limits for sand content finer than No. 40 sieve

of 10% exhibited by C100 soil was reduced to 3.2% for C50-S50 specimen and to almost 0% for C32-S68 specimen.

For the initial smaller fractions of sand added, the hydraulic conductivity values reduced as a result of the availability of enough clayey soil to swell and fill the pores between sand particles. With further increment in the percentage of sand added, the hydraulic conductivity values for all the soil specimens increased owing to the shortage of clay soil to occupy all the pores between sand particles during

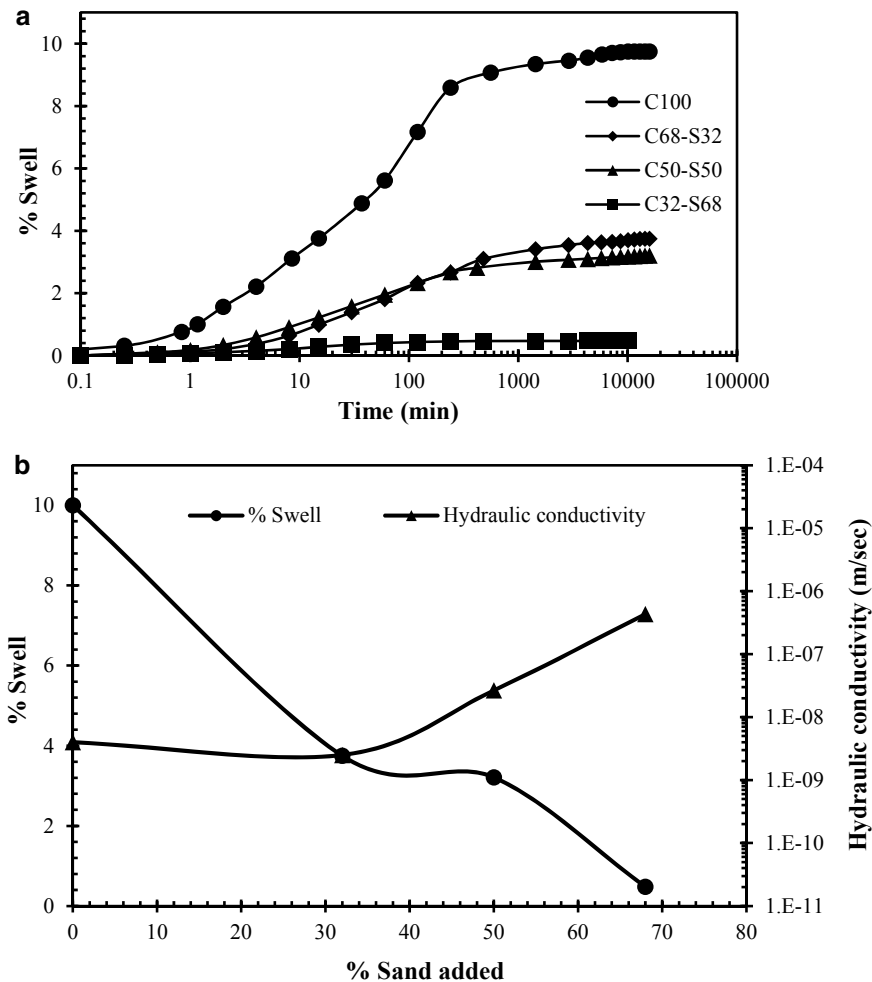


**Fig. 4 a** Influence of sand content on swell potential of clay-sand mixtures. **b** Influence of sand content on swell and hydraulic behaviour of clay-sand mixtures

swelling. Figure 4b explains the effect of addition of sand content on swell and hydraulic behaviour of different clay-sand mixtures. For C32-S68 specimen, the hydraulic conductivity increased by two orders of magnitude when the swell potential decreased to almost zero. The results obtained from both tests specify that the swelling and hydraulic behaviour of clay-sand mixtures are governed more by non-swelling fractions rather than plasticity and compaction characteristics.

## 4 Conclusions

Based on results obtained from the above experimental studies, we can conclude that.

- Liquid limit, plastic limit and plasticity index values of clay-sand mixtures decreased with increase in sand content. A smaller percentage of fine sand in the added sand resulted in only a smaller reduction in consistency limits. Therefore, the values of consistency limits of soils containing a higher proportion of coarser fractions are not reliable.
- The maximum dry unit weight increased and optimum moisture content reduced with the addition of sand. The denser packing of clay soil in the relatively less pore space of sand particles led to the increase in dry unit weight and the reduction in the amount of clay soil possessing higher water holding capacity decreased the moisture content.
- The swell potential of clay-sand mixtures reduced with an increase in sand content due to the replacement of clay particles with non-swelling sand fractions, swelling of clay particles within voids of sand and also due to restriction offered by bigger sand particles.
- The hydraulic conductivity values of clay-sand mixtures decreased for initial smaller percentages of added sand but later at higher percentages of sand, hydraulic conductivity values increased. At lesser percentages of sand, the mixture behaviour is controlled by clay particles and this results in lower hydraulic conductivity, whereas with the increase in sand proportion, the flow occurs through their voids and hydraulic conductivity increased.
- For soils with a more significant amount of non-swelling coarser fraction, their swelling and hydraulic behaviour are governed by non-swelling fraction rather than plasticity and compaction characteristics.

## References

1. ASTM D4318-17e1 (2017) Standard test methods for Liquid Limit, Plastic Limit, and Plasticity Index of soils. ASTM International, West Conshohocken, PA
2. ASTM D698-12e2 (2012) Standard test methods for laboratory compaction characteristics of soil using standard effort. ASTM International, West Conshohocken, PA
3. Benson CH, Trast JM (1995) Hydraulic conductivity of thirteen compacted clays. *Clays Clay Miner* 43(6):669–681
4. Benson CH, Daniel DE, Boutwell GP (1999) Field performance of compacted clay liners. *J Geotech Geoenviron Eng* 125(5):390–403
5. Cui YJ, Tang AM, Loiseau C, Delage P (2008) Determining the unsaturated hydraulic conductivity of a compacted sand-bentonite mixture under constant volume and free-swell conditions. *Phys Chem Earth* 33:S462–S471
6. Daniel DE, Benson CH (1990) Water content-density criteria for compacted soil liners. *J Geotech Eng* 116(12):1811–1830



7. Day RW (1994) Swell-shrink behaviour of compacted clay. *J Geotech Eng ASCE* 120(3):618–623
8. Kleppe JH, Olson RE (1985) Desiccation cracking of soil barriers. *Hydraulic Barriers in Soil and Rock*, ASTM STP 874:263–275
9. Lambe WT (1960) The character and identification of expansive soils. Technical studies report for Federal Housing Administration, 1–9
10. Omid GH, Prasad TV, Thomas JC, Brown KW (1996) The influence of amendments on the volumetric shrinkage and integrity of compacted clay soils used in landfill liners. *Water Air Soil Pollut* 86:263–274
11. Shaker AA, Elkady TY (2015) Hydraulic performance of sand-clay mixtures: soil fabric perspective. *Géotechnique Lett* 5:198–204
12. Sivapullaiah PV, Sridharan A (1985) Liquid limit of soil mixtures. *Geotech Test J* 8(3):111–116
13. Sivapullaiah PV, Sridharan A, Stalin VK (2000) Hydraulic conductivity of bentonite-sand mixtures. *Can Geotech J* 37(2):406–413
14. Srikanth V, Mishra AK (2016) A laboratory study on the geotechnical characteristics of sand-bentonite mixtures and the role of particle size of sand. *Int J Geosynthetics Ground Eng* 2(1):1–10
15. Tripathy S, Subba Rao KS (2009) Cyclic swell-shrink behaviour of a compacted expansive soil. *J Geotech Geological Eng ASCE* 27:89–103
16. UK Environmental Agency (2011) LFE04—Earthworks in landfill engineering. *Engineering Guidance*, 1–66
17. US EPA (2009) *Industrial Waste Management: Protecting Land, Ground Water, Surface Water, and Air*. Chapter 7, 7B-1- 7B-30

# Effect of Lime Treatment on Expansive Soils at High Initial Water Content



T. Ashok Kumar , T. Thyagaraj , and R. G. Robinson

**Abstract** Deep soil mixing is widely used technique for stabilizing thick deposits of soft clays. A laboratory trail was carried out to extend its application for stabilizing the expansive soils at high water content. Lime was used as a principal stabilizing agent and in addition to that pond ash was mixed at proportions of 10, 20 and 30% based on dry weight basis. The degree of shrinkage, swell and unconfined compressive strength characteristics were studied to evaluate the efficacy of the treatment method. The experimental findings show that the addition of 4–8% lime increased the unconfined compressive strength from 35 to 650 kPa at different initial water contents of 0.8–1.2 times the liquid limit ( $w_L$ ). The swell potential of the stabilized soil reduced to zero percentage on first wetting because of its high initial water content and pozzolanic reactions, but it showed a significant swell during second wetting which varied from 4.4 to 6.4% at 1.0  $w_L$ . The strength of lime-pond ash admixed soil shows a significant increment at 10% pond ash and further addition resulted in reduction in the strength characteristics. However, during the second wetting, the swell increased for 10 and 20% pond ash admixed soil and then it decreases for 30% pond ash admixed soil.

**Keywords** Expansive soil · Pond ash · Volume change · Stabilization

## 1 Introduction

The in-situ stabilized soil columns are generally formed through the mechanical mixing in which admixtures (lime/ cement) are mixed with the wet soil slurry by mixing blades. Deep mixing has been implemented in various applications like foundation improvement, seepage control, heave control, liquefaction mitigation, marine applications, etc., [5]. The deep soil mixing with designed guidelines was first implemented for the stabilization of marine clay for the construction of the Tokyo port in 1975 [7]. The diameter of the stabilized soil column varies from 0.5 to 1 m and the depth of treatment of soil ranges from 3 to 50 m [4]. The chemical interactions

---

T. A. Kumar (✉) · T. Thyagaraj · R. G. Robinson  
Department of Civil Engineering, Indian Institute of Technology Madras, Chennai 600036, India

between the soil and lime improve the soil properties by increasing the shear strength and reducing the compressibility than the untreated soil. Puppala et al. [6] studied the efficacy of cement-lime deep soil mixed (DSM) column in controlling the volume change of medium stiff expansive soils through the field study. It was reported that after the treatment, the swell pressure has reduced drastically when compared to the swell pressure of untreated soil sections. Madhyannapu et al. [3] performed laboratory and field studies to check the quality assessment and to examine the stiffness and strength properties of DSM stabilized soil. They found that the field stiffness and strength reduced by 30–60% and 20 to 30%, respectively, when compared to laboratory condition specimens. Bushra and Robinson [1] conducted laboratory study to utilize Class F fly ash along with the cement to study the consolidation and compressive strength behaviour of treated marine clay. They found that the optimum dosage of fly ash as 20% along with 10% cement, at a total clay water content of 1.25  $w_L$ . This paper brings out the strength and swell-shrink characteristics of expansive soil treated using DSM technique.

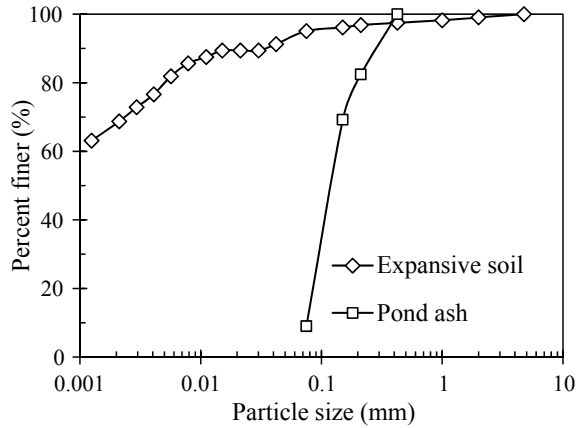
## 2 Materials and Experimental Protocol

The clay used for the experiments was obtained from Wellington Lake, near Tiruchirappalli, Tamil Nadu State. The procured soil was initially processed to remove any foreign matter, and then the soil was air-dried, pulverized and sieved through 425  $\mu\text{m}$  sieve. Table 1 summaries the properties of soil used for testing. The results of Atterberg limits and gradation show that the soil is high compressible clay (CH). Laboratory grade lime ( $\text{Ca}(\text{OH})_2$ ) is used as a primary stabilizer and pond ash as an additional admixture for the partial replacement to lime. The processed pond ash is sieved through 425  $\mu\text{m}$ , and the same is used for this present study. The pond ash

**Table 1** Physical properties of soil used for this study

Property	Values
Specific gravity	2.7
Atterberg limits (%)	
Liquid limit	95
Plastic limit	33
Shrinkage limit	8.5
Gradation (%)	
Sand	5
Silt	27
Clay	68
IS classification	CH
Differential free swell (%)	95

**Fig. 1** Particle size distribution curves of expansive soil and pond ash



is classified as poorly graded sand (SP) as it comprises 91% fine sand size particles. Figure 1 shows the particle size distribution curves of expansive soil and pond ash.

The required quantity of processed soil was taken and mixed with moisture contents of 0.8, 1.0 and 1.2 times of  $w_L$ . The amount of water required to prepare the wet soil slurry before adding lime and pond ash was calculated using the following equation:

$$\Delta W = \frac{WT}{1 + w_0}(w_r - w_0) \tag{1}$$

where  $\Delta W$  = weight of water to be added,  $W_T$  = weight of untreated soil,  $w_r$  = required remoulding water content and  $w_0$  = natural water content of soil. Then, the lime with water/binder ( $W/B$ ) ratio as 1.0 was mixed with soil paste in a mechanical mixer at 61 rpm for 10 min, and then, it was hand mixed for 2–3 min. The water content increases due to the additional moisture from the lime-pond ash slurry, and the total clay water content ( $w_t$ ) was determined by the following Eq. (2).

$$w_t = w_r + \left(\frac{W}{B}\right)A_w \tag{2}$$

where  $A_w$  is the amount of binder.

The prepared soil slurry was used for the determination of the degree of shrinkage, swell potential and strength. For the degree of shrinkage measurement, the soil paste was poured into the shrinkage cup and covered with cling film and stored in desiccators for 28 days. The specimens for oedometer swell potential determination were prepared by direct filling of soil–lime–pond ash paste into the acrylic rings of 76 mm diameter to a thickness of 20 mm in 30 mm thickness rings. After 24 h, the specimens along with the acrylic rings were wrapped with the cling film and placed in a desiccator for 28 days. The volume change behaviour of stabilized expansive soil was

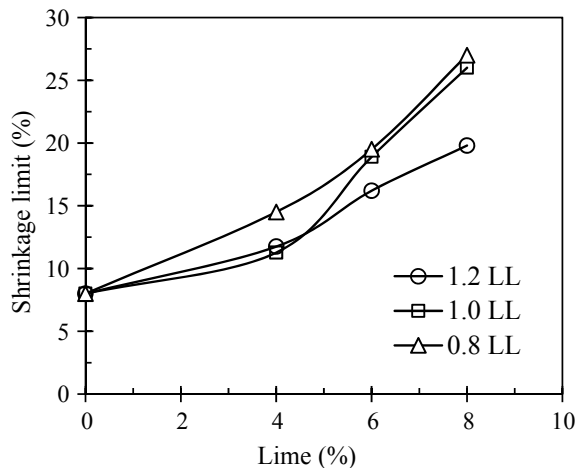
evaluated under a seating pressure of 6.25 kPa. The drying process was carried out in a hot air oven at  $45 \pm 5$  °C until the weight of the specimen remained unchanged. Due to the high workability of soil–lime-pond ash slurry paste, each soil specimen for the unconfined compression test was prepared by filling the wet soil slurry into 50 mm diameter and 120 mm height stainless steel mould. After 24 h, the specimens were ejected from the moulds and trimmed to 100 mm thickness and wrapped with a cling film. Three identical specimens were prepared and stored in a desiccator for 28 days for curing. The unconfined compression tests were carried out on 28 days cured specimens at a shearing rate of 0.625 mm/min.

### 3 Results and Discussion

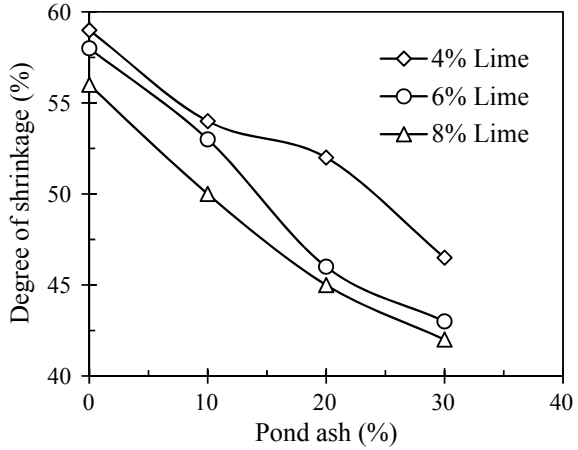
Figures 2 and 3 present the variation of shrinkage limit and degree of shrinkage with lime addition. The shrinkage limit of stabilized soil increased with increase in the lime content, but it decreased with increase in the initial total clay water content. The degree of shrinkage reduces to 56% (8% lime) from 60% (0% lime) for different lime proportions, and it further reduces to 42% for 8% lime and 30% pond ash at 1.0  $w_L$ . Also, the degree of shrinkage increases with an increase in initial moisture content for the fixed lime and pond ash percentage. The changes in the soil properties were attributed to the soil–lime reactions (pozzolanic reactions) and the changes in soil gradation due to the addition of pond ash.

Figure 4 brings out the effect of lime content and total clay water content on the unconfined compressive strength (UCS) of 28 days cured expansive soil. The UCS value increased with lime content but decreased with increase in remoulding total clay water content. The significant strength gain is mainly due to the effect of hydration and dissociation of calcium ions from the lime and reaction of calcium

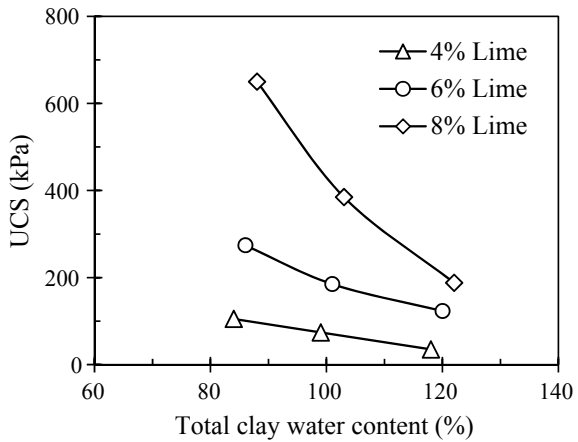
**Fig. 2** Variation in shrinkage limit with lime content at different initial water contents



**Fig. 3** Variation of degree of shrinkage with pond ash and lime contents at initial water content of 1.0  $w_L$



**Fig. 4** Variation of unconfined compressive strength with total clay water content at different lime contents



ions with the alumina and silica present in the soil to form cementitious products [2]. Figure 5 presents the stress–strain curves of lime and lime-pond ash stabilized expansive soil at 1.0  $w_L$ . With an initial addition of 4% lime and 10% pond ash, the UCS value increased, but the further increment of pond ash (20 and 30%) leads to a decrease in UCS value. The reduction in the strength might be due to the decrease in the pH value from 9.98 (4% lime) to 9.45 (4% lime + 30% pond ash) and an increased percentage of fine sand size particles in the soil due to pond ash. Because of the change in the soil–lime pH environment, it may affect the pozzolanic reactions.

To understand the volume change of stabilized soil, swell potential tests were performed at different total clay water contents. At a given initial water content, the swell potential remained zero at all lime contents of 4 to 8%. Figures 6 and 7 present the effect of wet-dry cycles on vertical deformation of soil stabilized with both lime and pond ash, respectively. There was no volume change during the first wetting

**Fig. 5** Stress–strain plots of soil stabilized with lime and pond ash at initial water content of 1.0  $w_L$

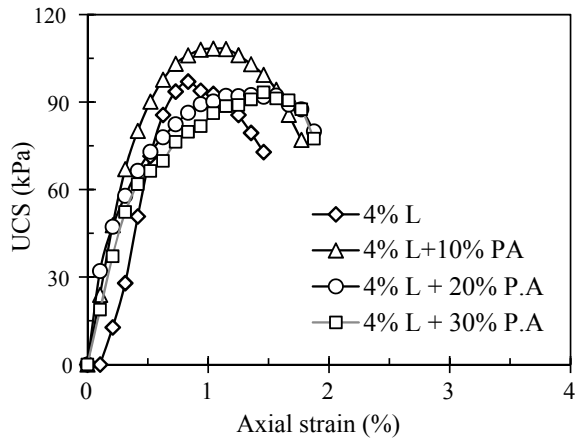


**Fig. 6** Effect of wet-dry cycles on vertical deformations of expansive soil stabilized with lime

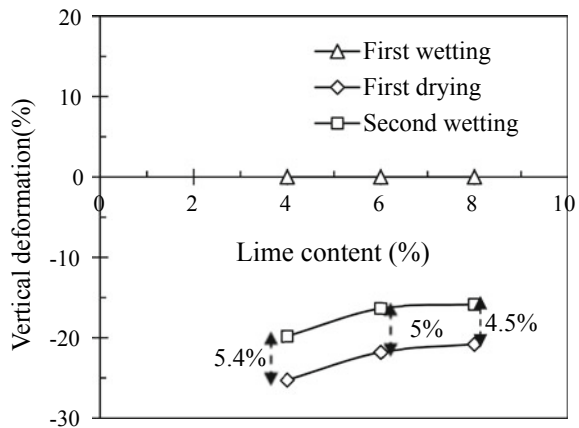
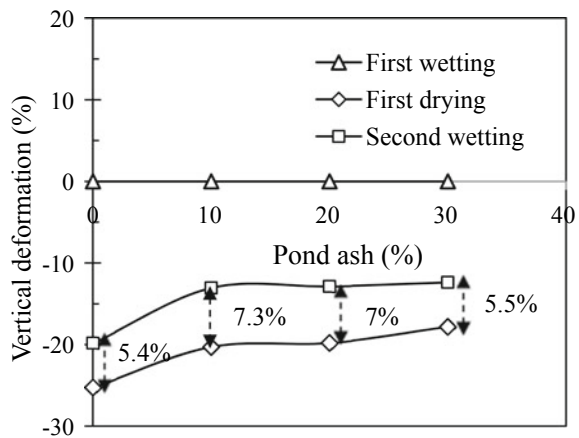


**Fig. 7** Effect of wet-dry cycles on vertical deformations of expansive soil stabilized with 4% lime and pond ash at water content of 1.0  $w_L$



cycle because of high initial water content and cementation effects. But during second wetting, the soil shows a significant vertical deformation and it decreases with increase in lime content as presented in Fig. 6. Similarly, from Fig. 7, it can be noticed that the initial addition of 10% pond ash increased the vertical deformation, and beyond 10% pond ash addition, the vertical deformation decreased, i.e. the bandwidth of 5.4% (4% lime) has increased to 7.3% for 10%, and it reduced to 5.5% for 30% pond ash addition.

## 4 Conclusions

In the current study, a laboratory trail is made to study the performance of expansive soil stabilized at higher moisture content. The following are the conclusions drawn from the series of laboratory trails.

- i. The shrinkage limit and degree of shrinkage results of stabilized soils show that the addition of lime and pond ash has improved the soil properties compared to untreated soil.
- ii. The strength of lime stabilized expansive soil improved substantially at water content of  $1.0 w_L$  and high lime contents. But, addition of pond ash beyond 10% did not show any significant strength improvement in the stabilized soil.
- iii. The swell potential upon first wetting remained zero for all the lime contents and the initial moisture content used in this study. But, the volume change occurs in the subsequent second wetting. Hence, the performance of lime stabilized expansive soils using deep soil mixing technique at high moisture contents during further wetting cycles needs further investigation.

## References

1. Bushra I, Robinson RG (2013) Effect of fly ash on cement admixture for a low plasticity marine soil. *Adv Civ Eng Mater* 2(1):608–621
2. Lorenzo GA, Bergado DT (2004) Fundamental parameters of cement-admixed clay—new approach. *J Geotech Geoenviron Eng* 130(10):1042–1050
3. Madhyannapu RS, Puppala AJ, Nazarian S, Yuan D (2010) Quality assessment and quality control of deep soil mixing construction for stabilizing expansive subsoils. *J Geotech Geoenviron Eng ASCE* 136(1):119–128
4. Moseley MP, Kirsch K (2004) *Ground improvement*. 2nd Edition, CRC Press, USA
5. Porbaha A (1998) State of the art in deep mixing technology: part I. Basic concepts and overview. *Proc Inst Civ Eng-Ground Improve* 2(2):81–92



6. Puppala AJ, Madhyannapu RS, Nazarian S, Yuan D, Hoyos L (2008) Deep soil mixing technology for mitigation of pavement roughness. Technical Report No. FHWA/TX-08/0-5179-1, Submitted to Texas Department of Transportation Research and Technology Implementation Office, The University of Texas at Arlington, Arlington, Texas
7. Terashi M (2002a) Development of deep mixing machine in Japan, Proceedings of Deep Mixing Workshop 2002 in Tokyo, Port and Airport Research Institute & Coastal Development Institute of Technology

# Sulfate Effects on Lime and Sulfate-Resistant Cement-Stabilized Expansive Soil



P. Sriram Karthick Raja  and T. Thyagaraj 

**Abstract** It is well demonstrated in the past that the lime or sulfate-resistant cement effectively controls the volume change and increases the strength of stabilized expansive soil due to both soil modification and pozzolanic reactions. Also, the rapid industrialization has increased the chances of contamination of stabilized soils with sulfate which significantly deteriorates the stabilized soil. Therefore, the effect of sodium sulfate intrusion into the lime and sulfate-resistant cement-stabilized soil on the volume change and strength behavior is brought out in this study. To achieve this objective, the expansive soil was stabilized with lime and sulfate-resistant cement and cured for 1, 7, and 28 days. Upon completion of the required curing period, the stabilized soils were contaminated with sulfate solutions of 5,000, 10,000, and 20,000 ppm for a period of 30 days before evaluating the volume change and strength properties. The current study reveals that the performance of the sulfate-resistant cement-stabilized specimens cured for long periods (28 days) was better than the lime-stabilized expansive soil in terms of the strength.

**Keywords** Sulfate · Expansive soil · Lime · Sulfate-resistant cement · Swell potential · Unconfined compressive strength

## 1 Introduction

Expansive soils occur in abundance in south India. As such these soils are very difficult to work with due to their inherent potential to swell when they are exposed to moisture. Hence, the need to stabilize this type of soils arises. In general, these soils are stabilized with the help mechanical, chemical, or structural modification of the soil [1]. Of the methods available for stabilization, the chemical stabilization is the fast, efficient, and reliable method of stabilization for ground improvement. Of the various chemical stabilizers used, lime is one of the most popular methods of

---

P. S. K. Raja (✉) · T. Thyagaraj  
Indian Institute of Technology Madras, Chennai 600036, India

© Springer Nature Singapore Pte Ltd. 2022  
A. K. Dey et al. (eds.), *Proceedings of the 7th Indian Young Geotechnical Engineers Conference*, Lecture Notes in Civil Engineering 195,  
[https://doi.org/10.1007/978-981-16-6456-4\\_14](https://doi.org/10.1007/978-981-16-6456-4_14)

stabilization for expansive soils owing to its ready availability and need for the less-skilled workforce for the stabilization projects [2–4]. Based on the literature available, the lime stabilization of the expansive soil is deemed reliable as long as the soil is not contaminated with sulfate salts. The availability of sulfate salts renders the lime-stabilized expansive soil ineffective by the formation of ettringite and thaumasite [5–7], whereas the studies on the post stabilization attack with sulfate on the lime-stabilized expansive soil are limited. Hence, this study aims at understanding the behavior of lime and sulfate-resistant cement-stabilized expansive soil attacked with external sulfate solution. The results of lime and cement-stabilized expansive soils are also compared.

## 2 Materials

Expansive soil used for the current study is obtained near the outskirts of Solagam-patti, Thiruchirapalli, Tamil Nadu, India, from a depth of 2 m below the ground surface. The expansive soil thus obtained was spread over a tarpaulin sheet for air-drying and made to pass through a 4.75 mm sieve to retain the coarse fraction, following which the processed soil was pulverized and made to pass through a 425  $\mu\text{m}$  sieve. This processed expansive soil was kept in airtight plastic bins and utilized for the current study. Based on the unified soil classification system, the expansive soil used in the current study is classified as fat clays or inorganic clay of high compressibility. Determination of initial consumption of lime (ICL) was carried out following the Eades and Grim [8] protocol, by which the ICL value was determined to be 3.5%. The cement used for the current study was Type V sulfate-resistant cement [9].

The chemicals used in the current study were laboratory grade sodium sulfate ( $\text{Na}_2\text{SO}_4$ ) and hydrated lime ( $\text{CaOH}_2$ ) with a purity of 99% and 90%, respectively. Among the sulfate salts available, sodium sulfate was selected as the contaminating solution due to its highest solubility in water (49.7 mg/100 ml) in comparison with all other sulfate salts.

## 3 Representative Expansive Soil Properties

The following properties such as physicochemical properties (pH and electrical conductivity), index properties (Atterberg limits), initial consumption of lime (ICL), grain size distribution, specific gravity ( $G_s$ ), differential free swell index (DFSI), and standard Proctor compaction characteristics were determined following the Indian standards (IS), and the experimental results are given in Table 1.

**Table 1** Basic properties of the expansive soil (after Raja and Thyagaraj [9])

Property	Value
pH	8.75
Specific gravity	2.7
Electrical conductivity (mS/cm)	2.77
<i>Atterberg limits (%)</i>	
Liquid limit	95
Plastic limit	21
Plasticity index	74
Shrinkage limit	7.5
Differential free swell index (%)	300
<i>Particle size distribution (%)</i>	
Fine sand	24.5
Fines (silt–clay fraction)	75.5
<i>Proctor compaction characteristics</i>	
Optimum moisture content (OMC) (%)	23
Maximum dry density (MDD) (kN/m <sup>3</sup> )	15.3
IS soil classification	CH

## 4 Testing Procedure

### 4.1 Unconfined Compression Tests

The soil specimens of 38 mm diameter and 76 mm height were used for unconfined compression tests. A measured quantity of 143.13 g of expansive soil, having a natural water content of 6.51%, was added with the desired quantity of stabilizer (i.e., 3.5% lime by dry weight/ 10% sulfate-resistant cement (SRC)) and water and statically compacted at the OMC to the corresponding MDD of the expansive soil. The mixtures were stored in airtight polythene bags and stored for curing in moisture-controlled desiccators. After the desired period of curing (1, 7, and 28 days), the stabilized soil specimens were carefully transferred into a sand bath of size 170 mm diameter and 300 mm in height. A single sand bath container can hold four identical specimens. The arrangement of the specimens inside the sand bath was made such that sufficient clearance was provided between specimens to deter the interaction between specimens. The procedure for the placement of the specimens is as follows. First, a thin layer of 10 mm thick fine clear sand was spread, on top of which the specimens were placed, providing a minimum clearance of 35 mm between each specimen. This was followed by filling up of the void space between the specimens with the clean fine sand. The clean sand was filled up to a height of 20 mm above the specimens. The specimens were then loaded with a surcharge of 6.25 kPa, and the sand bath was flooded with distilled water or sulfate contaminant (of 5,000, 10,000,

and 20,000 ppm). Separate containers were used for flooding with distilled water and sulfate contaminant of different concentration. This setup was left undisturbed for a period of 30 days, after which the specimens were carefully removed out and tested at a strain rate of 0.625 mm/min.

## 4.2 Oedometer Swell Tests

A measured quantity of 146.72 g of expansive soil with a natural water content of 6.51% was added with the desired quantity of stabilizer (3.5% lime or 10% sulfate-resistant cement), and then, the soil-stabilizer mix was mixed with the required quantity of water to bring the water content up to the OMC value. The soil-stabilizer mix was compacted to achieve a size of 75 mm diameter and 30 mm height in oedometer rings to the predetermined maximum density of the soil ( $1.637 \text{ Mg/m}^3$ ) in a single layer of  $20 \pm 0.5$  mm thickness. These compacted specimens were wrapped with a cling film so as to maintain the moisture content of the compacted soil specimens and are stored in desiccators for various curing periods of 1, 7, and 28 days. After the desired period of curing, the treated soil specimens were carefully transferred into oedometer test assemblies. The separate oedometer cells were filled with distilled water and sulfate solutions of desired concentration. After which, the swell measurements were monitored with time through a dial gauge assembly.

## 5 Results and Discussion

### 5.1 Unconfined Compressive Strength (UCS)

Figures 1a, 2a, and 3a highlight the effect of sulfate contamination on stress–strain plots of lime-stabilized soil specimens cured for 1, 7, and 28 days, respectively. The

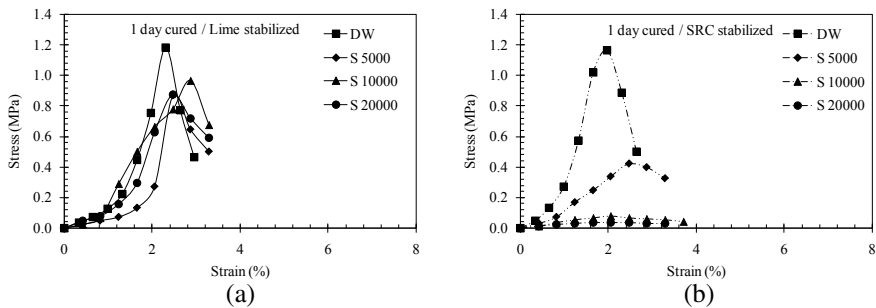


**Fig. 1** Effect of sulfate contamination on the stress–strain plots of 1 day cured: **a** lime-stabilized soil and **b** SRC stabilized soil

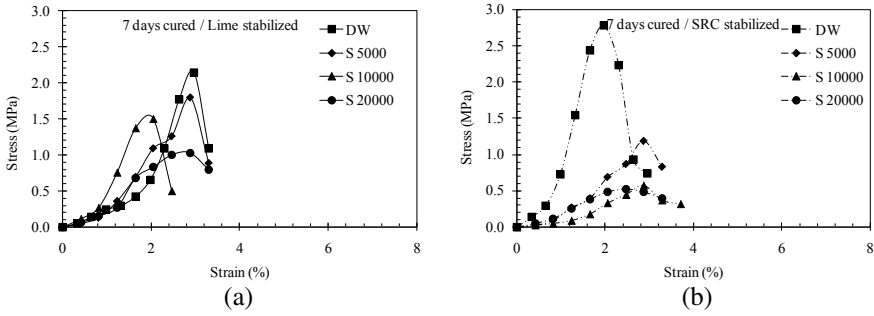


**Fig. 2** Effect of sulfate contamination on the stress–strain plots of 7 days cured: **a** lime-stabilized soil and **b** SRC stabilized soil

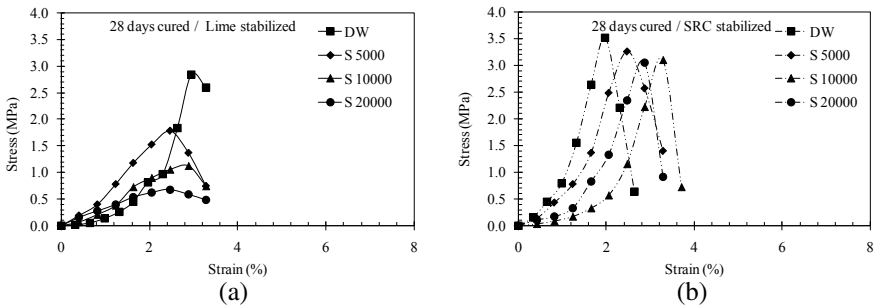


**Fig. 3** Effect of sulfate contamination on the stress–strain plots of 28 days cured: **a** lime-stabilized soil and **b** SRC stabilized soil

UCS of uncontaminated lime-stabilized specimens increased with curing period. This improvement in UCS is due to the admixed lime to the expansive soil, which increases its pH value, thus resulting in the silica (Si) and alumina (Al) ions dissolution in the clay lattice [10, 11], which aids in the development of different cementitious gels such as calcium silicate hydrate (CSH) and calcium aluminate hydrate (CAH) gels. These cementitious gels that are formed within the clay lattice cement them together. This cementation of the soil improves the strength of lime-stabilized soils [8, 11–14]. The strength of lime-stabilized specimens decreased upon sulfate contamination, and the lime-stabilized specimens cured for 7–28 days showed a significant reduction in strength. The reduction in UCS values of the lime-stabilized specimens cured for longer duration (7–28 days) is attributed to the decrease in pH upon the addition of sulfate solution, which in turn resulted in the leaching out of Ca ions from the cemented soil–lime mix.

Similarly, Figs. 1b, 2b, and 3b highlight the effect of sulfate contamination on stress–strain plots of sulfate-resistant cement-stabilized soil specimens cured for 1, 7, and 28 days, respectively. From the figures, it is clear that the strength of SRC

stabilized soil specimens increased with the curing period similar to that of the lime-stabilized specimens. However, the sulfate contamination decreased the strength of SRC stabilized specimens, and the decrease is significant for specimens cured for 1 and 7 days. The reduction in strength is negligible for specimens cured for long duration (28 days), which points that the reduction in the pH upon sulfate contamination is not significant enough to deter the cementation reactions occurring in the SRC stabilized specimens.

### 5.2 Swell Potential

Figures 4a, 5a, and 6a highlight the effect of sulfate contamination on the swell potential of lime-stabilized soil cured for 1, 7, and 28 days, respectively. The ion exchange process and the development of CSH and CAH cementation compounds in

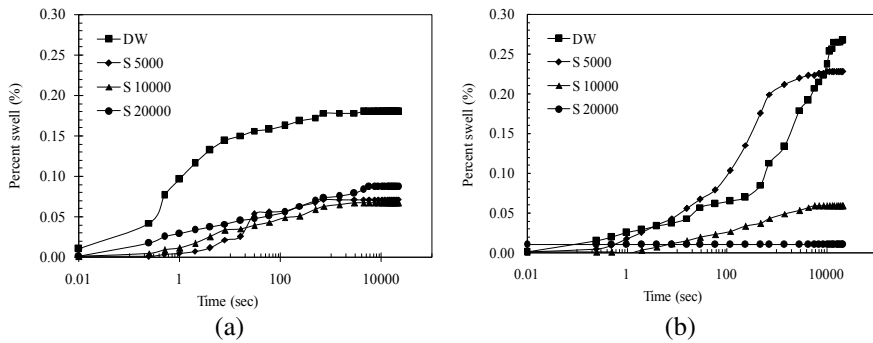


**Fig. 4** Effect of sulfate contamination on the vertical swell plots of 1 day cured: **a** lime-stabilized soil and **b** SRC stabilized soil

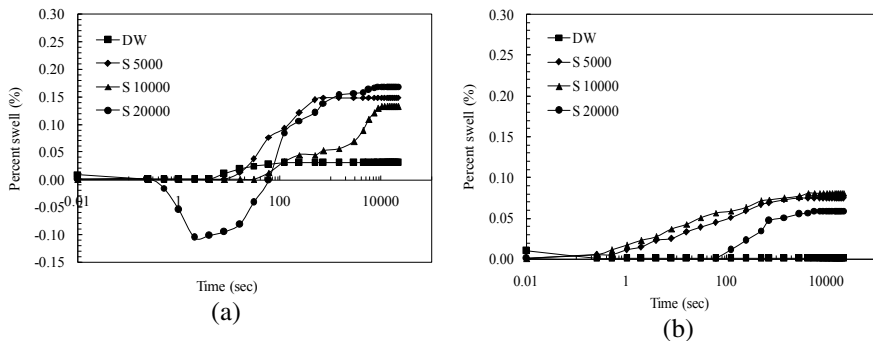


**Fig. 5** Effect of sulfate contamination on the vertical swell plots of 7 days cured: **a** lime-stabilized soil and **b** SRC stabilized soil

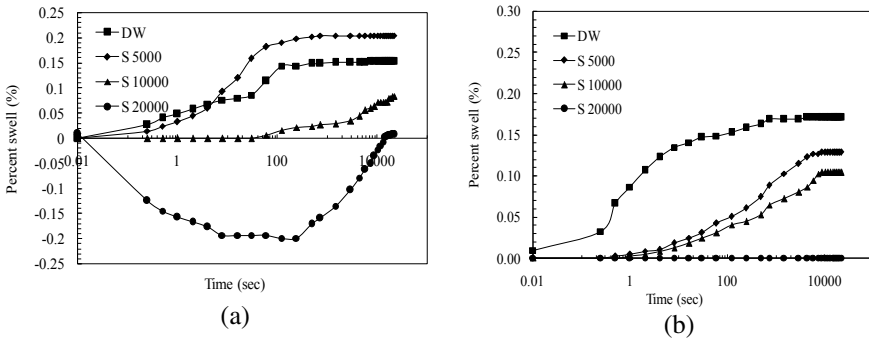


**Fig. 6** Effect of sulfate contamination on the vertical swell plots of 28 days cured: **a** lime-stabilized soil and **b** SRC stabilized soil

the 3.5% lime-stabilized soil and cured for 28 days decreased the swell potential from 33.2% to 0.15%. However, the specimens contaminated with sulfate contaminant of 20,000 ppm showed a compressive strain during the initial period, the compressive strain was leveled out after a long period of time. The initial compression of the soil may have been due to the difference in the osmotic gradient between the soil and the solution which might have been equaled out by the decrease in the matrix suction produced within the soil during the long period of curing. However, in the soils treated with SRC, there was no initial compression in the soil (Figs. 4b, 5b, and 6b). The soils cured for longer duration showed improved resistance to swelling.

## 6 Summary and Conclusions

Both the lime and SRC stabilized expansive soil exhibited improved resistance to the swelling and improved the unconfined compressive strength. The resistance to swelling and the strength increment was proportional with the curing period. Both lime and SRC stabilized expansive soil did not change their swelling characteristics even after 30 days of interaction with 20,000 ppm sodium sulfate solution, suggesting that the intrusion of the sulfate after the stabilization of the expansive soil will not have much effect on the swelling behavior of the stabilized soil cured up to 28 days. However, the decrease in strength of lime-stabilized expansive soil is considerable, suggesting that a long-term investigation is needed to completely understand the sulfate contamination and its effects on the lime and SRC stabilized expansive soil.

## References

1. Hausmann MR (1990) Engineering principles of ground modification. McGraw-Hill, New York



2. Diamond S, Kinter EB (1965) Mechanism of soil-lime stabilization. Bureau of public roads, U.S
3. Diamond S (1996) Delayed ettringite formation-processes and problems. *Cement Concrete Compos*
4. Osinubi KJ, Nwaiwu CMO (2006) Compaction delay effects on properties of lime-treated soil. *J Mater Civ Eng* 18:250–258
5. Hunter D (1988) Lime-induced heave in sulfate-bearing clay soils. *J Geotech Eng* 114(2):150–167
6. Puppala AJ, Griffin JA, Hoyos LR, Chomid S (2004) Studies on sulfate-resistant cement stabilization methods to address sulfate-induced soil heave. *J Geotech Geoenviron Eng* 130:391–402
7. Mccarthy M, Csetenyi LJ, Sachdeva A, Dhir RK (2012) Identifying the role of fly ash properties for minimizing sulfate-heave in lime-stabilized soils. *Fuel* 92(1):27–36
8. Eades JL, Grim RE (1996) A quick test to determine lime requirements for lime stabilization. highway research board. National Research Council, Washington DC 139, 61–72
9. Raja PSK, Thyagaraj T (2019) Effect of sulfate contamination on compaction and strength behavior of lime treated expansive soil. In: McCartney, John S, Hoyos LR (eds) Recent advancements on expansive soils. Proceedings of the 2nd GeoMEast international congress and exhibition on sustainable civil infrastructures 2018. Springer, Switzerland, . pp. 15–28
10. Boardman DI, Glendinning S, Rogers CDF (2001) Development of stabilisation and solidification in lime-clay mixes. *Geotechnique* 50(6):533–543
11. Barker JE, Rogers CD, Boardman DI (2006) Physio-chemical changes in clay caused by ion migration from lime piles. *J Mater Civil Eng* 18(2):182–189
12. Rajasekaran G, Narasimha Rao S (1990) Lime stabilization technique for the improvement of marine clay. *Soils Foundations, Japan* 37:97–104
13. Thyagaraj T, Zondinsanga S (2014) Swell-shrink behavior of lime precipitation treated soil. *Ground Improvement* 167(14):260–273
14. Diamond S, White JL, Dolch WL (1963) Transformation of clay minerals by calcium hydroxide attack. Joint Highway Research Project, Purdue University, Lafayette, Indiana31

# Cementation of Sand by Microbial Induced Calcite Precipitation



Vineeth Reddy Karnati, M. Sudhakar, Kalyan Kumar Gonavaram,  
and Amitava Bandhu

**Abstract** For any construction purpose, a strong and durable foundation is very much essential which requires a suitable sub soil condition. But the availability of competent soil conditions is not always possible. In such situations it needs to be stabilized in order to improve its properties. This study aims to analyze the effect of an innovative ground improvement technique by the use of Microbial Induced Calcite Precipitation (MICP) for improving the strength of a poorly graded sand. In this study, an attempt is made to study the effect of two different densities on the strength increase in the sand specimen. MICP is achieved through urea hydrolysis by the use of common soil bacterium *Sporosarcina Pasteurii*. The microbes were introduced into the specimens in liquid growth medium and urea +  $\text{CaCl}_2$  (cementitious solution) was injected later on. The optical density was studied during the injection. The injection of bacterial solutions and the cementitious solutions was carried out based on the standard procedure developed in various literature. The strength increase was found using the unconfined compressive testing and the precipitated minerals were identified using the X-ray diffraction analysis which confirms the formation of calcite crystals among the sand particles. The permeability of soil also is reduced by one order of magnitude.

**Keywords** MICP · Urea hydrolysis · Optical density · UCS and permeability

## 1 Introduction

The current development in the infrastructure demands satisfactory soil requirements to meet the ever-growing societal needs. But the adequate soil conditions are

---

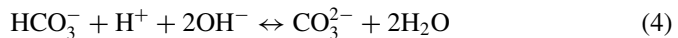
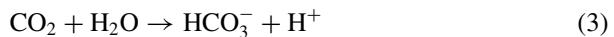
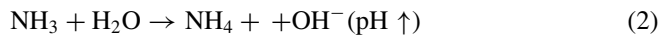
V. R. Karnati  
Anurag Group of Institutions, Hyderabad, Telangana 500038, India

M. Sudhakar · K. K. Gonavaram (✉) · A. Bandhu  
NIT Warangal, Warangal, Telangana 506004, India  
e-mail: [kalyan@nitw.ac.in](mailto:kalyan@nitw.ac.in)

© Springer Nature Singapore Pte Ltd. 2022  
A. K. Dey et al. (eds.), *Proceedings of the 7th Indian Young Geotechnical Engineers Conference*, Lecture Notes in Civil Engineering 195,  
[https://doi.org/10.1007/978-981-16-6456-4\\_15](https://doi.org/10.1007/978-981-16-6456-4_15)

127

not always easily available. In such a scenario, the available local soils with inadequate properties need to be modified using some improvement techniques. The modification of soil properties can be done conventionally by means of mechanical densification or by using grouting [17]. The traditional grout materials are mostly found to be costly and environmentally toxic. Hence, to avoid the environmental damages, a new and ingenious method of using Microbial Induced Calcite Precipitation (MICP) for soil stabilization is now being explored for its potential applications. By applying a biological process, it holds significant prospects in altering soil behavior besides reducing potential damage to the environment [22]. The existing research on the bioremediation of the contaminated ground needs to be focused at the interface between geo-mechanics and microbiology to develop intense ground improvement strategies and also to exploit the potential of microorganisms in bio-influenced foundation strategies [21]. Currently, rigorous research is being carried out to simulate biochemical processes aimed at modifying the soil properties on demand [6, 8, 16]. MICP process can be achieved through many means like urea hydrolysis, iron reduction, sulfate reduction, etc., among which urea hydrolysis is being followed by many researchers because of its fast reactions and high efficiency [18]. Hydrolysis of urea is a slow reaction in general which can be catalyzed in the presence of urease enzyme [1]. Introduction of urease enzyme into the soil medium becomes a costly and difficult process. Hence, this process is achieved through the introduction of urease positive soil microorganisms. MICP through urea hydrolysis involves the injection of bacterial cell solution and the cementitious solutions ( $\text{CaCl}_2 + \text{Urea}$ ). In the presence of urease enzyme secreted by the microorganism, urea ( $\text{CO}(\text{NH}_2)_2$ ) gets hydrolyzed into ammonium and carbonate ions increasing the pH of the whole medium. These carbonate ions will form calcite ( $\text{CaCO}_3$ ) crystals in the presence of supplied calcium source (in the form of  $\text{CaCl}_2$ ). This was explained with the following series of reactions:



Soil strengthening research by using biological processes has largely restricted to laboratory scale studies on the sand and further research is being carried out to evaluate the full potential of this technique. MICP was proven to be effective in soil improvement applications such as embankments, liquefiable soil deposits, and reinforcement in subgrade. Sand specimens treated using MICP reported reduction in

volumetric compression [5] increase in shear strength of soil [3, 4, 10] and improvement in soil stiffness [7, 19, 20]. To carry out field applications, it is necessary to understand the potential of this method thoroughly. In the current study, a common soil microorganism, *Sporosarcina pasteurii*, was used to stabilize the poorly graded sand available near the surroundings of NIT Warangal. The primary objective of this study is to investigate the effect of MICP on the engineering properties of the sand. A standard procedure was verified through various literature and adopted for bacterial cultivation and injection of these cells into the specimens.

## 2 Materials

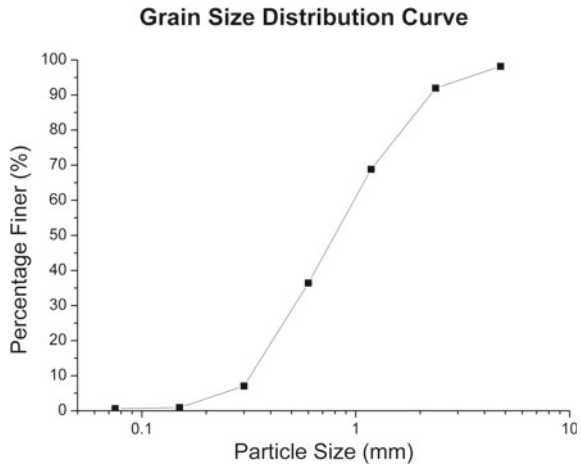
### 2.1 Sand

The sand used in the study was collected from the nearby site at NIT Warangal. The index properties of sand were found as per IS: 2720 [11, 12, 14] and presented in Table 1. The grain size distribution curve is presented in Fig. 1. The sand used in the study is classified as poorly graded sand (SP) as per IS soil classification.

**Table 1** Properties of sand used

Soil	Specific gravity	$C_u$	$C_c$	Soil type	$e_{min}$	$e_{max}$
Sand	2.65	3.06	0.83	SP	0.36	0.88

**Fig. 1** Grain size distribution curve



## **2.2 Bacterial Cells**

Freeze-dried vials of *Sporosarcina pasteurii* bacterium were procured from Microbial Type Culture Collection (MTCC) with catalogue number 1761. This bacterium is aerobic, urease positive common soil bacterium with biosafety level 1 ranking as per Centre for Disease Control and Prevention (CDC), USA and is suitable for laboratory use. These cells were rehydrated to liquid and solid nutrient mediums for future use.

## **3 Methodology**

### **3.1 Bacterial Cell Solution**

A seed culture was prepared from the stocks prepared and was inoculated to the main culture at a rate of 1 ml seeding for a 100 ml solution. This was incubated at 37 °C for about 32 h and then the cells were subjected to centrifugation at 4 °C to wash them with 0.1 M sodium phosphate solution in order to remove the metabolic waste. The bacterial cell solution comprising of  $\text{NH}_4\text{Cl}$  (10 g/l),  $\text{NaHCO}_3$  (2.12 g/l), Nutrient Broth (NB) (25 g/l), and Urea (20 g/l) was prepared and autoclaved. The cleaned cells were then transferred to bacterial cell solution and incubated for two hours. The optical density of the medium was found to be 0.87 before the injection of the specimen which indicates that *Sporosarcina Pasteurii* bacterium was sufficiently large in number.

### **3.2 Cementitious Solution**

The strength increase depends on the uniform distribution of calcite formed through the urea hydrolysis at the particle to particle interface. According to Inagaki et al. [9], the amount of calcite precipitation was largest when the concentration of Urea and Calcium Chloride ( $\text{CaCl}_2$ ) was 0.5 M. Hence, a cementitious solution concentration of 0.5 M was adopted for the study and standard stoichiometric calculations were made to calculate the weight of urea and  $\text{CaCl}_2$  required to be dissolved in distilled water.

### **3.3 Sample Preparation and Solution Injection**

PVC molds of size 55 mm diameter and D/L ratio 1:2 were cut to form split molds and joined to form a cylindrical shape as shown in Fig. 2. Scotch Brite of 10 mm thickness was used at the top and bottom to act as a porous plug for facilitating aeration and



**Fig. 2** Specimen preparation and injection of solutions

drainage. Now the sand was air pluviated to obtain the relative densities of 35% and 85%. The multi-stage injection process was adopted for the study as suggested by Harkes et al. [8]. One pore volume of bacterial cell solution was injected into the specimens at a very slow rate of about 10 ml/min and was allowed to drain after one day by the time which the bacterial cells would have been adsorbed to the soil grains. Then the cementitious solution was injected in pore volumes at the same rate with a duration of 12 h for two days. Then the sample was allowed for a curing period of 14 days.

### **3.4 Laboratory Tests**

The samples were drained and unconfined compression testing (UCS) was carried out according to IS: 2720—part 10 [13] as shown in Fig. 3 to verify the bio-stabilization. The permeability of the sand before and after stabilization was found using constant head permeability test according to IS: 2720—part 17 [15]. X-ray diffraction tests were carried out on the sand before and after treatment in order to ensure the formation of calcite mineral.

## **4 Results and Discussion**

The results of UCS tests and the permeability tests were presented in Table 2. Three samples of size 55 mm diameter and 110 mm long were tested for UCS and the average of values is presented. These values were comparable with those obtained from Cheng et al. [2]. The stress–strain graph was presented in Fig. 4. Incidentally,



**Fig. 3** Unconfined compression testing

**Table 2** UCS and permeability values of treated and untreated sand

Material	Relative density (%)	UCS (kPa)	Permeability (m/sec)
Untreated sand	35	–	$7.20 * 10^{-5}$
	85	–	$3.09 * 10^{-5}$
Treated sand	35	379	$6.83 * 10^{-6}$
	85	266	$8.61 * 10^{-6}$

a reduction of one order magnitude in permeability was observed in the treated samples. Similar reductions in permeability have been reported in various MICP studies conducted on the sand [23–25]. The result of XRD analysis was presented in Fig. 5. XRD analysis confirms the formation of calcite mineral which is responsible for the strength gain and reduction in permeability to clog the voids.

## 5 Conclusions

This paper shows the influence of multi-staged injection on the cementation of the sand particles with different degrees of packing. Microbial treatment has produced a significant average unconfined compressive strength of poorly graded sand which can be attributed to the formation of calcite through MICP. Permeability values were found to be reduced by about 75%. MICP through urea hydrolysis seems to

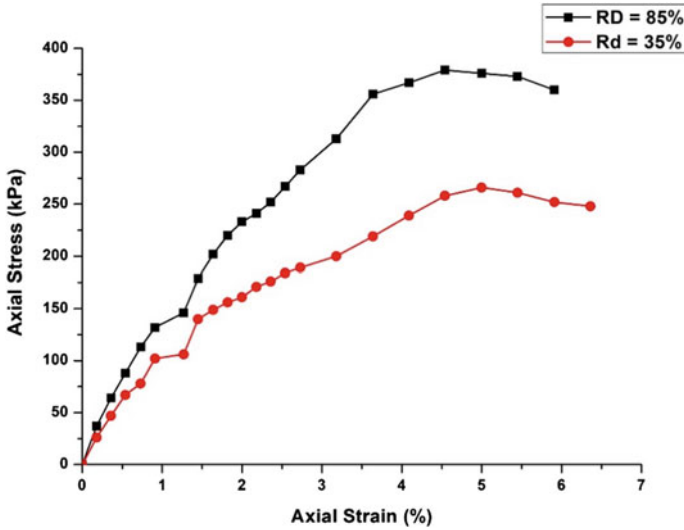


Fig. 4 Stress–strain response of treated sand

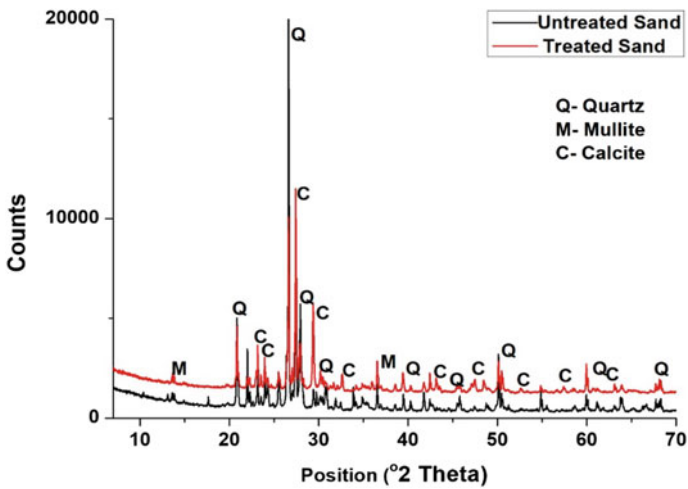


Fig. 5 XRD image of treated and untreated sand

be a promising and environmental friendly ground improvement technique. More research in terms of its uniformity of calcite precipitation is necessary for developing full-scale applications.



## References

1. Bachmeier KL, Williams AE, Warmington JR, Bang SS (2001) Urease activity in microbiologically-induced calcite precipitation. *J Biotechnol* 93:171–181
2. Cheng L, Cord-Ruwisch R, Shahin MA (2013) Cementation of sand soil by microbially induced calcite precipitation at various degrees of saturation. *Can Geotech J* 50(1):81–90
3. Chou CW, Seagren EA, Aydilek AH, Lai M (2011) Biocalcification of sand through ureolysis. *J Geotech Geoenviron Eng (ASCE)* GT 0000532:1179–1189
4. DeJong J, Fritzges M, Nüsslein K (2006) Microbially induced cementation to control sand response to undrained shear. *J Geotech Geoenviron Eng (ASCE)* 132(11):1381–1392
5. DeJong JT, Mortensen MB, Martinez BC, Nelson DC (2010) Bio-mediated soil improvement. *Ecol Eng* 36(2):197–210
6. DeJong JD et al (2013) Biogeochemical processes and geotechnical applications: progress, opportunities and challenges. *Geotechnique* 63(4):287–301
7. Feng K, Montoya BM (2015) Influence of confinement and cementation level on the behavior of microbial-induced calcite precipitated sands under monotonic drained loading. *J Geotech Geoenviron Eng* 142(1):04015057
8. Harkes MP, Van Paassen LA, Booster JL, Whiffin VS, Van Loosdrecht MC (2010) Fixation and distribution of bacterial activity in sand to induce carbonate precipitation for ground reinforcement. *Ecol Eng* 36(2):112–117
9. Inagaki Y, Tsukamoto M, Mori H, Sasaki T, Soga K, Qabany AA, Hata T (2011) The influence of injection conditions and soil types on soil improvement by microbial functions. In: *Geo-Frontiers 2011: Advances in Geotechnical Engineering*, pp 4021–4030
10. Ismail MA, Joer HA, Sim WH, Randolph MF (2002) Effect of cement type on shear behavior of cemented calcareous soil. *J Geotech Geoenviron Eng* 128(6)
11. IS 2720: Methods of Test for Soils: Part 3 determination of specific gravity/section 1 fine grained soils. Bureau of Indian Standards (1980)
12. IS 2720: Methods of test for soils: Part 4 grain size analysis. Bureau of Indian Standards (1985)
13. IS: 2720: Methods of test for soils: part 10 determination of unconfined compressive strength. Bureau of Indian Standards (1991)
14. IS 2720: Methods of test for soils: part 14 determination of density index (Relative density) of cohesionless soils. Bureau of Indian Standards (1983)
15. IS 2720: Methods of test for soils: part 17 laboratory determination of permeability. Bureau of Indian Standards (1985)
16. Ivanov V, Chu J (2008) Application of microorganisms to geotechnical engineering for bioclogging and biocementation of soil in situ. *Rev Environ Sci Biotechnol* 7:139–153
17. Karol RH, Berardinelli C (2003) Chemical grouting and soil stabilization. Revised and expanded. Vol. 12, Crc Press
18. Khodadadi, Tirkolaei H, Bilsel H (2015) Statistical modeling of environmental factors on microbial urea hydrolysis process for biocement production. *Adv Mater Sci Eng*
19. Lin H, Suleiman MT, Brown DG, Kavazanjian E (2016) Mechanical behavior of sands treated by microbially induced carbonate precipitation. *J Geotech Geoenviron Eng* 142(2):04015066
20. Montoya BM, DeJong JT (2015) Stress-strain behavior of sands cemented by microbially induced calcite precipitation. *J Geotech Geoenviron Eng* 141(6):04015019
21. Mitchell JK, Hon M, ASCE Santamarina JC (2005) M.ASCE: biological considerations in geotechnical engineering. *J Geotech Geoenviron Eng* 131(19):1222–1233
22. NRC.: Geological and geotechnical engineering in the new millennium: Opportunities for research and technological innovation, national research council, National Academies Press, Washington, DC(2006)
23. Soon WW, Hariharan M, Snyder MP (2013) High-throughput sequencing for biology and medicine. *Molecular Syst Biol* 9:640. Pmid: 2330846
24. Whiffin VS, Van Paassen LA, Harkes MP (2007) Microbial carbonate precipitation as a soil improvement technique. *Geomicrobiol J* 25:417–423

25. Yasuhara H, Hayashi K, Okamura M (2011) Evolution in mechanical and hydraulic properties of calcite-cemented sand mediated by biocatalyst. In: *Geo-Frontiers 2011: Adv Geotech Eng*, 3984–3992

# Strength and Deformation Aspects of Glass Fibre-Reinforced Clayey Soil



Suchit Kumar Patel  and Baleshwar Singh

**Abstract** Effect of glass fibre inclusion on the shear strength and deformation mode of clayey soil has been investigated in this study by conducting consolidated undrained triaxial test under varying confining pressure. Three different lengths of glass fibres (10, 20 and 30 mm) with 0.25% fibre content were used as reinforcement. Inclusion of glass fibre enhances the shear strength parameters and changes the specimen deformation mode which is also highly influenced by the confining pressure. 20 mm long fibres are found to provide optimum benefit in shear strength development. The positive pore pressure tends to develop more with longer fibre and under higher confining pressure. Inclusion of fibres progressively spreads the local bulging of unreinforced specimen to the entire specimen length. The bulging of specimen is reduced with longer fibre and higher confining pressure. The reinforced specimen seems to stand like an intact column at 400 kPa confining pressure with least bulging.

**Keywords** Glass fibre · Fibre length · Shear strength · Deformation mode

## 1 Introduction

A wide range of reinforcements in different form is in use to improve soil engineering behaviour across the globe. Conventionally, reinforcement has been provided as tension materials in the form of strip, sheet, bars, grid, etc., oriented in preferred direction. Fibre-reinforced soil is relatively newly developed soil improvement methods which are gaining popularity from the last 30–35 years. Randomly, distributed fibres maintain strength isotropy within soil by restricting the development of any potential weak plane. The fibre-reinforced soil can be used efficiently in different structures

---

S. K. Patel (✉)

Central University of Jharkhand, Ranchi, Jharkhand 835205, India

e-mail: [p.suchit@iitg.ac.in](mailto:p.suchit@iitg.ac.in)

B. Singh

Indian Institute of Technology Guwahati, Guwahati, Assam 781039, India

© Springer Nature Singapore Pte Ltd. 2022

A. K. Dey et al. (eds.), *Proceedings of the 7th Indian Young Geotechnical Engineers*

*Conference*, Lecture Notes in Civil Engineering 195,

[https://doi.org/10.1007/978-981-16-6456-4\\_16](https://doi.org/10.1007/978-981-16-6456-4_16)

including road pavements, soil retaining structures, clay liner and cover system [1–4]. Initial investigation of fibre-reinforced soil was mostly with sandy soils. Latter, fibre reinforcement effect on the performance of clayey soil is studied by unconfined compression tests [5–7], CBR test [8, 9] and triaxial tests [10–12]. Past studies tell that the mixing of fibres enhances the deviator stress-axial strain response, compressive strength, unconfined compression strength, extensibility and soil ductility by reducing the strength drop after peak. The contribution of fibres in strength improvement of soil is noted to be dependent on the percentage of mixed fibres, fibre aspect ratio and surficial interaction of soil and fibre. Maher and Gray [13] found that the benefit of fibre to the sand strength increases with increase in coefficient of uniformity and decrease of average particle size and particle sphericity.

In past investigation, the influence of fibre addition on clayey soil has mostly been focussed on the shear strength of soil. The effects of fibres mixing on the deformation aspects of clayey soil are not examined properly, and it needs further investigation. Therefore, in this paper, the influence of glass fibre on the shear strength along with deformation performance of clayey soil under varying confining pressure has been investigated. Glass fibres have been used as reinforcement as it has some added advantage over other fibres. It is more resistant to ageing, heat and aggressive chemical environment and has very good tensile strength.

## 2 Materials and Method

Locally, available clayey soil was collected from nearby hill slopes of IIT Guwahati campus of Northeastern India. The liquid limit and plastic limit of soil are as 46% and 24%, respectively, and the soil is found as low plastic clay (CL). The specific gravity, optimum moisture content (OMC) and maximum dry unit weight (MDU) are 2.63, 19.4% and 16.8 kN/m<sup>3</sup>, respectively. Glass fibres of 10, 20 and 30 mm lengths, 0.15 mm diameter and 2.57 specific gravity are being used as reinforcement. The tensile strength, elastic modulus and fracture strain of glass fibre are 1.53 GN/m<sup>2</sup>, 112.3 GN/m<sup>2</sup> and 1.8%, respectively.

Triaxial tests under undrained condition were performed to study the influence of fibre length under different confinement ( $\sigma_3 = 100, 200$  and 400 kPa) on the shear strength and deformation response. Glass fibre of 0.25% content was mixed in the soil, and specimens (38 mm  $\times$  76 mm) were compacted at OMC and MDU of parent soil. Back pressure methods were used to saturate the specimen maintaining 20 kPa positive head till Skempton pore pressure parameter B reaches at least 0.95. The specimens were consolidated under effective confinement of 100, 200 and 400 kPa prior to shearing. Static triaxial tests under undrained condition were performed according to ASTM D4767 [14] by maintaining a strain rate of 0.158% per minute.

### 3 Results and Discussion

The results have been analyzed and discussed under (1) deviator stress-axial strain and pore pressure variation, (2) shear strength parameters and (3) deformation mode. The criteria used to define failure of the test specimen is the maximum Deviatoric stress, which is taken as either the peak stress observed within 10% strain or deviator stress at 10% axial strain, if no prominent peak is noticed up to 10% axial strain.

#### 3.1 Stress–Strain and Pore Pressure Variation

**Effect of fibre length:** Figure 1a, b present the outcome of fibre length variation on deviator stress ( $\sigma_1 - \sigma_3$ )-axial strain and pore pressure-axial strain development during triaxial shearing, respectively, at 100 kPa confinement. The resistance against external loading of parent soil specimen is noted to increase significantly with longer fibres, and 20 mm long fibre contributes maximum in strength improvement. The deviator stress with 30 mm fibre decreases, however, it remains higher than that of 10 mm fibre reinforcement. For both unreinforced and reinforced specimens, no clear peak appears even up to 20% axial strain. Similar stress-strain response has been found for specimens sheared under other confining pressure. Ahmad et al. [15] found similar behavior where there was non-linear increase of shear strength with fibre length, and the increment was only up to 30 mm fibres, and then reduced with fibres of 45 mm length in the specimens of 50 mm diameter. From the pore pressure response, it has been noted that all specimens are showing positive pore pressure

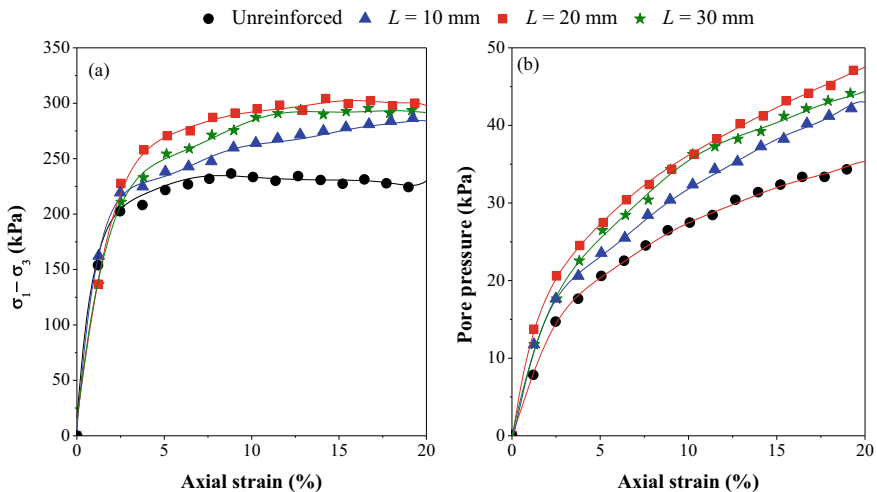


**Fig. 1** Outcomes of fibre length variation under 100 kPa confinement on **a** deviator stress variation; **b** pore pressure variation

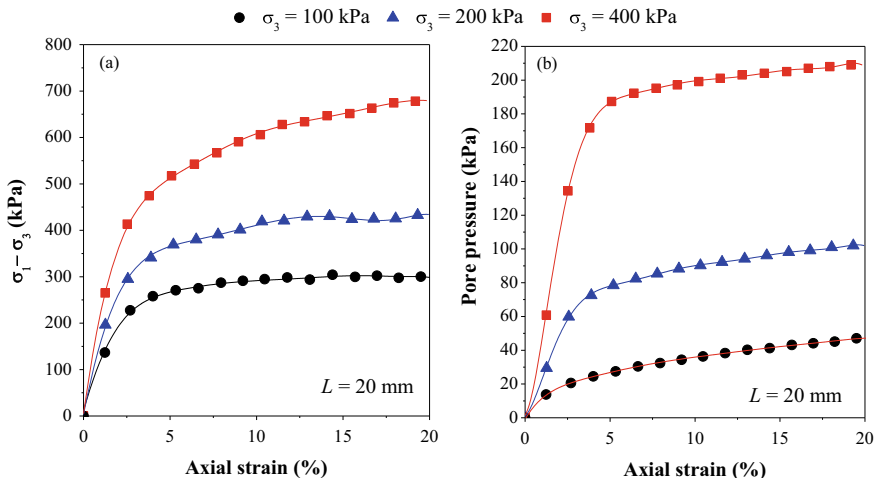


**Fig. 2** Effect of confining pressure for 20 mm fibre-reinforced specimen: **a** deviator stress variation; **b** pore pressure variation

which developed continuously with increasing axial strain and also noted to develop more with glass fibre reinforcement, signifying additional contractive behaviour of the soil with glass fibre reinforcement.

**Effect of confining pressure** Fig. 2a, b show the typical response of confining pressure variation on deviator stress-axial strain and pore pressure-axial strain behaviour, respectively, for the specimens mixed with 20 mm fibre. At higher confinement, the deviator stress and developed positive pore pressure increase (Fig. 2a, b). With increasing confinement, the area of interfacial contact amongst soil grains and individual fibre increases. The increased interaction area increases the degree of the interfacial friction and adhesion [16]. Racana et al. [17] noted an increase in friction between soil and geotextile strip when normal stress increases whilst conducting a pullout tests of geotextile strips in soil. Similarly, at higher confinement, the surface friction amongst the clayey particles and glass fibres is enhanced, causing more improvement in the specimen strength (Fig. 2a). The improved interfacial bonding and associated friction amongst clay particles and the fibres increases the contraction behaviour of the specimen, which results in the development of higher positive pore pressure at higher confinement (Fig. 2b).

### 3.2 Shear Strength Parameters

Stress path in  $p-q$  plot ( $p = (\sigma_1 + \sigma_3)/2$  and  $q = (\sigma_1 - \sigma_3)/2$ ) was drawn to evaluate the parameters of shear strength. The component shear strength calculated along with fibre contribution has been shown in Table 1. Fibre contribution is the additional value

**Table 1** Shear strength parameters value

Fibre length	Cohesion intercept, $c$ (kPa)	Friction angle, $\varphi$ ( $^{\circ}$ )
Unreinforced	45	25.8
10 mm	52	27.1
Fibre contribution	7	1.3
20 mm	56	30.4
Fibre contribution	11	4.6
30 mm	51	28.8
Fibre contribution	6	3

of shear strength parameters due to glass fibre inclusion above the value of parent soil. The value of shear strength parameters is found to increase with glass fibre inclusion and noted to be maximum with 20 mm long fibre. The cohesion intercept and friction angle value increase by 11 kPa and  $4.6^{\circ}$ , respectively, to reach a highest magnitude of 56 kPa and  $30.4^{\circ}$  with 20 mm fibre (Table 1).

### 3.3 Deformation Mode

**Effect of fibre length:** The deformation modes of the specimens of Fig. 1 are shown in Fig. 3 showing the effect of fibre length. There is bulging in only the upper half part of the unreinforced specimen (Fig. 3a). With inclusion of 10 mm fibres, the bulging spreads in the larger part of the specimen along its length (Fig. 3b) indicating that fibres cause uniform distribution of stress all along the specimen length. As the specimen is reinforced with 20 mm and 30 mm fibres (Figs. 3c and 3d), the bulging of the specimen is progressively restricted. With increasing fibre length, the frictional resistance and bond strength between soil grain and individual

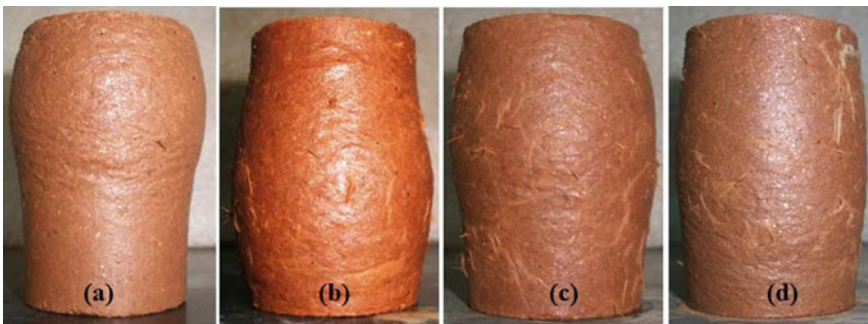


**Fig. 3** Variation in deformation mode with varying fibre length at 100 kPa confining pressure: **a** unreinforced; **b**  $L = 10$  mm; **c**  $L = 20$  mm; **d**  $L = 30$  mm

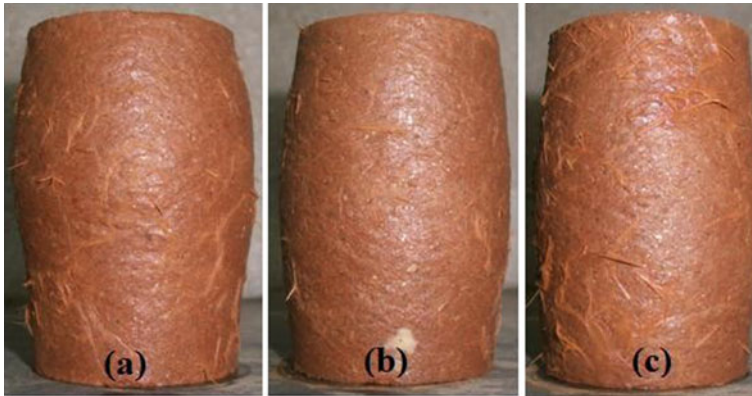


**Fig. 4** Variation in deformation mode with varying confining pressure: **a**  $\sigma_3 = 100$  kPa; **b**  $\sigma_3 = 200$  kPa; **c**  $\sigma_3 = 400$  kPa

fibres increase, restricting the lateral spreading of soil particles. Also, the increased bond strength controls the sliding of fibres through higher interlocking of the soil particles, limiting the specimen bulging.

**Effect of confining pressure:** The deformation patterns of the specimens of Fig. 2 are depicted in Fig. 4, presenting the effect of confining pressure. The increasing pore pressure or more contractive behaviour due to increased confinement as found in Fig. 2b can also be noted in the deformation patterns of the specimens (Fig. 4). There is bulging along the length of specimens under any confining pressure. Nevertheless, as confining pressure increases, the bulging of specimen reduces gradually. The bulging at 400 kPa confining pressure (Fig. 4c) is clearly smaller compared to that at 100 kPa (Fig. 4a), and the soil sample is noted to appear like an intact column at 400 kPa.

## 4 Conclusions

From the results of triaxial tests on clayey soil with glass fibre inclusion under undrained condition, it has been noted that the glass fibre significantly improves the shear strength of clayey soil. 20 mm long fibres provide the maximum contribution in shear strength enhancement. Inclusion of fibres causes uniform distribution of stresses within the specimen length. Glass fibres increase the positive pore water pressure development, indicating more contractive behaviour of specimens which further enhances with increasing confining pressure. Inclusion of glass fibres restricts the bulging of soil, and the bulging noted to be further hampered with increase of fibre length and confining pressure. Glass fibre can be a good alternative for soil reinforcement for its application as subgrade material, behind retaining wall and within shallow foundation.



## References

1. Rifai SM (2000) Impact of polypropylene fibers on desiccation cracking and hydraulic conductivity of compacted clay liners. Ph.D. thesis, Wayne State University, Detroit, United States
2. Santoni RL, Webster SL (2001) Airfields and roads construction using fibre stabilization of sands. *J Transp Eng* 127(2):96–104
3. Park T, Tan SA (2005) Enhanced performance of reinforced soil walls by the inclusion of short fibre. *Getetiles Geomembranes* 23(4):348–361
4. Rafalko SD, Brandon TL, Filz GM, Mitchell JK (2006) Fibre reinforcement for rapid stabilization of soft clay soils. Technical Report AFRL-RX-TY-TP-2009–4603, Department of Civil and Environmental Engineering Virginia Polytechnic Institute and State University Blacksburg, VA 24060–0105
5. Freitag DR (1986) Soil randomly reinforced with fibres. *J Geotech Eng* 112(8):823–826
6. Nataraj MS, McMain KL (1997) Strength and deformation properties of soils reinforced with fibrillated fibres. *Geosynthetic Int* 4(1):65–79
7. Patel SK, Singh B (2017) Strength and deformation behavior of fiber-reinforced cohesive soil under varying moisture and compaction states. *Geotech Geol Eng* 35(4):1767–1781
8. Hazirbaba K, Gullu H (2010) California Bearing Ratio improvement and freeze-thaw performance of fine-grained soils treated with geofibre and synthetic fluid. *Cold Reg Sci Technol* 63(1):50–60
9. Patel SK, Sing HB (2017) Experimental investigation on the behaviour of glass fibre—reinforced cohesive soil for application as pavement subgrade material. *Int J Geosynthetics Ground Eng* 3(2):1–12
10. Ozkul ZH, Baykal G (2006) Shear strength of clay with rubber fibre inclusions. *Geosynth Int* 13(5):173–180
11. Prabakar J, Sridhar RS (2002) Effect of random inclusion of sisal fibre on strength behaviour of soil. *Constr Build Mater* 16(2):123–131
12. Patel SK, Singh B (2019) Shear strength and deformation behaviour of glass fibre-reinforced cohesive soil with varying dry unit weight. *Indian Geotech J* 49(3):241–254
13. Maher MH, Gray DH (1990) Static response of sand reinforced with randomly distributed fibers. *J Geotech Eng* 116(11):1661–1677
14. ASTM D4767: Standard test method for consolidated undrained triaxial compression test for cohesive soils. ASTM International, West Conshohocken, PA, USA (2011)
15. Ahmad F, Bateni F, Azmi M (2010) Performance evaluation of silty sand reinforced with fibres. *Geotext Geomembr* 28(1):93–99
16. Dove JE, Frost JD (1999) Peak friction behavior of smooth geomembrane-particle interface. *J Geotech Geoenviron Eng* 129(7):544–555
17. Racana N, Grédiac M, Gourvès R (2003) Pull-out response of corrugated geotextile strips. *Geotext Geomembr* 21(5):265–288

# Behavior of Geosynthetic Encased Stone Column



Mrinal Bhaumik , Suresh Prasad Singh , and Preetynanda Nanda 

**Abstract** The satisfactory advantages of the stone column have enhanced the popularity as a ground improvement technique, particularly for soft soil. This technique is best suited for structures that can tolerate some amount of settlement. The effectiveness of the granular column becomes limited because of low confinement of the surrounding soil. Here, the significant improvement of load-carrying capacity due to partial encapsulation of normal stone column has been investigated. In this study, the effects of vertical circumferential encasement have been analyzed using finite element package Plaxis. To simulate with the field condition, stone column unit cell model of diameter 1 m has been constructed in the clay layer of 15 m thick. The load-carrying capacity of a floating stone column was found to be increased significantly up to a length of four times the diameter and beyond this length; no remarkable increment of bearing capacity has been observed due to lateral bulging. If bulging is restrained by circumferential encasement, the load-carrying capacity continues to increase with the length. From the study, it was found that the full encasement is not economical and the encasement at the top 25–30% of the total length is sufficient to mobilize full performance. Bearing pressure and stress concentration in the column material increases with the stiffness of the circumferential encasement. The shape of the hoop tension distribution diagram in geogrid is similar to the bulging pattern.

**Keywords** Stone column · Critical length · Geogrid · Optimum encasement depth · Bearing capacity

---

M. Bhaumik · S. P. Singh (✉)  
National Institute of Technology, Rourkela, Odisha, India  
e-mail: [spsingh@nitrkl.ac.in](mailto:spsingh@nitrkl.ac.in)

P. Nanda  
KIIT University, Bhubaneswar, Odisha, India  
e-mail: [preety.nandafce@kiit.ac.in](mailto:preety.nandafce@kiit.ac.in)

## 1 Introduction

Stone column treatment is one of the widely accepted ground improvement technique used in case of soft soil-like marine clay. Stone column technique is adopted for those structures which can sustain some amount of settlement, such as, storage tank, embankment, and lightweight structure. The construction of stone column consists of replacement of some amount of soft soil by available crushed stone [3, 13]. Depending upon the various factors, stone column experiences various mode of failures such as general shear failure, bulging failure, and sliding failure. The bulging type of failure is most predominant in longer stone column [1]. The effectiveness of stone column depends upon the lateral confinement. In soft soil, stone column generally failed by bulging due to low confinement. Circumferential confinement may increase the performance of stone column. Geosynthetic encased stone column has been successfully implemented in various geotechnical engineering aspects [4–8, 10, 11, 14]. Sharma et al. [16] conducted an experimental test on horizontally geosynthetic reinforced stone column, and reported it is more efficient than normal stone column. Raithel and Kempfert [15] investigated the effect of encasement and proposed a numerical approach for design-encased granular column. Murugesan and Rajagopal [11] analyzed the stress-settlement behavior of an isolated geosynthetic encased end bearing stone column using finite element package GEOFEM.

However, there are very limited literature on the analytical solution of an encased stone column and very less number of information available on performance of encased floating stone column. Most of the studies in the literature are based on end bearing stone column. Though, in case of large depth of soft clay layer, a floating stone column may be beneficial. In the present study, a 2D finite element analysis was implemented to replicate with the field condition by using Plaxis 2D V9.02. The influences of encasement, encasement depth, encasement stiffness at various strain level of the floating stone column have been studied.

## 2 Numerical Analyses

### 2.1 Description of Model

The numerical simulation was carried out using the finite element package Plaxis 2D 2012. An axisymmetric model analysis was performed using unit cell concept. Soft soil and stone columns were discretized to 15 node triangular elements. From the sensitivity analyses, the medium size mesh was found as effective. Mohr–Column failure criterion was adopted considering bilinear elastoplastic behavior of the materials. All the materials were assumed as a drained material, considering the analyses was carried out after sufficient time of construction.  $K_0$  procedure was adapted to generate lateral earth pressure at rest. No interface element was considered due to clay soil intermixing at the periphery of the non-encased stone column. Further, the

**Table 1** Soil and column properties [2]

Materials	$E$ (kPa)	$C_u$ (kPa)	$\phi$ ( $^{\circ}$ )	$\psi$ ( $^{\circ}$ )	$\mu$	$\gamma_{dry}$ (kN/m $^3$ )	$\gamma_{bulk}$ (kN/m $^3$ )
Clay	2150	7	0	0	0.47	13.6	18.3
Stone	55,000	0.3	43	10	0.3	16.62	-

clay may enter through the grid opening of geogrid encased stone column, and due to lack of information about this interaction, no interface element was taken.

## 2.2 Reference Case

A single isolated floating stone column was adopted from a large number of group of stone column. In this reference case, the stone column was considered at the center of the unit cell. Assuming the triangular pattern distribution of stone column, the diameter of the unit cell is calculated from the equivalent hexagonal tributary area of the stone column. Considering the long-term behavior and stress concentration effect on stone column, the loading is done on stone column area only. All the simulations were carried out in a 15 m thick clay stratum. This analysis focused only on the floating stone column, i.e., the length of the column is less than 15 m. Stone column diameter ( $D$ ) of 1 m was chosen for the whole study. The length of the column ( $L$ ) was taken having a broad range of variation from  $L/D = 0-12$ . Effect of the water table was not considered here. The properties of the soft clay and column material used for the idealized case are shown in Table 1. Axial stiffness ( $J$ ) of uniaxial geogrid was taken as 200, 500, 1000, 2000 kN/m.

## 2.3 Validation

The current model was verified by the load-settlement curve obtained from the experimental study conducted by Narasimha Rao et al. [12]. In their study, they used a tank of 650 mm diameter and 350 mm in height. A rigid plate of diameter two times the diameter of column was selected to apply load. To simulate the study in Plaxis, an axisymmetric model analysis was carried out (Fig. 1). The load-settlement curve obtained from the numerical study was well matched with the experimental one (Fig. 2).

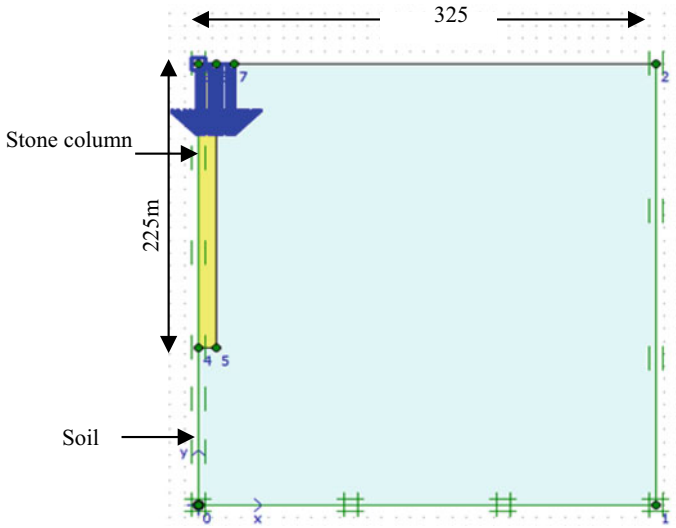


Fig. 1 Model for validation

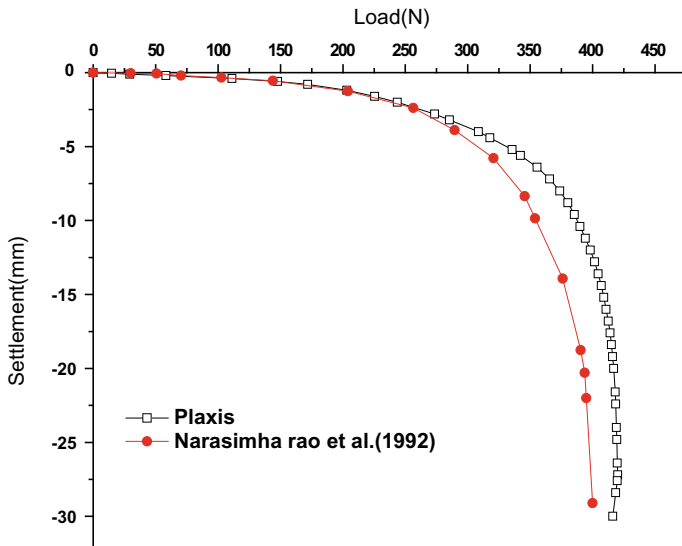


Fig. 2 Load-settlement curve obtain from experimental study and numerical model

### 3 Result and Analyses

#### 3.1 Column Length

In the first step of the parametric study, the influence of column length was studied. Load-carrying capacity of a stone column usually increases with increase in length. But after a certain length, increase in bearing capacity is negligible. Critical length is the maximum length up to which load-carrying capacity increases. Again, up to critical length, punching failure is predominant, and beyond this, value failure occurred by bulging of stone column.

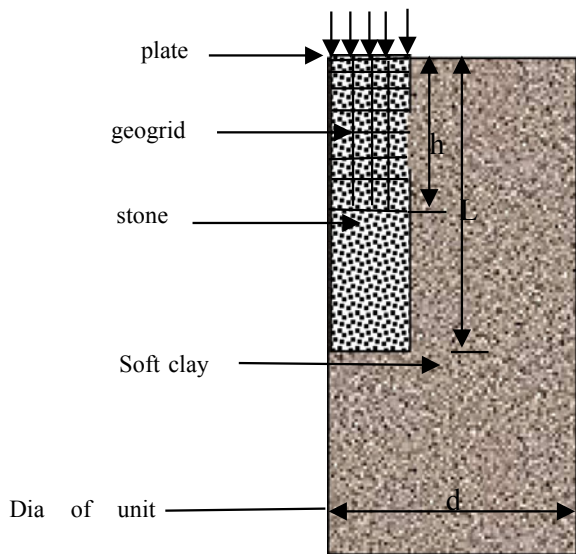
As the circumferential encasement resist the bulging, so encasement is effective only when the stone column length exceeds the critical length.

Figure 3 shows a typical geometric model of the stone column. In order to check the critical length, the length of the floating stone columns was varing such that  $L/d$  equal to 0, 2, 3, 4, 10. Figure 4 shows that the bearing value is not increasing beyond  $L/d = 4$ . By changing the various model properties, the same result also found. Hughes et al. [7] reported  $L_{cr}/d = 4.1$  from their experimental study. Mitra and Chattopadhyay [9] found the critical length lies between 4–5 times the diameter of stone column. So, it shows a good agreement with the literature.

##### a. Effect of Encasement

So, it is clear that even for a very long stone column, only a certain length is effective for bearing capacity improvement, and the rest of the length have no contribution on the same. Although the whole length may be effective in settlement improvement, this study is focused on the load-carrying capacity improvement. The stone columns

Fig. 3 Stone column geometric model



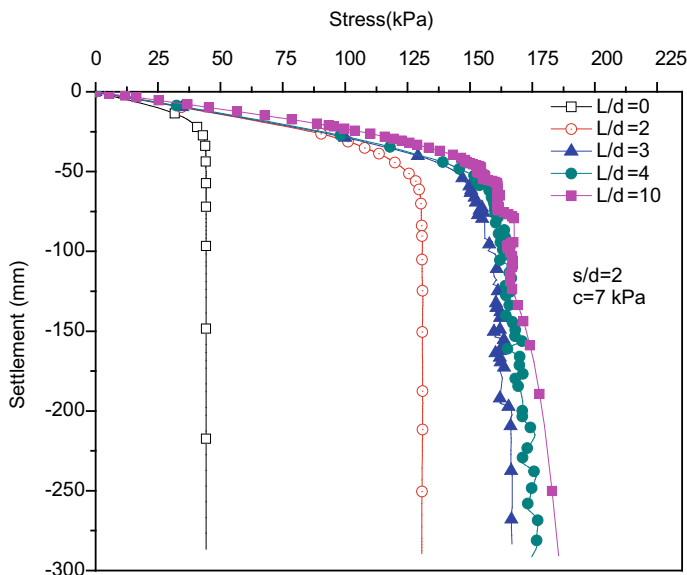


**Fig. 4** Stress-settlement response for different length of stone column

usually failed in bulging near the top, and this is due to very low confinement of the soil. To increase the lateral confinement, it was decided to encase the stone column with geogrid of various stiffness. To compare the response of both types of stone column, a series of prescribed displacement were applied on the plate at the top of the column, and the load–displacement curve was plotted accordingly. For the sake of simplicity, the stone columns were encased up to the full length. In Fig. 5, the load-carrying capacity of encased stone column was found to be more than two times the bearing capacity of non-encased one. A clear failure of the non-encased stone column was observed at very low strain, whereas an encased floating stone column failed at very high strain level, and it behaves like a semi-rigid pile. The almost uniform vertical settlement was observed along the length. It can be noted that the full length of the stone column can be utilized by the encasement.

**b. Effect of Encasement Depth**

The circumferential encasement around the stone column restricts the lateral spreading of stones and resists the bulging of column, and as a result, hoop tension force gets generated in the geogrid. From the hoop tension distribution diagram along the length of the encasement, it was found that maximum tensile stress get generated near the top portion within a length of equal to one diameter of the column. The hoop stress diminishes within two times the diameter. So, the full encasement of the stone column may not be economical. To find the effective depth of encasement, stone column was encased up to different depth (*h*) and the load-settlement response was analyzed. Figure 6 shows the load-settlement curve of stone columns with various depths of encasement. It is interesting that improvement of bearing capacity was

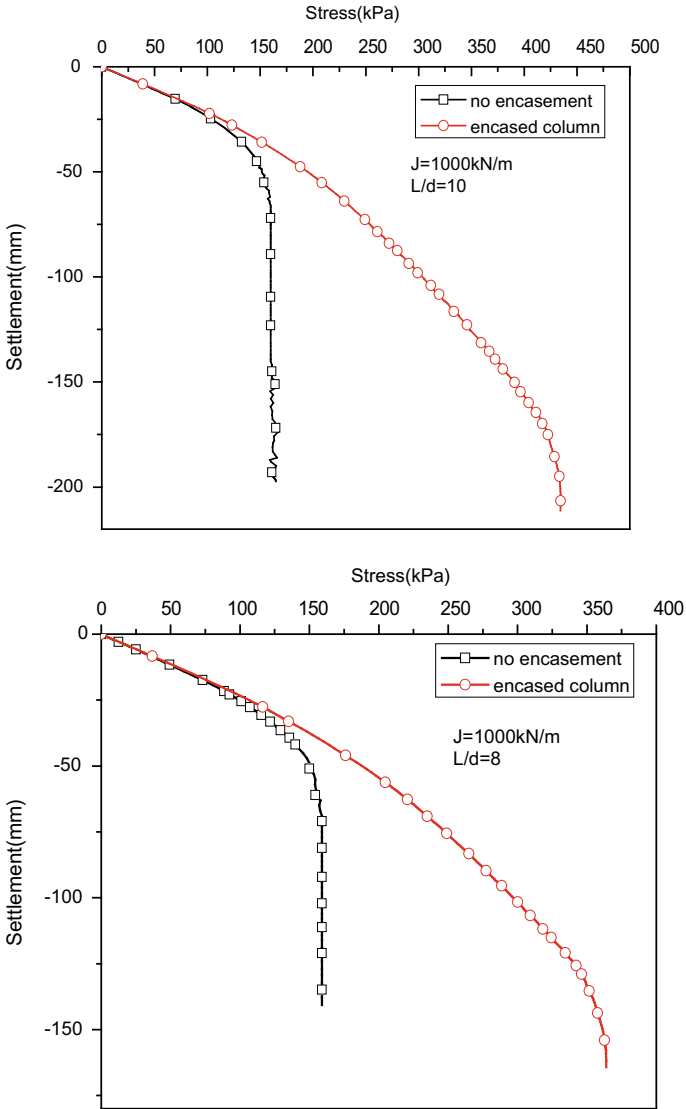
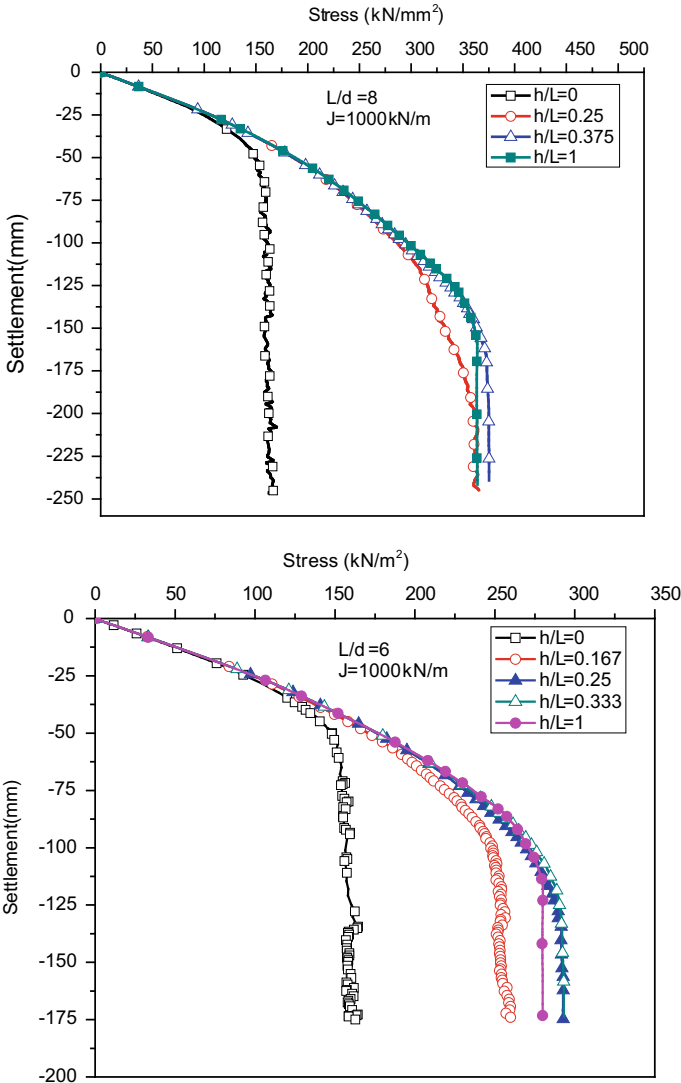


Fig. 5 Stress-settlement response of a single normal and encased stone column of  $L/d = 8$  and 10

found to be significant only up to an encasement depth equal to 25–30% of stone column length from the top, and after this, no increase in bearing capacity was observed. So, the encasement of 25–30% of the length is sufficient to mobilize the full performance of an encased stone column.





**Fig. 6** Effect of encasement depth for different lengths of stone column

c. Influence of Length of Partially Encased Stone Column

From the previous section, the optimum encasement depth has been found to be 25–30% of the length. In this parametric study, different lengths of encased stone columns were used, and each of the stone columns was encased only up to the optimum depth. The length of the optimally encased floating stone column was taken

as  $L/d = 4, 6, 8, 10,$  and  $12,$  and the loading was applied up to failure. The degree of improvement in each cases can be quantified by a non-dimensional improvement factor, as expressed below,

$$\text{Improvement factor } (\alpha) = \frac{\text{load carrying capacity of encased stone column}}{\text{load carrying capacity of non - encased stone column}}$$

Figure 7 shows a nearly linear increment of improvement factor with an increment of length of encased stone column.

d. Influence of Encasement Stiffness

As the performance of the longer stone column is greatly influenced by the circumferential confinement, stiffer confinement may result the better load-carrying capacity. Here, different column length have been used, and the encasement was provided upto the optimum depth as calculated earlier. A wide range of stiffness value was chosen from 200 to 2000 kN/m (Fig. 8). The study was further extended to investigate the stiffness effect at different strain level. As one can expect, the result shows that greater the encasement stiffness higher will be the compressive capacity of stone column. But, it is interesting to show that this improvement is a function of column length and strain level also. It shows the increment of improvement factor is more rapid for  $L/d = 10$  and  $8,$  and the influence goes to decrease for shorter stone column. So, it is clear that higher stiff encasement is meaningful for longer stone column only. Again, the mobilization of full resistance depends upon the strain level

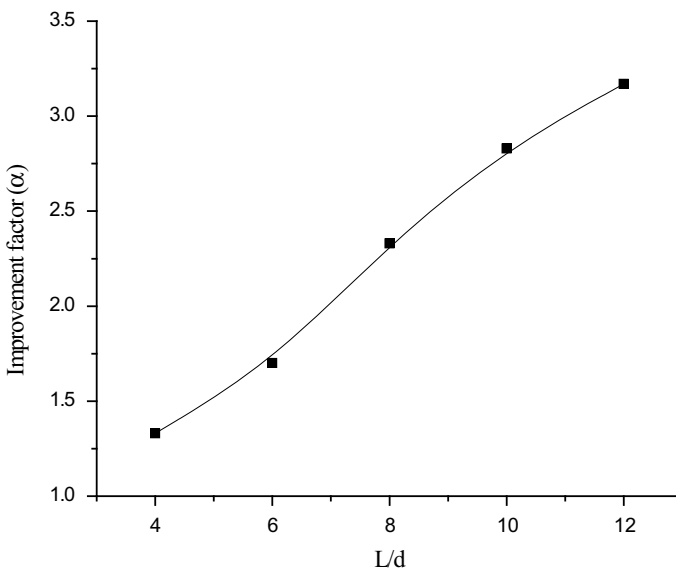
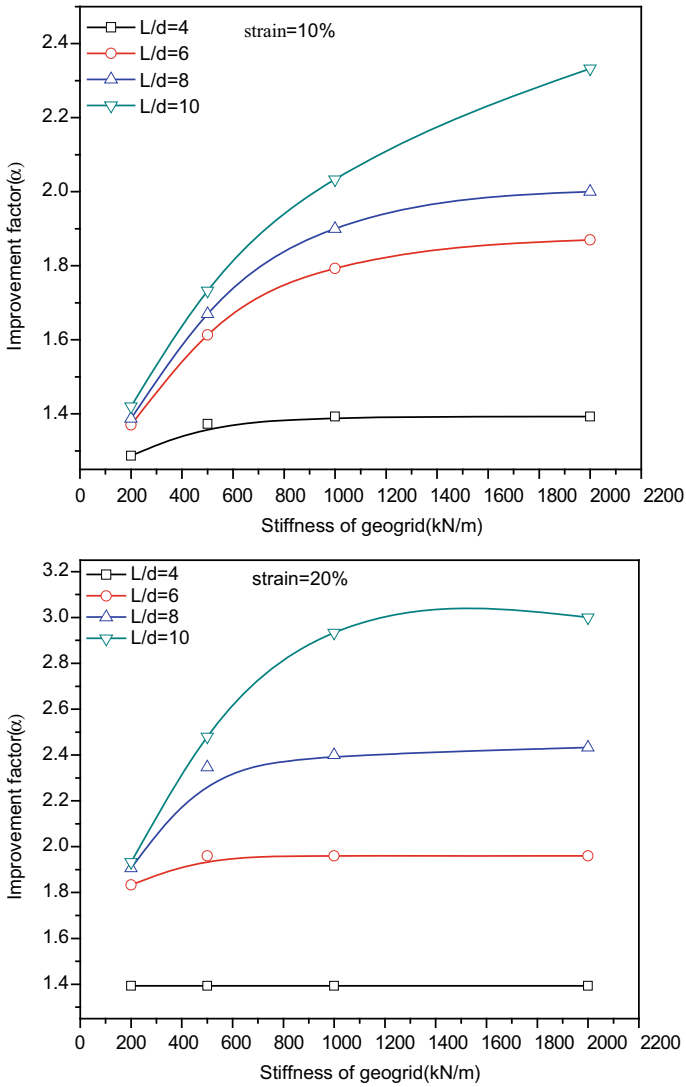


Fig. 7 Improvement factor for different length of stone column



**Fig. 8** Variation of improvement factor with stiffness of geogrid

up to which the column has been loaded. For shorter stone column, the bearing resistance mobilizes earlier than longer stone column. Again at higher strain condition, effect of encasement stiffness is very less.

## 4 Conclusion

In this study, we have compared the performance of normal and encased stone column. And the effect of various design parameters has been quantified. Depending upon the numerical analysis results and the trends of the obtained graphs, following conclusion can be summarized as:

For the column length more than the critical value ( $L/d = 4$ ), surrounding soil doesn't has adequate lateral confinement to resist the lateral bulging. Geosynthetic encasement can be employed as an effective solution, and it improves the compressive capacity more than two times.

The maximum hoop pressure in encasement remains within a length equal to two times the diameter near the top. So, an encasement depth of 25–30% of stone column length from top is sufficient to mobilize full performance of the encased stone column.

An appropriate stiffness value of encasement needs to be chosen depending upon the length of the column and allowable strain level. A higher stiff encasement is suitable for a longer stone column. Again, if a higher strain is allowed, then the stiffness can also be reduced.

## References

1. Aboshi H, Ichimoto E, Harada Y, Enoki M (1979) The compozer, a method to improve characteristics of soft clays by inclusion of large diameter sand columns. Proceedings of 1st international conference on soil reinforcement, Paris, 1, pp 211–216
2. Ambily AP, Gandhi SR (2007) Behavior of stone columns based on experimental and FEM analyses. *J Geotech Geo-Environ Eng* 133(4):405–415
3. Bouassida M, Carter J (2014) Optimization of design of column-reinforced foundations. *Int J Geomechan* 14:04014031
4. Castro J, Karstunen M (2010) Numerical simulations of stone column installation. *Can Geotech J* 47(10):1127–1138
5. Fattah M, Zabar B, Hassan H (2016) Experimental analysis of embankment on ordinary and encased stone columns. *Int J Geomech* 16(4):04015102
6. Gniel J, Bouazza A (2009) Improvement of soft soils using geogrid encased stone columns. *Geotext Geomembr* 27(3):167–175
7. Hughes JMO, Withers NJ, Greenwood DA (1975) A field trial of the reinforcing effect of a stone column in soil. *Geotechnique* 25(1):31–44
8. Khabbazian M, Kaliakin VN, Meehan CL (2009) 3D numerical analyses of geosynthetic encased stone columns. Contemporary topics in ground modification, problem soils, and geo-support, Geotechnical Special Publication, pp 201–208
9. Mitra S, Chattopadhyay BC (1999) Stone columns and design limitations. Proceedings on Indian geotechnical conference, Calcutta, India, 201–205
10. Murugesan S, Rajagopal K (2007) Model tests on geosynthetic encased stone columns. *Geosynth Int* 14(6):346–354
11. Murugesan S, Rajagopal K (2010) Studies on the behavior of single and group of geosynthetic encased stone columns. *J Geotech Geo-Environ Eng* 136(1):129–139
12. Narasimha Rao S, Madhiyan M, Prasad YVSN (1992) Influence of bearing area on the behavior of stone columns. Proceedings on indian geotechnical conference, Calcutta, India, pp 235–237

13. Priebe HJ (1995) The design of vibro replacement. *Ground Eng* 28(10):31
14. Pulko B, Majes B, Logar J (2011) Geosynthetic-encased stone columns: analytical calculation model. *Geotextiles Geomembranes* 29(1):29–39
15. Raithe M, Kempfert HG (2000) Calculation models for dam foundations with geotextile coated sand columns. *Proc Intl Conference on Geotechnical and Geological Engineering, Melbourne*
16. Sharma RS, Kumar BP, Nagendra G (2004) Compressive load response of granular piles reinforced with geogrids. *Can Geotech J* 41(1):187–192

# Evaluating the Utility of Pond Ash as an Alternative Foundation Material Partially Replacing Sand for Foundation Layers



Aditya Shankar Ghosh and Tapash Kumar Roy

**Abstract** The target of cent-percent utilization of the coal combustion ash likely to be generated in India in the upcoming years is definitely going to be a daunting task with its disquieting production and defined usage. Moreover, the harmful environmental and human health impact of the coal combustion ash stored in ash lagoons (Pond Ash) is demanding some immediate step for its effective bulk usage in a more eco-friendly way. The Supreme Court of India's order of imposing regulation on unconstrained fine aggregate excavation have turned the attention of the researchers toward Pond Ash (PA) and its potential usage as partial replacement of the Conventional Granular Material (CGM) for foundation layers. In this investigation the samples of PA were collected from Kolaghat Thermal Power Station (KTPS) ash pond in India and tested for its engineering properties (Specific gravity, Compaction behavior, Hydraulic conductivity, and Shear strength) along with gradation. Five mixtures of PA and zone-III sand with different mixture ratios (3, 6, 9, 12 and 15% PA content by weight of zone-III sand) were prepared for testing. Mineralogical analysis (XRD and FTIR) of the Virgin PA sample was conducted for verifying the pozzolanic nature of the collected PA sample. The test results showed favorable comparison of ash with the conventional granular material and PA is a promising Non-Conventional Granular Material (NCGM) which can be used effectively as well as economically by the industries as a foundation layer material, which will also address its disposal problems.

**Keywords** Pond ash · Chemical composition · Engineering properties · XRD · FTIR

## 1 Introduction

The year 1920 marked the beginning of burning of coal for the power generation which spread worldwide, yielding huge amounts of ash and associated by-products

---

A. S. Ghosh (✉) · T. K. Roy  
Department of Civil Engineering, Indian Institute of Engineering Science and Technology,  
Shibpur, West Bengal 711103, India

© Springer Nature Singapore Pte Ltd. 2022  
A. K. Dey et al. (eds.), *Proceedings of the 7th Indian Young Geotechnical Engineers Conference*, Lecture Notes in Civil Engineering 195,  
[https://doi.org/10.1007/978-981-16-6456-4\\_18](https://doi.org/10.1007/978-981-16-6456-4_18)

at an alarming rate. Incineration of coal itself generates 780 MTs of ash all around the globe, possessing a serious disposal issue. The ash generated is stored in ash ponds to prevent dust escaping, which bears tremendous initial investment. Researchers have already investigated that 1 megawatt (MW) of a thermal power plant's installed capacity consumes 0.4 ha storage space [1, 2]. The review of the reserved lives of the countries producing major amount of coal, based on their current production level revealed that, most of the developing countries have to confront this mounting problem in the upcoming decades [2].

The thermal power plants in India are mostly dependent on the combustion of bituminous coal having ash contents of 40–50% [3]. The ever more increasing capacity of coal-fired thermal power plants spurs the quantity of ash generation abruptly. Its rate of generation which is 130 MTs hugely surpasses the rate of its use of 60 MTs [1].

In the upcoming years, the cent-percent target of utilization of the ash likely to be generated is an intimidating task. The projected volume of ash production over the coming years is immense, and the planning as well as execution of using it has to be far more stimulating than what is perceived today. Conventional utilization strategies need to be backed up with newer avenues of bulk usage of the generated ash. This paper makes an attempt to determine the physio-chemical and engineering characteristics of ash collected from the ash pond of KTPS, West Bengal, India and showcase its prospects as alternate foundation materials where it can find bulk usage.

## ***1.1 Indian Scenario***

With the Honorable Supreme Court of India imposing total ban on sand mining in November 2017, resulted in scarcity of one of the most crucial foundation layer construction ingredients. This has also lead to manifold increase in the prices of the available sand, and altogether badly hit the running projects [India Today August 13, 2018]. These circumstances invoke the utilization of the Pond Ash (PA) from the ash ponds as an alternate foundation layer material, replacing the sand partially or fully, where it can find bulk utility and additionally can also reduce the construction cost hence become economically more beneficial.

## **2 Methodology**

The sample collection, determination of preliminary properties of the sample, and testing methods undertaken for this study are mentioned below.

**Sampling of Pond Ash.** PA samples for this study have been extracted from KTPS shown below in Fig. 1 directly from near the place where the ash mixed with water are getting discharged using a sampling scoop. The sampling was done following



**Fig. 1** Map showing the location of the Kolaghat Thermal Power Station Ash Pond

IS: 6491–1972. This was done to separate out arbitrarily the finer and comparatively coarser ash particles.

**Chemical composition analysis of virgin Pond Ash.** The chemical composition analysis of the collected ash sample was carried out by volumetric titration in the chemistry laboratory of IEST, Shibpur and the results are provided in Table 1 given below.

**Grain size analysis.** The ash ponds usually contain silt-size fraction more than sand-size fraction. Investigators have however observed that the bottom ashes predominantly contain sand-size fractions along with fractional silt-size fractions [2]. Explanations have also been made in their work about the predominance of particle size in the settlement of coal slurry, which directly affects the rheological behavior [2, 4]. In this study the grain size analysis was performed on pond ash, sand and pond ash/ sand mixtures. PA content of the mixtures was 100% (Virgin), 97, 94, 91, 88 and 85% by weight of the sand. The grain size of the samples was obtained using IS: 383–1970. The grain size analysis of the fractions passing 75 $\mu$  IS sieve is carried out according to Hydrometer Method, conforming to IS: 2720 part-IV (1985).

**Table 1** Chemical properties of Kolaghat pond ash

Constituents in percentage	Kolaghat pond ash (%)
Silica (SiO <sub>2</sub> )	70.00
Alumina (Al <sub>2</sub> O <sub>3</sub> )	1.20
Magnesium Oxide (MgO)	0.30
Iron (II) Oxide (Fe <sub>2</sub> O <sub>3</sub> )	10.00
Calcium Oxide (CaO)	1.00
Loss on Ignition	1.00



**Specific gravity, Compaction behavior and Permeability.** Investigational studies have stated that specific gravity of coal ash varies considerably depending on grain size distribution, particle shape and chemical composition [5, 6]. The specific gravity of the pond ash, sand and the sand/ ash mixtures was determined using IS: 2386 part-III (1963). The removal of the lower specific gravity PA particles was prevented by removal of air gaps, which was done by very slow heating.

Standard compaction tests were performed following IS: 2720 part-VII (1980). Premeasured quantities of PA and sand were prepared conforming to the requirements of IS: 460 part-I (1978) and were slowly hand-mixed at first, then suitable amount of water was sprayed gradually along with the slow mixing on a steel plate. The blended samples were then compacted in a standard compaction mold.

The permeability of the ash, sand and the ash/ sand mixtures was measured by the falling head tests as described by IS: 11,209–1985. The test was conformed to IS: 2720 part-17 (1986). The ash mixtures were compacted to 95% of the maximum density in the mold permeameter that was obtained from the standard proctor compaction test.

**Shear strength test.** In their study, the researchers stated this parameter to be one of the most important as shear strength characteristics is the main factor on which, the problems occurring in the field with slope stability of embankments, design of pavements, retaining structures and bearing capacity depends [7]. The shear strength behavior study of the ash samples for this study has been performed using Direct Shear Strength Test conforming to IS: 2720 part-13 (1986). Investigators in their work obtained the friction angle value to be in the range  $26^{\circ}$ – $42^{\circ}$  for pozzolanic coal-based ashes [8, 9].

**X-ray diffraction (XRD) and Fourier Transform Infrared spectroscopy (FTIR) analysis.** XRD measurement was performed on PA sample using the ULTIMA IV X-RAY DIFFRACTOMETER (RigakuKyowaglas-XA, Japan), automated with Cu-K $\alpha$  radiations. XRD samples were prepared by back loading technique. This minimizes preferred orientation [10]. The readings were taken in vertical Bragg–Brentano ( $2\theta$ ) geometry between  $10^{\circ}$  and  $80^{\circ}$  at  $0.02^{\circ}$  step size at 1 step/second, which resulted in a time of total measurement of 36 min/scan [11]. The X-Ray Tube Generator was operated at 40 kV and 40 mA [12].

The quantitative FTIR analysis of PA samples prepared alike as the XRD analysis, pressed into KBr pellets was done in a Nicolet 7199 FT-IR. For quantitative analysis of such spectra, a curve analysis program was employed to synthesize the IR spectra over a wide spectral range ( $450$ – $4000\text{ cm}^{-1}$ ).

### 3 Test Results and Discussion

The experimental data analysis for this study has been discussed accordingly.

**Grain size analysis.** Figure 2 below shows the grain size distributions for each PA, sand zone-III, as well as the PA/ sand mixtures, ranging from mostly silt to fine sand sizes. The grain size distribution curves of the ash mixtures shown in Fig. 2 are quite similar. Their sizes ranged from sand to small-size gravel. Table 2 represents the variation of Uniformity Coefficient ( $C_u$ ), Coefficient of Curvature ( $C_c$ ) and Effective size of the particles ( $D_{10}$ ).

**Specific gravity, Compaction behavior and Permeability.** The values of the specific gravity of the PA, Sand and PA/ sand mixtures are briefed in the Table 3. These values ranged from 2.501 to 2.856, that have been explained as a result of presence of PA particles with porous textures [13]. The higher specific gravity values are due to the presence of high iron oxide content. On examining the chemical composition, it revealed that the hollow ash particles have lower iron content and are also affected by the porosity of its particles [14, 13].

Table 3 shows that, as the PA content increases, the Maximum Dry unit weight ( $\gamma_{d,max}$ ) (MDD) increases, while the Optimum Moisture Content (OMC) decreases.

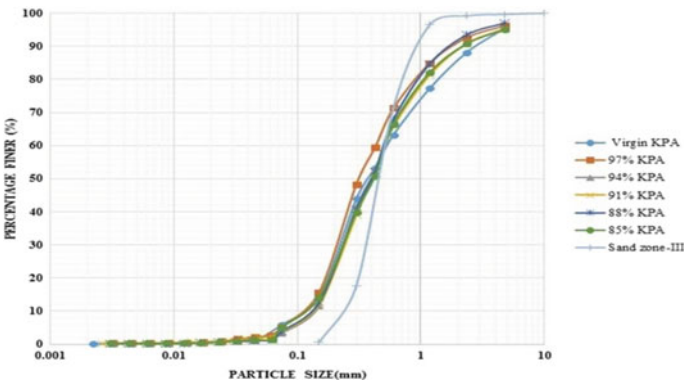


Fig. 2 Particle size distribution of pond ash, sand and pond ash/ sand mixtures

Table 2 Gradation analysis of the experimental samples

Description	$D_{10}$ (mm)	$C_u$	$C_c$
Virgin Kolaghat PA	0.135	3.926	0.7075
97% KPA + 3% Sand	0.110	3.730	0.9320
94% KPA + 6% Sand	0.140	3.570	0.6914
91% KPA + 9% Sand	0.130	3.846	0.7446
88% KPA + 12% Sand	0.120	4.167	0.8067
85% KPA + 15% Sand	0.110	4.550	0.8800
Sand zone-III	0.150	2.318	0.9700

**Table 3** Specific gravity, OMC, MDD, permeability data of pond ash, sand and pond ash/sand mixtures

Description	Specific Gravity	OMC	MDD (gm/cc)	Permeability (cm/sec)
Virgin Kolaghat PA	2.856	23.00%	1.53	0.00225934
97% KPA + 3% Sand	2.501	22.80%	1.56	0.00289355
94% KPA + 6% Sand	2.535	22.20%	1.58	0.00355713
91% KPA + 9% Sand	2.585	22.00%	1.62	0.00365988
88% KPA + 12% Sand	2.703	21.80%	1.68	0.00221749
85% KPA + 15% Sand	2.706	21.60%	1.72	0.00309080
Sand zone-III	2.675	12.50%	1.58	0.00743891

Studies revealed that for silty sands  $Y_{d,max}$  increases with increasing fines. They occupy the gaps in between the sand particles, and addition of PA results in a more well-graded size distribution. It allowing the ash to associate more closely, hence increasing the  $Y_{d,max}$  [15, 16] and [17].

Table 3 shows the value of permeability for compacted PA, sand and PA/ sand mixtures. The measured values varied from 0.002259335 cm/s to 0.007438907 cm/s, the former one is of the virgin PA and the latter is of zone-III sand respectively. With the increase of PA content in sand the permeability decreases. Researchers also supported this fact by stating that the larger specific surface of the PA particles causes increasing resistance to the water flow through the voids [13]. They also found out that the fines in the PA have a huge effect on the permeability [18, 13].

**Shear strength analysis.** The stress–strain behaviors of PA, sand and PA/sand mixtures, compacted in the shear box, conforming to IS: 11,229 (1985) and sheared in Direct Shear Strength testing machine, performing the CU Test, are represented by Fig. 3a–c. Table 4 shows the Cohesion ( $C$ ) and Friction Angle ( $\varphi$ ) data obtained. It is clearly observed from the shearing stress v/s strain graph under all the Normal stress conditions, that there is very small variation of effective friction angle [7]. Studies have revealed that, high shear strength parameters of these ashes prove to be favorable for their use in the field [5, 7] and [19].

**XRD and FTIR analysis.** The XRD studies are carried out primarily to identify the mineral phases of the PA sample. Figure 4a shows the presence of Mullite

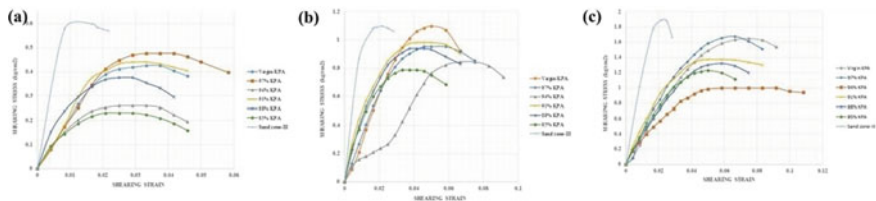


**Fig. 3** Shearing stress versus strain graph under normal stress **a** 0.5 kg/cm<sup>2</sup>, **b** 1.5 kg/cm<sup>2</sup> and **c** 2.5 kg/cm<sup>2</sup>

**Table 4** Direct shear test data of pond ash, sand and pond ash/ sand mixtures

Description	Cohesion (C) kg/cm <sup>2</sup>	Friction Angle ( $\phi$ )
Virgin Kolaghat PA	0.1883	31.17
97% KPA + 3% Sand	0.1667	31.38
94% KPA + 6% Sand	0.1558	31.61
91% KPA + 9% Sand	0.1400	31.87
88% KPA + 12% Sand	0.0825	32.09
85% KPA + 15% Sand	0.0333	32.34
Sand zone-III	0.0000	40.00

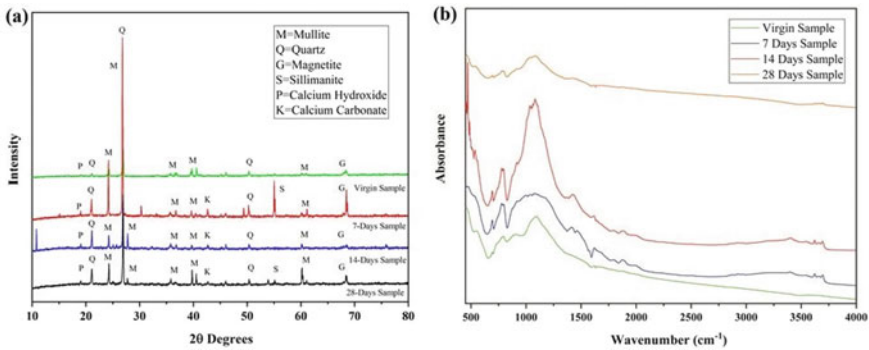


**Fig. 4** a XRD and b FTIR spectra of PA sample virgin, 7 days, 14 days and 28 days hydration

predominantly, followed up by partial presence of silica in crystalline form of Sillimanite and Quartz, combining with alumina as Mullite. Iron appears as the oxide of Magnetite. The figure also reveals the formation of peaks of Calcium Hydroxide and Calcium Carbonate which were found to match well with the Joint Committee on Powder Diffraction Standards (JCPDS File No. 44–1482) and (JCPDS File No. 85–1108) respectively [20].

FTIR Spectroscopy technique is used to obtain an infrared spectrum of absorption of the PA sample. The absorbance at 3440 cm<sup>-1</sup> and 1630 cm<sup>-1</sup> as shown in the Fig. 4b is due to the presence of (O–H) asymmetric stretching due to water and Silanol groups. Broad peak centered around 1083 cm<sup>-1</sup> is due to Si–O–Si bonds of amorphous silica which transform into Si–O–Al bonds of Poly-Sialate around 912 cm<sup>-1</sup> [11]. A shoulder at 1161 cm<sup>-1</sup> is marks the presence of Quartz.

## 4 Conclusions

The present study throws light on the chemical, physical and mineralogical properties of the PA collected from the KTPS. Tests are performed to analyze its pozzolanic properties and whether it could find effective application as alternate foundation material by partial replacement of fine aggregates. Besides these, the following conclusions are summarized based on this study:

- The chemical composition of the PA sample reveals higher percentage of Silica followed by Iron(II) Oxide and lower percentages of Alumina, Magnesium Oxide, Calcium Oxide and traces of some other compounds and elements.
- The grain size distribution of the experimental sample particles ranges between 0.001 and 0.075 mm. the increasing percentage of sand and decreasing percentage of PA in the blended mixture increases the  $C_u$  and  $C_c$  values of the mix.
- The specific gravity values of the experimental samples show steady increase with the increasing percentage of sand and decreasing percentage of PA in the blended mixture.
- The compaction test reveals that, as the PA content increases, the maximum dry unit weight increases, while the optimum moisture content decreases.
- The permeability results showed the larger specific surface of the PA particles causes more resistance to the flow of water through the voids, revealing the higher the percentage of PA in the mixture the lower is the permeability.
- The Direct Shear Test data shows that with an increase in the PA content the cohesive property of the blended sample increases however the friction angle decreases.
- In the mineralogical property analysis of the PA sample the XRD test followed up by the FTIR test performed to identify the mineral phases of the PA sample clearly reveals the pozzolanic nature of the PA sample.

## References

1. Chatterjee AK (2011) "Indian fly ashes: their characteristics and potential for mechanochemical activation for enhanced usability." *J Mater Civil Eng* 23(6):0899–1561, 783–788.
2. Moghal AAB (2017) "State-of-the-art review on the role of fly ashes in geotechnical and geoenvironmental applications." *J Mater Civil Eng* 29(8):04017072, 10.1061
3. British Petroleum (2015) "Statistical review of world energy, workbook, 2015"
4. Singh MK, Ratha D, Kumar S, Kumar D (2015) Influence of particle-size distribution and temperature on rheological behaviour of coal slurry. *Int J Coal Prep Util* 36(1):44–54
5. Gray DH, Lin YK (1972) Engineering properties of compacted fly ash. *J Soil Mech Found Div* 98(4):361–380
6. Pandian NS, Rajasekhar C, Sridharan A (1998) Studies on the specific gravity of some Indian coal ash- es. *J Test Eval* 26(3):177–186
7. Prakash K, Sridharan A (2009) "Beneficial properties of coal ashes and effective soil waste management." *Practice Periodical Hazardous Toxic Radioactive Waste Manage* 13(4):1090–025X, 239–248

8. DiGioia AM, McLaren RJ, Burns DL, Miller DE (1986) "Fly ash design manual for road and site application, vol. 1: Dry or conditioned placement." Manual prepared for EPRI, CS-4419, Research Project 2422- 2, Interim Report, Electric Power Research Institute, Palo Alto, Calif
9. Puppala A, Punthutaecha K, Vanapalli S (2006) "Soil-water characteristic curves of stabilized expansive soils." *J Geotech Geoenviron Eng* [https://doi.org/10.1061/\(ASCE\)1090-0241\(2006\)132:6\(736\)](https://doi.org/10.1061/(ASCE)1090-0241(2006)132:6(736)), 736–751
10. Singh GVPB, Subramaniam KVL (2016) "Quantitative XRD analysis of binary blends of siliceous fly ash and hydrated cement". *J Mater Civil Eng*
11. Abel ML (2004) "The influence of process parameters on the interfacial chemistry of  $\gamma$ -gips on aluminium: a review". *J Adhesion*
12. Singh GVPB, Subramaniam KVL (2016) "Quantitative XRD study of amorphous phase in alkaliactivated low calcium siliceous fly ash". *J Construct Build Mater*
13. Kim B, Prezzi M, Salgado R (2005) "Geotechnical properties of fly and bottom ash mixtures for use in highway embankments." *J Geotech Geoenviron Eng* [https://doi.org/10.1061/\(ASCE\)1090-0241\(2005\)131:7\(914\)](https://doi.org/10.1061/(ASCE)1090-0241(2005)131:7(914)), 914–92
14. Guo RQ, Rohatgi PK, Nath D (1996) Compacting characteristics of aluminium-fly ash power mix- tures. *J Mater Sci* 31:5513–5519
15. Kuerbis R, Negusse D, Vaid YP (1988) "Effect of gradation and fines content on the undrained response of sand." *Proc Hydraulic Fill Structures, Geotechnical Speccial Publication, No. 21, ASCE, New York*, 330–345
16. Lade P, Yamamuro J (1997) Effects of non-plastic fines on static liquefaction of sands. *Can Geotech J* 34(6):918–928
17. Salgado R, Bandini P, Karim A (2000) Shear strength and stiffness of silty sand. *J Geotech Geoenviron Eng* 126(5):451–462
18. Huang HW (1990) "The use of bottom ash in highway embankments, subgrade, and subbases." Joint Highway Research Project, Final Report, FHWA/IN/JHRP-90/4, Purdue Univ., W. Lafayette, Ind
19. Sridharan A, Pandian NS, Rao SS (1998) "Shear strength characteristics of some Indian fly ashes." *Ground Improv* 2(3)
20. Karvianto, Chow GM (2011) "The effects of surface and surface coatings on fluorescence properties of hollow NaYF:Yb, Er upconversion nanoparticles." *J Mater Res*

# pH and Electrical Conductivity of Cement-Treated Peat



Abhinaba Paul and Monowar Hussain

**Abstract** The constructional activities on peat soil are avoided which is due to its poor load-bearing capacity and high compressibility. Therefore, it always requires making the peat conducive in terms of its both strength and compressibility so as to undergo an infrastructural operation over it. However, apart from strength and compressibility criteria, there lie other two parameters (i.e., pH and electric conductivity) which also need to give emphasis while making any constructional activity over it. This paper studies the importance of accounting the pH and electric conductivity (EC) of peat soils as a significant parameter from the constructional point of view. Moreover, the change in behavior of pH and EC with cement addition is also analyzed. Simultaneously, it also attempted to make a correlation between this two which finally can help to understand the process of peat-cement reactions. From the results, it has been seen that pH and electric conductivity are a good indicative parameter through which the variations of other important parameters can be related. Finally, from the correlation, it is seen that irrespective of all curing days, the electric conductivity increases with increase in pH. However, this increase in EC with pH increment is found to be high at higher percent of cement.

**Keywords** Organic content · pH · Electric conductivity · Cement

## 1 Introduction

Peat is an exceptional type of problematic soil whose characteristics varies with a wide range of property difference hence making it a very poor kind of foundation material [6]. Therefore, it has become essential to comprehend the behavior of various properties of the peat so as to venture any constructional activity over it. In peat before processing any activity, few crucial parameters like bulk density, shear strength, void ratio, and compressibility which needed to understand. A number of studies have been done keeping these parameters as a sole concern in understanding the overall

---

A. Paul (✉) · M. Hussain

Department of Civil Engineering, National Institute of Technology, Silchar, Assam, India

© Springer Nature Singapore Pte Ltd. 2022

A. K. Dey et al. (eds.), *Proceedings of the 7th Indian Young Geotechnical Engineers Conference*, Lecture Notes in Civil Engineering 195,

[https://doi.org/10.1007/978-981-16-6456-4\\_19](https://doi.org/10.1007/978-981-16-6456-4_19)

peat behavior and also from the design point of view. However, apart from this there lie few other parameters like pH and EC which also need a significant attention while discussing or understanding the nature of peat. pH of a soil gives the measure of its acidity, neutrality, or alkalinity in terms of hydrogen ion concentrations in the soil–water system. A hydrogen ion is actually an acid cation which larger in proportion in the solution tells a high acidity in the solution. Peat acidity is highly influenced by the origin of rock, origin of plants, extent of oxygen supply, and concentration of humic acid. The acidity in the peatland occurs through two processes, one by microbial deterioration process and other through cation exchange capacity. The first process, there occurs the breakdown of the fiber, dead parts of roots, and plants by the bacteria and fungi which finally discharge acid solution into nearby zone. However, in the second process, the prevailing occurrence of peat moss (incompletely putrefied rotten plant life) acidifies to its nearby by cation exchange. Apart from this, the large accretion of organic substance, disintegration, and the firm release of acids (humic and fulvic) may be one another cause for low pH in peat. The typical pH value of different types of peat varies from 3.2 to 6.81 [7, 15]. Construction projects in acidic soils zones can be challenging to accomplish. Acidic soil appearing as acid sulfate soils is unconsolidated estuarine clays and muds, similar to gel-like traits and poor load-carrying ability [10]. Constructions or earthworks executed on such constituents may keep on settling or subsiding in a slow and uneven manner. A cautious engineering is vital to avert problems with subsidence, which can make highways to slump and foundations to crack. Electrical conductivity (EC) is the capability of soil in carrying electric current, and it is generally expressed in microSiemens ( $\mu\text{S}/\text{m}$ ) per distance. It is generally influenced by many different aspects such as temperature, organic content, pH, cation exchange capacity, and moisture content. Further, there occurs a strong correlation between the texture type and particle size with conductivity. It is observed that minerals changing from clay to sand exhibits from high to low conductivity values, respectively [9]. The literatures reported that regardless of decomposition stage, electric conductivity of peat reduces with increment in organic content [2]. Peat with high stage of decomposition holds more negative charge and high colloidal portion, which increases significantly the electrical conductance [2]. Robert et al. [16] mentioned that the electrical conductivity also varies depending upon the quantity of water seized in soil. Electrical conductance of soil is used in geotechnical engineering for site characterization, further it gives provide useful information for predicting other geotechnical parameters [4].

Moreover, it is seen to be connected with numerous hydraulic properties comprising degree of saturation, water content, pore structure, bulk density [8], and also helps to get idea of hydraulic conductivity [3]. Apart from this, some data have reported that it can measure consolidation [12] and degree of compaction [11] for certain soil categories. Further, micro-scale characterization of soil in examining the anisotropy effects has also done by using electric conductivity [12]. In addition, investigators have endeavored to describe liquefaction susceptibility and structural arrangement of sands using electrical measurements at higher frequencies (i.e., > 1 MHz), with considerate degree of success [1].



Nevertheless, apart from understanding the behavioral aspect of peat, it has also become necessary to utilize peat as with growing civilization and infrastructural development it is no longer remains an option to avoid such kind of soil. Various remedial measures have been adopted to deal with this kind of soil such as excavation-displacement or replacement, vertical drains and preloading, RCC piles, stone columns, light weight foundation system, and chemical stabilization technique [14].

However, out of all these, chemical stabilization/solidification process is a commonly used technique for the remediation of peat soil. In this process, peat soils mixed with a binders (like cement, lime and fly ash) to lower the organic matter content which finally enhances the chemisorption, soil strength through precipitation, physical encapsulation and ion exchange. All through the literatures, the effectiveness of this chemical treatment was been discussed mostly by strength and compressibility criteria. However, there occurs very less record of study where they have discussed pH and electric conductivity criteria. Therefore, considering all the previous history, this present study focuses in analyzing mainly on two aspects. One is considering the importance of discussing pH and EC of peat soil in engineering prospect and other to analyzing its changing pattern after the chemical treatment with use of cement. Further, this study also highlighted the correlation between the pH and EC of cement-treated peat.

## 2 Material and Methods

### 2.1 Peat

Peat collected in this study is from two districts in the state of Assam, one is from Cachar and other is from Hailakandi. In Cachar, it is collected from National highway 39 (NH39) locations, and in Hailakandi, it is collected from Kalinagar tea estate (KTE) area. It was noticed that the deposition of peat occurs at a depth of 1–2 m below the ground level and with the mean thickness of its layer is 1.5–6 m. The physicochemical properties of the studied peat are shown in Table 1. The cement

**Table 1** Physicochemical properties Indian peat

Parameters	NH39	KTE
Water content (%)	268	600
Organic content (%)	20	36
Specific gravity	2.03	1.9
Fiber content (%)	8.11	77.4
pH	5.1	5.5
Electric conductivity (MicroSimen/cm)	199	204
Degree of humification	H <sub>8</sub> –H <sub>10</sub>	H <sub>1</sub> –H <sub>4</sub>

**Table 2** Chemical composition of ordinary Portland cement

Chemical composition	Amount (%)
Calcium Oxide (CaO)	63.78
Silicon Dioxide (SiO <sub>2</sub> )	21.08
Ferric Oxide (Al <sub>2</sub> O <sub>3</sub> )	3.71
Aluminum Oxide (Al <sub>2</sub> O <sub>3</sub> )	4.42
Sulfuric Trioxide (SO <sub>3</sub> )	2.43
Magnesium Oxide (MgO)	1.6

used for the chemical treatment purpose is of ordinary Portland cement (OPC) of 43 grade. The chemical constituents of the OPC in percentage on a dry weight basis are shown in Table 2. The water used throughout the study is the normal water, except where standard specifications require distilled water.

The pH and EC were evaluated at different percentages (5, 10, 15, 20, and 30%) of cement which corresponds to maximum dry density (MDD)—optimum moisture content (OMC) and with varying curing days (i.e., 0, 7, 14, 28, 60, and 90 days). Further, they were evaluated out by using a pH and conductivity meter, respectively, according to the ASTM D 2976. A 3–5 g of the finely powdered soil sample is mixing with 50 ml of distilled water (having pH~ 6.5–7.5) and is poured into 100 ml beaker. The mixture is then allowed to get stirred for some minutes in electrical stirrer at 110–130 rotations/minute followed by a gentle filtration. The pH and EC meter are calibrated at their respective standard, and finally, readings are taken from the solution.

### 3 Results and Discussion

#### 3.1 PH and EC of Cement Treated Peat

pH variation with cement content at various curing days is shown in the Fig. 1 a, b. It is seen from the figure that the pH increases with increase in the cement content. The reason behind this increase is due to the hydration of free lime (CaO) that remains in cement releases calcium ion (Ca<sup>++</sup>) to pore fluid which increases the pH and finally making a basic environment in the solution. A similar variation has been informed by Erikus et al. [5] and Rahgozar and Saberian [17]. However, at advanced curing days, the pH value is found to get decreased. This is actually owing to the fact that at early curing days there occurs the consumption of free lime by the organic matter which leaves no such or very few lime to make any further hydration process. This decrement in the pH value with higher curing days is also mentioned by Taku et al. [18] The highest increment for pH is observed for NH39 is 5.1–12.3, and for KTE is 5.5–10.9, which tells that as with organic matter increment in the soil, the extent of pH increment got reduced.

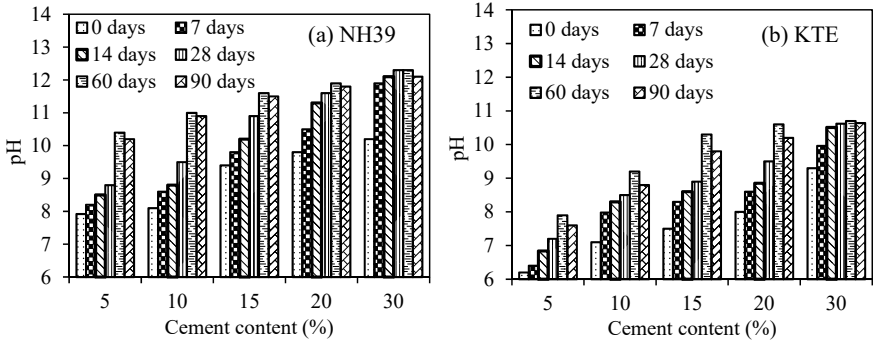


Fig. 1 pH variation with cement content at various curing periods

Figure 2 a, b shows the variation of EC with cement content at different curing periods. It is observed that for both the peats EC increases with increase in the cement content. This increase is due to the effect of calcium and hydroxyl ions ( $Ca^{2+}$  and  $OH^-$ ) that produced by the dissolution of cement in the soil pore structure. Further, this increase of EC with cement content can be explained by the inverse relation between electric conductivity and organic content. Since, it is well-known fact that with increase in cement organic content decreases so eventually it increasing the EC value. However, the reduction of EC at higher curing days can be explained due to the reason that at advanced curing days there happens the consumption of  $Ca^{2+}$  ion in the pozzolonic reaction which finally shortens the resultant ion activity in the soil pore structure [13].

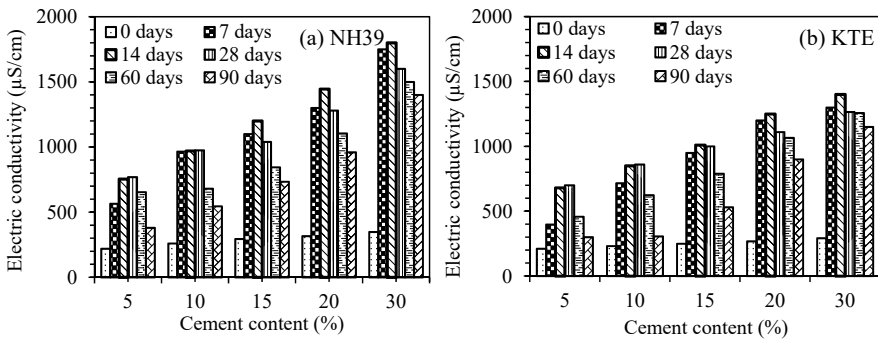
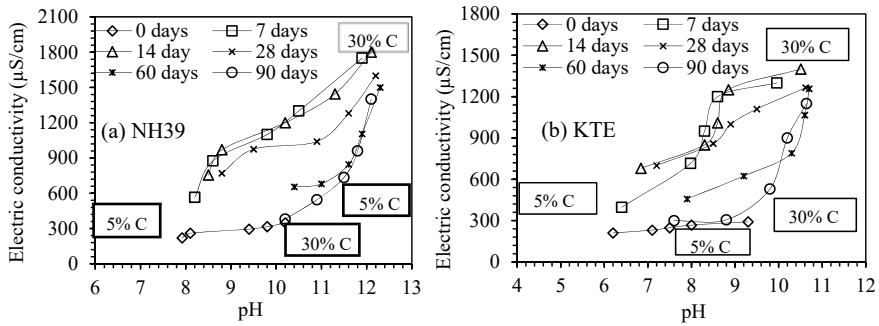


Fig. 2 Electric conductivity variations with cement content at various curing periods



**Fig. 3** Relationship between pH and EC with cement content at different curing periods

### 3.2 Correlation Between pH and EC

Figure 3 shows a typical relationship between pH and electric conductivity of cement-treated Indian peat. It can be seen from the figure that irrespective of all curing days, the electric conductivity increases with increase in pH. However, it is also observed that the relative steepness of the curve goes higher with increasing percentage of cement (>10% C) in both the peats. This indicates a small change in pH brings about a large change of EC.

## 4 Conclusion

To adequately characterize different types of peat for foundation of structures, it is necessary to accumulate sufficient data regarding soil properties which invariably includes chemical parameters also. Thus, pH and EC of soil are very essential for construction-related issues. The pH of soil is the measurement of its acidity and alkalinity. A low pH (<7) that is acidic soil can cause severe impacts to the environs and to infrastructure. Further, the presence of acid can also bring damage to steel and concrete, gradually abolishing roads, pipes, bridges, and constructions. In expanses before construction where acid sulfate soils are not given due concern, a costly repairs may be needed, or structure must be to be substituted well before the end of its envisioned life period. The need of electrical conductance of soil is quite important in the field of geotechnical engineering for site characterization. Although its direct application has not been found much, but it helps in giving information of prophesying other geotechnical parameters. The improvement in the quality of peat in terms of strength after the cement treatment can be well supported by through pH and EC variation. The generation of alkaline environment due to rise in pH after cement addition kindles largely the dissolution of silica and alumina in the solution finally rendering formation of cementitious gel which held responsible for the development of strength. Further, the increase in EC of the cement-treated peat gives much better

ability to store and hold onto cation which itself supports the mechanism where the release of  $\text{Ca}^{++}$  ion from cement in the solution reacts with soil pozzolans to produce strength enhancing products. Finally, it is seen that regardless of all curing days, the electric conductivity increases with increase in pH.

## References

1. Arulanandan K, Muraleetharan KK (1988) Level ground soil liquefaction analysis using in situ properties. *J Geotech Eng* 114(7):753–770
2. Asadi A, Huat BBK (2009) Electrical resistivity of tropical peat. *Electron J Geotech Eng* 14:1–9
3. Abu-Hassanein HS, Benson CH, Blotz LR (1996) The electrical resistivity of compacted clays. *J Geotech Eng* 122(5):397–406
4. Bryson LS, Bathe A (2009) Determination of selected geotechnical, properties of soil using electrical conductivity testing. *Geotech Testing J* 32(3):1–10
5. Erikcius DT, Leong EC, Rahardjo H (2001) Shear strength of peaty soil-cement mixes. In: *Proceedings of the third international conference on soft soil engineering, Hong Kong*, 551–556
6. Huat BBK, Afshin A, Kazemian S (2009) Experimental investigation on geomechanical properties of tropical organic soils and peat. *Am J Eng Appl Sci* 2(1):184–188
7. Kolay PK, Aminur MR, Taib SNL, Zain MISM (2011) Stabilization of tropical peat soil from Sarawak with different stabilizing agents. *Geotech Geological Eng* 29:1135–1141
8. Kalinski RJ, Kelly WE (1993) Estimating water content of soils from electrical resistivity. *Geotech Test J* 16(3):323–329
9. Ponziani M, Slob EC, Nagen-Tillard DJM, Vanhala H (2011) Influence of water content on the electrical conductivity of peat. *Int Water Technol J* 1(1):14–21
10. Muller PG, Coutts JA (2005) Acid sulfate soils and estuarine water quality of the Mackay district. *Land Res Bull* 1:77
11. McCarter WJ (1984) The electrical resistivity characteristics of compacted clays. *Geotechnique* 34(2):263–267
12. McCarter WJ, Desmazes P (1997) Soil characterization using electrical measurements. *Geotechnique* 47(1):179–183
13. Mukhtar F, Bhat MA, Bashir R, Chisti H (2014) Assessment of surface water quality by evaluating the physico-chemical parameters and by checking the water quality index of Nigeen Basin and Brari Nambal Lagoon of Dal Lake Kashmir. *J Mater Environ Sci* 5(4):1178–1187
14. Rowe RK (ed) (2012) *Geotechnical and geoenvironmental engineering handbook*. Springer Science and Business Media
15. Rahman ZA, Lee JYY, Rahim SA, Lihan T, Idris WMR (2015) Application of gypsum and fly ash as additives in stabilization of tropical peat soil. *J Appl Sci* 15(7):1006–1012
16. Robert BG, Mark Alley GW, Holshouser D, Thomason W (2009) Precision farming tools: soil electrical conductivity. *Virginia cooperative extension, Virginia*, 442–508
17. Rahgozar MA, Saberian M (2016) Geotechnical properties of peat soil stabilised with shredded waste tyre chips. *Mires Peat* 18:1–12
18. Taku KJ, Amartey DY, Kassari T (2015) Effect of acidic curing environment on the strength and durability of concrete. *Civ Environ Res* 7:8–13

# Bearing Capacity of Circular Footing on Geonatural and Geosynthetic Reinforced Sand



B. Venkatesh and T. Thyagaraj

**Abstract** This paper brings out the effect of tensile strength of reinforcement on the bearing capacity of circular footing in sand. In order to achieve this objective, a series of laboratory model tests were performed using natural jute and synthetic polypropylene geotextiles in a rigid steel tank of 900 mm × 900 mm × 800 mm size. A circular footing of 150 mm diameter ( $D$ ) was used for the model tests. The geotextile reinforcement sheets were placed as planar layers with the placement depth of first reinforcement layer ( $u$ ) as  $0.31D$  and spacing between the planar layers ( $h$ ) as  $0.3D$ . The number of layers used within the reinforced zone ( $N$ ) was 4, and the size of the reinforcement sheet ( $B_r$ ) was  $5D$  in the model tests. The placement of geotextile and quantity of geotextile used was same for all the tests. The experimental studies indicate that the stiffness of the reinforcement plays a significant role in load-carrying capacity improvement rather than the reinforcement material tensile strength.

**Keywords** Laboratory model tests · Circular footing · Geotextile reinforcement · Reinforced sand · Bearing capacity

## 1 Introduction

The bearing capacity of loose sands may not be sufficient to support the huge super-structure loads, even if the sand is densified to its maximum relative density. To increase the load-bearing capacity, one common practice is to reinforce the soil with a geosynthetic reinforcement layer(s). In the last few decades, a large number of laboratory studies have been carried out and reported in the literature which developed a cost-effective solution using geosynthetic reinforcement to increase the load-bearing capacity of shallow foundations, e.g., Binquet and Lee [2, 3], Guido et al. [5], Ghosh et al. [6], Latha and Somwanshi [9], Tavangar et al. [10].

The present study brings out the effect of low tensile strength natural woven jute geo-textile and high tensile strength synthetic woven polypropylene geotextile

---

B. Venkatesh (✉) · T. Thyagaraj  
Department of Civil Engineering, Indian Institute of Technology Madras, Chennai, India

**Table 1** Properties of sand

Property	Values
D <sub>10</sub> (mm)	0.25
D <sub>30</sub> (mm)	0.42
D <sub>60</sub> (mm)	0.95
C <sub>u</sub>	3.8
C <sub>c</sub>	0.743
Specific gravity, G	2.68
e <sub>max</sub>	0.666
e <sub>min</sub>	0.466
Classification	SP

reinforcements on the bearing capacity of circular footing by conducting laboratory model tests. The results of the laboratory model studies carried out on unreinforced and reinforced sand beds are presented in this paper. In order to ensure the repeatability of the model test results, most of the tests were repeated for two to three times.

## 2 Experimental Program

### 2.1 Materials Sand

The model tests were performed using clean-dry sand collected from Chennai locality. Table 1 summarizes the properties of sand.

### 2.2 Geotextiles

The model tests were performed on sand beds reinforced with natural woven jute geotextile (JGT) and synthetic woven polypropylene geotextile (PPGT). The photographic view of the geotextiles used in this study is shown in Fig. 1. The natural woven jute geotextile is obtained from the National Jute Board (NJB) approved company—Ballyfabs International Ltd Company, Chennai, India. The synthetic polypropylene geotextile was collected from the Techno Fabrics Geosynthetic (P) Ltd Company, Gujarat, India. The load-elongation curve of the geotextile was obtained from the standard wide-width tension test [1], and the test results (only machine direction) are presented in Fig. 2. The properties of geotextiles used for the laboratory model tests are presented in Table 2.



Fig. 1 Photographic view of woven jute geotextile and polypropylene geotextile

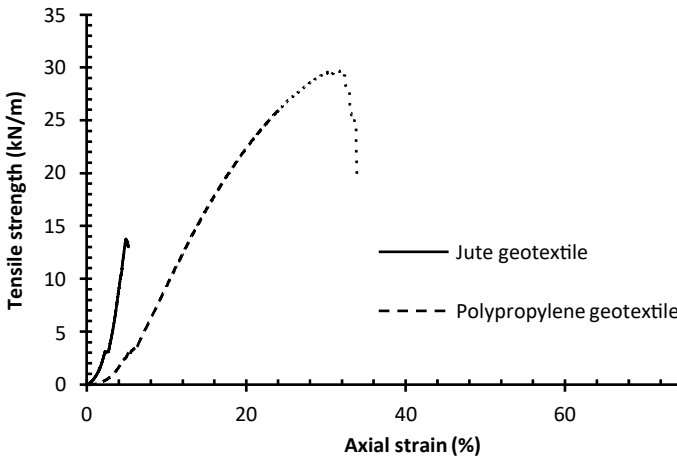


Fig. 2 Comparison of load-elongation behavior of jute and polypropylene geotextiles

### 2.3 Laboratory Test Setup

The load tests were performed on test sand beds using the loading frame test setup. The steel test tank with inner dimensions of 900 mm × 900 mm × 900 mm was used for the present study. The air-pluviation (raining) technique was adopted for the preparation of the sand bed in the test tanks up to 800 mm depth. The average dry unit weight and relative density of the sand bed were maintained constant at 17.23



**Table 2** Properties of geotextile reinforcement layers

Properties of geotextile	JGT	PPGT
<i>Physical properties</i>		
Thickness (mm)	1	0.4
Mass per unit area (g/m <sup>2</sup> )	315	130
<i>Mechanical property</i>		
Ultimate tensile strength MD x CMD (kN/m)	13.8 x 12.5	29.6 x 23.5
Failure strain MD x CMD (%)	4.9 x 5.9	30.2 x 21.4
Axial stiffness, EA (kN/m)	246	54

kN/m<sup>3</sup> and 70% for all the model tests, respectively. The model footing consisted of thick mild steel plate of 25 mm thick and 150 mm diameter (*D*). The model footing base was roughened by affixing a thin layer of sand with the help of araldite. The footing was pushed into the soil bed by means of a hydraulic jack.

Irrespective of type of geotextile material, a total of four geotextile reinforcement layers (*N*) of 750 mm size, *B<sub>r</sub>* (where *B<sub>r</sub>* is equal to 5*D*) was used. The depth of first reinforcement layer (*u*) and spacing between the reinforcement layers (*h*) were maintained as 0.31 times the diameter (*D*) (i.e., 46.5 mm) and 0.3*D* (i.e., 45 mm), as suggested by Ghosh et al. [6] and Tavangar et al. [10]. The load was applied on the footing using a precalibrated proving ring. Figure 3 shows the schematic diagram of the total test setup. The load application on the footing was in accordance to IS 1888–1982 [7]. The settlement of footing was monitored using dial gauges *Dg<sub>2</sub>* and *Dg<sub>3</sub>*.

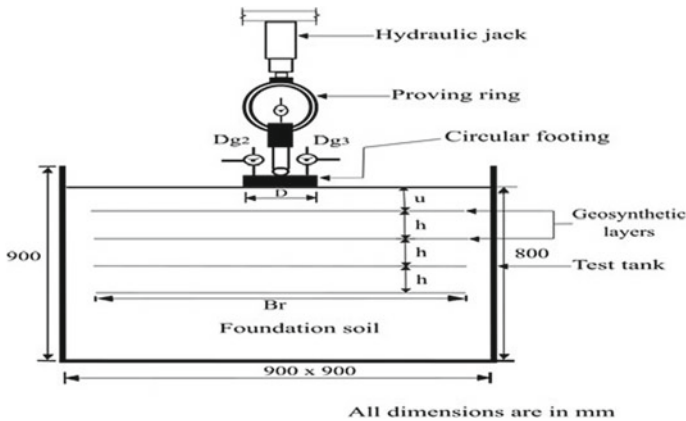


**Fig. 3** Geometry of the multi-layered planar reinforcement sand bed (after Buragadda and Thyagaraj [4])

### 3 Results and Discussion

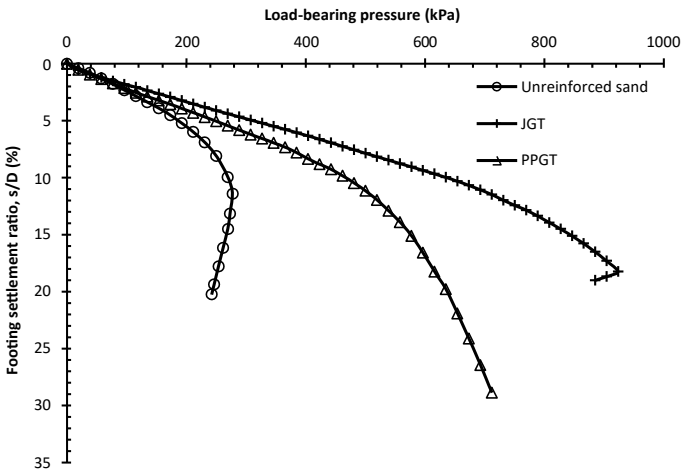
Bearing capacity ratio (BCR) is generally used to quantify the improvement in performance due to inclusion of reinforcement layers in the sand beds. The BCR is given by [2]:

$$BCR = q_{rs}/q_{us} \tag{1}$$

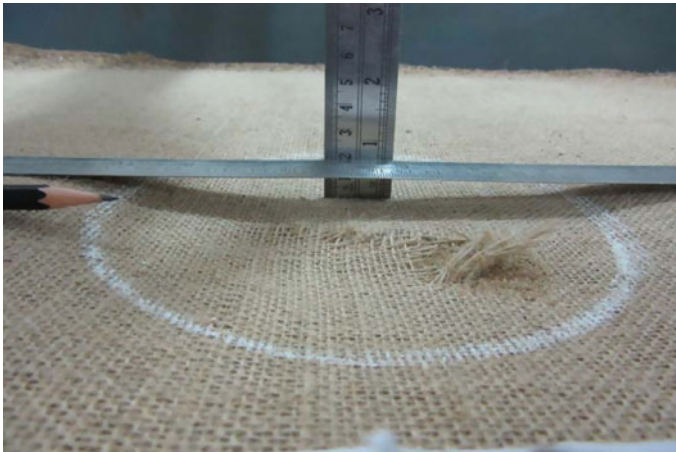
where  $q_{rs}$  and  $q_{us}$  are the bearing capacity of the reinforced and unreinforced sand beds at the same settlement(s), respectively. The footing ultimate bearing capacity ( $q_{ult}$ ) is used in place of  $q_{us}$  for settlements beyond the ultimate bearing capacity of the unreinforced soil ( $q_{ult}$ ).

Figure 4 compares the load-settlement response of unreinforced and geotextile reinforced sand beds. Irrespective of the geotextile material, the placement of geotextile and quantity of geotextile used was maintained same in all the model tests. From Fig. 4, it can be seen that the load-settlement response of the unreinforced sand bed and reinforced sand with natural jute geotextile shows a pronounced peak, indicating that the soil has undergone failure. However, a clear failure is not noticed in synthetic geotextile reinforced sand even up to a settlement as high as 30% of the footing diameter. The jute geotextile reinforced sand shows a pronounced peak due to earlier rupture of jute geotextile reinforcement layer because of its low tensile strength as shown in Fig. 5. The variation of BCR with footing settlement ratio ( $s/D$ ) is shown in Fig. 6.

In most of the cases, the settlement governs the shallow foundation design rather than the bearing capacity. In most practical circumstances, the amount of settlement



**Fig. 4** Comparison of load-settlement curves of unreinforced and geotextile reinforced sand beds ( $u/D = 0.31$ ,  $h/D = 0.3$ ,  $N = 4$ ,  $B_r/D = 5$ )



**Fig. 5** Failure of the jute geotextile after plate load test

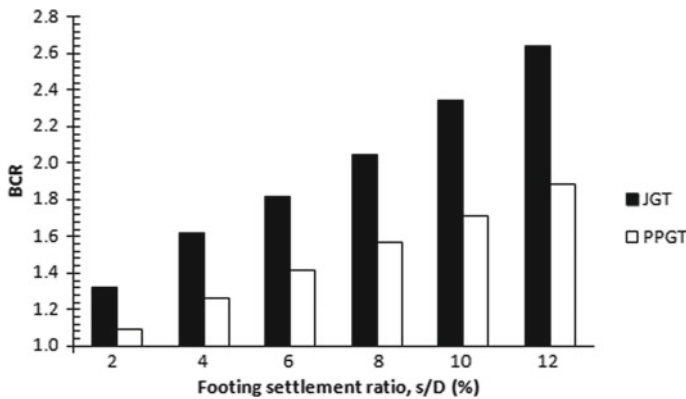


**Fig. 6** Variation of the BCR with footing settlement ratios of jute and polypropylene geo-textile reinforcement layers

should not be high. It should be between 10 to 15% of footing diameter ( $D$ ) for the design of the footings [8]. Hence, the BCR with footing settlement ratio ( $s/D$ ) is shown only up to settlement of 12% of footing diameter in Fig. 6. However, irrespective of any footing settlement ratio ( $s/D$ ), the load pressure-settlement response and BCR of reinforced sand with low tensile strength jute geotextile reinforcement layers are found to be greater than the unreinforced and synthetic reinforced sand.

This behavior could be due to the variation in tensile stiffness of the reinforcement. It is presented in terms of axial stiffness of the reinforcement layers. The jute geotextile is having higher axial stiffness value in comparison with the polypropylene geotextile as given in Table 2. The sand bed reinforced with natural jute geotextile

performed better than the synthetic polypropylene geotextile, though the ultimate load-carrying capacity is attained at lower settlement comparatively.

## 4 Summary and Conclusions

The experimental studies indicate that the stiffness of the reinforcement has a key role in the improvement of load-carrying capacity rather than the reinforcement tensile strength. As seen from the test results, the sand reinforced with low tensile strength natural jute geotextile performed better than the high tensile strength synthetic polypropylene geotextile reinforcement due to high tensile stiffness of jute geotextile.

## References

1. ASTM Standard D 4595–11 Standard test method for tensile properties of geotextiles by the wide-width strip method. American society for testing and materials, Pennsylvania, USA
2. Binquet J, Lee KL (1975) Bearing capacity tests on reinforced earth slabs. *J Geotech Eng Division ASCE* 101(12):1241–1255
3. Binquet J, Lee KL (1975) Bearing capacity analysis of reinforced earth slabs. *J Geotech Eng Division ASCE* 101(12):1257–1276
4. Buragadda V, Thyagaraj T (2019) Bearing capacity of jute geotextile-reinforced sand bed. *Int J Geosynthetics Ground Eng* 5:27. <https://doi.org/10.1007/s40891-019-0178-6>
5. Guido VA, Chang DK, Sweeney MA (1986) Comparison of geogrid and geotextile reinforced slabs. *Can Geotech J* 23:435–440
6. Ghosh A, Ghosh A, Bera AK (2005) Bearing capacity of square footing on pond ash reinforced with jute-geotextile. *Geotext Geomembr* 23(2):144–173
7. IS 1888–1982 Method of load test on soils. Determination of bearing capacity of soils and its settlement. Bureau of Indian Standards
8. IS 1904–1986 Code of practice for design and construction of foundations in soils: General requirements. Bureau of Indian standards
9. Latha M, Somwanshi A (2009) Bearing capacity of square footings on geosynthetic reinforced sand. *Geotext Geomembr* 27(4):281–294
10. Tavangar Y, Shooshpasha I (2016) Experimental and numerical study of bearing capacity and effect of specimen size on uniform sand with medium density, reinforced with nonwoven geotextile. *Arab J Sci Eng* 41(10):4127–4137

# **Geo-environmental Engineering**

# Mechanical Characterization of a Bio-enzyme Treated Granular Lateritic Soil for Application in Low Volume Roads



Vishal Khanna, Brundaban Beriha, and Umesh Chandra Sahoo

**Abstract** Traditionally cement, lime and fly ash or combinations of these materials have been used for stabilization of soils and granular materials. Studies on bio-enzyme stabilization suggest that it has the potential to replace these chemicals with more economical as well as environmental friendly solution for potential application in pavement structural layers of low volume roads. Use of bio-enzyme is one such sustainable method which facilitates cation exchange which in turn leads to reduction in adsorbed water on the clay particles. In this, clay (the substrate) is hydrolyzed into calcium silicate hydrate (reaction product), in the presence of bio-enzyme. The formation of reaction product depends upon the concentration of clay particles, dosage of bio-enzyme and environmental factors. In the present study, a commercial bio-enzyme, known as TerraZyme (extracted from sugar molasses) was used with and without addition of cement, to study its effect on strength and durability characteristics of a granular lateritic soil collected from eastern part of India. Effect of curing period, curing temperature and bio-enzyme dosage on the strength and durability properties of the soil was investigated. Mechanical properties of the stabilized soil were evaluated in terms of unconfined compressive strength (UCS) and flexural strength (FS). Results indicate that bio-enzyme is effective in stabilization of granular lateritic soils for application in structural layers of low volume road pavements. However, the strength of the bio-enzyme stabilized specimens under soaked condition needs to be evaluated to recommend it for areas subjected to poor drainage conditions.

**Keywords** Bio-enzyme stabilization · Unconfined compressive strength · Flexural strength · Durability · Low volume road · Lateritic soil

---

V. Khanna (✉) · B. Beriha · U. C. Sahoo  
School of Infrastructure, IIT Bhubaneswar, Bhubaneswar, India  
e-mail: [Vk30@iitbbs.ac.in](mailto:Vk30@iitbbs.ac.in)

© Springer Nature Singapore Pte Ltd. 2022  
A. K. Dey et al. (eds.), *Proceedings of the 7th Indian Young Geotechnical Engineers Conference*, Lecture Notes in Civil Engineering 195,  
[https://doi.org/10.1007/978-981-16-6456-4\\_21](https://doi.org/10.1007/978-981-16-6456-4_21)

## 1 Introduction

Granular lateritic soils are available in many parts of the world including India and usually this does not meet the specifications for aggregates used in unbound granular layers of pavements. With depletion of the sources of good quality aggregates, it has become imperative to use such marginal materials in pavement structural layers through proper stabilization. Traditionally cement, lime, fly ash have been used for stabilization of soils and granular materials [6, 9, 35]. The major advantage associated with these treatments includes cost effectiveness, readily availability and ease in application [9, 17, 22, 28]. On the flip side, usage of these materials has been found to consume huge human resources or natural resources and at times combination of duo [20, 23]. They are also found to have adverse environmental impacts including emission of huge amount of greenhouse gases, particulate matter, dust and increase in the pH of soil due to the release of OH-ions during hydration [15, 16, 21]. The mechanism of soil stabilization using lime states that lime helps in binding the silicate clay particles by changing their surface mineralogy through the cation-exchange process. This helps in decreasing the plasticity as well as moisture-holding capacity of soil which in turn gives rise to higher stability of soil [4, 24, 26]. Though lime has worked well in this aspect, the adverse effects can't be turned down. Lime carbonation, sulfate-salt reactions and caustic effects are few problems that lead to the weakening and breaking of bonds between the soils particles over the period of time [7, 18, 30]. Moreover, researchers have found that production of one metric ton of portland cement releases approximately one metric ton of carbon dioxide and the production of one metric ton of lime releases about 0.86 metric ton of carbon dioxide making it second largest contributor to humanity's production of greenhouse gas worldwide [16, 31]. At this juncture, there is an urgent need to devise novel techniques and/or substitute these materials partially with certain additives that can effectively strengthen the soil being environmentally cordial. One such newfangled technique is the stabilization of marginal soil by the enzymatic application. The present study focuses on strengthening lateritic soil using bio-enzyme independently as well as combined with cement.

### *1.1 Enzymatic Mechanism of Soil Stabilization*

Enzymes are hydrophilic organic catalyst which do not actively take part in chemical reactions but have a significant role in accelerating the rate of reaction by lowering the reaction activation energy [34] as well as by errand certain geometries in the transition state. Almost all the metabolic pathways in the living organisms are aided by various enzymes which are substrate specific and increase the rate of reaction exponentially [25]. Apart from having a significant role in the body of living organisms, enzymes are also used in the manufacturing of several industrial products. Their applications are well noticed in the brewing, baking and leather industries [19,

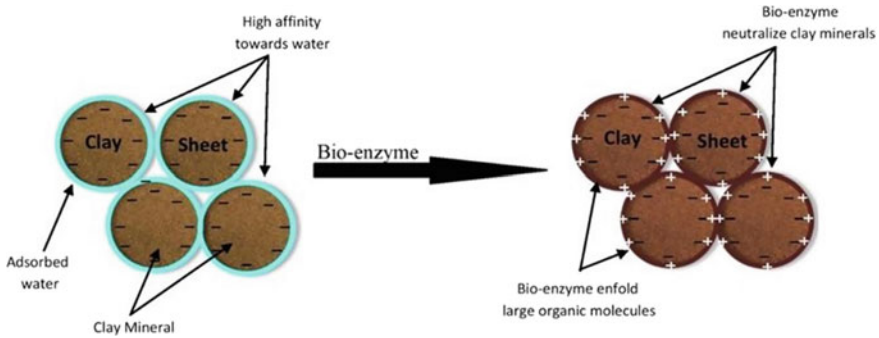


**Fig. 1** Enzymatic mechanism of soil stabilization

27, 33]. Enzymatic stabilizer due to advantages like biodegradability, non-toxicity, non-corrosive, ease in handling and ability to reduce carbon footprint have become a subject of interest to the researchers [1, 8]. Enzyme stabilizer agglomerates the clay particles by getting attached on the large organic molecules [5]. These large organic molecules get attracted to the clay minerals due to their net negative charge, which in turn neutralize the negative charge of clay minerals and thereby reducing the water affinity of the same [29, 32]. The above stated mechanism reduces, pore space, swelling and shrinkage, optimum moisture content and increases stability of the soil. In this paper an attempt has been made to evaluate the stabilization effect of bio-enzyme at different dosage, curing time and temperature on the lateritic soil. Figure 1 shows illustration of clay mineral affinity toward water, adsorbed water, enfolding of large organic molecules due to bio-enzyme leading to neutralization of clay mineral.

## 2 Materials and Methodology

### 2.1 Materials

**Lateritic Soil.** Granular lateritic soil sample was procured locally from the state of Odisha, India (20.17040N, 85.70590E). While collecting the soil samples, sufficient care was taken to obtain the representative sample from a reasonable depth after removing the vegetation and trimming the top layer of organic soils.

**Bio-enzyme.** A commercially available bio-enzyme product, named as TerraZyme (5X) was procured from M/s Avijeet Agencies, Chennai, India. Bio-enzyme is a non-flammable, non-toxic, non-corrosive, liquid enzyme manufactured from fermentation of vegetable extracts (Sugar molasses). Since, these enzymes do not directly take part in the reaction and are found to be highly substrate dependent very little quantity is requisite, making them economical for the pavement application.



## 2.2 Methodology

Procured soil samples were air dried for seven days succeeded by wet sieving to have precise particle size analysis, as per IS 2720 (Part-4). Particle size distribution curve of the soil sample is shown in Figure 2. To ensure uniform gradation for soil specimens, the grading were reproduced each time. Engineering properties of the tested soil and TerraZyme are shown in Tables 1 and 2, respectively.

Remolded samples for Unconfined Compressive Strength (UCS) on specimens of 100 mm diameter and 115 mm height, Flexural Strength (FS) on specimens of size  $75 \times 75 \times 285$  mm were prepared at maximum dry density (MDD) optimum moisture content (OMC) with varying dosage of the bio-enzyme. In order to avoid loss of moisture through evaporation, samples were wrapped with polythene for different curing periods. Four dosages the bio-enzyme (denoted as D1, D2, D3, and

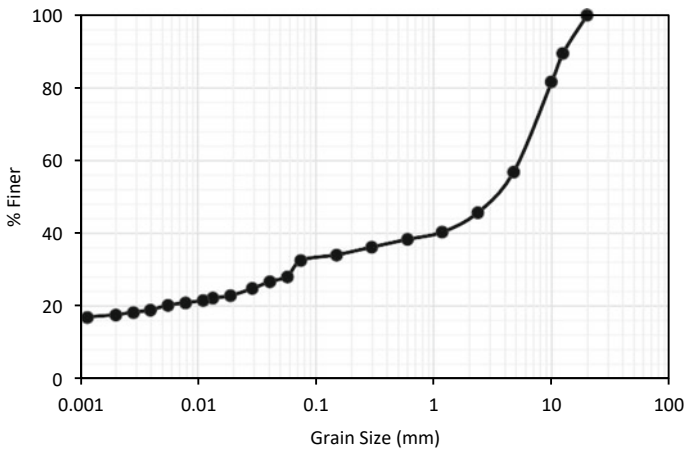


**Fig. 2** Particle size distribution of the lateritic soil

**Table 1** Engineering properties of lateritic soil

Properties	Results	Reference code
Specific gravity	2.75	IS 2720: Part III:1980
Maximum dry density (MDD)	20.01 (KN/m <sup>3</sup> )	IS 2720: Part VIII: 1980
Optimum moisture content	10.95%	IS 2720: Part VIII: 1980
Liquid limit	50	IS 2720: Part V: 1985
Plastic limit	23	IS 2720: Part V: 1985
Plasticity index (PI)	27	IS 2720: Part V: 1985
Classification	SC: clayey sand	IS 1498:1970

**Table 2** General properties of bio-enzyme

Properties	Result
Specific gravity	1–1.08
Color	Dark brown
Solubility in water	Close to 100%
Boiling point	212 F
Rate of evaporation	Same as water

D4) was considered initially to determine the optimum dosage based on the UCS value. D1, D2, D3 and D4 correspond to 0.0019, 0.0023, 0.0028 and 0.0038 percent by weight of sample respectively. The dosage that yielded highest average UCS after 1, 2, 4, 8 weeks was deemed as optimum dosage and was further considered for other tests. The detailed experimental investigation has been presented in a graphical form in Figure 3.

Cement with different dosages, i.e. 2% (C1) and 3% (C2) by weight of soil sample was used in combination with D2 and D3 enzyme dosages. Hereby, the above mentioned combination is called as enzymatic cement. UCS and FS were performed as per ASTM D1633 [2] and ASTM D1635 [3] respectively. Durability test was performed in accordance to method 1 described in IRC SP: 89 [10] for stabilized material. To study effect of temperature on the rate of gain of strength, samples were kept in incubator at 30, 40 and 50 °C with 98% humidity to avoid loss of moisture

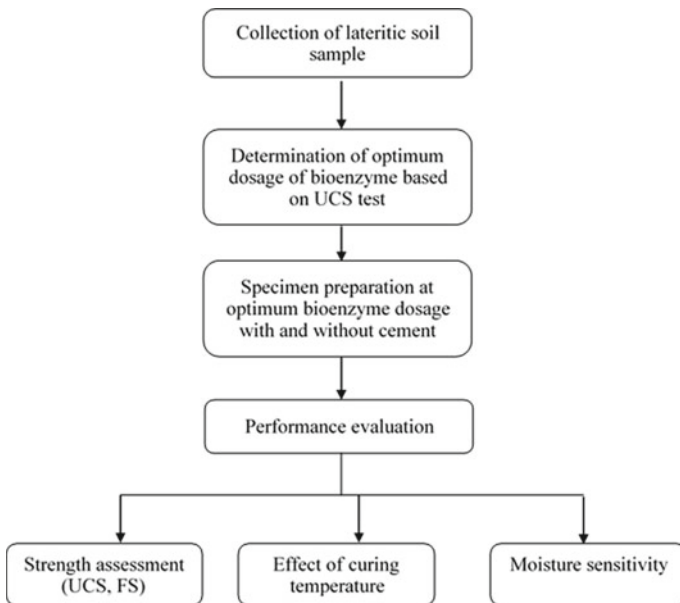


**Fig. 3** Flow chart showing the details of the experimental investigation

for 7 days. After their respective curing time, samples were removed from incubator and were tested within 60 min.

### 3 Results and Discussion

#### 3.1 UCS and FS

Figures 4 and 5 show the strength gain in terms of UCS and FS respectively, for the samples treated with varying dosages of bio-enzyme and enzymatic cement. Significant improvement in the strength with the period of curing is clearly visible in case of both bio-enzyme and enzymatic cement treated samples. The above stated improvement may be attributed to the encapsulation of clay mineral by the large

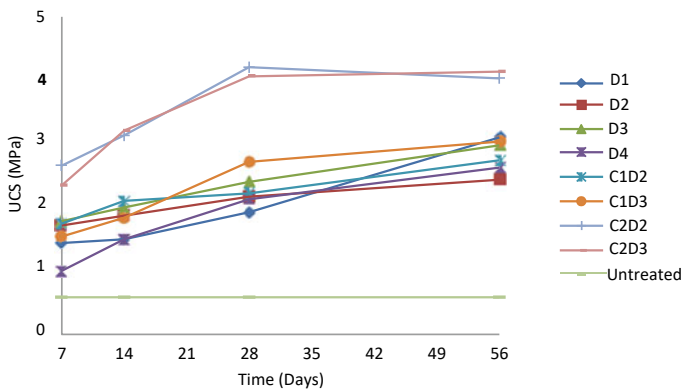


Fig. 4 UCS at different curing time of samples treated with different Bio-enzyme and enzymatic cement dosage

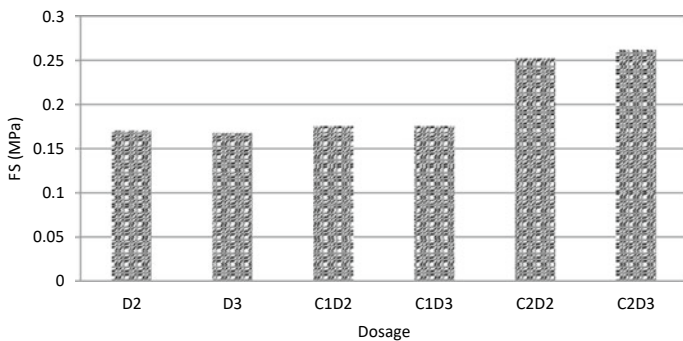
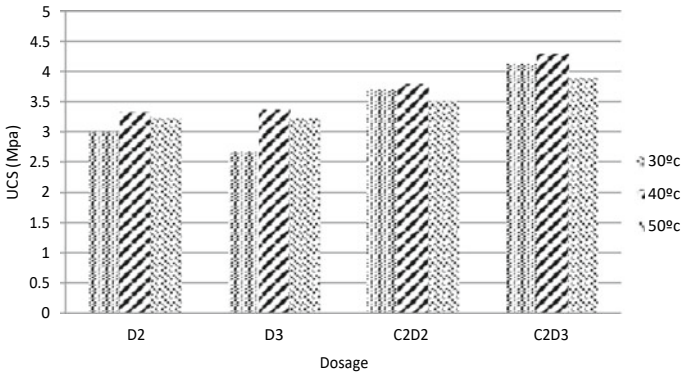


Fig. 5 Flexural strength of enzymatic stabilized soil sample after 28 days of curing



**Fig. 6** Effect of temperature on the UCS

organic molecules that reduced its affinity toward water and due to the formulation of calcium silicate hydrate gel. Aforementioned mechanism also leads to reduction in inter-particle space, void ratio, moisture holding capacity, plasticity, swelling and shrinkage making them some of the prime factors leading to strength gain [1, 8].

### 3.2 *Effect of Curing Temperature*

In order to further investigate the effect of curing temperature on the enzymatic reaction, seven day incubated samples were tested for UCS. Figure 6 shows 7 day UCS result of enzymatic treated sample incubated at various temperatures. It may be observed that at 40 °C, the rate of enzymatic reaction is better, which led to higher strength. A decrease in strength was also observed with increase in temperature beyond 40 °C. Moreover, influence can be seen greatly dependent on the initial bio-enzyme dosage, higher reduction in strength was seen in the samples treated with higher enzyme dosage. To have a better analysis microscopic studies are suggested for the future work.

### 3.3 *Moisture Sensitivity*

Specimens prepared with D3 and C2D3 dosages (three for each) were cured for 7 days and then immersed in water to check the moisture sensitivity. Initial signs of disintegration of the specimens were observed after one day of immersion. This indicates that bio-enzyme treated soils do not have enough structural integrity at 7 days of curing and therefore needs to be cured for longer durations and also efforts should be made to enhance the performance of the enzyme stabilized specimens in

presence of water, so that the same can be recommended for areas experiencing long hours of submergence.

## 4 Conclusions

Both enzyme and enzymatic cement stabilized samples resulted in strength values, which can be suitably used for sub-base and base layers of low volume road pavements. The major advantages associated with the use of enzyme treatment are ease of handling, environment friendly and reasonable price. From the laboratory tests conducted on the same soil with only 3% cement, the UCS value after 28 days was found to be around 2 MPa compared to 4.13 MPa obtained from enzymatic cement stabilization. However, it is recommended to go for stabilization only with bio-enzyme if the desired strength is achieved, else addition of cement or lime may be considered. UCS test results indicated that TerraZyme dosage of 0.0023–0.0028% by weight the soil is optimum and increase in strength with addition of cement was observed. While examining effect of curing temperature, 40 °C was found to be the most favorable temperature for the reactions to take place. However, the strength of the bio-enzyme stabilized specimens under soaked condition needs to be evaluated to recommend it for areas subjected to poor drainage conditions.

## References

1. Agarwal P, Kaur S (2014) Effect of bio-enzyme stabilization on unconfined compressive strength of expansive soil. *Int J Res Eng Technol* 3(5):30–33
2. ASTM D 1633 (2017) Standard Test Methods for compressive strength of molded soil-cement cylinders. ASTM International West Conshohocken, Pennsylvania
3. ASTM D1635/D1635M (2012) Flexural strength of soil-cement using simple beam with third-point loading. ASTM International West Conshohocken, Pennsylvania
4. Bell FG (1966) Lime stabilization of clay minerals and soils. *Eng Geol* 42(4):223–237
5. Choudalakis G, Gotsis AD (2009) Permeability of polymer/clay nanocomposites: a review. *Eur polym J* 45(4):967–984
6. Croft JB (1967) The structures of soils stabilized with cementitious agents. *Eng Geol* 2(2):63–80
7. Eujine GN, Chandrakaran S, Sankar N (2017) Accelerated subgrade stabilization using enzymatic lime technique. *J Mater Civ Eng* 29(9)
8. Greeshma C, Varun R, Sreekumaran E (2017) Supplementation of zinc induces retinoic acid-mediated differentiation of rat bone marrow mesenchymal stem cells (MSCS) in to insulin producing cells (IPCS) in-vitro. *Int J Res Ayurveda Pharm* 8 (Suppl 1)
9. Herrin M, Mitchell H (1961) Lime-soil mixtures. *Highw Res Board Bull* 304
10. IRC: SP 89 (2010) Guidelines for soil and granular material stabilization using cement, lime and fly ash. The Indian Roads Congress, New Delhi, India
11. IS: 2720 (Part III) (1980) Determination of specific gravity. Bureau of Indian Standards, New Delhi, India (Reaffirmed 2002)
12. IS: 2720 (Part V) (1985) Determination of specific liquid limit and plastic limit. Bureau of Indian Standards, New Delhi, India (Reaffirmed 2006)

13. IS: 2720 (Part VIII) (1983) Determination of water content-dry density relation using heavy compaction. Bureau of Indian Standards, New Delhi, India (Reaffirmed 2006)
14. IS: 1498. 1970 (Reaffirmed 2002) Classification and identification of soils for general engineering purposes. Bureau of Indian Standards, New Delhi, India
15. Jawad IT, Taha MR, Majeed ZH, Khan TA (2014) Soil stabilization using lime: advantages, disadvantages and proposing a potential alternative. *Res J Appl Sci, Eng Technol* 8(4):510–520
16. Joel M, Agbede IO (2010) Mechanical-cement stabilization of laterite for use as flexible pavement material. *J Mater Civ Eng* 23(2):146–152
17. Kennedy TW, Smith R, Holmgreen Jr RJ, Tahmoressi M (1987) An evaluation of lime and cement stabilization. *Transp Res Rec* 1119
18. Khalid N, Arshad MF, Mukri M, Kamarudin F, Ghani AHA (2014) California bearing ratio (CBR) value for banting soft soil subgrade stabilized using lime-pofa mixtures. *Electron J Geotech Eng* 19:155–163
19. Kirk O, Borchert TV, Fuglsang CC (2002) Industrial enzyme applications. *Curr Opin Biotechnol* 13(4):345–351
20. Kirsch K, Bell A (eds) (2012) *Ground improvement*. CRC Press
21. Leip A, Billen G, Garnier J, Grizzetti B, Lassaletta L, Reis S, Simpson D, Sutton MA, Vries W, Weiss F (2015) Impacts of European livestock production: nitrogen, sulphur, phosphorus and greenhouse gas emissions, land-use, water eutrophication and biodiversity. *Environ Res Lett* 10(11)
22. Mainfort RC (1955) Soil stabilization with resins and chemicals. *Highw Res Board Bull* 108
23. Mitchell JK (1970) In-place treatment of foundation soils. *J Soil Mech Found Div* 96(1):73–110
24. Mohammadinia A, Arulrajah A, Haghghi H, Horpibulsuk S (2017) Effect of lime stabilization on the mechanical and micro-scale properties of recycled demolition materials. *Sustain Cities Soc* 30:58–65
25. Rajoria V, Kaur S (2014) A review on stabilization of soil using Bio-enzyme. *Int J Res Eng Technol*. <https://doi.org/10.15623/IJRET.2014.0301011>
26. Rosone M, Celauro C, Ferrari A (2018) Microstructure and shear strength evolution of a lime-treated clay for use in road construction. *Int J Pavement Eng* 1–12
27. Rouau X (1993) Investigations into the effects of an enzyme preparation for baking on wheat flour dough pento-sans. *J Cereal Sci* 18(2):145–157
28. Sariosseiri F, Muhunthan B (2009) Effect of cement treatment on geotechnical properties of some Washington State soils. *Eng Geol* 104(1–2):119–125
29. Scholen DE (1995) Stabilizer mechanisms in nonstandard stabilizers. In: *Transportation research board conference proceedings* (No. 6)
30. Sherwood P (1993) Soil stabilization with cement and lime. State of the art review. Technical Report, Transport Research Laboratory, HMSO, London
31. Thangaraj R, Thenmozhi R (2013) Industrial and environmental application of high volume fly ash in concrete production. *Nat Environ Pollut Technol* 12(2):315–320
32. Tingle J, Newman J, Larson S, Weiss C, Rushing J (2007) Stabilization mechanisms of nontraditional additives. *Trans Res Rec: J Transp Res Board* 1989:59–67
33. Van Der Maarel MJ, Van der Veen B, Uitdehaag JC, Leemhuis H, Dijkhuizen L (2002) Properties and applications of starch-converting enzymes of the  $\alpha$ -amylase family. *J Biotechnol* 94(2):137–155
34. Venkatasubramanian C, Dhinakaran G (2011) Effect of bio-enzymatic soil stabilization on unconfined compressive strength and California bearing ratio. *J Eng Appl Sci* 6(5):295–298
35. Wang JWH, Mateos M, Davidson DT (1963) Comparative effects of hydraulic, calcitic and dolomitic limes and cement in soil stabilization. National Research Council. *Highw Res Rec Bull* 59:42–54

# Study of Municipal Solid Waste in Road Embankment



Parul Rawat and Supriya Mohanty

**Abstract** In developing country like India, waste generation and management have become a serious problem. The volume of waste projected to increase from 64 to 72 million tons at present to nearly twice by 2031. Improper disposal of these wastes causes adverse effect on the environment. To reduce their impact on natural ground these have been under the utilization process in the field of civil engineering such as; road material, cement, and other applications. In the present study, an attempt has been made to investigate the use of municipal solid waste (MSW) as a fill material for road embankment. A comparative study of embankment filled with MSW and natural soil over soft subsoil has been done. The numerical modeling of the embankment and foundation soil system has been carried out using 2-dimensional finite element software PLAXIS 2D. The numerical analysis of embankment has been performed under both static and seismic loading condition. The Chamoli earthquake (Mw 6.4) has been considered as input motion for the seismic analysis of embankment foundation system. In this study, the effective use of municipal solid waste for road embankment construction is presented.

**Keywords** Municipal solid waste · Finite element method · PLAXIS 2D · Embankment

## 1 Introduction

Slope instability in road embankment is a very common phenomenon, which causes ultimate failure of the embankment. In general the embankment fill comprise of different soil mixes like clayey sand, loamy sand, silty clay etc. Due to different factors like climate change, water table variation, swelling and shrinkage, varying

---

P. Rawat (✉) · S. Mohanty  
Department of Civil Engineering, Indian Institute of Technology (BHU), Varanasi, Uttar Pradesh  
221005, India  
e-mail: [parulrawat.rs.civ18@itbhu.ac.in](mailto:parulrawat.rs.civ18@itbhu.ac.in)

© Springer Nature Singapore Pte Ltd. 2022  
A. K. Dey et al. (eds.), *Proceedings of the 7th Indian Young Geotechnical Engineers Conference*, Lecture Notes in Civil Engineering 195,  
[https://doi.org/10.1007/978-981-16-6456-4\\_22](https://doi.org/10.1007/978-981-16-6456-4_22)

load and other parameters of soils underneath the structure like pavement or embankment cause the settlement. This causes cracking and undulations on the surface ultimately causing difficult driving condition on highways.

Countries all over the world are dealing with the problem of disposal of Municipal Solid Waste (MSW) and easiest solution is to dispose off the waste in landfill sites. Indian MSW generally consists of house hold wastes, industrial wastes, agricultural wastes, medical wastes etc., which makes MSW highly non homogeneous and variable in its content. Working with MSW is very difficult because of dependency of test results on the source site, particle size, age, and content of the waste. The particle size of MSW is very large as compared to the laboratory equipments, so segregation of MSW is required before using it as a fill material. In addition, the volume of solid waste is increasing day by day and is projected to increase from 64 to 72 million tons at present to nearly twice by 2031 [1]. Dixon and Jones [5] studied the effect of different parameters like compressibility, shear strength, lateral stiffness, in-situ horizontal stress, and hydraulic conductivity on landfill lining system design and performance. Havangi et al. [6] concluded MSW to be a coarse grained material with 70% particles to be retained on 75 micron IS sieve and recommended about 65–75% segregated waste can be used for embankment construction. Naveen et al. [10] showed damping ratio of dumped waste varies from 14 to 32% and for dry waste it varies from 14 to 18%. Ramaiah and Ramana [13] conducted cone penetration testing with pore pressure measurement (CPTU) on Ghazipur land fill site, Delhi and compared the results with the reported data from other landfill sites. They noticed that, the average tip resistance of the site varied from 1.5 to 2 MPa (upto 5 m) and 3–4 MPa from 5 to 13 m.

Numerical modeling of highway embankment by using Plaxis 2D on different embankment fills has been done by many researchers. There are study which shows slope stability of embankment filled with different soils on Plaxis 2D and gives factor of safety for different fill material [9]. Wang and Miao [14] proposed a light weight fill material for embankment using cement-treated Yang-zi river sand and expanded polystyrene (EPS) beads. Numerical analysis by PlaxisV8 concluded that, settlement of new light weight embankment was less than the general lime stabilized soil embankment. Analysis for settlement and factor of safety on fly ash fill embankment with geogrids under static and seismic loading conditions was conducted and parameters like maximum acceleration, vertical and horizontal displacement were found to be least at crest, toe, and bottom of embankment [7, 8]. There are few on Plaxis 2D to simulate dynamic traffic loading on embankment filled with different soil models [4]. Numerical simulation on geosynthetic reinforced embankment over locally weak zones was also conducted [3]. They analyzed the road embankment with foundation soil of high compressibility, low bearing capacity, and locally weak zones of limited extent. Settlement analysis of the embankment was carried out. The results show improvement in settlement due to the combination of the membrane strength effect of the geosynthetic and the arching effect within the embankment fill. Aseeja [2] analyzed the consolidation behavior of embankment on soft soil and compared the results with field data. In addition, they performed a parametric study to check the effectiveness of ground improvement techniques (preloading, stone columns and



prefabricated vertical drain). They found that, PVD shows better results by fast consolidation rate and minimum pore water pressure generation.

There are various studies have been done for MSW landfill stabilization but, very limited work has been done on utilization of MSW as a fill material. In the present study, a comparison has been made between a normal soil fill and MSW as a fill material for embankment under both static and seismic loading conditions.

## 2 Numerical Simulation of Road Embankment

For numerical modeling of road embankment, Plaxis 2D 2018 [11, 12] version has been used which is a finite element program for geotechnical applications. 15 noded triangular elements are used for the discretization of the embankment as well as foundation soil. Because of the symmetry of the problem only half part of the embankment is considered for numerical modeling. The width of the crest of the embankment is about 8.5 m and height is of 5 m with side slope of 2H: 1 V. The optimum finite element mesh of the embankment section obtained after convergence analysis (see Fig. 1). Staged construction has been adopted for the construction of embankment with two equal parts. Consolidation period of 60 days are allowed for the dissipation of excess pore water pressure. Water table is considered to be at 5 m below the ground surface. Analysis has been carried out for both static and seismic conditions under Chamoli earthquake motion.

### 2.1 Properties of Subsoil

The subsoil layer considered upto 15 m depth consisting of 3 layered soils. Thickness of each layer as follows:

Subsoil layer 1(sand) = 5 m

Subsoil layer 2(clay) = 5 m

Subsoil layer 3(sand) = 5 m.

**Fig. 1** Finite element mesh of the road embankment

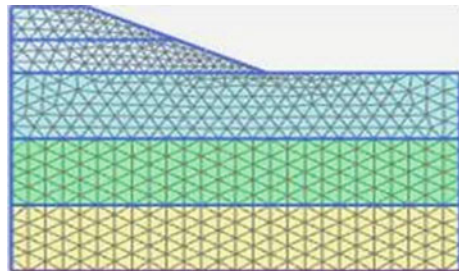


**Table 1** Parameters of foundation soil

Parameter	Foundation soil	
	Clay	Sand
Material model	Soft soil	Hardening soil
Material behavior	Undrained (A)	Drained
$\gamma_{\text{Dry}}$ (kN/m <sup>3</sup> )	15	17
$\gamma_{\text{Sat}}$ (kN/m <sup>3</sup> )	18	20
$c$ (kN/m <sup>2</sup> )	1	0
$\phi$ (°)	25	33
$e_o$	1	0.5
$k$ (m/day)	0.04752	7.128
Damping ratio	12.74	10

Properties of foundation soil are listed in Table 1.

## 2.2 Properties of Fill Material

Two different fill materials have been considered for the embankment construction. One is normal soil fill and other one is MSW fill. The properties of fill materials are listed in Table 2. The general properties of MSW in this study are taken from the Ghazipur landfill site, East Delhi [6]. The stiffness is computed with the correlations of average resistance of the same site with SPT values [13].

**Table 2** Parameters of the embankment fill material

Parameter	Embankment fill material	
	Soil	MSW
Material model	Hardening soil	Mohr-columb
material behavior	Drained	Drained
$\gamma_{\text{Dry}}$ (kN/m <sup>3</sup> )	16	16
$\gamma_{\text{Sat}}$ (kN/m <sup>3</sup> )	19	18.25
$E$ (kN/m <sup>2</sup> )	2.5E4	19,122.96
$c$ (kN/m <sup>2</sup> )	1	25
$\phi$ (°)	30	28
$e_o$	0.5	0.8
$k$ (m/day)	3.499	1.0454E-3
Damping ratio	10	15

### 2.3 Input Motion

For seismic analysis of the road embankment, Chamoli earthquake (Mw: 6.4) is considered as input motion. The Peak Ground Acceleration (PGA) of the input motion is about  $2 \text{ m/s}^2$  at 5 s and the total time duration of the motion is 25.4 s (Fig. 2).

## 3 Results and Discussions

The results of the numerical analysis summarized comparison between the two different fill materials based on settlement, acceleration, excess pore water pressure and stresses under static, and seismic loading conditions. Table 3 shows the comparative results between the soil and MSW fill embankment.

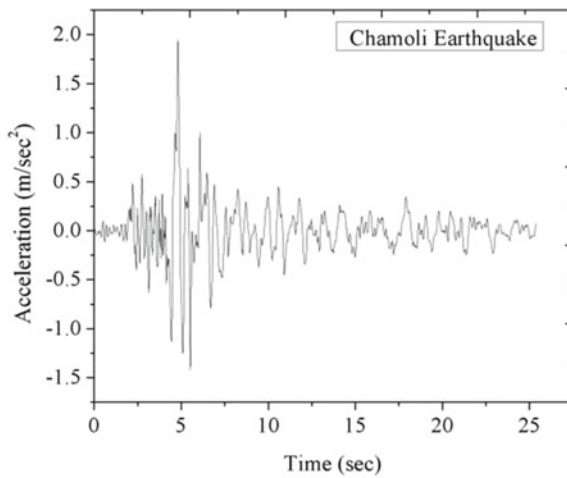


Fig. 2 Chamoli earthquake input motion

Table 3 Comparisons of results between soil and MSW fill embankment

	Deformation (m)		$\sigma'(yy)$ (kN/m <sup>2</sup> )		P (excess) (kN/m <sup>2</sup> )		$a_x$ (m/s <sup>2</sup> )
	Static	Seismic	Static	Seismic	Static	Seismic	Seismic
Soil	0.1516	0.3263	- 218.2	- 239.6	0.8684	38.51	0.6733
MSW	0.1444	0.2362	- 216.9	- 234.9	0.9798	39.52	0.4198

### 3.1 Deformation Variation

At the end of static analysis maximum horizontal displacement ( $U_x$ ) for soil and MSW fill embankment are comes out to be 0.02361 m and 0.02005 m, respectively, which shows more deformation for soil embankment. At the end of seismic analysis, the variation of horizontal displacement ( $U_x$ ) with depth at different horizontal distances ( $X = 0, 9$  and  $14.25$  m) for both soil and MSW embankment are presented in Figs. 3 and 4. The figures show that, horizontal displacement is minimum at center ( $X = 0$  m) at a depth of 5 m where as it increases toward the toe for both the cases.

Fig. 3  $U_x$  variation with depth for soil

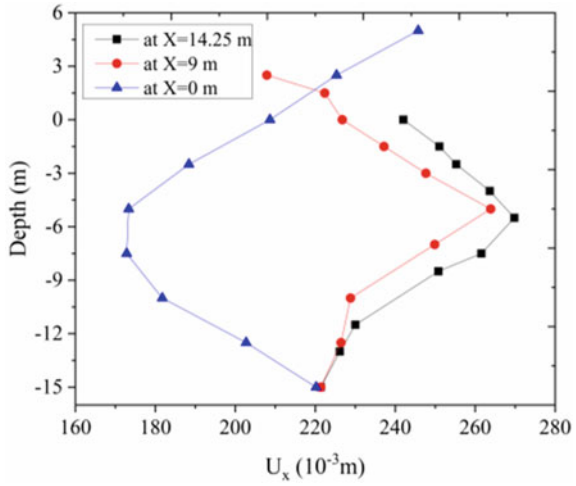
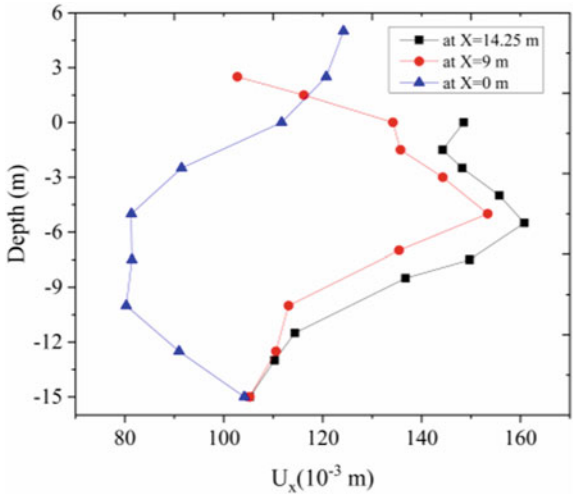


Fig. 4  $U_x$  variation with depth for MSW



Vertical displacement ( $U_y$ ) at the end of static analysis shows maximum values of 0.1516 m and 0.1444 m for soil and MSW filled embankment, respectively. Figures 5 and 6 show the variation of vertical displacement with depth at the end of seismic analysis for soil and MSW filled embankment. Vertical displacement for both fill material goes on decreasing toward the toe of the embankment due to decrease in the overburden pressure.

The maximum resultant displacement  $|U|$  after the static analysis gives values 0.1516 m and 0.1444 m for soil and MSW filled embankment, respectively. Similarly, at the end of seismic analysis, it increases to 0.3263 m and 0.2362 m, respectively, for soil and MSW fill embankment. Figures 7 and 8 show the variation of resultant

Fig. 5  $U_y$  variation with depth for soil

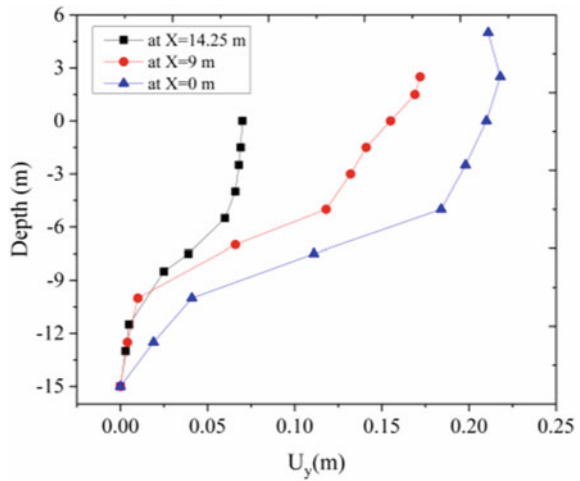
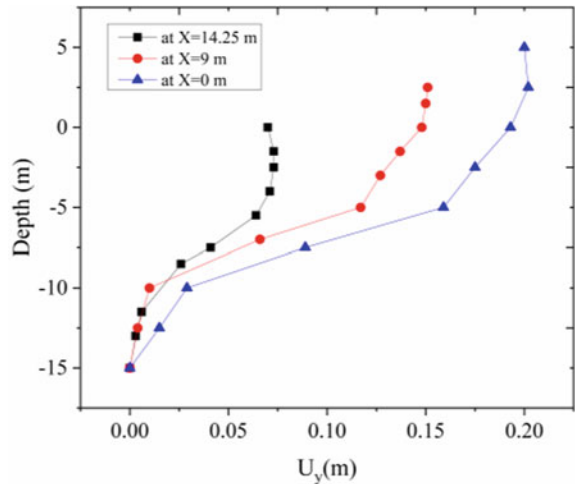
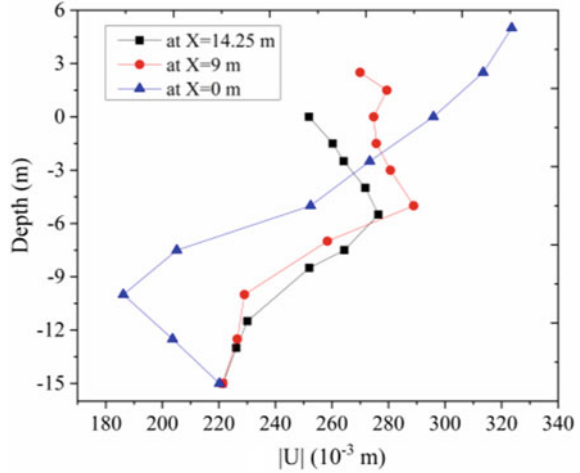


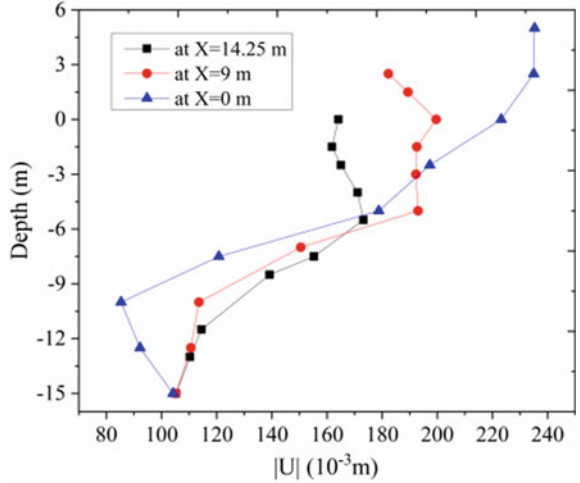
Fig. 6  $U_y$  variation with depth for MSW



**Fig. 7** Variation of  $|U|$  with depth for soil



**Fig. 8** Variation of  $|U|$  with depth for MSW



displacement  $|U|$  with the depth with varying horizontal distances ( $X = 0, 9$  and  $14.25$  m) for both soil and MSW fill embankments.

### 3.2 Acceleration Variation

At the end of seismic analysis, the absolute maximum horizontal acceleration is observed at different locations of the embankment. The variation of horizontal acceleration with depth is shown in Figs. 9 and 10 at different horizontal distances ( $X =$

**Fig. 9** Variation of  $a_x$  with depth for soil

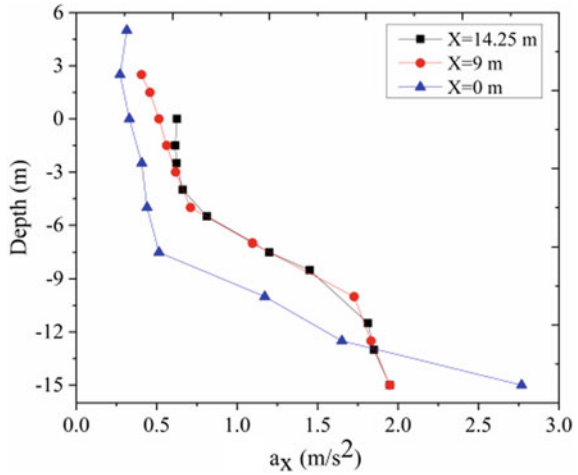
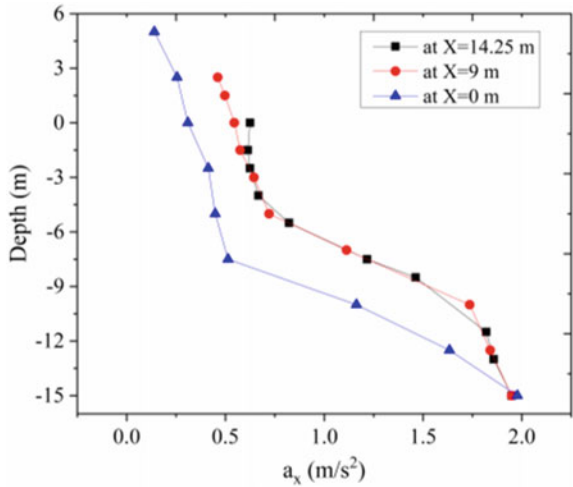


**Fig. 10** Variation of  $a_x$  with depth for MSW



0, 9 and 14.25 m) for both soil and MSW fill embankments. Horizontal acceleration increases as the depth and horizontal distance from the center of embankment increases.

### 3.3 Excess Pore Water Pressure Variation

At the end of static analysis, the excess pore water pressure is negligible and maximum values reaches upto 0.8684 kN/m<sup>2</sup> and 0.9798 kN/m<sup>2</sup> for soil and MSW

fill embankment, respectively. At the end of seismic analysis, the excess pore water pressure increases to the value of 38.51 kN/m<sup>2</sup> and 39.52 kN/m<sup>2</sup> for soil and MSW fill embankment, respectively. Figures 11 and 12 show typical variation of excess pore water pressure with depth with varying horizontal distances ( $X = 0, 9$  and  $14.25$  m). The maximum excess pore water is developed in between the foundation soil in clay layer.

**Fig.11** Variation of  $P_{\text{excess}}$  with depth for soil

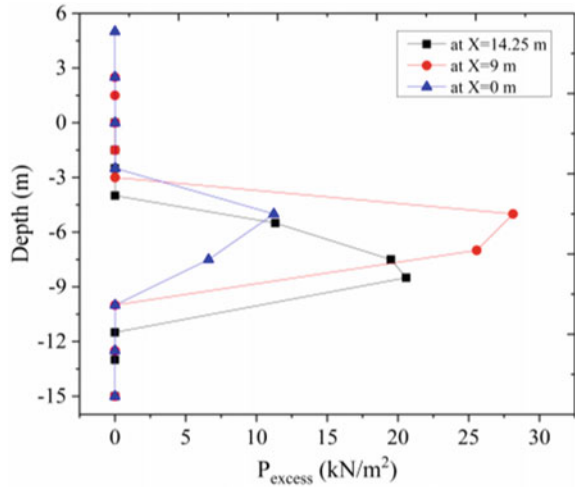
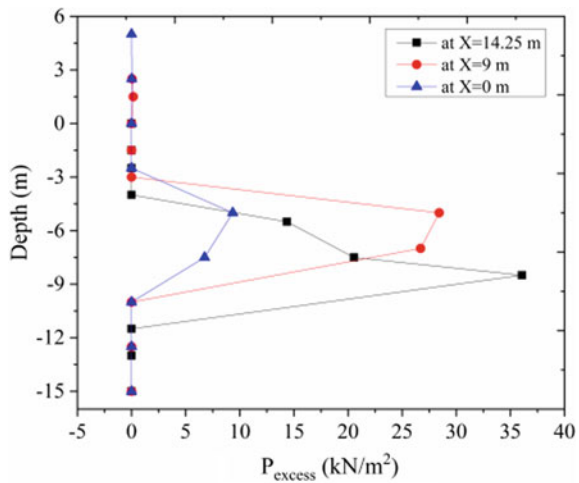


**Fig. 12** Variation of  $P_{\text{excess}}$  with depth for MSW





### 3.4 Effective Vertical Stress Variation

In static case, the maximum effective vertical stress is observed to be  $-218.2 \text{ kN/m}^2$  and  $-216.9 \text{ kN/m}^2$  for soil and MSW fill embankment, respectively, which increases to  $-239.6 \text{ kN/m}^2$  and  $-234.9 \text{ kN/m}^2$ , respectively for the seismic loading condition. Figures 13, 14, 15 and 16 show the contour fill of effective vertical stress in embankment and foundation soil after static and seismic analysis.

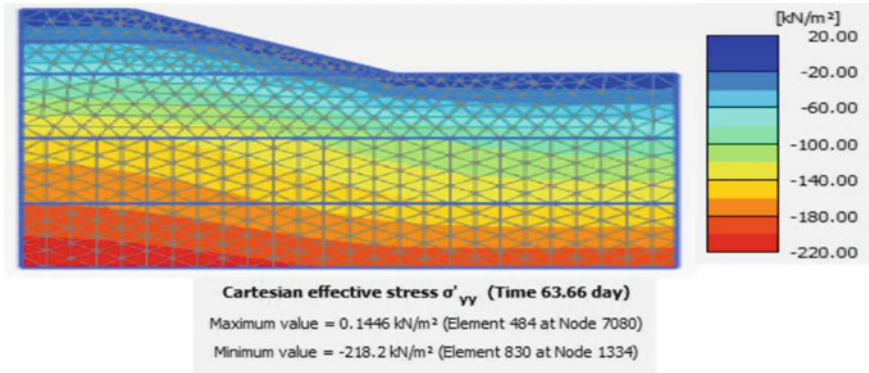


Fig. 13 Contour plot of effective vertical stress for embankment filled with soil (static analysis)

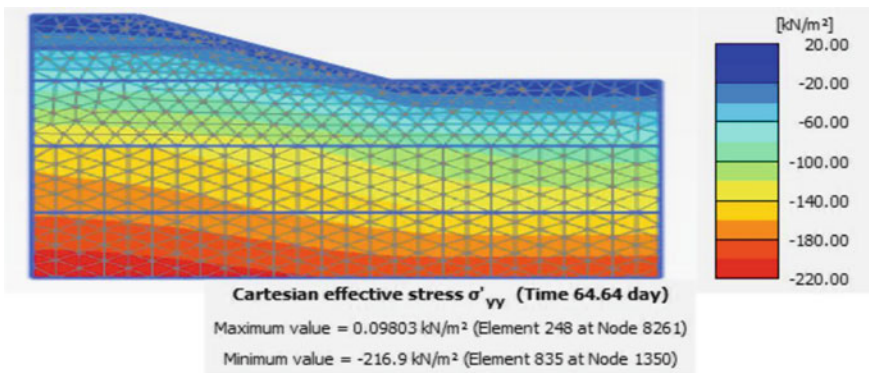
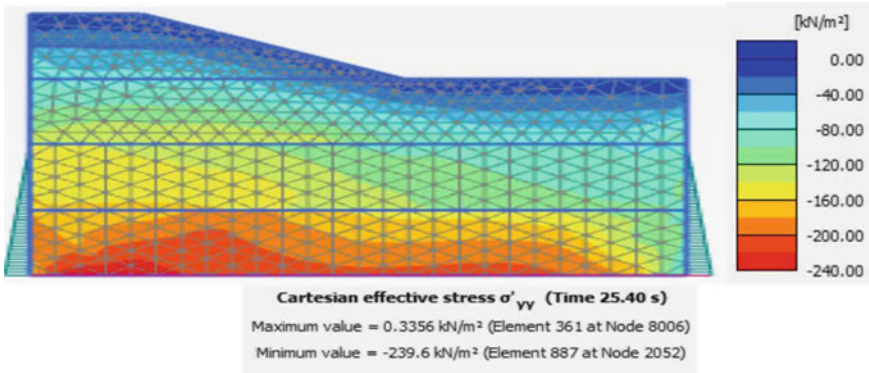
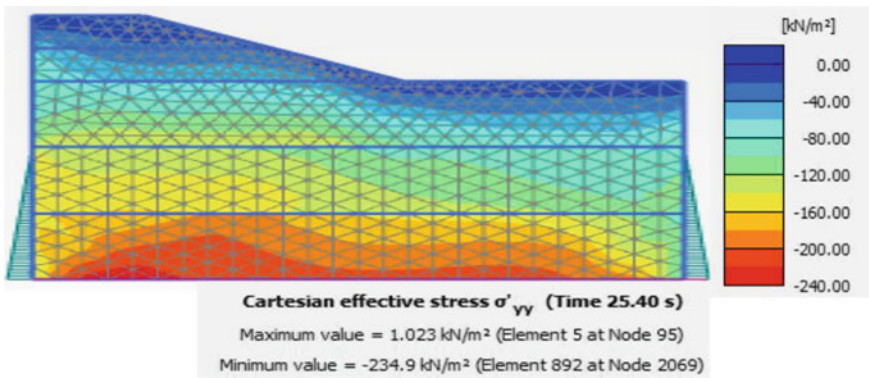


Fig. 14 Contour plot of effective vertical stress for embankment filled with MSW (static analysis)



**Fig. 15** Contour plot of effective vertical stress for embankment filled with soil (seismic analysis)



**Fig. 16** Contour plot of effective vertical stress for embankment filled with MSW (seismic analysis)

## 4 Conclusions

Following conclusions can be drawn from the results of the numerical analysis:

- MSW fill embankment shows less deformation both for static as well as seismic analysis as compared to that of soil fill embankment.
- Horizontal displacements are found to be more toward the sloping side where as vertical displacements are more at the center of the embankment.
- Horizontal acceleration increases with the increase in depth and found to be more at the base of foundation soil. Also, it is more toward the sloping side and shows less value for MSW fill as compared to the soil fill embankment.
- The maximum excess pore water pressure is observed in the clay layer during the seismic loading condition.
- The effective vertical stress increases with depth and found maximum at the base for both the cases.

The results of the numerical analysis show that MSW can be considered as a fill material for road embankment as it shows better results compared to the normal soil fill embankment. However, MSW is widely heterogeneous material and there are no proper codes and methods for characterization of MSW. Hence, further research is required in this field.

## References

1. Ahluwalia IJ, Patel U (2018) Solid waste management in India an assessment of resource recovery and environmental impact. Indian Council for Research on International Economic Relation (CRIER). Working Paper No. 356, pp 1–42
2. Aseeja PK (2016) Modelling consolidation behavior of embankment using Plaxis. *Int J Sci Eng Res* 7(4):70–75
3. Benmebarek S, Berrabah F, Benmebarek N (2015) Effect of geosynthetic reinforced embankment on locally weak zones by numerical approach. *Comput Geotech* 65:115–125
4. Camacho-Tauta J, Molina F, Reyes-Ortiza O (2015) Simulation of traffic loading on an embankment by the finite element method with different soil models. *Deformation Charact Geomater*, 737–744. <https://doi.org/10.3233/978-1-61499-601-9-737>
5. Dixon N, Jones DRV (2005) Engineering properties of municipal solid waste. *Geotext Geomem-br* 23:205–233
6. Havangi VG, Sinha AK, Parvathi GS, Chandra S (2017) Municipal solid waste in road embankment construction—a case study. *J Indian Road Congr*, Paper 669:79–90
7. Khan SA, Abbas SM (2014) Numerical modelling of highway embankment by different ground improvement techniques. *Int J Innov Res Adv Eng* 1(10):350–356
8. Khan SA, Abbas SM (2014) Seismic stability analysis of highway embankment by different ground modification techniques. *Int J Innov Res Adv Eng* 1(10):54–64
9. Laxminarayana A, Naresh M (2017) Analysis of embankment with different fill materials using Plaxis -2D. *Int J Eng Trends Technol* 45(6):280–284
10. Naveen BP, Sitharam TG, Sivapullaiah PV (2014) Evaluating the dynamic characteristics of municipal solid waste for geotechnical purpose. *Curr Adv Civ Eng* 2(1):28–34
11. Plaxis BV (2018) Plaxis 2D reference manual. The Netherlands
12. Plaxis BV (2018) Plaxis material models manual. The Netherlands
13. Ramaiah BJ, Ramana GV (2014) CPTu at a municipal solid waste site in Delhi, India. In: *Proceedings 3rd international symposium on cone penetration testing*, Las Vegas, Nevada, USA. pp 1083–1091
14. Wang F, Miao L (2009) A proposed lightweight fill for embankments using cement-treated Yangzi River sand and expanded polystyrene (EPS) beads. *Bull Eng Geol Environ* 68:517–524

# Hydraulic Conductivity of Steel Slag and Potential Influence of Leaching on Groundwater Alkalinity



Rituraj Devrani, Anant Aishwarya Dubey, K. Ravi, and Clint Thankachan

**Abstract** Steel slag is a coarse industrial solid waste obtained from steel manufacturing industries as by-product. The steel slag acquired from Tata Steel, Jamshedpur, India is investigated in this study. Recent studies have reported its potential for utilization as coarse aggregate in asphalt mixtures, embankments, landfills and sub-base material of highways & railways. This study emphasis on the assessment of saturated hydraulic conductivity with different proportions of sand mixtures and alkalinity exchange behaviour of steel slag through water outflow test. The steel slag obtained is observed to be heavy granular material and highly alkaline in nature. This study reports decrease in the hydraulic conductivity of sand from  $(15.70 \pm 0.66) \times 10^{-5}$  m/s to  $(4.505 \pm 0.17) \times 10^{-5}$  m/s with addition of 25% by weight of steel slag. This study also recommends for chemical treatment of the steel slag prior to its utilization in geotechnical applications as it may cause drastic change in the alkalinity of ground water.

**Keywords** Steel slag · Industrial waste · Hydraulic conductivity · Alkaline ex-change behaviour · Leaching

## 1 Introduction

Over the last few years, the functions and improvements in process technologies have led to a significant reduction in the volume of industrial waste generated. Also, the utilization of these by-products led us to the significant reduction of stress on the environment. The production of granulated slag is close to 10 million tonnes per annum from its existing steel plants [6]. Steel slag is the solid industrial waste produced during the separation of molten steel from impurities in steel-making furnaces during the production of steel. The slag is a complex solution of silicates and

---

R. Devrani (✉) · A. A. Dubey · K. Ravi  
Indian Institute of Technology, Guwahati, Guwahati, India

C. Thankachan  
Viswajyothi College of Engineering and Technology, Ernakulam, Kerala, India

oxides that solidifies upon cooling. The generation of steel slag will remain inevitable and emphasis on its recycling will remain one of the major concerns. These granular industrial waste materials may be utilized in large quantity in geotechnical applications as geo-material, however the major concern in its utilization as geo-material, is the environmental impact. Therefore, an efficient method of utilization of slag is necessary for sustainable development.

Several studies recommend utilization of steel slag in various engineering applications. Kandhal and Hoffman [11] incorporated the steel slag aggregates into the asphalt concrete. Chesner et al. [4] recommended to avoid any contamination of slag aggregate produced for its efficient utilization for sub-grade or sub-base construction in highway and pavement construction. Poh et al. [15] investigated the potential of utilization of steel slag in soil stabilization and it was reported that use of Blast oxygen steel (BOS) slag improves the strength, durability and reduces in the linear expansion. This study also suggested that a high percentage (15–20 %) of BOS slag and a long curing period are required for significant improvement. Asi et al. [2] recommended in their study that replacement of 75 % of limestone coarse aggregate with Steel Slag Aggregate (SSA) improved the mechanical properties of the asphalt mixes and suggested replacement of 25% Steel Slag Aggregate (SSA). Montenegro et al. [13] studied the expansive behaviour of ladle furnace slag in the construction of embankments. Anastasiou et al. [1] proposed the utilization of steel slag, fly ash in production of concrete and suggested the use of concrete produced for low-grade applications. Aziz et al. [3] indicated that the steel slag has hydrophobic property which provides good adhesion with bitumen binder and may help in resisting against stripping and other defects of roads. The steel slags are also employed as aggregates in road and pavement mixtures. Oluwasola et al. [14] introduced the electric arc furnace slag and copper mine tailings in asphalt mixes for road construction and observed increase in the performance of asphalt mixtures. Yildirim and Prezzi [16] reported that the utilization of both fresh and aged basic oxygen furnace (BOF) steel slag manifested superior strength and stiffness characteristics to conventional friction materials. Furthermore, the long-term swelling of fresh and aged basic oxygen furnace (BOF) steel slag when exposed to water, is due to the presence of free lime and magnesia. The application of fresh and aged steel slag as a railway ballast material was investigated by Koh et al. [12] and the study suggested that it can be used in place of natural crushed stone aggregate. Dubey et al. [5] discussed about the calcium leaching potential and high alkalinity behaviour of steel slag. The utilization of steel slag in geotechnical engineering applications without evaluation of its environmental aspects brings a concern for the sub-surface environment. Limited studies have been done on the leaching potential of steel slag after its utilization with soil for geotechnical applications. This study investigates the basic geotechnical characterization, alkalinity exchange behaviour and hydraulic conductivity behaviour of steel slag.

## 2 Materials and Methods

The steel slag used in the study was acquired from TATA Steel Plant, located in Jamshedpur, Jharkhand, India and the sand utilized in the study was Brahmaputra river shore sand. The study includes the geotechnical characterization such as grain size distribution analysis and classified according to Unified soil classification system (USCS). The specific gravity of steel slag was evaluated using kerosene instead of water because kerosene is bipolar in nature and using water may give deceptive observations. The relative density test was performed to determine the maximum and minimum density of steel slag. After that, the influence on the hydraulic behaviour of the sand with addition of different proportion of slag was examined using Falling head permeability test. The samples for the tests were prepared using quartering and coning method. All the tests were performed on triplicate samples. The specific gravity, grain size distribution, relative density and the falling permeability test were performed as per bureau of Indian Standards IS 2720 (Part 3/Sec 2)-1980; IS 2720 (Part 4)-1985; IS 2720 (Part 17)-1986; IS 2720 (Part 14)-1983 respectively. This study also assessed the alkalinity exchange behaviour of the water leaching from the steel slag as during the rainy season, the rainwater may percolate through non-engineered openly dumped steel slag to sub-surface and influence the alkalinity of the groundwater. The study was performed by collecting and examining the change in the alkaline behaviour of inflow and outflow of the water. Figure 1 illustrates the setup for alkalinity exchange behaviour of inflow and outflow study of water. The distilled water having pH of 6.8 was used in this test.

**Fig. 1** Alkalinity exchange behaviour setup of inflow and outflow of water

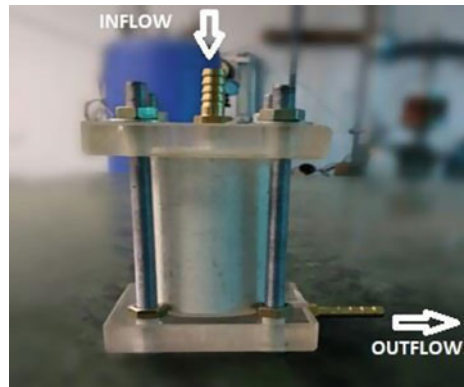


**Fig. 2** Grain size distribution curves of steel slag and sand

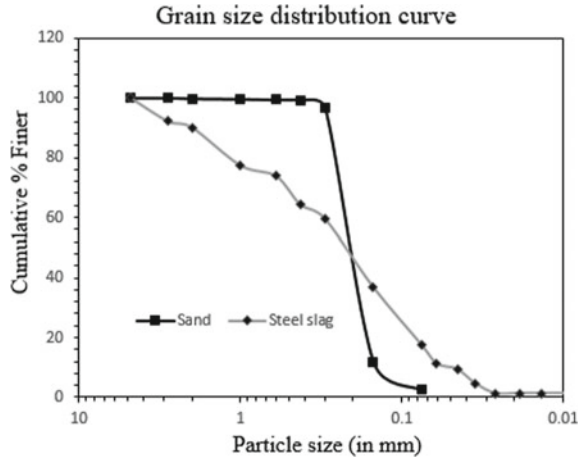


**Table 1** Grain size distribution measures of steel slag and sand

Gradation measures	Steel slag	Sand
Effective size, D <sub>10</sub> (mm)	0.050	0.136
D <sub>30</sub> (mm)	0.123	0.182
D <sub>60</sub> (mm)	0.308	0.235
Coefficient of uniformity (Cu)	6.114	1.717
Coefficient of curvature (Cc)	0.982	1.032

### 3 Results

#### 3.1 Grain Size Distribution Analysis

The grain size distribution curve of the Brahmaputra River shore sand and steel slag is shown in Figure 2. Steel slag was classified as Silty sand (SM) according to Unified Soil Classification System (USCS) as per ASTM D422-63, obtained is presented in Table 1. The grain size distribution based on dry sieve analysis classified Brahmaputra river shore sand as Poorly graded sand (SP) as per USCS with 2.4% of fine content. The gradation measures of sand are also presented in Table 1.

#### 3.2 Specific Gravity

The specific gravity of the steel slag was  $3.50 \pm 0.021$ . Whereas, the specific gravity of Brahmaputra river shore sand was obtained as  $2.75 \pm 0.015$ .



### 3.3 Relative Density

The density index of both sand and steel slag was determined. The maximum dry unit weight ( $\gamma_{d\_max}$ ) and minimum dry unit weight ( $\gamma_{d\_min}$ ) for sand were observed as 15.37 and 13.41 KN/m<sup>3</sup>. The Maximum dry unit weight ( $\gamma_{d\_max}$ ) and minimum dry unit weight ( $\gamma_{d\_min}$ ) for steel slag were obtained as 20.05 KN/m<sup>3</sup> and 16.07 KN/m<sup>3</sup>.

### 3.4 Saturated Hydraulic Conductivity

The saturated hydraulic conductivity of soil and steel slag are shown in Fig. 3. It also represents the rate of change in permeability with the incorporation of different ratio of steel slag with the sand. The saturated hydraulic conductivity of the bare sand was found as  $(15.70 \pm 0.66) \times 10^{-5}$  m/sec and of bare steel slag as  $(10.80 \pm 0.10) \times 10^{-5}$  m/s. The hydraulic conductivity was found to be decreased to  $(4.50 \pm 0.17) \times 10^{-5}$  m/s with the addition of steel slag to 25% by weight. The hydraulic conductivity decreases with the increase in the proportion of steel slag. The proportion of steel slag is added in small quantity during the preparation of mould for performing the test, in order to maintain the relative density of the sand-steel slag mixture. The hydraulic conductivity may be reduced due to the adjustment fine particles of steel slag in between the pores of sand particles.

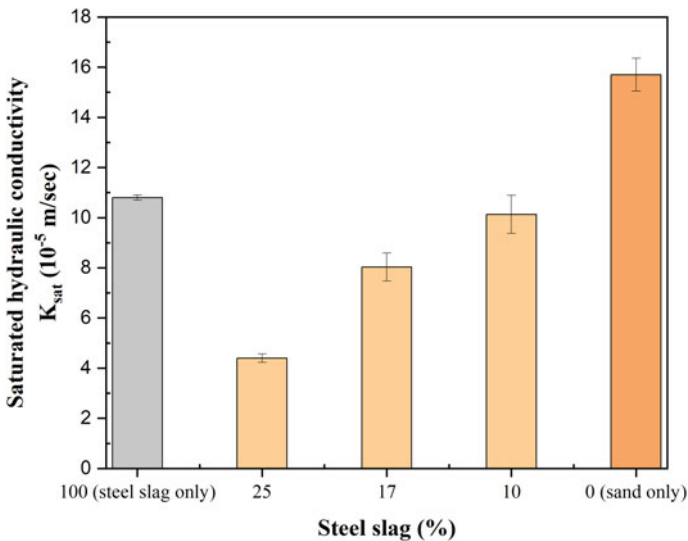


Fig. 3 Saturated hydraulic conductivity of sand, steel slag and their mixtures



### 3.5 Alkalinity Exchange Behaviour

It was observed that the pH of the distilled water (initial pH = 6.8) in inflow changes to (pH=11.84) in outflow through a sand column of 10 cm (diameter 3.8 cm). The results indicated that the utilization of steel slag in geotechnical applications without prior treatment may harm the ground water sources and nearby aquatic lives.

## 4 Conclusion

Steel slag is a coarse industrial waste obtained from steel production industries. The utilization of industrial granular waste in engineering applications aims to reduce the dumping of industrial waste in the geo-environment. The investigation of any industrial solid waste in environmental aspects is vital for sustainable development. This study helps to understand the alkalinity exchange capacity of steel slag due to leaching on the ground water pH. The drastic change in the alkalinity of ground water may affect the geo-environment adversely. Some of the major conclusions drawn from this study are reported as following-

- The hydraulic conductivity of the sand incorporated with different proportion of steel slag decreased with increase in steel slag proportion. This study also suggests that there are other factors which affect the hydraulic conductivity of the soil such as morphology of slag particles.
- The steel slag was observed to have significant alkaline exchange capacity as it changed the pH of the leaching water to highly alkaline (11.84) from neutral pH (6.8). The leaching of water through steel slag may affect the ground water sources adversely. This study suggests the treatment of steel slag prior to its use in the geotechnical applications such as in sub-base, sub-grade or in embankment construction.

The utilization of steel slag in the geotechnical applications must be considered as a sensitive issue as it can impact the geo-environment negatively. So, further investigation on the geo-environmental aspects of steel slag should be evaluated for better utility of slag as alternative geo-material.

**Acknowledgements** The authors would like to thank Abhinav Srivastava, Former researcher, Tata steel, Jamshedpur for providing the steel slag.

## References

1. Anastasiou E, Filikas KG, Stefanidou M (2014) Utilization of fine recycled aggregates in concrete with fly ash and steel slag. *Constr Build Mater* 50:154–161

2. Asi IM, Qasrawi HY, Shalabi FI (2007) Use of steel slag aggregate in asphalt concrete mixes. *Can J Civ Eng* 34(8):902–911
3. Aziz MMA, Hainin MR, Yaacob H, Ali Z, Chang FL, Adnan AM (2014) Characterisation and utilisation of steel slag for the construction of roads and highways. *Mater Res Innov* 18(sup6):S6-255
4. Chesner WH, Collins RJ, MacKay MH (1998) User guidelines for waste and by-product materials in pavement construction (No. FHWA-RD-97-148)
5. Dubey AA, Ravi K, Devrani R, Rathore S, Borthakur A (2020) Characterization of steel slag as geo-material. In: Latha Gali MPRR (eds) *Geotechnical characterization and modelling*. Lecture notes in civil engineering, vol 85. Springer, Singapore
6. Indian Minerals Yearbook (2017) Government of India, Ministry of Mines, Indian Bureau of Mines
7. IS 2720 (Part 14) (1983) Determination of density index (relative density) of cohesion-less soils, Indian Standard Code, Bureau of Indian Standard
8. IS 2720 (Part 3/Sec 2) (1980) Determination of specific gravity of fine, medium & coarse-grained soil. Methods of test for soil, Indian Standard Code, Bureau of Indian Standard
9. IS 2720 (Part 17) (1986) Determination of Permeability, Methods of test for soil, Indian Standard Code, Bureau of Indian Standard. Bureau of Indian Standard
10. IS 2720 (Part 4) (1985) Grain size analysis, Methods of test for soil, Indian Standard Code, Bureau of Indian Standard
11. Kandhal P, Hoffman G (1997) Evaluation of steel slag fine aggregate in hot-mix asphalt mixtures. *Transp Res Rec: J Transp Res Board* 1583:28–36
12. Koh T, Moon SW, Jung H, Jeong Y, Pyo S (2018) A feasibility study on the application of basic oxygen furnace (BOF) Steel Slag for railway ballast material. *Sustainability* 10(2):284
13. Montenegro JM, Celemín-Matachana M, Cañizal J, Setién J (2012) Ladle furnace slag in the construction of embankments: expansive behavior. *J Mater Civ Eng* 25(8):972–979
14. Oluwasola EA, Hainin MR, Aziz MMA (2015) Evaluation of asphalt mixtures incorporating electric arc furnace steel slag and copper mine tailings for road construction. *Transp Geotech* 2:47–55
15. Poh HY, Ghataora GS, Ghazireh N (2006) Soil stabilization using basic oxygen steel slag fines. *J Mater Civ Eng* 18(2):229–240
16. Yildirim IZ, Prezzi M (2015) Geotechnical properties of fresh and aged basic oxygen furnace steel slag. *J Mater Civ Eng* 27(12):04015046

# Evaluation of Geotechnical Properties of Mineral Oil-Contaminated Clay Soil



Atriya Chowdhury

**Abstract** Energy is essential for living and vital for the development of any country. Of the three main fossil fuels available—coal, petroleum and natural gas, petroleum is the most versatile and without which life may come to a standstill. Thus, there is a need for proper extraction, transportation and storage of petroleum. The accidental spilling of diesel or petrol from oil storage tanks at oil refilling sites is quite possible. In such situations due to leakage, the hydrocarbons present in oil may percolate into the subsurface and interact with the soil minerals thereby changing their properties. In the present study, interaction of hydrocarbon with fine grained soil was undertaken. The soil from an oil refilling station and the petroleum oil stored in the tank of that station were collected. The Atterberg's limits, compaction and shear strength characteristics for the contaminated and uncontaminated soil were examined. The amount of oil added was 5, 10 and 15% of the dry weight of the soil sample. The results showed a significant influence of petroleum oil on the properties of clayey soil studied. The Atterberg's limits, optimum moisture content, maximum dry density and undrained shear strength showed a decreasing trend with the increase in hydrocarbon content. The effective angle of internal friction ( $\phi'$ ) for uncontaminated soil samples exceeded the  $\phi'$  values of uncontaminated soils by  $8^\circ$ .

**Keywords** Hydrocarbons · Petroleum oil · Atterberg's limits · Shear strength

## 1 Introduction

Petroleum is an extremely important fossil fuel which is crucial for the growth and development of any nation. The need for proper extraction, transportation and storage of petroleum is thus very important. According to the Report of the Working Group on Petroleum and Natural Gas Sector for the XI plan, by the Ministry of Petroleum and Natural Gas [8], the Indian hydrocarbon industry is currently passing through a challenging phase. Increasing concern for energy security, increasingly stringent

---

A. Chowdhury (✉)

Civil Engineering Department, Jadavpur University, Kolkata 700032, India

© Springer Nature Singapore Pte Ltd. 2022

A. K. Dey et al. (eds.), *Proceedings of the 7th Indian Young Geotechnical Engineers Conference*, Lecture Notes in Civil Engineering 195,

[https://doi.org/10.1007/978-981-16-6456-4\\_24](https://doi.org/10.1007/978-981-16-6456-4_24)

217

environmental regulations, emergence of natural gas and soaring prices of crude oil and natural gas have thrown up both enormous challenges and opportunities to the Indian oil and gas industry. The prognosticated resources of hydrocarbon in India are about 28 billion tones as on 1.4.2006. The amount of recoverable balance of hydrocarbon is 1856 MMT. World oil use is expected to grow from 80 million barrels per day (mbpd) to 118 mbpd in 2030. The loss of petroleum by various ways has become an important issue which needs immediate attention for the survival of mankind. As much as 8 percent of total petroleum is lost during explorations, from oil vessels during transportation and accidents involving tankers. Among the sources of loss of petroleum, 33% comes from oil vessels during transportation, 2% during exploration and 12% from accidents involving oil tankers, which highlights a vital requirement for reducing the loss of oil during extraction, transport and storage.

An oil spill is an event resulting in the release of liquid petroleum into the ocean or land, mainly due to human activity. Some of the sources of oil spills are sinking or leakage of oil-carrying vessels or oil pipelines, leakage from oil storage units, illegal dumping by industries, terrorist activities and natural disasters. Crude oil after extraction is transported to oil filling stations for processing where it is stored in oil tanks. In case of accidental spilling the oil percolates into the soil, interacts with the soil minerals and changes the characteristic of the soil, which may become detrimental to the structure constructed or to be constructed over a particular soil deposit [6, 7, 10]. It is thus important to investigate the properties of oil-contaminated soil for assessment of its characteristics. Oil spills affect the surface of groundwater, covering it with a thick film of oil thereby affecting marine life. Oil spill affects the geotechnical properties of soil by reducing water content at liquid and plastic limits and tends to reduce the shear strength of the soil [9] which is unfavourable for geotechnical projects.

With this background, an oil refilling station of Hindustan Petroleum Corporation Limited in Budge Budge, South 24 Parganas District, West Bengal where oil spilling was evidenced from different containers at various time intervals was chosen as a test site. The objective of this study was to assess the impact of oil on the geotechnical properties of the locally available soil at the site and predicting the impact with varying the degree of contamination.

## 2 Materials and Methodology

Petroleum samples from the oil containers at the test site were collected. Soil samples up to a depth of 5 m were collected to determine the following index properties of the soil at the location:

- Moisture content
- Bulk density
- Atterberg's limits
- Particle size distribution

- Optimum moisture content
- Permeability (falling head).

### 3 Experimental Procedure

Particle size distribution of soil sample was determined by standard hydrometric analysis. Hydrometer conforming IS-2720-Part IV-1985 was used for the test. Liquid limit and plastic limit of the oven dried soil samples were determined according to IS-2720 (Part V)-1985. Falling head permeability test was carried out for determining the permeability of soil as per IS-2720-Part-17-1986 (Reaffirmed-1997). The specific gravity of the soil samples was determined by adopting standard procedure. The soil sample was dried in oven dried for 24 h and pulverized. The sample was then poured into a specific gravity bottle and topped up with distilled water. The specific gravity bottle was stirred and heated to eliminate air bubbles. The weight of the specific gravity bottle was recorded along with the temperature of the sample. For a falling head test arrangement, the specimen was connected through the top inlet to selected stand pipe. The bottom outlet was opened and the time interval required for the water level to fall from a known initial head to a known final head as measured above the centre of the outlet was recorded. Three successive observations were taken to the determination of permeability. Standard proctor tests were carried out in the laboratory as per IS-2720-Part VII-1985 in order to determine optimum moisture content corresponding to maximum dry density of soil. The triaxial test as described by Bishop and Henkel [1] typically consisting of three main stages, saturation, consolidation and shearing, were conducted. To determine the shear strength characteristics, CU (consolidated undrained) triaxial tests were conducted. The amount of oil added was 5, 10 and 15% of dried weight of the soil sample.

### 4 Results and Discussions

The liquid limit and plastic limit of soil were 45% and 25%, respectively, and the physio-chemical properties are given in Table 1.

The test results of oil (Petrol) analysis are presented in Table 2.

The soil was primarily cohesive in nature with high silt content (57%) and low permeability. Particle size analysis of the soil established that the clay content of the soil tested was 39% (see Fig. 1).

Using A-line chart, the soil was classified as clayey soil having medium plasticity (CM) (see Fig. 2).

The increase in the percentage of oil contamination led to decrease in the Atterberg's limits. The liquid limit and plastic limits reduced significantly with the liquid limits for 5, 10 and 15% oil contamination being 41%, 36% and 32%, respectively.

**Table 1** Physio-chemical properties of the soil

Soil property	Value
Liquid limit (%)	45
Plastic limit (%)	25
pH	7.52
Optimum moisture content (%)	21
Maximum dry density (kN/m <sup>3</sup> )	18.5
Specific gravity	2.61
Grain size distribution	4
Sand (%)	57
Silt (%)	39
Clay (%)	
Coefficient of permeability (cm/s)	$3 \times 10^{(-5)}$

**Table 2** Table captions should be placed above the tables

Property	Value
Density	0.830 g/cc
Pour point	3 °C
Flash point	35 °C (min)
Kinematic viscosity	3 cst at 40 °C
Polycyclic aromatic hydrocarbon content	10% maximum
Acidity	0.04 mg KOH/gm
Sulphur content	45 ppm maximum
pH of the oil	7.8

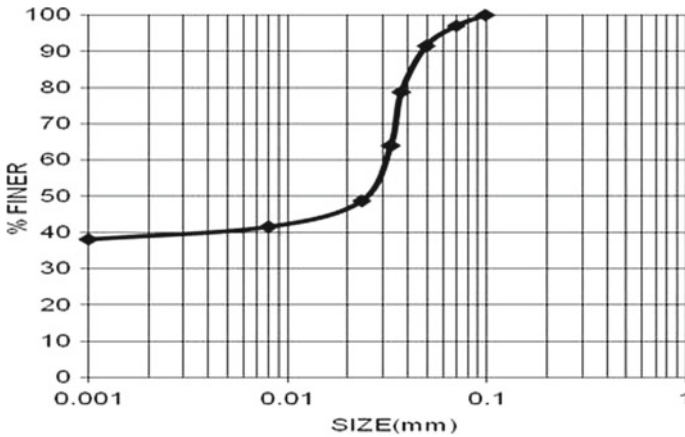


**Fig. 1** Particle size distribution curve

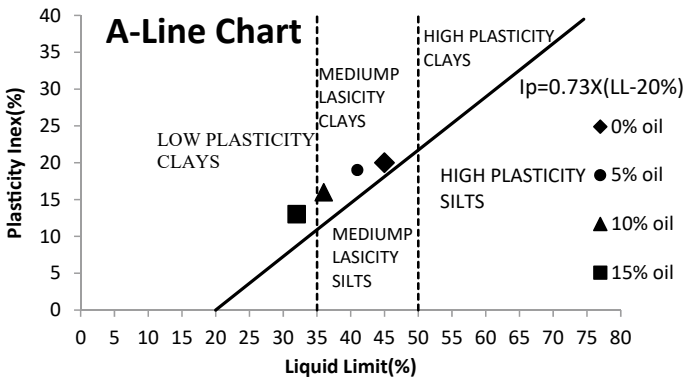
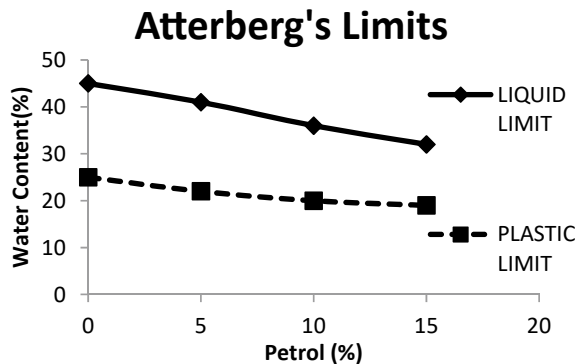


Fig. 2 Soil classification using A-line chart

The plastic limits were found to be 22, 20 and 19% for same percentages of contamination. The plasticity of the soil thus reduced with increasing hydrocarbon content. This behaviour is evident in Fig. 2 where the soil when contaminated with 15% oil is classified as clayey soil with low plasticity (CL). The variation in Atterberg’s Limit with oil content is depicted (see Fig. 3).

The maximum dry density (MDD) of the soil reduced with increasing oil content. The MDD value of uncontaminated soil was 18.5kN/m<sup>3</sup>. The MDD values decreased to 17.9, 17.3 and 17.1 kN/m<sup>3</sup> corresponding to 5, 10 and 15% oil contamination. The optimum moisture content (OMC) of the soil also showed a decreasing trend with increase in percentage of oil contamination. The OMC for 5, 10 and 15% oil contamination were 16.48%, 15.04% and 14.59%, respectively. The hydrocarbons present in petrol is a non-polar liquid and thus displaces the water (which is polar in nature) around the clay minerals thereby reducing the thickness of water film surrounding the clay minerals. This reduces the bonding between the clay particles as water acts a binding agent hence reducing the plasticity and water retaining capacities

Fig. 3 Variation in Atterberg’s limit with oil content



of cohesive soils. The variation in compaction characteristics of the cohesive soil due to oil contamination are presented below (see Fig. 4).

The results of the triaxial compression CU (consolidated undrained) tests conducted at effective confining pressures of 100 kPa and 200 kPa are presented in Fig. 5a, b, respectively. The maximum deviator stress for uncontaminated soil is appreciably more than contaminated soils for both confining pressures. For an effective confining pressure of 100 kPa, the peak deviator stress of uncontaminated, 5, 10 and 15% oil-contaminated soils was 92 kPa, 73 kPa, 63 kPa and 54 kPa, respectively. The corresponding peak deviator stresses for effective confining pressure of 200 were 179, 152, 135 and 126 kPa. The results of CU tests obtained are presented (see Fig. 5).

The effective stress parameters determined from Mohr's circles which gives the effective cohesion  $c'$  value as zero with only internal friction contributing to the strength as the soils studied are normally consolidated in nature. The ( $\phi'$ ) value decreases with the increase in petrol content thus indicating a reduction in shear

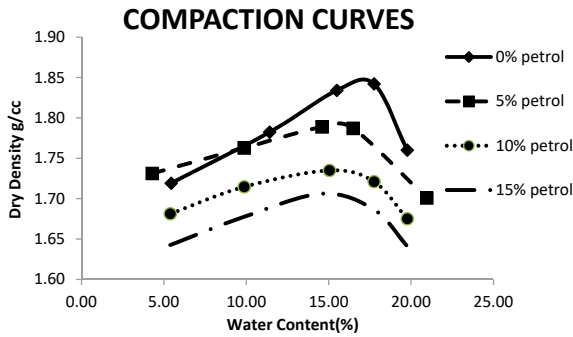


Fig. 4 Compaction curves obtained from standard Proctor tests

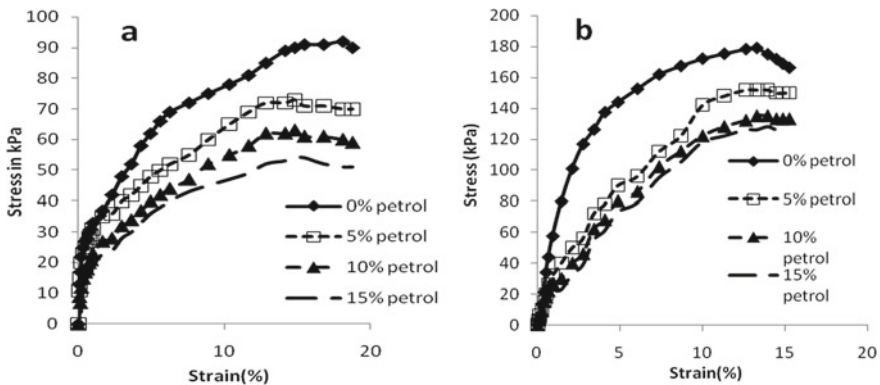
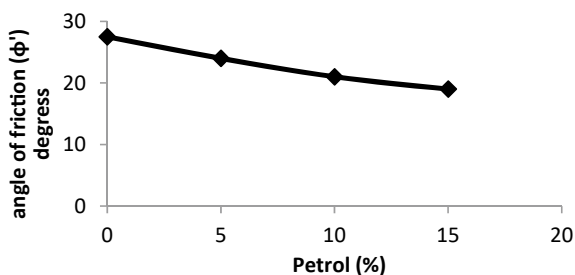


Fig. 5 a Stress–strain curves obtained from triaxial (CU) confining pressure 100 kPa, b stress–strain curves obtained from triaxial (CU) tests confining pressure 200 kPa



**Fig. 6** Variation of effective angle of internal friction ( $\phi'$ ) with oil content



strength. This is due to the reduction in water which acts as a binding agent between clay minerals. There is a significant decrease in shear strength as the ( $\phi'$ ) value reduces significantly for oil-contaminated soil. The ( $\phi'$ ) value for uncontaminated soil was found to be  $27.5^\circ$  and for 15% contaminated soil was  $19^\circ$ . The variations of effective angle of internal friction ( $\phi'$ ) with petrol percentage are presented (see Fig. 6).

## 5 Conclusions

1. Petroleum oil has a significant influence on geotechnical properties of clay soil.
2. The Atterberg's limits and the plasticity of the soil reduce with increase in oil content.
3. The maximum dry density, optimum moisture content and the shear strength of clay soil decrease with increase in oil contamination content. A significant drop in shear strength was evidenced with a difference of  $8^\circ$  in the effective angle of internal friction ( $\phi'$ ) values of uncontaminated and contaminated soil samples.

**Acknowledgements** I would like to thank the concerned authorities of the oil refilling station of Hindustan Petroleum Corporation Limited in Budge Budge, South 24 Parganas District, West Bengal, for allowing the collection of necessary samples required for carrying out this study.

## References

1. Bishop AW, Henkel DJ (1962) The measurement of soil properties in triaxial test. Edward Arnold
2. IS: 2720 (Part 4)—1985-Specification for methods of test for soils-code of practice
3. IS: 2720 (Part 5)—1985-specification for methods of test for soils-code of practice
4. IS: 2720 (Part 7)—1985-specification for methods of test for soils-code of practice
5. IS: 2720 (Part 17)—1985-specification for methods of test for soils-code of practice
6. Khamehchiyan M, Charkhabi Amir H, Tajik M (2007) Effects of crude oil contamination on geotechnical properties of clay and Sand soils. Eng Geol Sci Dir 89:220–229

7. Konečný F, Boháček Z, Müller P, Kovářová M, Sedláčková I (2003) Contamination of soils and groundwater by petroleum hydrocarbons and volatile organic compounds—case study: ELSLAV BRNO. *Bull Geosci* 78(3):225–323
8. Ministry of Petroleum and Natural Gas (2006) Report of the working group on petroleum and natural gas for the XI plan (2007–2012)
9. Rahman ZA, Hamzah U, Ahmad A (2010) Geotechnical characteristics of oil-contaminated granitic and metasedimentary soils. *Asian J Appl Sciences* 3(4):237–249
10. Tuncan A, Pamukeu S (1992) Predicted mechanism of crude oil and marine clay interactions in salt water. In: Conference on environmental geotechnology-CSME/Turkey, 109–112

# Plasticity Characteristics of Geopolymer Stabilized Expansive Soil



Manaswini Mishra, Soumyaprakash Sahoo , and Suresh Prasad Singh 

**Abstract** Marginal and weak soils are conventionally stabilized by cement and lime in civil engineering applications. However, the production process of these traditional stabilizers is energy intensive and it also serves as a major source of greenhouse gas emission leading to serious problems like global warming. But due to scarcity or non-availability of suitable soils at construction sites, use of cement is unavoidable. Geopolymer is a new generation alternative binding material for conventional cement. This is primarily produced from industrial wastes and rich in aluminosilicates when activated with alkalis. It has high strength, low cost, low energy consumption and it emits fewer greenhouse gases during synthesis. This study explores the efficiencies of ground granulated blast furnace slag (GGBS)-based geopolymer binder in stabilizing the expansive soil. The expansive soil is mixed with 0 to 20% of GGBS at 5% intervals and is activated with sodium hydroxide solutions of 0.5, 1, 2, 4, 6 and 8 M. The consistency limits, swelling and shrinkage characteristics of geopolymer treated soils are evaluated at curing periods of 0, 3, 7, 30 and 90 days. It is found that the plasticity characteristics and expansive properties of stabilized soil are strongly influenced by the geopolymer contents and the curing periods.

**Keywords** Expansive soil · Slag-based geopolymer · Consistency limits · Curing period

## 1 Introduction

Expansive soils are considered as problematic soils with their unpredictable performance in the presence of moisture. A little change in moisture content in this type of soil may lead to decrease in their shear strength associated with high swelling,

---

M. Mishra · S. Sahoo · S. P. Singh (✉)  
National Institute of Technology, Rourkela, Rourkela, Odisha, India  
e-mail: [spsingh@nitrrkl.ac.in](mailto:spsingh@nitrrkl.ac.in)

M. Mishra  
e-mail: [217ce1426@nitrrkl.ac.in](mailto:217ce1426@nitrrkl.ac.in)

shrinkage, settlement and consolidation. Improvement of expansive soils by treating with lime, cement, slag and fly ash is, nowadays, established methods which are used widely around the world. However, the production process of these traditional stabilizers is energy intensive and it also serves as a major source of carbon dioxide emission leading to serious problems like global warming.

Geopolymer is a new generation alternative binding material for conventional cement. The intense amount of work on geopolymeric binders derived from these industrial by-products have proved its utility having similar strength and durability properties that of conventional concrete. This alkali source provider, in the presence of alkaline medium forms geopolymerization products, that has comparable or even better characteristics than calcium-silicate-hydrate products of conventional concrete. Geopolymer is a type of inorganic material which is emerging as an analogues of thermosetting organic cross-linking materials [11]. The concept of geopolymers was proposed by Davidovits [1], who found that kaolinite could be polymerized by alkalis, producing a concrete-like material. High curing temperature and long curing time corresponded to higher compressive strength. The formation of geopolymer gel due to better geopolymerization enhanced the strength capabilities. The geopolymer structure became more rigid after curing for a certain period in comparison with its early stage [2]. Marginal lateritic soil could be stabilized by high calcium fly ash-based geopolymer and used as an environmentally friendly pavement material, which would furthermore decrease the need for high-carbon portland cement [10]. Increasing the molarity of alkali activator and alkali activator/clay improves the compressive strength of the geopolymer treated soil [3]. In this present study, an attempt has been made to study various mix parameters which control the stabilizing process in the soil geopolymer (Figs. 1 and 2).

## 2 Materials

### 2.1 *Expansive Soil*

Locally, available soil is collected from sector 19 area of Rourkela steel city. The soil is oven dried at least for 24 h at 110 °C and then pulverized in a ball mill and mixed thoroughly to bring homogeneity in the mass. It is passed through 425  $\mu\text{m}$  IS sieve before conducting experiments.

### 2.2 *Blast Furnace Slag*

Blast furnace slag is taken from Rourkela steel plant. It is grounded in ball mill for 4–5 h and mixed thoroughly to make it suitable for use in experimental works.

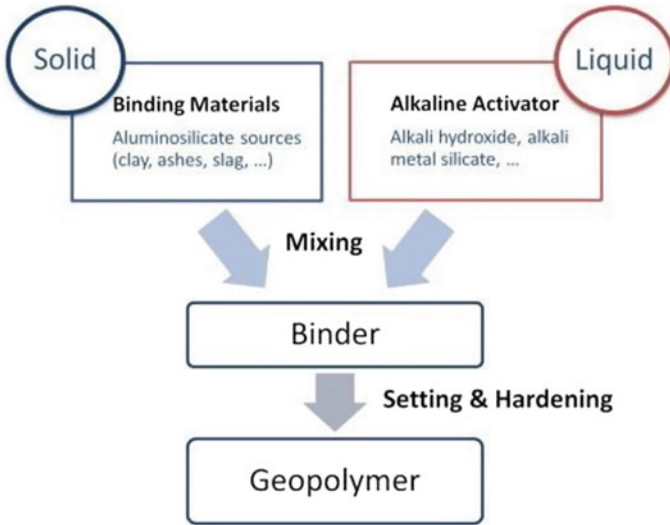


Fig. 1 Geopolymer components [8]

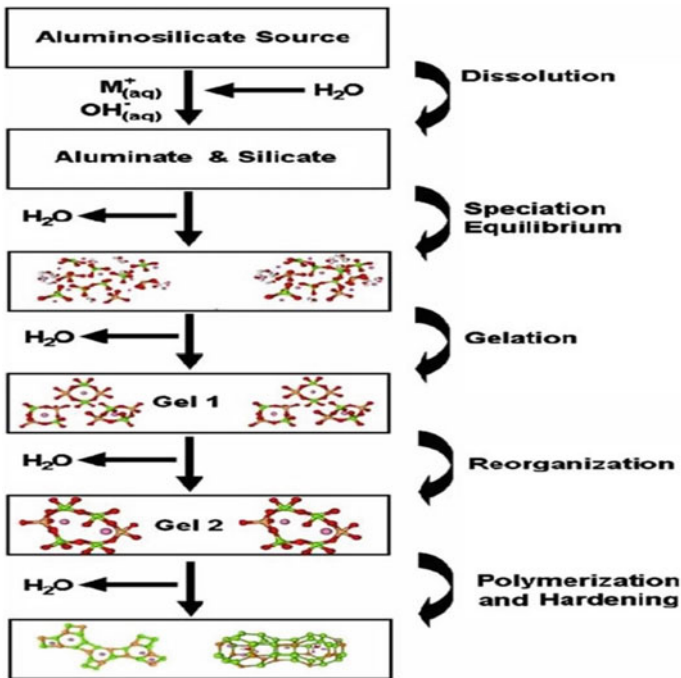


Fig. 2 Conceptual model of geopolymerization [9]

### 2.3 Alkali Activators

Sodium hydroxide solution is used as the alkali activator. Sodium hydroxide solutions of 1, 2, 4, 6 and 8 M are prepared 24 h prior to the experiments for homogeneous mixing and are kept in air tight containers.

## 3 Methodology

The experimental programme consists of treating the expansive soil with different percentages of blast furnace slag and different concentrations of sodium hydroxide solution. The varying percentages of slag used were 0–20% with an increment of 5%, and the concentration of sodium hydroxide used is 1, 2, 4, 6 and 8 M. The range of the slag contents and the concentration of the solution are chosen to study the effect of stabilization on a broader range. The soil is mixed with slag and sodium hydroxide solution and left for maturing at a constant temperature of 30 °C to conduct various tests at 0, 3, 7, 30 and 90 days. Atterberg limits [liquid limit (LL), plastic limit (PL) and plasticity index (PI)], differential free swell and pH are conducted following IS 2720 (part 5)-1985, IS 2720 (part 6)-1972, IS 2720 (part 40)-1977 and IS 2720 (part 26)-1987, respectively, to study the effect of stabilization on high swelling and shrinkage properties of soil (Table 1).

**Table 1** Characteristics of expansive soil

Specific gravity	2.78
Free swell index	110%
Linear shrinkage	20.8%
Shrinkage limit	10%
Plastic limit	28%
Liquid limit	78%
Light compaction test	OMC = 12.10%
	MDD = 1.972 g/cc
Heavy compaction test	OMC = 10.95%
	MDD = 2.072 g/cc

## 4 Result and Analyzes

### 4.1 Liquid Limit

The typical curves in Figs. 3 and 4 present liquid limit values of soil-slag mixtures treated with distilled water and NaOH solution for different curing periods. For a given concentration of NaOH solution, the liquid limit values decrease with slag content. The NaOH solution activates the slag, which produces calcium ions, and these calcium ions replace the exchangeable cations in the expansive soil and stabilize the surface charge causing the diffused double layer (DDL) to shrink. The increase in NaOH concentration and slag contents increases the reduction of DDL, thus decreasing the liquid limit values.

**Fig. 3** Liquid limit of soil-slag mix treated with distilled water

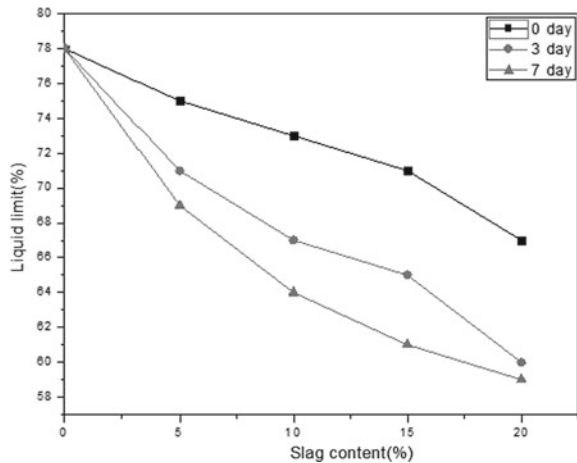
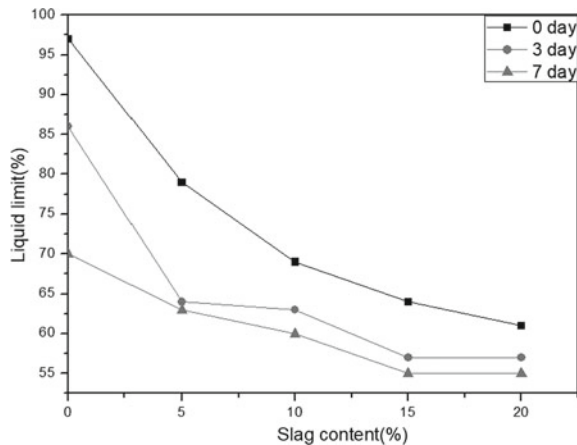


**Fig. 4** Liquid limit of soil-slag mix treated with 2 M NaOH solution



### 4.2 Plastic Limit

The typical curves presenting plasticity index values of soil-slag mixes with different contents of slag at a given concentration of sodium hydroxide (NaOH) are presented Figs. 5 and 6. It is seen that the plasticity index value decreases with slag content for a given concentration of NaOH solution with increase in curing period.

**Fig. 5** Plasticity index of soil-slag mix treated with distilled water

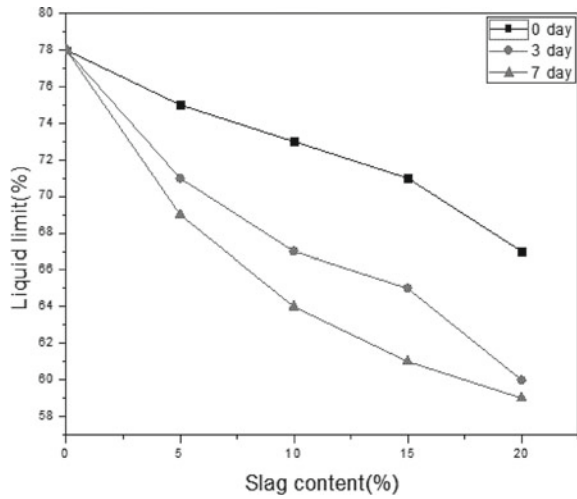
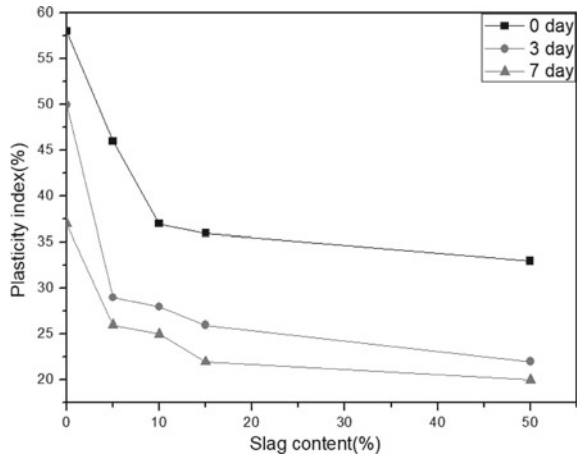


**Fig. 6** Plasticity index of soil-slag mix treated with 2 M NaOH solution





### 4.3 Shrinkage Limit

The set of curves representing shrinkage limit values of soil-slag mixes with different contents of slag at a given concentration of sodium hydroxide for different curing periods are presented in Figs. 7 and 8. It is seen that the shrinkage limit value increases with slag content for a given concentration of NaOH solution and it also increases with increase in curing period.

**Fig. 7** Shrinkage limit of soil-slag mix treated with distilled water

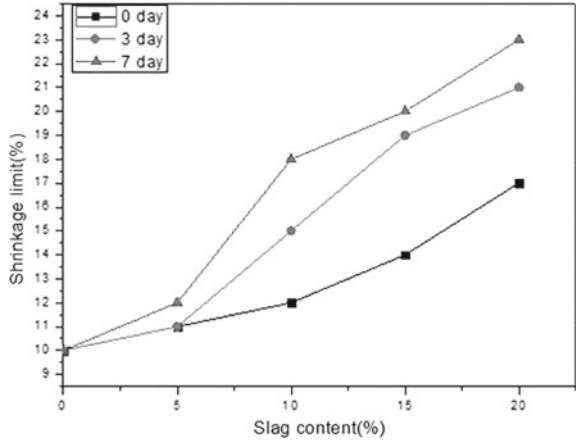


**Fig. 8** Shrinkage limit of soil-slag mix treated with 2 M NaOH solution

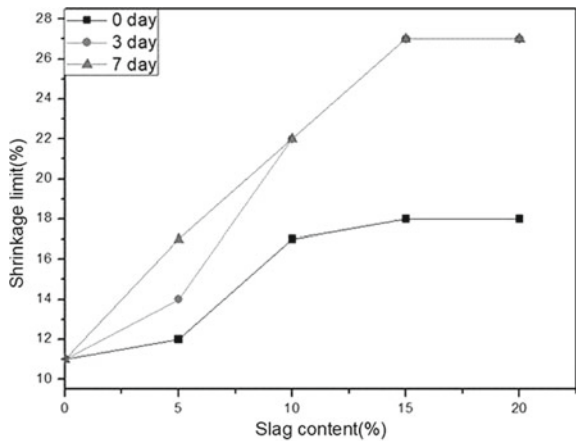
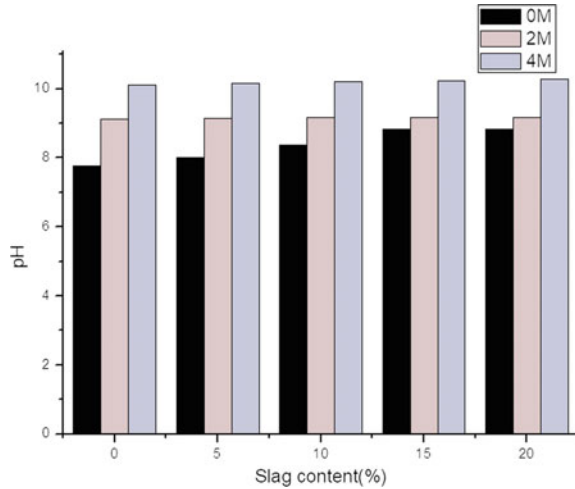


**Fig. 9** Variation of pH of soil-slag mixes with concentration of sodium hydroxide (NaOH) solution



#### 4.4 pH

The variation of pH values of soil-slag mixes with different contents of slag for different concentrations of sodium hydroxide solution is shown in the bar chart. There is not much increase in the pH values with increase in slag content for a given concentration of NaOH. With increase in concentration of NaOH, the pH value increases due to its alkaline nature (Fig. 9).

#### 4.5 Differential Free Swell

There is a decrease in the value of differential free swell (DFS) value with increase in slag content for soil-slag mixes. The DFS values also decrease with increase in concentration of sodium hydroxide solution and with increase in curing period (Fig. 10).

### 5 Conclusion

This paper investigated the influence of the mineral admixture slag and alkali activator on the plasticity and swelling characteristics of expansive soil.

- It is observed that both liquid limit and plasticity index are reduced significantly by adding sodium hydroxide solution. Further, both LL and PL reduce with increase in curing period.

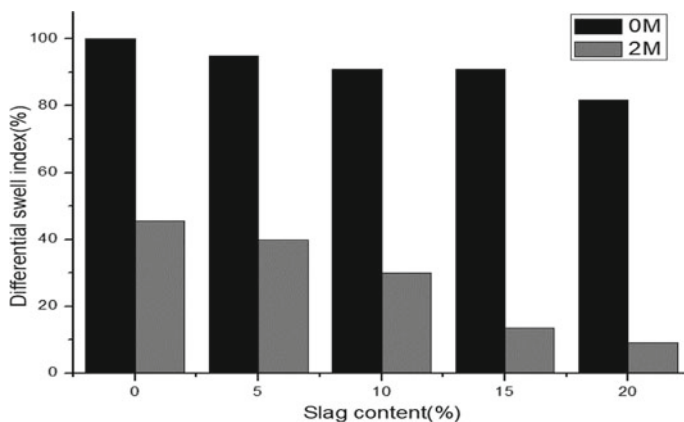


**Fig. 10** Variation of differential swell index of soil-slag mixes with concentration of NaOH solution

- Similarly, a reduction in swelling index is observed with increase in sodium hydroxide content and curing period.
- However, shrinkage limit increases when the slag content, concentration of NaOH solution and curing period increase.
- A marginal increase of pH value is observed with increase in slag content, whereas a substantial increase in pH is noticed with addition of NaOH concentration.

From the above observations, it is obvious that the sodium hydroxide (NaOH) solution activated slag is suitable as an alternative to conventional stabilizing agents. Addition of slag-based geopolymer to expansive soil modifies the plasticity and swelling properties of expansive soil. Geopolymer has hardly any harmful effect on environment.

## References

1. Davidovits J (2013) Geopolymer cement a review, published in geopolymer science and technics, Technical paper# 21, Geopolymer Institute Library
2. Diop MB, Molez L, Bouguerra A, Diouf AN, Grutzeck MW (2014) Manufacturing brick from attapulgite clay at low temperature by geopolymerization. Arab J Sci Eng 39(6):4351–4361
3. Ghadir P, Ranjbar N (2018) Clayey soil stabilization using geopolymer and Portland cement. Constr Build Mater 188:361–371
4. Indian Standard. IS: 2720 (Part 5)–1985. Methods of test for soils: determination of liquid and plastic limit (Second Revision)
5. Indian Standard. IS: 2720 (Part 6)-1972. Methods of test for soils: determination of shrinkage factors (First Revision)
6. Indian Standard. IS: 2720 (Part 26)-1987. Method of test for soils: determination of pH value (Second Revision)
7. Indian Standard. IS: 2720 (Part 40)-1977. Methods of test for soils: determination of free swell index of soils

8. Liew YM, Heah CY, Kamarudin H (2016) Structure and properties of clay-based geopolymer cements: a review. *Prog Mater Sci* 83:595–629
9. Petermann JC, Saeed A, Hammons MI (2010) Alkali-activated geopolymers: a literature review
10. Phummiphon I, Horpibulsuk S, Sukmak P, Chinkulkijniwat A, Arulrajah A, Shen SL (2016) Stabilisation of marginal lateritic soil using high calcium fly ash-based geopolymer. *Road Mater Pavement Des* 17(4):877–891
11. Sukmak P, Horpibulsuk S, Shen SL (2013) Strength development in clay–fly ash geopolymer. *Constr Build Mater* 40:566–574

# **Slope Stability and Landslides**

# Effect of Joint Orientation and Weathering on Static Stability of Rock Slope Having Transmission Tower



Mohammad Zaid  and Md. Rehan Sadique 

**Abstract** The youngest folded mountains of the Himalayas have the need to be studied for stability due to ongoing construction developments. Construction activity on these vulnerable slope leads toward greater instability. In the present case, the construction of a transmission tower has been considered. This paper focuses on the effect of joint orientation on the stability of slope. The weathering effect of rocks has also been considered. The slope studied is from the Karcham Wangtoo site in Kinnaur, Himachal Pradesh, India. The finite element software has been adopted for this study. The location of footing of transmission tower has been varied by increasing the distance between the footing and the edge of slope, starting from the edge. The angle of orientation of joint has initially been considered parallel ( $0^\circ$ ) and then varied till it became perpendicular to the slope ( $90^\circ$ ). The angle of dip is  $75^\circ$  with horizontal. The three-stepped geometry has been considered to be present at the site under consideration having road, Satluj river and footing. The basalt rock properties have been considered as input parameters for 2D plane strain elastoplastic model analysis. It was finally found out that weathering has significant effect on slope instability. This study also showcases the critical angle of orientation of joint with slope from instability point of view.

**Keywords** Slope stability · Rock · Finite element analysis · Joint

## 1 Introduction

The development of residential, institutional and industrial buildings in the hilly terrain are rising. Furthermore, the increasing demand of energy has called for increase in number of hydropower projects in hilly regions. Karcham Wangtoo hydro-power project (India) is one of the projects constructed to cater the need of power. The study on the stability of Himalayan rocky slope has been the area of research

---

M. Zaid (✉) · Md. Rehan Sadique  
Department of Civil Engineering, ZHCET, Aligarh Muslim University, Aligarh, U.P., India  
e-mail: [mohammadzaid1@zhcet.ac.in](mailto:mohammadzaid1@zhcet.ac.in)

interest. Several researchers have studied the effect of angle of friction between the rocks along the discontinuities for the stability of slope [1–3].

Mostly, the slopes lying in hilly regions are in earthquake prone zone, thus, stability of slope due to seismic loading has been studied by many researchers [4–10]. The adverse effects of rise in water table and increase in water content during the earthquake loading has been studied [10]. A study has also been carried out to analyze the stability of slope under earthquake for different inclination of slopes [8]. Soil slopes are even more problematic, and seismic loading and presence of clay make it more vulnerable to failure [7].

Development of computer-based programs have made it possible to carry out typical problem without any setup and without spending a plenty of resource for the study. A study has proved the efficiency and versatility of finite element over traditional approaches in the stability analysis of slope [11]. A research has been carried out for comparison between the elastoplastic methods of analysis of factor of safety calculation and location of critical failure surface [12]. Numerical approach has been adopted by many researchers for the study of slope stability under different conditions [9, 13, 14]. The influence of variation in the properties of the slope material has also been carried out [15].

The studies were carried out to present the combined effect of different orientations of joint, location of transmission tower footing, variation in the properties of rock-mass/effect of weathering. The analysis has been carried out using Abaqus/CAE.

## 2 Methodology

The paper has adopted the finite element method of analysis to carry out the stability study of jointed rock-slope. The process of analysis has been explained below.

### 2.1 Geology

The site of study lies near the river bank of Satluj river. The slope is near to the constructed Karcham Wangtoo Power House. The rock-mass considered for the study has been shown in the Table 1. The study focuses on the single major joint set. The slope has 75° dip with the horizontal [16]. And the major joint set has been varied with the slope by changing the angle of orientation of joint set with the slope at the rate of 15° up to 90° with the slope [17]. The study area lies in the Himalayan mountain belt. Since, Himalayas are young folded mountains, the study has been carried out for the stability of rock slope under static loading by considering the weathering of rock, which has been incorporated by change in mechanical and physical properties of rock (Fig. 1).

**Table 1** Input parameters for rock-mass

Rock-mass	Fresh basalt ( $W_0$ )	Slightly Weathered Basalt ( $W_1$ )	Medium weathered basalt ( $W_2$ )	Highly weathered basalt ( $W_3$ )
Density ( $\text{kg/m}^3$ )	2960	2740	2470	1820
Young's modulus (GPa)	46.5	20.6	2.8	0.6
Poisson ratio	0.186	0.26	0.272	0.272
Angle of internal friction				
(Degrees)	63.38	53.71	33.33	43.87
Cohesion (MPa)	26.25	18.5	8.08	1.64



**Fig. 1** Geological location of slope under Study [18]

## 2.2 Geometry of the Slope

The geometry of the slope has been adopted as of the geological location of the slope near Karcham Wangtoo hydroelectric power plant near the Satluj river. The geometry of the model has been shown in Fig. 2. The top horizontal base has been used for construction of transmission tower and here footing of transmission tower has been placed which has size of  $4.5 \text{ m} \times 4.5 \text{ m}$ . The footing was first placed at the edge of slope and the distance between the edge of slope and the footing increased up to  $d$



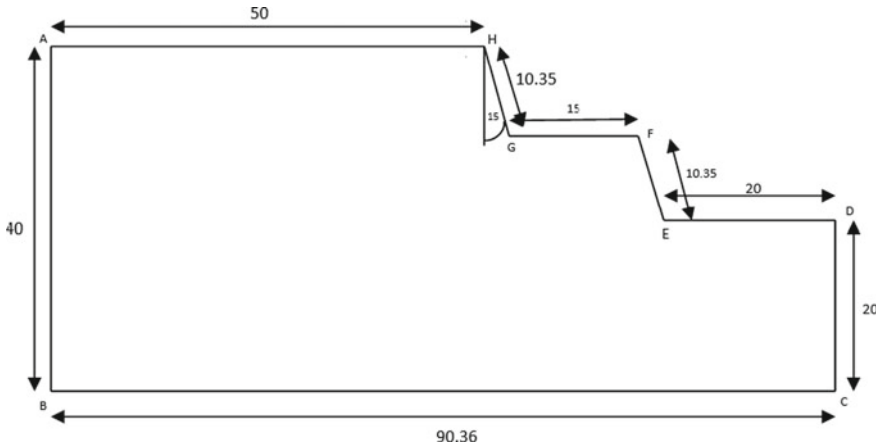


Fig. 2 Geometry of the slope [14]

=  $5d$  where  $d$  stands for the width of footing i.e.  $1d = 4.5$  m. The next step shown in the Figure meant for roadway passing nearby. Last step shows the span of Satluj river. The joint-set has orientation parallel to the slope which is at  $75^\circ$  dip angle, which is now onward referred as  $0^\circ$  orientation of joint with slope. The orientation of the joint has also varied from  $0^\circ$  angle of orientation with the slope to  $90^\circ$  angle of orientation with the slope [14].

### 2.3 Numerical Modelling

2D plane strain elasto-plastic model has been adopted for the stability analysis. The Mohr Coulomb theory of plasticity has been adopted for the plastic behavior of the rock-mass. The Nagpur fresh basalt, slightly weathered basalt, medium weathered basalt, and highly weathered basalt parameters of elasticity and plasticity has been adopted from Gahoi et al. [17, 19]. The elasticity model has been considered for footing of transmission tower having mass density of  $2400 \text{ kg/m}^3$ , modulus of elasticity of 25 GPa and Poisson’s ratio of 0.15.

Analysis step of Static, General type has been chosen for the static analysis. This step has time period of 1, initial increment size has been considered as 0.0001 and minimum increment size as  $1\text{E-}015$ . The direct method of equation solver has been adopted with asymmetric matrix storage. Full newton technique of solution has been considered.

General contact (standard) in the initial step has been assigned to the model with all self-type of included surfaces having contact properties of tangential contact property as 0.85 of friction coefficient, normal contact property has hard contact type of pressure overclosure. The general contact in Abaqus is adopted to apply the

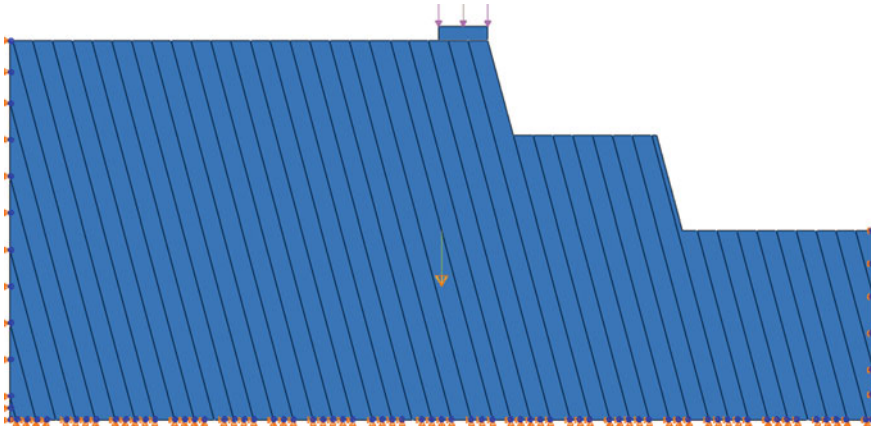


**Fig. 3** Loading and boundary conditions of the model

property of contact to whole model. Also, in addition to general contact, the hard contact property has to be applied to take into account the hardness of the material.

The total load of superstructure of transmission tower of 28,340 N/m has been applied as a line load on the footing. The gravity load of component  $-1$  has been applied to the whole model. The component of gravity loading is the value which is to be multiplied to value of gravitational acceleration, which has value of  $9.81 \text{ m/s}^2$ . The negative sign represents the direction of loading. The boundary condition on the left and right side of the slope has restrained in horizontal direction and allowed in  $y$ -direction (vertical direction). The base of the footing has been restrained in horizontal and vertical directions as the rock-mass has very large depth.

The footing of the transmission tower and the slope model of basalt rock has been meshed with element type of CPE3, A 3-node linear plane strain triangle having linear bulk viscosity as 0.06 and quadratic bulk viscosity as 1. The analysis has been done after above-mentioned parameters and the results are shown. Figure 3 shows the boundary conditions and the loading before the analysis has been carried out. Figure 3 is the visual representation of boundary conditions in user interface of Abaqus. Similarly, Fig. 4 represents the meshing of the finite element model of slope. The model has been modeled using triangular elements.

### 3 Results and Discussion

In the present paper the stability analysis has been performed, of jointed rock-slope on which transmission tower has been installed. The position of footing of the transmission tower has been varied from the edge of the slope which is denoted by  $0d$  to  $5d$  (where,  $d$  is equal to 4.5 m). Three rock parameters have been varied in the study, first is the joint orientation with the slope, second is the position of the footing of

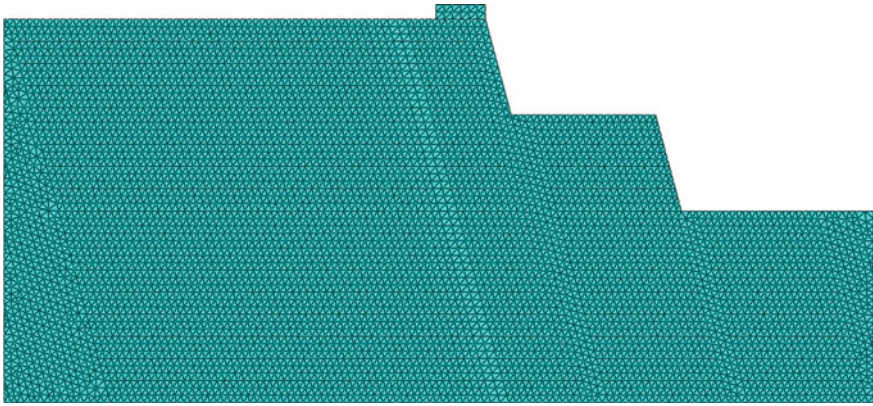


Fig. 4 Meshed rock-mass and footing of transmission tower

transmission tower, and third is the weathering class. Weathered properties of Basalt rock have been incorporated by change in properties (physical and mechanical) and strength due to weathering, as reported by Mishra et al. [20]. The slope stability analysis has been carried out in finite element software Abaqus/Standard.

Figure 5 shows for deformation versus orientation of joint for different position of footing. The Figure shows that there is slight decrease in deformation from 0° orientation (i.e. joint set parallel to slope) to 15° of joint orientation with the slope. After that, deformation increases giving maximum value of deformation at the 30°. The deformation later decreases, making slope stable.

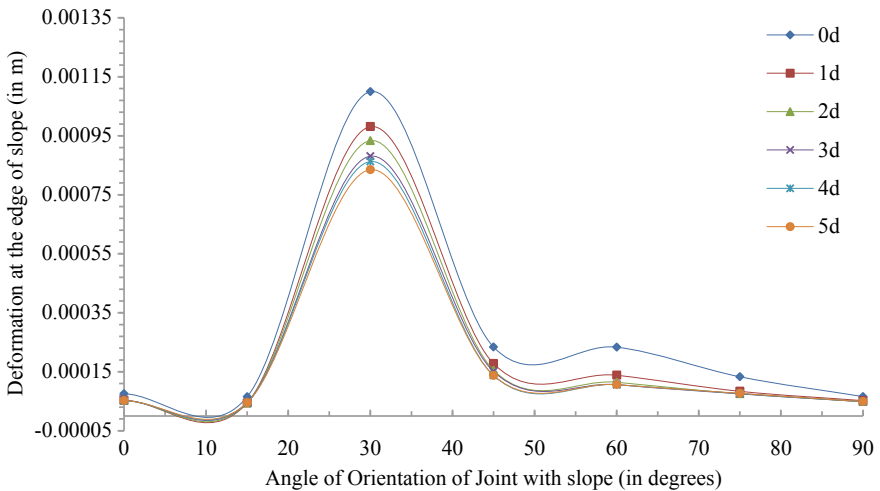


Fig. 5 Total maximum deformation at the edge of slope for different joint orientation with slope and varying location of footing for fresh basalt

Figure 6 also shows similar pattern of deformation as of Fig. 5. Thus, making the slope toward stability for the orientation of joint greater than 30° and lesser than 30°. The magnitude of deformation decreases from 30° of joint orientation to 90° of joint orientation.

The deformation at the edge of slope for different angle of orientation of joint and different positions of footing of transmission tower as shown in Fig. 7. There is a very small decrease in deformation from 0° to 15° of joint orientation and 45° of joint orientation has maximum magnitude of deformation.

A graph of deformation versus angle of joint orientation with slope for varying position of footing has been shown in Fig. 8. This figure is plotted for highly weathered basalt rock. Both, medium weathered basalt and highly weathered basalt shows similar kind of pattern.

Figure 9 shows different graphs for comparing deformation for different class of weathered rock-mass. The figure shows that there is significant change in deformation from  $W_1$  to  $W_2$  and from  $W_2$  to  $W_3$ . Highly weathered basalt rock ( $W_3$ ) has maximum deformation due to transmission tower footing.

Contours of maximum deformation for highly weathered basalt at 1d location of footing of transmission tower with varying orientations of joint with the slope are shown in Fig. 10. It shows a contour comparison for 1d location of footing for highly weathered basalt, as 1d location shows change in deformation and the deformation after that leads to stability. The maximum value of deformation has been observed in case of 45° which has value of 6.31 mm and the minimum value has been observed in case of 30°, having value of 0.98 mm. Thus, it can be stated that 30° of joint orientation with the face of slope is the safest in the case of present study and 45° of angle of joint orientation is critical of the present case.

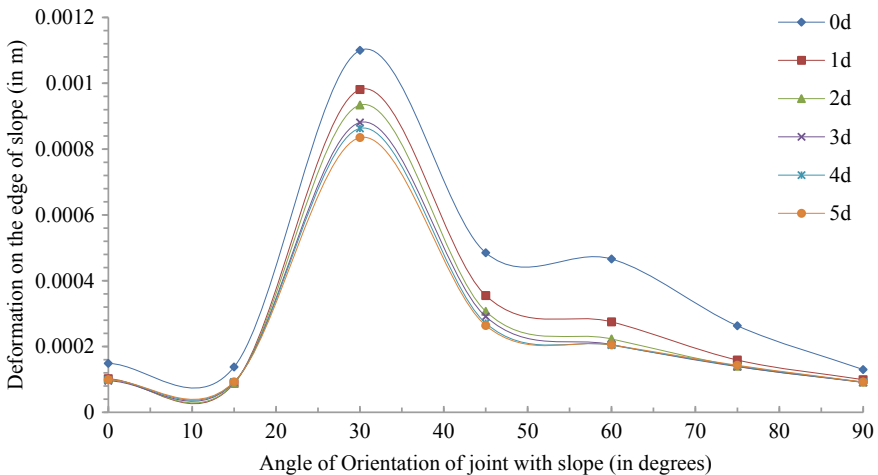
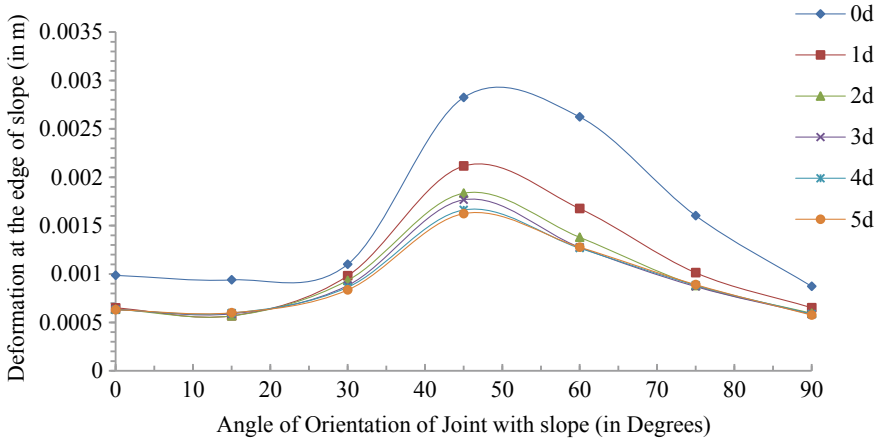
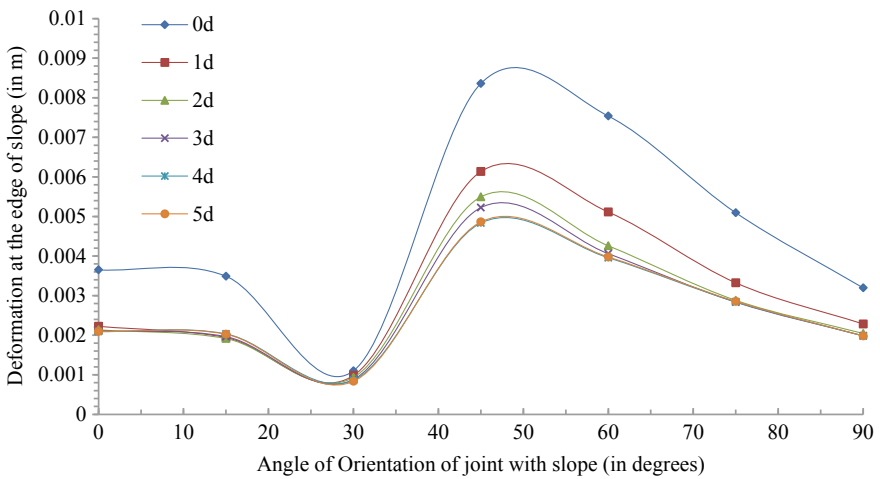


Fig. 6 Total maximum deformation at the edge of slope for different joint orientation with slope and varying location of footing for slightly weathered basalt



**Fig. 7** Total maximum deformation at the edge of slope for different joint orientation with slope and varying location of footing for medium weathered basalt



**Fig. 8** Total maximum deformation at the edge of slope for different joint orientation with slope and varying location of footing for highly weathered basalt

Figure 11 shows comparison contours for maximum deformation for weathering effect in case of 5d location of transmission tower from the edge of slope and 90° of orientation of joint with the slope. Although, the 5d location of transmission tower is in itself safest case but the effect of weathering has to be taken into account. The comparison of stated location in Fig. 11 for different stages of weathering of basalt rock shows that weathering has significant effect on the slope stability. Hence, it can be concluded that while studying the stability of the slope the effect of weathering must be taken into account.

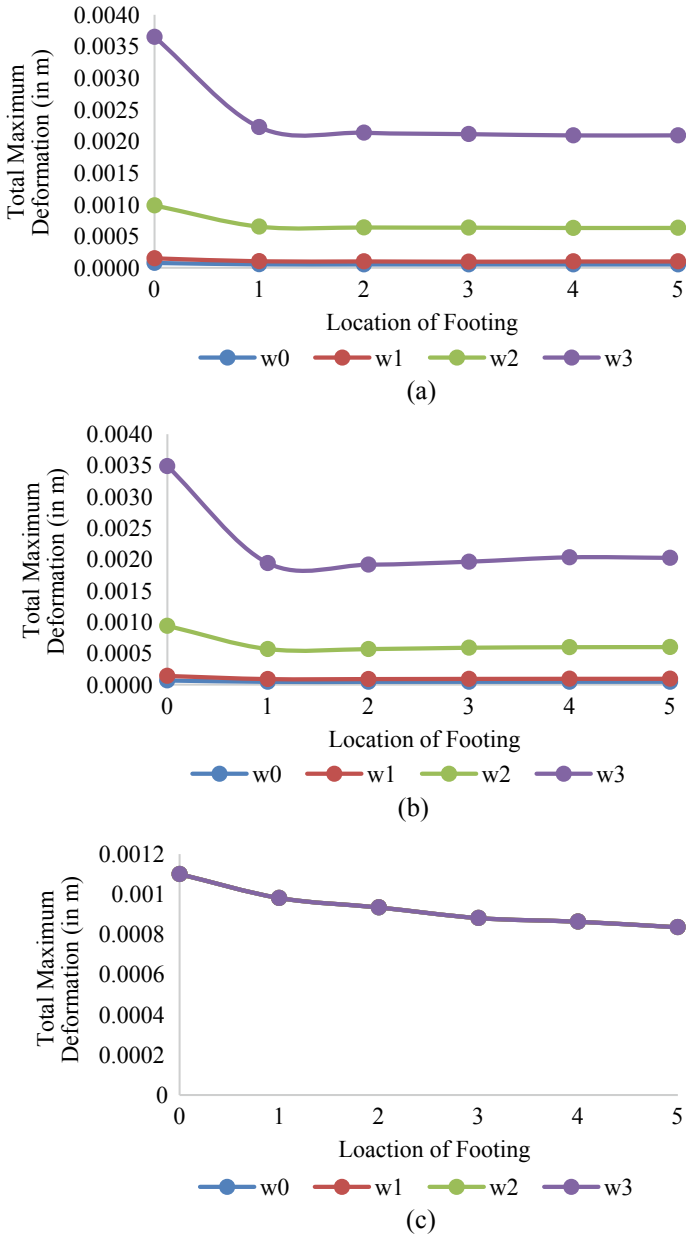


**Fig. 9** Comparison of total maximum deformation at the edge of slope of varying location of footing for different weathering stages of basalt rock for **a** 0°, **b** 15°, **c** 30°, **d** 45°, **e** 60°, **f** 75°, and **g** 90° angle of orientation of joint with the slope

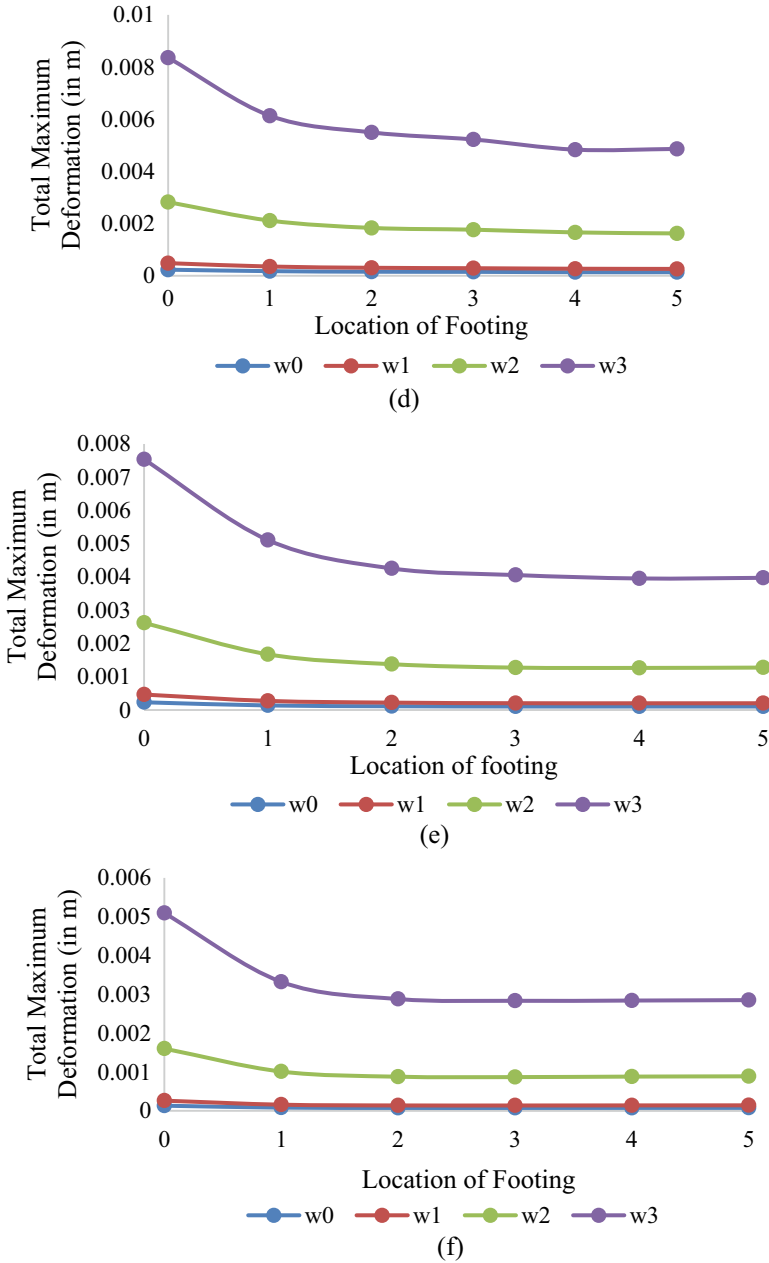


Fig. 9 (continued)

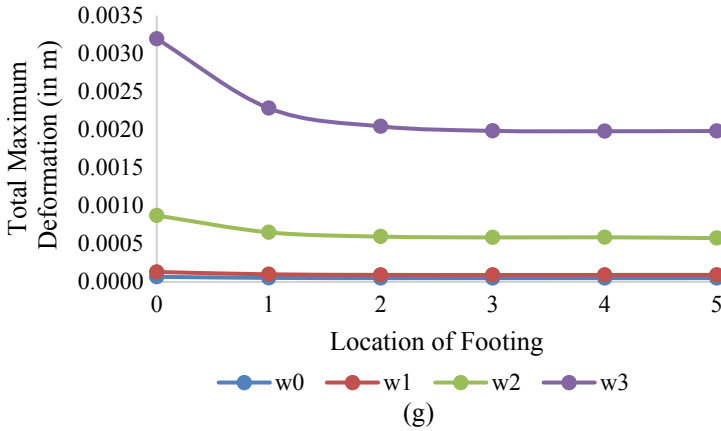


Fig. 9 (continued)

### 4 Conclusion

A two-dimensional finite element analysis has been performed to study the stability of rock slopes having transmission tower erected on its top. Rock-mass parameter has been adopted for fresh and weathered basalt. Topology of the region has been adopted from the Himalayan region. Further, it has been concluded:

- The 30° of orientation of joint with respect to the slope has been found to be critical in case of rock-mass of fresh basalt and slightly weathered basalt.
- Deformation shows similar pattern for each position of footing of transmission tower for both type of basalt.
- 1d location of footing of transmission tower has been found to be safer in all the cases analyzed in the present paper.
- Medium weathered basalt and highly weathered basalt shows similar behavior in terms of deformation.
- 0d location of footing of transmission tower i.e. at the edge of slope is the most critical in term of stability point of view.
- Weathering condition has no significant effect on the position of footing of transmission tower after 1d.



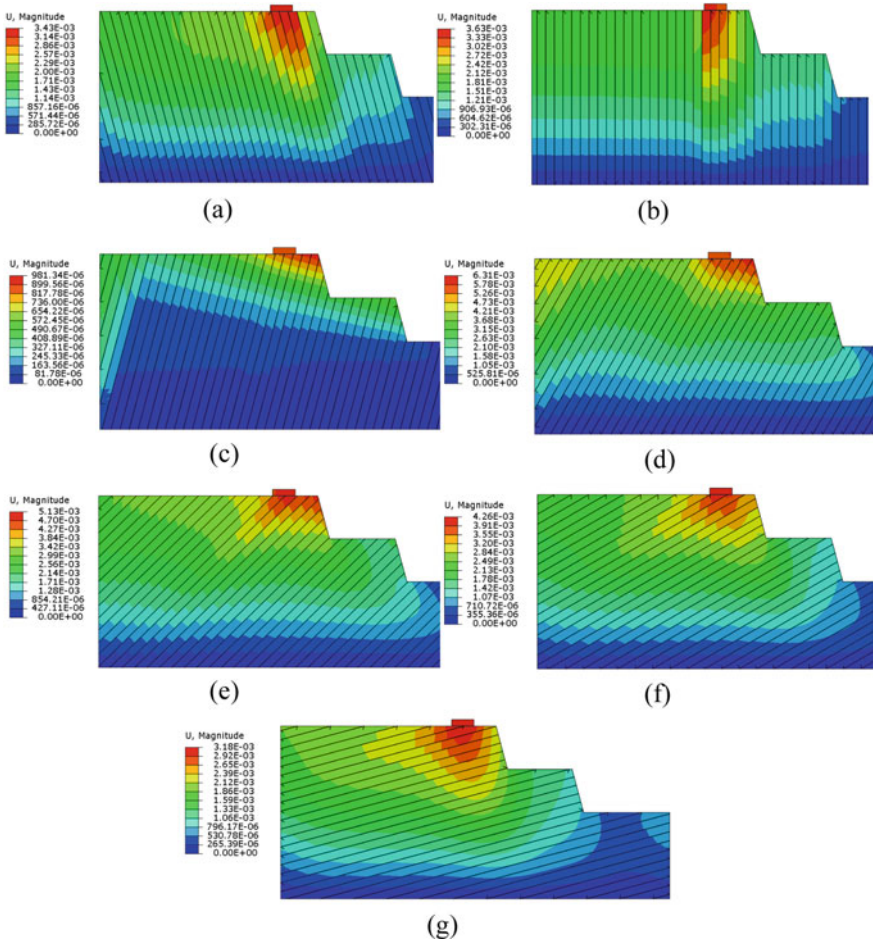


**Fig. 10** Total maximum deformation contours for highly weathered basalt at 1d Location of Footing with Varying Joint Orientation with the Slope **a** 0°, **b** 15°, **c** 30°, **d** 45°, **e** 60°, **f** 75°, and **g** 90°

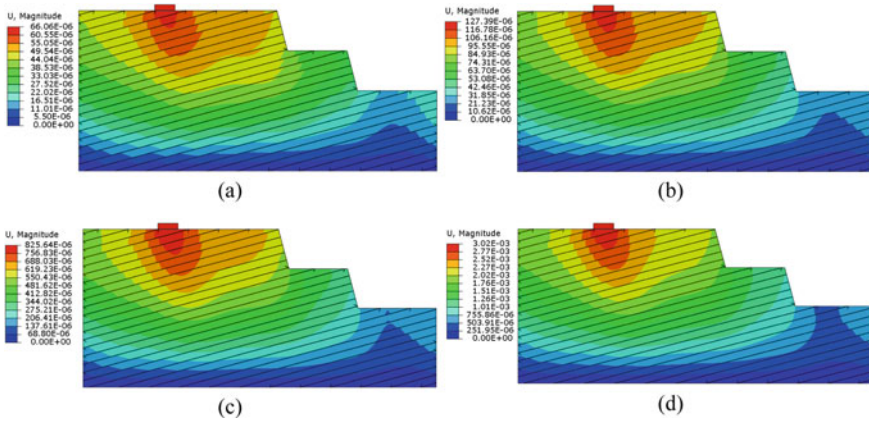


**Fig. 11** Contours for total maximum deformation for 5d location of transmission tower and 90° of orientation of joint with the slope for **a** Fresh basalt ( $W_0$ ), **b** slightly weathered basalt ( $W_1$ ), **c** medium weathered basalt ( $W_2$ ), and **d** highly weathered basalt ( $W_3$ )

## References

1. Byerlee J (1978) Friction of rocks. *Pure Appl Geophys* 116(4–5):615–626
2. Cundall PA (1988) Formulation of a three-dimensional distinct element model-Part I. A scheme to detect and represent contacts in a system composed of many polyhedral blocks. *Int J Rock Mech Min Sci* 25(3):107–116
3. Hart R, Cundall PA, Lemos J (1988) Formulation of a three-dimensional distinct element model-Part II. Mechanical calculations for motion and interaction of a system composed of many polyhedral blocks. *Int J Rock Mech Min Sci* 25(3):117–125
4. Cinioglu O, Erkli A (2018) Seismic bearing capacity of surficial foundations on sloping cohesive ground. *Soil Dyn Earthq Eng* 111(April):53–64
5. Azhari A, Ozbay U (2017) Investigating the effect of earthquakes on open pit mine slopes. *Int J Rock Mech Min Sci* 100(April):218–228
6. Lv Q, Liu Y, Yang Q (2017) Stability analysis of earthquake-induced rock slope based on back analysis of shear strength parameters of rock mass. *Eng Geol* 228(June):39–49
7. Zhou YG, Chen J, She Y, Kaynia AM, Huang B, Chen YM (2017) Earthquake response and sliding displacement of submarine sensitive clay slopes. *Eng Geol* 227(April):69–83
8. Zhao LH, Cheng X, Zhang Y, Li L, Li DJ (2016) Stability analysis of seismic slopes with cracks. *Comput Geotech* 77:77–90
9. Azzam WR (2015) Finite element analysis of skirted foundation adjacent to sand slope under earthquake loading. *HBRC J* 11(2):231–239
10. Lu L, Wang ZJ, Song ML, Arai K (2015) Stability analysis of slopes with ground water during earthquakes. *Eng Geol* 193:288–296
11. Griffiths DVV, Lane PAA (1999) Slope stability analysis by finite elements. *Géotechnique* 49(3):387–403
12. Zheng H, Liu DF, Li CG (2005) Slope stability analysis based on elasto-plastic finite element method. *Int J Numer Methods Eng* 64(14):1871–1888
13. Li LC, Tang CA, Zhu WC, Liang ZZ (2009) Numerical analysis of slope stability based on the gravity increase method. *Comput Geotech* 36(7):1246–1258
14. Zaid M, Talib A, Rehan Sadique Md (2018) Stability analysis of rock slope having transmission tower. *IJRECE* 6(2)

15. Du W, Wang G, Huang D (2018) Influence of slope property variabilities on seismic sliding displacement analysis. *Eng Geol* 242:121–129
16. Sadique MR (2010) Analysis of bridge pier foundation on jointed rocks. M. Tech Thesis, Indian Institute of Technology, Roorkee
17. Zaid M, Talib A, Sadique MR (2018) Effect of joint orientation on the seismic stability of rock slope with transmission tower. In: IGC-2018
18. <https://www.google.com/maps/place/Karcham+Wangtoo+Hydroelectric+Plant,+Yashang+Dhar,+Himachal+Pradesh+172104/@31.5433635,78.013884,924m/data=!3m1!1e3!4m5!3m4!1s0x390676ca35fd7d73:0xfc01027f78d95bf!8m2!3d31.543203!4d78.015222> Last seen 20th August 2018
19. Gahoi A, Zaid M, Mishra S, Rao KS (2017) Numerical analysis of the tunnels subjected to impact loading. In: INDOROCK, 2017
20. Mishra S, Rao KS, Gupta NK, Kumar A (2017) Damage to shallow tunnels in different geomaterials under static and dynamic loading. *Thin-Walled Struct* 126:138–149

# Stability of Slope During Rainfall: A Finite Element Approach



J. Sharailin Gidon  and Smurtirekha Sahoo 

**Abstract** The effects of different environmental factors, i.e., rainfall intensities, hydrological conditions and geological formation are inevitable while studying the stability of any slope. In this paper, these factors are taken into consideration, which consists of three different water levels, three different soil properties and five different rainfall intensities for analyzing a particular slope located in Meghalaya (i.e., one of the North Eastern states of India). A numerical analysis based on finite element method has been carried out on a slope formation found in Nongstoin, Meghalaya, India. The contribution of these parameters to the stability of the given slope is analyzed using finite element-based software (i.e., MIDAS GTX NX 2016). The variation of factor of safety with respect to time for different rainfall intensities are reported. Parametric studies based on different soil parameters are also being done. The results in terms of pore water pressure variation throughout the slope, lateral deformation of the slope have also been reported to have an insight into the response of the given slope due to various rainfall intensities and site characteristics.

**Keywords** Slope stability · Numerical analysis · Factor of safety · Finite element method

## 1 Introduction

The study of the effect of various environmental factors on the stability of slope is very common in the field of geotechnical engineering. These factors occur in different forms for, e.g., rainfall, melting of snow, earthquakes, geological factors, etc. Their impact directly or indirectly gives rise to instability to the surrounding slopes, which leads to the importance of study of slope stability. Equations and numerical models have been derived and developed to study the stability of saturated and unsaturated slopes [1]. One of the latest is the use of finite element method (FEM) [2] which can be used to virtually analyze complex slopes in two and three dimensions. FEM along

---

J. Sharailin Gidon (✉) · S. Sahoo  
NIT Meghalaya, Shillong, India

with an elasto-plastic (Mohr–Coulomb) strain–stress technique has been shown to be a reliable and sturdy method for studying the factor of safety of slopes [2]. In unsaturated slopes matric suction or negative pore water pressure plays an important role when it is exposed to rain [3]. In an unsaturated soil, when rainfall is infiltrated, the ground water level is increased and subsequently water pressure is increased or matric suction is decreased. The decrease in matric suction leads to the decrease in shear strength of soil, this in turn, possibly leads to the occurrence of slope failures [4].

In a state like Meghalaya, which holds the record for the wettest place on earth, rain is an important factor to be studied for slope stability. Under the present investigation, a two dimensional (2D) finite element analysis has been done on a slope situated in Nongstoin, Meghalaya, India. The objective of this paper is to study the effect of soil properties, different rainfall intensities and ground water table (GWT) position on the unsaturated hill slope of Meghalaya using finite element method for a period of 48 h. The unsaturated slope under study is subjected to five different rainfall intensities (16.4, 25.5, 196.1, 212.0 and 983.0 mm) and comparative studies were made to see the response of the slope. A parametric study was done and the results of the factor of safety (FOS), displacement and pore water pressure were compared for different GWT, rainfall intensities and soil properties.

## 2 Numerical Modeling of Slope

### 2.1 *Geometry and Location of Slope*

The slope under study is situated in Nongstoin, West Khasi Hills District, Meghalaya, situated in the Northeast part of India. It is located at  $25^{\circ} 10' N$  to  $25^{\circ} 51' N$  latitude and  $90^{\circ} 44' E$  to  $91^{\circ} 49' E$  longitude with an elevation of 1200 m [5]. The monsoon season starts from the month of April onwards and ends around the month of October. June and July receive the maximum average rainfall. The average rainfall for the whole year is given in Table 1. It can be seen from Table 1 that heavy rainfall occurs during the month of April to October whereas less rainfall occurs during the month of November to March.

### 2.2 *Geometry and Location of Slope*

Samples were collected from the site and the properties of soil were obtained through laboratory tests. The different shear strength parameters and unit weight are given in Table 3. For the analysis, slope angle of  $27^{\circ}$  and 15 m slope height were considered. A homogeneous slope was prepared in 2D using FEM (MIDAS GTX NX 2016) and analysis was carried out using strength reduction method (SRM). The principle

**Table 1** Average monthly rainfall and rainy days at Nongstoin, Meghalaya

Month	Rainfall (mm)	No. of rainy days
January	16.4	1.2
February	25.5	2.3
March	76.1	4.8
April	196.1	10.4
May	350.4	15.3
June	641.4	18.9
July	983.4	20.9
August	570.7	18.4
September	409.2	15.3
October	212.0	7.3
November	31.0	1.7
December	17.1	1.3

behind strength reduction method (SRM) is the reduction of the shear strength parameters until the slope starts to fail [6]. SRM is chosen since it gives a systematic stress analysis of the slope and thereby providing an ordered factor of safety values [7]. The meshing of the slope model has been done considering a higher order element during meshing; this is done in order to lessen the convergence error usually encountered while analyzing the model. A transient seepage analysis of 48 h has been carried out, which was divided into two-time intervals, in the first interval (i.e., 0–24 h) rainfall was provided and in the second interval (i.e., 24–48 h) rainfall was not provided.

Three parametric studies were carried out: (i) with different GWT positions, (ii) with different rainfall intensities and (iii) with different soil properties. The different GWT positions considered for this analysis are given in Table 2, where  $h_c$  = distance of the crest of slope from the GWT and  $h_t$  = distance of the toe of slope from the GWT. The GWT1 position was nearest to the ground surface and the farthest was for GWT3. The rainfall intensities of 16.4, 25.5, 196.1, 212.0 and 983.0 mm were applied to surface ground level to study how the slope responds to different intensities. The different soil properties used for parametric study are given in Table 3. Observations were made on the response of the slope 24 h after rainfall and this was done with all the three parametric studies.

**Table 2** Different ground water table positions

Name of different GWT positions	GWT1	GWT2	GWT3
$h_c$ (m)	10.5	12.75	15
$h_t$ (m)	4	5	6

**Table 3** Different soil properties

Soil properties	Cohesion (c) kN/m <sup>2</sup>	Angle of internal friction ( $\phi$ )°	Unit weight ( $\gamma$ ) kN/m <sup>3</sup>
Sample number			
Sample 1	6.5	42	16.5
Sample 2	7.2	42	16
Sample 3	7.3	43	16.8

### 3 Results and Discussion

#### 3.1 Parametric Studies with GWT Variation

Variations in factor of safety for different GWT positions are shown in Fig. 1. The variation shows that the factor of safety was highest for GWT3 throughout the period of 48 h and lowest for GWT1. It was observed from Fig. 1 that the initial value of FOS was 3.25 for GWT3 and initial FOS was 2.8 for GWT1. This is mainly due to the different ground water table positions. The increase in water pressure along the phreatic line led to the decrease in the shear strength of soil. The ground water level had less impact on the pattern of slope failure as observed in Fig. 1. The factor of safety values rapidly decreased in all the three positions; this is due to the high matric suction of the soil. From the figure, it was also observed that the FOS was minimum at 15 h and after the rain stopped the FOS was observed to increase gradually. In case of GWT2 and GWT1 the increase is almost constant which shows that even 24 h after the rain stopped, the slope fails to regain its original strength in the next 24 h,

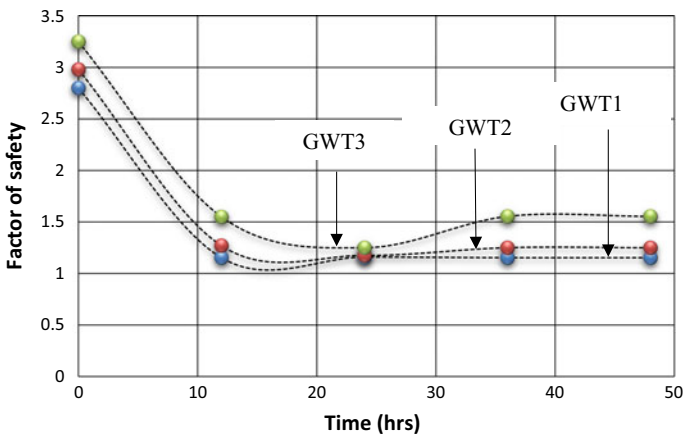


**Fig. 1** Variation of factor of safety with respect to a period of 48 h for different GWT

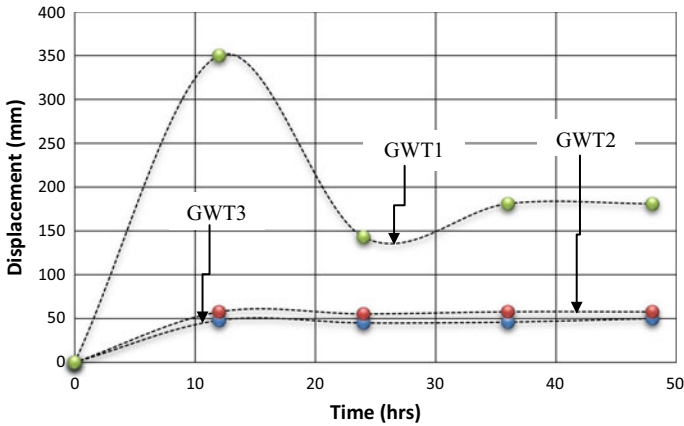


**Fig. 2** Variation of displacement with respect to a period of 48 h for different GWT

this was due to the high suction capacity of the soil and the high rainfall intensity (196.1 mm).

The transient seepage analysis performed in MIDAS GTX NX also provided the displacement of slopes for different GWT positions as shown in Fig. 2. The initial displacement was nil and with increasing time the displacement increased. For GWT2 and GWT3, the displacement along *x*-direction was comparatively low to that of GWT1. This is a result of the position of GWT with respect to the ground surface. In GWT1, the maximum displacement of the slope after 12 h of rainfall was 350 mm and after which displacement decreased suddenly to 140 mm at 26 h. This shows that at 12 h of rain the slope reached a level where it cannot be displaced anymore when the GWT is very near to the ground surface. In GWT3, when the GWT position was further away from the ground surface, the displacement was very less and remained constant throughout. This was the same case for GWT2. This can be due to the compaction of soil in after 12 h of rainfall. Since the rain was constant throughout the 24 h period the displacement of soil remained same even after the rain stopped. The position of GWT in these two cases did not have much effect to the displacements.

Negative pore water pressure was highest for GWT3 and lowest for GWT1. This is a direct result of the position of GWT. For the first 12 h of rainfall the pore water pressure decreases rapidly after which the negative pore pressure remained constant.

### 3.2 Parametric Studies with GWT Variation

Figure 3 shows the variation of FOS for different rainfall intensities for a total period of 48 h and the total duration of rainfall was 24 h. The rainfall intensities considered were 16.4, 25.5, 196.1, 212.0 and 983.0 mm. From the figure, it can be observed that



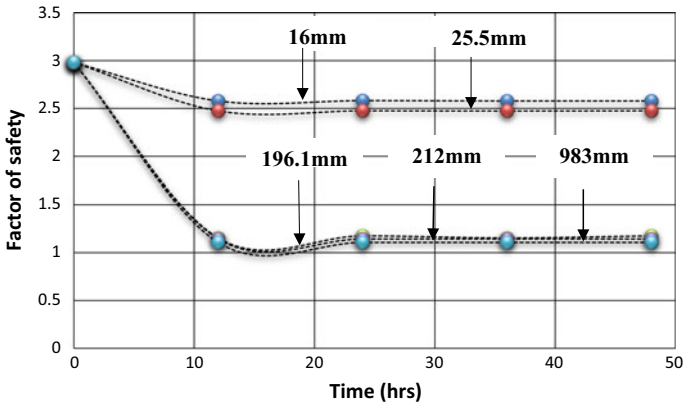


Fig. 3 Variation of factor of safety with respect to a period of 48 h for different rainfall intensities

the initial values of the factor of safety were same, because at this point rainfall has not occurred yet and all the slope properties were same. When rain started, the value of FOS for 16.4 and 25.5 mm rainfall intensities gradually decreased (as shown in Fig. 3) and achieved a minimum value of 2.6 and 2.4, respectively at 15 h. After 15 h the FOS value remained constant throughout. This shows that low intensity rainfall, did not has a substantial effect on the stability of the slope. For the rainfall intensities of 196.1, 212.0 and 983.0 mm the FOS suddenly decreased and the slope ultimately failed. The minimum value of FOS was observed at a time period of 14–18 h of rainfall and after the rain stopped, the FOS was constant and even during this period the slope failed to regain its original strength.

For different rainfall intensities, the maximum displacement was plotted as shown in Fig. 4. It was observed that for rainfall of less intensities, i.e., 16 and 25.5 mm, the resulting displacement was nil throughout the 48 h analysis. When rainfall intensities

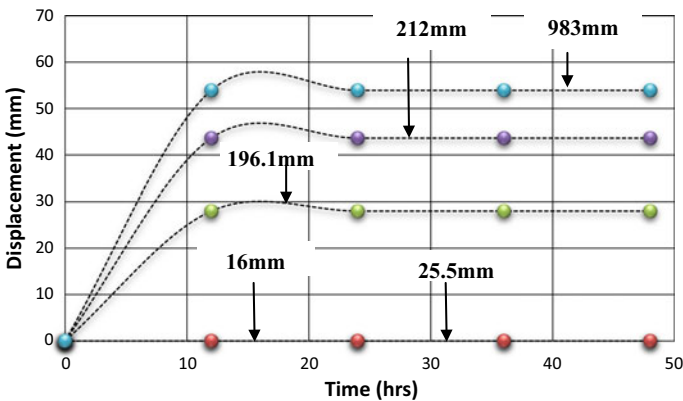


Fig. 4 Variation of displacement, with respect to a period of 48 h for different rainfall intensities

increase, the maximum displacement along x-direction keep on increasing and this increase was observed at the toe of the slope. The higher the rainfall intensity the more the pressure and ultimately the displacement will increase. The displacement along x-direction for rainfall intensity of 983, 212 and 196.1 mm was highest at 15 h of rainfall. From 15 to 24 h, the displacement decreases gradually and after 24 h the displacement remained constant. The red patch at the toe of the slope (Fig. 5) shows the occurrence of maximum displacement.

The pore water pressure was highest for the lowest rainfall intensity and as the intensity keep on increasing the pore water pressure decreased. This shows that, the higher the rainfall intensity, the lower the negative pore water pressure and this affected the shear strength of the soil. The pore water pressure variation is given in Fig. 6. The negative pore water pressure was lowest at the crest of the slope.

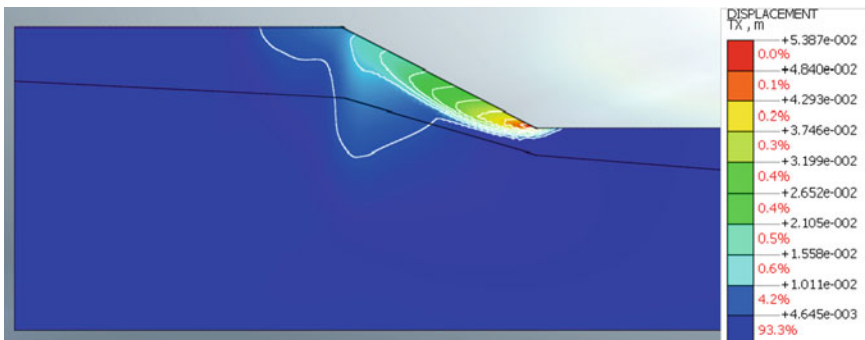


Fig. 5 Displacement contours diagram for 983 mm rainfall (highest intensity) at 48 h

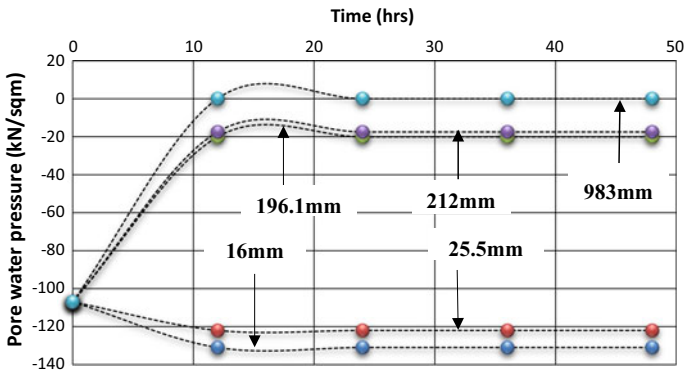


Fig. 6 Variation of pore water pressure with respect to a period of 48 h for different rainfall intensities

### 3.3 Parametric Studies with GWT Variation

The variation of FOS for different soil properties (as given in Table 2) is shown in Fig. 7 and the rainfall intensity in this case was 983 mm. The failure pattern is the same for all the three soil properties and sample 3 having the highest cohesion (7.3 kN/m<sup>2</sup>) and angle of internal friction (43°) have the highest factor of safety values. Since the samples were taken from the same site location, the shear strength parameters had very little difference; because of this the factor of safety values did not show much variation.

Maximum displacement along x-direction for different soil samples are plotted in Fig. 8. Initially the displacement was zero and the displacement showed a substantial

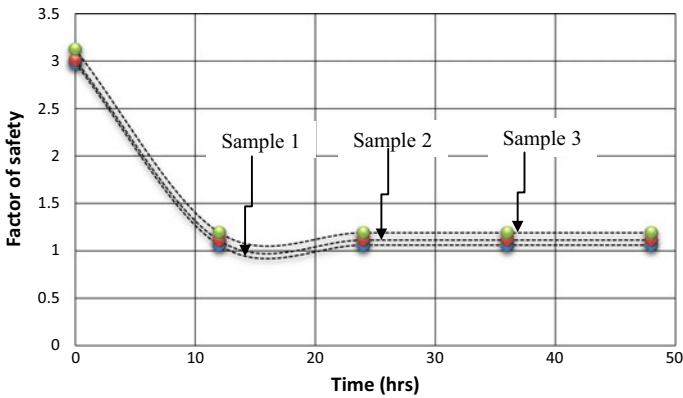


Fig. 7 Variation of factor of safety with respect to a period of 48 h for different soil properties

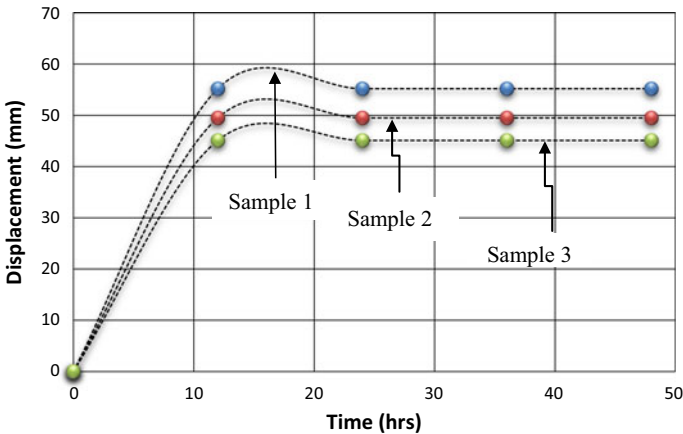


Fig. 8 Variation of displacement, with respect to a period of 48 h for different soil properties

increased during the first 12 h of rainfall. From 12 h the displacement gradually decreased till 24 h and after which it attained a constant value. Since the displacement pattern was same and the values did not vary much for all the three samples it can be concluded that the different soil properties have similar effect on the slope.

The negative pore water pressures for all the three soil parameters were the same throughout the analysis of 48 h. Initially the negative pore water pressure was  $-107 \text{ kN/m}^2$  and as the rain started, the value decreases steadily and attains a constant value of  $-20.1 \text{ kN/m}^2$  after rain. In the case of pore water pressure also, the shear strength parameters did not have significant effect to the slope.

## 4 Conclusions

The variation of GWT and rainfall intensities showed a very significant effect to the slope at Nongstoin, Meghalaya, whereas the different soil properties did not show a noticeable effect. The overall results can be summarized below as.

1. Initial values of FOS for all analysis are quite high, hence during the dry season, the chances that the slope will fail is very low. This is due to the high value of negative pore water pressure. When rain is applied, the negative pore water pressure or matric suction decreases over the time which directly affected the slope stability. It can be observed that as the matric suction decreases, FOS also decreases and attains a minimum value around 14–18 h during heavy rainfall intensities.
2. It can also be noted that during high rainfall the FOS rapidly changed with time, which is the result of the high permeability of the soil in the area, leading to the rapid seepage of rain water when the intensity of rainfall is high. The slope under study appears to be vulnerable to the high rain intensity, hence proper remedial measures needed to be taken to the slope under consideration in order to avoid any hazards during heavy rainfall.
3. The displacement was highly affected by the high GWT position. When the rainfall intensities were high the observed displacement along  $x$ -direction was higher.
4. Since all the three soil samples were collected from the same area, the different soil parameters did not show any significant effect to the slope under consideration.

## References

1. Ng CWW, Shi Q (1998) A numerical investigation of the stability of unsaturated soil slopes subjected to transient seepage. *Comput Geotech* 22:1–28
2. Griffiths DV, Lane PA (1999) Slope stability analysis by finite elements. *Geotechnique* 49(3):387–403

3. Fredlund DG, Rahardjo H (1993) Soil mechanics for unsaturated soils. Wiley, New York
4. Cai F, Ugai K (2004) Numerical analysis of rainfall effects on slope stability. *Int J Geomech*, 4(2):69–78 (2004). ©ASCE
5. Lala IP, Ray PK, Bora AK, Singh NJ, Singh R, Feroze SM (2014) Rainfall characteristics, pattern and distribution of central Meghalaya. *J Indian Water Resour Soc* 34(2):9–16
6. Matsui T, San KC (1992) Finite element slope stability analysis by shear strength reduction technique. *Jpn Soc Soil Mech Found Eng* 32(1):59–70
7. Hammah RE, Yacoub TE, Corkum BC (2005) The shear strength reduction method for the generalized hoek-brown criterion, American Rock Mechanics Association (ARMA)

# Landslide Early Warning System in Kalimpong, West Bengal



Abhirup Dikshit  and Neelima Satyam 

**Abstract** Landslides can be triggered either by rainfall or earthquake which have been intensified by the increase in human activities. Majority of the landslides in Indian Himalayas are initiated by heavy monsoonal precipitation. Several attempts have been made to determine the relationship between precipitation and landslide occurrences using various empirical or statistical methods. However, a comprehensive study on the relationship using an effective monitoring system is yet to be conducted. The present work analyses the results obtained from a reliable and robust monitoring system and analyse its applicability. The monitoring system consists of Microelectromechanical Systems (MEMS) tilt sensor and volumetric water content sensor. The MEMS-based sensor determines the tilting angle which is places at shallow depths. The change in the tilting angle reflects to the lateral displacement at the surface. Thus, the amount of tilting angle which exceeds critical value would reflect various stages of slope failure. The results obtained from the monitoring system would help in setting up a warning system and eventually save human lives.

**Keywords** Kalimpong · Monitoring system · Shallow landslides

## 1 Introduction

Landslides are hazardous natural disaster affecting human lives, property and agricultural land. The two main triggering factors for landslide initiation is rainfall and earthquake. This study deals with rainfall triggered landslides as more than 70% of the landslides are initiated by rainfall [1]. The study on rainfall induced landslides can be broadly classified in three categories conducted on either temporal or spatial scale: (i) determining the thresholds for landslide triggering (ii) hazard/susceptibility zonation (iii) monitoring system. (These studies are equally relevant and important for analysing landslide mechanism. Globally, emphasis has been on determining thresholds and understand landslide mechanism using statistical or physical models

---

A. Dikshit (✉) · N. Satyam

Discipline of Civil Engineering, Indian Institute of Technology Indore, Indore 452020, India

© Springer Nature Singapore Pte Ltd. 2022

A. K. Dey et al. (eds.), *Proceedings of the 7th Indian Young Geotechnical Engineers*

*Conference*, Lecture Notes in Civil Engineering 195,

[https://doi.org/10.1007/978-981-16-6456-4\\_28](https://doi.org/10.1007/978-981-16-6456-4_28)

[3, 5]. In context of Indian Himalayan scenario, focus has been more on zonation using various techniques. Very few studies have been conducted on threshold estimation using several approaches like statistical, probabilistic, and algorithm-based. However, a comprehensive study on understanding the mechanism of landslide initiation for long-term is yet to be attempted.

Landslide monitoring is probably the most important aspect for landslide hazard assessment as this is directly linked to the movement of slopes. It can be conducted using either remote sensing techniques, in situ ground observation or change in topography. This study deals with an in situ ground observation technique using tilt meters for real-time monitoring of unstable slopes. It would also help in understanding the relationship between the precipitation occurrences and landslide mechanism for various time periods.

## 2 Study Area

The study area is Chibo ( $27^{\circ} 03'$ ,  $88^{\circ} 27' 30''$ ) which is in the south-western part of Kalimpong situated in the Darjeeling Himalayas (Fig. 1). The region has suffered numerous landslides triggered by monsoonal precipitation (2000–4000 mm) and improper drainage system [2]. A large section of the area falls under moderate susceptible zones and the region drained by mountain rivulets (known as jhoras) generally falls under high susceptible zones. The jhoras occupy less than 1% but drains more than 10% of the region, one-third of the region is damp with more than half of the area being wet (GSI Report, 2018). The monitoring system was installed surrounding the two major destructive jhoras (Pyarieni and OC jhora). A comprehensive field visit was conducted in October 2016 to identify the monitoring sections and the instrumentation was thereby setup.

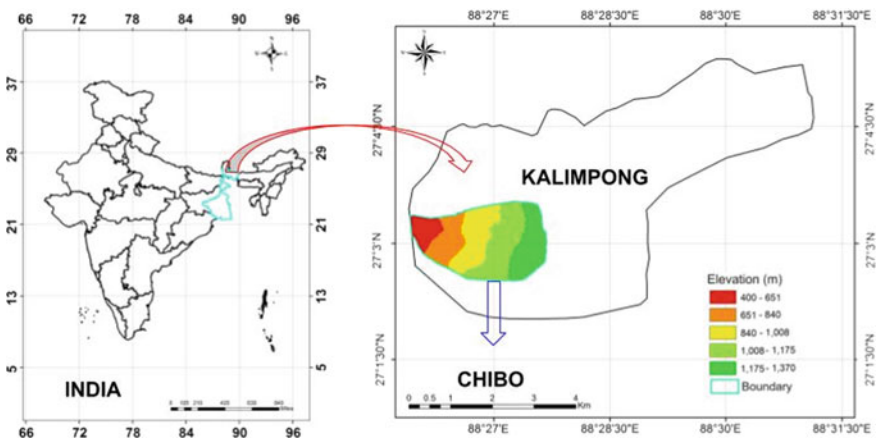


Fig. 1 Location of the study region

### 3 Monitoring System

The present study utilizes a monitoring system equipped with MEMS technology comprising of tilt sensors, volumetric water content sensor, data logger and rain gauge [6, 7]. The setup comprised of steel poles, tilt sensor enclosed in a box, volumetric water content sensor and wireless transmission kit. The tilt and volumetric sensor are tied at the bottom of pole which are installed at shallow depths of upto 1.5 m. On the top of the rod, a wireless transmission kit which uses radio communication is tied to send the data collected every 10 min to data logger. The data collected at the data logger from all the sensors is transferred to server via Internet using a cell phone network. The detailed installation and working of the monitoring setup can be found at Dikshit et al. [3], Dikshit and Satyam, [4]. The sensor location along with an illustration of the monitoring system is depicted in Fig. 2a, b.

### 4 Results and Discussion

The monitoring system has been installed for over a year (15 June 2017–9 September 2018) and the analysis has been conducted for two monsoon seasons. Such an analysis would help in understanding the sections which are susceptible to landslide initiation and determine the future slope failure. The tilting rates in  $X$  and  $Y$  direction for the study period along with volumetric water content sensor values are illustrated in Fig. 3. During investigated period, sensor 2 and 3 have shown an average tilting rate of  $0.000657^\circ/\text{h}$  and  $0.000126^\circ/\text{h}$  in parallel direction to slope and for perpendicular to slope, it has  $0.00032^\circ/\text{hr}$  and  $0.000087^\circ/\text{hr}$ , respectively. The data obtained from all the sensors clearly depict that the tilting rate was maximum at the top of the slope (sensor 2) followed at the centre (sensor 3) and then at the bottom. In case of Sensor 2, there were primarily two scenarios where the variation is significant (Fig. 4). The two cases are (13/08/2017–17/08/2017) (circled in orange) and (02/08/2018–05/08/2018) (circled in black). The initial time period had tilting rate of  $0.081^\circ/\text{h}$  and  $0.017^\circ/\text{h}$  in parallel and perpendicular direction to slope. In case of the latter time period, the tilting rate in  $X$  and  $Y$  direction was  $0.0057^\circ/\text{h}$  and  $0.0037^\circ/\text{h}$ . The major difference between the two displacement periods is the amount of rainfall. The total precipitation during the initial and latter time period was 25.15 mm and 10.9 mm, respectively.

For Sensor 3, the tilting rates are generally average movement rate during monsoon of 2018 is very less compared to monsoon of 2017 for both parallel and perpendicular direction of slope. Whereas the tilting rates is higher for pre-monsoon compared to post monsoon in both the directions to slope. This ascertains that the top of the slope or the region around Sensor 2 is at higher risk compared to Sensor 3 even for low rainfall seasons.

The fluctuating record for sensor 5 in 2018 suggests that the soil condition around this sensor became soft in 2018 and possibly local conditions affected this sensor. The



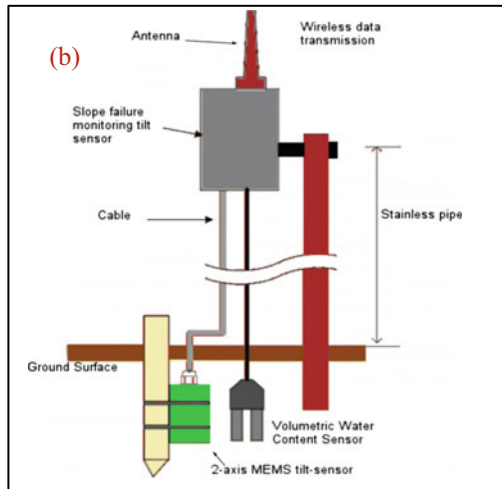
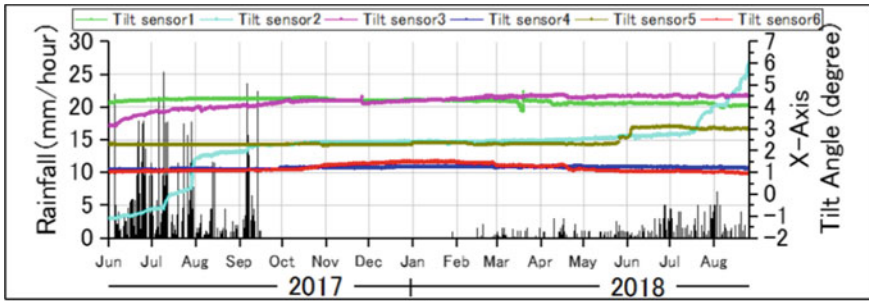
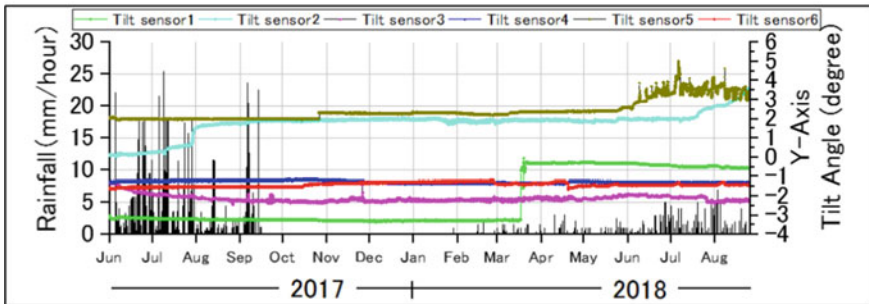


**Fig. 2 a** Location of the sensors and data logger. *Source* Google Earth, **b** MEMS sensor and volumetric water content sensor (Dikshit et al. 2018)

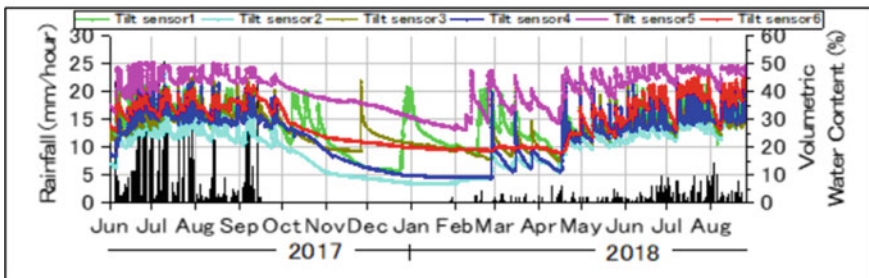
examination of the tilting rates across both the monsoon season depicts that rainfall can be considered as the main inducement of landslide or slope failure, however other important factors like ground water level, ground crack, active fault or unstable slope vegetation can also affect instability.



(a)



(b)



(c)

**Fig. 3** Detailed time history of **a** Tilting angle in parallel direction, **b** tilting angle in perpendicular direction, **c** volumetric moisture content

## 5 Conclusions

The study aims to develop an early warning system for rainfall induced landslides for Chibo, Kalimpong of Darjeeling Himalayas. To develop a warning system, MEMS-based tilt sensors and volumetric water content sensors were used. These sensors measured the variation in the tilt of instrument installed at shallow depths and the data was transferred to a server on Internet through mobile network. A major benefit

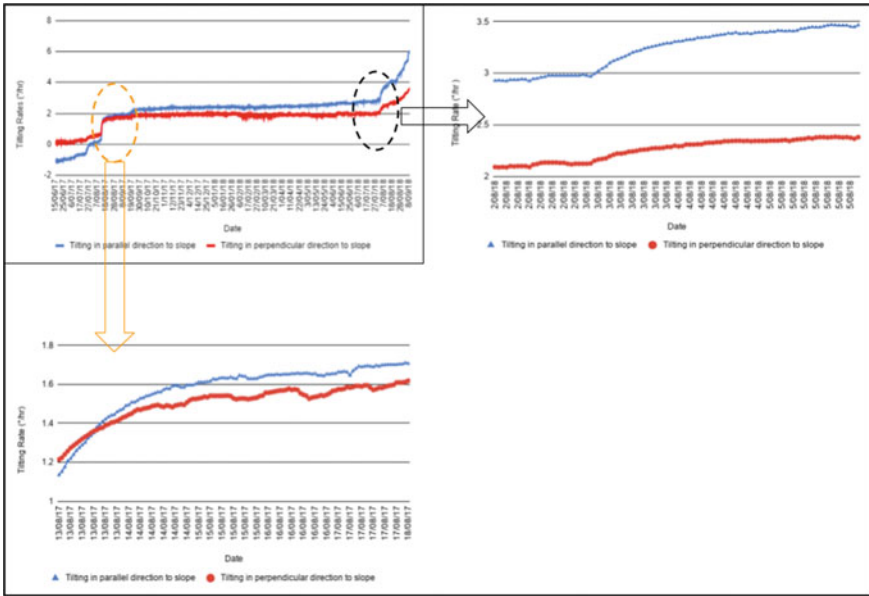


Fig. 4 Variation of tilting rates of Sensor 2

of using such instrumentation against the traditional monitoring instruments is due to its low cost and predicting the exact failure location and time. Six sensors were installed across the major sinking zones in the region and the results showed the area under 2 sensors are on the verge of failure. The field visit after monsoon 2017 was in corroboration with the tilting rates. Preventive measures need to be taken around these sensors to avoid future slope failure. The results could also help in calibrating the regional or local thresholds calculated for the region.

### References

1. Dikshit A, Satyam DN (2018) Estimation of rainfall thresholds for landslide occurrences in Kalimpong, India. *Innov Infrastruct Solut* 3:24. <https://doi.org/10.1007/s41062-018-0132-9>
2. Dikshit A, Satyam DN, Towhata I (2018) Early warning system using tilt sensors in Chibo, Kalimpong, Darjeeling Himalayas, India. *Nat Hazards* 94:727–741. <https://doi.org/10.1007/s11069-018-3417-6>
3. Dikshit A, Sarkar R, Satyam N (2018) Probabilistic approach toward Darjeeling Himalayas landslides—a case study. *Cogent Eng* 5:1–11. <https://doi.org/10.1080/23311916.2018.1537539>
4. Dikshit A, Satyam N (2019) Probabilistic rainfall thresholds in Chibo, India: estimation and validation using monitoring system, *J Mt Sci* 16:870–883. <https://doi.org/10.1007/s11629-018-5189-6>
5. Segoni S, Picciullo L, Gariano SL (2018) A review of the recent literature on rainfall thresholds for landslide occurrence. *Landslides* 15:1483. <https://doi.org/10.1007/s10346-018-0966-4>

6. Uchimura T, Towhata I, Wang L, Seko I (2009) Development of low-cost early warning system of slope instability for civilian use. In: Proceedings of the 17th ISSMGE, Alexandria, vol 3, pp 1897–1900
7. Uchimura T, Towhata I, Trinh TLA, Fukuda J, Bautista CJB, Wang L, Seko I, Uchida T, Matsu-oka A, Ito Y, Onda Y, Iwagami S, Kim MS, Sakai N (2010) Simple monitoring method for precaution of landslides watching tilting and water contents on slopes surface. *Landslides* 7(3):351–358

# Investigating the Influence of Groundwater Level Variation on Performance of Soil Nailed Slopes



Meletetsega Gashaw and A. Murali Krishna

**Abstract** The use of soil-nailing is one of the methods adopted for the stabilization of slopes and supporting the deep excavations. Many design guidelines and manuals suggested the suitable and favorable conditions for the application of soil-nailing techniques, among which groundwater level is the main concern. But most of the studies failed to show how this groundwater level and its fluctuation in the slope will affect the serviceability and ultimate limit state criteria which include the deflection, the axial forces developed in the nails, the distribution of tensile force along the nails and safety factors as a whole. Hence, in the present study, the influence of the variation of groundwater level on the behavior of soil nailed slopes using a finite element modeling software 'RS2-Rocscience' is studied. For this study, a homogeneous unstable slope for three different soils with different strength and hydraulic properties are analyzed and soil nail support systems are designed as per the FHWA soil nail design manual. Then, the variations of slope deformation developed axial forces and factor of safety for the variation of the groundwater level are presented. The results of numerical modeling show that the increase in the groundwater table will decrease the critical factor of safety and increase the horizontal deformation and the peak axial force on the nails. Further in case of unsaturated soils, due to the presence of the groundwater the top nails are all under compression (negative axial force) and the increase in stability is offered by the lower nails only.

**Keywords** Soil nail · Slope stabilization · Groundwater variation · RS2-Rocscience · Slope stability

## 1 Introduction

Soil-nailing is a technique that involves reinforcing and strengthening of unstable slopes and deep excavations by installing closely spaced steel bars, termed as soil nails. The construction method proceeds from top to bottom. This technique has

---

M. Gashaw (✉) · A. Murali Krishna  
Department of Civil Engineering, Indian Institute of Technology Guwahati, Guwahati, India

several advantages, over other stabilization techniques, such as cost, ease of construction, time of construction, construction flexibility, environmental/esthetic considerations, requirement of limited access area etc. [1, 2]. The reinforcing action of soil nails develops through the development of tensile force in passive reinforcement as the result of lateral deformation of the structure as construction goes from top to down [2–5].

Shaw-Shong [6], Tan and Chow [8] discussed the design requirements, available manuals for design and other important considerations that should be considered while designing the soil nails. The manuals widely referred in designing the soil-nailing strengthening work are: (a) BS8006:1995 Code of practice for Strengthened/reinforcement soils and other fills, (b) Federal Highway Administration (FHWA) Manual for Design & Construction Monitoring of Soil Nail Walls, and (c) BS8081:1989 Code of practice for Ground Anchorage [6, 8]. These different design manuals specified the favorable and suitable ground conditions for the application of soil nails. Among these conditions, the soil type and the groundwater conditions are the main concerns. Many studies have been conducted to study how the soil type affects the nail performance. But studies related to groundwater effect on the performance of soil nails and these structures are very rare. Byrne et al. [1] and Lazarte et al. [4] recommended locating the nails above the groundwater level and if it exists in case, it should not affect the face of excavation, the bond between the ground and the soil nails. The groundwater level inside the slope mass will vary for various changes in hydrological conditions. The aim of this study is therefore to investigate the influence of groundwater variation on the general performance of slopes stabilized with soil nails including the axial forces developed in the nails, the critical factor of safety, the displacement and the variation in suction inside the slope mass.

## 1.1 Problem Statement

Three different soils (Soil-A, Soil-B & Soil-C) representing a homogenous  $c-\phi'$  soils with different mechanical and hydraulic properties are adopted in the study. The slope geometry and soil properties adopted for the study are listed in (Fig. 1, Tables 1 and 2) respectively. Initially the slope is analyzed assuming the dry condition (the groundwater is at infinite depth from the slope) for the three soil types. Then the groundwater level starts to rise from the base of the slope to the toe of the slope which is located at 10 m from the base of the slope. Five different locations of groundwater table were considered. The 'Z' term in (Fig. 1) represents the depth of the groundwater level at a particular location. The five cases considered are: (a)  $Z = 0$  m, (b)  $Z = 2$  m, (c)  $Z = 4$  m, (d)  $Z = 6$  m, (e)  $Z = 8$  m and (f)  $Z = 10$  m. Then the slope is designed for its dry condition state using soil nails to improve the safety factor thereby stabilizing it using Byrne et al. [1] and Lazarte et al. [3, 4] soil nail design guidelines. Finally, with the set of assumptions with regard to in-situ conditions, the reinforced slope is numerically simulated using two-dimensional finite element

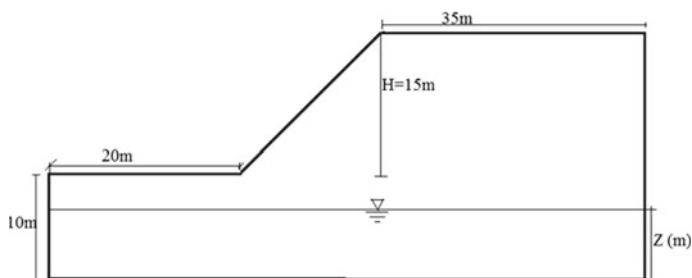


**Fig. 1** Geometry of slope

**Table 1** Mechanical properties soils

Soil type	$\gamma$ (kN/ $\mu^3$ )	$c'$ (kPa)	$\phi'$ ( $^\circ$ )	$\phi b$ ( $^\circ$ )	$E$ (MPa)	$\gamma$
Soil-A	18	8	25	25	100	0.3
Soil-B	20	10	30	30	50	0.33
Soil-C	20	20	20	20	75	0.35

**Table 2** Hydraulic properties of soils

Soil type	$\alpha$ ( $m^{-1}$ )	$n$	$\theta_r$	$\Theta_s$	$k_s$ (m/s)
Soil-A	7.087	0.005	0.049	0.304	$1.8292e^{-05}$
Soil-B	1.6	1.37	0.034	0.46	$2.39e^{-06}$
Soil-C	0.5	1.09	0.070	0.36	$5.5e^{-08}$

based computational tool RS2 Phase 2 V.9 (Rocscience2018) software for different groundwater levels and results are discussed in detail. The modeling approach used for this study was first verified by validating a model proposed by Zolqadr et al. [9].

Slope stability analysis is performed by strength reduction method followed by transient seepage analysis using coupled solid-fluid interaction analysis. In a coupled analysis, the changes in pore pressure and the effective stresses affect the deformation but not the pore pressure. A fully drained condition which defines a condition of zero excess pore pressure is considered. After seepage analysis has been done, the results of the pore pressure distribution including negative pore water pressure known as matric suction in the unsaturated zone above the water table are used to determine the stability of the slope through the strength reduction method.

## 2 Numerical Model

### 2.1 Validation of Model

Numerical model is developed using finite element method base numerical package RS2 (Rock and soil 2-dimensional) used for soil and rock applications. One of the major features of RS2 is a finite element slope stability analysis using shear strength reduction (SSR) method which automatically determines the most critical failure mode and the corresponding safety factor. To verify the results of the numerical model, a soil nailed wall constructed to support underground excavation [9] was modeled in RS2 and the horizontal deformation of the model is compared with reported data. Properties used for the validation model are presented in (Tables 3 and 4).

The modeling approach consists of simulating soil behavior by Mohr-coulomb model which exhibits linear-elastic and perfectly plastic soil behavior; applying fully grouted tie back bolts (with 100% bond length) for modeling soil nails; applying liners of standard beam as elastic material for modeling of temporary facings (shotcrete); using denser mesh in the vicinity of soil nails; and no interface element to model both soil-facing and soil-nailing interaction. The values of modulus of elasticity for

**Table 3** Input parameters for Seattle wall [9]

Soil layer	Layer 1	Layer 2	Layer 3	Layer 4	Layer 5
Thickness (m)	4	3.6	3.6	3.6	3.6
$c$ (kPa)	9.6	9.6	9.6	9.6	9.6
$\phi$ (°)	40	40	40	40	40
$\gamma$ (kN/m <sup>3</sup> )	21.6	21.6	21.6	21.6	21.6
$E$ (MPa)	40.7	95.7	143.5	358.8	923.4
$\nu$	0.34	0.32	0.29	0.234	0.2

**Table 4** Input parameters used for soil nails and shotcrete

Bolt type	Tieback
Bolt diameter (mm)	50
Bolt modulus, (kPa)	4,222,698.95
Bond shear stiffness, kN/m/m	3000
Bond strength (kN/m)	1000
Borehole diameter (mm)	150
Liner type	Standard beam
Young's modulus, $E$ (kPa)	1,628,878.28
Poisson's ratio	0.18
Thickness (m)	0.1



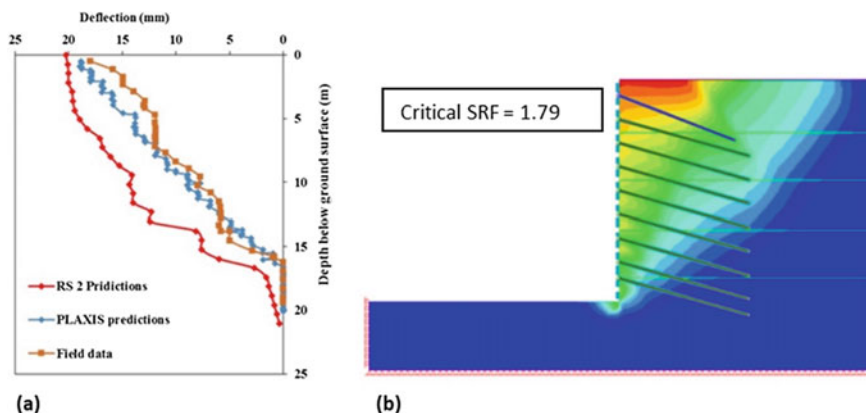


**Fig. 2** **a** Comparisons of horizontal deformations, **b** numerical model of Seattle wall

both shotcrete element and tieback were calculated from the axial stiffness (EA in kN/m) values given from Zolqadr et al. [9].

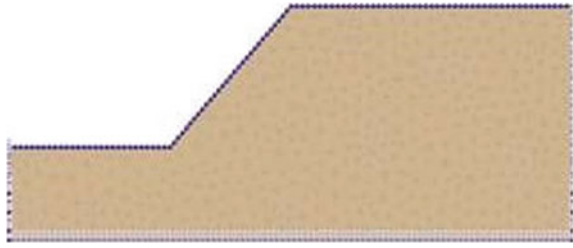
The reported final horizontal deformation at the end of construction from Zolqadr et al. [9] was 18 mm from field inclinometer measurements and 19.7 mm from PLAXIS FEM predictions. The RS2 deformation prediction of the same model was found to be 20.22 mm at the end of construction. Comparing the three results, it shows that the numerical predicted horizontal displacement by RS2 is acceptable (Fig. 2).

## 2.2 Analysis of Unreinforced Slope

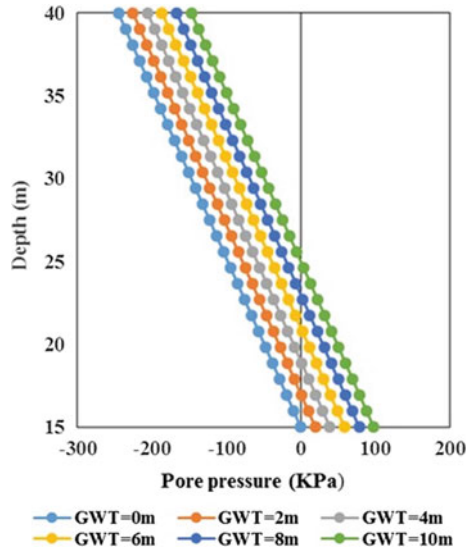
Numerical model of homogenous slope has been prepared to study the effect of groundwater rise in unreinforced slope for the three different soils through a finite element model using RS2 Phase-2 (Rocscience, 2018) software using coupled analysis followed by strength reduction analysis. A uniform mesh type with 1500 six noded triangular elements is used for both slope stability and groundwater analysis. The bottom boundaries were assigned fixed boundary condition and left and right sides of slope were assigned roller boundary conditions to allow movement in the vertical direction for stability analysis. And for seepage analysis, each level of groundwater is defined as a total head boundary at the left and right side of the model. The boundaries above the groundwater table are defined as a nodal flow rate with seepage face condition. The face of slope is assigned undefined flow rate and the bottom boundary is assigned a nodal flow rate except for the conditions when the groundwater table is at the base of the slope as shown in (Fig. 3).

Figure 4 illustrates the pore pressure profile variation with the change in the groundwater table. It is observed that with the rise in the groundwater table the pore pressure changes from zero which was the case when groundwater table was fixed

**Fig. 3** Numerical model of seepage analysis



**Fig. 4** Porewater pressure variation with increase in groundwater level



at the base of the slope to 98.1 kPa when the water reaches the toe of the slope at the same time the negative pore pressure which is known as matric suction is decreasing with the increase in the groundwater table. Matric suction changes from 245.24 kPa when groundwater table was fixed at the base of the slope to 147.15 kPa when water table reaches the toe of the slope. The decrease in the suction results in decrease of effective stresses which is the cause of reduction of strength of soil.

Figure 5a depicts the change in critical factor of safety with the rise in the groundwater level. Due to the inherent suction, the factor of safety of the soils are very high at higher suction levels compared to the ideal dry condition which is difficult to find in real case. But with the rise in the groundwater table, the safety factor reduces for all soils considered in the study. But depending on the strength and unsaturated properties of the soils the stability of soils varies. For example, for Soil-A, the factor of safety of the slope changes from 2.46 to 1.34, for Soil-B from 2.89 to 1.58 and for Soil-C from 2.1 to 1.33 when the groundwater rises from the base of slope (0 m) to toe of the slope (10 m). Soil-B is more stable than Soil-A and Soil-C. This shows

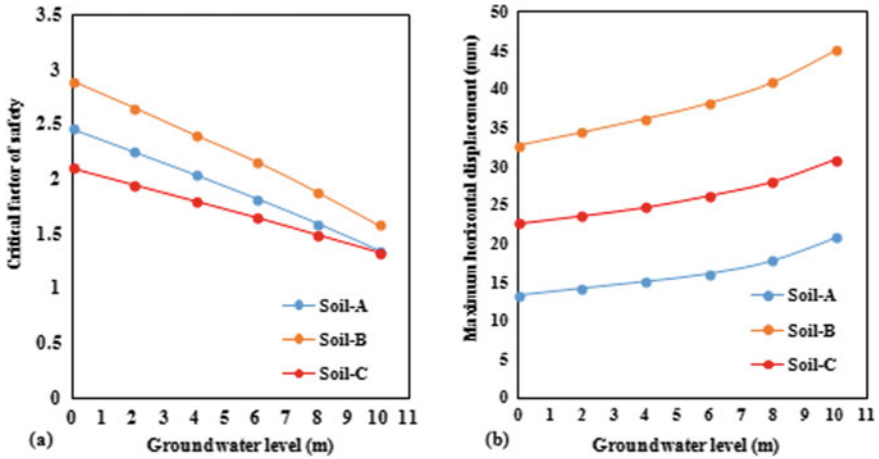


Fig. 5 a Variation of critical factor of safety of unreinforced slope with groundwater increase, b variation of maximum horizontal deformation of unreinforced slope with groundwater increase

that the strength parameters together with the unsaturated shear strength parameter will result different response of the slope subjected to similar seepage condition.

Figure 5b depicts the maximum horizontal deformations at different groundwater levels. Since the deformations are the results of the changes in the pore pressure and effective stress, the decrease in effective stresses and increase in pore pressure will result in more deformation. The maximum horizontal deformation increases from 13.3 mm to 20.8 mm, 32.7 mm to 45.1 mm and 22.6 mm to 30.9 mm for Soil-A, Soil-B and Soil-C respectively when the groundwater increases from the base to toe of slope. The values of horizontal deformations also show that deformations in finite element analysis are directly influenced by deformation properties of soils (E and  $\nu$ ).

### 2.3 Design of Reinforced Slope

The design of the soil nail support for the three soil types system is carried out based on the [1, 3] soil nail design manual. The allowable stress/load design method and the simplified wedge failure method of design [7] are used. For soils the design of soil nails is done for the dry condition where the groundwater is neglected. The design parameters used and the outputs of the design for all soils considered in the study are presented in Tables 5, 6, 7 and 8.

**Table 5** General material properties and performance requirements used for design

Parameter	Value
Height of the slope (m)	15
Slope of backfill, $\beta(^{\circ})$	0
Face batter, $\alpha(^{\circ})$	45
Nail installation method	Rotary drilled
Nail distribution at wall face	Uniform
Grade of steel	Fe-420
Modulus of elasticity of nail EN, GPa	200
Nail spacing, $S_V$ and $S_H$ (m)	$1 \times 1$
Nail inclination from the horizontal $i$ , ( $^{\circ}$ )	15
Drill hole diameter, $D_{DH}$ , mm	150
Compressive strength of grout, $f_{ck}$ , MPa	30
Ultimate bond strength, $q_u$ , kPa	150
Modulus of elasticity of grout, $E_g$ , GPa	30
FS for global stability, $F_{SG}$	1.35
FS for pullout, $FS_P$	2.0
FS for tensile strength, $FS_T$	1.8
FS for flexural failure, $FS_{FF}$	1.35
FS for punching shear, $FS_{FP}$	1.35

**Table 6** Summary of design for nails

Design parameter	Soil-A	Soil-B	Soil-C
Length $L$ , m	14	14	15
Diameter $D$ , mm	32	32	32
Max. axial force $T_{max}$ , kN	105.93	97	142.18
Axial force at the head, kN	63.56	58	85.31
Pullout capacity $Q_U$ , kN/m	70.65	70.65	70.65
Max. tensile load capacity $R_T$ , kN	337.78	337.784	337.784
FOS against pullout, $FS_P$	9.28	10.18	7.4
FOS against tensile strength, $FS_T$	3.2	3.5	2.4

**Table 7** Summary of design for facing

Type	Temporary shotcrete		
Thickness, $h$ , mm	200		
Reinforcement	102 $\times$ 102-MW26 $\times$ MW26		
Other reinforcement	Waller bars 2 $\times$ 10 mm (2 $\times$ #10)		
Bearing plate grade	Fe-420		
Bearing plate dimension	225 mm $\times$ 225 mm $\times$ 25 mm		
Flexural capacity $R_{FF}$ , kN	260.56	260.56	260.56
Punching shear capacity $R_{FP}$ , kN	440.60	440.60	440.60
FS against flexural failure, $FS_{FF}$	4.1	4.5	3.05
FS against punching shear, $FS_{FP}$	6.9	7.6	5.16

**Table 8** Factor of safety of unreinforced and reinforced slope for dry condition

Soil type	FOS of unreinforced slope	FOS of reinforced slope
Soil-A	0.89	1.9
Soil-B	1.02	2.37
Soil-C	1.01	1.74

**Table 9** Soil nail and facing properties used in numerical modeling

<i>Nail properties</i>	
Bolt type	Tieback
Bolt diameter, (mm)	32
Bolt modulus, $E$ (GPa)	200
Tensile capacity (kN)	300
Bond shear stiffness (kN/m/m)	20,000
Bond strength (kN/m)	150
<i>Facing properties</i>	
Liner type	Standard beam
Young's modulus (kPa)	$3 \times 10^7$
Poisson's ratio	0.25
Thickness (m)	0.2

## 2.4 Analysis of Reinforced Slope

Using the same numerical modeling approach in the case of unreinforced slope the reinforced slopes are modeled in RS2. The soil nails are modeled as tieback bolts with 100% bond length and the facing are modeled as standard beam of elastic material. The input parameters used for the soil nails and facing are shown in Table 9.

Figure 6a depicts the variation of critical factor of safety of the reinforced slope with groundwater table increase. As in the case of unreinforced slope, the factor of safety reduces with groundwater rise. The factor of safety of reinforced slope changes from 2.63 to 1.55 for Soil-A, 3.14 to 1.94 for Soil-B and 2.33 to 1.54 for Soil-C when the groundwater keeps increasing from base of the slope to toe of the slope. The changes in horizontal deformation of reinforced slope are also shown in (Fig. 6b). The maximum horizontal deformation changes from 12.5 mm to 17.9 mm for Soil-A, from 29.1 mm to 37 mm for Soil-B and from 20.4 mm to 26.5 mm or Soil-C.

For soil nails to develop their reinforcing action, the axial tension force that is developed in the nails as the result of the interaction between soil and soil nail as the ground deforms is required. Figure 7 depicts the changes in the peak axial loads with increase in the groundwater table. Since the displacement of the slope is increasing with groundwater rise, the axial force that develops on the nails increases because the nail forces are mobilized when there is enough displacement. Therefore, the peak axial load that develops at the lower nails is increasing.

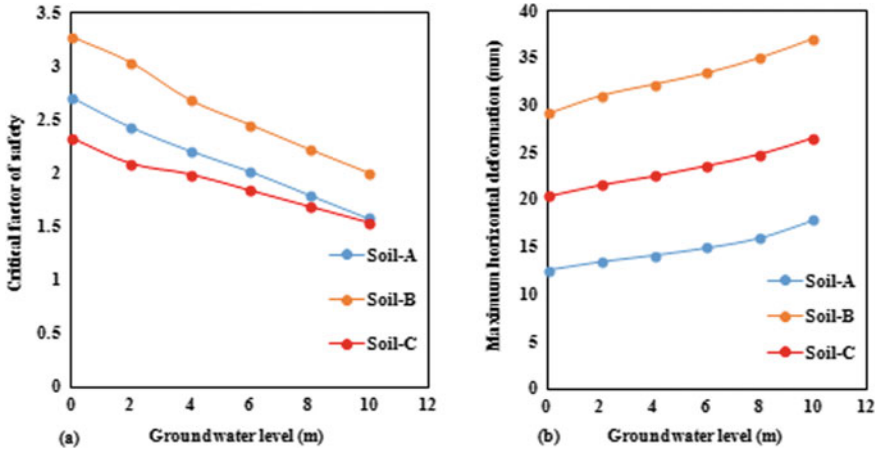


Fig. 6 a Variation of critical factor of safety of reinforced slope with groundwater increase, b variation of maximum horizontal deformation of reinforced slope with groundwater increase

Fig. 7 Variation of peak axial force with groundwater increase

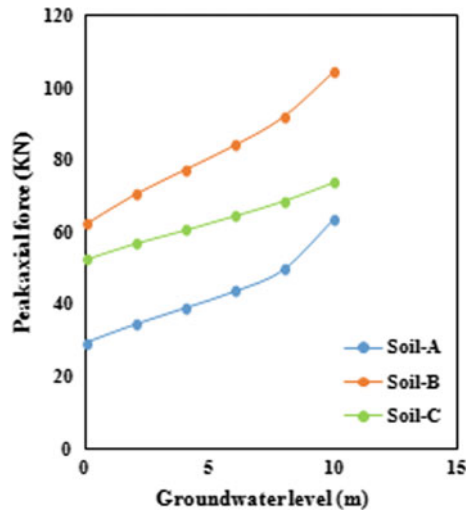
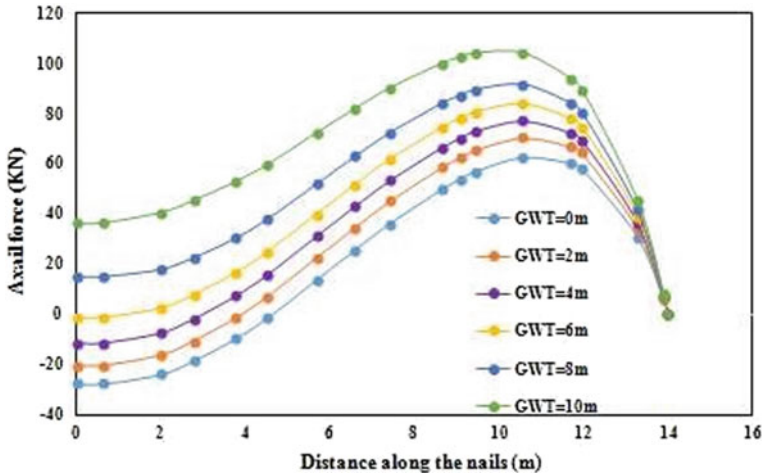


Figure 8 shows the axial force distribution along the bottom nail for different groundwater levels. It is clearly seen that the axial force along the nails increases with groundwater rise. But it was also observed that due to the presence of the groundwater the top nails in the unsaturated zone are all under compression (negative axial force) and the increase in stability is offered by the lower nails only. The top nails are not providing any resistance since the axial forces are not mobilized in the nails unlike the dry case where groundwater is neglected. In this case, it can be observed that in the case of unsaturated soils relatively large displacements are required to mobilize



**Fig. 8** Axial force variation with groundwater changes along the nail length for the bottom nail (Soil-B)

the nail forces. If the more axial force develops on the nails, then only there will be increase in the stability of the slope. This observation is seen in (Fig. 9).

### 3 Conclusions

Three different homogenous soils with different mechanical and hydraulic properties were modeled to study the effects of groundwater variations in soil nailed slopes. From the results, it can be concluded that with the increase in the groundwater table the factor of safety reduces, and the deformations increase as the result of reduction in suction for both reinforced and unreinforced slopes. In the case of reinforced slopes, the peak axial force that develops in the bottom nails also increases with rise in the groundwater as the result of large deformations. The results also show how the performance of the nails in mobilizing their axial force is affected by the presence of seepage compared to the dry soil conditions. The axial forces that are the main sources of stability for soil nailed structures are not mobilized as required in the case of the presence of groundwater flow. For the axial forces in the nails and basic reinforcement mechanism of nails to develop a relatively larger displacements are required in case of unsaturated soils. But this again has to be checked from serviceability criteria where the deformations should lay within the acceptable ranges.

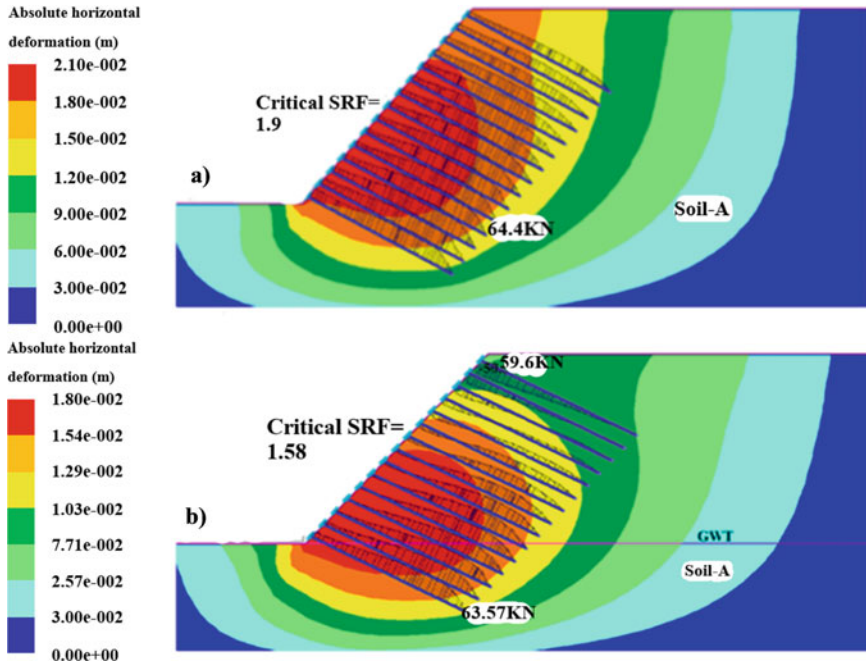


**Fig. 9** Axial force distribution along the nails for Soil-A **a** Under dry condition, **b** groundwater at 10 m

## References

1. Byrne RJ, Cotton D, Porterfield J, Wolschlag C, Ueblacker G (1998) Soil manual for design and construction monitoring of soil nail walls. Manual of the Federal Highway Administration Division, No. FHWA-SA-96-069R
2. Dey A (2014) Issues and aspects of soil nailing. QIP-STC on challenges and recent advances in geotechnical engineering research and practices: December
3. Lazarte CA, Elias V, Espinoza RD, Sabatini PJ (2003) Geotechnical engineering circular no. 7: soil nail walls. Federal Highway Administration, Washington, DC
4. Lazarte CA, Robinson H, Gómez JE, Baxter A, Cadden A, Berg R (2015) Soil nail walls reference manual (No.FHWA-NHI-14-007)
5. Prashant A, Mukherjee M (2010) Soil nailing for stabilization of steep slopes near railway tracks. Research Design and Standard Organisation, Lucknow
6. Shaw-Shong L (2005) Soil nailing for slope strengthening. Geotechnical Engineering, Gue& Partners SdnBhd, Kuala Lumpur, Malaysia, 30–31
7. Sheahan TC, Ho CL (2003) Simplified trial wedge method for soil nailed wall analysis. J Geotech Geoenviron Eng 129(2):117–124
8. Tan YC, Chow CM (2004) Slope stabilization using soil nails: design assumptions and construction realities. In: Malaysia-Japan symposium on geohazards and geoenvironmental engineering, Bangi, Malaysia, pp 13–14
9. Zolqadr E, Yasrobi SS, NorouzOlyaei M (2016) Analysis of soil nail walls performance—case study. Geomech Geoeng 11(1):1–12



# Effect of Vertical Seismic Coefficient in Slope Stability Analysis



Sukanta Das and B. K. Maheshwari

**Abstract** From the major earthquakes in hilly areas, the researchers have focused on the need of consideration of vertical seismic acceleration component in seismic slope stability analysis. The conventional pseudo-static method is quite common because of its simplicity. The earthquake force is considered as an equivalent static force (two seismic acceleration components) within the soil mass. The horizontal seismic acceleration coefficient is always considered acting away from the slope and the criticality of the direction of vertical seismic acceleration coefficient depends on the soil properties. The conventional pseudo-static method is considered in this study. The variation of factor of safety due to change in direction of vertical seismic coefficient for different soil properties is examined. Moreover, the critical direction of vertical seismic coefficient ( $k_v$ ) for different types of soil has been investigated throughout this study.

**Keywords** Factor of safety · Pseudo-static method · Seismic slope stability · Type of soil

## 1 Introduction

The earthquake induced ground shaking may lead slopes to fail which are marginally stable before shaking. Although, stability of a natural or man-made slope depends on material properties, geometry and geological conditions of the slope [1]. Several methods have been adopted for stability analysis of slopes. Limit equilibrium is the method where the factor of safety (FS) can be estimated but no information is obtained regarding slope deformations. The stress deformation method gives the information about factor of safety as well as deformation. In pseudo-static method, to check the seismic stability of slopes, the earthquake force is considered as equivalent static force acting within the soil mass. Newmark Sliding block method is also adopted for seismic slope stability and permanent displacement assessment for seismic condition

---

S. Das (✉) · B. K. Maheshwari  
Department of Earthquake Engineering, IIT Roorkee, Roorkee, India

[2]. The horizontal seismic acceleration component ( $k_h$ ) significantly reduces the FS of a slope. The recent earthquake damages in hilly areas have influenced researchers to focus on the vertical seismic coefficient ( $k_v$ ) for the stability analysis of slopes. The vertical seismic coefficient is quite strong enough to influence the conventional stability analysis [3–5]. Sarma [6] determined the critical acceleration taking into account both seismic components for different soil conditions. Many researches have been conducted to check the effect of ' $k_v$ ' on slope stability analysis but those are mostly based on a particular soil type [7, 8].

No study has been found which directly suggests for considering the direction of ' $k_v$ ' for different types of soil in a common platform. In the present study, the effect of vertical seismic coefficient ' $k_v$ ' on conventional pseudo-static method for different types of soil has been discussed through analytical expressions and graphically. The effect of direction of ' $k_v$ ' on slope stability analysis for all types of soil has been summarized in the present work.

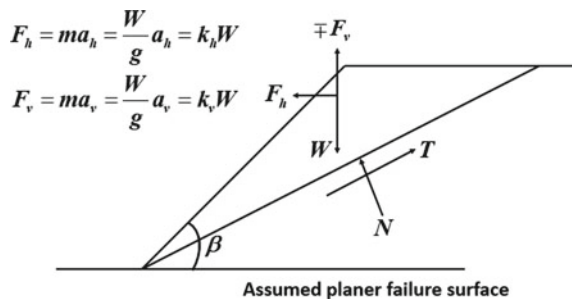
## 2 Pseudo-static Method

In Fig. 1, a typical planer failure surface has been presented and forces acting on the plane are shown with the as per direction. FS is a ratio of resisting force to the disturbing force acting on the failure plane.  $F_v$  and  $F_h$  are the seismic forces in vertical and horizontal directions, respectively,  $W$  is weight of the soil mass and  $N$  is the reaction force acting on the soil mass. General equation for FS can be obtained by resolving all the forces acting on the failure plane.

### 2.1 Factor of Safety

After resolving force acting along the failure surface of the slope, the equations for FS is obtained to evaluate the FS for  $c$ - $\phi$ , pure cohesionless and cohesive soil. The  $c$  and  $\phi$  are cohesion and internal friction of the soil is used as in conventional method

**Fig. 1** Assumed failure surface in pseudo-static method



of pseudo-static analysis. Where  $W$  is weight of the soil,  $T$  is resisting force acting along the plane,  $N$  is reaction force acting perpendicular to the plane and  $\beta$  is slope angle. The direction of vertical seismic coefficient is positive in downward direction and negative in upward direction.

FS for  $c$ - $\emptyset$  soil

$$FS = \frac{CL + [(W \mp F_V)\text{Cos}\beta - F_h\text{Sin}\beta] \tan \phi}{(W \mp F_V)\text{Sin}\beta + F_h\text{Cos}\beta} \quad (1)$$

In Eq. 1, the FS depends on soil strength parameters, slope angle and seismic forces. The  $\text{Cos}\beta$ , term is effected by direction of ( $k_v$ ) thus the FS is also effected. For  $c$ - $\phi$  soil, in normalized form is given in Eq. 2.

$$FS = \frac{\frac{CL}{W} + [(1 \mp K_V)\text{Cos}\beta - K_h\text{Sin}\beta] \tan \phi}{(1 \mp K_V)\text{Sin}\beta + K_h\text{Cos}\beta} \quad (2)$$

FS is strongly influenced by cohesion in Eq. 3. The ' $\text{Sin}\beta$ ' denominator term is effected by direction of ' $k_v$ ' and the FS is also influenced.

FS for  $\phi = 0$  soil

$$FS = \frac{\frac{CL}{W}}{(1 \mp K_V)\text{Sin}\beta + K_h\text{Cos}\beta} \quad (3)$$

In Eq. 4, numerator and denominator both are influenced by the FS but the numerator is influenced much because of its 'cos' component.

FS for  $c = 0$  soil

$$FS = \frac{[(1 \mp K_V)\text{Cos}\beta - K_h\text{Sin}\beta] \tan \phi}{(1 \mp K_V)\text{Sin}\beta + K_h\text{Cos}\beta} \quad (4)$$

### 3 Results and Discussion

In this present study, FS of slopes is obtained using commercial tool *Geostudio*, 2012. The ordinary slice method has been considered and the critical slip circle is obtained by several trial. The Mohr-Column failure criteria is considered and FS for different types of soil has been examined. The variation of FS with the change of direction of  $k_v$  for different soils has been presented subsequently.

### 3.1 For Cohesionless Soil ( $c = 0$ )

In this study, the value of vertical seismic coefficient is assumed as half of the horizontal seismic coefficient. Thus, Indian standard code 1893 [9] suggests that the value of ' $k_v$ ' should be taken as half or two third of the ' $k_h$ '. The Fig. 2a, d shows the effect of vertical seismic coefficient on factor of safety for cohesionless soil with different value of angle of internal frictions. It can be observed that when ' $k_v$ ' is acting upward, the FS decrease with increase in value of ' $k_v$ '. While when ' $k_v$ ' is acting downward, the FS increase with increase in value of ' $k_v$ '. Thus, there is a clear effect of direction of ' $k_v$ ' and the difference in FS (for ' $k_v$ ' upward and for ' $k_v$ ' download cases) increase with increase in ' $k_v$ '. As expected, with the increase in ' $k_v$ ' the difference of FS also increases and this phenomenon becomes strong when  $\phi$  value increases. The critical FS is observed when the ' $k_v$ ' acts against the gravity. The change of critical FS is much stronger at higher value of the vertical seismic

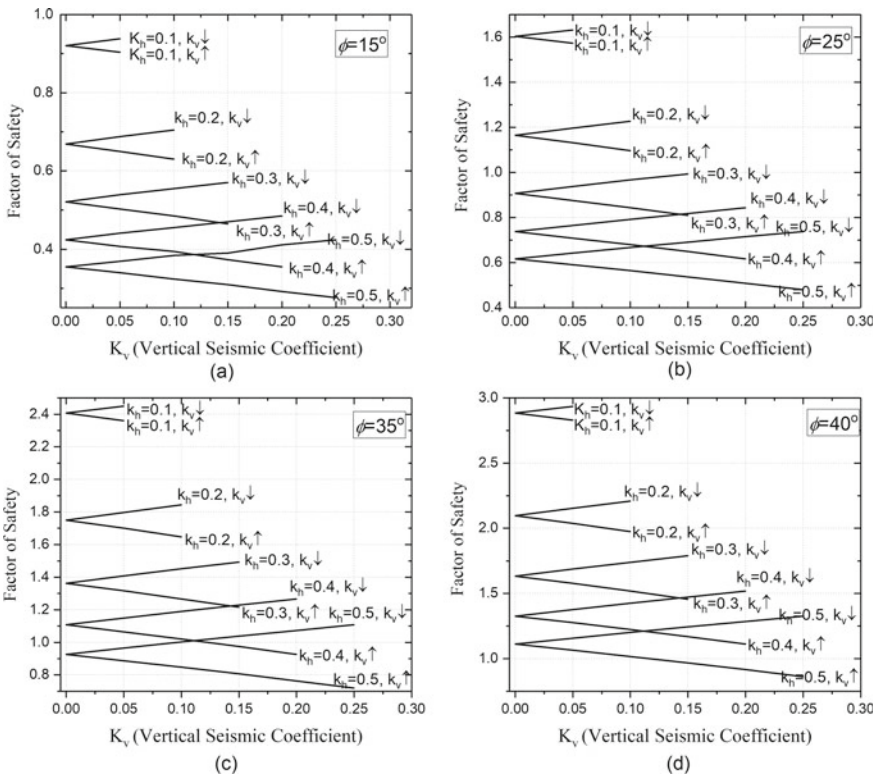


**Fig. 2** Variation of factor of safety (FS) with vertical seismic coefficient ( $k_v$ ) towards  $\downarrow$  and against  $\uparrow$  the direction of gravity for cohesionless soil and for  $c = 0$ ,  $\gamma = 17 \text{ kN/m}^3$ ,  $\beta = 26^\circ$ , **a**  $\phi = 15^\circ$ , **b**  $\phi = 25^\circ$ , **c**  $\phi = 35^\circ$ , **d**  $\phi = 40^\circ$

coefficient. Therefore, ' $k_v$ ' should be considered in upward direction or against the gravity for estimating of minimum or critical FS for cohesionless soil.

### 3.2 For Cohesive Soil ( $\phi = 0$ )

The variation of FS with the direction of ' $k_v$ ' for pure cohesive soil has been shown in Fig. 3. For pure cohesive soil, the critical FS has been found when the direction of ' $k_v$ ' is the that of the gravity. The trend of the results for cohesive soil are opposite to that of cohesionless soil. Similar phenomena has been observed throughout the graph with the increase of cohesion the FS increasing.

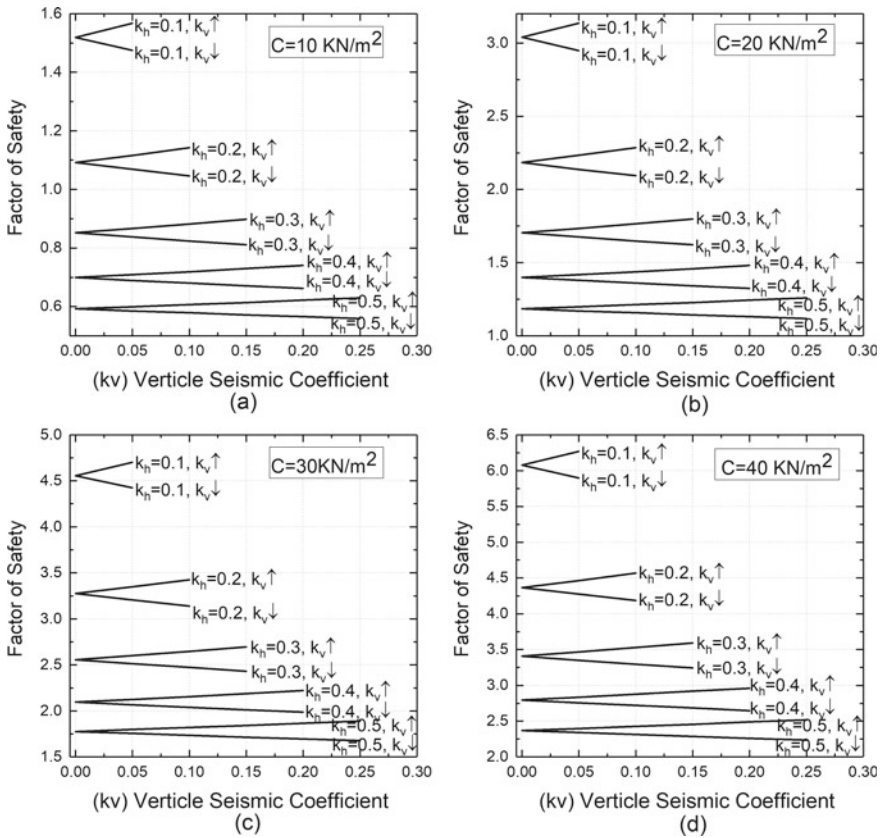


**Fig. 3** Variation of factor of safety (FS) with vertical seismic coefficient ( $k_v$ ) towards  $\downarrow$  and against  $\uparrow$  the direction of gravity for cohesive soil and for  $\phi=0$ ,  $\gamma=26 \text{ kN/m}^3$ ,  $\beta=26^\circ$ , **a**  $c = 10 \text{ kN/m}^2$ , **b**  $c = 20 \text{ kN/m}^2$ , **c**  $c = 30 \text{ kN/m}^2$ , **d**  $c = 40 \text{ kN/m}^2$

### 3.3 For $c-\phi$ Soil

The change of FS with different slope angles for ' $c-\phi$ ' soil is shown in the Fig. 4a, d. From Fig. 4a, the variation of FS increases due to change of direction of ' $k_v$ ' with the increase of ' $k_h$ '. The upward direction of ' $k_v$ ' is giving critical factor of safety in most of the cases for lower value of  $\beta$ . However, with the increase of slope angle the critical FS has been observed in downward direction of ' $k_v$ ' at a certain value of ' $k_h$ ' and after that upward direction of ' $k_v$ ' gives the critical FS.

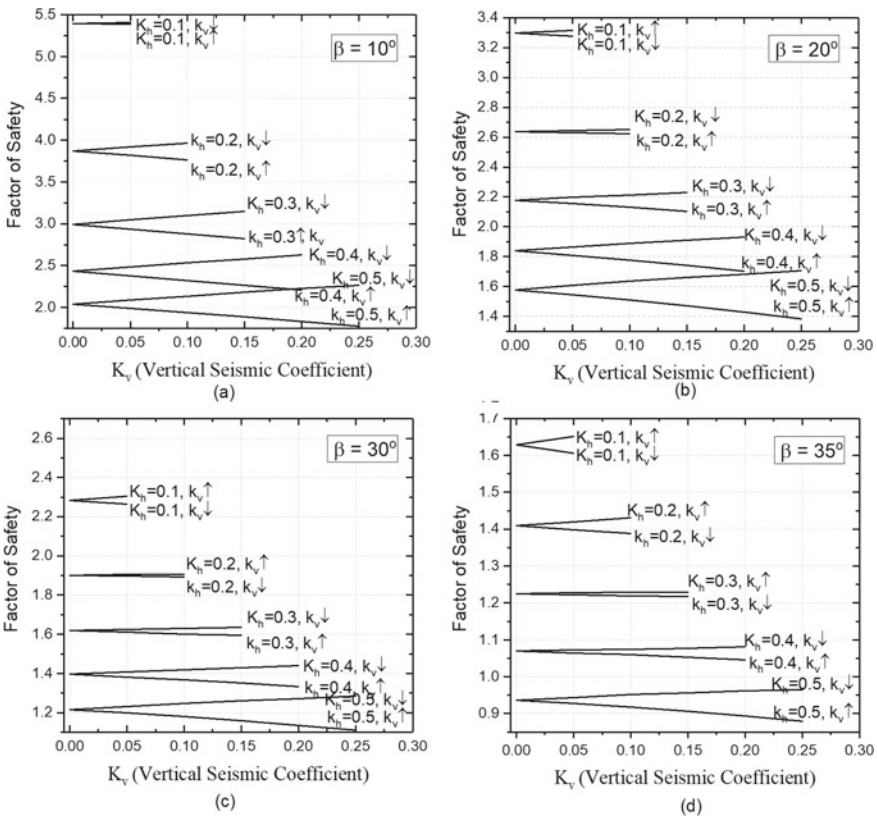


**Fig. 4** Variation of factor of safety (FS) with vertical seismic coefficient ( $k_v$ ) towards  $\downarrow$  and against  $\uparrow$  the direction of gravity for  $c-\phi$  soil and for  $c = 10 \text{ kN/m}^2$ ,  $\gamma = 17 \text{ kN/m}^3$  and  $\phi = 40^\circ$ , **a** =  $\beta 10^\circ$ , **b** =  $\beta 20^\circ$ , **c** =  $\beta 30^\circ$ , **d** =  $\beta 35^\circ$

## 4 Conclusions

From the above study the following conclusions can be drawn:

For a given cohesionless soil slope, the critical direction of vertical seismic coefficient is upward direction or against the gravity which gives the minimum factor of safety. While the minimum FS is observed in the downward direction of vertical seismic coefficient for cohesive soil slope.

In case of ' $c-\phi$ ' soil slope, the critical direction of vertical seismic coefficient depends on the domination parameter between  $c$  and  $\phi$ . However, the critical direction of vertical seismic coefficient depends on the slope angle for a constant  $c-\phi$  value.

## References

1. Kramer SL (1996) Geotechnical earthquake engineering. Prentice Hall, Upper Saddle River NJ
2. Newmark NM (1965) Effects of earthquakes on dams and embankments. *Geotechnique* 15(2):139–160
3. Chopra AK (1966) The importance of vertical component of earthquake motion. *Bull Seismol Soc Am* 56(5):1163–1175
4. Jibson RW (2011) Methods for assessing the stability of slopes during earthquakes—a retrospective. *Eng Geol* 122(1):43–50
5. Leschinsky D, Ling HI, Wang JP (2009) Equivalent seismic coefficient in geocell retention systems. *Geotext Geomembr* 27(1):9–18
6. Sarma SK (1999) Seismic slope stability—the critical acceleration. In: Proceedings of the second international conference on earthquake geotechnical engineering. Balkema, Lisbon. pp 1077–1082 Standard (BIS). New Delhi, India
7. Sahoo PP, Shukla SK, Mohyeddin A (2018) Analytical expressions for determining the stability of cohesionless soil slope under generalized seismic conditions *J Mountain Sci* 15(3)
8. Malla S (2017) Consistent application of horizontal and vertical earthquake components in analysis of a block sliding down an inclined plane. *Soil Dyn Earthq Eng* 101:176–181
9. IS: 1983 (2016) Indian standards criteria for earthquake resistant design of structures. Part 1, Bureau of Indian

# Prediction of Stability of Hill Slope Through Electrical Resistivity Tomography



Arindam Saha, Ashim Kanti Dey, Bedanta Kalita, Surya Pratap Vishwakarma, and Nayan Ahmed

**Abstract** Landslides are very common events along NH 54, i.e., Silchar Halflong road. There are many sliding zones like Reko, Phiangpui, Muolhoi Digrik, Debarai, Nutan Basti, Mahadev tilla, Durbin Tilla, Synod turning, Tankaram turning, etc. where landslides occur almost every year. The state PWD removes debris every year with an assumption that the slides become stable and will not recur. No investigation has ever been done to evaluate the depth of the loose debris and the potential of future slides due to rains. In the present study, one potential slide area namely, Durbin tilla has been chosen for investigation. An electrical resistivity tomography (ERT) was conducted on the area during the winter season. Forty-eight numbers of electrodes at a spacing of 0.6 m center to the center were laid along the slope and electrical resistivity survey was conducted. It was observed that the top surface consists of loose gravelly sand of resistivity around 400  $\Omega$  m. Some pockets of loose boulders with high resistivity 3000  $\Omega$  m were also observed. High resistivity area near the top end of the slope was observed. The slope stability analysis was performed using GEO5 software using different methods like Bishop method, Sharma method and Spencer method. The possible slip surface and the factors of safety were determined in GEO5 software with the present groundwater table condition. It is observed that the slope is stable in its present condition but becomes unstable during rainy season due to rise in water table.

**Keywords** Landslide · Electrical resistivity survey · Slope stability analysis · GEO5

## 1 Introduction

Rainfall induced landslides cause huge loss of life and property every year in Assam, India. There are many factors affecting initiation of landslides like geometry of the slopes, the geotechnical properties of soil, magnitude and intensity of the rainfall

---

A. Saha (✉) · A. K. Dey · B. Kalita · S. P. Vishwakarma · N. Ahmed  
National Institute of Technology Silchar, Silchar, Assam, India  
e-mail: [lncs@springer.com](mailto:lncs@springer.com)

© Springer Nature Singapore Pte Ltd. 2022  
A. K. Dey et al. (eds.), *Proceedings of the 7th Indian Young Geotechnical Engineers Conference*, Lecture Notes in Civil Engineering 195,  
[https://doi.org/10.1007/978-981-16-6456-4\\_31](https://doi.org/10.1007/978-981-16-6456-4_31)



over the area, level of ground water table, etc. Investigating landslide prone area with conventional methods like borehole technique or cone penetration test is very difficult, risky and uneconomical. In such situation, noninvasive geophysical technique like electrical resistivity tomography (ERT) can prove to be an easy and efficient way. ERT has been greatly used in characterizing the subsurface condition on the basis of its resistivity to current flow [9]. Information about the resistivity gives us information about soil type, lithology [14], water content [2], degree of saturation, porosity [8], detection of cracks [11], etc. ERT can successfully separate integrated rock and weathered rock [5]. These utilities of electrical resistivity tomography made it a useful tool for investigation at landslide site [3, 4].

In this paper, a detail electrical resistivity tomography study was conducted in a landslide prone area, namely, Durbin Tilla located in the Silchar-Haflong road in the state of Assam, India. A 2D electrical resistivity survey along a profile over a landslide mass was carried out using Wenner Schlumberger array configuration which yielded some important results regarding the characteristic of the soil and geometry of the profile. The geotechnical properties were determined in the laboratory. The stratification and geotechnical property were incorporated in GEO5 software and the stability of the slope was determined.

## 2 Geology and Site Characteristics at Durbin Tilla

The coordinates of the site are 25.006818 N, 92.760188 E. On one side of the road lies the Jatinga river and on the other side lies the selected site for this study. The vegetation is mostly tropical evergreen and there is a large tract of rainforest in this part of Assam. The region receives an average rainfall of 1300 mm per annum. The soil is nonlateritic in the flat alluvial area to lateritic in topographically high areas. It ranges from sandy to clayey loam in nature. The rock present in the site is well jointed and highly fractured. Groundwater manifests in the forms of perennial and seasonal springs and the discharge of the spring and seepage depends on the amount of precipitation in the area. The area represents a high run-off zone. By conducting a survey using a theodolite, the slope of the site was found out to be around 34° in the study area and with degree of slope increasing at the top of hill (Fig. 1).

## 3 Electrical Resistivity Tomography (ERT)

The electrical resistivity tomography is performed by passing an electric current into the ground surface through a pair of electrodes and the resulting potential difference was measured by other pair of potential electrodes. Forty-eight numbers of electrodes in the ground surface were used. These electrodes were connected with each other via a multi-cable wire and were connected to a control machine named Syscal Junior. The pattern of taking this resistivity data depends upon the type of array created in

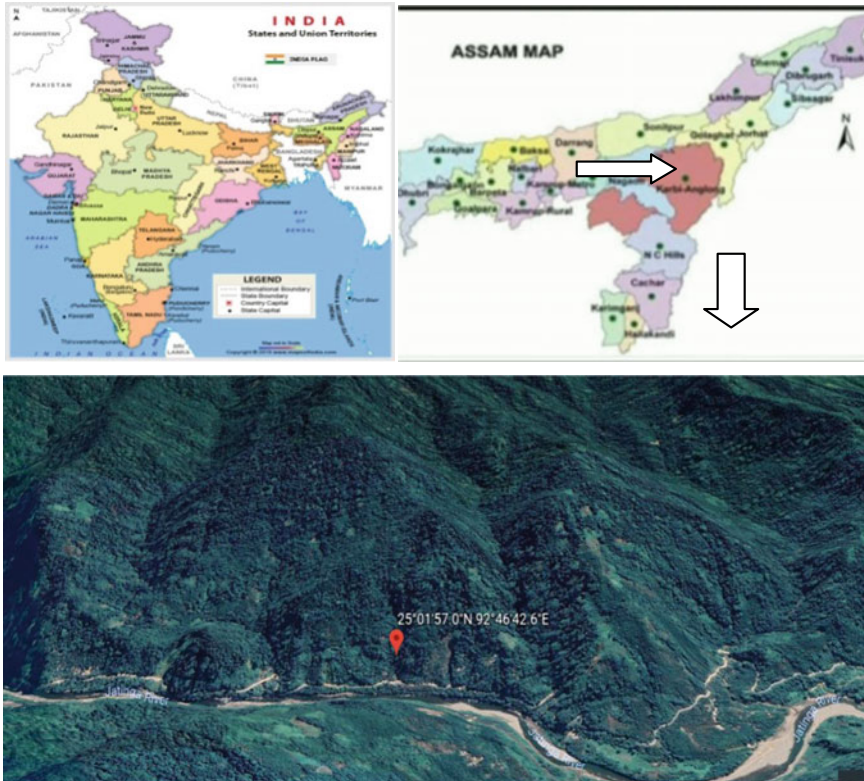


**Fig. 1** Showing the location and satellite image of the mountain

the syscal junior machine by Electro Pro software. The electrodes were inserted in a linear pattern at a horizontal spacing of 0.6 m. A smaller inter electrode spacing was kept to obtain the subsurface condition with a greater resolution. The elevation of each electrodes position was also noted down and was used during the calculation of true resistivity in software. The survey covered a length of 24 m along the slope which showed a vertical distance of 18 m from the existing road level. The survey could not be done beyond this length due to the presence of steep boulders and rock. A profile of 12 m depth was obtained from the survey. For better horizontal and vertical resolution, Wenner Schlumberger array was used [7]. As in a landslide area, the heterogeneity of the medium is very large; a high number of stacking was used, as stacking increases the appropriateness of the field data. A minimum of 6 and a maximum of 8 stackings with a confidence limit of 99.5 percent were maintained during the acquisition of filed data. The data collected here are apparent resistivity. The resistivities stored in syscal junior were downloaded in a laptop by prosys software. The bad data points are deleted using this software. The resistivity values were transferred to the next software called RES2D, where inversion of the field data gives the true resistivity of the site area.

**Table 1** Index properties of soil

S. No.	Parameter	Value
1	Water content	16%
2	In situ density	17.5 KN/m <sup>3</sup>
3	Gravel content	44.6%
4	Sand content	33.2%
5	Silt content	8.2%
6	Clay content	13.5%
7	Liquid limit	25%
9	Plastic limit	Nonplastic
10	Specific gravity	2.61

## 4 Geotechnical Properties

For landslide prediction, geotechnical properties and the position of groundwater play an important role. The in situ density was determined by core cutter method following IS: 2720 (Part 29). The in situ water content of the soil was determined by oven dry method following IS code IS: 2720 (Part 2). The grain size distribution was determined following IS: 2720 (Part 4). Wet sieving was carried out to separate the fine grain particles from the coarse grain particles by washing it on a 75-micron sieve. Dry sieve analysis was carried out on particles retained on 75-micron sieve. Hydrometer analysis was then carried out on soil fraction which was finer than 75 microns to determine the percentage of silt and clay. The atterberg limits and specific gravity were determined following IS: 2720 (Part 5) and IS: 2720 (Part 3), respectively. The liquid limit was determined by Casagrande apparatus and specific gravity was determined by 50 ml density bottle. Properties of the soil are shown in Table 1.

## 5 GEO 5 Software and Slope Stability Methods

The slope stability analysis was performed with the help of GEO5 software. It enables design and analysis of slope stability with circular or polygonal surfaces and automatic optimization of the slip surface. Considering circular slip surface, Bishop method was used to determine the stability of slope while for polygonal slip surface, Sharma method and Spencer method were used. Bishop method uses the method of slices to discrete the soil mass and determine the factor of safety. This method satisfies vertical force equilibrium for each slice and overall moment equilibrium about the center of the circular trial surface. The Sharma method is based on limit equilibrium condition for the forces and calculates moment in the individual wedges created above a polygonal slip surface [12]. Spencer satisfies the conditions of equilibrium for both forces and moments and assumes that the interslice forces are parallel [13].

## 6 Results and Discussion

High resolution subsurface image was obtained using electrical resistivity tomography. ERT can successfully separate integrated rock and weathered rock on the basis of their resistivity range. Resistivity depends on the type of soil. The resistivity of clayey soil generally varies between 10 and 100 Ω m, where the silty soil varies from 10 to 150 Ω m, sandy soil and gravel varies from 400 to 4000 Ω m and resistivity of rock may range above 4000 Ω m [6]. Also Archie’s law was originally developed and used to link resistivity with pore water, porosity and degree of saturation of surrounding petroleum reservoir rocks. The correlation between these factors is depicted by classical, empirical [1] equation as given in Eq. 1:

$$\rho_a = a \cdot \rho_w \cdot n^{-m} \cdot s^{-1} \tag{1}$$

where,

- $\rho_a$  Is the resistivity of rocks or soils,
- $\rho_w$  The resistivity of pore water,
- $n$  Porosity,
- $s$  The degree of saturation,
- $m$  Cementation factor and
- $\alpha$  Tortuosity.

From the above equation, it can be stated that the resistivity of a medium decreases with the increase in degree of saturation. Below groundwater table, the soil becomes completely saturated. This causes a decrease in electrical resistivity value below the groundwater table. Thus many researchers have predicted the depth of groundwater table based on this correlation [10]. The electrical resistivity tomography obtained at the present site is shown in Fig. 2.

In this figure, high resistivity zone could be observed in the top end of the profile. The resistivity of this region ranges above 4000 Ω m which indicates the presence of intact rock. In the middle portion of the figure, a resistivity zone ranging between 1600 and 4000 Ω m could be observed. This resistivity ranges indicates the presences of boulders which could be also verified from visual experience. The resistivity of the remaining portion ranges in between 50 Ω and 1600 Ω m which indicates the presence of sandy gravel soil with traces of silty and clay. Below 2–2.5 m depth, there is a decrease in resistivity value which indicated the presence of groundwater table. From the resistivity image, the area can be broadly classified into three portions, the unweathered rock on the top of the hill, the soil and the boulders. The stratification of the layer is shown in Fig. 3.

The shear strength of the soil, boulders and unweathered rock plays an important role in determining the possibility of landslide occurrence. These shear strength parameters are incorporated in GEO 5 software to determine the factor of safety. The effective cohesion and effective angle of internal friction of soil as determine in laboratory using direct shear are 10 kPa and 35°, respectively. The shear strength

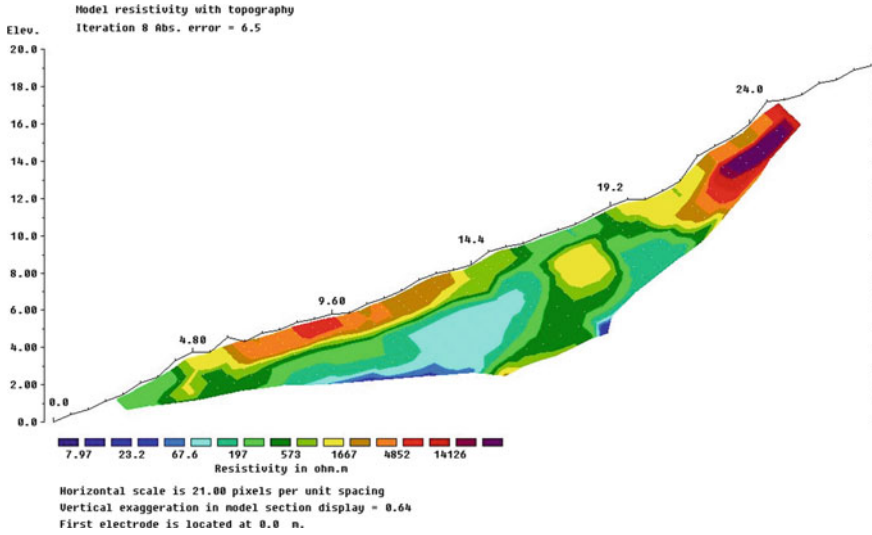


Fig. 2 The electrical resistivity tomography of the present landslide area

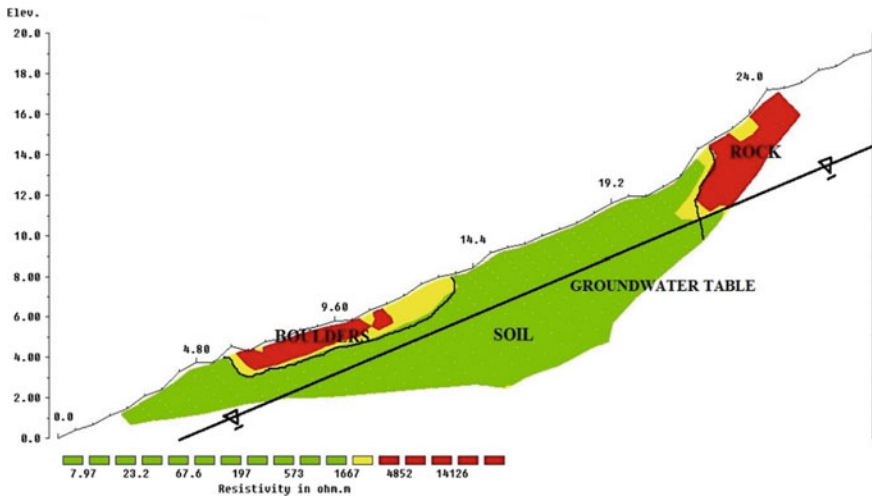


Fig. 3 Stratification of hill slope based on electrical resistivity tomography

parameter of boulders and unweathered rock could not be determined in laboratory and therefore the values are taken from literature. The effective cohesion and effective angle of internal friction of boulders are taken as 5 kPa and 39°, respectively and that of unweathered rock is taken as 200 kPa and 15°, respectively. The unsaturated and saturated unit weights of unweathered rock were 24 KN/m<sup>3</sup> and 22.5 KN/m<sup>3</sup>,

respectively and that of boulder was 20KN/m<sup>3</sup> and 22 KN/m<sup>3</sup>, respectively. The index properties of the soil are shown in Table 1.

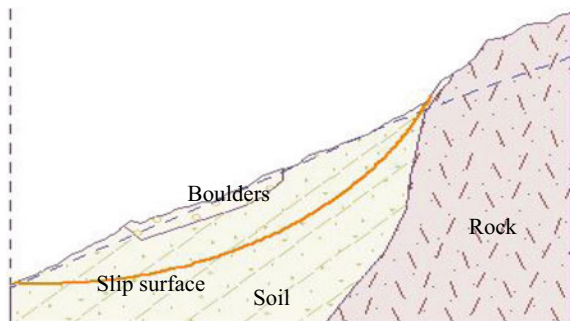
### 7 Stability Analysis of the Slope

The stability of the slope is determined as the ratio of the resisting movement which ensuring the stability of slope to those driving movement that threatening the slope stability. The stratification obtained from electrical resistivity tomography is modeled in GEO5 software. Three main interface is formed, the unweathered rock, the soil and the boulders. The unit weight and shear strength parameters of rock, soil and boulders are also incorporated using the GEO5 software. The groundwater level obtained from electrical resistivity tomography was also incorporated. As the landslide occurred in this region is rainfall induced, the stability of the slope was checked by increasing the level of groundwater table. The stability analysis of the slope for different ground-water level determined by Bishop method, Spencer method and Sharma method in GEO5 software are tabulated in Table 2. The slip surface is predicted from optimization technique having the least factor of safety. A typical slip surface predicted by Bishop method when the groundwater table is just near the ground surface is shown in Fig. 4.

**Table 2** Stability analysis of the slope

S. No.	Methods	Factors of safety		
		When water table is in existing condition	When water table just 1 m above the existing condition	When water table is just below the ground surface
1	Bishop method	1.54	1.41	1.11
2	Spacer method	1.55	1.41	1.10
3	Sharma method	1.57	1.44	1.13

**Fig. 4** Showing slip surface developed in GEO5 software using Bishop method



## 8 Conclusions

The following conclusions are drawn:

1. The factor of safety of the slope predicted for the existing groundwater table using Bishop, Spencer and Sharma method are coming 1.54, 1.55 and 1.57, respectively which suggest that the slope is stable in the prevailing condition.
2. With the increase in groundwater table, the factor of safety decreases.
3. The stratification obtained from electrical resistivity matches with the borehole data and with visual experience.
4. ERT reduces the number of boreholes required to know the actual site condition and made the investigation economical.
5. The stratification obtained from the electrical resistivity tomography helps in predicting the possible slip surface.

## References

1. Archie GE (1942) The electrical resistivity log as an aid in determining some reservoir characteristics. *Trans AIME* 146(01):54–62. <https://doi.org/10.2118/942054-G>
2. Chambers J, Gunn DA, Wilkinson PB, Meldrum P, Haslam E, Holyoake S, Kirkham M, Kuras O, Merritt A, Wragg J (2014) 4D electrical resistivity tomography monitoring of soil moisture dynamics in an operational railway embankment. *Near Surface Geophys* 12(1):61–72. <https://doi.org/10.3997/1873-0604.2013002>
3. Crawford MM, Bryson LS (2018) Assessment of active landslides using field electrical measurements. *Eng Geol* 233:146–159. <https://doi.org/10.1016/j.enggeo.2017.11.012>
4. Friedel S, Thielen A, Springman SM (2006) Investigation of a slope endangered by rainfall-induced landslides using 3D resistivity tomography and geotechnical testing. *J Appl Geophys* 60:100–114. <https://doi.org/10.1016/j.jappgeo.2006.01.001>
5. Giao PH, Weller A, Hien DH, Adisornsupawat K (2008) An approach to construct the weathering profile in a hilly granitic terrain based on electrical imaging. *J Appl Geophys* 65:30–38. <https://doi.org/10.1016/j.jappgeo.2008.03.004>
6. IEEE (1981) IEEE guide and for soil and thermal resistivity and measurements. A IEEE Std 442-1981 (Reaffirmed 1996), 1981(reaffirmed). <https://doi.org/10.1127/0028-3649/2003/2003-0556>
7. Loke MH (2000) Electrical imaging surveys for environmental and engineering studies—a practical guide to 2-D and 3-D surveys. [https://www.academia.edu/11991713/Electrical\\_imaging\\_surveys\\_for\\_environmental\\_and\\_engineering\\_studies\\_A\\_practical\\_guide\\_to\\_2\\_D\\_and\\_3\\_D\\_surveys](https://www.academia.edu/11991713/Electrical_imaging_surveys_for_environmental_and_engineering_studies_A_practical_guide_to_2_D_and_3_D_surveys)
8. Mota R, Santos FAM (2010) 2D sections of porosity and water saturation from integrated resistivity and seismic surveys. *Near Surface Geophys* 8:575–584. <https://doi.org/10.3997/1873-0604.2010042>
9. Rinaldi V, Guichon M, Ferrero V, Serrano C, Ponti N (2006) Resistivity survey of the subsurface conditions in the estuary of the rio de la plata. *J Geotech Geoenviron Eng* 132(1):72–79
10. Saad R, Nawawi MN, Mohamad E (2012) Groundwater detection in alluvium using 2-D electrical resistivity tomography (ERT) 2-D electrical resistivity tomography. *Electron J Geotech Eng* 17:369–376

11. Samouelian A, Cousin I, Richard G, Tabbagh A, Bruand A (2003) Electrical resistivity imaging for detecting soil cracking at the centimetric scale. *Soil Sci Soc Am J* 67(5):1319–1326. <https://doi.org/10.2136/sssaj2003.1319>
12. Sarma SK (1973) Stability analysis of embankments and slopes. *Geotechnique* 23(3):423–433. <https://doi.org/10.1680/geot.1973.23.3.423>
13. Spencer E (1967) A method of analysis of the stability of embankments assuming parallel inter-slice forces. *Geotechnique* 17:11–26
14. Stan D, Stan-Kłeczek I (2014) Application of electrical resistivity tomography to map lithological differences and subsurface structures (Eastern Sudetes, Czech Republic). *Geomorphology* 221:113–123. <https://doi.org/10.1016/j.geomorph.2014.05.027>



# **Soil Dynamics and Earthquake Engineering**

# Effect of Excavation Depths on Soil Pressure Acting on Embedded Cantilever Retaining Walls Under Dynamic Loadings



Sanku Konai

**Abstract** In this study, the effect of various excavation depths ( $D_e$ ) on resultant lateral soil pressure acting on cantilever retaining wall embedded in sand has been investigated. A finite difference program (FLAC-2D) is used for the present study. Numerical analysis in plane strain condition is performed by assuming the soil to behave as a linearly elastic perfectly plastic material obeying Mohr–Coulomb failure criterion. Sinusoidal dynamic acceleration with peak acceleration of 0.3 g, where g is the acceleration due to gravity and frequency 3 Hz are applied for 7 s at bottom grid of the numerical model. The net pressure acting on cantilever retaining wall is observed after the dynamic event. From this numerical study, it is observed that the behavior of left wall and right wall are different under post dynamic conditions. It is also found that under static condition the rate of increment of maximum earth pressure is less with the increment of excavation depth ( $D_e$ ) although under dynamic condition the rate of increment of maximum earth pressure is decreased for left wall and increased for right wall. It is also found that the maximum net pressure lies between excavation level and the toe of the embedded cantilever wall.

**Keywords** Flexible cantilever retaining wall · Numerical modeling · Soil pressure · Depth of excavation

## 1 Introduction

Earth excavation is necessary for almost all types of construction work and use of flexible retaining wall is in common practice. In many cases these walls can experience dynamic loading due to earthquake. Generally, Mononobe-Okabe method is used to calculate the dynamic earth pressure acting on embedded retaining wall. From experimental study under dynamic loading condition researchers found that active earth pressure measured in the experiments are close to the calculated active earth pressure by M–O methods [1, 2] but the pressure distributions are not hydrostatic in

---

S. Konai (✉)

Department of Civil Engineering, Bennett University, Greater Noida, U.P. 201310, India

© Springer Nature Singapore Pte Ltd. 2022

A. K. Dey et al. (eds.), *Proceedings of the 7th Indian Young Geotechnical Engineers*

*Conference*, Lecture Notes in Civil Engineering 195,

[https://doi.org/10.1007/978-981-16-6456-4\\_32](https://doi.org/10.1007/978-981-16-6456-4_32)

most of the cases. From a series of non-linear explicit finite difference study [3] it is found lateral stress acting on the wall did not correspond with Mononobe-Okabe predicted lateral stress. Significant studies were done for estimating dynamic earth pressure [4–8]. Some experiments and analytical programs are performed to find out the distribution of lateral earth pressure on cantilever retaining structure and found that the maximum dynamic earth pressure increased with depth and can be approximated by triangular distribution [9]. For the structural design of cantilever retaining wall the maximum bending moment and lateral displacement realistic distribution of earth pressure should be considered. Earth pressure distribution depends on many important factors, but excavation depth is one of the most important factors which severely influences the lateral earth pressure in static as well as dynamic condition. A numerical study is conducted to understand the effect of excavation depth on lateral earth pressure act against embedded cantilever wall.

## 2 Modeling

A small-scale numerical model (two dimensional) of flexible embedded cantilever wall based on finite difference analysis is developed using FLAC2D [10]. Numerical model is generated considering plane strain condition. Two cantilever walls are modeled with 200 mm total depth and 2.4 mm thickness of plexiglass material. These walls are discretized by 10 numbers of element which are two-dimensional beam elements. Numerical model dimensions are identical with experimental analysis as described in Konai et al. [11]. In the present numerical analyses, using  $E_{pp} = E_p/(1 - \mu_c^2)$  [10], Young's modulus of the walls is found out. Value of Young's Modulus of plexiglass ( $E_p$ ) is as  $6.333 \times 10^9$  N/m<sup>2</sup> and value of Poisson ratio ( $\mu_p$ ) is 0.35 in this analysis. The element size of mesh in plane strain numerical grid (800 mm  $\times$  400 mm), within which the cantilever walls are located, is 20 mm  $\times$  20 mm. Figure 1 shows the grid developed for the present numerical study. The “*sigmoidal (sig4)*” model is defined as follows [10] in FLAC 2D.

$$M_s = y_0 + \frac{a}{1 + \exp[-(L - x_0)/b]} \quad (1)$$

where  $a$ ,  $b$ ,  $x_0$  and  $y_0$  used in Eq. 1 are the curve fitting parameters, and their values are 0.984,  $-0.686$ ,  $-2.77$  and  $-0.0899$ , respectively. The logarithmic strain  $L$  in Eq. 1 is given as  $L = \log_{10}(\gamma)$ . As a dynamic loading input a 7 s sinusoidal acceleration time history with peak acceleration of 0.3 g and frequency of 3 Hz is applied to understand the resultant lateral earth pressure acting on cantilever wall. Acceleration time history applied to the bottom grid of numerical model is shown in Fig. 2. Acceleration time history used in numerical analysis is similar to the dynamic input used in experimental analysis described in Konai et al. [11].

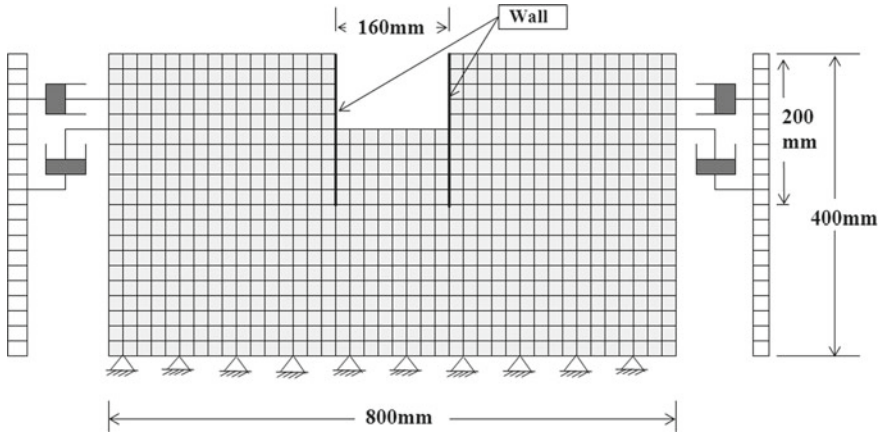
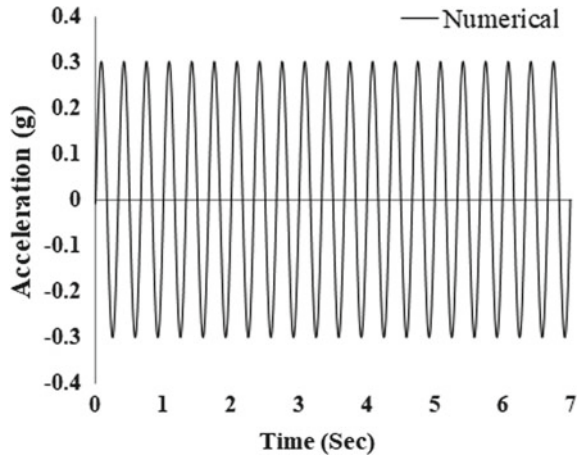


Fig. 1 Adopted Grid for numerical analysis on embedded cantilever wall

Fig. 2 Sinusoidal acceleration applied as input loading for numerical analysis

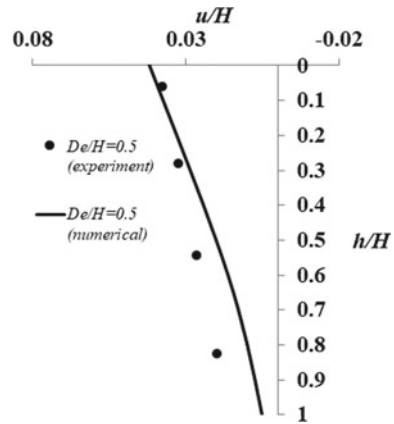


In this analysis, uniform grained dry sand is considered, and the specific gravity of the soil is 2.7. The maximum dry unit weight  $\gamma_{d(max)}$  is  $16.7 \text{ kN/m}^3$ , and the minimum dry unit weight  $\gamma_{d(min)}$  is  $14.03 \text{ kN/m}^3$ . The effective cohesion ( $c'$ ) and the effective angle of friction ( $\varphi'$ ) used for this study is 0.05 kPa and  $38^\circ$ , respectively.

The interaction between the soil and structure is modeled by using a shear and a normal spring at each node of the structure. The normal and shear stiffness ( $K_n$  and  $K_s$ ) used in this study are given [10] as

$$K_n = K_s = 10 \max \left[ \frac{(K + \frac{4}{3}G)}{\Delta z_{min.}} \right]$$

**Fig. 3** Lateral deformation profile of right cantilever wall [11]



where,  $K$ ,  $G$  are the bulk modulus and the shear modulus of the soil, respectively.  $\Delta z_{\min}$  is the smallest width (20 mm) of the adjoining zone in the normal direction to the interface between soil and structure. The values of the normal and shear stiffness ( $K_n$  and  $K_s$ ) used here are  $2.9 \times 10^9$  Pa/m. Interface friction angle of  $20^\circ$  is used between plexiglass and sand considered. The coefficient of lateral earth pressure for the soil is 0.38 which is found out using the well-known formula  $K_h = 1 - \sin(\phi')$ . The elastic modulus of the soil ( $E$ ) is found out from the equation proposed by Janbu [12] which is as follows

$$E = P_{\text{ref}} K \left[ \frac{(\sigma_c)}{P_{\text{ref}}} \right]^n$$

where  $P_{\text{ref}} = 100$  kPa and  $\sigma_c =$  Confining pressure. Values of  $K$  and  $n$  are taken as 402 and 0.5, respectively which are obtained from laboratory drained triaxial test [11].

Validation of this numerical model is done with respect to experimental analysis which is described in Konai et al. [11]. Figure 3 (ref. to Konai et al. [11]) showing the comparison with the lateral displacement of the right wall obtained from numerical analysis as well as experimental analysis which shows reasonable agreement with each other.

### 3 Results and Discussion

From numerical analysis resultant lateral earth pressures acting on left and right cantilever wall are obtained. The total depth of the wall ( $H$ ) considered in numerical analysis is 200 mm and lateral earth pressure obtained for various excavation depths ( $D_e/H = 0.3, 0.4, 0.5$ ). Figure 4a, b shows the static lateral earth pressure acting

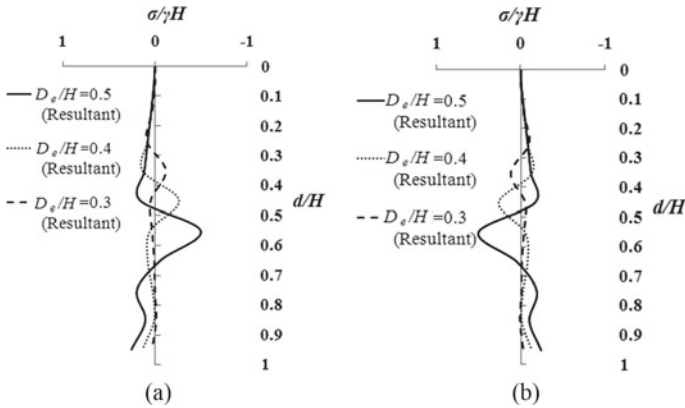


**Fig. 4** Distribution of resultant (net) lateral earth pressure acting on **a** left wall and **b** right wall under different excavation depths in static condition

on the left and the right wall, respectively and it is found that the resultant lateral earth pressure distribution for both the walls are same. It can also be seen that under static condition when  $D_e/H$  increases from 0.3 to 0.4 the maximum value of resultant lateral earth pressure increased by 129% but when  $D_e/H$  increases from 0.4 m to 0.5 the maximum value of resultant lateral earth pressure increased by 91% for left and right wall both so the rate of increment of maximum earth pressure is less with the increment of  $D_e/H$ .

Figure 5a, b shows post dynamic resultant lateral earth pressure acting on the left and the right wall, respectively. At the end of dynamic event when  $D_e/H$  increases from 0.3 to 0.4, the maximum value of resultant lateral earth pressure increased 144% and 19.5% but when  $D_e/H$  increases from 0.4 to 0.5 the maximum value of resultant

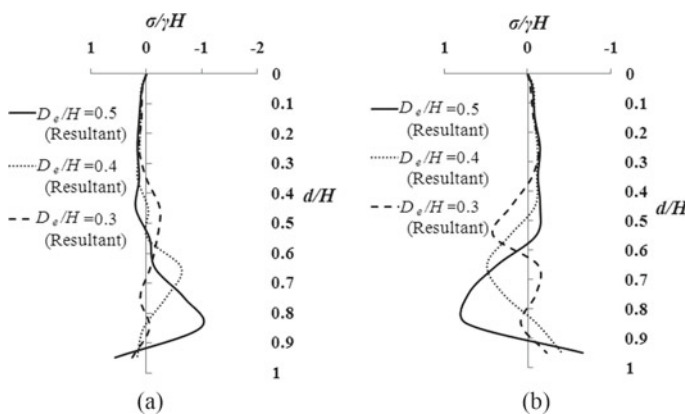


**Fig. 5** Distribution of resultant (net) lateral earth pressure acting on **a** left wall and **b** right under different excavation depths at the end of dynamic loadings

lateral earth pressure increased 55% and 48% for left and right wall, respectively. Therefore, the rate of increment of maximum earth pressure is decreased for left wall but on contrary increased for right wall. There is huge difference in the developed resultant earth pressure after excavation (before dynamic event) and after the dynamic event. It is found that for  $D_e/H = 0.5$ , resultant earth pressure after dynamic event is 3.9 and 2.9 times more than static stage (after excavation) for left and right wall, respectively. Therefore, Earth pressure acting on left and right wall is almost same in static condition as shown in Fig. 4a and b, but they are different in post dynamic condition as shown in Fig. 5a, b. It is also found that the maximum resultant pressure lies between excavation level and the toe of the embedded cantilever wall.

## 4 Conclusions

The effect of various depth of excavation ( $D_e$ ) on resultant lateral soil pressure acting on embedded flexible cantilever retaining wall in dry sand has been performed using FLAC 2D which is based on finite difference program (FLAC-2D). From the numerical study performed under sinusoidal dynamic acceleration, it is observed that the maximum net pressure lies between excavation level and the toe of the embedded cantilever wall. It is also found from the study that under static condition the rate of increment of maximum earth pressure is less with the increment of  $D_e/H$ . But when dynamic loading is applied the rate of increment of maximum earth pressure is decreased for left wall and for right wall it is increased. Unlike static condition, it is seen that the behavior of left wall and right wall are different under post dynamic conditions. The difference in earth pressure acting on left wall and right wall in post dynamic condition will causes different lateral displacement and bending moment of the wall and different ground settlement beside the wall. Further studies are needed in these directions to properly design the embedded cantilever wall.

## References


1. Mononobe N, Matsuo H (1929) On the determination of earth pressure during earthquakes. In: Proceedings of World Engineering Congress, vol 9, pp 177–185
2. Okabe S (1924) General theory of earth pressures. J Jpn Soc Civ Eng 10(6):1277–1323
3. Green RA, Olgun CG, Cameron WI (2008) Response and modeling of cantilever wall subjected to dynamic motions. Comput Aided Civ Infrastruct Eng 23:309–322
4. Nadim F, Whitman RV (1983) Dynamic induced movement of retaining walls. J Geotech Eng ASCE 109(7):915–931
5. Ostadan F (2005) Dynamic soil pressure for building walls an updated approach. Soil Dyn Earthq Eng 25:785–793
6. Richards RJ, Elms D (1979) Dynamic behavior of gravity retaining wall. J Geotech Eng Div ASCE 150(GT4):449–464
7. Wood JH (1973) Earthquake induced soil pressure on structure. Doctoral thesis, California Institute of Technology, Pasadena

8. Veletsos A, Younan AH (1994) Dynamic soil pressure on rigid vertical walls. *Earthq Eng Struct Dynam* 23:275–301
9. Callisto L, Soccodato FM (2010) Dynamic design of flexible cantilever retaining walls. *J Geotech Geoenviron Eng* 136(2):344–354
10. Itasca (2005) *FLAC Fast Lagrangian Analysis of Continua*, v. 5.0, User's Manual
11. Konai S, Sengupta A, Deb K (2017) Effect of excavation depths on ground surface settlement for embedded cantilever retaining structure due to dynamic loading. *Procedia Eng* 199:2342–2347
12. Janbu N (1963) Soil compressibility as determined by oedometer and triaxial tests. In: *European conference on soil mechanics & foundation engineering*, Wiesbaden, Germany, vol 1, pp 19–25



# Earthquake Response Analysis of Sites Using DEEPSOIL



D. Nishanth Kiran, Mohammad Muzzaffar Khan ,  
M. Madhu Sudhan Reddy, and Gonavaram Kalyan Kumar

**Abstract** Earthquakes are one of the natural disasters that cause a huge amount of loss in terms of economy and human life. The local site conditions such as the topographic condition and soil profile play an important role in amplifying earthquake waves thereby causing severe damage at particular site compared to other site. To achieve safety against natural disasters like earthquake, it is necessary to construct the building considering geotechnical problems like site effects. The site effects usually amplify the seismic waves which can be assessed by ground response analysis studies. In the present study, 1D earthquake response analysis has been carried out in different sites of Andhra Pradesh capital seed area of 16.5 km<sup>2</sup> in Amaravathi city in Guntur district. To evaluate site effects, borehole data up to a depth of 15 m has been collected. The earthquake time histories were used as input motion. The site amplification at surface has been assessed by using the equivalent linear approach in DEEPSOIL software. In addition to that, response spectra and variations of strain (%) time histories, PGA, and maximum strain (%) with depth were assessed. These results are used for dynamic analysis and design of earthquake-resistant structures. In this study, it is observed that waves are amplified at high level, and it results in high peak ground acceleration when compared to bedrock-level acceleration.

**Keywords** Ground response analysis · Amplification · Guntur

## 1 Introduction

Earthquakes are one of the devastating hazards in the world. The 1993 Latur earthquake (MW 6.3), 1997 Jabalpur earthquake (MW 6.0), 1997 Koyana earthquake (MW 6.5), and 2001 Bhuj earthquake (MW 7.9) are some of the recent earthquakes

---

D. Nishanth Kiran · M. Muzzaffar Khan · G. Kalyan Kumar (✉)  
Department of Civil Engineering, NIT Warangal, Warangal 506004, India  
e-mail: [kalyan@nitw.ac.in](mailto:kalyan@nitw.ac.in)

M. Madhu Sudhan Reddy  
Department of Civil Engineering, KL University, Guntur 522502, India

occurred in peninsular India. This recent seismicity has revealed that the Indian peninsular shield which was considered to be stable is also prone to devastating earthquakes. Earthquake causes huge damage to the regions by ground shaking, landslides, tsunamis, etc. Therefore, there is a need for amplification studies to analyze the amount of destruction caused due to earthquake [1]. Seismic waves are the reasons for major destructions during earthquake. These waves travel several meters from a few meters in soil to a few kilometers in rock. Therefore, soil has a key role in the estimation of ground response analysis and its characteristics. It is evident from past earthquakes that response of soil is different at different locations to ground motions imposed by earthquake loading [2]. Therefore, there is a need to model the soil to characterize and analyze the cyclic behavior of soil by these studies. Ground response analysis are generally analyzed by 1D response assuming the waves generated by an earthquake travel vertically through soil layers [5]. 1D response modeling can be analyzed by (i) linear, (ii) equivalent linear, and (iii) nonlinear approach. Equivalent linear approach is mostly used and it is an approximation of nonlinear behavior of soil [6]. This analysis is carried out in SHAKE, DEEPSOIL computer software which are popularly used. In equivalent linear approach, initial estimates of shear modulus and shear strain are estimated. These estimates are used to compute the peak strain, and from this peak strain, effective strain is computed which will be used to find the new shear modulus and damping ratio from standard curves given by Seed and Idriss [8] and Vucetic and Dobry [9]. This procedure is performed repeatedly until the values variation comes narrow and these parameters are taken as equivalent shear modulus and equivalent damping ratio to perform dynamic analyses. These parameters are used in evaluating the local site effects which play an important role in our study. The results obtained can be used to construct earthquake-resistant buildings and liquefaction analysis and various dynamic analysis [7].

## 2 Study Area and Data Collection

The study area under scope is a location having an area of 16.5 km<sup>2</sup> in the villages of Lingayapalem, Udandarayapalem, and Thalayapalem in Thullurmandal of Guntur district, and map view of area is shown in Fig. 1 representing the locations of boreholes. It is located between 80°33'3.19"E, 16°31'15.03"N and 80°29'2.31"E, 16°32'37.37"N. It is the third most populous district in Andhra Pradesh. River Krishna is also partly flowing in the district, and there are other small rivers and channels flowing in the district. There are hills in surrounding areas and can be found forest reserves in the North East region. Guntur will come in zone 3 according to IS 1893 part-I [4] which makes moderate earthquake having magnitude from 4.9 to 6 Mw. For detailed estimation of local site effects, geotechnical data is collected from SPT test conducted at study area up to a depth of 15 m and detailed soil strata is shown in Fig. 2. In this study, first three boreholes were considered in each grid (A, B, C as shown in Fig. 1) for analysis of local site effects.

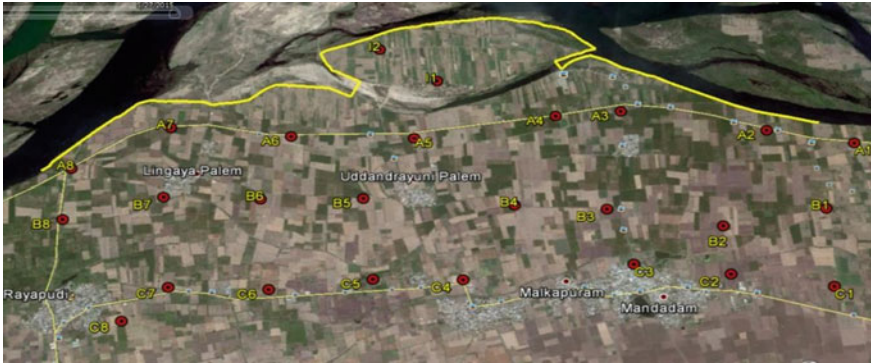


Fig. 1 Map view of study area with borehole locations

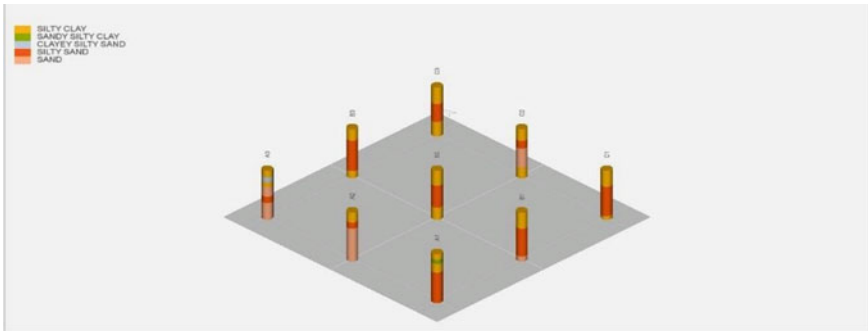


Fig. 2 Detailed soil strata at boreholes

### 3 Geotechnical Details

In the study area, SPT test was performed at different locations as shown in Fig. 1. Bedrock was observed at 15 m depth in few locations and extended to 30 m others. Site was characterized with different soils like silty clay (residual soils), silty sand, sand (alluvial soils), and stiff clay which were mostly found in eastern side, and with addition to this, soil, pebbles, and yellowish soft disintegrated rock can be found in the western side of the area. Undisturbed and disturbed samples were collected from test site and analyzed in laboratory. SPT-N values for every strata of entire soil depth were given in Fig. 3. Ground water table influences the site effects which should be considered. Water table levels are shallow, having depth up to 3–4 m at all the boreholes. It infers that their location is at the upstream side of the river.

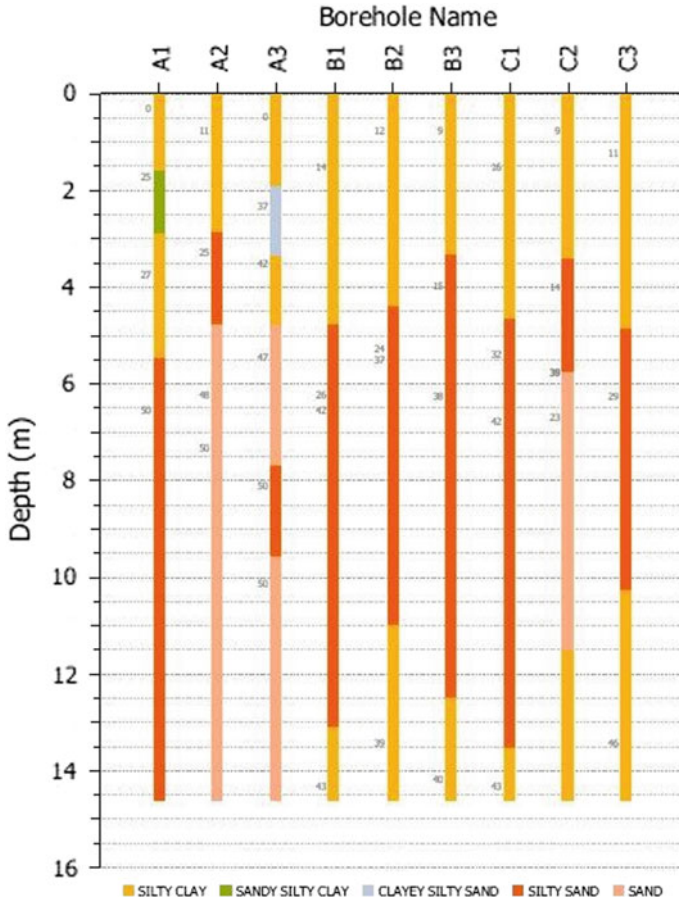


Fig. 3 SPT-N values along depth

### 4 Input Motions

Input motions are selected based upon regional seismicity and PGA values. The study area comes under zone 3 having a maximum PGA value of 0.16 g [4]. Chamoli earthquake ( $M_b = 5.4$  and  $PGA = 0.11$  g) of March 29, 1999, is selected as the input ground motion to analyze soil effects and is applied at hard stratum shown in Fig. 4.

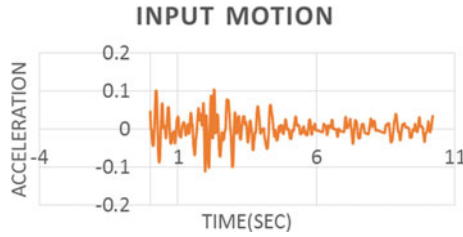


Fig. 4 “Chamoli” earthquake input motion

## 5 Results

### 5.1 Surface Acceleration Time Histories

The surface acceleration time history attained at these boreholes in response to Chamoli earthquake motion shown in Fig. 5a–c. The peak ground acceleration (PGA) observed as 0.2 g, 0.18 g, and 0.17 g at A1, A2, A3 boreholes. PGA at B1, B2, B3 boreholes are 0.23 g, 0.22 g, and 0.21 g. Similarly, at C1, C2, C3 boreholes was 0.18 g, 0.2 g, 0.21 g. PGA values are quite high at B and C to values at A, and it is due to the presence of clayey layers at these boreholes. The amplification is higher at all boreholes, due to availability of hard stratum at shallower depth (nearly 15 m) at all borehole locations.

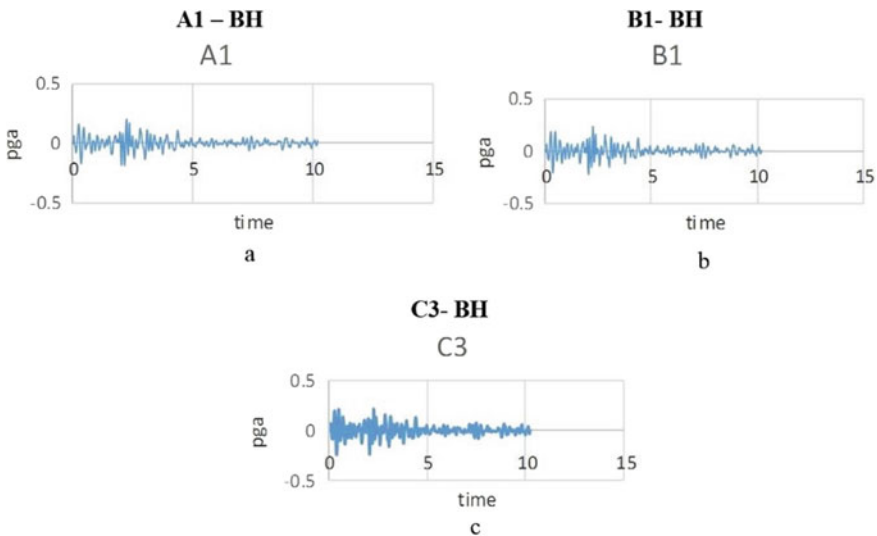


Fig. 5 a–c Surface acceleration time histories at boreholes A1, B1, and C3

### 5.2 Response Spectrum

Response spectrum is defined as the locus of maximum response for a particular damping ratio to a single degree of freedom system. The response spectrum at 5% damping at ground surface for these boreholes was shown in Fig. 6. The IS 1893-part I (2016) spectrum for medium soils and zone III is shown for comparison. It is found that the IS spectrum is unconservative in low period range for all grids (A, B, C). It is analyzed that seismic design is mostly used for soil having lower period. This usually affects the structures of low to medium rise buildings, where the fundamental periods are generally less in comparison with high rise buildings. Further, considering only PGA in seismic design requirements is not reliable, since the soil present at a particular site of interest plays important role in amplifying the seismic waves thereby increasing the overall acceleration effect on the structures.

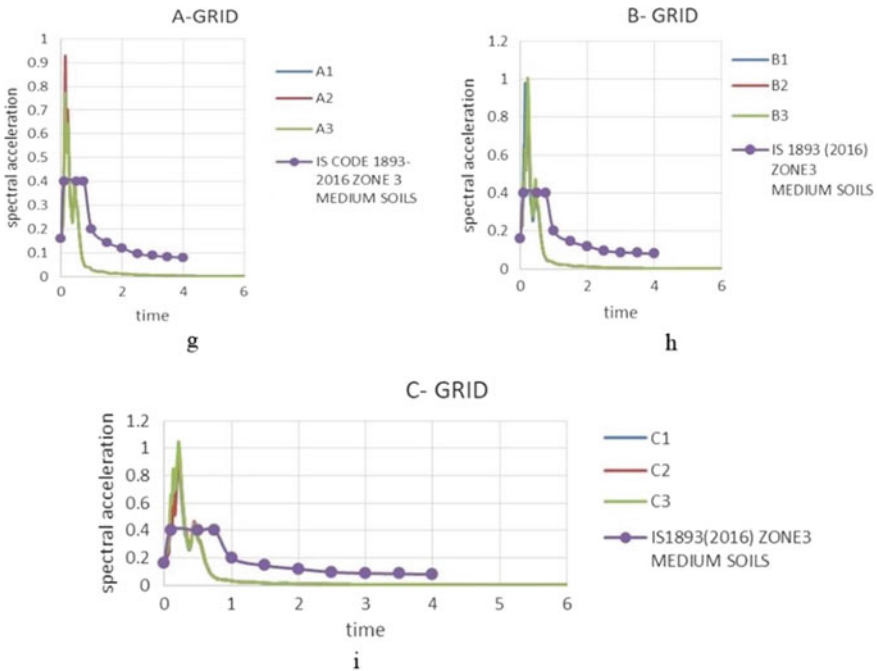


Fig. 6 Response spectra at different grids (A, B, and C)

## 6 Conclusions

This analysis is used to find the effect of local site effects at Guntur by using 1D equivalent linear approach using DEEPSOIL software [3]. The acceleration time histories of Chamoli earthquake has been used as input motion.

- (i) The peak ground acceleration for same earthquake motion is different at different boreholes. The higher amplification were found (greater than 0.2) which shows the effect of local site effects on the seismic waves. These amplification is due to deposition of residual soils like silty clay at larger amount. These PGA values will be used for designing under drain pipes, sunderground structures.
- (ii) Response spectrum for 5% damping have been obtained for different borehole locations. The variation of response spectrum in terms of spectral acceleration and time period are noted. It can be used as design guideline for different type of structures at these locations.
- (iii) From the analysis, it is found that IS 1893 part (2016) codal spectrum for zone III is found to be unconservative at all boreholes.
- (iv) It is found essential to consider local site effects in seismic design at all these locations.

## References

1. Anbazhagan P, Sitharam TG (2008) Site characterization and site response studies using shear wave velocity. *J Seismolog Earthq Eng* 10(2):53–67
2. Desai SS, Choudhury D (2015) Site-specific seismic ground response study for nuclear power plants and ports in Mumbai. *Nat Hazard Rev* 16(4):04015002
3. Hashash YM, Musgrove MI, Harmon JA, Groholski DR, Phillips CA, Park D (2016) DEEPSOIL 6.1, user manual. Urbana, IL, Board of Trustees of University of Illinois at Urbana-Champaign
4. IS 1893 (2016) Part 1: criteria for earthquake resistant design of structures—part 1: general provisions and building. Bureau of Indian Standards
5. Mahajan AK (2009) NEHRP soil classification and estimation of 1-D site effect of Dehradun fan deposits using shear wave velocity. *Eng Geol* 104(3–4):232–240
6. Puri N, Jain A, Mohanty P, Bhattacharya S (2018) Earthquake response analysis of sites in state of Haryana using DEEPSOIL software. *Procedia Comput Sci* 125:357–366
7. Putti SP, Satyam N (2018) Ground response analysis and liquefaction hazard assessment for Vishakhapatnam city. *Innovative Infrastruct Solutions* 3(1):12
8. Seed HB, Idriss IM (1970, December) Soil moduli and damping factors for dynamic response analysis. Report No. EERC 70–10, University of California, Berkeley
9. Vucetic M, Dobry R (1991) Effect of soil plasticity on cyclic response. *J Geotech Eng* 117(1):89–107

# Evaluation of Dynamics Properties and Liquefaction Potential of Kasai River Sand by Cyclic Triaxial Test



Satya Prakash Vikal and Paramita Bhattacharya 

**Abstract** The present research work examines the dynamics shear modulus, cyclic pore pressure ratio and liquefaction potential of locally available Kasai river sand at medium dense state and at high strain level ( $>10^{-4}$ ) by displacement-controlled cyclic triaxial test. Kasai river is located in Paschim Medinipur district of West Bengal. This region is seismically bounded by several faults such as Garhmayna Khanda-Ghosh fault, Pingla fault and Eocene Hinge zone. Although this area is under Seismic Zone III, a good number of earthquakes of magnitude around 5.0 in Richter scale have been experienced in recent past. It is known that earthquakes destruction is largely dependent upon dynamic properties. Therefore the study is carried out to keep in mind the safety of the important structures. The dynamic shear modulus and excess pore pressure ratio of Kasai river sand at fully saturated state have been determined for different values of shear strain and confining pressure. The tested sand specimen has been prepared at relative density of 50%. In the displacement-controlled cyclic test, the axial strain amplitude is chosen to be 0.2, 0.3 and 0.5% and frequency is 1 Hz. The shear modulus is decreased and excess pore pressure ratio is increased due to an increase in number of cycles of loading. However the excess pore pressure ratio depends on the magnitude of cyclic shear strain.

**Keywords** Shear modulus · Excess pore pressure ratio · Liquefaction potential · Kasai river sand · Medium dense sand · Cyclic triaxial

## 1 Introduction

Soil liquefaction is commonly occurred in saturated soil for the loss of its effective stress and stiffness during earthquake. During liquefaction the effective stress ( $\sigma'3$ ) of the saturated soil reduces to zero. A series of investigations available in the literature related to dynamic properties of soils are divided into (i) large strain ( $>10^{-4}$ ) analysis [6, 12, 14, 16] and (ii) small strain ( $<10^{-4}$ ) analysis [5, 9, 10]. These work deal with

---

S. P. Vikal (✉) · P. Bhattacharya  
Indian Institute of Technology Kharagpur, Kharagpur WB721302, India

© Springer Nature Singapore Pte Ltd. 2022  
A. K. Dey et al. (eds.), *Proceedings of the 7th Indian Young Geotechnical Engineers Conference*, Lecture Notes in Civil Engineering 195,  
[https://doi.org/10.1007/978-981-16-6456-4\\_34](https://doi.org/10.1007/978-981-16-6456-4_34)



the damping ratio and dynamic shear modulus for sand prepared at different relative densities and cycles of load. There are few research works available on pore pressure generation by Belkhatir et al. [4], Xenaki and Athanaspoulos [15]. These works basically deal with variations of pore pressure with void ratios, relative densities and fine contents. There are some research works in literature by Ishihara et al. [8, 11, 13] dealing with in-situ soil characteristics for evaluation of residual strength, safety factor, liquefaction potential indices and critical depth required for liquefaction.

From literature it is understood that the study of dynamic properties of foundation soils and its liquefaction are important for the safety of any structures built over it. Several important structures like road and rail bridges, embankment etc. are existing over the Kasai river. There is a twin bridge located at either banks of the Kasai river which eventually connect Kharagpur and Medinipur cities in Paschim Medinipur district of West Bengal. Although the study area is under Zone-III in the Map designed based on the seismic activity in India, a good number of earthquakes are recorded in recent past of magnitude around 5.0 in Richter scale. Moreover the presence of several faults such as Garhmayna-Khanda-Ghosh fault, Pingla fault and Eocene Hinge zone has increased the possibility of seismic activity in this region. Since there is no data available on building up of pore pressure and dynamic shear modulus of Kasai river sand under displacement-controlled (strain controlled) cyclic loading so the present work has studied the liquefaction potential, pore pressure ratio and dynamic shear modulus of Kasai river sand at medium dense state under cyclic loading at high strain rate ( $> 10^{-4}$ ).

## 2 Soil Characterization

Dry sand sample from Kasai river bed was collected. Sand sample passing through 4.75 mm sieve and retained by 75  $\mu\text{m}$  was used for sample preparation. Fig. 1 shows

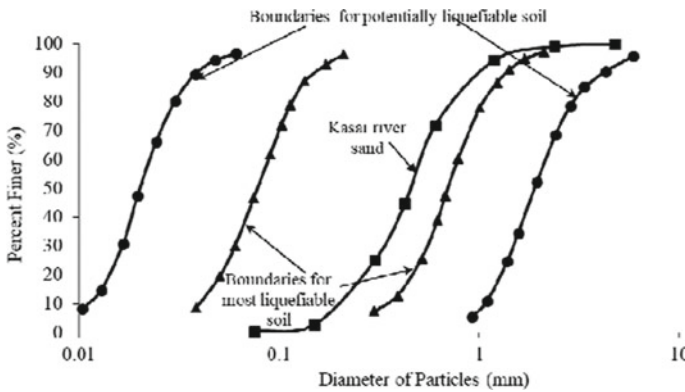


Fig. 1 Grain size distribution curve

**Table 1** Characterization of soil

Soil parameter	Value
Specific gravity	2.67
Uniformity coefficient, $C_u$	2.5
Coefficient of curvature, $C_c$	1.16
Maximum void ratio, $e_{max}$	0.84

a typical grain size distribution curve of the sample. Table 1 provides the index properties of the sample.

### 2.1 Index Properties and Gradation of Sand

The distribution of soil grain is shown in Fig. 1. It shows the soil sample is poorly graded sand. Moreover this distribution curve of grain size is found to lie within the bounds for potentially liquefiable soil.

### 2.2 Shear Strength Parameters of Kasai River Sand by CD Triaxial Test

The peak friction angle ( $\phi_{peak}$ ) and critical state friction angle ( $\phi_{cr}$ ) of sand sample have been determined by conducting consolidated drained (CD) triaxial tests. Total four CD tests have been performed at relative density  $R_d = 50\%$  for confining pressures ( $\sigma'_3$ ) equal to 50, 100, 150 and 200 kPa. The strain rate at all CD tests is kept at 1.25 mm/min as per ASTM D7181-11 [1]. The CD test results are shown in Fig. 2. The values of  $\phi_{peak}$  and  $\phi_{cr}$  determined from experiments are  $34.6^\circ$  and  $5^\circ$ , respectively.

**Fig. 2** Deviation stress versus axial strain in CD triaxial test at  $R_d = 50\%$

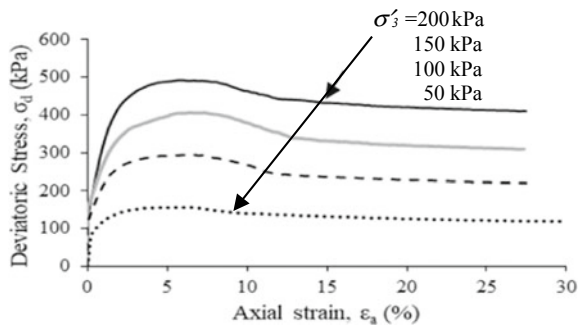
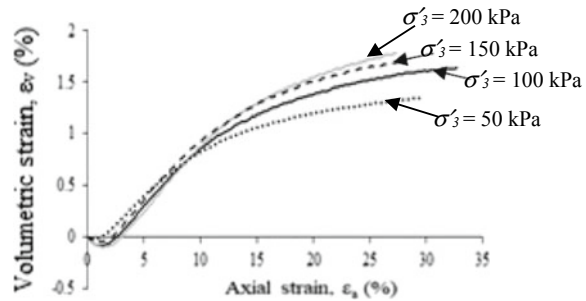


**Fig. 3** Volumetric strain versus axial strain curve at  $R_d = 50\%$



### 3 Sample Preparation

Each cylindrical sand specimen of size 50 mm  $\times$  100 mm has been prepared and placed on the pedestal. The specimen has been covered by a rubber membrane with the help of split mould. In this case the size of the split mould used is 50 mm (dia.)  $\times$  100 mm (height). First weight of oven dried sand at 50% relative density is calculated. The tamping method described in ASTM D5311-11 [2] was used for the sample preparation. In this method the soil sample was prepared in three layers of oven dried sand. So the required dry weight of the sand for each layer was determined. Then the weighed sand was allowed to pour through a funnel with long tube to the mould maintaining zero dropping height. Thereafter each layer of the poured sand in the mould is tamped so that the every layer has a height equal to 1/3rd of the mould's height. The second and third layers are filled in the mould following similar steps. In order to keep the sample stiff and ensure minimum disturbance of the specimen at the time of removal a little suction is provided to the specimen. Then the split mould is removed. Then de-aired water is used to saturate the sample. Back pressure is applied to accelerate the saturation process. Keeping  $\sigma'_3$  around 15–20 kPa the amount of applied back pressure was gradually increased as long as the Skempton's parameter related to pore pressure  $B$  ( $= \Delta u / \Delta \sigma$ ,  $\Delta u$  = change in pore pressure,  $\Delta \sigma$  = change in confining pressure) becomes equal to or more than 0.95. Thereafter the sand specimens were isotropically consolidated at a required  $\sigma'_3$  (Fig. 3).

### 4 Testing Procedure

The experiment has been conducted by the automated hydraulic cyclic triaxial testing equipment made by M/s. HEICO, India. The loading system is comprised of a loading frame of maximum 50 kN load carrying capacity and a hydraulic actuator which is capable to perform both strain and stress-controlled tests for a wide range of frequency varying from 0.1 to 10 Hz. The automated triaxial testing system has six transducers including one submersible type load cell of  $\pm 5$  kN capacity for monitoring the axial load, a displacement transducer of  $\pm 50$  mm capacity

for measuring the vertical displacement, four transducers for recording pore water pressure, confining pressure, back pressure and volume change. The data acquisition card and analysis software confining ASTM 3999 [3] and ASTM 5311 [2] are also provided for analysis purpose. Cyclic loading is applied to the sample using displacement-controlled method so that the frequency of the sinusoidal axial displacement remains constant at 1 Hz. The tests have been performed at different amplitudes of cyclic axial strain such as 0.2%, 0.3% and 0.5% and  $\sigma'_3$  values of 100 and 200 kPa. Using the results obtained from the tests the analysis software plotted the deviator stress versus axial strain curve. The nature of this curve is hysteresis loop for every loading cycle. The dynamic Young's modulus ( $E$ ) in Eq. (1) is defined by the slope of the secant line which connects two extreme points of the loop:

$$E = \frac{\sigma_d}{\varepsilon_a} \quad (1)$$

where  $\sigma'_d$  and  $\varepsilon_a$  are amplitude of deviator stress at any cycle of loading and amplitude of axial strain, respectively. Thereafter the dynamic shear modulus  $G$  and amplitude of cyclic shear strain ( $\gamma$ ) are calculated by using the theory of elasticity as written below:

$$G = \frac{E}{2(1 + \mu)} \quad (2)$$

$$\gamma = (1 + \mu)\varepsilon_a \quad (3)$$

here  $\mu$  is Poisson's ratio of soil which equals to 0.5 for saturated sand.

## 5 Results and Discussions

A series of displacement-controlled dynamic triaxial tests have been performed with sand collected from Kasai river bed at 50% relative density considering two different  $\sigma'_3$  values say 100 and 200 kPa and for three different axial strain amplitude say, 0.2, 0.3 and 0.5%. All the dynamic tests have been conducted with sinusoidal wave with 1 Hz frequency. Figures 4, 5, 6, 7, 8 and 9 represent the test results of sand sample.

Figures 4 and 5 show the variation of dynamic shear modulus with number of loading cycles at  $\sigma'_3 = 100$  kPa and 200 kPa, respectively. The magnitude of dynamic shear modulus of soil decreases due to an increase in number of loading cycle for constant values of  $\sigma'_3$ .

The dynamic shear modulus has been reduced considerably at 10th cycle. The reduction of dynamic shear modulus is found to be more prominent in case of higher strain amplitude for both  $\sigma'_3$ . The effect of number of loading cycles on pore pressure ratio for Kasai river sand at 50% relative density has been presented in Figs. 6 and

**Fig. 4** Shear modulus versus no. of cycles at  $\sigma_3' = 100$  kPa

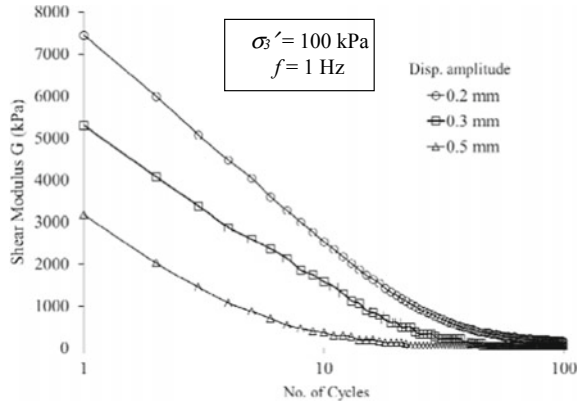


**Fig. 5** Shear modulus versus no. of cycles at  $\sigma_3' = 200$  kPa

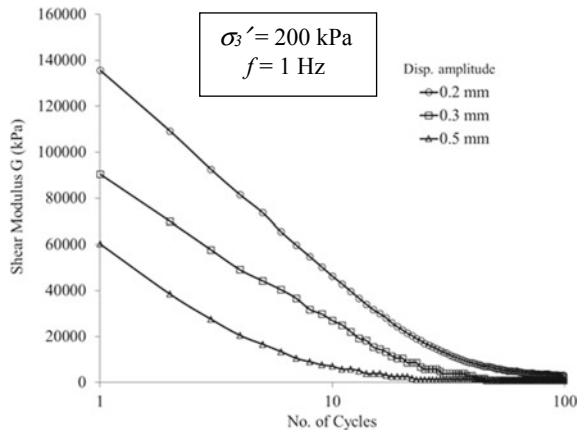


**Fig. 6** Pore pressure ratio versus no. of cycle at  $\sigma_3' = 100$  kPa

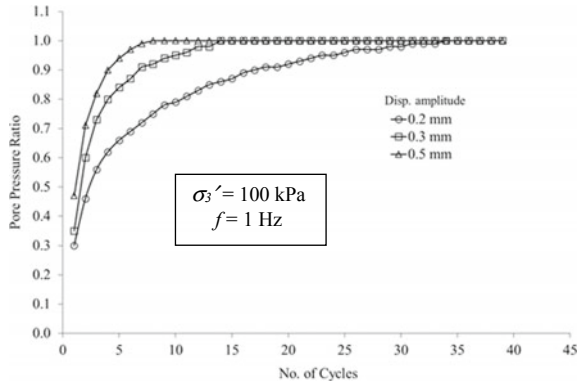


**Fig. 7** Pore pressure ratio versus no. of cycle at  $\sigma_3' = 200$  kPa

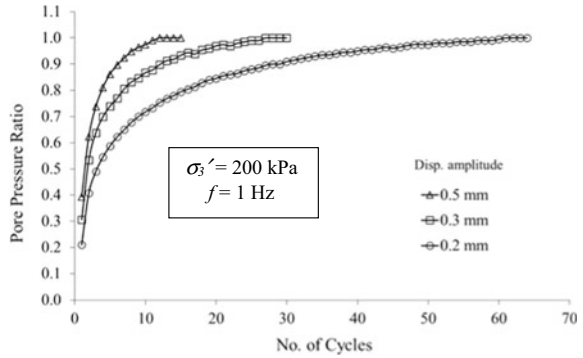


**Fig. 8** Cyclic resistance curve for Kasai river sand at 50% relative density

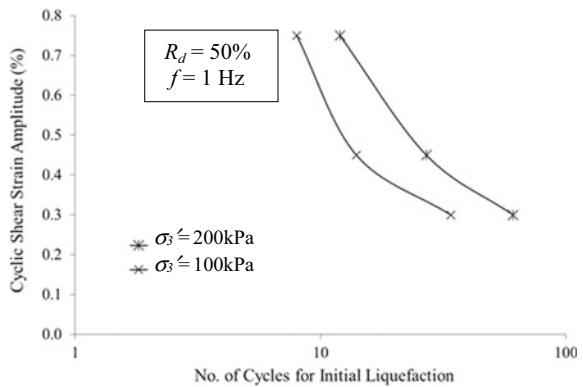
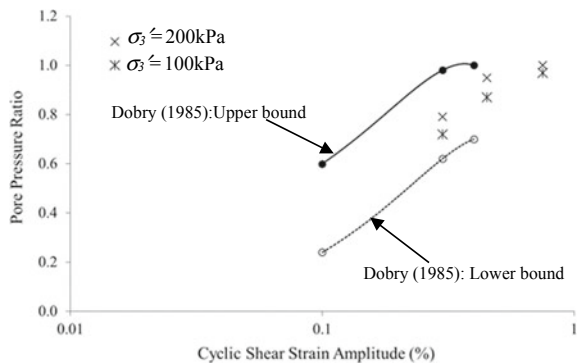


**Fig. 9** Variation of pore pressure ratio with cyclic shear strain amplitude for Kasai river sand at 50% relative density



7 for  $\sigma_3' = 100$  kPa and 200 kPa, respectively. When the excess pore pressure ratio defined as the ratio of excess pore pressure to confining pressure becomes equal to 1, the liquefaction of soil sample occurs. In this case the pore pressure ratio increases continuously due to an increase in loading cycle till liquefaction of soil initiates.

The number of cycles for initial soil liquefaction versus amplitude of  $\gamma$  has been presented in Fig. 8 for  $\sigma_3' = 100$  and 200 kPa. In this case for 0.75% cyclic shear strain Kasai river sand at 50% relative density can liquefy at 8 no. of cycles and 12 no. of cycles for confining pressure equals to 100 kPa and 200 kPa, respectively. Similarly for  $\gamma = 0.3\%$  Kasai river sand at 50% relative density can liquefy at 35 no. of cycles and 61 no. of cycles for  $\sigma_3' = 100$  kPa and 200 kPa, respectively. Hence the Kasai river sand can easily liquefy at less number of loading cycles for higher magnitude of cyclic shear strain. Fig. 9 illustrates the variation of pore pressure ratio with cyclic shear strain at 10th loading cycle for the Kasai river sand. Dobry [7] provided the upper and lower bound curves for variation of pore pressure with  $\gamma$  at 10th loading cycle which is shown here. The present results are found to match well with the range provided by Dobry [7].

## 6 Conclusions

The present experimental work reveals that the cyclic shear strain and confining pressures are the two important factors on which liquefaction potential of Kasai river sand depends for a particular relative density. The magnitude of cyclic shear strain amplitude has greatest influence in the value of dynamic shear modulus reduction and pore pressure generation. From the experiments it has been found that Kasai river sand is highly liquefiable at higher cyclic shear strains at 50% relative density and for  $\sigma_3' = 100\text{--}200$  kPa. The built up pore water pressure is also found to be a function of cyclic shear strain at 10th loading cycle and lies between the upper and lower bounds proposed by Dobry 1985. Therefore proper care is necessary prior to construction of important structure on this soil.

## References

1. ASTM, D. 7181-11 (2011) Method for consolidated drained triaxial compression test for soils. Annual Book of ASTM Standards, vol 4
2. ASTM, D. 5311-92 (2004) Standard test methods for load controlled cyclic triaxial strength of soil. Annual Book of ASTM Standards, vol 11
3. ASTM, D. 3999-91 (2003) Standard test method for the determination of the modulus and damping properties of soils using the cyclic triaxial apparatus. Annual Book of ASTM Standards 4
4. Belkhatir M, Schanz T, Arab A, Delta N, Kadri A (2014) Insight into the effects of gradation on the pore pressure generation of sand silt mixtures. *Geotech Test J* 37(5):922–931
5. Chattaraj R, Sengupta A (2016) Liquefaction potential and strain dependent dynamic properties of Kasai River Sand. *Soil Dyn Earthq Eng* 90:467–475
6. Dash HK, Sitharam TG (2011) Undrained monotonic response of sand silt mixtures: effect of non plastic fines. *Geomech Geoengineering Int J* 6(1):47–58
7. Dobry R (1985) Liquefaction of soils under earthquakes. Committee on Earthquake Engineering, Commission on Engineering and Technical Systems, National Research Council, National Academy Press, Washington, D.C.

8. Ishihara K, Tatsuoka F, Yasuda S (1975) Undrained deformation and liquefaction of sand under cyclic stresses. *Soils Found* 15(1):29–44
9. Khan Z, El Naggar MH, Cascante G (2011) Frequency dependent dynamic properties from resonant column and cyclic triaxial tests. *J Franklin Inst* 348(7):1363–1376
10. Khosravi A, McCartney JS (2011) Resonant column test for unsaturated soils with suction-saturation control. *Geotech Test J* 34(6):730–739
11. Ladd RS, Dobry R, Dutko P, Yokel FY, Chung RM (1989) Pore water pressure buildup in clean sands because of cyclic straining. *Geotech Test J* 12(1):76–81
12. Okur DV, Ansal A (2007) Stiffness degradation of natural fine grained soils during cyclic loading. *Soil Dyn Earthq Eng* 27(9):843–854
13. Seed HB (1987) Design problems in soil liquefaction. *J Geotech Eng* 113(8):827–845
14. Sitharam TG, Govindaraju L, Srinivasa Murthy BR (2004) Evaluation of liquefaction potential and dynamic properties of sandy soil using cyclic triaxial testing. *ASTM Geotech Test J* 27(5):427–429
15. Xenaki VC, Athanasopoulous GA (2003) Liquefaction resistance of sand silt mixtures: an experimental investigation of the effect of fines. *Soil Dyn Earthq Eng* 23(3):183–194
16. Zhou Y, Chen Y (2005) Influence of seismic cyclic loading history on small strain shear modulus of saturated sand. *Soil Dyn Earthq Eng* 25(5):341–353



# Determination of Geometric Attenuation Parameters of Surface Amplitude in Soil Medium Due to Installation of Impact Pile Casing



B. Vinoth

**Abstract** This paper mainly concerns the field study, to assess the geometric attenuation parameters of surface amplitude due to installation of impact pile casing driving for two cases, like (1) single pile casing driving (2) simultaneous two pile casing driving. The peak particle velocity (PPV) have been monitored at different radial distances (0–30 m) for varying depth of pile driving (0–28 m). The geometric attenuation parameters have been determined by considering the three important aspects (1) effects on amplitude of motion of soil particles with respect to radial distances (2) effects on peak particle velocity versus vibration energy for the corresponding radial distance (Energy-Attenuation Model) and (3) effects on ratio of vibration amplitude with respect to corresponding ratio of radial distances (velocity ratio model). Finally, the values of geometric attenuation parameters have been compared with previous research studies and existing theoretical attenuation laws.

**Keywords** Construction induced vibration · Geometric attenuation parameters · Surface amplitude · Peak particle velocity (PPV) · Impact pile casing driving

## 1 Introduction

Ground vibration associated with man-made construction activities has become a major area of research. These vibrations are mostly being generated from various construction activities such as vibratory or impact pile casings, sheet pile, blasting, excavation, demolition, and dynamic compaction. This may lead to occurrence of damages in adjacent structures as well as disturbances in surrounding environment. Hence it is essential to study the behavior of soil on or before the construction activities and to minimize their effects, so as to avoid any damages during construction. In order to effectively control vibration related problems in urban areas or nearby existing structures, the study on characteristic of wave propagation in soil medium and attenuation characteristics of ground vibration is essential to predict the critical

---

B. Vinoth (✉)

Department of Civil Engineering, Indian Institute of Engineering Science and Technology, Shibpur, India

© Springer Nature Singapore Pte Ltd. 2022

A. K. Dey et al. (eds.), *Proceedings of the 7th Indian Young Geotechnical Engineers Conference*, Lecture Notes in Civil Engineering 195,  
[https://doi.org/10.1007/978-981-16-6456-4\\_35](https://doi.org/10.1007/978-981-16-6456-4_35)

327

or safest distance from the construction activities in the field. The vibration amplitudes are to be monitored in construction site is to keep it within the permissible limits as per the guidelines [7, 10, 11].

Vibration propagates from a piece of construction equipment through the ground predominantly by means of Rayleigh waves and secondarily by means of body waves. The amplitude of these waves diminishes with increases in radial distance from the vibration source. Thus, source of vibration and geo-environmental condition of a specific site plays an important role in vibration related problems and its ground vibration propagation [3, 4, 6]. For the proper assessment of impact on ground vibration the site-specific vibration measurements are warranted. In man-made ground vibration measurement, it has been found that to be convenient to describe the intensity of ground vibration by means of the peak value of the particle velocity (mm/s) and the reason for this choice is the well-established correlation which has been established theoretically by the fact that the strain induced in the ground during vibration is proportional to the particle velocity [2, 8]. In past three decades several researchers have carried out study in the area of construction induce vibration to develop the relation between propagation and attenuation characteristics of soil under various dynamic conditions [1, 13, 14]. Thus, the Prerequisite relationship is required to predict construction induced vibration in field upon site response and behavior of soil under dynamic loading. So, present study is mainly focused on evaluation of geometric attenuation parameters of surface wave amplitude (Peak Particle Velocity, mm/s) due to impact pile case driving for two different phenomena in field during construction activities.

## **2 Field Investigation**

### ***2.1 Test Site***

The test site is located at Newtown, Kolkata, West Bengal. The construction activities mainly involve, the impact pile casing driving carried out with Impact Hammer up to depth of 28 m from ground level. The vibration generated during pile casing driving had been observed on the surrounding environment as well as the soil medium due to close proximity of the existing structures. Figure 1 shows the schematic diagram of the proposed site and the existing structure of the nearby construction activities.

### ***2.2 Soil Strata at Test Site***

The soil conditions for the proposed site have been eventually same for all over the place and one typical bore log profile of the soil exploration data is as follows.

**Fig. 1** Construction site



- Stratum—I varying between depths from 0 to 1 m and consists greyish brown silty clay.
- Stratum—II varying between depth from 1 to 3.15 m and consists Loose/soft greyish brown silty clay / clayey silt and silty fine sand with some mica flakes.
- Stratum—III varying between depths from 3.15 to 33.75 m and consists Loose to dense bluish grey silty clay and micaceous silty fine sand.
- Stratum—IV varying between depths from 33.75 to 43.25 m and consists of Very dense, yellowish brown silty clay/fine sand with mica flakes.
- Stratum—V varying between depths from 43.25 to 50.45 m and consists of Very stiff, bluish grey, silty clay with thin laminations of yellowish silt and very fine sand.

The ground water table was located at about 2.0 m depth below the ground surface. The SPT value of the construction site ranges from 7–20 up to 10.0 m and below that higher values of SPT about 50 at termination depth of pile. It is revealed that mostly silty clay with fine sand has been encountered during pile driving in the site and the typical bore log profile has been presented in Fig. 2.

### 2.3 Source of Vibration and Pile Properties

Impact hammer being used to drive the pile casing up to a depth of about 28.0 m. The mass of the hammers used in this project in the range of 4.2 ton. The height of fall

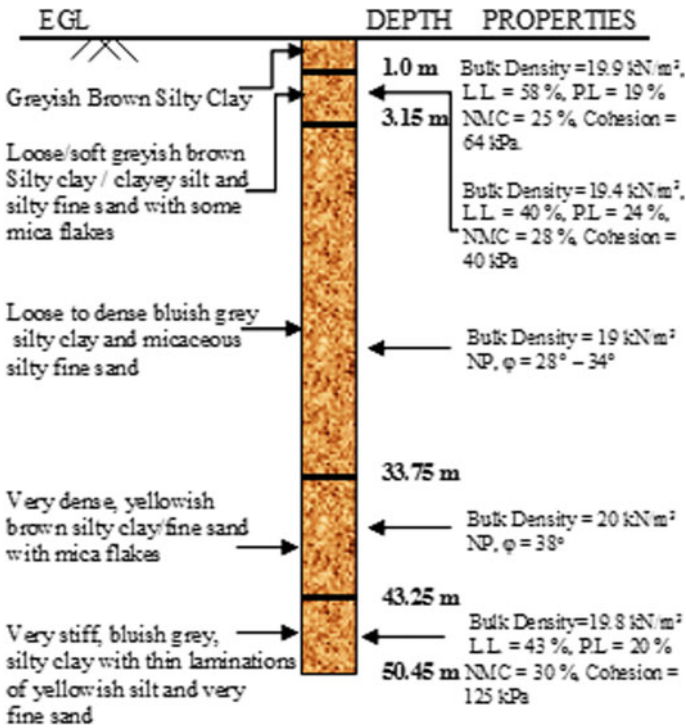


Fig. 2 Soil profile

from the hammer is 1.5 m. The diameter of pile casing is 500 mm and total length of pile is 30 m but the driving depth of pile is up to 28 m in all over the construction site.

### 3 Test Program and Analysis Procedure

This section addresses the test program and analysis procedure that has been used to determine the geometric attenuation parameters of soil.

#### 3.1 Test Program

During construction, the existing building structures have been situated very close proximity to the pile casing driving in all over the construction sites whose radial distance varies from 20 to 90 m has shown in Fig. 1. Vibration Meter VM-82 has been

used in the site for measuring peak particle velocity (mm/s). The vibration meter VM-82 is designed for a wide range of applications and it is particularly suited for routine maintenance and monitoring of vibration, as well as for performance testing during construction activities. Acceleration (mm/s<sup>2</sup>), Velocity (mm/s), and Displacement (mm) can be easily monitored and precise evaluation of construction vibration in sites. The present study mainly focussed on monitoring ground vibration motion in eastern sides of the construction sites during various phases of construction activity and to determine the decay of surface wave amplitude (Geometric Attenuation parameters) for following two cases.

- Monitored peak particle velocity (PPV, mm/s) on soil surface for varying radial distance (0–30 m) due to single pile casing driving (the depth of pile driving is 0–28 m).
- Monitored peak particle velocity (PPV, mm/s) on soil surface for varying radial distance (0–30 m) due to simultaneous two pile casing driving (the depth of pile driving is 0–28 m).

### 3.2 Analysis Procedure

According to Richart et al. [9] showed that, there are two main factors that govern the attenuation of surface wave vibration amplitude in the soil medium, one is due to the geometric attenuation and other is due to material attenuation. Geometric attenuation occurs, where the decay of vibration in the soil medium due to geometric spreading of the wave front with respect to increase in the radial distance from the vibration source. The geometric attenuation depends upon type of propagating wave, shape of associated wave front and types of excitation source generate in the soil medium. Energy density of the wave front attenuate due to internal damping effect in the soil medium, that caused by internal friction and cohesion of the soil particles as wave propagate through, this phenomenon is known as material attenuation. The following two models have been used here to determine the geometric attenuation parameters of soil.

Velocity Ratio Model: In this model simple expression is used to determine geometric attenuation coefficient ( $\gamma$ ) based on the ratio of peak particle velocity and the radial distances as given below.

$$V_b = V_a \left( \sqrt{\frac{R_a}{R_b}} \right). \tag{1}$$

Above equation can be modified as:

$$V_b = V_a \left( \frac{R_a}{R_b} \right)^\gamma \tag{2}$$

$$\gamma = \frac{\ln\left(\frac{V_b}{V_a}\right)}{\ln\left(\frac{R_a}{R_b}\right)} \quad (3)$$

where,  $V_a$  is amplitude of ground motion at a distance  $R_a$  and  $V_b$  is amplitude of ground motion at a distance  $R_b$ .  $\gamma$  is geometric attenuation coefficient depends on type of wave and its associated wave front.

Energy Attenuation Model or Scaled Distance Approach: This model is to explore the relationship for construction vibration in field by considering the sources of construction vibrations, effect of transmitting medium, and the effects upon receiver from the vibration sources. Wiss [12, 13] suggested simple wave attenuation model, which is a scale-distance method that neglects the type of wave propagation and only considers the effect of source of energy on media and radial distance away from the source. Based on his field experimental data, he proposed a simple expression between peak particle velocity (mm/s) versus energy source (J) and the radial distance (m).

$$V = CE^\alpha. \quad (4)$$

$$V = kD^{-n} \quad (5)$$

where, the value of  $\alpha$  has been found one half (1/2) from his experimental study. The above two models, can be combined into single model and expressed from energy attenuation relationship as follows.

$$V = K \times \left(\frac{D}{\sqrt{E}}\right)^{-N} \quad V = K \times \left(\frac{D}{\sqrt{E}}\right)^{-N} \quad V = K \times \left(\frac{D}{\sqrt{E}}\right)^{-N} \quad (6)$$

where,  $V$  is the peak particle velocity (mm/s),  $D$  is Radial distance away from the vibration source,  $E$  is energy from vibration source,  $k$  is the attenuation constant or intercept in terms of velocity at one unit of distance,  $N$  is slope or Pseudo attenuation rate, which is the slope of  $V$  and  $\frac{r}{\sqrt{E}} \frac{D}{\sqrt{E}}$  plotted in log-log scale. Later onwards woods and Jedele [14] and Jedele [5] supplement the energy attenuation model from various site data and determine the  $k$  and  $N$  value based on their studies. Among that, Energy—Attenuation model is simplest and appropriate model to assess the construction induced vibration in site and to predict the safest distance from the vibration source easily.

Gutowiski and Dym [4] developed a series of theoretical models, to determine the geometric attenuation coefficient of soil by varying placement condition of different vibration source in the soil medium (i.e., point source on surface, line load and point source at depth). Based on his theoretical models, he concluded that due to point source on surface the amplitude of the Rayleigh wave decay with inversely

proportional to the square root of the distance and the amplitude of the body wave decay with inversely proportional to the square of the distance from the source.

## 4 Test Results

In this section the test results have been presented in graphical presentation for the following two major cases, (1) single pile casing driving (2) simultaneously two pile casing driving. In each case, the vibration has been monitoring at different depth of pile driving (0–28 m) for the varying radial distances.

### 4.1 PPV (mm/s) Versus Radial Distance (M)

Figure 3a, b is plotted between PPV value (mm/s) and radial distance (m) for single pile casing driving and simultaneous pile casing driving. From the graphical presentation it has been observed that the peak particle velocity decreases with increase in radial distance away from the vibration source. The amplitude of motion of soil particles attenuate due to geometric dependence of the soil medium depends on characteristics of the soil and the energy source. The simple linear model has been developed to determine the attenuation factor between peak particle velocity (mm/s) and the radial distance away from the vibration sources for both the cases. The attenuation factor ( $n$ ) for single pile casing driving is obtained 1.1–1.8 with respect to depth of pile driving and same for simultaneous pile casing driving the  $n$  values has been obtained 1.2–2.0 and both the cases the attenuation factor ( $n$ ) gradually increases with respect to increase in vibration energy and this is complied with above energy attenuation model.

## 5 Discussion

This section presents the attenuation parameters obtained through field study and the values of the attenuation parameters have been validated with existing methodologies. The average soil profile of the site mainly consists of silty clay with mixture of fine sand. The attenuation parameter has been determined from three analytical model, (1) Attenuation decay coefficient ( $n$ ) value obtained from the measured peak particle velocity (mm/s) with respect to radial distance (m) (2) Geometric attenuation coefficient ( $\gamma$ ) from velocity ratio model and 3. Pseudo attenuation coefficient ( $N$ ) from scaled distance approach and the obtained attenuation parameters from above models have been formulated in Table 1.

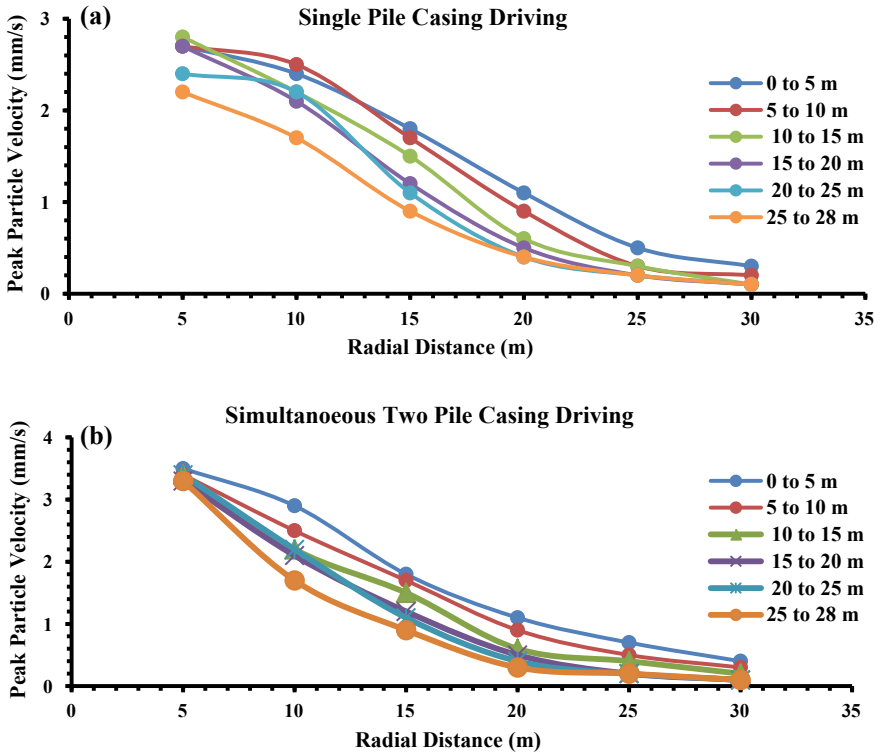


**Fig. 3** **a** Represents the peak particle velocity (mm/s) versus radial distance (m) for varying depth of pile driving (m). **b** Represents the peak particle velocity (mm/s) versus radial distance (m) for varying depth of pile driving (m)

### 5.1 Attenuation Decay Coefficient ( $N$ ) Due to Radial Distance

- The attenuation coefficient mainly depends on radial distance, energy source, and soil condition. According to increasing radial distance, the significant reduction in particle velocity observed and variation of reduction or attenuation decay ( $n$ ) with respect to soil condition is plotted in Fig. 3a, b.
- The average increase in percentage (%) of the peak particle velocity value from single to simultaneous pile casing driving varies from 22 to 31% due to increase in vibration energy.
- From this method, the obtained attenuation coefficient ( $n$ ) value was overestimated from other methods because, in this relation it does not contain any soil characteristics, vibration energy, and wave propagation parameters.



**Table 1** Summary of the field test results compared with past literature study

Past literature study		Present study		
Authors	Geometric attenuation coefficient	Based on PPV versus radial distance ( $n$ ) value	Based on velocity ratio ( $\gamma$ ) value	Based on scaled distance model ( $N$ ) value
Field and theoretical studies (Soil type: clay and firm soil)		Soil profile: silty clay with mixture of fine sand		
Wiss [12]	1.50	Single pile casing driving $n = 1.1-1.8$	Single pile casing driving $\gamma = 1.310-1.653$	Single pile casing driving $N = 1.378$
Attewell and Farmer [1]	1.00	Simultaneous pile casing driving $n = 1.2-2.0$	Simultaneous pile casing driving $\gamma = 1.450-1.732$	Simultaneous pile casing driving $N = 1.467$
Kim and Lee [6]	1.00			
Jedele [5]	1.27			
Gutowiski and Dym [4]	0.5			

### 5.2 Geometric Attenuation coefficient ( $\gamma$ )

- The geometric attenuation coefficient ( $\gamma$ ) has been evaluated by using Eq. 3 and the obtained test results have been plotted in Fig. 4a, b. For single pile casing driving the obtained geometric attenuation coefficient ( $\gamma$ ) values vary from 1.310 to 1.653 and for simultaneous two pile casing driving the geometric attenuation coefficient ( $\gamma$ ) varies from 1.450 to 1.732. From Fig. 4a for single pile casing driving, it shows the maximum particle velocity ratio ( $V_b/V_a$ ) is obtained on 0.223 (i.e., ratio of  $\ln(R_a/R_b)$ ) for the corresponding depth of pile driving (m) and after that particle velocity ratio decreases proportionally with respect to increasing radial distance from vibration source and it can be observed that we can approximately predict the critical distance ( $D_c$ ) from single pile casing driving is 15–20 m where the maximum particle velocity ratio. In the same way Fig. 4b for simultaneous pile casing driving, the approximate critical distance ( $D_c$ ) is obtained on 20–25 m radial distance from vibration sources and for the corresponding maximum particle velocity ratio is obtained ( $V_b/V_a$ ) 0.290 (i.e., ratio of  $\ln(R_a/R_b)$ ).

### 5.3 Pseudo-Attenuation Coefficient ( $N$ )

The Pseudo attenuation coefficient has been determined from Eq. 6 and the test results have been presented in Fig. 5a, b plotted between Peak Particle Velocity (mm/s) versus scaled distance (m/ $\sqrt{J}$ ) in log–log scale and the ( $N$ ) values have been

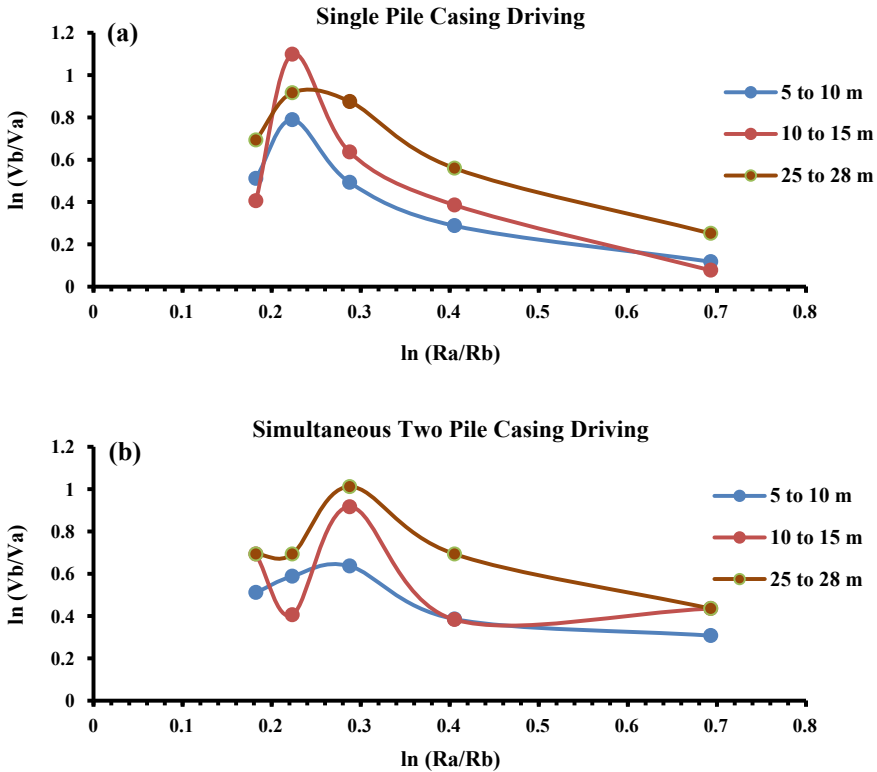


**Fig. 4** **a** Represents the ratio of vibration amplitude (PPV, mm/s) versus radial distance (m) for varying depth of pile driving (m). **b** Represents the ratio of vibration amplitude (PPV, mm/s) versus radial distance (m) for varying depth of pile driving (m)

obtained through simple linear regression analysis. The variation in *N* values has been observed for both the cases due to higher amount of vibration energy in simultaneous pile casing driving.

## 6 Conclusion

Based on the present study the following conclusion has been drawn.

- The Peak Particle velocity (mm/s) increases with increasing in vibration energy level from the vibration source with respect to the same radial distance in varying different depth of pile diving. The attenuation decay coefficient (*n*) increases with respect to increase in vibration energy. The single pile driving the attenuation coefficient (*n*) is observed 1.10–1.80 and simultaneous two pile casing driving 1.20–2.0.

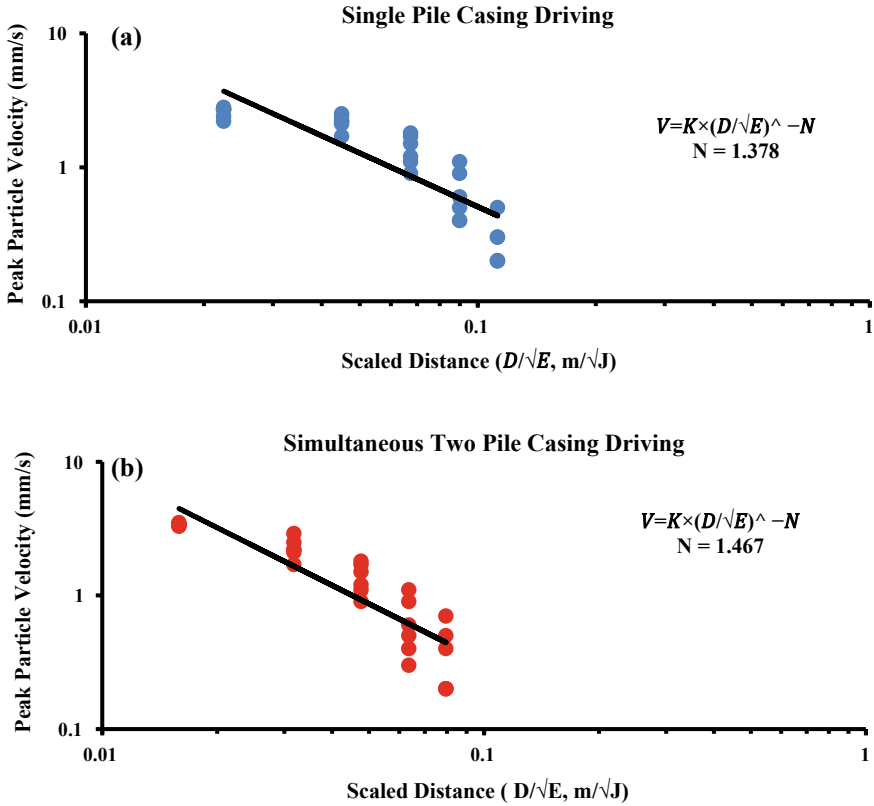


**Fig. 5** **a** Represents the peak particle velocity (mm/s) versus scaled distance ( $m/\sqrt{J}$ ) for single pile casing driving. **b** Represents the peak particle velocity (mm/s) versus scaled distance ( $m/\sqrt{J}$ ) for simultaneous two pile casing driving

- The values of Geometric attenuation coefficient ( $\gamma$ ) from velocity ratio model were observed 1.310–1.653 of single pile casing driving and 1.450–1.732 of simultaneous two pile casing driving.
- The values of Pseudo attenuation coefficient ( $N$ ) from energy attenuation model have observed 1.378 for single pile casing driving and 1.467 for simultaneous two pile casing driving.

**Acknowledgements** I would like to express my sincere gratitude to Prof. Ambarish Ghosh, Department of Civil Engineering in IEST, Shibpur for his support throughout in this research work.

## References

1. Attewell PB, Farmer IW (1973) Attenuation of ground vibrations from pile driving part two. *Ground Eng* 6(4):26–29
2. Athanasopoulos GA, Pelekis PC (2000) Ground vibrations from sheet pile driving in urban environment: measurements, analysis and effects on buildings and occupants. *Soil Dyn Earthq Eng* 19(4):371–387
3. Amick H, Gendreau M (2000) Construction vibrations and their impact on vibration-sensitive facilities. In: ASCE construction congress, vol 6, Orlando, Florida, pp 1–10
4. Gutowski TG, Dym CL (1976) Propagation of ground vibration. *J Sound Vib* 49(2):179–193
5. Jedele LP (2005) Energy-attenuation relationships from construction vibrations revisited. In: Proceedings of soil dynamics symposium in honor of Professor Richard D. Woods, geo-frontiers congress 2005. ASCE, Austin, Texas, pp 1–14
6. Kim DS, Lee JS (2000) Propagation and attenuation characteristics of various ground vibrations. *J Soil Dyn Earthq Eng* 19:115–126
7. Massarsch KR (1993) Man-made vibrations and solutions. In: 3rd International conference on case histories in geotechnical engineering, St. Louis, Missouri, pp 1393–1405
8. Massarsch KR, Fellenius, BH (2014) Ground vibrations from pile and sheet pile driving (Part 2–Review of vibration standards). In: Proceedings of the DFI/EFFC international conference on piling and deep foundations, Stockholm, pp 487–501
9. Richart FE, Hall JR, Woods RD (1970) *Vibrations of soils and foundations*. Prentice-Hall Upper Saddle River, New Jersey
10. Svinkin MR (2004) Minimizing construction vibration effects. *Practice Period Struct Des Constr ASCE* 9(2):108–115
11. Svinkin MR (2013) Tolerable limits of construction vibrations. *J Struct Des Constr ASCE* 20(2):1–7
12. Wiss JF (1967) Damage Effects of Pile Driving Vibration. *Highway Research Board Record* 155:14–20.
13. Wiss JF (1981) Construction vibrations: state of the art. *J Geotech Div ASCE* 107:167–181
14. Woods RD, Jedele LP (1985) Energy-attenuation relationships from construction vibrations. In: Proceedings of a symposium on vibration problems in geotechnical engineering. ASCE, Detroit, Michigan, pp 229–246

# Numerical Analysis of Layered Soil-Ash-Foundation System



Amit Kumar Ram and Supriya Mohanty

**Abstract** As earthquake events are unpredictable, necessity of seismic response analysis of ground has become important these days. In this study, nonlinear 1D-ground response analysis of a layered soil-ash system has been performed using Cyclic1D software. Cyclic1D is based on nonlinear finite element principle for one-dimensional (1D) horizontal seismic site-response analysis. In addition, behavior of a shallow foundation placed on the layered soil-ash system has been analyzed using two-dimensional numerical analysis software CyclicTP. The seismic analysis of the layered soil-ash and soil-ash-foundation system has been performed considering the seismic excitation of Uttarkashi earthquake input motion (Mw-6.5). The results of the numerical analysis are demonstrated in the form of acceleration response, displacement response, and excess pore pressure variation for both 1D and 2D analysis. The results of the present studies may be of help in seismic design of foundation constructed with soil-ash deposit to minimize the disposal problem.

**Keywords** Response analysis · Soil-ash-foundation system · Finite element method · Earthquake loading

## 1 Introduction

The present scenario of site characterization study for time varying load like earthquake, landslides, tsunami, etc., is very much significant for geotechnical engineer and it is generally carried out by ground response analysis of the complex system subjected to different excitations. Out of these, earthquake is much frequent and can't be neglected nowadays because of its devastating effects on the structure resting on the top surface of earth's crust, structure beneath the ground surface and the structure on sloping surface of the ground which makes the structure unfit for their use in future. The behavior of soil forming the layered complex ground system is nonlinear

---

A. K. Ram (✉) · S. Mohanty  
Department of Civil Engineering, Indian Institute of Technology (BHU), Varanasi, Uttar Pradesh  
221005, India  
e-mail: [amitkumarram.rs.civ18@itbhu.ac.in](mailto:amitkumarram.rs.civ18@itbhu.ac.in)

© Springer Nature Singapore Pte Ltd. 2022  
A. K. Dey et al. (eds.), *Proceedings of the 7th Indian Young Geotechnical Engineers Conference*, Lecture Notes in Civil Engineering 195,  
[https://doi.org/10.1007/978-981-16-6456-4\\_36](https://doi.org/10.1007/978-981-16-6456-4_36)

339

in nature and its behavior depends on soil type, types of load applied, amplitude of loading and in situ condition of the ground. Hashash et al. [4] studied the recent developments in material model and also discussed the difficulty in measuring the small and large strain damping parameters of soil. Asgari et al. [1] performed the numerical analysis of shallow depth foundation resting on loose silt and silty sand deposit subjected to three different earthquake loadings and discovered that excess pore pressure and deformation plays very important role in soil liquefaction analysis. Yoshimoto et al. [12] investigated the granulated coal ash applicability as reclaimed material by performing pseudo-dynamic response tests. In addition, they compared the results of coal ash with Toyoura sand and come to know that the rate of development of excess pore pressure was slower for coal ash as compared to Toyoura sand. The behavior of Indian pond ash under different earthquake loadings and cyclic loadings has also been investigated in past [7, 8].

In addition to ground response analysis, seismic analysis of liquefaction potential of the existing soil plays a major role in order to understand the resistance of soil under seismic excitations. Seed et al. [11] investigated the use of standard penetration data for the computation of liquefaction potential of silty sand deposits. Liu and Dobry [6] carried out some experimental centrifuge model test to study the settlement of shallow foundation caused due to liquefaction of sandy soil. They found that, when the soil permeability decreases, the excess pore pressure increases under the footing but the total foundation settlement doesn't change. Hashash and Park [3] studied nonlinear 1D ground response analysis in the Mississippi embayment. From this analysis they found that, spectral amplification factor is greater than one in period between 2 and 10 s. Mohanty and Patra [9] investigated liquefaction and seismic response analysis of Panipat pond ash compacted embankment in India. It was observed for upstream case the excess pore pressure ratio is equals to one whereas for downstream side it was observed greater than one. Mohanty and Patra [10] studied liquefaction and ground response analysis of Panki pond ash in India using in situ shear wave velocity measurements under four different earthquake loadings. Both liquefaction and amplification in PGA were noticed under the excitation of given earthquakes. Zand et al. [13] investigated the liquefaction potential of impounded fly ash by conducting cyclic triaxial tests under different confining pressures and densities. The results after the analysis show that, the cyclic loading given by earthquake was lower than the cyclic strength of the fly ash material. Response analysis on layered soil ash and soil-ash-foundation systems is limited. Hence, current study has been focused on the response of soil-ash and soil-ash-foundation system under seismic excitation.

The numerical analysis of soil-ash column of 20 m depth has been carried out by using one-dimensional (1D) nonlinear ground response analysis software Cyclic1D. The seismic response of soil-ash-foundation system of size 20 m × 20 m has been done using plane strain (2D) finite element software CyclicTP under seismic loading. For both 1D and 2D analysis, it is divided into two cases, in which Case-1 represents partially saturated soil condition (water table is at 5 m below the top surface) and Case-2 represents dry condition (water table at bottom of the soil domain). The input motion considered for the present study is Uttarkashi earthquake (Mw-6.5). The

soil domain is divided into four layers; in which fly ash is considered as top layer underlain by sand and cohesive stiff soil resting on hard rock strata. The outcomes of the numerical investigation are expressed in form of acceleration, horizontal/vertical displacement, and excess pore pressure along the depth for both the cases.

## 2 Material Properties

The seismic response analysis has been studied by considering a layered soil-ash and soil-ash-foundation systems having four layer soil systems. The width and height of the soil domain are  $20\text{ m} \times 20\text{ m}$  with water table at 5 m and 20 m below the ground surface. The fly ash has been considered as the top layer in the layered soil system underlain by sand having different densities and cohesive stiff soil at the bottom layer which is supported on hard rock base. The subsurface layer is divided into 5 m thickness. The detailed properties of the layered soil-ash system are shown in Table 1.

The shallow foundation has been considered to carry out the seismic response of soil-ash-foundation systems. The footing is made of concrete having modulus of elasticity of  $25E + 6\text{ kPa}$ , Poisson's ratio of 0.15, and mass density of  $2400\text{ kg/m}^3$ . The width of the footing is 1 m and height above and below the ground surface is 1 m.

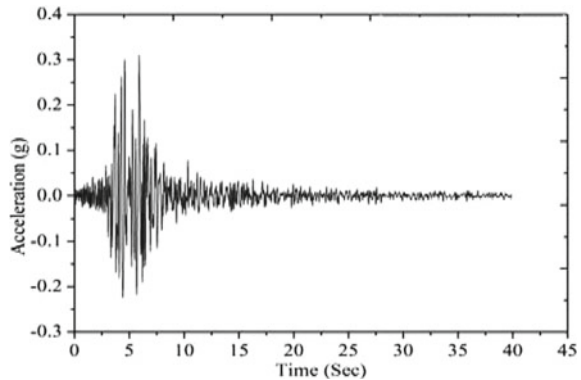
### 2.1 Earthquake Motion

The input motion applied to the layered soil-ash and soil-ash-foundation system is Uttarkashi earthquake and it is also known as Garhwali earthquake. Uttarkashi is a district in Uttarakhand (India). The earthquake occurs in the early morning time having epicenter around 107 km away from Uttarkashi. The magnitude and duration of the earthquake are Mw-6.5 and 39.9 s, respectively. The peak ground acceleration

**Table 1** Soil properties considered for the current study

Layer No.	Layer thickness (m)	Soil type	Shear wave velocity (m/s)	Mass density ( $\text{kg/m}^3$ )
1	5	Fly ash	116.62	1589
2	5	Medium sand permeability	205	1900
3	5	Medium dense sand permeability	225	2000
4	5	Cohesive stiff	300	1800

**Fig. 1** Acceleration time history of Uttarkashi earthquake (Mw: 6.5)



of this earthquake is 0.31 g at 5.9 s. The acceleration time history of the Uttarkashi earthquake used for the present study is shown below in Fig. 1.

### 3 Finite Element Modeling

The finite element software Cyclic1D and CyclicTP was used for the 1D and 2D response/behavior analysis of the soil-ash and soil-ash-foundation system under the excitation of Uttarkashi earthquake. The Cyclic1D used was nonlinear finite element software for one-dimensional (1D) site-response analysis. The number of elements considered in Cyclic1D were 200. The numerical study consists of two different cases, in Case-1 water table was situated at 5 m below ground whereas in Case-2 the water table was situated at bottom of the soil domain. CyclicTP is a two-dimensional finite element software used for numerical analysis of shallow foundation subjected to earthquake excitation. With the help of this software linear and nonlinear analysis can be easily executed. In CyclicTP the lateral mesh borders experience shear beam type motions. The meshing can be done with 9 (solid phase) and 4 (fluid phase) noded quadratic element mesh. The considered domain has been discretized into 2256 number of element. Typical representation of discretized mesh of soil-ash-foundation system considered is shown in Fig. 2.

### 4 Results and Discussions

Results of 1D and 2D numerical analysis of the layered soil-ash and soil-ash-foundation system under the excitation of Uttarkashi earthquake have been discussed in terms of acceleration, horizontal/vertical displacement, and variation of excess pore pressure with depth. Results were presented in both tabular and graphical format in the following sections.



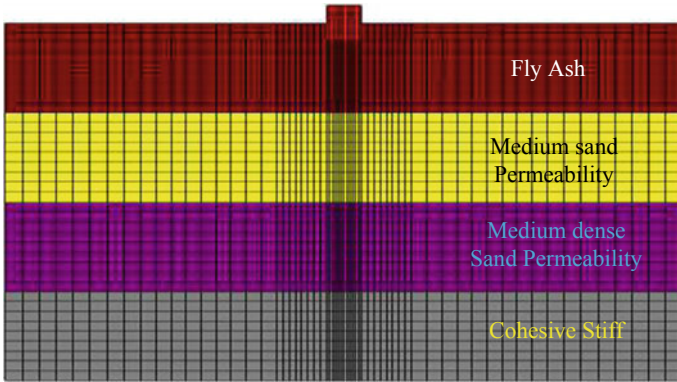
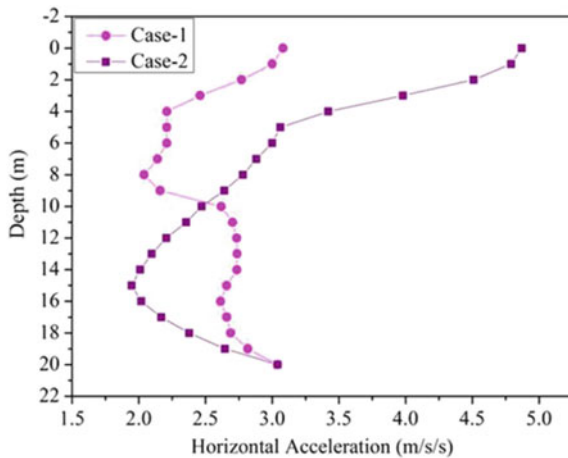


Fig. 2 Discretized mesh of soil-ash-foundation system using CyclicTP

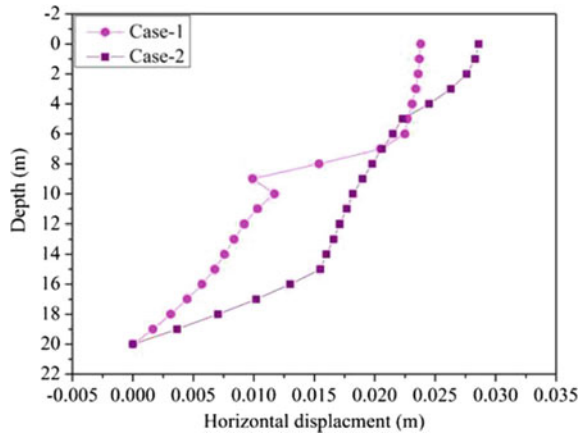
### 4.1 Results of 1D Ground Response Analysis of Soil-Ash System Using Cyclic1D

**Variation of Acceleration** Horizontal acceleration is one of the parameters used for the seismic design of the structure. Hence, in the present study variation of horizontal acceleration with depth at different water table conditions was recorded. The peak ground acceleration (PGA) for the Case-1, i.e., partially saturated system (GWT = 5 m below top surface) is  $3.08 \text{ m/s}^2$ . Similarly, the PGA value for the Case-2, i.e., dry condition (GWT at bottom of the soil domain) is  $4.87 \text{ m/s}^2$  when excited by Uttarkashi earthquake motion. Graphical representation of horizontal acceleration with depth for both the cases for 1D analysis was shown in Fig. 3.

Fig. 3 Variation of horizontal acceleration with depth for 1D analysis



**Fig. 4** Representation of horizontal displacement variation with depth for 1D analysis



**Variation of Horizontal Displacement** Horizontal displacement response noticed at different depths of considered soil-ash system with varied water table conditions was presented in this section. The peak value of the horizontal acceleration for the Case-1, i.e., partially saturated state (GWT = 5 m below the top surface) was 0.0238 m. Similarly, for Case-2, i.e., dry condition (water table at bottom of the soil domain) the peak horizontal displacement value was 0.0286 m when excited by Uttarkashi earthquake. Graphical plot of horizontal displacement with depth for both the cases for 1D analysis was shown in Fig. 4.

**Variation of Excess Pore Pressure** In Cyclic1D, results were recorded at regular intervals of depth for both the cases. Development of excess pore pressure was observed only for the Case-1, i.e., partially saturated state (GWT = 5 m below the top surface). Peak value of EPP is 116.22 kPa at the depth of 10 m from top. Excess pore pressure variation of soil-ash system with depth for Case 1 was presented in Fig. 5.

In addition, peak values of horizontal acceleration, horizontal displacement and excess pore pressure were represented in Table 2 for 1D analysis using Cyclic1D.

## 4.2 Results of Seismic Response of Soil-Ash-Foundation System Using CyclicTP

**Variation of Acceleration Responses** Acceleration responses were obtained in the same manner like Cyclic1D but the only difference is that 2D size of composite system and their variation was plotted with different depth and different lateral distances from the center of the footing under Uttarkashi earthquake as input motion. The acceleration values are recorded at Centre, 0.5B, 2B, 6B away from the footing center on either side of the footing. Peak acceleration values in Case-1 and Case-2

**Fig. 5** Representation of excess pore pressure variation with depth for 1D analysis

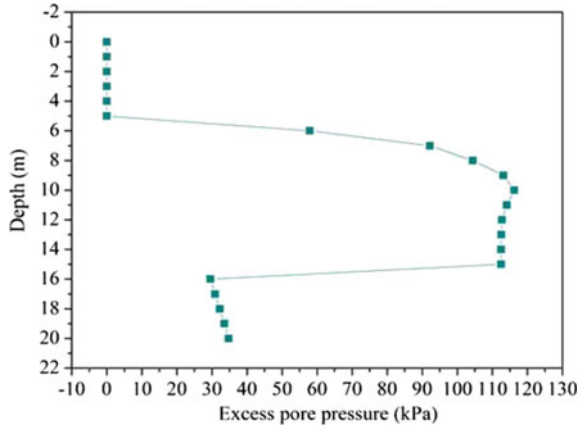


**Table 2** Table captions should be placed above the tables

Cases	Horizontal acceleration (m/s/s)	Horizontal displacement (m)	Excess pore pressure (kPa)
Case-1	3.08	0.0238	116.22
Case-2	4.87	0.0286	0

were  $3.77 \text{ m/s}^2$  and  $4.54 \text{ m/s}^2$ , respectively, when the water table was at 5 and 20 m below ground surface. It is observed from linear and nonlinear ground response analysis that, the PGA remains similar for the soil having high stiffness [5] but in soil-ash-foundation system fly ash has lesser stiffness because of which it is showing increasing trend below the water table. Typical variation of acceleration response along the depth at different locations on either side from center of footing for both the cases was represented in Figs. 6 and 7. Peak values of acceleration at different locations from center of footing for both the cases were presented in Table 3.

**Lateral Displacement Responses** Lateral displacement responses were recorded at different depths on either side from center of the footing for the soil-ash-foundation system when excited by Uttarkashi earthquake. Peak lateral displacements observed for Case-1 and Case-2 were 0.0344 m and 0.0298 m, respectively, when water table was situated at 5 and 20 m below ground surface. Lateral displacement variation with depth on either side from center of the footing for both the cases was represented in Figs. 8 and 9. Peak lateral displacements on either side from center of footing for both the cases were presented in Table 4.

**Variation of Vertical Displacement** Vertical displacement responses were recorded at different depths on either side from center of the footing for the soil-ash-foundation system when excited by Uttarkashi earthquake. It was found that, the vertical displacement is more away from the footing as compared with center of footing. Peak vertical displacements for Case-1 and Case-2 were 0.00871 m and 0.0137 m,

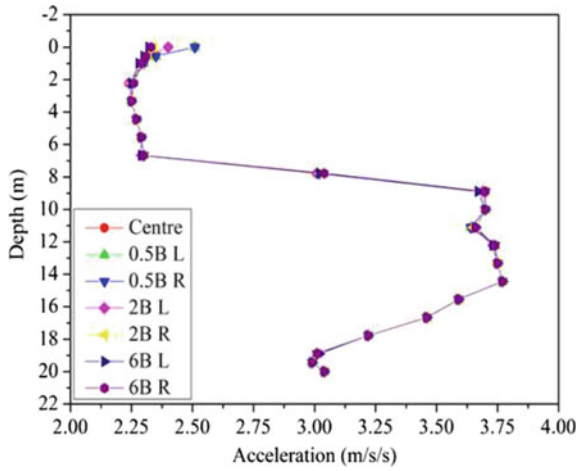


Fig. 6 Typical representation of acceleration variation with depth for Case-1 for 2D analysis

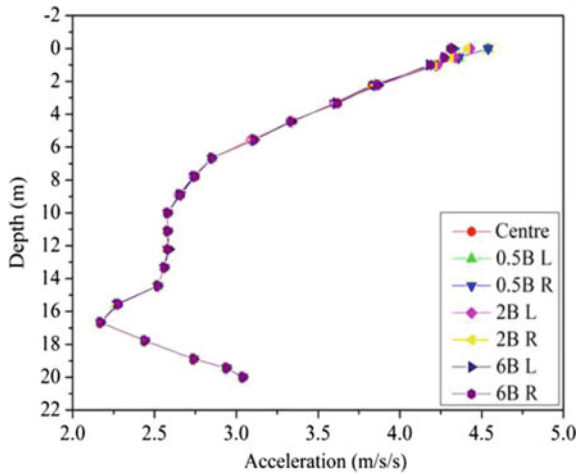


Fig. 7 Typical representation of acceleration variation with depth for Case-2 for 2D analysis

Table 3 Peak acceleration values observed in Case 1 and Case 2 for 2D analysis

Cases	Acceleration (m/s/s)						
	Centre	0.5B L	0.5B R	2B L	2B R	6B L	6B R
1	3.77	3.77	3.77	3.77	3.77	3.77	3.77
2	4.54	4.54	4.54	4.43	4.41	4.33	4.31

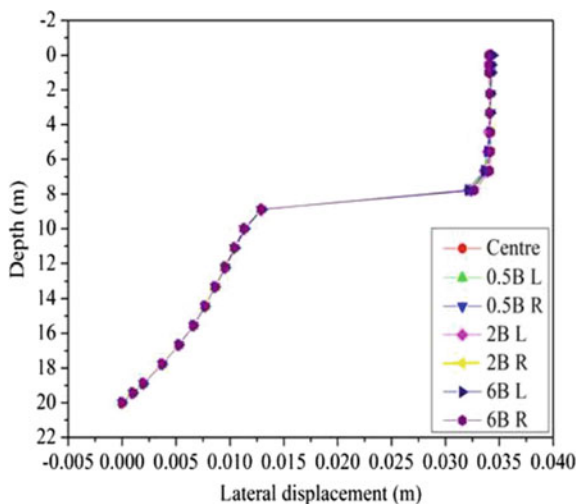


Fig. 8 Typical representation of lateral displacement variation with depth for Case-1 for 2D analysis

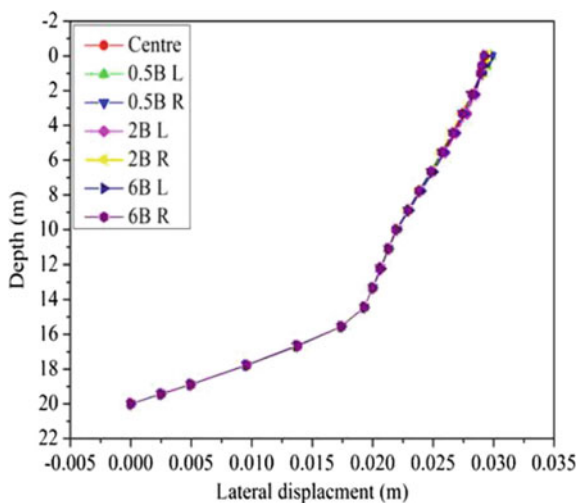


Fig. 9 Typical representation of lateral displacement variation with depth for Case-2 for 2D analysis

Table 4 Peak values of lateral displacement for Case 1 and Case 2 for 2D analysis

Cases	Lateral displacement (m)						
Location from center of footing	Centre	0.5B L	0.5B R	2B L	2B R	6B L	6B R
1	0.0342	0.0342	0.0342	0.0343	0.0342	0.0344	0.0342
2	0.0298	0.0298	0.0298	0.0294	0.0295	0.0293	0.0292

respectively, when water table was 5 and 20 m below ground surface. Lateral displacement variation with depth on either side from center of the footing for both the cases was represented in Figs. 10 and 11. Peak lateral displacements on either side from center of footing for both the cases were presented in Table 5.

**Variation of Excess Pore Pressure** Pore pressure generation was noticed in Case-1 as no water table was present in Case-2. Peak excess pore pressure value was

**Fig. 10** Typical representation of vertical displacement variation with depth for Case-1 for 2D analysis

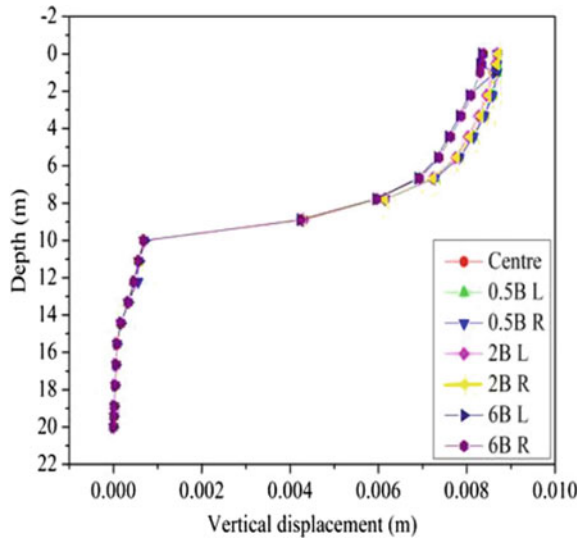


**Fig. 11** Typical representation of vertical displacement variation with depth for Case-2 for 2D analysis

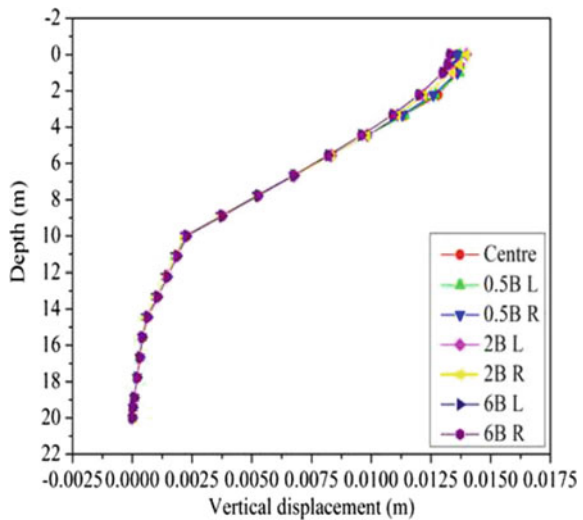


**Table 5** Peak values of vertical displacement for Case 1 and Case 2 for 2D analysis

Cases	Vertical displacement (m)						
	Centre	0.5B L	0.5B R	2B L	2B R	6B L	6B R
1	0.00869	0.00869	0.00869	0.00869	0.00871	0.00864	0.00838
2	0.0136	0.0137	0.0136	0.014	0.014	0.0133	0.0133

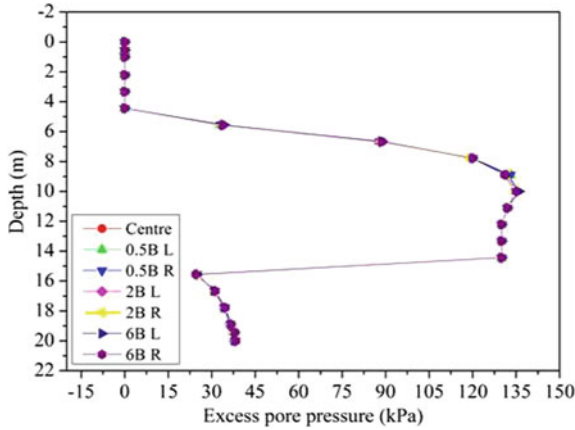


**Fig. 12.** Typical representation of excess pore pressure variation with depth for Case-1 for 2D analysis

observed as 136 kPa for Case-1. Excess pore pressure variation with depth on either side from center of the footing for case-1 was represented in Fig. 12.

Results obtained from 1 and 2D response analysis of soil-ash and soil-ash-foundation system were compared and presented in Table 6. High values of displacement and excess pore pressure were noticed for Case-1, i.e., partially saturated state in 2D analysis. This may be due to the saturated condition of the soil-ash system. Also, presence of footing in 2D analysis case may increase in external loading on soil-ash deposit which in turn results in increase of displacement and excess pore pressure values. However, peak values of acceleration were observed to be more for

**Table 6** Peak values of acceleration, displacement and excess pore presses for Case-1 and Case-2 for 1D and 2D analysis

Cases	Acceleration (m/s/s)		Displacement (m)		Excess pore pressure (kPa)	
	1D	2D	1D	2D	1D	2D
Case-1	3.08	3.77	0.0238	0.0344	116.22	136.00
Case-2	4.87	4.54	0.0286	0.0298	0	0

Case-2, i.e., dry condition for both 1D and 2D analysis. Similar observations have also been noticed by Mohanty and Patra [9].

## 5 Conclusions

The present paper investigated 1D and 2D response analysis of a layered soil-ash and soil-ash-foundation system under the excitation of Uttarkashi earthquake using the finite element software Cyclic1D and CyclicTP with partially saturated and dry conditions. From 1 and 2D analysis, the acceleration values are found to be more in Case-2 than Case-1. However, lateral displacement was higher in Case-1 than Case-2 in 2D analysis. From 1D analysis using Cyclic1D, the horizontal acceleration and horizontal displacement are found to be more in Case-2 deposit than Case-1 deposit. Horizontal displacement values (0.0344 m) were observed to be more when compared with vertical displacement (0.0137 m). Therefore, response analysis of the soil-ash and soil-ash-foundation system is very significant to know the behavior of the complex ground subjected to seismic excitations. From the above analysis, it can be concluded that, fly ash can be used as fill material with proper ground improvement techniques to minimize the waste disposal problem.

## References

1. Asgari A, Golshani A, Bagheri M (2014) Numerical evaluation of seismic response of shallow foundation on loose silt and silty sand. *J Earth Syst Sci* 123(2):365–379
2. Elgamal A, Yang Z, Lu J (2006) Cyclic1D: a computer program for seismic ground response. Report No. SSRP-06/05, Department of Structural Engineering, University of California, San Diego, La Jolla, CA (2006)
3. Hashash YMA, Park D (2001) Non-linear one-dimensional seismic ground motion propagation in the Mississippi embayment. *Eng Geol* 62:185–206
4. Hashash YMA, Phillips C, Groholski DR (2010) Recent advances in non-linear site response analysis. In: 5th International conference on recent advancement in geotechnical engineering and soil dynamics, pp 1–22. San Diego, California (2010)
5. Kumar SS, Dey A, Krishna AM (2014) Equivalent linear and nonlinear ground response analysis of two typical sites at Guwahati city. In: Indian geotechnical conference proceedings, IGC-2014, Kakinada, India, pp 1–10
6. Liu L, Dobry R (1997) Seismic response of shallow foundation on liquefiable sand. *J Geotech Geoenviron Eng* 123(6):557–567
7. Mohanty S, Patra NR (2012) Assessment of liquefaction potential of pond ash at Panipat in India using SHAKE2000. In: GeoCongress-2012 proceedings, state of the art and practice in geotechnical engineering, GSP: 225, ASCE, California, pp 1829–1838
8. Mohanty S, Patra NR (2014) Cyclic behavior and liquefaction potential of Indian pond ash located in seismic zone III and IV. *J Mater Civ Eng ASCE* 26(7):1–5
9. Mohanty S, Patra NR (2016) Liquefaction and earthquake response analysis of Panipat pond ash embankment in India. *J Earthquake Tsunami* 10(2):1–23



10. Mohanty S, Patra NR (2018) Liquefaction and ground response analysis of Indian pond ash using shear wave velocity measurements. In: Geotechnical earthquake engineering and soil dynamics proceedings V 2018, GSP: 291, ASCE, pp 504–513
11. Seed HB, Idriss IM, Arango I (1983) Evaluation of liquefaction potential using field performance data. *J Geotech Eng* 109(3):458–482
12. Yoshimoto N, Orense RP, Kanda H, Hyodo M (2008) Earthquake response of granulated coal ash by online testing. In: The 14th world conference on earthquake engineering proceedings, Beijing, China, pp 1–8
13. Zand B, Tu W, Amaya PJ, Wolfe WE, Butalia T (2007) Evaluation of liquefaction potential of impounded fly ash. In: Proceedings of world of coal ash (WOCA), Northern Kentucky, USA, pp 1–23

# Comparative Study on Static and Seismic Performance of Ash-Foundation System



M. V. Ravi Kishore Reddy, Supriya Mohanty, and Shaik Rehana

**Abstract** Utilization of coal ash under a foundation of structure deals with huge quantity of its usage that solves the issue of its disposal, which is trivial in most parts of the world. Adaptability of coal ash under foundation needs to be examined on a large scale. In this study, it is attempted to investigate static and seismic response of shallow foundation resting on pond ash deposit. Two-dimensional (2D) response analysis is carried out for the ash-foundation system by employing finite element software PLAXIS 2D. It has been recognized since decades that soil-foundation interaction or ash-foundation interaction is prime factor in the seismic response of structure or portions of structure. Ash-foundation system is excited under the influence of Nepal earthquake motion ( $M_w$ : 7.8) and North East India earthquake motion ( $M_w$ : 7.5). The displacement was observed more in case of North East India earthquake, i.e. 6.028 m. However, acceleration and excess pore pressure response were high in case of Nepal earthquake, i.e. 0.152 g and 129.16 kPa, respectively. These responses can be utilized to assess the performance of ash-foundation system.

**Keywords** Static and seismic response · Shallow foundation · Pond ash deposit · 2D response analysis · PLAXIS 2D

---

M. V. Ravi Kishore Reddy · S. Rehana  
Earthquake Engineering Research Centre, International Institute of Information Technology,  
Hyderabad, Telangana 500032, India  
e-mail: [meeгада.reddy@research.iiit.ac.in](mailto:meeгада.reddy@research.iiit.ac.in)

S. Rehana  
e-mail: [rehana.s@iiit.ac.in](mailto:rehana.s@iiit.ac.in)

S. Mohanty (✉)  
Department of Civil Engineering, Indian Institute of Technology (BHU), Varanasi, Uttar Pradesh  
221005, India  
e-mail: [supriya.civ@iitbhu.ac.in](mailto:supriya.civ@iitbhu.ac.in)

## 1 Introduction

Utilization of coal ash requires precise investigations using both laboratory and numerical studies. Many researchers have reported several studies related to geotechnical characterization of coal ash in comparable with soil [1–4]. Employability of coal ash in place of soil completely has not been established yet. Though several studies were available on seismic response analysis of coal ash deposits [4–9], further investigations on utilization of coal ash are lacking. In addition, it is required to investigate the utilization of coal ash under foundation. Investigation on response of complex system (soil-foundation or soil-foundation-structure) due to static loads or dynamic loads is of prime need and serious concern for stability of the system. Response of foundation depends on the medium surrounding it. In this study, ash has been considered under the foundation. When this system is subjected to either static or dynamic loads, response of ash influences foundation behaviour, in turn response of foundation influences ash behaviour, and so this can be referred as ash-foundation interaction. Several studies on static performance of ash-foundation system have been reported in the past that includes laboratory investigations and numerical studies [10, 11]. Numerical analyzes by finite element discretization of soil-foundation system under seismic condition revealed that seismic response is more for partially saturated state than that of dry state [12]. In addition, studies on foundation-soil-foundation interaction by boundary element method revealed that this phenomenon affects the dynamic behaviour of adjacent footings [13]. Seismic performance of ash-foundation system draws much attention of researchers, as it is uncommon using ash under foundation. It has been observed that studies on seismic performance of ash-foundation system are limited.

Present study comprises comparison of static and seismic performance of a partially saturated ash-foundation system (water table located at a depth 4.5 m from ground level). This comparative study is made for the parameters like acceleration, displacement, excess pore pressure variation under different earthquake excitations, i.e. Nepal earthquake (Mw: 7.8) and North East India earthquake (Mw: 7.5) motions.

## 2 Input Data

Parameters considered for the present study on static and seismic performance of ash-foundation system are as follows.

### 2.1 Foundation Parameters

Foundation parameters adopted for the current study are stated in the following Table 1.

**Table 1** Details of adopted foundation parameters for present study

Parameter		Units
Foundation	Shallow (Strip foundation)	–
Width, $b$	1.5	M
Thickness, $d$	0.8	M
Weight, $w$	36	kN/m/m
Normal stiffness, EA	$37.5 \times 10^6$	kN/m
Flexural rigidity, EI	$2 \times 10^6$	kN m <sup>2</sup> /m
Poisson's ratio, $\nu$	0.2	–

**Table 2** Details of ash material properties for present study

Parameter	Value	Units
Unsaturated unit weight, $\gamma_{\text{unsat}}$	10.76	kN/m <sup>3</sup>
Saturated unit weight, $\gamma_{\text{sat}}$	14.74	kN/m <sup>3</sup>
Void ratio, $e_{\text{init}}$	0.72	–
Cohesion, $c$	22.54	kPa
Angle of internal friction, $\phi$	36.29	°
Permeability, $k$	$2.13 \times 10^{-6}$	m/s

## 2.2 Ash Parameters

Ash material considered in this study is pond ash, which was collected at pond ash site of Talcher thermal power plant, Odisha, India. The site comes under seismic zone-III (moderate earthquake zone,  $a_{\text{max}} = 0.16$  g). Properties of ash material considered are listed in Table 2.

## 2.3 Earthquake Motion

Two earthquake motions are considered for the study of seismic performance of ash-foundation system. Nepal earthquake motion (Mw: 7.8, 2015) and North East India earthquake motion (Mw: 7.5, 1988). Peak ground acceleration (PGA) value of Nepal earthquake motion is 0.1639 g and it observed at 49.31 s. Similarly, PGA value of North East India earthquake is 0.1743 g and it observed at 28.86 s. Duration of Nepal earthquake motion and North East India earthquake motion is 149.996 s and 119.66 s, respectively. Accelerogram of Nepal earthquake and North East India earthquake is presented in Fig. 1.

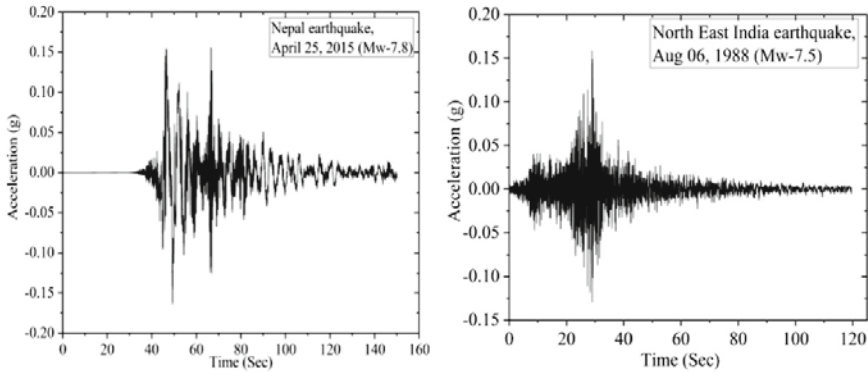


**Fig. 1** Acceleration time history of Nepal earthquake (Mw: 7.8) and North East India earthquake (Mw: 7.5)

### 3 Methodology

Static and seismic performance of ash-foundation system are investigated numerically by employing PLAXIS 2D software. PLAXIS 2D [14, 15] is a finite element source intended of simulating soil behaviour by various soil models for varied applications in the field of geotechnical engineering. Hardening soil small model with small-strain stiffness (HSsmall) has been chosen for simulating soil behaviour subjected for dynamic loads. For accurate description of stiffness of soil, parameters like the triaxial loading stiffness  $E_{50}$ , triaxial unloading stiffness,  $E_{ur}$  and oedometer loading stiffness,  $E_{oed}$ , small-strain shear modulus,  $G_0^{ref}$  are used. In dynamic applications, when this model is used, it introduces hysteretic material damping. This model gives more reliable responses for such complex systems. PLAXIS 2D is also a user-friendly software with good graphical user interface.

Ash-foundation system is discretized into 2032 elements in case of both Nepal and North East India earthquakes as input motions. Optimum number of element, i.e. 2032 was chosen based on the results of convergence study. In PLAXIS, earthquake motion (acceleration time history) was applied in terms of displacement multiplier with  $m/sec^2$  as its units. Pond ash deposit was discretized into number of elements for 2D analysis such that it satisfies criteria according to Eq. (1) [16, 17].

$$\lambda/8 < l_e < \lambda/5 \tag{1}$$

$l_e$  Maximum dimension of any element in vertical direction

$\lambda$  Least wavelength for the analysis =  $V_s/f$ .

where  $V_s$  is the shear wave velocity considered for the study (m/s) and  $f$  is frequency (Hz).

In dynamic analysis to avoid distortions of computed results caused by reflection of stress waves, the domain size of  $80\text{ m} \times 20\text{ m}$  was adopted in this study. Foundation

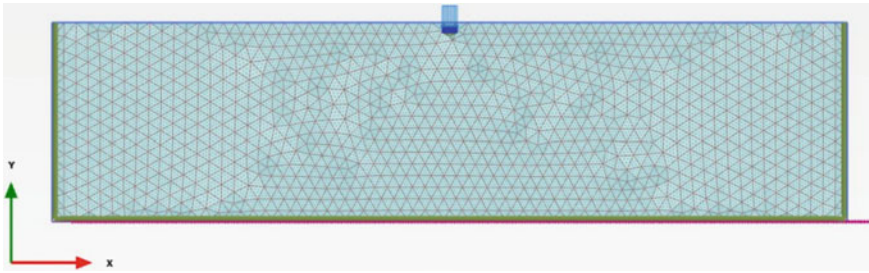


**Fig. 2** View of discretized mesh of ash-foundation system

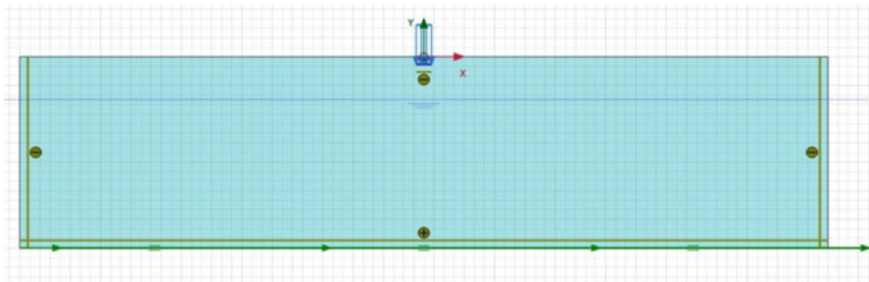


**Fig. 3** Model of created ash-foundation system

is of size ( $b \times d$ )  $1.5 \text{ m} \times 0.8 \text{ m}$ . Response of ash-foundation system due to static load and due to earthquake load is discussed in the following sections. Seismic performance of ash-foundation system in terms of peak ground acceleration, peak ground displacement and excess pore pressure generation under excitation of two input motions (i.e. Nepal and North East India earthquake) is discussed in detailed in the following sections. Discretized mesh and created ash-foundation system are presented in Figs. 2 and 3.

## 4 Results and Discussion

Static and seismic performance of ash-foundation system and its comparative study have been presented in this section. Variation of parameters like acceleration ( $g$ ), displacement ( $m$ ) and excess pore pressure ( $kPa$ ) with respect to depth around centre of ash-foundation system under two earthquake loading conditions has been discussed in the following sections.

### 4.1 Response of Ash-Foundation System Under Static Load

Static load (line load) of 64.21 kN/m/m was applied on the foundation experiencing a displacement of 29.53 mm. The maximum displacement of 29.53 mm was observed at location (0.75, -0.8 m). Similar observations were noticed from the studies on fly ash and soil by past researchers [11, 18] using PLAXIS 2D. Excess pore pressure was minimal as location of water table is beyond the impact of foundation and superimposed load. Variation of displacement close to footing centre is plotted against depth and presented below in Fig. 4. View of deformed mesh is shown in Fig. 5.

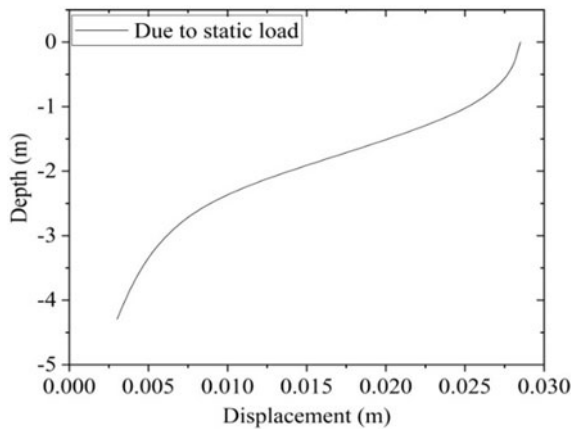


Fig. 4 Variation of displacement of ash-foundation system with depth under static load

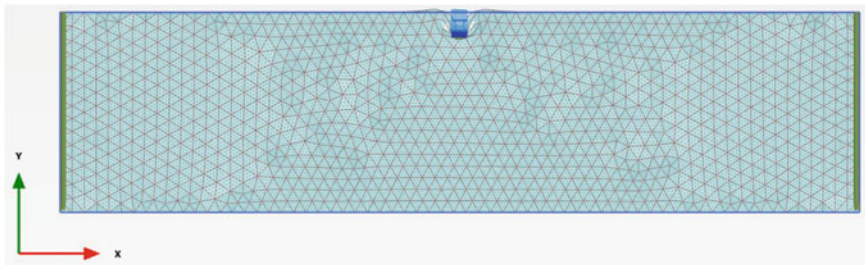
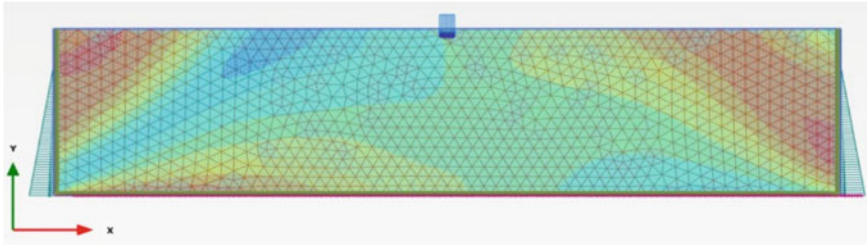


Fig. 5 Typical view of deformed mesh for ash-foundation system under static load



**Fig. 6** Typical view of shadings of displacement for ash-foundation system under dynamic loading (Nepal input motion)

## 4.2 Response of Ash-Foundation System Under Dynamic Loading

**Displacement Variation** The peak displacement observed in case of Nepal earthquake as input motion was 0.535 m, whereas in case of North East India earthquake, it was 6.028 m. High PGA value of North East India earthquake (0.1743 g) when compared with Nepal earthquake (0.1639 g) input motion may cause high displacement. It may be due to excitation of ash-foundation system with high amplitude of motion initially (North East India earthquake) from inception of event when compared. Similar result of high magnitude of displacement in case of North East India earthquake was observed in the past studies by Khanna and Mohanty [6] on 2D seismic response analysis of pond ash deposits. Figure 6 represents typical shadings of displacement for Nepal earthquake motions.

**Acceleration Variation** The peak acceleration observed in case of Nepal earthquake as input motion was 0.152 g, whereas in case of North East India earthquake was 0.087 g at ground surface. High value observed in case of Nepal earthquake motion is due to small time step of earthquake motion, i.e. 0.005 s and also may be due to high magnitude of Nepal input motion (Mw: 7.8). In addition, in case of Nepal input motion acceleration value was observed to be increased a little below water table and then decreases with depth whereas in case of North East India earthquake acceleration value was observed to be decreased with depth. Amplification of acceleration between bottom and top of the ash-foundation system was observed with a mean value of 0.145, 0.074 g for Nepal earthquake and North East India earthquake, respectively. It was similar to the recent past studies of pond ash embankments [9]. Variation of acceleration of ash-foundation system with depth is presented in Table 3.

**Excess Pore Pressure Variation** Excess pore pressure was observed high in case of Nepal input motion, i.e. 129.16 kPa, whereas under North East India earthquake was 92.89 kPa. It may be short period of time of excitation of Nepal earthquake motion. Excess pore pressure variation of ash-foundation system with depth is presented in Table 4.



**Table 3** Variation of acceleration of ash-foundation system with depth when subjected to two input motions, respectively

Depth (m)	Acceleration ( $a_x$ ) (g)	
	Nepal earthquake (Mw: 7.8)	North East India earthquake (Mw: 7.5)
0	0.152	0.087
-1.05	0.148	0.086
-2.18	0.143	0.084
-3.64	0.145	0.080
-4.93	0.147	0.075
-6.19	0.148	0.069
-7.41	0.147	0.065
-8.61	0.145	0.066
-9.79	0.140	0.065
-10.38	0.137	0.066
-12.15	0.140	0.067

**Table 4** Excess pore pressure variation of ash-foundation system with depth when subjected to two input motions, respectively

Depth (m)	Excess pore pressure (kPa)	
	Nepal earthquake (Mw: 7.8)	North East India earthquake (Mw: 7.5)
-5.08	2.806	22.393
-6.19	13.566	27.788
-7.03	19.780	32.077
-8.01	25.251	36.618
-9.07	26.645	40.939
-9.93	13.913	45.082
-10.97	25.649	50.529
-11.93	09.261	55.684
-13.32	26.566	63.220
-14.78	41.982	70.892
-15.94	83.800	76.840
-17.1	67.109	82.590
-18.26	102.549	90.229
-18.99	129.163	92.896

## 5 Conclusions

Studies on static performance of ash-foundation system were experienced by many researchers extensively in laboratories and very few under numerical analyzes. Here, it is attempted to study the performance of ash-foundation system for static loads and also to know the system’s response under dynamic loads especially earthquake load

with the presence of water table. In this study, two earthquake motions were considered for numerical analysis of ash-foundation system and the analysis is performed using numerical analysis software PLAXIS 2D. Response was evaluated with the parameters like displacement, acceleration and excess pore pressure variation at various locations within ash-foundation system. Displacement of approximately 30 mm was experienced in case of static load, whereas a very high value around 6 m was experienced in case of dynamic load when subjected on the ash-foundation system. A variation of almost 5.5 m is observed between the peak displacement values of ash-foundation system when subjected to dynamic loads, i.e. Nepal earthquake (0.535 m) and North East India earthquake (6.028 m), respectively. Acceleration value was observed to be more in case of Nepal earthquake, i.e. 0.152 g, and variation of acceleration value was observed to be almost double when compared with that of North East India earthquake with an acceleration value of 0.087 g. Excess pore pressure was observed high in case of Nepal earthquake as base excitation, i.e. 129.46 kPa, whereas under North East India earthquake was 92.89 kPa. The variation in excess pore pressure is about 40%. It was concluded from results that seismic performance of ash-foundation system has to be investigated prior to the construction of structure on ash deposit.

## References

1. Das SK, Yudhbir (2005) Geotechnical characterization of some Indian fly ashes. *J Mater Civil Eng* 17(5):544–552
2. Jakka RS, Ramana GV, Datta M (2010) Shear behavior of loose and compacted pond ash. *Geotech Geol Eng* 28:763–778
3. Kim B, Prezzi M, Salgado R (2005) Geotechnical properties of fly and bottom ash mixtures for use in highway embankments. *J Geotech Geoenviron Eng* 131(7):914–924
4. Mohanty S, Patra NR (2015) Geotechnical characterization of Panki and Panipat pond ash in India. *Int J Geo-Eng* 6(13):1–18
5. Amorosi A, Boldini D, Elia G (2010) Parametric study on seismic ground response by finite element modelling. *Comput Geotech* 37:515–528
6. Khanna A, Mohanty S (2017) 2D ground response analysis of pond ash deposits. In: *Geotechnical frontiers*, GSP-276. ASCE, pp 387–396
7. Mohanty S, Patra NR (2014) Cyclic behavior and liquefaction potential of Indian pond ash located in seismic zones III and IV. *J Mater Civ Eng* 06014012:1–5
8. Reddy MVRK, Mohanty S, Shaik R (2018) Comparative study of 1D, 2D and 3D ground response analysis of pond ash from Odisha under different earthquake motions. In: *Indian geotechnical conference 2018, India*, pp 1–8
9. Vijayasri T, Raychowdhury P, Patra NR (2016) Seismic response analysis of Renusagar pond ash embankment in Northern India. *Int J Geomech* 17(6):1–12
10. Ghosh A, Ghosh A, Bera AK (2005) Bearing capacity of square footing on pond ash reinforced with jute—Geotextile. *Geotect Geomembr* 23:144–173
11. Gill KS, Choudhary AK, Shukla SK (2012) Load bearing capacity of footing resting on the fly ash slope with multilayer reinforcements. In: *GEOCONGRESS 2012, ASCE*, pp 4262–4271
12. Reddy MVRK, Mohanty S, Ramancharla PK (2019) Comparative study of dynamic response analysis of shallow foundation on layered soils. In: *Soil dynamics and earthquake geotechnical engineering. Lecture notes in civil engineering*, vol 15. Springer, Singapore, pp 91–99

13. Karabalis DL, Mohammadi M (1998) 3-D dynamic foundation-soil-foundation interaction on layered soil. *Soil Dyn Earthq Eng* 17:139–152
14. Brinkgreve RBJ, Kumarswamy S, Swolfs WM, Foria F (2018) *Plaxis 2D reference manual*. The Netherlands
15. Brinkgreve RBJ, Kumarswamy S, Swolfs WM, Foria F (2018) *Plaxis 2D material models manual*. The Netherlands
16. Kuhlemeyer RL, Lysmer J (1973) Finite element method accuracy for wave propagation problems. *J Soil Dyn Div* 99:421–427
17. Lysmer J, Udaka T, Tsai CF, Seed HB (1975) *FLUSH: a computer program for approximate 3-D analysis of soil-structure interaction problems*. Report EERC 75-30, Berkeley, p 83
18. Raviteja KVNS, Umashankar B, Ramu K, Babu RD (2014) Bearing capacity of a strip footing resting on treated and untreated soils. In: *Indian geotechnical conference 2014, India*, pp 1–6

# Influence of Bedrock on Site Response



Bhavesh Pandey , Ravi S. Jakka, and Ashok Kumar

**Abstract** Seismic hazard assessment study cannot be completed without complete understanding of site response of the particular site. Empirically,  $V_{S30}$  is one of the most important parameter for estimation of site response. Site response of two sites having similar  $V_{S30}$  may vary significantly. These variations or uncertainties mainly arise from the variations in dynamic properties and thickness of individual layers and depth of bedrock. This study focuses on the aspect of influence of bedrock depth on site amplification. For this study, strong motion stations of Kik-Net dataset are used, due to availability of surface and downhole sensors and complete information regarding the properties of subsurface soil stratum. These sites are grouped as per  $V_{S30}$  and bedrock depth. Theoretical ground response analysis (GRA) was performed for all these sites using equivalent linear approach. Amplification function obtained from GRA is compared with amplification function obtained from standard spectral ratio (SSR) and horizontal to vertical spectral ratio of surface records (HVSR). Results obtained were presented in the form of variation in amplification spectrum with respect to bedrock depth.

**Keywords** Site amplification · Bedrock · HVSR · Shear-wave velocity

## 1 Introduction

It has been observed and reported by several researchers that soil conditions modify ground motion and may cause high amplifications and change in frequency content along with the duration of shaking. The oldest documented account of the effect of soil conditions and subsequent modifications were first reported by MacMurdo [1]. He observed that buildings over hard rock experienced lesser damage in comparison

---

B. Pandey (✉)

Civil Engineering Department, BT Kumaon Institute of Technology, Dwarahat, Uttarakhand, India  
e-mail: [bpandey@eq.iitr.ac.in](mailto:bpandey@eq.iitr.ac.in)

B. Pandey · R. S. Jakka · A. Kumar

Department of Earthquake Engineering, Indian Institute of Technology, Roorkee, India

© Springer Nature Singapore Pte Ltd. 2022

A. K. Dey et al. (eds.), *Proceedings of the 7th Indian Young Geotechnical Engineers Conference*, Lecture Notes in Civil Engineering 195,  
[https://doi.org/10.1007/978-981-16-6456-4\\_38](https://doi.org/10.1007/978-981-16-6456-4_38)

363

to buildings which were on soft soil sites. Similar observations were later reported in several other earthquakes such as “September 19, 1985, Michoacan Earthquake” [2], “October 19, 1989 Loma Pieta earthquake” [3], and “January 26, 2001 Bhuj Earthquake” [4].

Researchers and practicing engineers Paulay and Priestley [5], Adhikary and Singh [6], Pandey et al. [7, 8] etc., all around the globe, tirelessly working for several years to standardize the solutions to be used in for accounting site effects while designing of structures. Such solutions are generally known as “Design Codes” or “Design Standards” (such as Eurocode 8, [9, 10], NEHRP Guidelines 1997; [11, 12]; IITK-GDM [13–16] etc.) which are published and publicized by responsible government agencies. Most of these standards use shear-wave velocity or other soil parameters to characterize the site. It is not always practically possible to drill a hole and find out the exact depth of such layer, hence, several geophysical methods are used to estimate shear-wave velocity ( $V_s$ ) profiles of the soil column.  $V_s$  being directly proportional to the shear stiffness of soil makes this a useful parameter for site classification. Table 1 presents the soil classification scheme from different codes of practice. Subsequently, loads are defined as per these site classes to be applied for the design of structures.

As per different codes of practice (Table 1), sites are typically classified as per their  $V_{s30}$  value except in IS 1893:2002.  $V_{s30}$  is defined as average shear-wave velocity of the top 30 m depth soil strata calculated using average travel time of shear-wave velocity. On the basis of these classes, loads in terms of response spectra are assigned to be used for the design of structures for seismic loading. Also, it can be seen that there are different kind of rock sites defined mostly having  $V_s$  greater than  $\sim 800$  m/s.

Even though depth and stiffness of bedrock is such an important parameter which influences ground motion, still no clear-cut guideline is available in the literature to incorporate this parameter for amplification study. Most of the modern attenuation relations such as Chiou and Youngs [19] considered depths of different  $V_s$  for reference site. Steidl et al. [20] questioned what could be considered as a reference site for given site conditions. Even after so many years, the question is still relevant. Most of the studies, either related to GMPE or seismic hazard assessment, consider some layer with a local velocity between 760 and 1500 m/s (NEHRP class B sites) as a reference site or bedrock. But, there are no definite criteria to select a reference site (in case of standard spectral ratio) or half-space for theoretical ground response analysis.

This work primarily deals with the effect of depth of EB/bedrock on site amplification. Further, this study also explores the idea of what should be considered as the depth of EB that could be a good approximation for most of the engineering purposes. For this study, nine sites from Kik-Net dataset were used. Sites from Kik-Net database are selected due to the availability of records at top of the soil surface and inside a borehole at the top of bedrock.

**Table 1** Comparison of site classes in different codes of practice

Building seismic safety Council (BSSC) [17]		EUROCODE 8 [18]		New Zealand Code [12]		Indian seismic code (BIS 2002) IS 1893 [10]	
SC	Description	SC	Description	SC	Description	SC	Description
A	Hard rock: $V_{S30} > 1500$ m/s	A	Rock and rock-like geological formation: $V_{S30} > 800$ m/s	A	Strong to extremely strong rock: $V_{S30} > 1500$ m/s; $c_u > 50$ kPa; Not underlain by $< 18$ MPa or $V_s$ 600 m/s materials	Type-I	Rock or hard soil. Well-graded gravel and sand-gravel mixtures with or without clay binder, and clayey sands
B	Rock: $760 < V_{S30} < 1500$ m/s	B	Deposits of very dense sand, gravel, or very stiff clay: $360 < V_{S30} < 800$ m/s; $N > 50$ ; $c_u > 250$ kPa	B	Rock: $V_{S30} > 360$ m/s; $1 < c_u < 50$ kPa and not underlain by $< 0.8$ MPa or $V_s$ 300 m/s materials, a surface layer no more than 3 m depth		poorly graded or sand-clay mixtures $N > 30$
C	Very dense soil and soft rock: $360 < V_{S30} < 760$ m/s; $N > 50$ ; $\bar{c}_u > 100$ kPa						

(continued)

**Table 1** (continued)

Building seismic safety Council (BSSC) [17]		EUROCODE 8 [18]		New Zealand Code [12]		Indian seismic code (BIS 2002) IS 1893 [10]	
SC	Description	SC	Description	SC	Description	SC	Description
D	Stiff soil: $180 < V_{S30} < 360$ m/s; $15 < N < 50$ ; $50 < \bar{c}_u < 100$ kPa	C	Deep deposits of dense or medium dense sand, gravel or stiff clay: $180 < V_{S30} < 360$ m/s; $15 < N < 50$ ; $70 < c_u < 250$ kPa	C	Not class A, B, or E, low amplitude natural period $\leq 0.6$ s	Type-II	Medium soils, i.e., poorly graded sands or gravelly sands with little or no fines $10 < N < 30$ or $N > 15$
E	Soft clay soil: $V_{S30} < 180$ m/s; $N < 15$ ; $\bar{c}_u < 50$ kPa; or any profile having depth $> 3$ m of soft clay defined as soil with $PI > 20$ , $w \geq 40\%$ , and $c_u < 25$ kPa	D	Deposits of loose-to-medium cohesion less soil or soft to firm cohesive soil: $V_{S30} < 180$ m/s; $c_u < 70$ kPa	E	Very soft soil sites with depth $> 10$ m and $V_{S30} < 150$ m/s or $N < 6$ or $Cu < 12.5$ kPa	Type-III	Soft soils $N < 10$

## 2 Methodology

As discussed above, this paper’s prime objective is to study the effect of depth of bedrock and its stiffness or  $V_s$  on site amplification. For this study, nine sites from Kik-net database were selected, and they had been grouped as per their corresponding depth of EB which is defined as the layer having local shear-wave velocity equal to or greater than 760 m/s. Hence, the three groups of selected sites were formed as follows:

- The first group consists of sites having the depth of EB less than 50 m.
- The second group consists of sites having the depth of EB between 50 and 100 m.
- The third group of sites is those which have the depth of EB a more than 100 m.

The available shear-wave velocity profile of the sites is modified by extracting multiple shear-wave velocity profiles from the original profile so that each extracted profile has a different depth and half-space as shown in Fig. 1. Using the available records and extracted profiles, transfer functions or amplification functions were estimated for the site by using the following methods:

- The transfer function for each extracted profile of a site is calculated by ground response analysis using equivalent linear approach.
- Horizontal to vertical spectral ratio was also calculated for each site.
- Standard spectral ratio using Kagami’s ratio technique was also estimated for each site.

A brief description of each method is provided below:

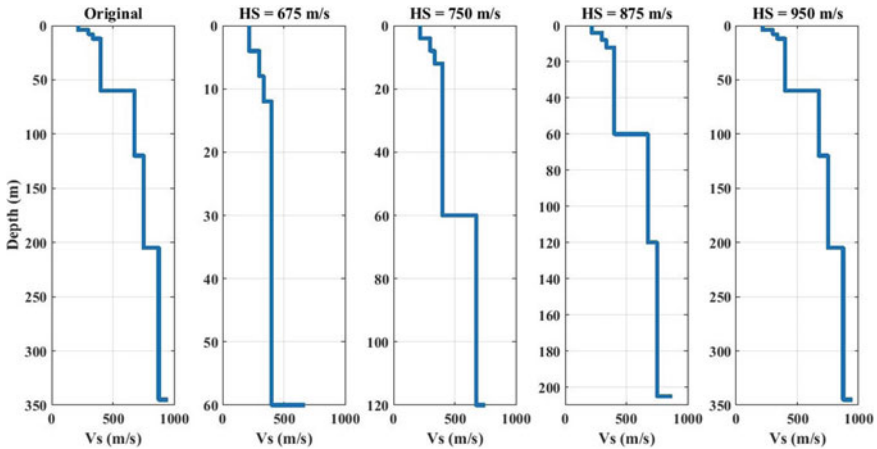


**Fig. 1** Typical example of different  $V_s$  models used to study effect of bedrock depth for a site. From the original profile, several shear-wave velocity profiles had been extracted having different half-space (depth), and amplification function for all the profiles including the original one was estimated and compared using GRA



### **Equivalent Linear 1-dimensional Ground Response Analysis (GRA)**

For performing analysis using GRA parameters such as the shear-wave velocity, density, the material damping factor, and the thickness of each layer are required. These parameters may be computed through the various geotechnical and geophysical field and laboratory tests. These analyses may be performed considering either linear or non-linear behavior for the soil. For considering non-linear behavior of soil, usually, equivalent linear method is used. This method uses an iterative procedure to adopt soil parameters (i.e., stiffness and damping) to the strain level that each particular soil layer experiences during a specific earthquake motion. For accounting non-linearity with an increase in shear strain level, specific curves expressing the degradation of shear modulus  $G$  ( $G/G_{max}$ ) and the respective increase of material damping with the increasing shear strain level are used. Such curves for different types of soils had been proposed by numerous researchers.

To perform such analysis, several computer programs are available such as SHAKE2000, STRATA, and DEEPSOIL. For this study, STRATA [21] has been used. STRATA is very user-friendly open-source software to perform 1D ground response analysis.

Using the shear-wave velocity profile and other details, as provided in the Kik-net database, transfer functions were calculated for each of the extracted profile. The surface ground motion was used as input motion at top of the profile, and the transfer function is estimated between surface and top of half-space (HS).

### **Standard Spectral Ratio (SSR)**

Standard spectral ratio (SSR), proposed by Borchardt [22], has been the most popular and widely used technique to characterize site amplification. SSR is calculated by taking the ratio of the spectral values of a soil-site record to that of a nearby rock-site record from the same earthquake and component of motion. The nearby rock site is generally termed as a reference site, hence, this methodology is also known as reference-site technique. This methodology considers two assumptions, first is that path, and source effect for both the stations is the same, and the other is reference site station does not have any site effects. The basis of the first assumption, the close distance between the stations in comparison to the distance from the source. The second assumption is the reason that the reference station is selected on a rock outcrop. However, it is very difficult to find out any such site, which is totally free from any site effects due to which it becomes very difficult to locate reference site [20]. This is the huge drawback of this methodology.

As it is very difficult to find out a perfect reference site, the problem could have been solved if the surface to downhole spectral ratio is used, considering the downhole record as a reference record. This ratio is also known as Kagami's ratio [23]. In Kagami's ratio, a correction needs to be applied to overcome the problem of feedback from the surface and intermediate layers to the downhole sensor. A downhole sensor time history also records reflected waves from upper layers along with the incident wave due to which it differs from the surface record significantly. This can be easily corrected by multiplying the ratio by coherence function of input and output, which

is given by the following equation:

$$C_{12}^2 = |X_{s,b}(f)|^2 / (X_{s,s}(f)X_{b,b}(f)) \tag{1}$$

where  $X_{s,b}(f)$  is defined as Fourier transform of cross correlation of signals recorded at surface and borehole,  $X_{s,s}(f)$  and  $X_{b,b}(f)$  are Fourier transform of auto-correlation of surface and borehole records. For this study, SSR is performed by Kagami’s approach [23].

**Horizontal-to-Vertical Spectral Ratio (HVSR)**

Horizontal-to-vertical spectral ratio of microtremor technique named after Nakamura [24], who proposed to use microtremors for studying site amplification and hence, site characterization. This technique requires only, one three-component sensor, hence, this technique is also known as a single-station method. It was found that the peak frequency of the ambient vibration H/V spectrum (HVamb) for a site almost corresponds to the fundamental frequency of that site [25]. HVamb technique was first introduced by Nogoshi and Igarashi [26], but Nakamura [24] developed and used it for the purpose of estimation of site response. The similar methodology was used by Langston [27], using earthquake records to understand the crustal and upper-mantle structure of earth using teleseismic recordings. Due to the requirement of records from only one station, this method is also known as the single-station method or non-reference site technique. This feature makes this methodology very user-friendly and time-saving, which in turn makes it very popular among earthquake engineers and seismologists.

Later, earthquake records are also being used for estimation of local site effects using HVSR, and it was found by many researchers that the shape of site response curve obtained from SSR and HVSR was most of the time found to be similar when S-wave part of the seismogram is used in several comparative studies (such as [28–33]). Though, both the methods were found to be consistent in estimating the fundamental resonance frequency of the site, their estimated amplification levels differ.

For the estimation of SSR and HVSR for this study, resultant horizontal record is used given as:

$$Acc_{Hor} = EW + iNS \tag{2}$$

where  $Acc_{Hor}$  is a resultant horizontal record;  $EW$  is East–West component of the record, and  $NS$  is North–South component. To take care of the effect of feedback, from the surface, in downhole sensor record SSR is multiplied by coherence function as defined in Eq. (2). Only those earthquake records which has PGA less than 30 gals and signal-to-noise ratio more than 2 at the surface are used for the study.

Further Konno-Omachi [34] smoothing function is used. This smoothing function ensures a constant number of points at low and high frequency, hence, it is mostly preferred for frequency analysis.

### 3 Results

For G1 group, four sites are selected having  $V_{S30}$  equal to 238 m/s (AOMH05), 261 m/s (AOMH09), 243 m/s (KKWH11), and 355 m/s (KKWH13), respectively. The  $V_S$  profile for these sites is shown in Fig. 2. All these sites have a fundamental frequency at more than 2 Hz except KKWH13, which shows fundamental frequency estimated using HVSR and SSR at around 5 Hz. In the case of KKWH13 (Fig. 2), it seems that the top layer, which has  $V_S$  equal to 230 m/s, and depth equal to 8 m are governing the response of used ground motion. The theoretical frequency calculated for this layer would be equal to 7.2 Hz ( $f = V_S/4H$ ), which is similar to the frequency obtained by HVSR and SSR. The fundamental frequency from the transfer function obtained from GRA is also around 3 Hz, which is similar to the theoretical fundamental frequency calculated using  $f = V_S/4H$  (3.25 Hz) for 24 m

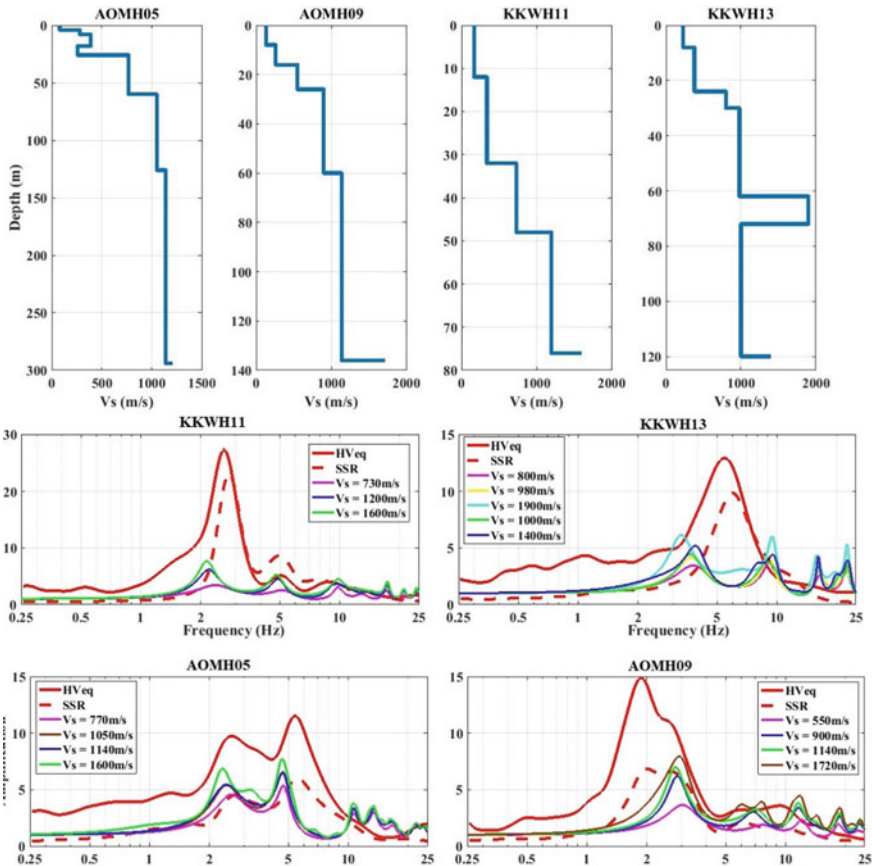


**Fig. 2** Shear-wave velocity profiles and comparison of TF between surface and internal layer from GRA, having high  $V_S$ , as outcrop (reference site) with SSR and HVSR for G1 sites

depth. There is no significant change observed in fundamental frequency obtained from GRA which were performed by using HS more than 800 m/s (and depth more than 24 m). Although amplification seems to increase for profiles having deeper and stiffer HS due to which, 800 m/s may not be a good HS for estimation of amplification although fundamental frequency can be obtained using such a profile. Similarly, for AOMH05 (Fig. 2), a dominant peak is observed next to the first peak, which seems to be representing the topmost layer of  $V_s$  equal to 80 m/s and depth 4 m. This peak was found to be present in the transfer functions obtained from all three methods. All these results suggest an HS or reference site of  $V_s$  more than 1000–1200 m/s is must for  $G1$  sites even if they have low  $V_{S30}$  values.

Shear-wave velocity profiles and the results of the analysis of  $G2$  sites are shown in Fig. 3. In  $G2$  group, for sites MYGH05 and NMRH02 (Fig. 3), the peak frequency seems to be guided by the very soft top layer ( $V_s = 120$  m/s and thickness = 2 m for MYGH05 and  $V_s = 110$  m/s and thickness = 4 m for NMRH02). The effect of the top layer is evident in the transfer functions produced by all three methods. Though the effect of the top layer is significant in these cases, still the transfer function cannot rely only on the top layer, which causes amplification at high frequency. The lower frequency peaks in SSR and HVSr are caused by the influence of lower layers, which is also evident in the transfer function produced by GRA using EB as HS.

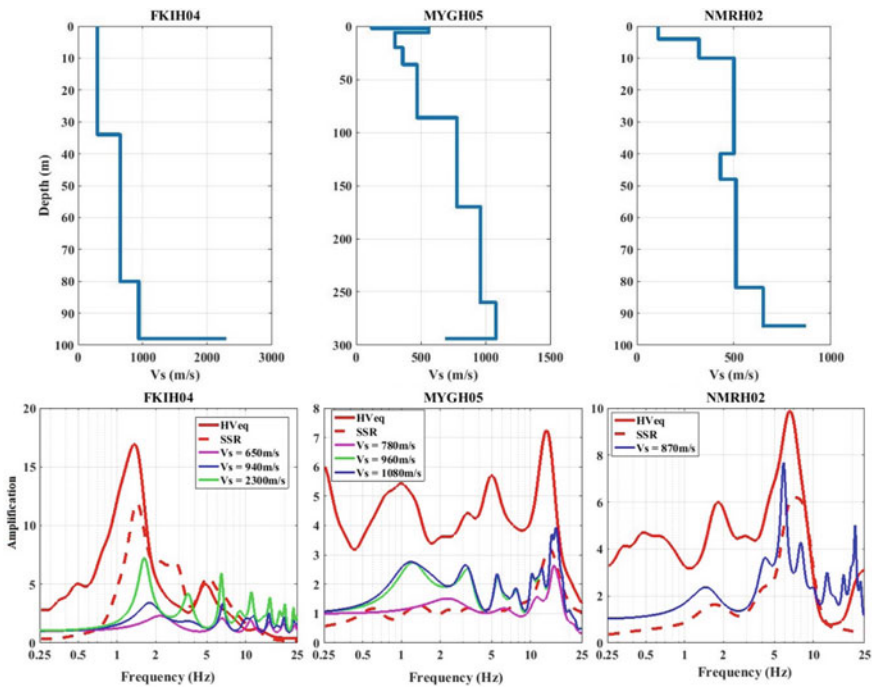


**Fig. 3** Shear-wave velocity profiles and comparison of TF between surface and internal layer from GRA, having high  $V_s$ , as outcrop (reference site) with SSR and HVSr for  $G2$  sites

Considering the results of both the sites, it can be said that an HS of 1000 m/s or more could be good enough for such sites. The analysis of transfer functions obtained for FKIHO4 (Fig. 3), having  $V_{S30} = 300$  m/s, deviates from this conclusion. For this site, the sudden and huge change in the stiffness/ $V_s$  of the layer (of the order of more than twice) at the depth of 98 m seems to be guiding the amplification. Typically, such changes occur in the top layers of the soil strata having lower  $V_s$  values; hence, most of the times those layers govern the peak frequency of the transfer function. Although such kind of deviations is rare and they are the reminder to the scientific community that generalization of nature is very difficult.

The sites used in the *G3* group (Fig. 4) have a fundamental frequency corresponding to more than 2 Hz. Due to this, the results of *G3* sites from the Kik-Net database helps to explore the involvement of sharp impedance contrast at low depths. Only two sites are considered in this group from the Kik-Net database to evaluate the effects of such sharp contrast. From GRA transfer functions, it can be clearly seen that the peak frequency can be easily estimated using the first sharp impedance contrast. Although just using that layer, as HS cannot provide a good estimate of amplification as can be seen for site AICH23. For this site, the profile having HS of

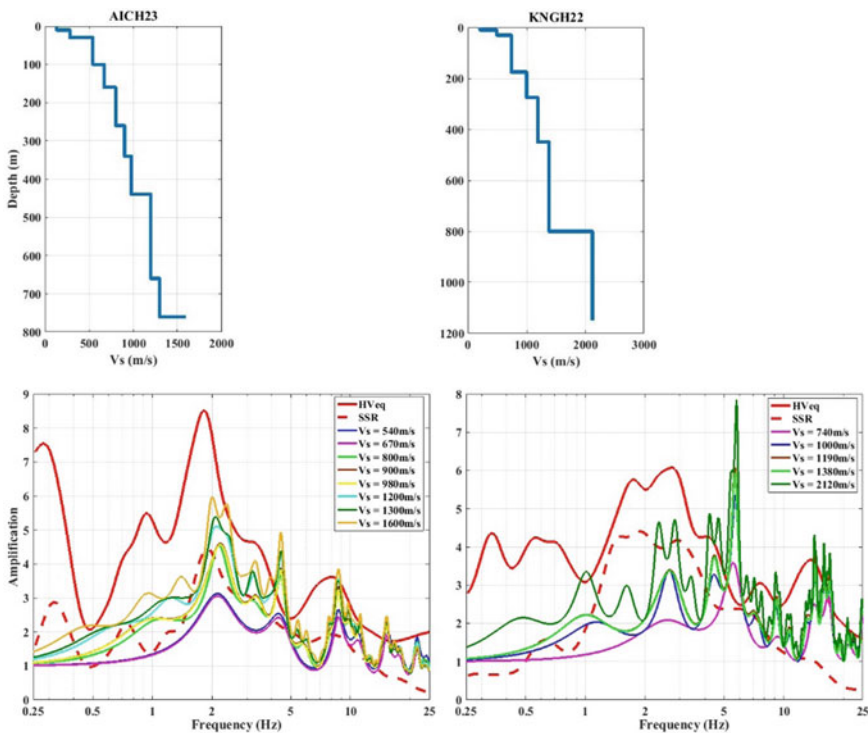


**Fig. 4** Shear-wave velocity profiles and comparison of TF between surface and internal layer from GRA, having high  $V_s$ , as outcrop (reference site) with SSR and HVSR for *G3* sites

540 m/s at the depth of 30 m provides HS of 1200 m/s or more seems to be necessary; otherwise, the estimate of amplification may go wrong.

## 4 Summary and Conclusion

The main aim of this study was to find out the effect of bedrock depth and its stiffness on site amplification. Site amplification has two components, one is the fundamental frequency which can be defined as the first maxima in the amplification function. The second component is amplification amplitude. This fundamental frequency of the site is a very important parameter in any engineering analysis which is further used for calculation of the design load of the building. All the site classes have been created so that different kind of sites having similar fundamental frequencies can be grouped together. This makes it easier to define loads as it has to be defined for a lesser number of cases.

As discussed earlier, most of the codes have five kinds of site classes as per their  $V_{S30}$  values. These site classes do not consider the depth of bedrock. Few attenuation relations have used depth of bedrock as a parameter in their models and each considers different  $V_S$  value to be bedrock.

This study suggests the fundamental frequency response of any site is dependent only upon few meters of the soil cover which may or may not be extending up to the top of soft/hard rock (site class B/A). Hence, it may be advisable that we may reconsider the depth of the bedrock parameter for the seismic hazard studies. This study is on a very preliminary stage, and with more analysis, we may come up with some standard solution for this problem.

**Acknowledgements** The authors would like to thank the Department of Earthquake Engineering, IIT Roorkee for the support provided. We would also like to thank the Department of Civil Engineering, BT Kumaon Institute of Technology, Dwarahat, Uttarakhand, India for support. The authors would also like to thank the National Research Institute for Earth Science and Disaster Resilience, Japan for providing the earthquake records from Kik-Net Database.

## References

1. MacMurdo J (1824) Papers relating to earthquake which occurred in India in 1819. *Phil Mag* 63:105–177
2. Stone WC, Yokel FY, Celebi M, Hanks T, Leyendecker EV (1987) *Engineering aspects of the September 19, 1985 Mexico earthquake*. NBS Building Science Series 165, National Bureau of Standards, Washington, DC
3. Seed RB, Dickenson SE, Reimer MF, Bray JD, Sitar N, Mitchell JK, Idriss IM, Kayen RE, Kropp A, Harder LF, Power MS (1990) Preliminary report on the principal geotechnical aspects of the October 17, 1989 Loma Prieta earthquake. Report UCB/EERC-90/05, Earthquake Engineering Research Center, University of California, Berkeley, p 137

4. Sitharam TG, Govindraju L (2004) Geotechnical aspects and ground response studies in Bhuj earthquake, India. *Geotech Geol Eng* 22:(439–455)
5. Paulay T, Priestley MJN (1992) *Seismic design of reinforced concrete and masonry buildings*. Wiley, New York
6. Adhikary S, Singh Y (2012) Limitations of soil amplification provisions in the 2002 Indian seismic code. *J Earthq Eng* 16(1):1–14
7. Pandey B, Jakka RS, Kumar A (2016a) Influence of local site conditions on strong ground motion characteristics at Tarai region of Uttarakhand, India. *Nat Hazards* 81(2). <https://doi.org/10.1007/s11069-015-2120-0>
8. Pandey B, Jakka RS, Kumar A, Mittal H (2016) Site characterization of strong-motion recording stations of Delhi using joint inversion of phase velocity dispersion and H/V Curve. *Bull Seismol Soc Am* 106(3):1254–1266. <https://doi.org/10.1785/0120150135>
9. IS:13920 (1993) Indian standard code of practice for ductile detailing of reinforced concrete structures subjected to seismic forces. Bureau of Indian Standards, New Delhi
10. IS:1893 (Part 1) (2016) Indian standard criteria for earthquake resistant design of structures. Bureau of Indian Standards, New Delhi
11. New Zealand Government Print (1992) *Regulations to the Building Act*, Wellington
12. New Zealand Standards (NZS 1170.5), (2004) *Structural design actions, Part 5: earthquake actions—New Zealand, Standards*. Wellington, New Zealand
13. IITK-GDM (2005) IITK-GSDMA guidelines for proposed draft code and commentary on Indian Seismic Code IS:1893 (Part 1), IITK-GSDMA-EQ05-V4.0, August 2005, Indian Institute of Technology Kanpur and Gujarat State Disaster Mitigation Authority, Gandhinagar, India
14. Canadian Concrete Association (1994) *Design of concrete structures for buildings*. CAN-A23.3-M84. Rexdale, Ontario
15. International Conference of Building Officials (1997) *Uniform building code*. Whittier, California
16. Standards Australia (1988) *Earthquake loads*. AS 1170.4. Homebush, Sydney
17. Building Safety Standards Committee (2001) *NEHRP recommended provisions for seismic regulations for new buildings and other structures*. 2000 Edition, Part 1: Provisions. Building Seismic Safety Council for the Federal Emergency Management Agency (Report FEMA 368), Washington, DC
18. Comité Européen de Normalisation (CEN EN 1998-1) (2004) *Eurocode 8: design of structures for earthquake resistance—part 1: general rules, seismic actions, and rules for buildings*. European Committee for Standardization, Brussels, Belgium
19. Chiou BSJ, Youngs RR (2008) Update of the Chiou and Youngs NGA model for the average horizontal component of peak ground motion and response spectra. *Earthq Spectra* 24(1):173–215. <https://doi.org/10.1193/072813EQS219M>
20. Steidl JH, Tumarkin AG, Archuleta R (1996) What is a reference site? *Bull Seism Soc Am* 86(6):1733–1748
21. Kottke AR, Wang X, Rathje EM (2013) *Technical manual of STRATA*. Department of Civil, Architectural and Environmental Engineering, University of Texas, Geotechnical Engineering Center
22. Borcherdt RD (1970) Effects of local geology on ground motion near San Francisco Bay. *Bull Seism Soc Am* 60:29–61
23. Kagami H, Duke CM, Liang GC, Ohta Y (1982) Observation of 1- to 5-second microtremors and their application to earthquake engineering. Part II evaluation of site effect upon seismic wave amplification due to extremely deep soil deposits. *Bull Seismol Soc Am* 72–3:987–998
24. Nakamura Y (1989) A method for dynamic characteristics estimation of subsurface using microtremor on the ground surface. *Quarterly Report of the Railway Technical Research Institute*, vol 30
25. Lachet C, Bard P-Y (1994) Numerical and theoretical investigations on the possibilities and limitations of Nakamura's technique. *J Phys Earth* 42(5):377–397. <https://doi.org/10.4294/jpe.1952.42.377>

26. Nogoshi M, Igarashi T (1970) On the propagation characteristics of microtremors. *J Seism Soc Jpn* 23:264–280 (in Japanese with English abstract)
27. Langston CA (1979) Structure under Mount Rainier, Washington, inferred from teleseismic body waves. *J Geophys Res* 84:4749–4762
28. Bonilla LF, Steidl JH, Lindley GT, Tumarkin AG, Archuleta RJ (1997) Site amplification in the San Fernando Valley, California: variability of site effect estimation using S-wave, coda, and H/V methods. *Bull Seism Soc Am* 87:710–730
29. Field EH, Jacob KH (1995) A comparison and test of various site response estimation techniques, including three that are non reference- site dependent. *Bull Seism Soc Am* 86:991–1005
30. Parolai S, Richwalski SM, Milkereit C, Bormann P (2004) Assessment of the stability of H/V spectral ratio from ambient noise and comparison with earthquake data in the Cologne area (Germany). *Tectonophysics* 390:57–73
31. Parolai S, Bindi D, Troiani L (2001) Site response for the RSM seismic network and source parameters in the Central Apennines (Italy). *Pure Appl Geophys* 158:695–715
32. Parolai S, Bindi D, Augliera P (2000) Application of the generalized inversion technique (GIT) to a microzonation study: numerical simulations and comparison with different site-estimation techniques. *Bull Seism Soc Am* 90(2):286–297
33. Triantafyllidis P, Hatzidimitriou PM, Theodulidis M, Suhadolc P, Papazachos C, Raptakis D, Lontzetidis K (1999) Site effects in the city of Thessaloniki (Greece) estimated from acceleration data and 1D local soil profiles. *Bull Seism Soc Am* 89:521–537
34. Konno K, Ohmachi T (1998) Ground-motion characteristics estimated from spectral ratio between horizontal and vertical components of microtremor. *Bull Seismol Soc Am* 88(1):228–241



# Comparative Seismic Fragility Study of Railway Concrete Bridge Piers Without and with the Effect of Soil-Structure Interaction



Saranika Das and Arjun Sil

**Abstract** This paper is a comparative case study of seismic fragility surfaces of a railway-bridge piers considering without and with the soil-structure interaction effect. Lateral and horizontal stiffness has been calculated layer-wise as the soil profile. Dynamic shear modulus has been calculated using EERA. 3D modelling of the bridge has been formed in the CSiBridge and the stiffness due to soil has been applied as spring models. The pier tip displacement and rotation are considered as the guiding parameters for the study. A set of scaled ground-motion data has been used to perform non-linear time history analysis. Lognormal relationship has been established between the demand spectral acceleration  $S_a$  with the control parameters by multiple linear regression method. Fragility surfaces have been generated for both the cases. The result shows that soil-structure interaction effect reduces the damage probability. The effect depends on soil type. The variation is marginal in soft soil case. The pier tip rotation is guiding criteria for without soil effect but rotation effects more in soil effect.

**Keywords** Seismic fragility surfaces · Soil-structure interaction · Nonlinear time history analysis · Bridge pier

## 1 Introduction

One of the important inventions of Civil engineering is bridges that overcomes any physical obstruction without disturbing the region underneath it. The bridges are constructed for the ease of transportation. Thus, their safety and maintenance are of great concern. Fragility analysis of bridges is useful for seismic risk assessment of bridges and is defined as the probability that a non-structural, structural, geotechnical system subjected to specified intensity seismic event violates at least a limit state. There had been several studies regarding the fragility analysis of bridge piers. A

---

S. Das · A. Sil (✉)  
National Institute of Technology, Silchar, India

comparative study of seismic fragility considering soil-structure interaction of a rail-bridge piers has been presented in this paper. Earlier, rail bridges were designed to carry 25T axle load but with the recent development the bridges are getting modified and these new bridges are designed to carry 32.5T axle load also known as DFC loading. So, from the aspect of safety of bridges failure pattern, the capacity of the bridges due to earthquake loading need to be determined. Pier tip displacement and rotation are considered as the main guiding parameters in the study.

## 2 Study Area Details

The study consists of a 3-span continuous rail bridge located across river Pandu Fig. 1 in Uttar Pradesh, India has been considered. It is located near to the city of Allahabad connecting Howrah and Delhi DFC loading rail track. The bridge location comes under seismic zone III. The geology of the region is Gangetic plain with minor faults. The region is located near to the Himalayan ranges which are seismically active. The area is deposited by river sediments, such that soil is soft. Thus, it can be summarized that the soil, geology conditions of the zone may cause adverse scenario to the structure during earthquake.

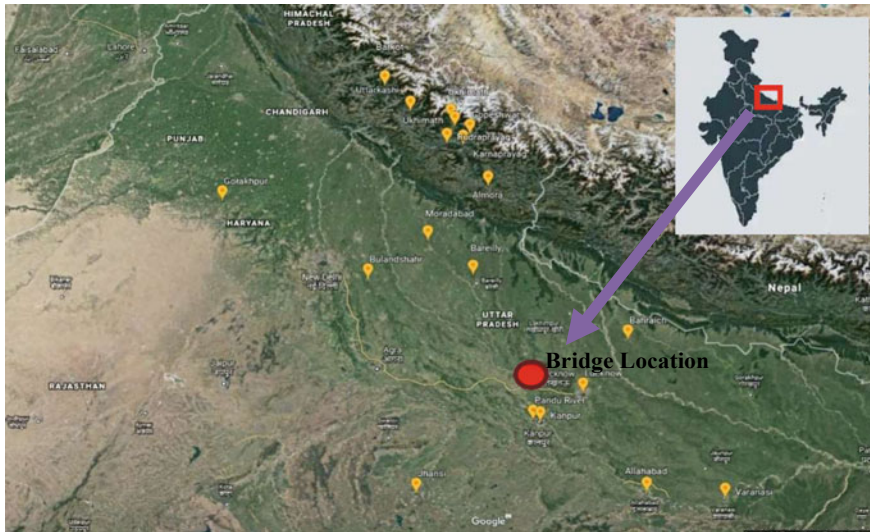


**Fig. 1** Location of the rail bridge across river Pandu and the nearest seismic stations in the region as obtained from Google Earth

### 3 Data for Study

Depth (m)	Soil description	$N$ value	Bulk density (g/cc)	$c$ (kg/cm <sup>2</sup> )	$\phi^0$	Soil modulus (kg/cm <sup>2</sup> )
2.5	Sandy soil with low plasticity	10	1.66	0.51	10	383
5.5	Sandy soil with low plasticity	23	1.69	0.59	8	443
8.5	Sandy soil with low plasticity	32	1.71	0.65	8	488
11.5	Sandy soil with low plasticity	36	1.74	0.74	7	555
14.5	Clayey silt with medium plasticity	42	1.76	0.86	5	645
17.5	Clayey silt with medium plasticity	47	1.79	0.81	6	608
20.5	Clayey silt with medium plasticity	63	1.81	0.83	5	623
23.5	Clayey silt with medium plasticity	60	1.82	0.94	3	705
26.5	Clayey silt with medium plasticity	65	1.83	0.92	3	690

#### *Ground-motion Data*

Ground-motion data of 2015 Nepal earthquake (Table 1) has been collected from Strong Motion Virtual Data Centre. 65 sets of strong ground-motion data of magnitude ranged 4.0–5.5. Scaled seismic data has been considered for the analysis.

#### *Structural Data*

The structural drawing and designs have been collected so that almost exact structure can be replicated for the study. The general arrangement of the bridge is shown in Fig. 2.

Details of the bridge:

- Span configuration:  $1 \times 20.84 \text{ m} + 1 \times 14.08 \text{ m} + 1 \times 20.84 \text{ m}$

**Table 1** Details of ground-motion data considered in the analysis of the concerned bridge

Earthquake name	Location	Depth of epicenter	Recorded station	Magnitude range	Date of occurrence
2015 Nepal earthquake	Latitude 28.08°, Longitude 84.76°	10 km	Kathmandu	4.0–5.5	25.04.2015 and after-shocks till 2016

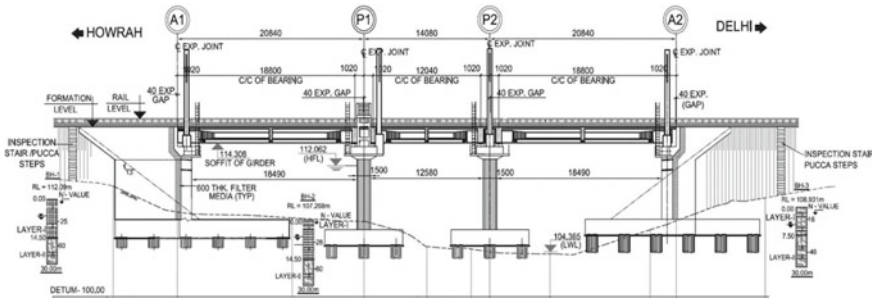


**Fig. 2** Longitudinal Elevation of the three-span railway bridge (20.84 m + 14.08 m + 20.84 m) across river Pandu with pier heights of 8 m and pile depth of 38 m as prepared by STUP Consultants Pvt. Ltd

- Pile diameter: 1.2 m, Pile depth: 38 m
- Vertical pile capacity: 244 T at abutment location, 265 T at pier location
- Pile, pile cap: M35, Pier, pier cap: M40, HYSD bars: Grade Fe 500 MPa.

### 4 Methodology

The structural dynamic response induces supporting soil deformation. The methodology consists of determination of soil stiffness parameters and analysis of bridge.

#### *Determination of horizontal and rotational soil stiffness*

The stiffness values of the soil are determined from the following formulas of the modulus of subgrade reaction for laterally loaded pile. Ashford et al. [1] gave the modulus of subgrade reaction as

$$K_S = \frac{E_S}{1 - \mu^2} \left[ \frac{E_S D^4}{E_P I_P} \right]^{1/4} \tag{1}$$

Prendergast and Gavin [2] gave Biot’s solution of coefficient of subgrade reaction K from the correlation between Winkler model and continuum elastic theory as

$$K_S = \frac{0.95 E_S}{D (1 - \mu^2)} \left[ \frac{E_S D^4}{(1 - \mu^2) E_P I_P} \right]^{0.108} \tag{2}$$

They also suggested the equation derived from Vesic’s approach [2] by matching displacements of the models and is given as

$$K_S = \frac{0.65 E_S}{D (1 - \mu^2)} \left[ \frac{E_S D^4}{E_P I_P} \right]^{1/12} \tag{3}$$

Tongaonkar and Jangid [3] proposed the horizontal stiffness ( $K_h$ ) and rotational stiffness ( $K_\phi$ ) as

$$K_h = \frac{8Ga (1 + \frac{1}{2H'})}{2 - \mu} \quad (4)$$

$$K_\phi = \frac{8Ga^3}{3(1 - \mu)} \quad (5)$$

Choudhury et al. [4] proposed similar equations for horizontal and rotational stiffness as

$$K_h = \frac{8Ga}{2 - \mu} \quad (6)$$

$$K_\phi = \frac{8Ga^3 (1 + \frac{6}{H'})}{3 (1 - \mu)} \quad (7)$$

IS 2911 (Part1/Sec2):2010, Annex C (Clause 6.5.2) C-2.1 [5] gives lateral resistance for normally-consolidated clay and granular soils with varying modulus of soil.

#### *Seismic analysis procedure*

The main methods of analysis are nonlinear time history analysis and pushover analysis, such that for bridge fragility studies nonlinear time history analysis is mainly recommended. The fragility function can be explained in a simpler form in Eq. (8).

$$F_d(x) = \phi \left[ \frac{\ln(x/\mu)}{\beta} \right] \quad (8)$$

where  $F_d$  is a fragility function for damage state  $d$  evaluated at ' $x$ ',  $\mu$  is the median capacity of asset to resist damage state ' $d$ ', ' $\beta$ ' is standard deviation of natural logarithm of the capacity to resist ' $d$ '.

## **5 Analysis Procedure**

The analysis procedure has been broadly classified into three sections and are calculation of the soil stiffness data, scaling of the strong ground-motion data, modelling of the structure and analysis.

#### *Calculation of soil stiffness data*

The stiffness properties of the soil springs have been calculated from the various references discussed in the Sect. 4.1.1. Shear wave-velocity  $V_s$  (m/s) has been obtained

from [6] depending on the SPT values ( $N$ ) of the soil at different depths.

$$V_s = 79.217 * N^{0.3699} \tag{9}$$

The dynamic shear-modulus ( $N/m^2$ ) of soil has been generated layer by layer using the tool EERA [7] using ground-motion data of magnitude of 4.5, 5.0 and 5.5. The average lateral soil stiffness for different magnitude range has been shown in Fig. 3.

*Scaling of strong ground-motion data*

The seismic data has been scaled as per IS 1893:2000, Part I to the maximum capacity of the structure considering fundamental time period (as in Fig. 4) 2.8 s and soft soil. The has been normalized by dividing with the PGA and has been scaled up to 0.6 g by increment of 0.1 g gradually.

*Modelling and analysis of the structure*

The bridge has been modelled with the software tool CSiBridge 2017.

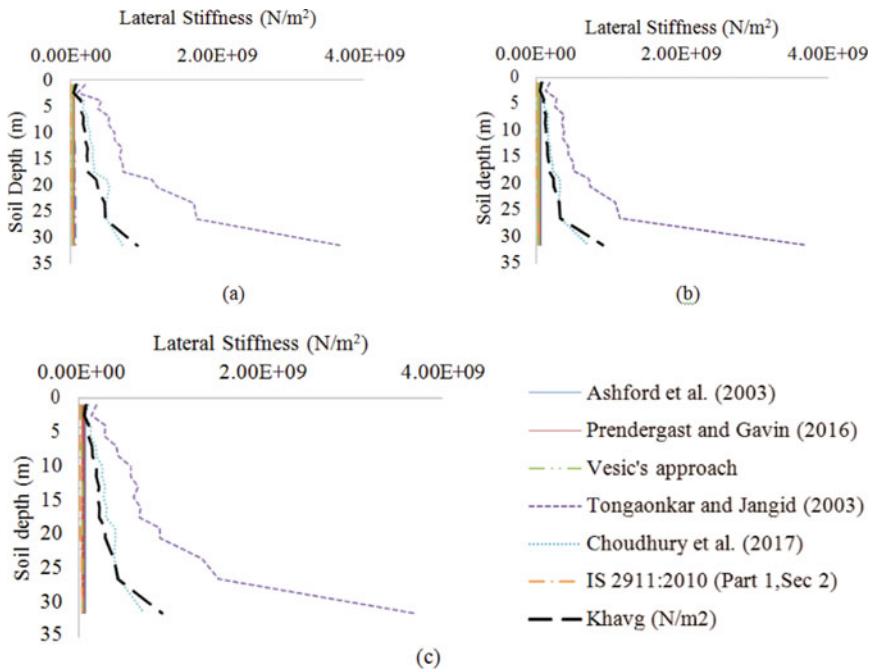
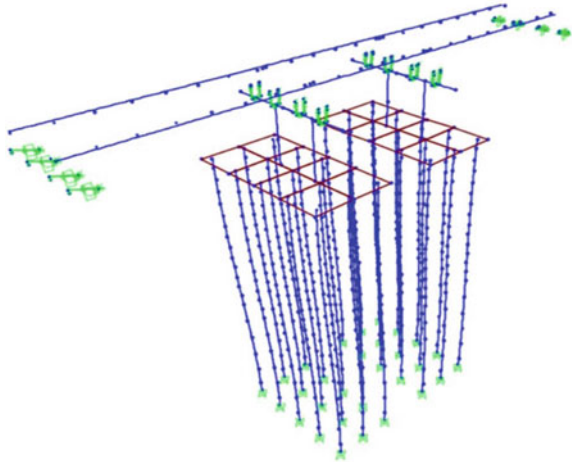


**Fig. 3** Lateral stiffness versus depth  $P_1$  for earthquake magnitude **a** 4.0–4.5, **b** 4.5–5.0, **c** 5.0–5.5

**Fig. 4** First mode shape of the bridge with fundamental time period of 2.8 s



## 6 Results

Lognormal relationship for both the cases has been established between the demand spectral acceleration  $S_a$  with the control parameters by multiple linear regression method in Origin Pro. Fragility surfaces have been generated depending on the two parameters i.e. pier tip displacement  $d$  (cm) and rotation  $r$  (rad). The relationship for without soil-structure interaction effect is given as

$$\ln(S_a) = 9.1347 + 0.162 \ln(d) + 0.4969 \ln(r) \tag{10}$$

The relationship for with soil-structure interaction effect is given as

$$\ln(S_a) = 2.434 + 0.31705 \ln(d) + 0.17365 \ln(r) \tag{11}$$

The probability of exceedance of the damaged state of the structure has been calculated from the observed data by using the Eqs. (10) and (11) for the comparative study of without and with the soil-structure interaction effect respectively (Fig. 5).

## 7 Conclusions

This case study concludes that the probability of damage reduces due to the soil-structure interaction effect. Here for same ground-motion data the difference in probability of exceedance of damage considering without and with soil-structure interaction effect is marginal as soft soil has been modelled. Probability of exceedance of damage state is 0.505 with soil-structure interaction effect and 0.511 without soil effect. The difference will be effective as the soil properties changes from medium

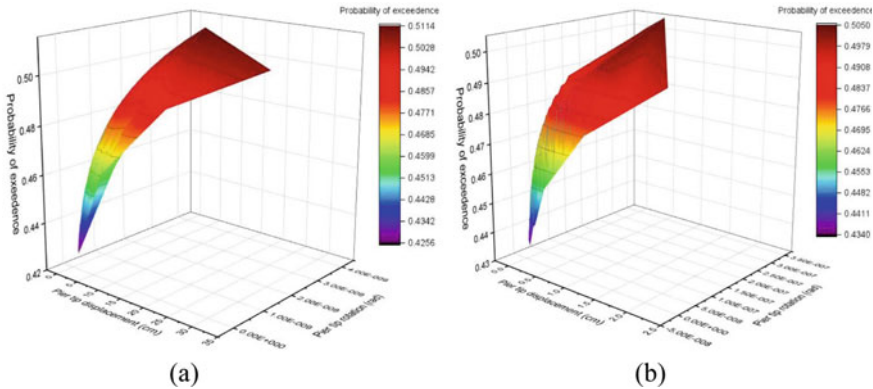


**Fig. 5** Fragility surface representing probability of exceedance of spectral acceleration of pier tip depending on pier tip displacement (cm) and rotation (rad) considering **a** without soil-structure interaction and **b** with soil-structure interaction

to hard type of soil that can be predicted. Among the two parameters, the displacement is guiding criteria without the soil-structure interaction effect consideration but rotation overpowers the fragility surface for with soil-structure interaction effect.

## References

1. Ashford SA, Juirnarongrit T (2003) Evaluation of pile diameter effect on initial modulus of subgrade reaction. *J Geotech Geoenviron Eng* © ASCE 129(3):234–242
2. Prenderga LJ, Gavin K (2016) A comparison of initial stiffness formulations for small-strain soil–pile dynamic Winkler modelling. *Soil Dyn Earthq Eng* 81:27–41
3. Tongaonkar NP, Jangid RS (2003) Seismic response of isolated bridges with soil–structure interaction. *Soil Dyn Earthq Eng* 23:287–302
4. Chowdhury I, Tarafdar R, Ghosh A, Dasgupta SP (2017) Dynamic soil- structure interaction of bridge piers supported on well foundation. *Soil Dyn Earthq Eng* 97:251–265
5. IS 2911 (Part 1/Sec 2) (2010) Design and construction of pile foundations — code of practice ,Part 1 concrete piles , Section 2 Bored cast in-situ concrete piles, B U R E A U O F I N D I A N S T A N D A R D S
6. Sil A, Haloi J (2017) Empirical correlations with standard penetration test (SPT)-N for estimating shear wave velocity applicable to any region *Int. J Geosynth Ground Eng* 3:22
7. Bardet JP, Ichii K, Lin CH (2000) EERA A computer program for equivalent-linear earthquake site response analyses of layered soil deposits. University of Southern California, California



# **Site Investigation and Case Studies**

# Stabilization of Railway Tracks Using Geosynthetics—A Review



Rajashekar Mallikarjun Hubballi

**Abstract** The Railway forms one of the predominant and well connected transportation networks in India, serving all economic classes of people. Railway fosters the proliferation of our Country's economy by transporting bulk commodities related to industrial, agricultural and energy sectors. For the efficient and safe movement of trains on railway tracks, the latter's strength and stability are very important. Indian government has initiated the roll-out of projects to connect routes with a high traffic density using super-fast trains. For the safe operation of such super-fast trains, the tracks must be strong, stable and durable. Hence, this paper presents a glimpse of the seminal geosynthetics based research attempts related to stabilization and drainage of railway tracks. The paper can be used as a quick reference by research scholars, engineers and students to comprehend geosynthetic techniques for stabilizing both existing old tracks and newly constructed tracks.

**Keywords** Railway track stabilization · Geosynthetics · Geotechnical engineering · Railway track drainage · Mud pumping · Ballast fouling · Differential settlement

## 1 Introduction

Rail transportation plays a vital role for the social, cultural and economic development of any country. It serves people from all economic classes. Mass and rapid transportation of goods and passengers can be accomplished through rail transportation. It helps in the growth of industrial sector by supplying raw materials to the industries and transporting finished products to various outlets. Agricultural sector is supplied with raw materials like seeds, fertilizers, farm equipment through rail transportation and grown crops are transported to consumer markets. Rail transportation plays a very important role in power sector by transporting raw materials like coal and petrol. Hence, for the fast and balanced development of any nation, efficient

---

R. M. Hubballi (✉)

Department of Civil Engineering, Central Institute of Technology, Kokrajhar, India  
e-mail: [rm.hubballi@cit.ac.in](mailto:rm.hubballi@cit.ac.in)

© Springer Nature Singapore Pte Ltd. 2022

A. K. Dey et al. (eds.), *Proceedings of the 7th Indian Young Geotechnical Engineers Conference*, Lecture Notes in Civil Engineering 195,  
[https://doi.org/10.1007/978-981-16-6456-4\\_40](https://doi.org/10.1007/978-981-16-6456-4_40)

387

rail transportation system is inevitable. India has the fourth largest rail network in the world. Indian government is undertaking more advanced rail projects for the rapid growth of the nation. For the fast and safe movement of trains, strong and stable railway tracks are required. However, for a railway track to be strong and stable, all its components namely, rails, sleepers, fastenings, ballast should be strong and durable. Subgrade i.e. the level ground on which railway track rests should be strong enough to safely withstand the load from the railway track and train coming on it. Subgrade should remain strong during adverse weather conditions like heavy rainfall. In some situations, design and construction of strong and stable track with conventional materials and technology becomes difficult because of extreme weather conditions and/or weak subgrade. Such tracks can be efficiently and economically stabilized with the help of geosynthetics.

This paper is organized as follows: Sect. 2 describes the structure of a railway track along with a brief discussion on its constituent components. The next section discusses about the problems encountered by different layers of railway tracks. This is followed by an overview of the prominent techniques proposed in the literature to mitigate the problems and to subsequently stabilize tracks. The paper is concluded with pointers to future research and summary.

## 2 Components of a Railway Track

Figure 1 depicts the following components of railway tracks: subgrade, subballast, ballast, sleepers, fastenings and rails [26].

Subgrade is the levelled platform on which entire track structure is constructed. Subgrade can be natural ground or placed soil. Weight of the track and train are finally transferred onto the subgrade.

The layer of ballast between subgrade and ballast is called ‘subballast’. Generally, sand gravel mixtures or crushed stone aggregates or slag forms the subballast material. It offers the following advantages towards maintaining track stability:

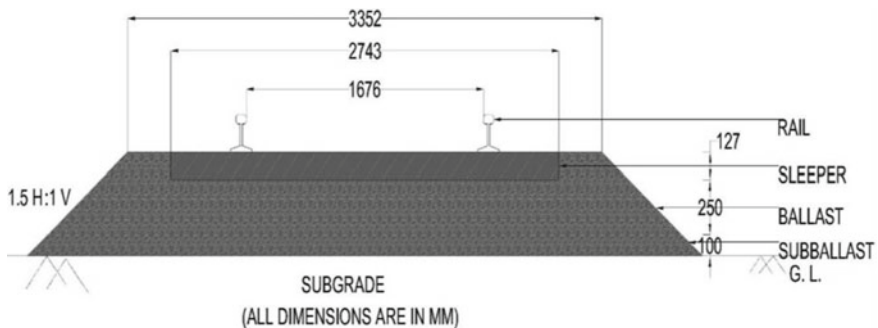


**Fig. 1** Components of a railway track

1. It prevents the penetration of ballast stones into the subgrade.
2. It inhibits the movement of fine materials from the subgrade into the ballast.
3. It prevents mud pumping by avoiding penetration of ballast stone into the subgrade in the presence of water.
4. It facilitates the cross drainage of surface and subsurface water into the side drains.
5. It checks the upward movement of subsurface water from the subgrade.

Ballast is the granular material in which sleepers are embedded. Generally angular, crushed stone aggregates form a good ballast material. The functions of the ballast are to retain the sleepers in their position, to provide quick drainage, to distribute the load on to the large area of subgrade and to act as an elastic medium to absorb shocks and reduce noise.

This paper focuses on problems related to ballast, subballast and subgrade components of railway tracks without prejudice to the problems associated with the other components.

### 3 Causes for Track Instability

Generally, instability in the track can be caused due to the following reasons:

1. Mud pumping
2. Ballast fouling
3. Differential settlement
4. Poor drainage.

Mud pumping is the accumulation of fine soil particles on the track from the subgrade. Typically, it occurs if the subgrade is a clayey soil. When saturated clayey subgrade is subjected to dynamic train load, it builds up excess pore water pressure in the soil subgrade. The water oozing out from the subgrade soil enters into the ballast along with fines. Later water either drains out or evaporates leaving fines in the ballast. These fines fill the voids in the ballast and reduce its porosity and decrease drainage property. Track stability decreases with the loss of free draining property [27]. Figure 2a illustrates the phenomenon of mud pumping [30].

Ballast fouling is a condition where performance of the ballast is affected due to accumulation of fines in the voids of the ballast. Here performance implies free drainage and shock absorption due to moving train. Ballast is crushed into fine particles due to repetitive heavy train load. These crushed particles occupy the voids between large ballast and decrease their porosity and elasticity. This can also happen due to mud pumping [4]. Figure 2b depicts the ballast fouling problem [31].

Subgrade in case of tracks is generally natural ground whose property varies from place to place. When track passes through weak subgrade, it may undergo settlement due to heavy train load. If the subgrade is clayey soil, under saturated condition excess pore water pressure may build up due to train load. This excess pore water pressure

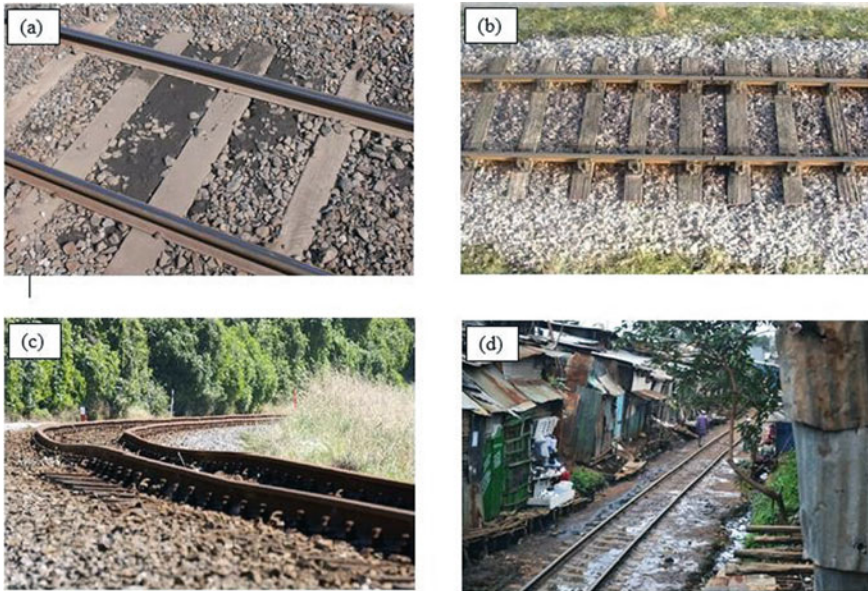


**Fig. 2** a Mud pumping (Source Wiki-A); b Ballast fouling (Source Wiki-B); c differential settlement (Source Wiki-C); d poor drainage (Source Wiki-D)

when dissipated results in settlement of track. Track may also undergo settlement due to settlement of ballast. When heavy train load acts on the ballast it breaks its sharp corners leading to settlement. Settlement is more if recycled ballast is used than fresh ballast [14, 28]. Figure 2c shows the negative impacts of differential settlement [32].

Improper drainage in tracks leads to decrease in strength of subgrade. Water accumulation in tracks decreases the bearing capacity of subgrade and results in track settlement. Water accumulated over ballast acts as lubricant and results in more settlement due to train load. Poor drainage may be due to ballast fouling and/or poorly designed or insufficient side drains [13, 27]. Track instability due to poor drainage can be visualized in Figure 2d [33].

## 4 Stabilization Techniques

Seminal research works carried out to address the aforementioned problems using geosynthetics are discussed in the following sub-sections

**Table 1** Criteria for effective filtration of fines through geotextile [19]

Soil characteristics		Suggested characteristics of the filter layer
% clay	Soil type	
>30	Non-dispersive	OST[100%] <0.1 mm and OST[95%] <DS[50%] and OST[95%] <DS[90%]
	Dispersive	Lay 50–150 mm of fine sand over the subgrade and consider the fine sand layer as part of the subgrade
<30	Plastic	Depending on the double- hydrometer-ratio (DHR) test value for the subgrade, adopt either of the two suggestions for dispersive/non-dispersive soil type with greater than 30% clay
	Non-plastic	OST[95%] < DS[50%]

### 4.1 Mud Pumping Mitigation

By using geosynthetic layer at the interface between the subballast and the subgrade mud pumping can be mitigated. A geosynthetic should be such that it should allow movement of water across its plane at the same time it should retain soil particles on its upstream side [18]. Geotextiles are effective in preventing entry of coarse-grained soil particles from the subgrade into the ballast however they cannot prevent the entry of clay sized fine grained particles [5]. By following the guidelines given in Table 1, entry of fine particles from the subgrade into the subballast through geotextile can be effectively avoided [19]. In Table 1, let OST[ $x\%$ ] denote the upper bound on the size of at least  $x\%$  openings in the geotextile. Similarly, let DS[ $y\%$ ] denote the upper bound on the diameter of at least  $y\%$  of the subgrade particles.

### 4.2 Solution for Differential Settlement

Settlement of the track takes place either due to settlement of subgrade or settlement of ballast. Settlement of subgrade takes place due to consolidation of subgrade under train load. When accelerated rate of primary consolidation is required, geosynthetic Prefabricated Vertical Drains (PVD) can be adopted. By using PVDs, radial drainage path can be decreased thus increasing the rate of consolidation. This results in a subsequent increase of the subgrade shear strength and its bearing capacity. PVDs have high discharge capacity, low well-resistance and can filter fine particles from entering the drain [8]. With the installation of PVDs excess pore water pressure continues to dissipate even after the passage of a train [16].

Application of repetitive train load leads to settlement of ballast. Based on large-scale triaxial tests it was concluded that behaviour of ballast under the action of cyclic load is highly nonlinear [10, 11]. To understand the settlement behaviour of ballast under cyclic load, tests were conducted using large test chamber where walls

of the chamber are fixed and rigid [1]. However, in field, ballast moves freely in the lateral direction. To account for this, tests were conducted on ballast using large test chamber where walls of the chamber are free to move in the lateral direction. The geosynthetic used in the tests was a geocomposite (geogrid bonded with non-woven geotextile). In the geocomposite reinforcement, geogrid provides mechanical interlock with the ballast and prevents their lateral movement whereas non-woven geotextile acts as filter against the entry of fines from the subgrade and subballast, thereby avoiding ballast fouling. Geosynthetics can be placed anywhere in the ballast however keeping it 150 mm below the sleeper would be convenient for the tamping operation. Based on the Finite Element analyses the optimum depth of reinforcement from the sleeper is found to be 200 mm, beyond or below which geosynthetic will have insignificant effect on the ballast settlement reduction. By providing a depth of 200 mm, a convenient depth of 150 mm is made available for the tamping operation [15].

Through large-scale prismatic triaxial rig experiments, it was inferred that recycled ballast reinforced with geogrid bonded with non-woven geotextile, when subjected to 500,000 load cycles showed lesser total settlement as compared to fresh unreinforced ballast subjected to the same load cycles [13]. Lateral strain of the recycled ballast reinforced with geotextile or geocomposite is lesser than that of the unreinforced fresh ballast subjected to same load cycles [13].

McDowell modelled the interaction between geogrid and ballast using Discrete Element Method and pull-out tests data. Based on the model study it was inferred that the size of the geogrid opening should be 40% more than the typical size of the ballast, to have a good ballast geogrid interlocking [21]. Brown, by using Composite Element Test (CET) equipment conducted series of tests to understand influence of various parameters of the geogrid such as stiffness, grid geometry, strength at junction and cross-sectional area of the rib on the ballast settlement reduction under cyclic loading. Geogrid with tensile strength of 30 kN/m and nominal aperture size of 65 mm is found to be the most efficient for ballast reinforcement [3]. Geogrids are effective in reducing ballast deformation, especially when the ratio of geogrid aperture size to average size of ballast is 1.1 (Indraratna et al. 2016). For attaining the maximum reduction in lateral displacement of the ballast, geogrids should be placed 65 mm above the subballast [17].

Fatahi and Khabbaz studied the influence of shoulder ballast along with geosynthetics on the reduction of total track settlement under the train load. They concluded that track performance can be improved by adopting wider shoulder ballast with geosynthetic layer [7]. Biabani conducted large-scale pull-out tests on the geocell reinforced subballast. Geocells used in the tests were made from geogrid and geomembrane. He concluded that geocell inclusion in the subballast provides more passive resistance under pull-out force [2]. When ballast is to be laid over concrete bridge deck, inclusion of a rubber mat at the interface between the concrete bridge deck and ballast reduces both lateral and vertical plastic deformation of the ballast [6].

Based on the techniques proposed in the literature the following recommendations can be made to solve the differential track settlement problem:

1. Depth of the geosynthetic reinforcement should be 200 mm from the sleeper.
2. Geocomposite is preferable than geogrid and geotextile as it performs the functions of both reinforcement and filtration.
3. The ratio of geogrid aperture size to the nominal size of the ballast should be 1.4.
4. More width of shoulder ballast is recommended to derive better advantages from geosynthetics.

### 4.3 Ballast Fouling Prevention

Ballast fouling can be prevented by avoiding ballast degradation and mud pumping. Marshal had performed large-scale triaxial tests and subsequently concluded that geosynthetic reinforced recycled and fresh ballast show good resistance to degradation compared to unreinforced ballast. Ballast breakage can be reduced up to 50% by reinforcing recycled ballast with geocomposites [20]. Since breakage and disturbance of the ballast reduces with inclusion of geosynthetic reinforcement, less maintenance overhead is required and the frequency of maintenance operation also reduces [29].

If a sand layer is used between subgrade and subballast, it should be overlain by geotextile which prevents intermixing of sand with subballast [5, 24, 25]. Geosynthetic reinforcement reduces breakage index of fresh as well as recycled ballast in both wet and dry conditions. However, the effect of reinforcement is significant for the recycled ballast in wet condition as shown in Table 2 [12].

When heavy repetitive train load acts on the ballast, its particles are crushed. Crushed fine particles enter into the void spaces of the ballast. This reduces the porosity of the ballast and affects its drainage properties. Recycled ballast has less angularity number as their sharp corners might have been broken due to past train load cycles. Hence, settlement and lateral strain of the recycled ballast is more than that of the fresh ballast [15]. Degradation of ballast can be further reduced by using shock mats such as rubber pads on the top and bottom surface of ballast. These shock mats dampen repetitive dynamic load from the train and decreases ballast degradation [14, 23].

**Table 2** Breakage Index (%) with and without geosynthetic reinforcements [12]

		Condition of ballast					
		Dry			Wet		
Fresh Ballast	Unreinforced	1.50			1.63		
	Reinforced	Geogrid	Geotextile	Geocomposite	–		
		1.49	1.54	1.42			
Recycled Ballast	Unreinforced	2.96			3.19		
	Reinforced	–			Geogrid	Geotextile	Geocomposite
					1.88	1.64	1.6



Inclusion of geogrid in the ballast layer reduces the pressure on the ballast below the geogrid and hence reduces their breakage. Geogrids are effective to avoid the deformation of ballast over soft subgrade whereas rubber mats are effective when ballast is laid over a concrete bridge deck [22]. Reduction in the ballast degradation by about 35–45% can be achieved by inclusion of rubber mats at the interface between the concrete bridge deck and ballast [6].

Some of the suggested techniques to offset ballast fouling include but not limited to the following:

5. Use a geocomposite in the interface between subgrade and subballast.
6. Preferably the geocomposite can be biaxial geogrid bonded with non-woven geotextile.
7. Use shock mats to encapsulate the ballast from its adjacent layers.

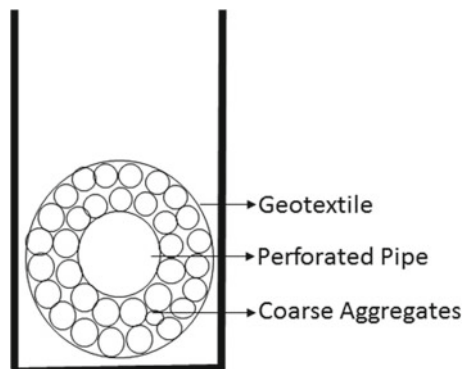
#### 4.4 Facilitation of Drainage

For proper drainage of railway tracks, surface and subsurface water coming on to it should be discharged quickly and efficiently. Drainage of surface water can be accomplished by providing side drains along the length of the track. Where there is a possibility of erosion of side drains, they can be lined with geosynthetic materials. Usage of the bituminous geomembrane for water-proofing the track subgrade is found to be very effective in field [9]. For drainage of subsurface water, deep side drain such as French drain is required. These drains consist of a perforated pipe surrounded by coarse aggregates. This entire assembly is wrapped within a geotextile filter as shown in Fig. 3 [26].

Therefore, for the drainage of railway tracks the following techniques can be adopted:

1. Side drains lined with geosynthetics should be provided.
2. Deep side drains wrapped with geotextile can be constructed.

**Fig. 3** Deep side drain



## 5 Conclusions

This paper describes the importance of using geosynthetics in stabilizing railway tracks. By leveraging proper geosynthetic reinforced designs, problems associated with tracks such as mud pumping, differential settlement, ballast fouling and poor drainage can be mitigated efficiently and cost-effectively. By adopting the recommendations cited in this paper, the frequency of maintenance operations and hence the maintenance costs are reduced drastically. However, the field conditions to a major extent determine the type and the design of the geosynthetic reinforcement adopted for track stabilization. Predominantly, the geosynthetic materials used for track stabilization are geogrids, geotextiles and geomembranes. However, the potential to leverage other geosynthetics for track stabilization could be researched and explored.

## References

1. Atalar C, Das BM, Shin EC, Kim DH (2001) Settlement of geogrid reinforced railroad bed due to cyclic load. In: Proceedings of the 15th international conference on soil mechanics and geotechnical engineering. Istanbul, pp 2045–2048
2. Biabani MM, Ngo NT, Indraratna B (2016) Performance evaluation of railway subballast stabilised with geocell based on pull-out testing. *Geotext Geomembr* 44(4):579–591
3. Brown SF, Kwanb J, Thom NH (2007) Identifying the key parameters that influence geogrid reinforcement of railway ballast. *Geotext Geomembr* 25(6):326–335
4. Bruzek R, Stark TD, Wilk ST, Thompson HB, Sussmann TR (2016) Fouled Ballast definitions and parameters. In: Proceedings of the joint rail conference. Columbia SC, USA, pp 1–7
5. Byrne BJ (1989) Evaluation of the ability of geotextiles to prevent pumping of fines into ballast. Msc project. Department of Civil Engineering, University of Massachusetts at Amherst, USA
6. Diyaljee V (2018) Use of rubber mats to improve the deformation and degradation behavior of rail ballast under cyclic loading. *J Geotech Geoenviron Eng* 144(7):1–15
7. Fatahi B, Khabbaz H (2011) Enhancement of ballasted rail track performance using geosynthetics. In: Proceedings of the geo human international conference. ASCE, Hunan, China, pp 222–230
8. Hansbo S (1981) Consolidation of fine-grained soils by prefabricated drains. In: Proceedings of the 10th international conference on soil mechanics and foundation engineering. Balkema, Rotterdam, the Netherlands, pp 677–682
9. Imbert B, Breul B, Herment R (1996) More than 20 years of experience in using a bituminous geomembrane beneath French railway ballast. *Geosynthetics: applications, design and construction*. Balkema, Rotterdam, pp 283–286
10. Indraratna B, Redana IW (2000) Numerical modeling of vertical drains with smear and well resistance installed in soft clay. *Can Geotech J* 37(1):132–145
11. Indraratna B, Ionescu D, Christie D (1998) Shear behavior of railway ballast based on large-scale tri-axial tests. *Geotech Geoenviron Eng ASCE* 124(5):439–439
12. Indraratna B, Khabbaz H, Salim W (2004) A laboratory study on improvement of railway ballast using geosynthetics. In: Proceedings of the international conference on geotechnical engineering for transportation projects. Los Angeles, California, USA, pp 617–626
13. Indraratna B, Khabbaz H, Salim W, Christie D (2006) Geotechnical properties of ballast and the role of geosynthetics in rail track stabilization. *Ground Improvement* 10(3):91–101

14. Indraratna B, Nimbalkar S, Rujikiatkamjorn C (2012) Track stabilisation with geosynthetics and geodrains and performance verification through field monitoring and numerical modelling. *Int J Railw Technol* 1(1):195–219
15. Indraratna B, Shahin MA, Salim MW (2005) Use of geosynthetics for stabilizing recycled ballast in railway track substructures. In: *Proceedings of the North American geosynthetics Society (NAGS)-geosynthetics institute (GSI) conference*. Las Vegas, Nevada, pp 1–15
16. Indraratna B, Shahin MA, Salim W (2007) Stabilisation of granular media and formation soil using geosynthetics with special reference to railway engineering. *Ground Improvement* 11(1):27–43
17. Indraratna B, Hussaini SKK, Vinod JS (2013) The lateral displacement response of geogrid-reinforced ballast under cyclic loading. *Geotext Geomembr* 39(1):20–29
18. Koerner RM (1998) *Designing with geosynthetics*, 4th edn. Prentice Hall, New Jersey
19. Leuttich SM, Giroud JP, Bachus RC (1992) Geotextile filter design guide. *Geotext Geomembr* 11(4):19–34
20. Marshal RJ (1967) Large scale testing of rockfill materials. *J Soil Mech Foundation Eng ASCE* 93(2):27–43
21. McDowell GR, Harireche O, Konietzky H, Brown SF, Thom NH (2006) Discrete element modelling of geogrid-reinforced aggregates. *Proc Instit Civil Eng- Geotech Eng* 159(1):35–48
22. Ngo NT, Indraratna B, Ferreira FB, Rujikiatkamjorn C (2018) Improved performance of geosynthetics enhanced ballast: laboratory and numerical studies. *Proc Inst Civil Eng Ground Improvement* 171(4):202–222
23. Nimbalkar S, Indraratna B (2016) Improved performance of ballasted rail track using geosynthetics and rubber shockmat. *J Geotech Geoenviron Eng* 142(8):1–13
24. Raymond GP, Ismail I (2003) The effect of geogrid reinforcement on unbound aggregates. *Geotext Geomembr* 21(6):355–380
25. Raymond GP (2002) Reinforced ballast behaviour subjected to repeated load. *Geotext Geomembr* 20(1):39–61
26. Sanjay KS (2002) *Geosynthetics and their applications*, 1st edn. Thomas Telford Publishing, London
27. Selig ET, Waters JM (1994) *Track geotechnology and substructure management*, 1st edn, Thomas Telford Publishing, London, U.K
28. Suiker ASJ, Selig ET, Frenkel R (2005) Static and cyclic triaxial testing of ballast and subballast. *J Geotech Geoenviron Eng* 131(6):771–782
29. Walls JC, Galbreath LL (1987) Railroad ballast reinforcement using geogrids. In: *Proceedings of geosynthetics conference*. New Orleans, pp 38–45
30. Wiki-A, [https://commons.wikimedia.org/wiki/File:Railway\\_track\\_Mud\\_eruption.jpg](https://commons.wikimedia.org/wiki/File:Railway_track_Mud_eruption.jpg), last accessed 2019/11/11
31. Wiki-B, <http://www.cliffbarker.me.uk/Gauge1FineandStandardTrack.html>, last accessed 2019/11/11
32. Wiki-C, [https://de.wikipedia.org/wiki/Kaikoura\\_District](https://de.wikipedia.org/wiki/Kaikoura_District), last accessed 2019/11/11
33. Wiki-D, <https://en.wikipedia.org/wiki/Kibera>, last accessed 2019/11/11

# Micro-Piles as Foundation for G+10 Building at Chhattisgarh—A Case Study



Rutuj Chheda, Chhaya Kandpal, Harshita Anjana, Atharva Pisolkar, Aditya Soni, and Jigisha Vashi

**Abstract** Foundations are classified as shallow and deep. Their primary purpose is to provide support for super structure through transfer of load to layers of soil or rock, which have adequate bearing capacity. However, some ground conditions and site limitations make use of conventional foundations unsuitable. Micro-piles are the only alternative in this scenario. They can be used both as a ground improvement method and structural element designed as soil frictional piles and rock socketed piles either under tension or compression. They can be used in restricted access sites making them very favourable. The present paper is a case study of use of micro-pile for a G+10 commercial building where the access to the construction site is restricted and the ground conditions are unfavourable for conventional foundations. Also geotechnical and structural design of micro-pile are carried out using Indian codes in the present work.

**Keywords** Micro-pile · Foundation · Load carrying capacity

## List of Symbol

$d$	Effective depth
$D$	Overall depth
$A_p$	Area of pile toe
$D$	Diameter of pile in m
$e_{\min}$	Minimum eccentricity
$M_{ux}$	Design moment about $X-X$ axis
$M_{UY}$	Design moment about $Y-Y$ axis
$A_s$	Area of steel in column
$F_y$	Characteristic strength of steel

---

R. Chheda · C. Kandpal · H. Anjana · A. Pisolkar · A. Soni · J. Vashi (✉)  
SVKM's NMIMS, Mukesh Patel School of Technology Management & Engineering, Mumbai,  
India  
e-mail: [jigisha.vashi@nmims.edu](mailto:jigisha.vashi@nmims.edu)

$L$	Length of column
$L_{\text{eff}}$	Effective length of column
$F_{ck}$	Characteristic compressive strength of concrete
$A_g$	Gross area of section
$P_u$	Design axial load for limit state design (factored load)
$PP$	Percentage of tension reinforcement
$P$	Percentage of reinforcement
$K$	Constant or coefficient or factors
$Q_s$	Safe load capacity of pile in t
$q_c$	Uniaxial compressive strength of rock $t/m^2$
$N_d$	Depth factor = $0.8 + 0.2 l_s/D$ , limited to 2
$d'$	Distance of centroid of compression reinforcement from the extreme compression fiber of the concrete section
$p'$	3.14
$L_c$	Socket length into the rock in m
$\alpha$	Rock socket correction slide resistance reduction factor
$\beta$	Rock socket correction factor
$N_j$	Discontinuity in rocks values a per Fig. 2 of IS 12070
$A_{av}$	Total cross sectional area of stirrup legs or bent up bars within a distance $S_v$
$S_v$	Spacing of the stirrups or bent up bars along the length of the member
$b$	Breadth of the member which for flanged beam shall be taken as the breadth of the web
$f_y$	Characteristic strength of the stirrup or bent up reinforcement which shall not be taken greater than $415 \text{ N/mm}^2$
$P_b$	Axial load corresponding to the condition of maximum compressive strain
$P'$	Compression with bending

## 1 Introduction

The primary purpose of foundation is to provide support for super structure through transfer of load to layers of soil or rock, which have adequate bearing capacity. Shallow foundations can be made even in depths as small as 0.5 m, whilst deep foundations can be made at depths of 20–65 m. Shallow foundations are used for small, light buildings, whilst deep foundations are for large, heavy buildings. Deep foundations may also be needed in conditions where an adequate hard stratum is not available at shallow depth. For deep foundations, piles are employed. A pile essentially is a long cylinder of a strong material such as concrete that is pushed into the ground so that structures can be supported on top of it. Piles are employed when surface has a layer of weak soil, which cannot support weight of the building. Thus, load of the building has to bypass this layer and be transferred to the layer of stronger soil or rock that is below this weak layer.

However, certain ground conditions and site constraints make it difficult to use these conventional foundations such as weak soil present at shallow depths. In such situations, only alternative is to use micro-piles. A micro-pile is a pile having a smaller diameter than a conventional pile, typically less than 300 mm. It is heavily reinforced and carries most of its load on high capacity steel reinforcement. They can be used both as a ground improvement method and structural element designed as soil frictional piles and rock socketed piles either under tension or compression. They can be used in restricted access sites, thus making them very convenient.

Micro-piles find their application as shoring piles, for soil stabilization, for underpinning of structures with differential settlement, locations where conventional piling methods may not be feasible and headroom available is limited. They may also be used as temporary retaining structures for basement construction. Advantages of micro-piles are high carrying capacity, self-sustained operation, vibration free drilling method, only small volume of earth needs to be excavated, less site constraint problems and raking piles can be easily constructed.

The present paper is a case study of use of micro-piles as foundation for a G+10 commercial building at Chhattisgarh, India, where the access to the construction site is restricted and the ground conditions are unfavourable for conventional foundations. Geotechnical and structural design of micro-piles are carried out using Indian codes in the present work. The objectives of the paper are to understand usage and application of micro-pile, study design parameters of micro-piles for given project and design the micro-pile for practical application.

## 2 Methodology

The site at Chhattisgarh having filling material up to 3 m which is followed from 3 to 4 m by fractured rock and subsequently by soft rock up to 15 m. Ground water is located at 1.1 m from ground level. The typical sub soil profile is shown in Fig. 1. The pile cap arrangement with micro-pile is shown in Fig. 2. After referring to site investigation report and vicinity of the G+10 building, conventional foundation was found unfavourable. Therefore, feasibility of micro-pile foundation was examined and found very convenient and suitable. Hence both the geotechnical and structural aspect of micro pile was studied, analysed and designed in the present study for the structural loads coming on the footing.

## 3 Geotechnical Calculation

Assessment of vertical load of a single micro-pile based on geotechnical considerations:

- Diameter of pile = 0.3 m

Description of Strata	Symbol	Thick. (M)	From (M)	To (M)	Sample Depth (M)	Sample Type	Sample Ref. No.	SPT Record				Core Recovery (%)	R.Q.D.	SPT Curve
								0-150	150-300	300-450	N			
FILLING MATERIALS	[Symbol]	0.00-2.90	0.00	2.90	1.50	P	SPT-1	12cm in 50 blows, N>50						
FRACTURED ROCK	[Symbol]	3.00-4.00												
SOFT ROCK	[Symbol]	4.10-15.00	4.10	4.00	4.00	C	C-1					25.00	0.00	
					5.50	C	C-2					30.00	0.00	
					7.00	C	C-3					40.00	0.00	
					8.50	C	C-4					42.00	10.00	
					10.00	C	C-5					44.00	12.00	
					11.50	C	C-6					50.00	10.00	
					13.00	C	C-7					55.00	18.00	
					14.50	C	C-8					60.00	20.00	
Bore Hole Terminated at : 15.00														
D-Disturbed Sample, U-Undisturbed Sample, P-Standard Penetration Test, C-Core, W-Water Sample, V-V														

Fig. 1 Bore log data of G+10 building at Chhattisgarh

- Multiplication constant for socket length depending on rock strata = 4
- Socket length =  $4 \times 3 = 1.2$  m (From IS 14593)
- Uniaxial compressive strength of rock =  $730 \text{ t/m}^2$  (as per soil investigation report)
- Depth factor from formula = 1.6 (From page 3 of IS 14593)
- Maximum value of depth factor = 2
- Actual depth factor = 1.6
- Area of pile toe =  $\pi/4 \times 0.3 \times 0.3 = 0.070686 \text{ m}^2$
- Rock socket slide resistance reduction factor,  $\alpha = 0.1$  (From Fig. 1 of IS 14593)
- Rock socket correction factor,  $\beta = 0.4$  (From: Fig. 2 of IS 14593)
- $N_f$ , depending upon the discontinuity in rocks = 0.1 (From IS 12070)
- Total pile load capacity = 41.28 t
- Safe load considering neglecting end bearing = 33.02 t

Assessment of vertical load on Micro-pile group based on geotechnical pile capacity:

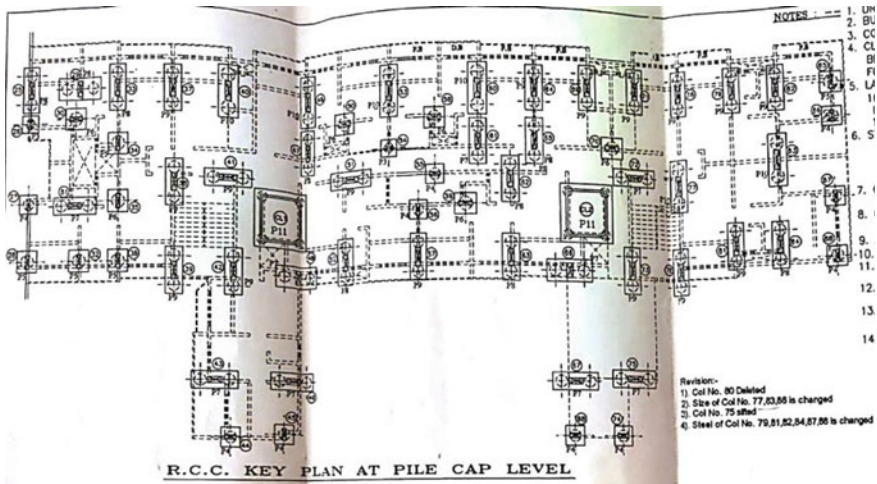


Fig. 2 Pile cap arrangement of micro-pile

- Allowable vertical load on pile group = number of piles × vertical load carry capacity of single micro-pile × efficiency factor
- Vertical load carry capacity of single micro-pile = safe load on single micro-pile = 33 t
- Minimum centre to centre distance between any two adjacent piles = 3 times diameter of pile =  $3 \times 0.3 = 0.9$  m
- Group efficiency factor = 1
- Number of micro-piles in a group = 3, 4, 5, 6, 7, 8
  - 3group micro-pile, group capacity =  $3 \times 33 \times 1 = 99$  t
  - 4group micro-pile, group capacity =  $4 \times 33 \times 1 = 132$  t
  - 5group micro-pile, group capacity =  $5 \times 33 \times 1 = 165$  t
  - 6group micro-pile, group capacity =  $6 \times 33 \times 1 = 198$  t
  - 7group micro-pile, group capacity =  $7 \times 33 \times 1 = 231$  t
  - 8group micro-pile, group capacity =  $8 \times 33 \times 1 = 264$  t

### 4 Structural Calculation

In the structural design of a micro-pile it is designed as a compression member carrying axial load. The slenderness ratio must be determined for the behaviour of pile and its failure as a long slender member or short member. The following structural design is carried out with the help of design aids for reinforced concrete SP 16 (1980) and IS 456: 1978 [1]. The parameters of pile taken for design purpose are as follows; length of the pile—8.5 m, axial load ( $P_u$ )—330 kN, grade of concrete M-30, ( $f_{ck} = 30$ ) and grade of steel—Fe 415, ( $f_y = 415$  MPa).



Assumption: The pile is effectively held in position and restrained against rotation at one end and at the other restrained against rotation but not held in position hence the effective length equals to 1.2 times the length of the pile (Ref.—Table 28 of IS 456: 2000) [2].

$$\text{Effective Length } (L_{\text{eff}}) = 1.2 \times 8.5 = 10.2 \text{ m}$$

$$\text{Slenderness Ratio } (L_{\text{eff}}/\text{Diameter of the pile}) = (10.2/0.3) = 34$$

Here, Slenderness Ratio = 34 > 12, the pile will fail as a slender member

Additional eccentricity  $e/D = (1/2000) \times (L_{\text{eff}}/D) \times 2 = 0.578 \sim 0.58$  (by interpolation) (Ref.—Table 1 Addition Eccentricity clause 3.4 of SP 16-1980)

$$M_u = P_u \times e = 330 \times 0.58 \times 0.3 = 57.42 \text{ kNm}$$

$$A_g = 300 \text{ mm dia pile} = 70650 \text{ mm}^2 = 706.5 \text{ cm}^2$$

Assumption: Nominal cover = 45 mm

$$d'/D = 45/300 = 0.15$$

Assumption: Reinforcement percentage = 0.9%

$$P_{uz}/A_g = 16 \text{ N/mm}^2$$

$$P_{uz} = 16 \times 70,650 = 1,130,400 \text{ N} = 1130.4 \text{ kN} \text{ (Ref.—Chart 63 from SP-16: 1980)}$$

$$P_u/(F_{ck} \times D \times D) = (330 \times 103/30 \times 300 \times 300) = 0.122$$

$$M_u/(F_{ck} \times D \times D \times D) = (57.4 \times 106/30 \times 300 \times 300 \times 300) = 0.070$$

From Graph =  $(p'/F_{ck}) = 0.07$  (Ref.—Chart 57 from SP-16: 1980)

$$p' = 0.07 \times 30 = 2.1$$

$$P_b = (K_1 + (K_2 \times p'/F_{ck})) F_{ck} D \times D$$

$$K_1 = 0.149 \text{ for circular column } (d'/D = 0.15)$$

$$K_2 = 0.201 \text{ for circular column } (d'/D = 0.15) \text{ (Ref.—Table 60 from SP 16-1980)}$$

$$P_b = (0.149 + (0.201 \times (2.5/30))) \times 30 \times 3502 = 438.45 \text{ kN}$$

$$K = (P_{uz}/P_u)/(P_{uz} - P_b) = (1130.4 - 330)/(1130.4 - 438.48) = 1.1567$$

$$\text{Additional Moment } M_a = 1.1567 \times 57.42 = 66.42 \text{ kNm}$$

$$\text{Minimum Eccentricity } e_{\text{min}} = (e/500) + (d/30) (8500/500) + (300/30) = 27 \text{ mm} > 20 \text{ mm}$$

$$\text{Moment due to minimum eccentricity } (M_{ux}) = 330 \times (2.7/100) = 8.91 \text{ kNm}$$

$$\text{Total Moment} = 8.91 + 66.42 = 75.33 \text{ kNm}$$

$$p'/f_{ck} = (2.1/30) = 0.07$$

$$P_u/(F_{ck} \times p' \times D \times D/4) = 0.1556$$

$$P_u/(F_{ck} \times b \times b) = 0.1222$$

$$M_u/(F_{ck} \times p' \times d \times d/4) = 0.12$$

$$M_{ux1} = (0.12 \times 30 \times p'/4 \times 0.3 \times 0.3) = 254.46 \text{ kNm}$$

$$(M_{ux}/M_{ux1}) = (75.33/254.46) = 0.296$$

$$(P_u/P_{uz}) = 330/1130.4 = 0.291$$

The value of  $(M_{ux}/M_{ux1})$  and  $(P_u/P_{uz})$  are very close

Assume % reinforcement = 0.9%

$$A_s = 2 \times (p'/4) \times (0.3 \times 0.3) = 1413.71 \text{ mm}^2$$

Provide 5–20 mm diameter Fe 415 Transverse Reinforcement

Pitch = 300

$$16 d = 16 \times 20 = 320$$

Least lateral dimension of the pile = 300 > 150 mm

Hence Ok

Diameter =  $0.25 \times 20 = 6$  mm

Provide 5–20 mm diameter bars with 8 mm ties spacing 300 mm c/c.

#### 4.1 Group Pile Calculation

Length of pile cap = 2.4 m = 2400 mm

Width of pile cap = 1.5 m = 1500 mm

Error in plan of position of piles = 120 mm

Assume overall depth = 800 mm

Effective depth =  $1000 - 75 - (25/2) = 912.5$  mm ~ 910 mm

$F_{ck} = 30$  N/mm<sup>2</sup>

$F_y = 415$  N/mm<sup>2</sup>

$L.A_{AA} = 900 - 300/2 + 120 = 870$  mm

$M_{AA} = 1700 \times 2 \times 0.87 = 2958$

$L.A_{BB} = (900/2) - (800/2) + 120 = 170$  mm

$M_{BB} = 1700 \times 3 \times 0.17 = 867$  kNm

$(M_{AA}/bd^2) = (867 \times 106/1500 \times 102) = 0.46$

By interpolation % pt = 0.1298 (Ref.—Table no: 19 Page no: 73 of IS 456: 2000)

[2]

$(100 A_{st}/bd) = 0.1298$

$A_{st} = 2756.952$  mm<sup>2</sup>

Provide 6 bars of 25 mm diameter and 8 mm stirrups @ 100 c/c

Critical Shear: Chart 60 of SP 16 (1980)

$v = (v/bd) = (1700 \times 103 \times 2)/(1500 \times 910) = 2.49$  N/mm<sup>2</sup>

$A_s = 10308.35$  mm<sup>2</sup>

$b = 1500$  mm

$d = 910$  mm

$(100 A_s/bd) = (100 \times 10308.35)/(1500 \times 910) = 0.755$  N/m<sup>2</sup>

$V_c = 0.755$ , therefore reinforcement is not required.

## 5 Conclusion

For the proposed G+10 building of 330 kN load, micro-pile was constructed as foundation with following geotechnical specifications:

- 3 no of pile can resist the capacity of 99 t
- 4 no of pile can resist the capacity of 132 t
- 5 no of pile can resist the capacity of 165 t

- (d) 6 no of pile can resist the capacity of 198 t
- (e) 7 no of pile can resist the capacity of 231 t
- (f) 8 no of pile can resist the capacity of 264 t

For the proposed G+10 building of 330 kN load, micro-pile was constructed as foundation with following structural specifications: 6 bars of 25 mm diameter and 8 mm stirrups @ 100 c/c.

**Acknowledgements** Sincere thanks to SVKM's NMIMS Mukesh Patel School of Technology Management & Engineering, Mumbai for providing good working Environment. We all are also thankful to Mr. Chandresh Chheda of Shilplekha Consultant and Mr. Ashwin Parmar of ITD Cementation for helping and guiding us and providing us with the necessary data.

## References

1. Bureau of Indian Standards, SP 16, Design aids for reinforced concrete to IS 456456, 47-148-142-171 (1978)
2. IS 456 (2000) Plain and reinforced concrete-code of practice (CED2: cement and concrete), pp 73-94
3. IS 14593 (1998) Design and construction of bored cast-in-situ piles founded on rocks-guide-lines (CED 48: rock mechanics), 3
4. IS 12070 (1987) Code of practice for design and construction of shallow foundations on rocks (CED 48: rock mechanics), 6
5. Tomlinson MJ (1995) Pile design and construction practice. Fourth edition, E & FN SPON

# Phosphogypsum Dumping Yards—A Review



K. Tulasi and C. N. V. Satyanarayana Reddy

**Abstract** Phosphogypsum is a high volume solid waste by-product generated when sulfuric acid reacts with the phosphate rock during manufacturing of phosphoric acid, which is a major constituent for many fertilizers. Phosphogypsum contains impurities such as Al, P, F, Si, Fe, rare earth elements, trace elements, and naturally occurring radionuclides. For producing one ton of phosphoric acid, nearly 4–5 tons of phosphogypsum is produced and thereby poses the problems of disposal. Till recent times, in our country, phosphogypsum is disposed within the plants in stack(s) on the existing ground. The extent of soil contamination that might have occurred so far because of direct dumping cannot be justified. However, few foreign countries have imposed restrictions on the disposal of phosphogypsum directly on the ground (US EPA in Potential uses of phosphogypsum and associated risks, 1989) [1]. Increasing environmental concerns demand for safe dumping of any industrial waste. Hence, safe disposal methods for phosphogypsum are to be adopted. To restrict seepage of leachate into the subsoil, Central Pollution Control Board (CPCB) stipulates that the phosphogypsum stack shall be constructed on bentonite blended natural clay above the ground level. For preparing the bottom layer or base lining of the phosphogypsum stack, in the absence of availability of suitable clay, completely stabilized phosphogypsum is suggested for use with the prior approval from CPCB. This technical paper focuses on issues related to past and present practices of phosphogypsum dumping at fertilizer manufacturing units. The issues of concern in forming base lining systems with different materials for phosphogypsum stacking are discussed.

**Keywords** Phosphogypsum · Engineered landfills · Geosynthetic clay liner

## 1 Introduction

Rapid industrialization has resulted in the generation of huge quantity of wastes and quite often, industrial wastes are deposited at the landfill sites without any base

---

K. Tulasi (✉) · C. N. V. Satyanarayana Reddy  
Civil Engineering Department, Andhra University, Visakhapatnam, India

© Springer Nature Singapore Pte Ltd. 2022  
A. K. Dey et al. (eds.), *Proceedings of the 7th Indian Young Geotechnical Engineers Conference*, Lecture Notes in Civil Engineering 195,  
[https://doi.org/10.1007/978-981-16-6456-4\\_42](https://doi.org/10.1007/978-981-16-6456-4_42)

405

lining systems. Unscientific disposal of such wastes is causing adverse effects on all components of the environment and human health. The major concerns in industrial landfills are the leaching of toxic materials into the subsoil and ground water pollution. When rainwater infiltrates into a landfill or when the moisture in the waste reacts with the constituents of the waste due to the probable chemical reactions, leachate containing dissolved and suspended materials is generated. This scenario necessitates adoption of “Engineered Landfills” for controlled disposal. Engineered landfill is a carefully designed isolated enclosed area with appropriate base and side lining systems created in the ground or built on top of the ground for facilitating safe disposal of waste.

## 2 Phosphogypsum

High volume solid waste by-product, phosphogypsum (PG), is generated at many fertilizer plants during the wet process manufacturing of phosphoric acid. Depending on the method employed for wet process, phosphogypsum is produced in dihydrate ( $\text{CaSO}_4 \cdot 2\text{H}_2\text{O}$ ) or hemihydrate form ( $\text{CaSO}_4 \cdot \frac{1}{2}\text{H}_2\text{O}$ ). Dihydrate methods were favored in the past, but hemihydrate methods are now being preferred as they produce phosphoric acid of higher strength (International Atomic Energy Agency-IAEA). The hemihydrate form changes to dihydrate form in presence of free water and hardens in to cemented mass when left undisturbed. Phosphogypsum generally has small residual amounts of phosphoric acid and sulfuric acid, and consequently, it exhibits acidic characteristics. Phosphogypsum also contains rare earth materials, trace elements, and small amounts of uranium and radium, which results in low levels of radiation. The United States Environmental Protection Agency (US EPA) categorizes phosphogypsum as “Technologically Enhanced Naturally Occurring Radioactive Material (TENORM),” whereas in India, the phosphogypsum has not been included in the hazardous waste category listed in the Hazardous waste rules, 2008, of Environment Protection Act, 1986. In the literature, the core problems regarding the management of phosphogypsum are reported to be its high fluoride concentration (0.5–1.5%), radioactivity, presence of heavy metals such as Cd, Cr, and Pb.

### 2.1 Production of Phosphogypsum

The production of phosphogypsum is increasing at global level, and it is estimated to touch 200–250 million tons in the next two decades (IAEA). At present, phosphogypsum generation in India is around 11 million tons per year (based on the consideration that 5 tons of phosphogypsum generation per ton of phosphoric acid production) [2]. The principal producers of phosphogypsum across the country listed in Indian Minerals Year Book, 2016 [3], are presented in Table 1.

**Table 1** Principal producers of phosphogypsum in India

State	Unit
Andhra Pradesh	Coromandel International Ltd., Visakhapatnam
Gujarat	(i) Gujarat state fertilizers and chemicals Ltd., Vadodara (ii) Hindalco Industries Ltd., Dahej
Kerala	Fertilizers and Chemicals Travancore Ltd., Ernakulam
Maharashtra	Rashtriya Chemicals and Fertilizers, Mumbai
Odisha	(i) Paradeep Phosphates Ltd (ii) IFFCO, Paradeep
Tamil Nadu	(i) Southern Petrochemical Industries Corporation Ltd., Thoothukudi (ii) Coromandel International Ltd., Thiruvallur (iii) Sterlite Industries (India) Ltd., Thoothukudi
West Bengal	Tata Chemicals Ltd., Haldia

## 2.2 Properties of Phosphogypsum

Phosphogypsum is a gray colored material comprised of silt or silt-sand sized particles. The particle size range of the material is 0.5–1.0 mm with 50–75% of the particles finer than 0.075 mm. The specific gravity of phosphogypsum is in the range of 2.3–2.6. The range of maximum dry density of the phosphogypsum from standard proctor tests is 1470–1670 kg/m<sup>3</sup>. Phosphogypsum contains free moisture content of 18–35%. The hydraulic conductivities of phosphogypsum in unstabilized and lime-stabilized forms are around  $1.3 \times 10^{-4}$  cm/s and  $2.1 \times 10^{-5}$  cm/s, respectively (CPCB). The addition of fly ash or Portland cement stabilizer to phosphogypsum is reported to increase the values of maximum dry density with slight increase in respective optimum moisture contents [4]. The shear parameters of phosphogypsum exhibit the average internal angle of friction as 32° and a cohesion value of 125 kPa in unstabilized form in unconsolidated undrained condition. The angle internal friction and cohesion of cement-stabilized phosphogypsum are reported to vary in the range of 28°–47° and 76–179 kPa respectively [5]. The purity of phosphogypsum ranges from 77 to 98% CaSO<sub>4</sub> · 2H<sub>2</sub>O. The pH value of the phosphogypsum generally ranges between 2.5 and 6 (IAEA). The important chemical components of phosphogypsum are presented in Table 2.

## 3 Earlier Practices of Phosphogypsum Disposal

### 3.1 Discharge into Water Bodies

Countries such as Morocco, Tunisia, South Africa, and Mexico discharge the waste phosphogypsum into the sea (Ardaman and Associates). It is reported that 1.8–3.0

**Table 2** Main chemical constituents of phosphogypsum

Constituent	Minimum (%)	Maximum (%)
CaO	24	34
SO <sub>4</sub>	48	58
SiO <sub>2</sub>	0.5	18
Na <sub>2</sub> O	0.12	10
C (organic)	0.1	2.5
F	0.1	1.8
P <sub>2</sub> O <sub>5</sub>	0.05	8
Al <sub>2</sub> O <sub>3</sub>	0.05	0.6
Cl	0.035	0.045
MgO	0.01	0.54
Fe <sub>2</sub> O <sub>3</sub>	0.01	0.25

billion tons, which constituted of 29–50% of the generated phosphogypsum till 2006 is disposed of by discharging into water bodies [6]. However the discharge of phosphogypsum into the water bodies is later banned by many countries due to its harmful effect on the water bodies (US EPA, European Union and London Convention of the International Maritime Organization).

### 3.2 *Dumping on Land Without Liners*

In many countries including India, phosphogypsum was dumped directly on the ground without any design standards due to lack of guidelines and awareness. It might have resulted in soil and ground water contamination in the neighborhood of phosphogypsum ponds.

## 4 Current Disposal Practices

Currently, the practice of discharge of phosphogypsum to water bodies is almost declined due to international regulations (London convention of International Maritime Organization (IMO), European Union Regulation and USEPA) which prohibit such activities. The ban imposed by US EPA on usage of phosphogypsum with concentration of <sup>226</sup>Ra beyond 10 picocurie/gram (0.4 Bq/g) has resulted in the large stacks of phosphogypsum.

Three common methods of disposal in use at present are.

- Dry stacking (USA, India)
- Wet stacking (Brazil, China, Finland, USA, Spain, South Africa)

- Backfill to the mine (North Carolina, USA—filled into quarries formed by the quarrying of the phosphate ore and backfilled with a blend of clay tailings)

CPCB [2] suggested the following procedure for stacking of phosphogypsum.

- The base lining of the phosphogypsum stack should have a single composite liner of HDPE geomembrane of thickness not less than 1.5 mm. Below HDPE membrane, a layer of compacted clay or any amended soil of thickness not less than 600 mm or bentonite blended local soil of adequate thickness with hydraulic conductivity less than  $10^{-7}$  cm/s should be laid.
- The second part of the composite liner system shall contain a layer of mechanically compacted, and neutralized phosphogypsum having hydraulic conductivity below  $1 \times 10^{-4}$  cm/s is placed above the drainage layer.

Figure 1 shows the liner system suggested by CPCB.

Regulations of Florida Department of Environmental Protection [7] for stacking of phosphogypsum are as given below.

- Phosphogypsum stack should consist of composite liner with cooling ponds and leachate control systems.
- The synthetic component of composite liners should consist of a geomembrane liner with thickness more than 1.5 mm.
- The other part of the composite liner should contain either a layer of 450 mm thick compacted soil placed below the geomembrane with a hydraulic conductivity less than  $1 \times 10^{-7}$  cm/s, constructed in 150 mm lifts.
- The geomembrane liner component should be installed on the compacted soil layer to check leachate migration if a leak in the flexible membrane liner occurs or a

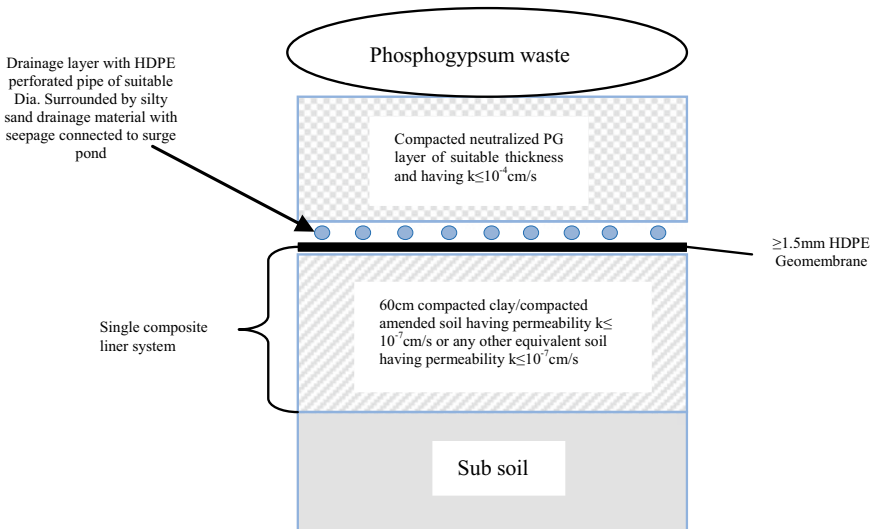


Fig. 1 Suggested liner system for the phosphogypsum stack



layer of mechanically compacted phosphogypsum having a minimum thickness of 600 mm should be placed above the geomembrane, with hydraulic conductivity less than  $1 \times 10^{-4}$  cm/s.

#### **4.1 Geosynthetic Clay Liners (GCL)**

As geosynthetic clay liners (GCL) are being used in the base lining systems of hazardous and non-hazardous landfills, it may be considered for use in phosphogypsum ponds where impervious clay is not available. However, the long-term performance of GCL in contact with phosphogypsum need detailed study as its permeability may increase due to the dissolution of clays due to the presence of fluoride containing solutions in the phosphogypsum. Dissolution of clays would result in contaminant transport, making the GCL less effective than the original design requirements [8]. Also the cation exchange between the bentonite in the GCL and the minerals such as Ca, Si, P, and Fe present in the phosphogypsum may result in increased permeability.

### **5 Conclusions**

Based on the prevailing scenario of the phosphogypsum stacks, it is essential to study the level of contamination of subsoil where open dumping is done. For using geosynthetic clay liner in the base lining system of phosphogypsum stacks, long-term impervious character of GCL need to be established. There is need to evolve alternate base lining systems which are not affected by phosphogypsum or amend phosphogypsum for making suitable for using it as impervious liner.

### **References**

1. United States Environmental Protection Agency (1939) Potential uses of phosphogypsum and associated risks
2. Guidelines for management, handling, utilisation and disposal of phosphogypsum generated from phosphoric acid plants, 2014. Central Pollution Control Board
3. Part III: Minerals review. 56th Edition. Minor minerals. Indian minerals year book, 2006
4. Taha R, Seals RK (1992) Engineering properties and potential uses of by-product phosphogypsum. Utilisation of waste materials in civil engineering construction. In: Proceedings of conference New York, 1992. American Society of Civil Engineers, New York, 250–263
5. Lopez AM, Seals RK (1992) The environmental and geotechnical aspects of phosphogypsum utilization and disposal. In: Environmental geotechnology (proceedings of mediterranean conference, Cesme, Turkey, 1992). A.A. Balkema, Rotterdam, pp 437–443
6. Safety reports series No. 78. Radiation protection and management of NORM residues in the phosphate industry, 2013. International Atomic Energy Agency
7. Florida Department of Environmental Protection (2005) New management requirements for phosphogypsum stack systems

8. Arocena JM, Dudas MJ, Poulsen L, Rutherford PM (1994) Weathering of clay minerals by fluoride-containing solutions from phosphogypsum by-product. *Can J Soil Sci*
9. Convention on the prevention of marine pollution by dumping of wastes and other matter, 1972, as amended 2006. International Maritime Organisation
10. Wissa AEZ. Phosphogypsum disposal and the environment. Ardaman and Associates, Orlando, FL

# Long-Term Deformations of Soft Clays: A Case Study



Atriya Chowdhury

**Abstract** Any material subjected to constant loading will deform in due course of time. The magnitude of time-dependent deformation depends upon the properties of individual materials. Creep is the time-dependent deformation phenomenon experienced in soft soils depending upon their consistency and magnitude of superimposed load. Clayey soils exhibit many rheological properties amongst which creep is one of the most widely observed phenomenon. The creep behaviour of clay has been extensively studied by many researchers and there are several cases on record where the consequences of rheological process of creep of soils have been disastrous for various types of structures constructed over them. In this paper, two case studies based on creep-related rheological phenomenon of soil have been presented, namely The Leaning Tower of Pisa, Italy and The San Jacinto Monument, Texas, U.S.A. The Leaning Tower of Pisa, Italy is an engineering marvel with the tower being inclined at a degree of 5.5 due to presence of the soft soil under one of the sides of the tower. The San Jacinto Monument was constructed in 1936 comprising of a 176.5 m tower resting on a square mat of 37.8 m. The settlement of the structure as recorded after 70 years was 0.329 m. Subsequently, the settlement behaviour of a typical foundation of Kolkata High court building constructed in the nineteenth century has been discussed in an attempt to highlight the effect of time-dependent deformation of typical soft clay deposit in Kolkata.

**Keywords** Creep · Rheological phenomenon · Kolkata · Time-dependent deformation

## 1 Introduction

Geotechnical projects are long-term installations, and soil is the most sensitive material as compared to the other construction materials whose properties remain more or less constant, and their behaviour can be determined to a high level of accuracy.

---

A. Chowdhury (✉)

Civil Engineering Department, Jadavpur University, Kolkata 700032, India

© Springer Nature Singapore Pte Ltd. 2022

A. K. Dey et al. (eds.), *Proceedings of the 7th Indian Young Geotechnical Engineers Conference*, Lecture Notes in Civil Engineering 195,

[https://doi.org/10.1007/978-981-16-6456-4\\_43](https://doi.org/10.1007/978-981-16-6456-4_43)

Natural soil is never uniform, and the omnipotence of theories ceases to exist. It is thus important to assess the “long-term” condition of soil to understand and predict the performance of the structure erected. The “end of construction” conditions of a soil can change with time due to variation in pore pressure and shear strength of the soil. There have been several instances in the past when the changes in in-situ conditions have adversely affected the stability of the structure and in some cases even led to failure [1]. Creep is the time-dependent deformation phenomenon of soil. After the completion of construction, the long-term strength and creep deformation of the soil are the two major geotechnical problems governing the stability of the superstructure. Creep behaviour study is thus very important for prediction of long-term behaviour and avoids problems of significant prolonged deformation which may even, sometimes, lead to failure.

Singh and Mitchell [2] first proposed the following equation for prediction of strain rate of soil during creep under undrained condition.

$$\dot{\varepsilon}_a = A e^{\alpha D} \left( \frac{t_1}{t} \right)^m \quad (1)$$

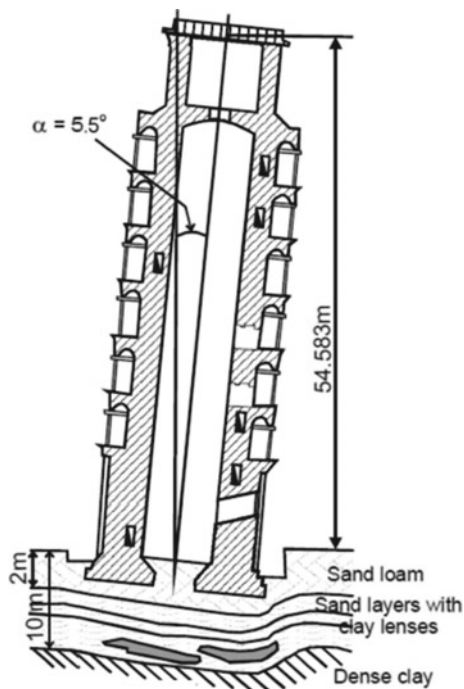
Please where  $A$ ,  $\alpha$  and  $m$  are a measure of the creep potential of a soil, for values of  $m < 1$  the chances of creep of soil exits. Lower the value higher the creep potential. This expression has been used by several researchers to predict long-term deformation characteristics of various old structures [3–5]. Slope of  $e$ - $\log \sigma'_v$  curve is defined as compression index and is denoted by  $c_c$ . The slope of linear part of void ratio versus logarithmic time curve beyond end of primary is defined as secondary compression index ( $c_\alpha$ ). Relation between  $c_\alpha/c_c$  for all the loading stages and times beyond the end of primary consolidation is constant [6–8]. The concept is based on the observation that the magnitude and behaviour of  $c_\alpha$  with time is directly related to that of  $c_c$  with consolidation pressure [9]. The value of  $c_\alpha$  varies with time and that of  $c_c$  varies with vertical effective stress ( $\sigma'_v$ ); secondary consolidation behaviour of all soils at any time after end of primary consolidation can be completely defined by the values of  $c_\alpha/c_c$  and  $e$ - $\log \sigma'_v$  relationship.

In this paper, the long-term settlement of The San Jacinto Monument, Texas, U.S.A has been presented along with the classical case of The Leaning Tower of Pisa, Italy where creep deformation of the soft clay soil under the southern side of the tower led to tilting of the tower. Further, settlement analysis of a typical foundation of the Kolkata High Court building constructed in 1872 has been presented in order to highlight the time-dependent behaviour of soft Normal Kolkata Deposit.

## 2 Leaning Tower of Pisa

The Leaning Tower of Pisa, Italy is a classic example of creep settlement of soil. It is an architectural marvel constructed during the years 1173–1370. The tower was constructed in three phases. The first four floors were constructed between the years

**Fig. 1** The leaning tower of Pisa sectional view [11]



1173–1178 following which the construction stopped. The next three floors were constructed in the second phase of construction during the years 1272–1278. The third and final phase of construction began in 1360, and the tower was completed in 1370. The area of ring foundation provided was  $280 \text{ m}^2$  with outer diameter of 19.35 m and inner diameter of 4 m. The net pressure on the soil below foundation was 505 kPa resting on soil having an undrained shear strength of 55 kPa [10]. The tower began to tilt during construction period when the pressure reached 331 kPa due to inadequate undrained strength below the foundation in the southern side. The sectional view of the tower is presented below (see Fig. 1).

## 2.1 Subsoil Conditions

The subsoil below the tower consisted of three main strata belonging to the Holocene and Pleistocene age [12]. The top layer is made of slightly clayey and sandy yellow silt with interbedded lenses and layers of sand and clay. The subsequent stratum is predominantly clayey in nature, and the third consists of slightly silty sand, which extends at least to a depth of 65–70 m below ground level. The unit weights of the soil in these strata were  $19 \text{ kN/m}^3$ ,  $16\text{--}20 \text{ kN/m}^3$ , and  $21 \text{ kN/m}^3$ . The liquid limits varied in the range of 28–42%, 34–78% for stratum one and two. The plasticity indices

ranged from 22 to 100% for the top stratum and was greater than 80% for the second stratum. Several researchers (e.g. [10–15] have extensively studied the settlement in order to determine the deformation mechanism. Due to the presence of soft plastic clay strata below the tower which was subjected to low overburden pressure pre-construction, the tower started to settle on application of superstructure loading. The tower continued to tilt for decades before the construction was completed. By the end of construction in the fourteenth century, the structure had already tilted by 2.1 m on one side. The tower continued to settle over the centuries after construction and is presently settling at 2 mm per year. The average settlement has been recorded over 1.5 m, and the tilt is 5.58 m. The tower is 54.583 m high from the ground on the low side and 56.29 m on the high side.

## 2.2 Settlement Analysis and Creep Potential Parameters of Pisa Clay

The settlement calculated using the expression given by Terzaghi [16] and Mesri [17] is given below:

$$\text{Immediate settlement} = qB(1-\gamma^2) I_\sigma / E \quad (2)$$

where

$q$  = average foundation pressure = 50.5 t/m<sup>2</sup>

$B$  = width of foundation = 7.5 m (Strip)

$\gamma$  = poisson's ratio = 0.5

$I_\sigma$  = influence factor = 2.0

$E$  = young's modulus = 2000 t/m<sup>2</sup>

So, immediate settlement = 284 mm

$$\text{Consolidation settlement} = c_c H \log\{(p + \Delta p)/p\} \quad (3)$$

where

$c_c$  = coefficient of compression

$H$  = thickness of influence zone

$p$  = overburden pressure

$\Delta p$  = increase in overburden pressure at the centre of influence zone

So, consolidation settlement = 742 mm.

Applying correction factors over immediate and consolidation settlements, the corrected settlement is 642 mm.

**Table 1** Singh and Mitchell parameter (from Mitchell and Soga [15])

Sample	Layer	$m$	$\alpha$	$A(\%/year)$
4 m	Clayey silt	0.89	5.81	0.09
6 m	Clayey silt	0.95	5.86	0.04
10 m	Clay	0.83	6.33	0.152
14 m	Clay	0.86	6.39	0.05
19 m	Clay	0.75	882	0.05

$$\text{Secondary consolidation settlement} = H c_{\alpha} \log(t_2/t_1) \tag{4}$$

where

$c_{\alpha}$  = coefficient of secondary compression = 0.023

$H$  = thickness of influence zone = 15 m

$t_2$  = time period after end of construction = 7000 years

$t_1$  = time for 95% consolidation in years = 37 years

So, secondary consolidation settlement = 789 mm.

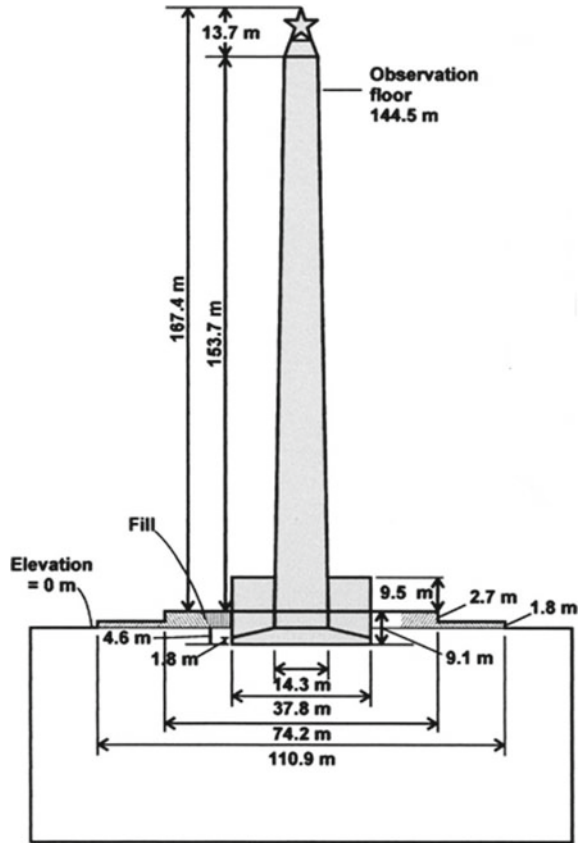
Thus, the total settlement estimated is 1431 mm which is close to the observed settlement of 1.5 m. Creep tests were conducted on Pisa clay by Bishop and Lovénbury [18] and Mitchell and Soga [15]. The Singh and Mitchell creep parameters  $A$ ,  $m$  and  $\alpha$  were determined as represented in Table 1.

Using the parameters presented in Table 1, Bai et al. [19] performed plane stress analysis to quantify the soil creep effects on the deformation of the tower. The results obtained showed creep accounted for 1.7° tilt out of the total 5.5°. The mean stresses increased by 20% in the upper clay layers and the stress states moved away from critical state. An additional 1 m settlement was caused due to creep of the soil.

### 3 San Jacinto Monument

The San Jacinto Monument, the tallest column monument in the world according to the Guinness Book of World Records was built in 1936 to honour the 100-year anniversary of the victory of the Texan army over the Mexican army. It consists of a 176.5 m high column founded on a large steel-reinforced square mat with each side of 37.8 m. The mat is 4.6 m thick at the centre having a width of 14.3 tapering to 1.8 m at the edges. The total weight including the column, a star at the top of the column, a museum at the base, and mat foundation was estimated to be 312.7 MN [20]. The foundation was designed by Raymond Dawson considering an average pressure of 223.8 kPa on the soil under the mat. The mat was laid at a depth of 4.6 m below ground level resulting in the net pressure acting on the soil below foundation being 141 kPa. (unit weight of the soil removed from above foundation was 18 kN/m<sup>3</sup>).

**Fig. 2** Dimensions of the San Jacinto Monument [21]



Dawson had setup settlement points on the mat foundation along with benchmarks away from the monument. The settlements recorded over the years were reported by Briaud et al. [21]. The settlements continued at a constant rate of 6 mm/year even 45 years after construction when the average settlement measured was 0.3 m. The settlement of the structure over 70 years was measured to 0.329 m. The dimension of the monument is shown. (see Fig. 2).

### 3.1 Subsoil Conditions

The subsoil at the site consisted of clay up to a depth of 20 m; a thin strip of clay with sand seams of average thickness 2 m was present in between this layer at depths 10–12 m. The borehole data collected at various time after construction till date depict a variation in ground water level was found to vary between depths of 0.61–11.9 m. The moisture content of the soil strata at depths 0–10 m was found to be close to 35%



and reduced to 20% at greater depths. The plasticity index of the top soil was as high as 55%. A reasonable estimate of a lower bound of undrained shear strength of soil at the site is about 100 kPa as obtained from soil investigations carried out in 1953, 1954, 1958, 1959, and 1962. The average of coefficient of compression determined from analysis was 0.255, and average  $c_v$  value was  $1.3 \times 10^{-7} \text{ m}^2/\text{s}$  [21].

### 3.2 Settlement Analysis and Creep Potential Parameters

Dawson predicted the long-term settlement of the structure to be 0.187 m. The component of the elastic, secondary consolidation, and creep settlement corresponding to the horizontal movement of soil under the structure was neglected as it does not occur in odometer tests due to ring confinement. The presence of intermediate sand layers and clay with sand seams at various depths along the soil profile is indicative of presence of drainage paths aiding elastic and primary settlements. The total settlement of the structure calculated predicts a settlement of 270 mm, thus 59 mm settlement less than the observed ground settlement. Using the settlement data presented in Briaud [21] the creep parameters  $m$ ,  $A$  and  $\alpha$  were calculated as shown in Table 2.

The corresponding axial strain rate against time has been plotted. (see Fig. 3).

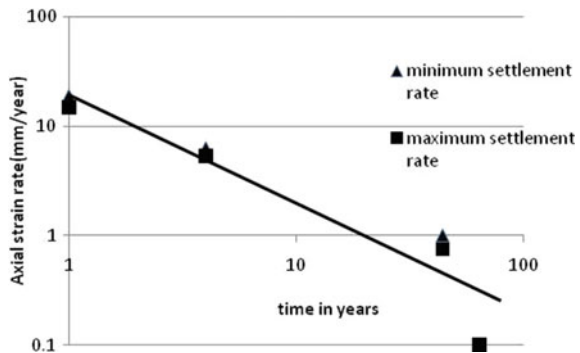
## 4 Kolkata High Court

The Calcutta High Court, the oldest High Court in India was constructed in neo-Gothic style between 1864 and 1868. It is a 150 years old brick structure constructed

**Table 2** Singh and Mitchell parameters

$m$	$A$ (mm/year)	$\alpha$
0.79	0.05	0.004

**Fig. 3** Axial strain rate versus time plot



close to the eastern bank of the Hooghly River. The dead load on the structure has increased over the years, probably attributed to the necessity to maintain a record of documents. The structure experienced excessive settlement which led to the development of distress cracks of certain structural members in the year 2014 [22]. In order to study and review the settlement, the soil investigation work around the main building of the High Court was conducted.

Kolkata soil profile comprises of Normal Kolkata Deposits and the river channel deposits. The river channel deposits are located along the banks of Adi Ganga with sand layer ranging up to a depth of 20–25 m. The Normal Kolkata Deposit consists of soft clay up to a depth of 15 m followed by a layer of medium/stiff clay of thickness 5–6 m, beyond which lies an intermediate sand layer followed by a deep hard clay layer. The settlement analysis for a typical foundation of the High Court building has also been presented in order to examine time-dependent behaviour of Normal Kolkata Deposit. The average soil profile along with the average properties at the site is given (see Fig. 4). Subsoil at the site comprises of a top fill of about 3 m followed by a thick compressible soft clay deposit of brownish grey/dark-grey silty clay/clayey silt down to a depth of 15 m below ground level (unpublished soil report Jadavpur University).

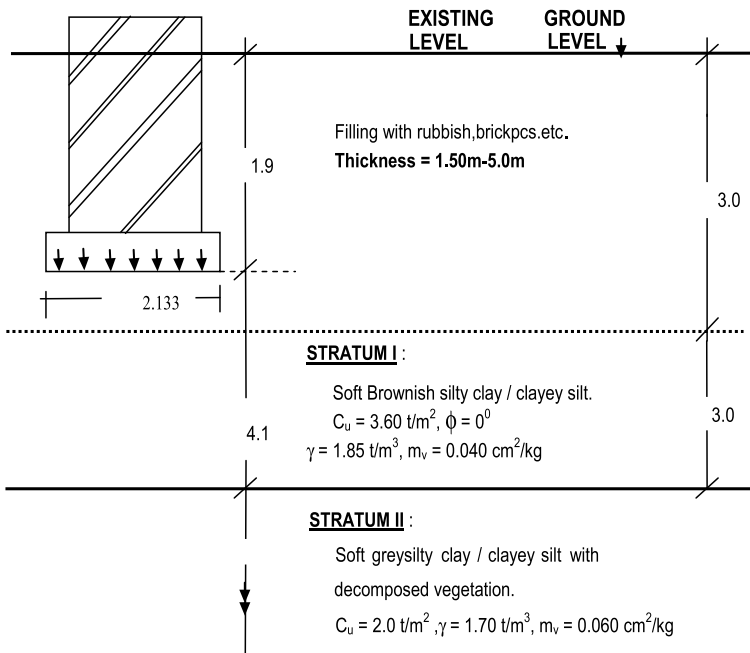


Fig. 4 Subsoil profile for settlement calculations

#### 4.1 Settlement Analysis of a Typical Foundation of the High Court Building

Considering the subsoil conditions and soil parameters as obtained from the soil investigation at the site settlement analysis of a typical strip foundation of width 2.13 m resting at a depth of 1.90 m (see Fig. 4) below existing ground level (reported to be found from excavation at a typical location of the building) has been done considering an average foundation pressure of 20 t/m<sup>2</sup> (see Fig. 4).

$$\text{Immediate settlement} = qB(1-\gamma^2)I_\sigma/E \quad (5)$$

where

$$\begin{aligned} q &= \text{average foundation pressure} = 20 \text{ t/m}^2 \\ B &= \text{width of foundation} = 2.13 \text{ m (Strip)} \\ \gamma &= \text{poisson's ratio} = 0.5 \\ I_\sigma &= \text{influence factor} = 2.0 \\ E &= \text{young's modulus} = 500 \times 3.6 = 1800 \text{ t/m}^2 \\ \text{So, immediate settlement} &= 36 \text{ mm} \end{aligned}$$

$$\text{Consolidation settlement} = m_v \Delta P H \quad (6)$$

where

$$\begin{aligned} m_v &= \text{coefficient of volume change} = 0.004 \text{ m}^2/\text{tonne} \\ \Delta P &= \text{increase in overburden pressure at the centre of influence zone} = 10 \text{ t/m}^2 \\ H &= \text{thickness of influence zone} = 4.26 \text{ m} \end{aligned}$$

So, consolidation settlement = 170 mm.

In addition to this, there was some secondary settlement as the High Court building was constructed about 150 years back, and its magnitude was estimated considering the ratio of  $c_\alpha/c_c = 0.04$  [23].

$$\text{Secondary consolidation settlement} = Hc_\alpha \log(t_2/t_1) \quad (7)$$

where

$$\begin{aligned} c_\alpha &= \text{coefficient of secondary compression} = 0.01 \\ H &= \text{thickness of influence zone} = 4.26 \text{ m} \\ t_2 &= \text{time period after end of construction} = 150 \text{ years} \\ t_1 &= \text{time for 95\% consolidation in years} = 3 \text{ years} \end{aligned}$$

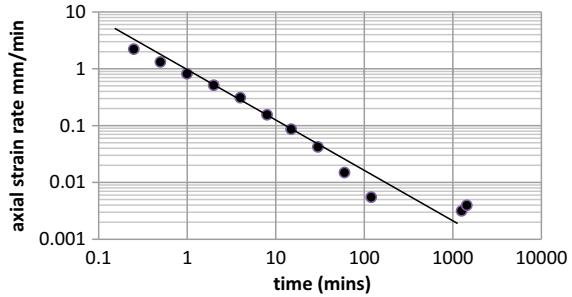
So, secondary consolidation settlement = 72 mm.

Thus, the total predicted settlement is about 250 mm, and thus, the secondary settlement was about 30% of the total settlement.

**Table 3** Singh and Mitchell creep potential parameters

$m$	$A$ (mm/min)	$\alpha$
0.70	0.02	0.0097

**Fig. 5** Axial strain rate versus time plot



Further, some long-term tests were also conducted to evaluate the Singh and Mitchell [2] parameters (Table 3) required for prediction of axial strain rate.

Using these parameters, the axial strain rate against time for the soil has been obtained. These parameters may be used for prediction of rate of deformation of similar types of structures constructed over soft Normal Kolkata Deposit. (see Fig. 5).

## 5 Conclusions

The importance of time-dependent deformation of soft clays was examined with the help of two well discussed case studies. The settlement analysis of the structures constructed over soft clays showed a significant contribution of creep settlement in the overall settlement of the structure. In case of the Kolkata High Court, creep settlement was estimated to be in the order of 30% of total settlement. It is thus important to consider creep settlement during the design of structures over soft clays as excessive deformations may affect the stability, serviceability and durability of structural members.

## References

1. Skempton AW (1964) Long-term stability of clay slopes (4th Rankine lecture). *Géotechnique* 14(2)
2. Singh A, Mitchell JK (1969) Creep potential and creep rupture of soils. In: *Proceedings 7th international conference on soil mechanics and foundation engineering*, vol 1, Mexico, pp. 379–384(1969).
3. Lai X, Wang S, Qin H, Liu X (2009) Unsaturated creep tests and empirical models for sliding

- zone soils of Qianjiangping landslide in the three gorges. *J Rock Mech Geotech Eng* 2(2):149–154
4. Zhao B, Huang W, Shu Z, Han M, Fong Y (2018) Experimental and theoretical studies on the creep behavior of Bayer red mud. *Adv Civil Eng* 2018(6327971):9
  5. Zhu J-G, Yin J-H, Luk ST (1999) Time-dependent behavior of Hong Kong marine deposits. *Geotech Testing J ASTM* 22(2):118–126
  6. Mesri G, Godlewski PM (1977) Time and stress compressibility interrelationships. *J Geotech Eng ASCE* 103(GT5):417–430
  7. Mesri G, Hedien JE, Shahien M (1997) Geotechnical characteristics and compression of Pisa clay. In: *Proceedings, 14th international conference in soil mechanics and foundation engineering, Hamburg, Germany*, pp. 373–376
  8. Mesri G, Stark TD, Ajlouni MA, Chen CS (1997) Secondary consolidation of Peat with and without Surcharging. *J Geotech Geo-environ Eng ASCE* 123(5): 411–421
  9. Mesri G, Castro A (1987)  $C_{\alpha}/C_c$  concept and  $K_0$  during secondary compression. *J Geotech Eng ASCE* 113(3):230–247
  10. Jamiolkowsky M (2006) Behavior of the leaning tower of Pisa during and after stabilization works. *The Ralph B. Peck Lecture, Atlanta*
  11. Meschyan SR (1995) Experimental rheology of clayey soils. *Balkema*
  12. Jamiolkowski M, Levi F, Lancellotta R (1993) Leaning tower of Pisa—updated information. In: *3rd International conference on case histories in geotechnical engineering, St. Louis, Missouri, vol 2*, pp 1319–1330
  13. Leonards GA (1979) Discussion of “Foundation performance of Tower of Pisa”. *ASCE J Geotech Eng Div* 105(GT1):95–105
  14. Mitchell JK, Vivatrat V, Lambe TW (1977) Foundation performance of tower of Pisa. *J Geotech Eng Div Proc ASCE* 103(GTS):227–249
  15. Mitchell JK, Soga K (1995) Numerical and experimental studies related to the performance and stabilization of the Tower of Pisa. In: *Report to the Consorzio Progetto Torre di Pisa*
  16. Terzaghi K (1943) *Theoretical soil mechanics*. Wiley, New York
  17. Mesri G (1973) Coefficient of secondary compression. *J Soil Mech Found Div Am Soc Civ Eng* 99(SM1):122–137
  18. Bishop AE, Lovenbury HT (1969) Creep characteristics of two undisturbed clays. In: *Proceedings of ICSMFE, vol 1*, pp 29–37
  19. Bai J, Morgenstern N, Chan D (2008) Three-dimensional creep analyses of the leaning tower of Pisa. *Soils Found* 48:195–205
  20. Cummins RJ (1937) A concrete shaft 564 feet high. *Houston, Tex*
  21. Briaud J-L, Nicks J, Rhee K, Stieben G (2007) San Jacinto Monument case history. *J Geotech Geoenviron Eng*. [https://doi.org/10.1061/\(ASCE\)1090-0241\(2007\)133:11\(1337\),1337-1351](https://doi.org/10.1061/(ASCE)1090-0241(2007)133:11(1337),1337-1351)
  22. Mittal S, SivakumarBabu GL (2018) Retrofitting of N–W corner of Kolkata high court heritage building—through micropiles and grouting. In: Krishna A, Dey A, Sreedeeep S (eds) *Geotechnics for natural and engineered sustainable technologies. Developments in Geotechnical Engineering*. Springer, Singapore (2018)
  23. Kotireddy B, Sahu RB, Ghosh S (2013) Consolidation behaviour of organic soil in normal Kolkata deposit. *Indian Geotech J*. <https://doi.org/10.1007/s40098-013-0076-0>

# Effect of Interface Connection on Performance of Narrow Shored Reinforced Earth Wall



Charmy Joshi, Sweta Dave, Shalini Singh, and Manish Shah

**Abstract** Narrow Reinforced Earth (RE) walls are usually constructed in limited space (a ratio of wall width  $L$  to wall height  $H$  is less than 0.7) and in front of existing stable walls. These walls are preferred in such situation where existing highway width is needed to be increased or in mountain terrain. Performance of such walls differs from conventional RE walls because of constrained space and interaction with existing stable walls. Many researchers evidenced that due to limited width ( $L$ ) of narrow RE wall, ample resistance against pull-out force in reinforcements was not fully mobilization. That led to pull-out failure and/or development of tension cracks in extreme loading conditions at the interface between narrow RE wall and shoring wall. However, experimental database especially with the interface connection is scarce. Thus, the main objective of this study is to understand the actual characteristics of narrow RE wall by load–displacement settlement tests having provision of interface connection between RE wall and shoring wall. For the connection between two walls, friction connection was used. Results indicated that friction-based connection for connecting narrow RE wall with existing shoring is an active measure to reduce the deformation in the narrow RE wall.

**Keywords** Narrow reinforced earth wall · Shoring wall · Load–displacement tests · Experimental study · Geogrid

## 1 Introduction

Due to advantages in construction techniques, esthetics, economic construction, seismic performance, and ability to tolerate large deformations without structural distress, Reinforced Earth (RE) walls have been widely designed and used all over the world. However, as population increases, traffic demand has also increased, which

---

C. Joshi (✉) · S. Singh · M. Shah  
Applied Mechanics Department, L.D. College of Engineering, Ahmedabad, India

S. Dave  
GEC Gandhinagar, Gandhinagar, India

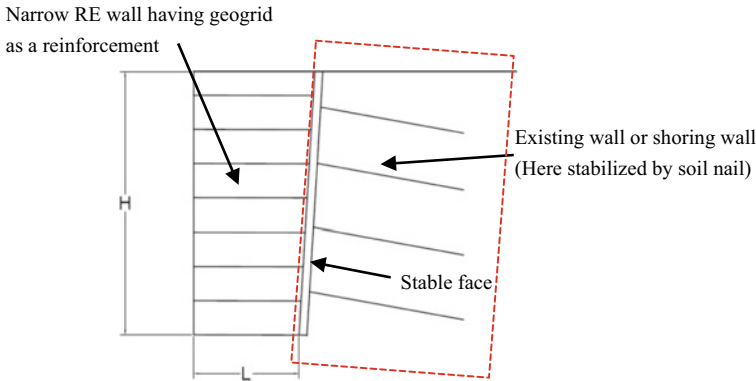


**Fig. 1** Illustration of new narrow RE wall in front of exiting stable face

has led to a widening of existing highway roads. One way is to construct a new RE wall in front of exiting stable wall in limited space to diminish the cost of construction. Such walls are referred to as narrow RE walls. According to Federal Highway Administration (FHWA) MSE-wall design guidelines, Narrow RE walls are referred to as RE walls having an aspect ratio  $L/H$  (ratio of wall width  $L$  to wall height  $H$ ) of less than 0.7 [1]. An example of a narrow RE wall is shown in Fig. 1.

Due to constrained space and interaction with existing stable walls, the behavior of narrow RE walls differs from conventional RE walls, which include a magnitude of earth pressure, failure modes, and distribution of tension along the reinforcement. Field-scale tests and centrifugal modeling tests on narrow RE walls suggested that there exists significant reduction in lateral earth pressure behind narrow RE wall [2, 5, 8]. And the reduction in earth pressure is mainly caused due to the “Arching” effect. Also, based on centrifugal modeling, Xu et al. [7] suggest that the critical failure plane of the narrow RE wall was bilinear and tangent to the stable existing wall, which was different from conventional RE walls. Researchers recommended mainly mechanical connection and frictional connections to avoid tension cracks at boundary zone between the existing stable walls and narrow RE wall. According to the measured field-scale data, Morrison et al. [4] reported that different connection forms had little effect on the deformation behavior of the Shored MSE wall. Thus, FHWA design guidelines for SMSE walls [4] suggested not applying mechanical connections for its complicated construction. Based on numerical modeling study, Tavakolian and Grien [6] used friction-based connection also known as a sandwich connection to connect the narrow RE wall with existing stable wall (i.e., shoring wall) to achieve the pull-out resistance force and increase the internal stability of combined wall systems. They reported that the presence of secondary reinforcement reduces the required resistance force in the primary reinforcement. Also, primary and secondary reinforcements are not directly connected so that the flexibility of the combined wall system can be maintained.

However, experimental based study on the interface connection between the narrow RE wall and existing stable wall (i.e., shoring wall) was not thoroughly investigated. Therefore, the main objective of this paper was to understand the behavior of narrow RE walls and to check the effect of interface connections using load displacement and load-settlement analysis. For the connection between two walls, a friction-based connection was used.

## 2 Experimental Program

### 2.1 Model of Narrow RE Wall

Model tank was fabricated of size 900 mm \* 400 mm \* 930 mm using angle sections and metal sheets. The model consists of a reinforced fill zone, and a shoring wall. The reinforced fill zone serves the purpose of narrow RE wall, and the shoring wall is mounted to act as shoring wall. Perspex sheets with a thickness of 20 mm were used at the sides to examine the failure surface, whereas the front and rear sides of the model tank were kept open to measure the displacements. To simulate the structure of the flexible shoring wall, a hollow structure was constructed with a front batter of 1:9 (H:V) from plywood sheets with a thickness of 20 mm containing filler material to obtain desired weight. Minimum geogrid reinforcement length (measured at the bottom of the wall) was 400 mm, corresponding to an aspect ratio (L/H) of approximately 0.44. The reinforcement length increased from bottom to top, with the largest reinforcement provided at the top of length 500 mm, corresponding to an aspect ratio (L/H) of 0.55. Figure 2 shows schematic diagram and actual prototype model of narrow RE wall.

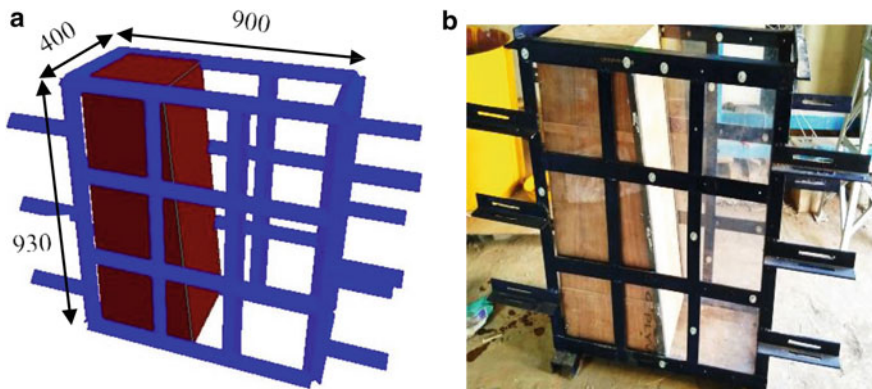


**Fig. 2** Model of narrow RE wall: **a** schematic diagram, **b** actual model (all dimensions are in mm)



### 2.2 Materials Used

**Sand.** The backfill material used in this study was dry cohesionless sand. The sieve analysis test was carried out according to IS 2720–4:1985 and particle size distribution curve for sand was shown in Fig. 3. Table 1 lists the index and engineering properties of backfill sand which were measured in accordance with the procedure mentioned in the Bureau of Indian Standards. Classification of sand was found as poorly graded sand (SP). Stage filling was considered to fill the model tank, and the density of the backfill was achieved by compaction using a vibratory motor. The target relative density of the backfill was kept to 80%.

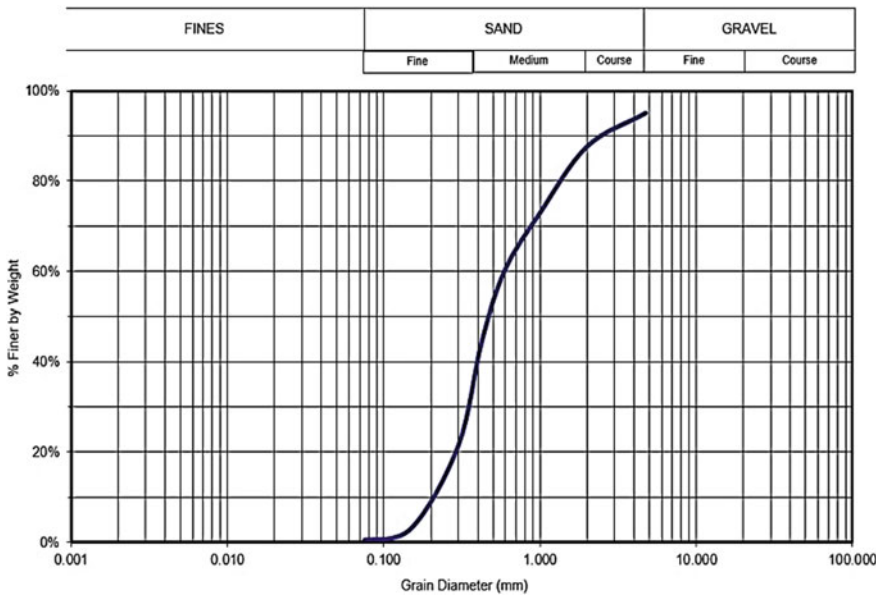


**Fig. 3** Particle size distribution curve for sand

**Table 1** Index and engineering properties of backfill sand

Parameter	Symbol	Value
Coefficient of uniformity	$C_u$	2.86
Coefficient of curvature	$C_c$	1.09
Specific Gravity	$G$	2.65
Maximum dry density (in $\text{kN/m}^3$ )	$\gamma_{\text{max}}$	19.10
Minimum dry density (in $\text{kN/m}^3$ )	$\gamma_{\text{min}}$	16.95
Friction angle	$\phi$	37.1°

**Table 2** Mechanical properties of uniaxial geogrid

Index properties	Value
Ultimate tensile strength-MD(kN/m)	40
Ultimate tensile strength-CMD(kN/m)	20
Creep reduction factor	1.49
Partial factor-installation damage	1.11
Partial factor-environmental effects	1.15
Pull-out interaction coefficient	0.8

**Geogrid.** Uni-axial geo grid composed of high tenacity polyester (PET) multifilament yarn was used as reinforcement material. The mechanical properties of geogrid are in Table 2.

### 2.3 Instrumentation and Test Setup

The main component of the apparatus is shown in Fig. 4. An aluminum plate of size 380 mm × 150 mm was used to simulate static footing condition. To obtain the plane strain condition, the length of the footing plate was almost equal to the width of the model tank. Geogrid was used as the reinforcement and was placed at the 0.4 H (225 mm) vertical distance of the facing panel. For connection between geogrid and facing panel, L shape angle section jointed back to back and geogrid was placed in between clamps and fixing it by steel nut bolt dia of 6 mm as displayed in Fig. 5. Under such a condition, the geogrid would not be pulled out from the facing between the clamps. Displacements and settlement measurements can be made using

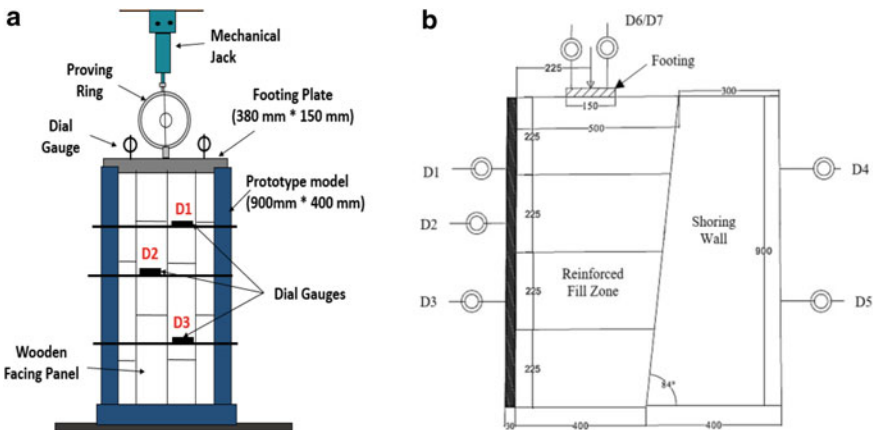


**Fig. 4** Schematic diagram of the test apparatus: **a** front view, **b** section view (all dimensions are in mm)

**Fig. 5** Mechanical connection between facing panel and geogrid



dial gauges of suitable capacity. Total 7 dial gauges were set up in narrow RE wall model. Dial gauge D1, D2, and D3 were placed at front face of model tank at a distance of 190 mm, 350 mm and 600 mm from top of the facing panel respectively whereas dial gauge D4 and D5 were located at back face of model at a vertical distance of 210 and 600 mm from top of the facing panel respectively. Two dial gauges D6 and D7 were placed diagonally at  $180^\circ$  apart on footing plate to measure the vertical settlement of footing plate.

## 2.4 Test Procedure

Load displacement and load-settlement tests were performed in a narrow RE wall model in order to know displacement and settlement characteristics. First, the tank was filled in four layers, and geogrid was placed in between sand layers. In each layer, the volume of the sand was calculated ahead, and by controlling the weight of corresponding soil mass, the relative density of 80% was further ensured. The unconnected system consists of a single layer of reinforcement connected to the facing panel via two L-shaped clamps placed back to back and fixing with 6 mm bolt with facing panel and cut down near shoring wall. For the connected system, secondary reinforcements were first connected to the shoring wall and overlapped upon associated primary reinforcement which was then connected to the facing panel.

A vertical downward load was applied using a mechanical jack on a footing plate which was placed at a horizontal distance from the facing panel was kept as 225 mm. A seating load of  $7 \text{ kN/m}^2$  was applied on the plate using a mechanical jack. When there was no perceptible increase in settlement or when the rate of settlement reduces to 0.02 mm per minute as given in IS 1888–1982, the dial gauge readings were noted [3]. Figure 6 shows an arrangement of test setup of mechanical jack, proving ring and dial gauges from front and backside. Load versus displacement and load/settlement graph were then plotted for both connected and unconnected systems.

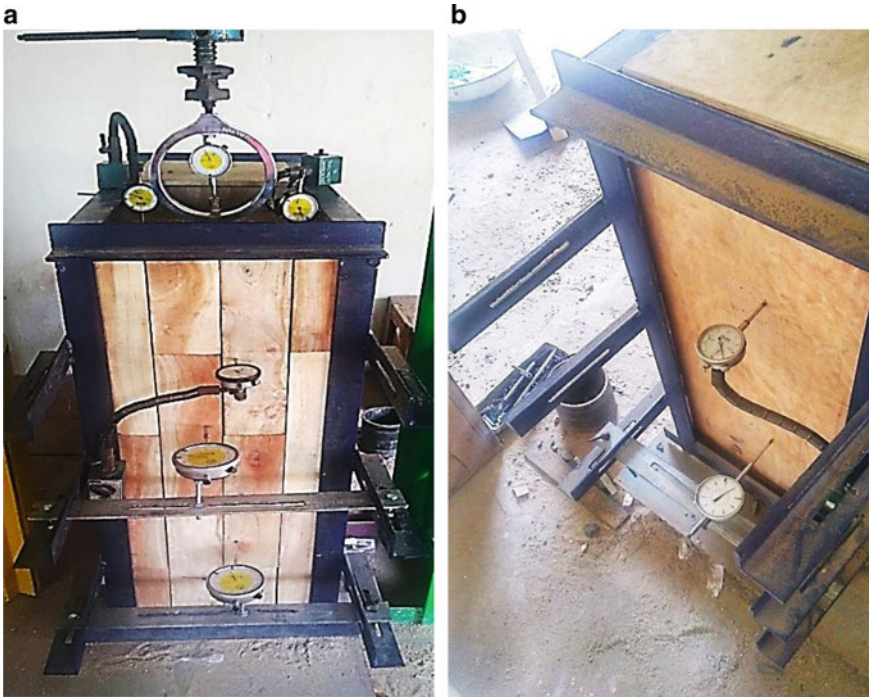


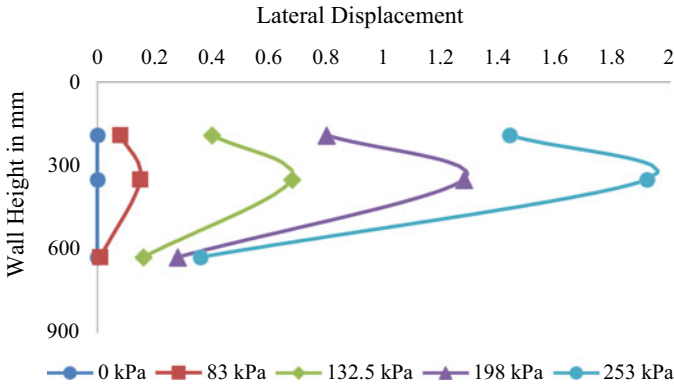
**Fig. 6** Arrangement of test setup: **a** front side, **b** back side

### 3 Results and Discussion

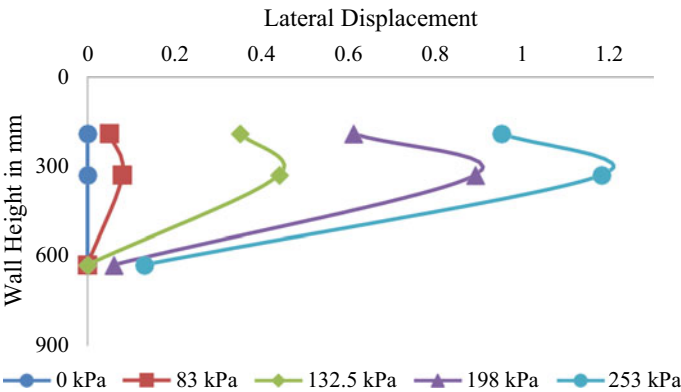
Tests were conducted on a narrow RE wall to check the effect of interface connection between narrow RE wall and shoring wall. All other parameters such as reinforcement length, spacing, soil density, position of loading were kept same. Load–Displacement and Load–Settlement curves have been obtained for unreinforced system as well as connected and unconnected system. Outcomes from the test are presented below.

Figure 7 and 8 show load versus displacement characteristic for an unconnected system and connected system at D1, D2, and D3 dial gauge location respectively.

From Fig. 7 and 8, it was observed that as surcharge load increases, lateral displacement also increases. Maximum lateral displacement was observed at surcharge loading of 253 kPa which was 1.92 mm and 1.18 mm for unconnected and connected system respectively. Also, the maximum displacement detected at center at D2 dial gauge location of narrow RE wall model. However, narrow RE wall model was designed for active earth pressure condition in which movement of facing panel is restricted only from bottom. But the maximum displacement reading at center portion was may be due to end constrains.



**Fig. 7** Lateral displacement versus wall height for unconnected system for different surcharge loading



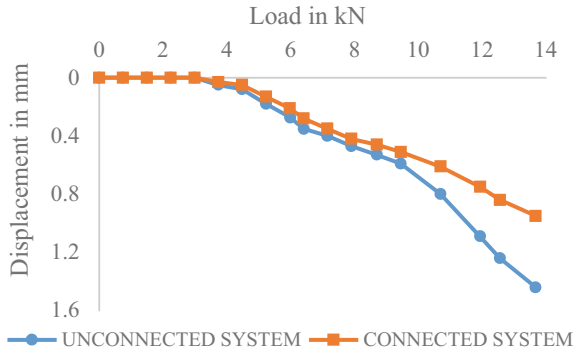
**Fig. 8** Lateral displacement versus wall height for connected system for different surcharge loading

### 3.1 Evaluation of Load–displacement Characteristics on Interface Connection of Combined Wall System

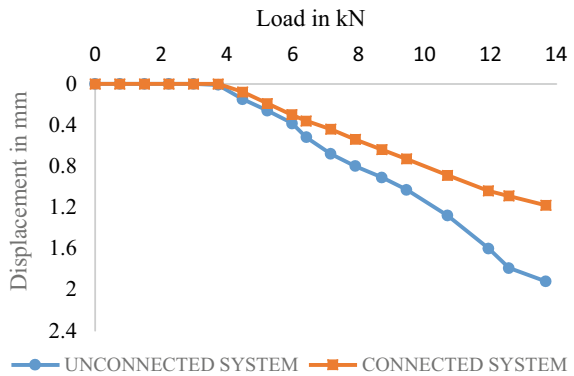
Figures 9, 10 and 11 show displacement characteristics of narrow RE wall for connected and unconnected systems at each dial gauge location of D1, D2, and D3 respectively.

From the graph, it is observed that a connected system has lower displacements compare to the unconnected system. Furthermore, displacement is more prominent at the center compared to the top and bottom dial gauge locations. Also, difference in lateral displacement for unconnected and connected systems is less at dial gauge location D1 than D2 and D3 dial gauge location. This can be related to the fact that more deformation takes place near the crest of the shoring wall as suggested

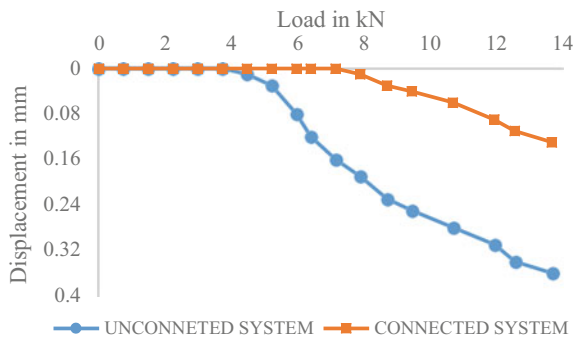
**Fig. 9** Load versus displacement characteristics for a connected and unconnected system at D1 dial gauge location



**Fig. 10** Load versus displacement characteristics for a connected and unconnected system at D2 dial gauge location



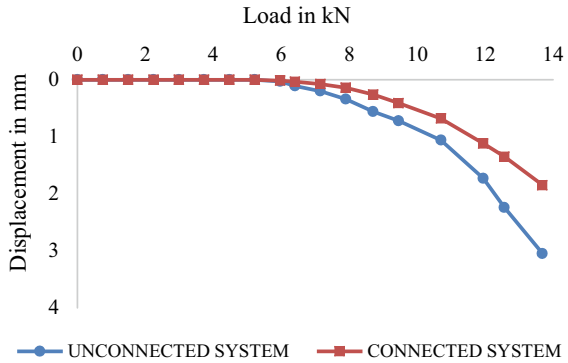
**Fig. 11** Load versus displacement characteristics for a connected and unconnected system at D3 dial gauge location



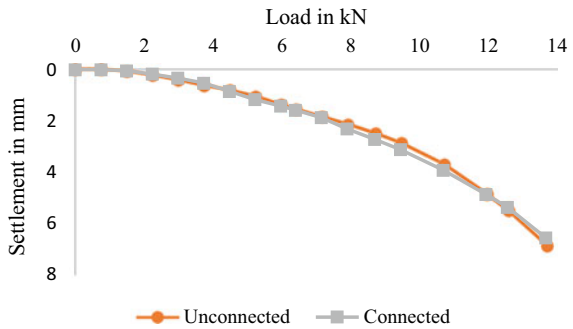
by Morrison et al. [4]. This means that for smaller loads, primary reinforcement is sufficient to take all the vertical loads. At higher loads, vertical loads will be transferred to secondary reinforcements. Thus, lateral displacement at D1 dial gauge location is found to be more for connected system.

Figure 12 represents the load versus displacement curve from D4 and D5 dial gauge locations for both connected and unconnected systems. The total displacement

**Fig. 12** Load versus displacement characteristics for the connected and unconnected system



**Fig. 13** Load versus settlement characteristics for the connected and unconnected system



at 13.7 kN load in the connected and unconnected system is 1.85 mm and 3.05 mm, respectively.

### 3.2 Load-Settlement Curve

Figure 13 displays the load-settlement behavior of narrow RE wall for connected and unconnected system. Total settlement at 13.7 kN load in connected and unconnected system was reported to be 6.57 mm and 6.87 mm respectively.

## 4 Conclusions

This paper presents instrumented model tests to investigate the effect of interface connections on the performance of the narrow RE wall subjected to static loading in-plane strain conditions. Influence factors were the connection between narrow RE wall and shoring wall. All other parameters such as type of the backfill material,

type of reinforcement, spacing, footing distance, footing size were kept constant. The lateral displacement of the wall facing and the settlement of the footing were measured. Following conclusions can be drawn from this study.

- The lateral displacement of the wall facing increased with the increase of footing load in all the model tests. In almost all the models, most of the wall facing displacements occurred at center dial gauge location which may be due to end constraints.
- Load displacement behavior of unconnected and connected system depicts that inclusion of geogrid reinforcement in between sand layers increases the lateral confinement of narrow RE wall. Thus lateral displacement decreases drastically.
- However, settlement is almost identical for connected and unconnected systems indicating that provision of second reinforcement layer only helps in reduction of lateral deformation of narrow RE wall system.
- Due to narrow width available, sufficient length is not available in upper portion of wall thus prone to pull-out failure. Thus, frictional based connection proven to be efficient and practical approach for connecting narrow RE wall to existing stable wall/shoring wall.

## References

1. Elias V, Christopher BR, Berg RR (2001) Mechanically stabilized earth walls and reinforced soil slopes design and construction guidelines. FHWA-NHI-00-043, National Highway Institute, Federal Highway Administration, Washington, DC
2. Frydman S, Keissar I (1987) Earth pressure on retaining walls near rock faces. *J Geotech Eng* 113:586–599. [https://doi.org/10.1061/\(asce\)0733-9410\(1987\)113:6\(586\)](https://doi.org/10.1061/(asce)0733-9410(1987)113:6(586))
3. Indian Standard. IS 1888(1982) Method of load test on soils. New Delhi, India
4. Morrison KF, Harrison FE, Collin JG, Dodds A, Arndt B (2006) Shored mechanically stabilized earth (SMSE) wall systems. FHWA-CFL/TD-06-001, Federal Highway Administration, Washington, DC
5. Take W, Valsangkar A (2001) Earth pressures on unyielding retaining walls of narrow backfill width. *Can Geotech J* 38:1220–1230. <https://doi.org/10.1139/t01-063>
6. Tavakolian R, Sankey J (2011) Sandwich connection design for shored reinforced earth walls. In: Proceedings of the 17th international conference on soil mechanics and geotechnical engineering. <https://doi.org/10.3233/978-1-60750-031-5-1441>
7. Xu C, Luo Y, Chen H, Jia B (2016) Effects of interface connections on narrowed mechanically stabilized earth walls. *Environ Earth Sci*. <https://doi.org/10.1007/s12665-016-6226-9>
8. Yang M., Xiao CT, ASCE AM (2017) Rigid retaining walls with narrow cohesionless backfills under various wall movement modes. *Int J Geomech* 17(11):04017098:1–12



# Analytical Methods for Predicting Load Carrying Capacity of Granular Piles—A Review



Murtaza Hasan and N. K. Samadhiya

**Abstract** Granular piles have been adopted as an effective technique for improving the engineering behaviour of soft clayey soils and loose silt deposits. The granular piles have been installed in various difficult sites to increase load carrying capacity, improve slope stability of embankments, reduce settlements and reduce lateral spreading. The granular pile derives load carrying capacity from the lateral confining pressure from the surrounding soft soils. The different modes of failures for a single granular pile installed in homogeneous soft soils are such as bulging; general shear failure, and sliding. Various researchers have performed laboratory model tests, analytical analyses, numerical modelling and field studies for the assessment of ordinary granular behaviour since early 1970s. This paper presents a review on analytical and design approaches published in various research papers that focus on load carrying capacity of ordinary granular piles. The review has been presented in chronological order. The objective of the present study is to assemble published analytical approaches in order to give an easy access to the information for researchers and designers.

**Keywords** Stone columns · Ground improvement · State of the art · Ultimate load analysis

## 1 Introduction

Ordinary granular piles (also known as conventional or unreinforced granular piles) generally replace 15–40% volume of the weak soil by using coarse gravel and coarser crushed stone aggregates compacted to a range of different densities, depending on site conditions and installation method. The installation of the granular pile creates

---

M. Hasan (✉)

Department of Civil Engineering, Chandigarh University, Mohali 140143, India

N. K. Samadhiya

Department of Civil Engineering, Indian Institute of Technology Roorkee, Roorkee 247667, India

e-mail: [nksamfce@iitr.ac.in](mailto:nksamfce@iitr.ac.in)

© Springer Nature Singapore Pte Ltd. 2022

A. K. Dey et al. (eds.), *Proceedings of the 7th Indian Young Geotechnical Engineers*

*Conference*, Lecture Notes in Civil Engineering 195,

[https://doi.org/10.1007/978-981-16-6456-4\\_45](https://doi.org/10.1007/978-981-16-6456-4_45)

a higher strength composite material of lower overall compressibility than the native soft soil alone [1–4]. The component material being granular and with higher permeability, granular piles have also been found to accelerate the consolidation settlements and minimise the post construction settlements [5–7]. The present paper investigates the analytical approaches developed by the various researchers for predicting ultimate load carrying capacity of granular piles installed in soft soils.

## 2 Analytical and Design Approaches

Greenwood [5] explained the load transfer mechanism in granular piles under bulging mode of failure. The author stated that improvement in the bearing capacity of granular piles treated ground depends on several factors such as lateral support provided by the surrounding clay to the pile, diameter and degree of compaction of the pile. Granular piles were assumed to be resting on firm clay, sand or harder ground. He proposed a formula to obtain the passive resistance by considering the earth pressure theory which is given by the Eq. 1.

$$\sigma_r = \gamma Z k_p + 2c_u \sqrt{k_p} \quad (1)$$

where,  $\sigma_r$  is the radial resistance of surrounding soils,  $\gamma$  is the bulk density of clay,  $Z$  is the average bulge depth,  $k_p$  is the coefficient of passive earth pressure,  $k_p = (1 + \sin \phi_s)/(1 - \sin \phi_s)$ .

$c_u$  is the undrained strength of soil and  $\phi_s$  is the angle of internal friction of the soil. Greenwood [5] also proposed an equation by taking into account a surcharge which is expressed as given in Eq. 1.1.

$$\sigma_r = \gamma Z k_p + 2c_u \sqrt{k_p} + q k_p \quad (1.1)$$

where,  $q$  is the surcharge load per unit area.

When granular pile approaches shear failure due to bulging, limiting axial stress (ultimate vertical stress or ultimate capacity) developed in the granular pile is expressed as:

$$q_u = \sigma_r \frac{1 + \sin \phi'}{1 - \sin \phi'} \quad (1.2)$$

where,  $\phi'$  is the angle of internal friction of pile material.

Vesic [8] developed a cavity expansion theory for cohesive and frictional soils. He proposed an expression to obtain ultimate lateral resistance provided by the surrounding soil which is given by Eq. 2.

$$\sigma_3 = cF'_c + qF'_q \quad (2)$$

where,  $q$  is the mean (isotropic) stress at the equivalent failure depth,  $c$  is the cohesion of the surrounding soil, are the cavity expansion factors which are function of the Rigidity Index,  $I_r$  and angle of internal friction of the surrounding soil.

$$I_r = \frac{E}{[2(1 + \nu)(c + q \tan \phi')]} \quad (2.1)$$

The long- as well as short-term ultimate load capacity of a granular pile may be calculated using cavity expansion theory. The ultimate capacity of the granular pile under bulging mode of failure surrounding is expressed as:

$$q_{ult} = \sigma_3 \frac{1 + \sin \phi_s}{1 - \sin \phi_s} \quad (2.2)$$

where,  $\phi_s$  is angle of internal friction of the surrounding soil.

Hughes and Withers [1] stated that the vertical loads are applied simultaneously on surrounding clay and pile in the practical applications. The authors idealised the mechanism of granular pile bulging as cylindrical cavity expansion in clay, similar to the behaviour of clay in a pressuremeter test. They proposed following expression which is widely used in practice to estimate the ultimate vertical stress that a granular pile can carry under the bulging mode of failure.

$$q_u = \frac{1 + \sin \phi'}{1 - \sin \phi'} (\sigma_{ro} - u + 4c) \quad (3)$$

where,  $c$  is the undrained strength of soil,  $u$  is the pore water pressure,  $\phi'$  is the angle of internal friction of pile material and  $\sigma_{ro}$  is the initial radial total stress in the native soil before pile construction.

Brauns [9] considered passive pressure within the soil and available to the aggregate pier is independent of depth. The author derived an equation to obtain the ultimate load capacity of pier by taking into account a surcharge which is given by Eq. 4.

$$q_{ult} = \left( q + \frac{2c}{\sin 2\delta_p} \right) \left( 1 + \frac{\tan \delta_p}{\tan \delta} \right) \tan^2 \delta_p \quad (4)$$

where,  $c$  is the undrained shear strength of the clay,  $q$  is the surcharge,  $\delta$  is the angle of the shear plane in the matrix soil and  $\delta_p = \left( 45 + \frac{\phi'}{2} \right)$  where  $\phi'$  is the angle of internal friction of pier material.

If surcharge loading is not acted on the granular piles, it can be expressed as:

$$\tan \delta (\tan^2 \delta - 1) = 2 \tan \delta_p \quad (4.1)$$

Madhav and Vitkar [2] considered a general shear failure type mechanism for the analysis of soft soil reinforced by a gravel trench or pile and proposed an equation for estimating the ultimate capacity of granular pile which is expressed as:

$$q_{\text{ult}} = \frac{\gamma_c B}{2} N_\gamma + c N_c + D_f \gamma_c N_q \quad (5)$$

where,  $\gamma_c$  is bulk unit weight of the clay, and  $N_c$ ,  $N_q$  and  $N_\gamma$  are the bearing capacity factors which depend on the properties of trench, soil material and the ratio of  $A/B$ . The study is limited to strip footings in cohesive soils.

Mitchell [10] proposed a simple and empirical method to calculate the ultimate load capacity of a single granular pile which is expressed as:

$$q_{\text{ult}} = c N_p \quad (6)$$

where,  $N_p$  is the bearing capacity factor. It was recommended as 25, whilst Datye et al. [11] recommended 25–30 for such piles. Datye et al. also recommended as 40 and 45–50 in the case of uncased and cased rammed granular piles respectively. Barksdale and Bachus [6] suggested in the range of 18–22 for vibrated aggregate piles.

Barksdale and Bachus [6] assumed unit cell idealisation and considered that the bearing capacity, a group of aggregate piers under square and strip footing, can be determined assuming bilinear failure surface. The average shear strength parameters ( $\phi_{\text{avg}}$  and  $c_{\text{avg}}$ ) are expressed as:

$$\phi_{\text{avg}} = \tan^{-1}(n a_r \tan \phi') \quad (7)$$

$$c_{\text{avg}} = (1 - a_r)c \quad (8)$$

where,  $n$  and  $a_r$  are stress concentration factor and area replacement ratio respectively. The confining stress resisting the failure wedge is expressed as:

$$\sigma_3 = 0.5 \gamma_s B \tan\left(45 + \frac{\phi_{\text{avg}}}{2}\right) + 2c \quad (9)$$

where,  $\gamma_s$  is the unit weight of the surrounding soil and  $B$  is the footing width. The bearing capacity of aggregate piers group is estimated by using Eq. 10.

$$q_{\text{group}} = \sigma_3 \tan^2\left(45 + \frac{\phi_{\text{avg}}}{2}\right) + 2c_{\text{avg}} \tan\left(45 + \frac{\phi_{\text{avg}}}{2}\right) \quad (10)$$

Watts et al. [12] modified an equation proposed by Hughes and Withers [1] assuming shear deformation (bulging failure) in the pile at a depth of  $h$ , which is expressed as:

$$q_{ult} = K_{pc} [K_o(\gamma_s h - u_{so}) + u_{so} - u_s + 4c_u] \quad (11)$$

where,  $K_{pc}$  is the coefficient of passive earth pressure =  $(1 + \sin \phi')/1 - \sin \phi'$ ,  $K_o$  is the coefficient of earth pressure at rest for native soil =  $(1 - \sin \phi_s)$ ,  $u_{so}$  is the initial pore water pressure at depth  $h$ , and  $u_s$  is the pore pressure at depth  $h$ .

Ambily and Gandhi [3] carried out experimental study coupled with FEM numerical analyses on the granular piles installed in soft clay assuming unit cell. Based on the results, design charts were developed. A design procedure also suggested which ensured a required factor of safety and checks the settlement proposed an equation to determine limiting axial capacity of the pile considering surcharge on surrounding clay which is expressed as given in Eq. 12.

$$\sigma_{suq} = \sigma_{su} + (0.0088\phi'^2 - 0.5067\phi' + 10.86)q \quad (12)$$

where,  $\sigma_{suq}$  is the limiting axial stress with surcharge ( $q$ ),  $\phi'$  is the angle of internal friction of pier material and  $\sigma_{su}$  is the limiting axial stress without surcharge.

Afshar and Ghazavi [13] introduced a simple analytical method, verified using FEM analysis for estimation of the ultimate bearing capacity of the granular pile under bulging mode of failure using Coulomb lateral earth pressure theory. Granular piles were converted into equivalent and continuous strips of width  $W$ . The method is based on the lateral earth pressure theorem and requires conventional Mohr-coulomb shear strength parameters of the granular pile material and the native soil to be reinforced. An imaginary retaining wall was assumed as stretched vertically from the stone pile edge. The developed method is simple, efficient and useful for estimation of the ultimate bearing capacity of granular piles. Although the predictions made by the developed simple solution were satisfactory. Authors recommend that more laboratory and field tests and sophisticated numerical analyses should perform to quantify the predictions of the developed solution. The ultimate bearing capacity of the granular pile is expressed by the relation:

$$q_{ult} = cN_c + \bar{q}N_q + \frac{1}{2}W\gamma_c N_\gamma \quad (13)$$

where,  $c$  is the cohesion of surrounding soils,  $q$  is the surcharge pressure on passive region surface.  $\gamma_c$  is the unit weight of clay and  $N_c$ ,  $N_q$  and  $N_\gamma$  are the bearing capacity factors which depend on friction angle of the pile material and native soil.

Fattah et al. [14] presented a general equation which was obtained by carrying out statistical analysis using the SPSS (Statistical Package for the Social Sciences) program from conducting an experimental work and previous studies The propose

equation is used to estimate the bearing capacity ( $q_u$ ) of floating granular piles group installed in clays having different undrained shear strengths between (4 and 25) kPa and with different diameters and  $L/D$  ratios constructed by cased bored method, which is expressed as:

$$q_u = 15.34c_u^{0.401} A_s^{0.266} N_s^{0.084} (L/D)^{0.526} \tag{14}$$

where,  $c_u$  is the undrained shear strength of surrounding soils,  $N_s$  is the number of granular piles,  $A_s$  is the area replacement ratio and  $L/D$  is the length to pile diameter ratio.

### 3 Conclusion

The estimation of ultimate load capacity of granular pile through suggested formula by various researchers has been presented in Table 1.

**Table 1** Estimation of ultimate load capacity of granular piles by various researchers

Failure mode	Suggested formula	References
Bulging failure	$q_{ult} = (\gamma Z K_p + 2c_u \sqrt{K_p}) \frac{1+\sin \phi'}{1-\sin \phi'}$	Greenwood [12]
	$q_{ult} = (cF'_c + qF'_q) \frac{1+\sin \phi_s}{1-\sin \phi_s}$	Vesic [8]
	$q_{ult} = \frac{1+\sin \phi'}{1-\sin \phi'} (\sigma_{ro} - u + 4c)$	Hughes and Withers [1]
	$q_{ult} = K_{pc} [K_o (\gamma_s h - u_{so}) + u_{so} - u_s + 4C_u]$	Watts et al. [12]
	$q_{ult} = cN_c + \bar{q}N_q + \frac{1}{2} W \gamma_c N_\gamma$	Afshar and Ghazavi [13]
General shear	$q_{ult} = \left( q + \frac{2c}{\sin 2\delta_p} \right) \left( 1 + \frac{\tan \delta_p}{\tan \delta} \right) \tan^2 \delta_p$	Brauns [9]
Failure	$q_{ult} = \frac{\gamma_c B}{2} N_\gamma + cN_c + D_f \gamma_c N_q$	Madhav and Vitkar [2]
	$c_{avg} = (1 - a_r)c$ and $\phi_{avg} = \tan^{-1}(na_r \tan \phi')$	Barksdale and Bachus [6]
	$q_{group} = \sigma_3 \tan^2 \left( 45 + \frac{\phi_{avg}}{2} \right) + 2c_{avg} \tan \left( 45 + \frac{\phi_{avg}}{2} \right)$	
Sliding surface	$q = (1 - A_s)C_0 + (\gamma_s z + \mu_s \sigma_z) A_s \tan \phi_s \cos^2 \theta$ $\mu_s = \frac{n}{1+(n-1)A_s}$	Aboshi et al. [15]
General equation	$q_u = 15.34c_u^{0.401} A_s^{0.266} N_s^{0.084} (L/D)^{0.526}$	Fattah et al. [14]

## References

1. Hughes JMO, Withers NJ (1974) Reinforcing of soft cohesive soils with stone columns. *Ground Eng* 7(3):42–49
2. Madhav MR, Vitkar PP (1978) Strip footing on weak clay stabilized with a granular trench or pile. *Canadian Geotech J* 15(4):605–609
3. Ambily AP, Gandhi SR (2007) Behavior of stone columns based on experimental and FEM analysis. *J Geotech Geoenviron Eng ASCE* 133(4):405–415
4. Hasan M, Samadhiya NK (2017) Performance of geosynthetic-reinforced granular piles in soft clays: model tests and numerical analysis. *Comput Geotech* 87:178–187
5. Greenwood DA (1970) Mechanical improvement of soils below ground surfaces. In: *Proceedings of ground engineering conference, institution of civil engineers*, pp 11–22. London
6. Barksdale RD, Bachus RC (1983) Design and construction of stone columns: final Report SCEGIT-83–104. Federal Highway Administration, Washington DC
7. Han J, Ye SL (2001) Simplified method for consolidation rate of stone column reinforced foundation. *J Geotech Geoenviron Eng ASCE* 127(7):597–603
8. Vesic AS (1972) Expansion of cavities in infinite soil mass. *J Soil Mech Found Div ASCE* 98(3):265–290
9. Brauns J (1978) Initial bearing capacity of stone columns and sand piles. In: *Soil reinforcing and stabilizing techniques in engineering practice*, pp 497–512. Sydney
10. Mitchell JK (1981) Soil improvement-state-of-the-art report. In: *Proceedings of the tenth international conference on soil mechanics and foundation engineering*, vol 4, pp 506–565. Stockholm
11. Datye KR (1982) Settlement and bearing capacity of foundation system with stone columns. In: *Symposium on recent developments in ground improvement techniques*, pp 85–101. Bangkok
12. Watts KS, Johnson D, Wood LA, Saadi A (2000) An instrumental trial of vibro ground treatment supporting strip foundations in a variable fill. *Geotechnique* 50(6):699–708
13. Afshar JN, Ghazavi M (2014) A simple analytical method for calculation of bearing capacity of stone-column. *Int J Civil Eng* 12(1):15–25
14. Fattah MY, Al-Neami MA, Al-Suhaily AS (2017) Estimation of bearing capacity of floating group of stone columns. *Eng Sci Technol Int J* 20(3):1166–1172
15. Aboshi H, Ichimoto E, Harada K, Emoki M (1979) The composer-a method to improve the characteristics of soft clays by inclusion of large diameter sand columns. In: *Proceedings of the international conference on soil reinforcement. E.N.P.C.*, pp 211–216. Paris

# A Season-Wise Geotechnical and Morphological Study of Alteration in Coastal Profile Along the Shores of Puducherry, India



Nazeel Sabah, Arjun Sil, and G. Vijayakumar

**Abstract** Soil erosion in the coastal area (coastal erosion) is often a crucial issue in geotechnical aspects mainly with regards to the sediment transport phenomena accompanied by turbulent characteristics of breaking sea waves. This study takes into account a stretch of 1 km of coastline along Veerampattinam coastal stretch essentially to examine the erosion and accretion characteristics which would further lead to the estimation of sediment budgeting for the study area. A study of coastal wave dynamics was performed to understand the seasonal variations of the wave characteristics. The changes in the coastal morphology of the area have been studied periodically using a GPS device and this quantifies the volumetric changes in the beach morphology. The net sediment transport rate and also the quantity of the suspended sediments in motion is also estimated. The experimental results which suggest accretion along the southern part of the Veerampattinam breakwater and thereby erosion along the northern part are quite coherent with the practical observations. The study reveals that in the north-easterly monsoon and post-monsoon seasons, the zone of study experiences rampant erosion with around 20,000 m<sup>3</sup> of coastal sediment deposition. The study reveals that the phenomena of coastal erosion in the study area can be addressed by a sediment transfer amounting 24,436 m<sup>3</sup> of beach sand from the south side to the northern side of the breakwater.

**Keywords** Sediment transport rate · Suspended sediments · Wave-climate study · Coastal erosion · Accretion · Artificial beach nourishment

---

N. Sabah · A. Sil (✉)  
National Institute of Technology Silchar, Silchar, India  
e-mail: [arjun@civil.nits.ac.in](mailto:arjun@civil.nits.ac.in)

G. Vijayakumar  
Pondicherry Engineering College, Pondicherry, India  
e-mail: [gvk@pec.edu](mailto:gvk@pec.edu)



## 1 Introduction

Located along the Coromandel Coast, between latitudes  $11^{\circ}45'N$  and  $12^{\circ}03'N$  and longitudes  $79^{\circ}37'E$  and  $79^{\circ}53'E$ , Pondicherry has been a world-renowned tourist attraction since ages. The virgin beaches of this international city were renowned to be extraordinarily spectacular by the tourists. But since recent past, this tourism legacy is turning into a nightmare with the beaches getting crippled with a multitude of changes. Contamination, erosion, seawater intrusion and a countless number of other issues are arising day by day. This could prove to be a blot on the rich tourism legacy of the town. A lot of man-made intervention and natural phenomena are posing a great threat to this urban agglomeration. With the needs rising for a commercial harbor in the town, the harm to nature is in contrast with the so-called urban development.

Though a harsh coastal wave climate prevails only for less than a week in Puducherry (Upon observation of historic wave climate data), the effect of coastal erosion in the city is felt across a stretch of 6 km. Things worsened after a fishing harbor and its breakwaters were constructed at Thengaithittu, at the southern part of the city. Thereafter, the coastal erosion along the northern part of the city aggravated drastically. As an interim remedy, the government of Puducherry has constructed seawalls using massive boulders and plain cement concrete tetrapods to absorb the energy of the breaking waves. Coastal engineers are assigned a mammoth task of combating coastal erosion.

## 2 Need for Study

As a result of the construction of structures like groynes and breakwaters, the entire coastline particularly the beaches experience severe erosion and constant shorelines changes, the outcomes being drastic. The northern part of the coastline is experiencing erosion, whereas the southern part is either stable or undergoing accretion. The beaches, the lifeline of the town are slowly losing their pristine identity. In addition, there is supposed to be a remarkable tidal wave variation which is greatly impacting the fishermen folk. The beach land is getting engulfed by the sea water which is replacing the shoreline of Puducherry. The town is facing a reduction in the tourist economy. Every year a large amount of land area is being occupied by the sea. Various natural and man-made activities are primarily responsible for an unstable coastal zone. Longshore sediment transport, controlled mainly by nearshore topography and wave characteristics is an important factor which governs beach erosion. Waves generated deep in the ocean propagate to the nearshore and dissipate their energy on the coast leading to the sediments being lifted which further generate longshore currents and result in littoral sediment transport.

### 3 Wave Climate Measurement

There exists a wide variety of instruments for wave measurements, some of which are placed either at or below the sea-level. There exist some field instruments too to measure wave height and wave directions. The use of such instruments depend upon the required accuracy, repeatability and range of instrumentation needed. The prevailing environmental conditions are also crucial in deciding the choice of instrumentation. Previous works by Chen et al. [1] and (Katz) suggest some of the available instrumentation methods for coastal wave climate measurement. For the current study, online surf data from NIOT [2] and Magicseaweed [3] were collected periodically which claim that the data were procured from buoys installed in the nearshore environment of Pondicherry.

### 4 Definition of Wave Parameters

The actual processing of wave information is involved in the determination of wave statistics. The goal is producing a statistical estimate from the analyzed time series data to describe an irregular sea state in simple parametric form. The characteristic height  $H$  and characteristic period  $T$  are the two most important parameters necessary for adequately quantifying a given sea state. Other derived parameters from  $H$  and  $T$  may also be put to use in the parametric representation of the irregular seas. The definition of characteristic height includes the mean height and the root-mean-square height. Of these, the most commonly used height is the significant height which is quite similar to the visual height estimated by an experienced observer [4].

#### 4.1 Significant Wave Height

$H_s$  (or  $H1/3$ ), the significant wave height is the most important quantity to describe the state of a sea. Previous work by Sverdrup and Munk [5] gives an introduction to the concept of the significant wave height. The simplest method of calculating the significant wave height is by observing and ranking the waves in a wave record and then choosing the highest one-third waves. The average of the chosen wave gives the significant wave height as follows

$$H_s = \frac{1}{N/3} \sum_{i=1}^{N/3} H_i \quad (1)$$

## 5 Profile Calculation

The focus of our study was a kilometer long stretch of beach starting from the southern limb of the Veerampattinam breakwater southwards to Veerampattinam fishermen bay (see Fig. 1). The initial point chosen was chosen as the western face of the first visible column of the southern breakwater. The final point was at an offset of 64 m from the central column of the fishermen bay on the Veerampattinam coast. The stretch of around 1 km was further divided into intervals of 200 m. The Line of Sight was established by using a Vernier theodolite.

The study of the profile was continued across the three monsoon seasons namely pre-monsoon, post- monsoon and non-monsoon barring the months of November and December 2015 due to incessant rains in the region. The observation of the profile was done every fortnight when the tidal conditions were normal. After the line of sight was traced out, the profile observation was carried out with GARMIN E-TREX (see Fig. 2) G.P.S by procuring the Northing, Easting and Elevation details at fixed points.

Along the 1 km stretch, offsets at intervals of 5 m each were marked at every 200 m toward the sea till the point wetted by the sea water. The G.P.S was employed to obtain the coordinates and elevation at the offsets. The difference between the G.P.S elevations between corresponding fortnights gives an idea of the morphological changes of the beach profile. With the changes in beach profile obtained across the various weeks, the volumetric changes in the beach profile could be obtained and this could be later used for calculating the sediment budgeting which is defined as the accounting of sources, sinks and redistribution pathways of sediments in a unit region over unit time [6].



**Fig. 1** The southern experimental zone. *Source* Developed from Google Maps



**Fig. 2** GARMIN E-TREX G.P.S

Figures 3, 4, 5 and 6 above show the variation in beach morphology in longitudinal and transverse directions across various months corresponding to Monsoon and Post-Monsoon seasons.

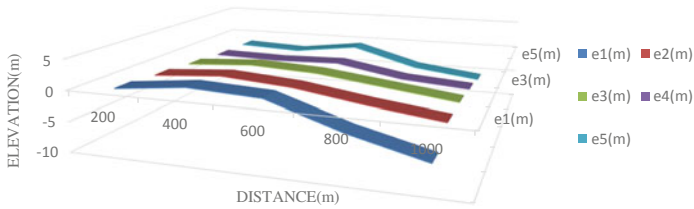


**Fig. 3** Coastal profile of Veerampattinam stretch (dated 5th September, 2015). e1, e2, e3, e4, e5 being offsets at 5 m intervals in seaward direction

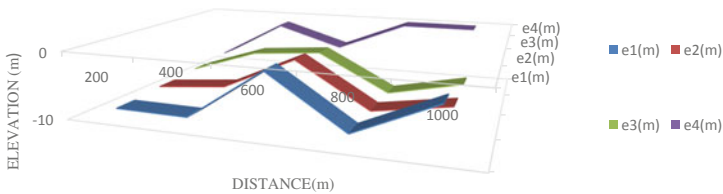


**Fig. 4** Coastal profile of Veerampattinam stretch (dated 17th October, 2015). e1, e2, e3, e4 being offsets at 5 m intervals in seaward direction

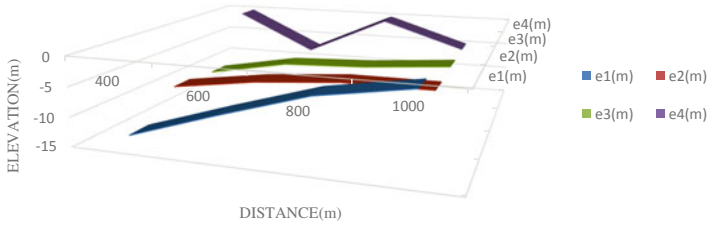


**Fig. 5** Coastal profile of Veerampattinam stretch (dated 31st January, 2015). e1, e2, e3, e4 being offsets at 5 m intervals in seaward direction

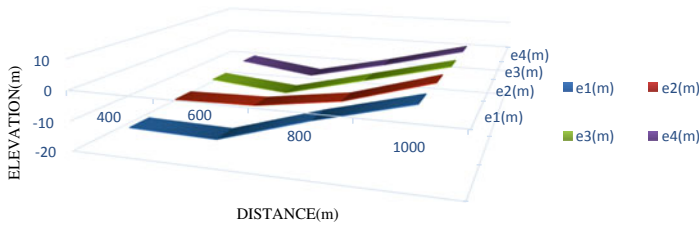


**Fig. 6** Coastal profile of Veerampattinam stretch (dated 28th February, 2015). e1, e2, e3, e4 being offsets at 5 m intervals in seaward direction

## 6 Measurement of Sediment Transport Rate

Tracers are one of the means of obtaining alongshore sediment transport rate, but the process gets difficult in practice as in most cases they (tracers) get buried or lost in transit. Another possible means to arrive at the sediment transport rate is from the measured volume of deposited sand. But this process also lacks practical feasibility. For the current study, a set-up was made to collect suspended sediments and sand samples which are presented in the following clauses.

### 6.1 Sediment Samples Collecting System

As the area of study was a stretch of only a kilometer, the scope of sand trap [7] (an indigenously developed tool for trapping suspended sediments) was undermined and the collection of sediment samples were performed manually with sampling bottles and the number of suspended sand particles per  $m^3$  of water sample were found out.

## 6.2 Collection of Sand Samples

The sand sediments are collected from the study area at every 200 m intervals. The sand sampling is done at both the intermediate zone and the splash zone. In the situation of lack of sand trap, the collection done is manual assuring that only top layer sand up to a depth of 1 mm only was obtained. After obtaining the sand samples, they were subjected to sieve analysis to obtain the predominant particle size at each zone. This could give a rough idea of the predominant size of the particles in motion in both intermediate and splash zones. The collected sand was carefully preserved in sealed sampling bags, and later subjected to laboratory sieve analysis for obtaining the predominant particle size. The predominant particle size is obtained by computing D10, D30 and D60 values from the semi-log plot of sieve analysis.

## 7 Calculation of Wave Parameters, Potential Sediment Transport Rate and Profile Volume

The wave parameters such as wave height and direction are referred from on-line wave surf data Magicseaweed [3], NIOT [2] and calculations are made.

The longshore sediment transport takes place by beach drifting and transport in the breaker zone. The longshore sediment transport rate may be computed by employing energy flux methods which relate sediment transport with wave-generated momentum or energy gradient. CERC method as used by Vijayakumar et al. [8] was found suitable for this study area. The CERC method for bulk sediment transport rate is expressed in Eq. 2.

$$Q_{th} = 330H_{sb}^{5/2} \sin^2 \alpha_b (m^3/hr) \quad (2)$$

where  $H_{sb}$  is the near shore-breaking wave height,  $\alpha_b$  is the breaker angle. It can be seen that  $Q_{th}$  is a function of 'H' and  $\alpha$  only.

The elevation of total profile near the shoreline and just above shoreline is taken using GPS for the entire stretch. The elevations of various grids are known and its area is calculated using Simpson formula (Eq. 3) [9] and thereafter volume of the sections are calculated (Eq. 4) as follows

$$\text{Area} = \left( \frac{e_1 + e_n}{2} + e_2 + e_3 + \dots \right) * D \quad (3)$$

where  $e_1, e_2 \dots$  = elevation of the sections;  $D$  = interval between elevations

$$\text{Volume} = (A_1 + A_2) * D \quad (4)$$

where  $A_1, A_2$  = area of the section.

## 8 Results

The result obtained from the calculation of the net sediment transport at Veerampattinam coastal stretch can be highlighted as follows:

- During the month of July–September, i.e. south-westerly Monsoon, the net sediment movement is southerly and hence most of the sediments get trapped on the up-drift side of the breakwater field which results in the formation of beach till the mouth of the breakwater. The net drift is 5126.87 **m<sup>3</sup>/day** which is towards South. For this season, the predominant particle size in the intermediate zone was 0.177 mm and that in the Splash zone was 0.157 mm. The amount of suspended sediments obtained in this season is 3.0139 kg/m<sup>3</sup>.
- During the month of October–December i.e. north-easterly Monsoon, the sediment movement is northerly and the net drift is 3417.72 **m<sup>3</sup>/day** North direction. For this season, the predominant particle size in the intermediate zone was 0.1446 mm and that in the Splash zone was 0.0948 mm. The amount of suspended sediments obtained in this season is 1.86 kg/m<sup>3</sup>.
- During the month of January–March, i.e. non monsoon or post-monsoon period the sediment movement is predominantly northerly and the net drift is 3139.71 **m<sup>3</sup>/day** North direction. For this season, the predominant particle size in the intermediate zone was 0.1304 mm and that in the Splash zone was 0.108 mm. The amount of suspended sediments obtained in this season is 2.4786 kg/m<sup>3</sup>.
- It was observed from the volumetric profile calculation that there was a significant difference between the beach profiles for various monsoon seasons. There was significant growth in the volume of the beach during the north-westerly and Non-Monsoon season, thereby indicating accretion in the southern zone and erosion in the Northern zone.

The results so obtained are summarized in the following tables (Tables 1 and 2)

## 9 Conclusion

From the results the following conclusion can be drawn:

- Construction of breakwater field at the Veerampattinam region has created an imbalance situation in the coastal stretch of about 1 km.

**Table 1** Volumetric difference of the profile across various seasons

Season	Months	Wedge volume for two observations in a season (m <sup>3</sup> )	The difference in volume (m <sup>3</sup> )	Accretion/erosion at southern zone
South-Westerly monsoon	Jul–Sept 2015	1. –110,645.2 2. –152,716.1	–42,070.9	Erosion
North-Easterly monsoon	Oct–Dec 2015	3. –213,350.6 4. –194,286.3	+19,064.3	Accretion
Post-monsoon	Jan–Mar 2016	1. –145,574.7 2. –123,811.8	+21,763.7	Accretion

**Table 2** Net Sediment transport rate and amount of suspended sediments

Type of monsoon	Months	Net average sediment transport rate (Q <sub>net</sub> ) (in m <sup>3</sup> /day)	Predominant particle size collected		Amount of suspended sediments (kg/m <sup>3</sup> )
			Intermediate zone (mm)	Splash zone (mm)	
South-westerly	July–September 2015	–5126.87 (Erosion at southern zone)	0.1772	0.1576	3.0139
North-easterly	October–December 2015	3417.72 (accretion at southern zone)	0.1446	0.0948	1.86
Non-Monsoon	January–March 2016	3139.71 (accretion at southern zone)	0.1304	0.108	2.4786

- Since the predominant movement of sediment is northerly, there is a predominant accretion in the southern region and pronounced erosion in the northern zone
- According to the volumetric calculations performed, a sediment transfer amounting 24,436 m<sup>3</sup> of beach sand from south side to the northern side has to be performed.
- Sediment by-passing (a technique of transferring the excessive accreted sand from the accreting zone to the eroding zone) is the best alternative than the conventional hard solutions as this turns to be a more feasible one.
- If this situation continues, the entire coastal stretch with natural beaches will be destroyed and it will lead to a threat to biodiversity.



## References

1. Chen G-Y, Chien H-C (2008) Measuring progressive edge wave by a single instrument: applications in tsunami and typhoon waves. In: 2008 Taiwan-polish joint seminar on coastal protection, pp. A37-A48
2. NIOT (2015–2016, July-March) Ocean observation systems. Retrieved from National Institute of Ocean Technology: <https://www.niot.res.in/index.php/node/index/128/>
3. Magicseaweed (2015–2016, July-March) Wave buoys and weather stations. Retrieved from magicseaweed.com: <https://magicseaweed.com/Sri-Lanka-Wave-Buoys/54/?wave=true&wind=true&ll=7.74%2C80.69&zoom=7>
4. Kinsman B (1965) Wind waves. In: Kinsman B (eds) *The Generation and propagation on the ocean surface*. Prentice Hall Incorporated
5. Sverdrup H, Munk W (1974) *Wind, sea and swell: theory of relations for forecasting*. Hydrographic Office Publications, U.S department of Navy, p 44
6. Slaymaker O (2003) The sediment budget as conceptual framework and management tool: the interactions between sediments and water (Guest Editor: Brian Kronvang). *Hydrobiologia*, pp 1–3
7. Verhoeven R, Huygens M, Poucke LV, Witter J, Hakvoort H (1996) Design of a smart sand trap construction as a part of an interregional environmental study. *Trans Eng Sci*
8. Vijayakumar G, Rajasekaran C, Sundararajan T, Govindarajulu D (2014) Studies on the dynamic response of coastal sediments due to natural and manmade activities for the Puducherry coast. *Indian J Mar Sci*
9. Cook M, Rimmer (1993) *Maths Xtra*. Stafford College, Stafford, katz, I. (n.d.). Ocean wave measurements. *APL technical Digest*

# **Computational Geomechanics**

# Numerical Analysis of Hybrid Back-To-Back MSE Wall with Select and Marginal Backfill



Gopika Rajagopal and T. K. Sudheesh

**Abstract** Back-to-back mechanically stabilized earth (MSE) walls are extensively used in transportation development projects worldwide due to their effectiveness, ease of construction, and cost efficiency. As per Federal Highway Administration (FHWA) guidelines, such MSE walls are to be backfilled with high-quality select fill in both reinforced and retained zones. However, considering the scarcity of high-quality fill and increased cost associated with the procurement of such material, the Indian Roads Congress (IRC) has recommended the use of inferior soil ( $\phi \geq 25^\circ$  and  $PI \leq 20\%$ ) in specific configuration in the retained zone for six lane projects. The present study investigates the deformation response and global stability of back-to-back MSE wall due to the inclusion of marginal soil fill in the central region of the wall. Numerical analysis using finite element software PLAXIS 2D was carried out by varying the size of marginal fill zone to investigate their effect on the behavior of wall. Specifically, the analysis was performed by varying the quality and relative dimensions of marginal soil zone to examine their effect on factor of safety and horizontal and vertical deformations. The results indicated that the quality and height of retained soil has minimal influence on global safety factor and horizontal deformation when the marginal fill is within the retained zone. However, notable increase in deformation and decrease in safety factor were observed for base width beyond 2.2H. Also, differential surface settlement of hybrid wall was found to be less than that of conventional MSE wall.

**Keywords** Back-to-back MSE walls · Reinforced fill · Marginal fill · Numerical analysis · Soil deformation

## 1 Introduction

Mechanically stabilized earth walls have gained acceptance in roadway projects as in bridge abutments, wing walls, and a way to minimize the right-of-way requirements.

---

G. Rajagopal (✉) · T. K. Sudheesh  
Indian Institute of Technology, Palakkad, Kerala, India

Back-to-back configuration of MSE walls are typically used in highway ramps and embankments approaching bridges. According to FHWA classification, such type of wall is categorized under complex geometry [1]. Hence, limited number of resources are available in literature describing the detailed design procedure of back-to-back MSE walls. FHWA [1] suggests independent design of each wall if the distance between the walls ( $D$ ) is greater than interaction distance,  $D_i$  (Eq. 1) as active thrust behind each wall is completely mobilized in this scenario.

$$D_i = H \cdot \tan(45 - \phi/2) \quad (1)$$

where  $H$  and  $\phi$  are height of the wall and angle of internal friction of backfill, respectively.

Another important factor considered in the design of MSE wall is the quality of backfill material. As per various codal provisions [1–3], select granular fill (fine content < 15%, Plasticity Index (PI)  $\leq$  6%) should be used in the reinforced zone. However, particularly for back-to-back MSE walls, FHWA [1] has recommended to use high-quality select fills in both reinforced and retained zones if the width of retained zone is less than half of the wall height. Indian Roads Congress [3] has suggested specific configuration of retained fill ( $\phi \geq 25^\circ$  and PI  $\leq 20\%$ ) for highways having six lanes and more. But, no detailed studies are available in literature on such hybrid combination of reinforced and retained fills in back-to-back MSE walls.

Still, considering the ease of availability and substantial cost savings, marginal soils are commonly used as reinforced and retained backfill. Owing to the fact that 50–75% of total cost is taken by backfill, ample cost reduction up to 20–30% can be achieved by using locally available soil [4, 5]. Several studies were reported on the behavior of MSE walls with marginal fill and efficacy of various methods such as use of electrokinetic geosynthetics, sand cushion, encapsulated geogrid, and hybrid geosynthetics to improve their overall performance [6–10]. However, it is alarming that most of the reported case studies regarding reinforced wall failure was associated with marginal backfill. It is evident from the recently published database of geosynthetic reinforced wall failures that more than 60% of total 171 failure cases were due to the improper drainage behind the reinforced zone [11]. The poor drainage results in developing positive pore water pressure in the fill, which in turn causes excessive deformation and reduces the strength, stiffness, and interfacial shear resistance of reinforcement [4, 12–14].

It is expected that a trade-off between cost and stability can be achieved by using well graded granular soil in the critical regions of MSE wall where it is inevitable and marginal soil in the remaining areas of backfill. Such partial replacement results in a hybrid combination of select and marginal fill. This paper presents the numerical analysis performed to study the deformation behavior and global stability factor of such hybrid back-to-back MSE walls in drained condition. The influence of varying width and height of marginal fill zone on the behavior of the wall was investigated.

## 2 Numerical Modeling

The study of back-to-back MSE wall was carried out using numerical two-dimensional finite element software, PLAXIS 2D. The geometric dimensions and parametric properties of baseline model (Fig. 1a) were taken from the literature [15, 16]. The W/H ratio, height, and length of the reinforcement were considered as 3, 6 m, and 0.7H, respectively.

In conformity with IRC recommendations [3], a back-to-back wall with central trapezoidal marginal fill zone was selected as the hybrid configuration in the present study (Fig. 1b). Different combinations of base width and vertical height were considered for trapezoidal marginal fill zone in the analysis. However, the slant height of the trapezoidal zone was always governed by Rankine’s failure line. The first set of analysis was performed for trapezoidal marginal fill zone with base width equal to the distance between reinforced zone (i.e.,  $b = 1.6H$ ). The height of the marginal fill was varied from 0.5H to 1H. Then, the analysis was repeated by increasing the base width at an increment of 0.2H up to 2.8H. Also, three types of marginal fill material with different friction angle ( $\phi = 25^\circ, 20^\circ$  and  $15^\circ$ ) was chosen in the analysis. The influence of properties, height, and base width of marginal fill zone on factor of safety, horizontal, and vertical deformations were investigated.

The wall was simulated using plane strain model with 15-noded triangular elements. The facing panel and reinforcement were modeled as plate and geogrid elements, respectively. A total of four panels each of 1.5 m height and 0.14 m thickness were used. The foundation soil was considered as hard stratum. The simulation of the real field construction of wall was completed in multiple stages using staged construction calculation type. A lift thickness of 0.375 m was adopted. Subsequent to the simulation of construction, an additional phase was created to perform safety analysis. The parametric properties of materials used for modeling are given in Table 1.

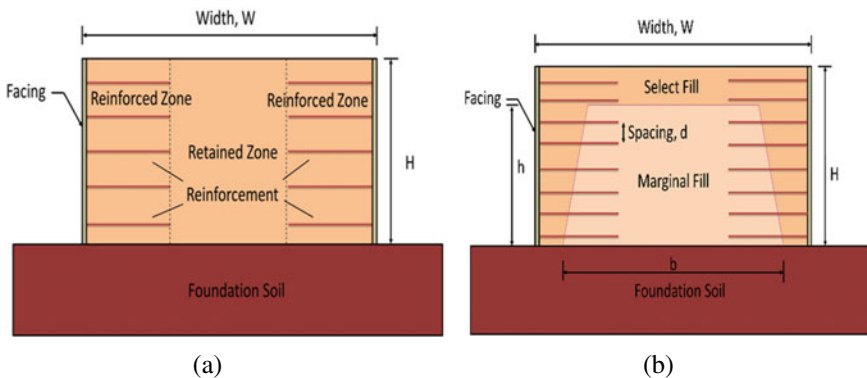


**Fig. 1** a Baseline wall with complete select fill; b hybrid wall with marginal core surrounded by select fill

**Table 1** Parametric properties for finite element modeling

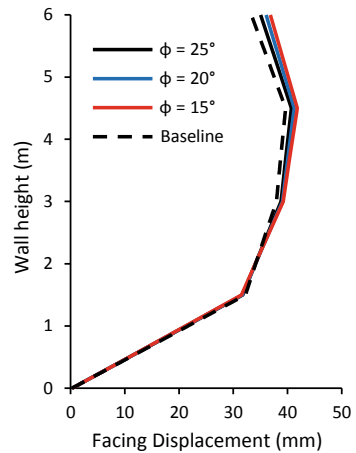
Material	Foundation soil	Select fill	Marginal fill	Geogrid	Facing panel
Model	Mohr–coulomb	Mohr–Coulomb	Mohr–coulomb	Elasto-plastic	Elastic
Drainage	Drained	Drained	Drained	–	–
Unit weight (kN/m <sup>3</sup> )	22	18	18	–	–
Cohesion (kN/m <sup>2</sup> )	100	0	0	–	–
Friction angle (°)	30	35	25, 20, 15	–	–
Dilation angle (°)	0	5	5	–	–
Axial stiffness (kN/m)	–	–	–	1100	$3.5 \times 10^6$
Bending stiffness (kN m <sup>2</sup> /m)	–	–	–	–	5717

### 3 Results

#### 3.1 Horizontal Facing Displacement

The variation of horizontal displacement along the wall facing for different types of marginal fills ( $\phi = 25^\circ, 20^\circ, 15^\circ$ ) in trapezoidal core with height,  $h = 0.5H$ , and base width,  $b = 1.6H$  are presented (Fig. 2). As evident from the figure, quality of the

**Fig. 2** Variation of facing displacement with decreasing quality of marginal fill (marginal core base width = 1.6H and height = 0.5H)



core has minimal influence on the horizontal deformation of the wall. The maximum lateral movement along the walls varied as 40–42 mm from the baseline model to hybrid model with marginal fill ( $\phi = 15^\circ$ ) and was located approximately 4.5 m from the base of the wall.

The variation of horizontal displacement along the wall facing with increase in the height of the marginal fill zone for a constant friction angle of  $25^\circ$  was plotted (Fig. 3). No significant increase in horizontal displacement was noticed by increasing the height of marginal fill zone with a base width of 1.6H. Similar responses were

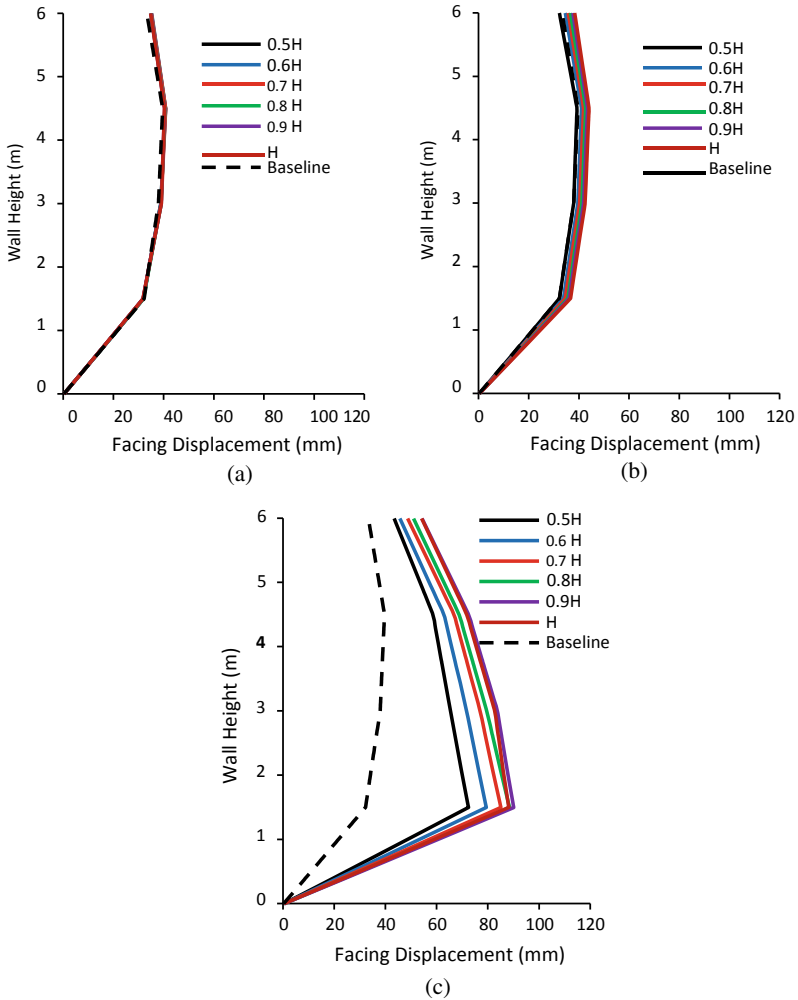
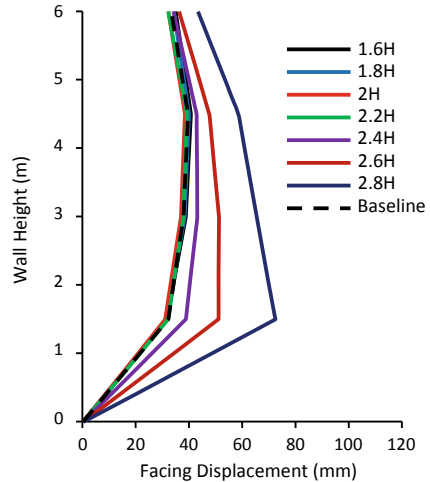


**Fig. 3** Variation of facing displacement with increasing height of marginal fill core ( $\phi = 25^\circ$ ). **a** Base width = 1.6H; **b** base width = 2.2H; **c** base width = 2.8H

**Fig. 4** Variation of facing displacement with increasing base width of marginal fill core ( $\phi = 25^\circ$ ;  $h = 0.5H$ )



noticed for other base width as well. However, the variation of horizontal deformation with increase in fill height was more pronounced at larger base width ( $>2.2H$ ).

Similarly, graph was plotted by varying the base width of marginal fill zone (Fig. 4) for a constant height of  $0.5H$  and friction angle  $25^\circ$ . As can be seen from figure, no much variation in displacement profile was observed until a base width of  $2.2H$ , whereas there was a major deviation beyond  $2.2H$ .

### 3.2 Vertical Surface Settlement

The variation in surface settlement for hybrid models having two different marginal fill base width for varying height are presented along with that of baseline model (Fig. 5). The surface settlement of the reinforced zone was not significantly increased by the inclusion of marginal fill in the retained zone. However, an increase in settlement of the reinforced zone was identified with the increase of marginal fill base width. This is due to the fact that the marginal fill occupies some portion of the reinforced zone as base width increases. Interestingly, the observed differential surface settlement of the hybrid back-to-back walls with marginal fill base width up to  $2.4H$  was less than that of baseline model. The influence of marginal fill height on the differential settlement of the walls was found to be minimal. It should be noted that the observed surface settlement was only due to the vertical deformation of MSE fill as the foundation soil was modeled as hard stratum.

Surface settlement profile of different marginal fill base width is depicted in Fig. 6. As can be seen from figure, the surface settlement within the reinforced zone was observed to be comparable up to a marginal fill base width of  $2.4H$ . However, considerable increase was noticed beyond a base width of  $2.4H$ . As mentioned previously,



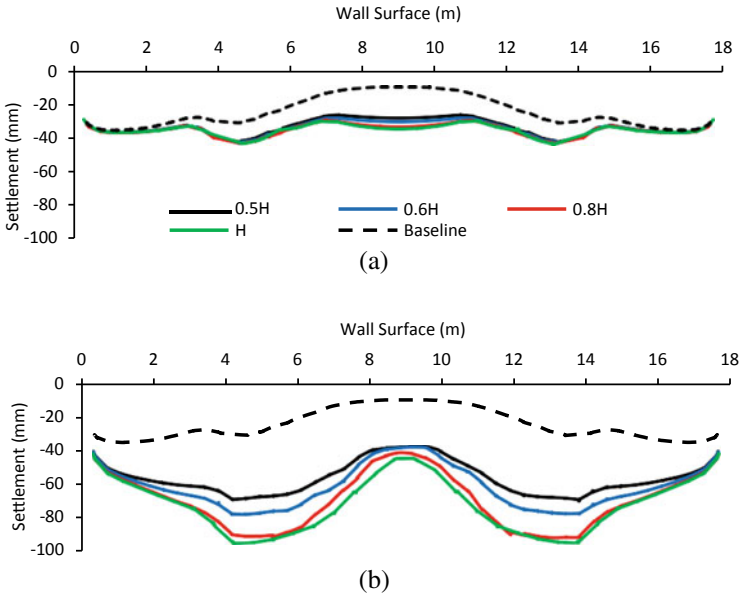


**Fig. 5** Variation of surface settlement with increasing height of marginal fill core ( $\phi = 25^\circ$ ). **a** Base width = 1.6H; **b** base width = 2.8H

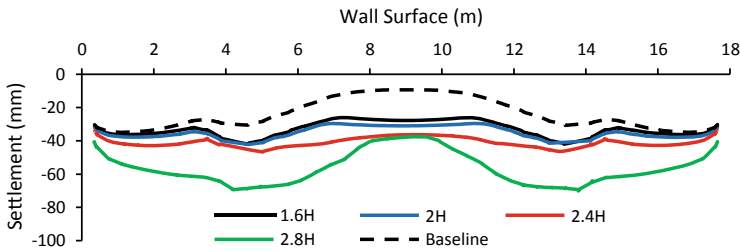


**Fig. 6** Variation of surface settlement with increasing base width of marginal fill core ( $\phi = 25^\circ$ ;  $h = 0.5H$ )

the differential surface settlement was not significant for base width in the range of 1.6H to 2.4H compared to the baseline model. The differential settlement increases with further increase in the base width.

### 3.3 Factor of Safety

Following the simulation of construction phase, a strength reduction analysis ( $c$ - $\phi$  reduction) method implemented in PLAXIS 2D was adopted to determine the global

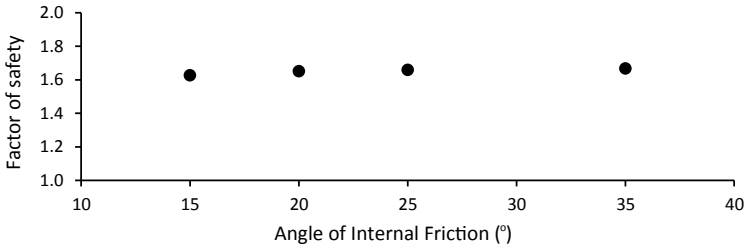


**Fig. 7** Variation of factor of safety with decreasing quality of marginal fill core ( $\phi = 25^\circ$ ;  $h = 0.5H$ )

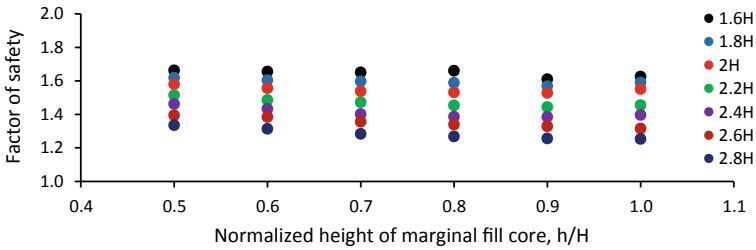


**Fig. 8** Variation of factor of safety with increasing height and base width of marginal fill core ( $\phi = 25^\circ$ )

safety factor of the system. The global failure surface for the model was obtained from incremental shear strain plot after safety analysis [17]. The variation of global factor of safety of hybrid model (marginal fill base width = 1.6H and height = 0.5H) with different quality of marginal fill material is presented in Fig. 7. Although the factor of safety decreased with the decrease in angle of internal friction of the fill, the difference was found to be marginal (1.67 for baseline vs. 1.63 for 15° marginal fill).

The variation of factor of safety with increasing the base width and height of marginal fill zone is summarized in the plot (Fig. 8). No considerable decrease of factor of safety was identified with increase in fill height. Similarly, reduction in factor of safety was minimal with increase of marginal fill base width up to 2.0H. Notable decrease in safety factor was observed with further increase of base width.

### 4 Conclusion

This study investigated the behavior of back-to-back MSE wall with hybrid combination of select fill and marginal sandy soil with less fines under drained condition. The analysis considered a trapezoidal marginal fill zone in the middle of back-to-back wall. The influence of marginal fill quality and dimensions on factor of safety

and horizontal and vertical deformation are analyzed. It was noticed that base width of marginal core has more influence than its height and thus found to be an important factor in designing hybrid back-to-back MSE wall. Following observations are recorded from the present analysis:

1. Horizontal deformation of the wall was minimally influenced by the quality and height of marginal fill having a maximum base width of  $2.2H$ .
2. Differential surface settlement of hybrid back-to-back walls with marginal fill base width up to  $2.4H$  was less than that of conventional fill walls.
3. The global safety factor of the proposed hybrid configuration was comparable with that of conventional system up to a maximum marginal fill base width of  $2.0H$ .

## References

1. Berg R, Christopher B, Samtani N (2009) Design of mechanically stabilized earth walls and reinforced soil slopes I, FHWA
2. AASHTO (2012) American Association of State Highway and Transportation Officials, Washington DC, USA
3. IRC:SP:102 (2014) Guidelines for design and construction of reinforced soil walls. Indian Roads Congress
4. Christopher B, Stulgis R (2005) Low permeable backfill soils in geosynthetic reinforced soil walls: state-of-the-practice in North America. In: Proceedings of North American geo-synthetics conference (NAGS 2005), pp 14–16
5. Koerner J, Soong T-Y, Koerner R (1998) Earth retaining wall costs in the USA. Geosynthetic Research Institute
6. Abdi M, Arjomand M (2011) Pullout tests conducted on clay reinforced with geogrid encapsulated in thin layers of sand. *Geotext Geomembr* 29(6):588–595
7. Bhattacharjee D, Viswanadham B (2015) Numerical studies on the performance of hybrid-geosynthetic-reinforced soil slopes subjected to rainfall. *Geosynthetics Int* 22(6):411–427
8. Glendinning S, Jones C, Pugh R (2005) Reinforced soil using cohesive fill and electrokinetic geosynthetics. *Int J Geomech* 5(2):138–146
9. Raisinghani D, Viswanadham B (2010) Evaluation of permeability characteristics of a geosynthetic-reinforced soil through laboratory tests. *Geotext Geomembr* 28(6):579–588
10. Raisinghani D, Viswanadham B (2011) Centrifuge model study on low permeable slope reinforced by hybrid geosynthetics. *Geotext Geomembr* 29(6):567–580
11. Koerner RM, Koerner GR (2013) A data base, statistics and recommendations regarding 171 failed geosynthetic reinforced mechanically stabilized earth (mse) walls. *Geotext Geomembr* 40:20–27
12. Chen H-T, Hung W-Y, Chang C-C, Chen Y-J, Lee C-J (2007) Centrifuge modeling test of a geotextile-reinforced wall with a very wet clayey backfill. *Geotext Geomembr* 25(6):346–359
13. Koerner R, Koerner G (2011) The importance of drainage control for geosynthetic reinforced mechanically stabilized earth walls. *J GeoEngineering* 6(1):3–13
14. Yoo C, Jung H-Y (2006) Case history of geosynthetic reinforced segmental retaining wall failure. *J Geotech Geoenviron Eng* 132(12):1538–1548

15. Benmebarek S, Attallaoui S, Benmebarek N (2016) Interaction analysis of back-to-back mechanically stabilized earth walls. *J Rock Mech Geotech Eng* 8(5):697–702
16. Han J, Leshchinsky D (2010) Analysis of back-to-back mechanically stabilized earth walls. *Geotext Geomembr* 28(3):262–267
17. Guler E, Hamderi M, Demirkan M (2007) Numerical analysis of reinforced soil-retaining wall structures with cohesive and granular backfills. *Geosynthetics Int* 14(6):330–345

# Numerical Modeling by Finite Elements for a Pile Foundation Under Tension Load



B. K. Huchegowda, Chethan Bagoor, and G. Kalyan Kumar

**Abstract** The pull out test is a rare test conducted on pile foundation. It is generally conducted to evaluate the resistance of a pile against the various uplift forces generated. Some of the major uplift forces generated are due to seismic activity, wind loads, and unstable sand conditions such as quick sand condition. The geotechnical investigations are conducted for the proposed 60 MW solar PV plant at Tamil Nadu. Field tests were carried out to determine uplift capacity of concrete piles of 0.3 and 0.35 m diameters of L/D ratio 4–5. Totally, eight number of piles were tested in the field. In the preset study, an attempt has been made to determine pull out capacity of piles by numerical modeling using PLAXIS 2D software. A comparative study on uplift capacity of piles has been carried out with the field data. The results obtained from the study indicated that the pile surface characteristics, pile–soil friction angle, and earth pressure coefficient are all significant variables affecting the ultimate uplift capacity of a pile foundation. Further, it is found from the study that there is a close agreement of uplift resistance of piles obtained from the numerical studies with respect to field results.

**Keywords** PLAXIS 2D · Field test · Young's modulus · Short pile

## 1 Introduction

Deep foundations in the form of piles are used when soft compressible strata exist near the ground surface and extend up to large depths. Long piles are used to transfer the heavy load from super structure to ground below the weak soil or to hard rock or below the water to the high bearing capacity. Piles are normally used on normal

---

B. K. Huchegowda  
IIT Hyderabad, Hyderabad, Telangana, India

C. Bagoor · G. Kalyan Kumar (✉)  
NIT Warangal, Warangal, Telangana, India  
e-mail: [kalyan@nitw.ac.in](mailto:kalyan@nitw.ac.in)

ground level to resist the uplift load and the horizontal load of multi-storied buildings, high towers, earth walls, bridge abutments, and dolphins. Piles also provide a convenient method of construction of works over water, such as jetties or bridge piers. Piles are sometimes used to control earth movements. Pile group is a combination of the pile cap and piles. Piles are made up of wood, steel, and concrete. Pile foundations are often subjected to axial loads, lateral loads, moments, and uplift. Piles are designed, depending upon the type of the soil, pile material, and loading condition. Load transmission from the pile is depending on the pile–soil interaction, but understanding of this problem is very complicated [1, 2]. The phenomenon is a function of pile material, its surface characteristics, L/D ratio, soil–pile interaction angle, shape of pile and group, installation conditions and boundary conditions, consolidation, shear properties of soil, location of water table, and type of loading [3]. Excessive theoretical and experimental investigations are available on the behavior of single piles and pile groups subjected to axial, inclined, and lateral compressive loads. Uplift piles are used to resist the water pressure in dams, wind load from the high rise building, anchors of towers, and bulkheads. Laterally loaded capacity of single and group piles are evaluated using PLAXIS and FDM method; it shows that the numerical results are well comparable with the field results [4]. In case, the lateral loads are large incremental of diameter which is effective than the length [5]. Pull out test is a rare test conducted on pile foundation. It is generally conducted to evaluate the resistance of a pile against the various uplift forces generated. Some of the major uplift forces generated are due to seismic activity, wind loads, unstable sand conditions such as quick sand condition etc. In areas where the top soil is not of much strength and hard strata are available at a greater depth and foundation is to be installed at economic rate, piles are most suited. In areas of high winds, the forces caused by the wind causes uproot of the pile from the ground surface. Pull out test is such a test which simulates the field condition of wind pressure by pulling out the pile and causing the pile to uproot from the soil to be tested. The main objectives of the study are: To study the effect of surface characteristics on 300 and 350 mm diameter piles. The numerical results of the piles have been compared with the experimental results and predicted values. Present state of knowledge on soil–pile–uplift load as critically reviewed from the literature [6]. Identifications of the parameters effect on the uplift behavior of piles are carried out in this study. Research problems with shortcoming are addressed for future work.

## 2 Properties of Soil

In this analysis, the required field data have been taken from the technical report on the geotechnical and geophysical investigation for the proposed 60 MW solar PV plant at Tamil Nadu, India. The different laboratory tests on soils are given below. Geological observations are made in the proposed site and nearby areas. Geologically, the area consists of Granitic Gneisses of Precambrian age. Few outcrops are seen in the area, and majority of the out crops show Gneissic textures. Grain size analysis

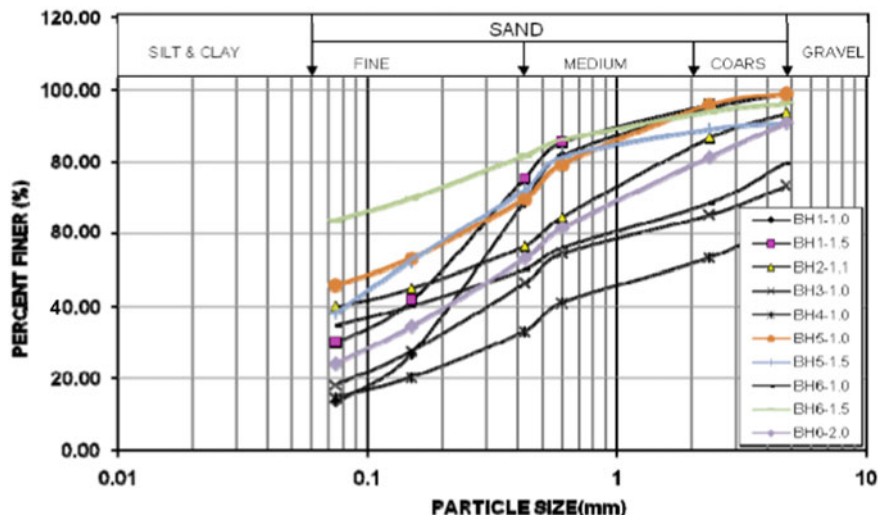


Fig. 1 Grain size analysis

is shown in Fig. 1, and detailed soil parameters are given in Table 1. Safe bearing capacity has been determined based on both shear and settlement criteria [7] as per

Table 1 Properties of soil

Bore hole	Depth (m)	SPT	Dry density (g/cc)	Sp. gravity	Voids ratio ( $e$ )	C (Kpa)	$\phi^\circ$
BH1	1		1.93	2.66	0.38	0	31
	1.5	>50	-	-	-	-	-
BH2	1.1	>50	-	-	-	-	-
BH3	1	>50	-	-	-	-	-
BH4	1	>50	-	-	-	-	-
BH5	1	30	-	-	-	-	-
	1.5	>50	-	-	-	-	-
BH6	1		1.85	2.68	0.45	2	32
	1.5	18	-	-	-	-	-
	2	>50	-	-	-	-	-
BH7	1		1.89	2.67	0.41	2	33
	1.5	37	-	-	-	-	-
	2	>50	-	-	-	-	-
BH8	1		1.92	2.67	0.39	1	32
	1.5	>50	-	-	-	-	-
BH9	0.5	>50	-	-	-	-	-

**Table 2** Safe bearing capacity of soil in different location

Borehole NO	Depth below GL (m)	Types of strata	SBC (t/m <sup>2</sup> )
BH1, BH2, BH3, BH4, BH5, BH8, BH9	1.5	Soft disintegrated weathered rock	20
BH6	1.5	Silty sand	15
	2.0	Soft disintegrated weathered rock	22
BH7	1.5	Silty sand with gravel	17
	2.0	Soft disintegrated weathered rock	22

relevant IS codes. SBC calculations have been carried out for footing of width 1.5 m for 25 mm settlement. The  $N$ -values from SPT at various depths are given in Table 1. The safe bearing pressures determined are given in Table 2.

### 3 Evaluation of Uplift Capacity

#### 3.1 Theoretical Estimation of Uplift Capacity of Pile (Pile No 1, BH1)

Based on the geotechnical investigation report, the following parameters have been selected to arrive at the uplift capacity of pile.

Data pile diameter = 300 mm.

Pile length = 1.45 m.

Angle of internal friction =  $\phi = 31^\circ$ .

Dry density =  $\gamma_d = 19.3 \text{ KN/m}^3$ .

Friction factor =  $\delta = 3/4 \times 31 = 23.25^\circ$ .

Earth pressure coefficient =  $K = 1.5$ .

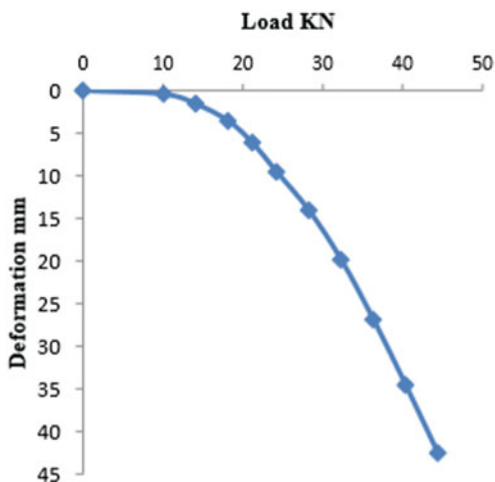
Ultimate pull out resistance of pile

$$\begin{aligned}
 Q_{ut} &= A_s K \sigma'_v \tan \delta + \text{Weight of pile} \\
 &= (\pi \times 0.3 \times 1.45 \times 1.5 \times 0.5 \times 1.45 \times 19.3 \times \tan 23.5) \\
 &\quad + (\pi/4 \times 0.32 \times 1.45 \times 24) \\
 &= 12.32 + 2.46 \\
 &= 14.78 \text{ KN}
 \end{aligned}$$

Safe capacity of Pile =  $14.78/2.5 = 5.89 \text{ KN}$ .



**Fig. 2** Variation of uplift load with lateral deflection for pile 1 (field test)



### 3.2 Field Test for Estimation of Uplift Capacity of Pile (Is 2911 Part 4)

Pile number 1 near BH1 having 0.3 m diameter was tested for determining the pull out capacity. The length of pile is 1.45 m. Load versus deformation curve from the field test is shown in Fig. 2

### 3.3 Finite Element Method

Pull out test was carried out using PLAXIS 2D. The detailed parameters [8] are given in Table 3, model of pile is shown in Fig. 3 and load versus deformation curve obtained from Plaxis analysis is shown in Fig. 4.

**Table 3** Parameter of soil and pile used in PLAXIS for pile 1

Parameter	Name	Sand	Pile	Units
Soil unit weight above phreatic level	$\gamma_{unsat}$	19.30	24.0	KN/m <sup>3</sup>
Young's modulus	$E$	50–81	30,000	MPa
Poisson's ratio	$\mu$	0.3	0.1	–
Cohesion	$C$	0	–	KN/m <sup>2</sup>
Friction angle	$\phi$	31	–	°
Interfaces reduction factor	$R_{inter}$	0.715	1	–

**Fig. 3** Model of pile with boundary condition

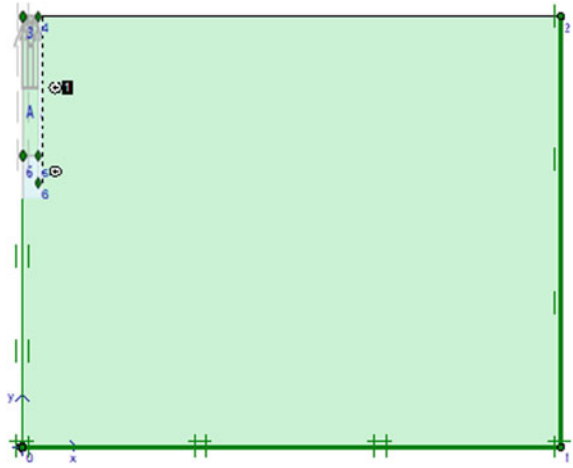
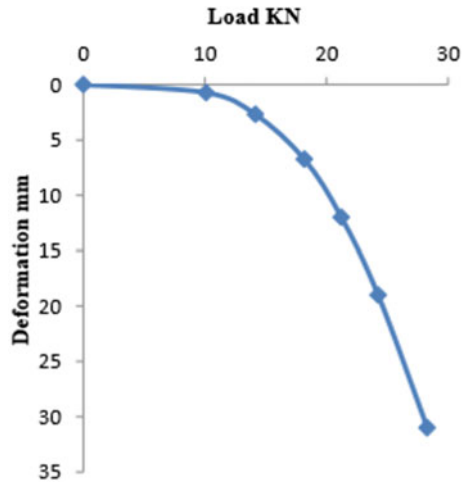


**Fig. 4** Variation of uplift load with lateral deflection for pile 1 using PLAXIS



### 4 Results and Discussion

The ultimate pull out load is defined as the load at which the pile was completely pulled out or initially the load–displacement plot became practically constant and even it proves in PLAXIS software if further increasing the load–displacement curve will be varied. A total of eight tests were conducted in this study under different conditions. The load–displacement graphs were plotted for all the piles shown in Fig. 5. At an early stage, displacement is linear, but later for small incremental loading, displacement values increase gradually, and with constant load, displacement increases which shows the failure of the pile. It can be observed from the experiment and PLAXIS that the uplift capacity is significantly affected by the state

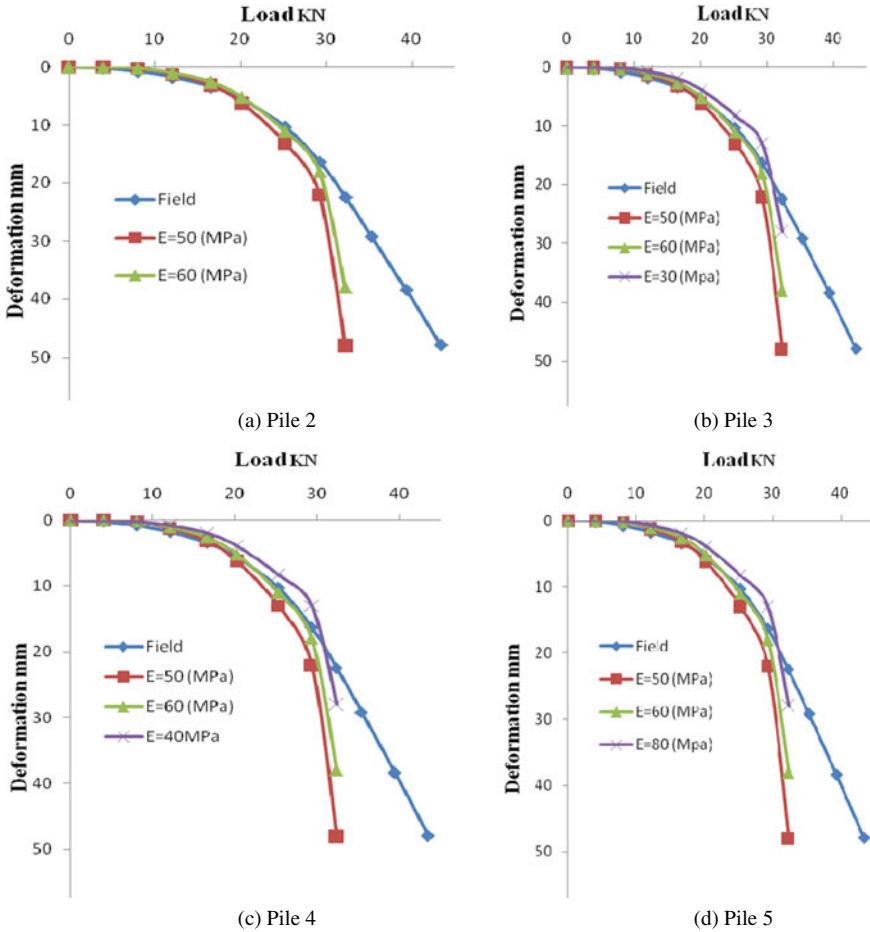


Fig. 5 Deformation curve for different pile

of the soil [9]. From the load–displacement curve, ultimate load was selected to corresponding to the 12 mm upward displacement [10].

Safe load has been estimated based on two-thirds of the load at which the total displacement is 12 mm as per IS: 2911(Part-4)—1985 as given in Table 4. However, this safe load is subject to vary corresponding to a specified permissible uplift. Uplift capacity is maximum when the soil is compacted to maximum dry density. The uplift capacity is also found to be high for a fully embedded rough pile of maximum weight [11]. When compared with the surface characteristics, the effect of embedment length-to-diameter ratio is observed to be predominant. The experimental result shows that the state of the soil and embedment length-to-diameter ratio plays a vital role in determining the uplift capacity of piles. The short piles are failed due to the uplift load Rader than the compression load because short piles are designed for

**Table 4** Ultimate pull out capacity of piles

Test pile no	Location	Theoretical		Field test at 12 mm settlement		Numerical at 12 mm settlement	
		Ultimate pull out capacity (KN)	Safe load (KN)	Ultimate pull out capacity (KN)	Safe load (KN)	Ultimate pull out capacity (KN)	Safe load (KN)
P1	Near BH1	14.78	5.89	26.5	17.6	22.44	14.96
P2	Near BH4	22.50	9.00	28.0	18.7	31.44	20.96
P3	Near BH6	18.75	7.50	30.0	20.0	27.54	18.36
P4	Near BH7	13.51	5.40	20.0	13.3	20.20	13.47
P5	Near BH8	13.30	5.32	26.5	17.6	25.82	17.21
P6	Near BH8	17.50	7.00	36.0	24.0	35.35	23.56
P7	Near BH9	13.75	5.50	30.0	20.0	24.24	16.16
P8	Near BH9	11.50	4.60	24.0	16.0	23.50	15.7

less vertical load, but in some places near to costal area wind pressure is dramatic. Lateral pile and uplift piles are depending on the skin friction of pile, if the soil strength reduces due to water content of the top soil, the capacity is reduces. Different Young's modulus are used for this analysis represents the different soil strength due to various effect.

## 5 Conclusions

Based on numerical analysis in comparison with field results, following conclusions were drawn:

- The load–displacement response and uplift capacity under axial uplift load depend on embedment length-to-diameter ratio ( $L/D$ ). Larger the  $L/D$  ratio, higher is the uplift load.
- The result clearly shows that the state of the soil has significant influence on the uplift capacity of the pile.
- The ultimate uplift capacity is also found to depend on the Young's modulus and poison ratio.
- The ultimate uplift capacity also varied with the pile diameter. Piles with larger diameter were found to be more resistant to uplift load since the self-weight of larger diameter piles were also larger.
- The theoretical or predicted values of uplift capacity were observed to be much smaller than the experimental or measured uplift capacity, but numerical analysis values are nearly equal experimental values.

## References

1. Faizi K et al (2015) Determination of pile failure mechanism under pullout test in loose sand. *J Cent S Univ* 22(4):1490–1501
2. Faizi K et al (2015) Deformation model of sand around short piles under pullout test. *Measurement* 63:110–119
3. Chattopadhyay BC, Pise PJ (1986) Uplift capacity of piles in sand. *J Geotech Eng* 112(9):888–895
4. Huchegowda BK, Teja M, Kalyan Kumar G (2020) Evaluation of lateral capacity of pile foundation using finite element method in layered soil. *Adv Geotech Transp Eng* (Springer, Singapore) 79–84
5. Krishna B, Patra NR (2006) Effect of compressive load on oblique pull-out capacity of model piles in sand. *Geotech Geol Eng* 24(3):593–614
6. Lo K, Ong D, Oh E (2018) The response of piles under tension loads based on analytical method and finite element analysis. *Int J Geomate* 15(52):129–136
7. Jung G, Jung SJ, Kwon OS, Kim MM (2006) Evaluation of full-sized cast-in-place pile capacity with artificial defects. *J Transp Res Board* 1975
8. Bowles JE (1988) *Foundation analysis and design*. McGraw-hill
9. Zhou W-H, Yin J-H, Hong C-Y (2011) Finite element modelling of pullout testing on a soil nail in a pullout box under different overburden and grouting pressures. *Can Geotech J* 48(4):557–567
10. IS 2911 (Part-4) (1985) Indian Standard Code of practice for design and construction of pile foundation—load test on piles stimulates an experiment on pile pull out test
11. Kong GQ et al (2008) Uplift capacity of single piles embedded in clay: prediction and application. In: *Proceedings of the international young scholars' symposium on rock mechanics-boundaries of rock mechanics recent advances and challenges for the 21st century*

# Prediction of Settlement of Shallow Foundation on Cohesionless Soil Using Artificial Neural Network



Sinjan Debnath  and Parbin Sultana 

**Abstract** In this paper, Artificial Neural Network (ANN) has been used effectively to predict the settlement of shallow foundation on cohesionless soil. Using 199 test data which have been collected from various published literature, an ANN model has been built. A model equation for the determination of shallow foundation settlement on cohesionless soil has been developed from the ANN model. Sensitivity analysis has been carried out to find out the order of importance of input parameters on the output parameter.

**Keywords** Shallow foundation · Settlement · ANN

## 1 Introduction

The two main criteria for the design of shallow foundation are the bearing capacity of the underlying soil and the settlement of the foundation. However, in case of cohesionless soil deposit, the settlement of shallow foundation governs the foundation design process considering the width of foundation exceeds 1.2 m [1]. That is why, accurate prediction of the shallow foundation settlement on cohesionless soil is of prime concern.

In this paper, Artificial Neural Network (ANN) has been adopted to predict the settlement of shallow foundation on cohesionless soil. A two-layer feed-forward neural network with Tan-sigmoid transfer function for both the hidden and output layers has been created in MATLAB R2013b environment to predict the shallow foundation settlement. The following network has been trained with Bayesian Regularization (BR) backpropagation learning algorithm.

---

S. Debnath · P. Sultana (✉)  
National Institute of Technology Silchar, Silchar, Assam, India

**Table 1** Sources of the collected data

Sources	Number of cases
Bazaraa [2]	5
D'Appolonia et al. [3]	10
Burbidge [4]	22
Burland and Burbidge [5]	125
Picornell and del Monte [6]	1
Wahls [7]	30
Maugeri et al. [8]	2
Briaud and Gibbens [9]	4

## 2 Sequence of Modelling

The following sequence has been followed for building the ANN model—

- Collection of data
- Determination of model inputs
- Division of data
- Optimizing the number of hidden nodes

### 2.1 Collection of Data

199 actual cases of measured shallow foundation settlement have been collected from various published literature (Table 1). Each set contains width, length and embedment depth of the footing; net applied pressure on the footing, average SPT blow count and the corresponding measured settlement of the footing.

### 2.2 Determination of Model Inputs

The five parameters which have been considered as input parameters for constructing the ANN model are as follows—

- Length of the footing ( $L$ )
- Breadth of the footing ( $B$ )
- Embedment depth of the footing ( $D$ )
- Net applied pressure on the footing ( $q$ )
- Average SPT blow count ( $N$ )

**Table 2** Statistical parameters of training and testing set

Model parameters and dataset	Mean	Standard deviation	Maximum	Minimum
<i>Footing width B (m)</i>				
Training set	8.757	10.291	60	0.8
Testing set	8.433	9.221	42.7	0.9
<i>Footing length L (m)</i>				
Training set	16.290	18.782	101	0.8
Testing set	15.756	16.903	75	0.9
<i>Embedment depth D (m)</i>				
Training set	2.443	2.037	10.7	0
Testing set	2.186	1.703	7.3	0
<i>Net applied pressure q (kPa)</i>				
Training set	185.794	123.096	697	18.32
Testing set	189.142	114.884	576	25
<i>Average SPT blow count N</i>				
Training set	24.413	13.510	60	4
Testing set	24.196	12.664	60	6
<i>Measured settlement S (mm)</i>				
Training set	18.792	24.929	121	0.6
Testing set	22.203	28.547	120	1.3

### 2.3 Division of Data

The whole database has been subdivided into two sets—(a) Training set (b) Testing set. 70% of the whole database (138 cases) has been allocated to the training set and the remaining 30% of the whole database (61 cases) has been allocated to the testing set. The training set has been used to adjust the weights of connections of nodes in ANN and the testing set has been used to provide an unbiased evaluation of the trained model. Statistical consistency of both the sets has been maintained i.e. mean and standard deviation of all the parameters of both the sets have been kept as close as possible (Table 2).

### 2.4 Optimizing the Number of Hidden Nodes

Finding out the optimum number of hidden nodes is necessary to ensure the optimal performance of the ANN model. The upper limit of the number of hidden nodes may be taken as  $(2i + 1)$ , where  $i$  is the number of input parameters [10]. As we have five input parameters in this case, several ANN models with number of hidden nodes



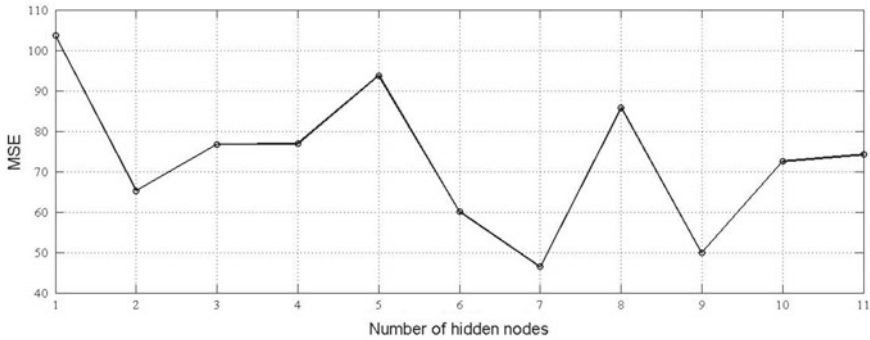


**Fig. 1** Plot between MSE and number of hidden nodes

starting from 1 to 11 have been created and the ANN model having the lowest mean squared error (MSE) has been taken into account and the corresponding number of hidden nodes has been chosen as the optimum number of hidden nodes which is seven in this case (Fig. 1).

### 3 Building the Best Performing ANN Model

The best performing ANN model has been obtained by employing seven hidden nodes (optimum number of hidden nodes). Tan-sigmoid transfer function has been used in both hidden and output layers. The following network has been trained with Bayesian Regularization (BR) backpropagation learning algorithm. In this paper, the best performing ANN model obtained has been designated as ANN-5-7-1. An architecture diagram of the model (Fig. 2) has been provided for better understanding.

Some performance measuring functions which have been used here to assess the performance of the network are as follows.

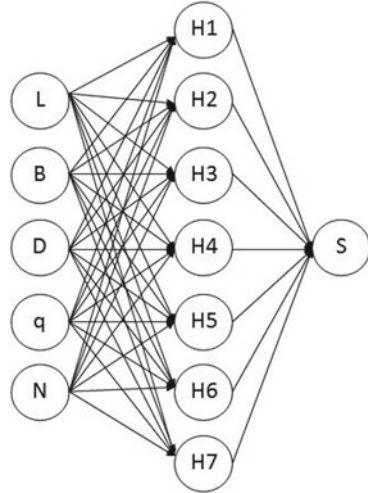
Coefficient of Correlation ( $R$ )

$$R = \sqrt{\frac{\sum Y_m^2 - \sum (Y_m - Y_p)^2}{\sum Y_m^2}}$$

Mean Squared Error (MSE)

$$MSE = \frac{\sum (Y_m - Y_p)^2}{N}$$

**Fig. 2** Architecture of ANN-5-7-1 model



Mean Absolute Error (MAE)

$$MAE = \frac{\sum |Y_m - Y_p|}{N}$$

Coefficient of Correlation ( $R$ ) measures relative correlation and goodness of linear fit between the actual measured target values ( $Y_m$ ) and the predicted output values ( $Y_p$ ). Therefore, it should be as high as possible. MSE and MAE are error measuring functions, these functions should be as low as possible.

According to Smith [11], If  $R > 0.8$ , Strong correlation exists between two sets of variables. If  $0.8 > R > 0.2$ , Correlation exists between two sets of variables. If  $0.2 > R$ , Weak correlation exists between two sets of variables.

From Tables 3 and 4, it can be seen that there has been significant improvement in terms of performance in case of ANN-5-7-1 model. The coefficient of correlation ( $R$ ) of both training and testing set of ANN-5-7-1 model is greater than that of Shahin et al. [12] ANN model. The values of MSE and MAE which measure errors are also

**Table 3** Performance of the training and testing set of ANN-5-7-1 model

Dataset	$R$	MSE (mm <sup>2</sup> )	MAE (mm)
Training set	0.966	40.918	4.152
Testing set	0.960	64.277	5.388

**Table 4** Performance of the training and testing set of Shahin et al. [12] ANN model

Dataset	$R$	MSE (mm <sup>2</sup> )	MAE (mm)
Training set	0.930	100.2	6.87
Testing set	0.929	102.414	6.43

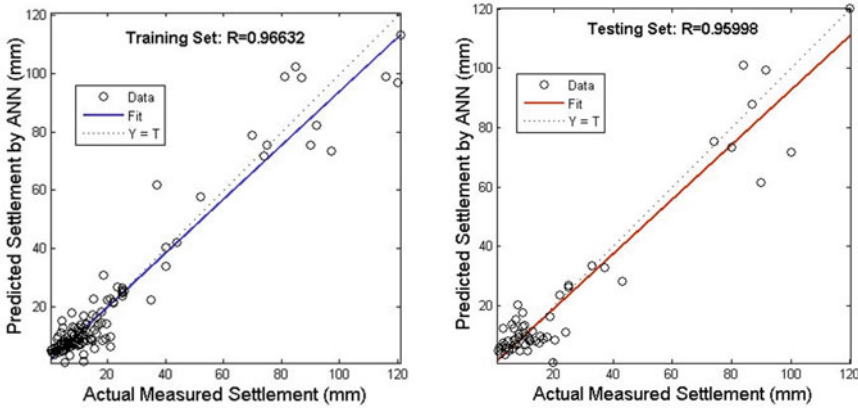


**Fig. 3 a, b** Plot between predicted settlement and actual measured settlement of training and testing set of ANN-5-7-1 model

lower in case of ANN-5-7-1 model. Thus, it can be said that the current ANN-5-7-1 model is more efficient than that of Shahin et al. [12] ANN model in terms of settlement prediction (Fig. 3).

### 4 Development of Settlement Prediction Equation from ANN-5-7-1 Model

The mathematical equation as suggested by Goh et al. [13] involving all the input variables and the output variable as per the ANN model is written as

$$Y_n = f_o \left\{ b_o + \sum_{k=1}^h \left[ w_k f_h \left( b_{hk} + \sum_{i=1}^m w_{ik} X_{ni} \right) \right] \right\} \tag{1}$$

where

- $Y_n$  Predicted output parameter.
- $f_h$  and  $f_o$  Tan-sigmoid transfer function for hidden and output layer respectively.
- $b_o$  Output nodal bias.
- $w_k$  Connection weight between the  $k$ th hidden node and the output node.
- $b_{hk}$  Bias of the  $k$ th hidden node.
- $w_{ik}$  Connection weight between the  $i$ th input node and the  $k$ th hidden node.
- $X_{ni}$   $i$ th input parameter.

By substituting the values of weights and biases shown in Table 5 in Eq. (1), the model equation for the prediction of settlement has been developed. The following equations can be written to arrive at a correlation of the output parameter with the

**Table 5** Weights and biases of the ANN-5-7-1 model

Hidden node	Input-hidden weight					Hidden-output weight	Bias	
	<i>B</i>	<i>L</i>	<i>q</i>	<i>N</i>	<i>D</i>		Hidden	Output
1	0.629	0.25	0.927	-0.984	-1.227	-2.168	0.497	-1.336
2	-0.623	-2.125	0.453	3.88	-0.718	-1.884	0.901	
3	0.602	0.333	1.231	-0.248	-0.21	1.711	1.008	
4	1.827	0.057	-0.236	1.201	0.394	-1.879	1.561	
5	-0.594	3.186	-0.882	-1.365	0.951	-2.152	0.235	
6	1.827	0.146	0.104	0.259	-1.084	1.865	0.974	
7	0.234	1.165	-0.315	-0.186	0.346	1.55	1.387	

input parameters.

$$a = 0.629B + 0.25L + 0.927q - 0.984N - 1.227D + 0.497 \tag{2}$$

$$b = -0.623B - 2.125L + 0.453q + 3.88N - 0.718D + 0.901 \tag{3}$$

$$c = 0.602B + 0.333L + 1.231q - 0.248N - 0.21D + 1.008 \tag{4}$$

$$d = 1.827B + 0.057L - 0.236q + 1.201N + 0.394D + 1.561 \tag{5}$$

$$e = -0.594B + 3.186L - 0.882q - 1.365N + 0.951D + 0.235 \tag{6}$$

$$f = 1.827B + 0.146L + 0.104q + 0.259N - 1.084D + 0.974 \tag{7}$$

$$g = 0.234B + 1.165L - 0.315q - 0.186N + 0.346D + 1.387 \tag{8}$$

All the values of input parameters are needed to be normalized in the range of  $[-1, 1]$  before substituting in the above Eqs. (2)–(8) using Eq. (12) and the limits of the training data presented in Table 2.

$$x = -2.168 \tanh(a) - 1.884 \tanh(b) + 1.711 \tanh(c) - 1.879 \tanh(d) - 2.152 \tanh(e) + 1.865 \tanh(f) + 1.55 \tanh(g) - 1.336 \tag{9}$$

$$\text{Settlement, } S \text{ (Normalized)} = \tanh(x) \tag{10}$$

Equation (10) has been de-normalized to Eq. (11) using Eq. (12) and the limits of the settlement (Training set).

$$\text{Settlement, } S(\text{mm}) = 60.2 \tanh(x) + 60.8 \quad (11)$$

The equation for normalization is given as

$$X_n = \frac{2(X - X_{\min})}{X_{\max} - X_{\min}} - 1 \quad (12)$$

where

$X_n$  Normalized input parameter data in the range of  $[-1, 1]$ .

$X$  Actual given input parameter data.

$X_{\max}, X_{\min}$  Limits of the input parameter.

## 5 Numerical Example

A numerical example has been provided to explain the process of settlement calculation using the developed equations.

A square test footing having dimensions  $1.1 \text{ m} \times 1.1 \text{ m}$  is founded at a depth of  $0.825 \text{ m}$  from the ground surface in a cohesionless soil deposit. The net applied load exerted on the footing is  $274 \text{ kPa}$  and the average value of SPT blow count is  $9$ . Predict the settlement of the foundation.

Solution:

Given data: Breadth of the footing ( $B$ ) =  $1.1 \text{ m}$ , Length of the footing ( $L$ ) =  $1.1 \text{ m}$ , Embedment depth of the footing ( $D$ ) =  $0.825 \text{ m}$ , Net applied pressure on the footing ( $q$ ) =  $274 \text{ kPa}$ , Average value of SPT blow count ( $N$ ) =  $9$ .

Step 1: Normalize the given data in the range of  $[-1, 1]$  using Eq. (12) given and the limits of the input parameters given in Table 2.

Step 2: Substitute the normalized data into Eqs. (2)–(8) and solve for  $a, b, c, d, e, f$  and  $g$ .

Step 3: Substitute the calculated values of  $a, b, c, d, e, f$  and  $g$  into Eq. (9) and solve for  $x$ .

Step 4: Now, substitute the value of  $x$  into Eq. (11) and solve for  $S$ .

The value of predicted settlement obtained from Eq. (11) is found to be  $11.25 \text{ mm}$ .

The data of the example has been obtained from a real-life in-situ test [1] whose settlement was found to be  $12.7 \text{ mm}$ .

Therefore, error in prediction is  $11.41\%$  which is acceptable.

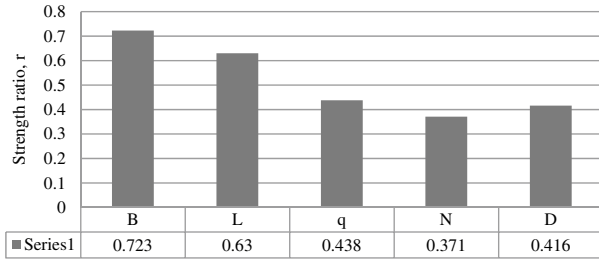


Fig. 4 Histogram showing strength ratios of different input parameters

### 6 Sensitivity Analysis

Sensitivity analysis has been carried out on the database using Cosine Amplitude Method [14] in order to find out the order of influence of input parameters on the dependent output parameter (i.e. Settlement).

In this method, strength ratio ( $r$ ) between each independent input variable and dependent output variable has been calculated using Eq. (13) and accordingly a graph has been plotted (Fig. 4).

$$\text{Strength ratio, } r = \frac{\sum(\text{Input} * \text{Target Settlement})}{\sqrt{\sum(\text{Input})^2 * \sum(\text{Target Settlement})^2}} \tag{13}$$

Order of importance of independent input variables as per the Cosine Amplitude Method is as follows.

Footing width ( $B$ ) > Footing length ( $L$ ) > Net applied pressure on the footing ( $q$ ) > Embedment depth of the footing ( $D$ ) > Average SPT blow count ( $N$ ).

### 7 Conclusions

The conclusions which can be drawn from this work are as follows—

- ANN has proved to be an effective tool in predicting the future shallow foundation settlements.
- The developed model equation for the prediction of shallow foundation settlement works effectively within the specified limits.
- In case of cohesionless soil, footing width has the maximum influence on the settlement and average SPT value has the least.

It should be noted that this ANN model is alike yet an improvement over the ANN model reported by Shahin et al. [12].

## References

1. Schmertmann JH (1970) Static cone to compute static settlement over sand. *J Soil Mech Found Div* 96(3):1011–1043
2. Bazaraa ARSS (1967) Use of the standard penetration test for estimating settlements of shallow foundations on sand. Ph.D. thesis, University of Illinois, Urbana, Illinois
3. D'Appolonia DJ, D'Appolonia E, Brissette RF (1968) Settlement of spread footings on sand. *J Soil Mech Found Div* 94(3):735–762
4. Burbidge MC (1982) A case study review of settlements on granular soil. M.Sc. thesis, Imperial College of Science and Technology, University of London, London
5. Burland JB, Burbidge MC (1985) Settlement of foundations on sand and gravel. *Proc ICE* 78(6):1325–1381
6. Picornell M, Del Monte E (1988) Prediction of settlements of cohesive granular soils. In: *Proceedings of measured performance of shallow foundations*, Nashville, Tennessee, pp 55–72
7. Wahls HE (1997) Settlement analysis for shallow foundations on sand. In: *Proceedings of the 3rd international geotechnical engineering conference*, Cairo, Egypt, pp 7–28
8. Maugeri M, Castelli F, Massimino MR, Verona G (1998) Observed and computed settlements of two shallow foundations on sand. *J Geotech Geoenviron Eng* 124(7):595–605
9. Briaud JL, Gibbens R (1999) Behavior of five large spread footings in sand. *J Geotech Geoenviron Eng* 125(9):787–796
10. Hecht-Nielsen R (1989) Theory of the backpropagation neural network. *International joint conference on neural networks*, Washington, DC, USA 1:593–605
11. Smith GN (1986) *Probability and statistics in civil engineering: an introduction*. Collins, London
12. Shahin MA, Jaksza MB, Maier HR (2002) Artificial neural network-based settlement prediction formula for shallow foundations on granular soils. *Aust Geomech J* 37(4):45–52
13. Goh ATC, Kulhawy FH, Chua CG (2005) Bayesian neural network analysis of undrained side resistance of drilled shafts. *J Geotech Geoenviron Eng* 131(1):84–93
14. Monjezi M, Hasanipanah M, Khandelwal M (2013) Evaluation and prediction of blast-induced ground vibration at Shur river dam, Iran, by artificial neural network. *Neural Comput Appl* 22:1637–1643

# Finite Element Modelling of Piled Raft in Sand Under Earthquake Load



Prasun Halder and Bappaditya Manna

**Abstract** In this paper, finite element (FE) simulations are carried out in PLAXIS to investigate the seismic response of piled raft embedded in sand using pseudo-static approach. A three-dimensional FE model of piled raft, verified with published data in literature, is utilized to study the response of piled raft for Uttarkashi (1991) and Sikkim (2011) earthquake pseudo-static loading conditions. This pseudo-static load is applied at the level of the raft in addition to the vertical load. Based on the numerical results, the piles are found to carry about 60–75% of the applied pseudo-static load. This pile load proportion increases with increasing magnitude of pseudo-static load for different earthquake events. Lateral displacement and bending moment are observed to attain their maximum values at the pile head. The bending moment of the pile is found to change from positive to negative along the length of the pile and finally becomes zero at the pile tip.

**Keywords** Piled raft system · Pseudo-static approach · Earthquake load · Finite element modelling

## 1 Introduction

The performance of piled rafts as the foundation for the high-rise buildings is effective and economic because of simultaneous load sharing between the raft and piles under vertical load. As a result, the settlement of the raft can be reduced to acceptable limit by using the piles under the raft. The concept of using such settlement reducing piles under the raft was first proposed by Burland et al. [1]. Following this concept, a number of design methods and guidelines regarding piled raft foundations subjected to vertical load have been reported by several researchers [2, 3]. Response of piled rafts under lateral load has also been documented by researchers. Horikoshi et al. [4] reported the centrifuge test results describing the behaviour of piled rafts under static vertical and horizontal loads. Horikoshi et al. [5] investigated the response of

---

P. Halder (✉) · B. Manna  
Indian Institute of Technology Delhi, Hauz Khas, New Delhi 110016, India



piled rafts under seismic loading using centrifuge shake table tests. Zeng et al. [6] analytically examined the behaviour of piles under various shaped impulse loads. However, very few literatures have been published regarding the complex behaviour of piled raft subjected to real earthquake loading conditions. Summarily, it can be said that the studies related to the seismic analysis of piled raft foundations are very few and therefore needs to be investigated further using earthquake loads.

### ***1.1 Objective and Scope of the Study***

The prime objective of the present study is to understand the seismic response of piled rafts using the pseudo-static approach. To achieve this goal, a 3D FE model of piled raft, verified with published data in literature, is utilized to study the response of piled raft for Uttarkashi (1991) and Sikkim (2011) earthquake pseudo-static loading conditions. The responses of piled raft are presented in terms of pile-raft load sharing, lateral displacement and bending moment under pseudo-static load.

## **2 Finite Element Modelling and Loading Condition**

This segment presents the details of finite element modelling along with necessary boundary conditions, constitutive models, model validation and pseudo-static loading conditions.

### ***2.1 Boundary Conditions and Constitutive Models***

The numerical modelling of the present study is done using PLAXIS 3D [7] which is an efficient finite element tool to deal with soil-structure interaction problem. The schematic diagram of the 3D finite element (FE) model is presented in Fig. 1. Sides of the model are restricted to lateral movement, and the base is restrained from both horizontal and vertical movements.

Soil domain is modelled using 10-noded tetrahedral soil elements. The conventional Mohr-Coulomb model is used to simulate the behaviour of the sand [8–10]. The linear elastic portion of the model is based on Hooke's law of isotropic elasticity. The perfectly plastic part is governed by the Mohr-Coulomb failure criterion. A 4 m square raft having 1m thickness is modelled using a plate element. The embedded pile element option is used to model 4 no. of 9 m long piles having 500 mm diameter (d). The piles are placed at 2 m centre-to-centre spacing under the raft. Rigid connection is considered between the raft and pile heads. A mesh convergence study is performed using the non-dimensional average element lengths to find out the optimal mesh size for the FE model. Medium meshing scheme is selected for the model. A vertical load

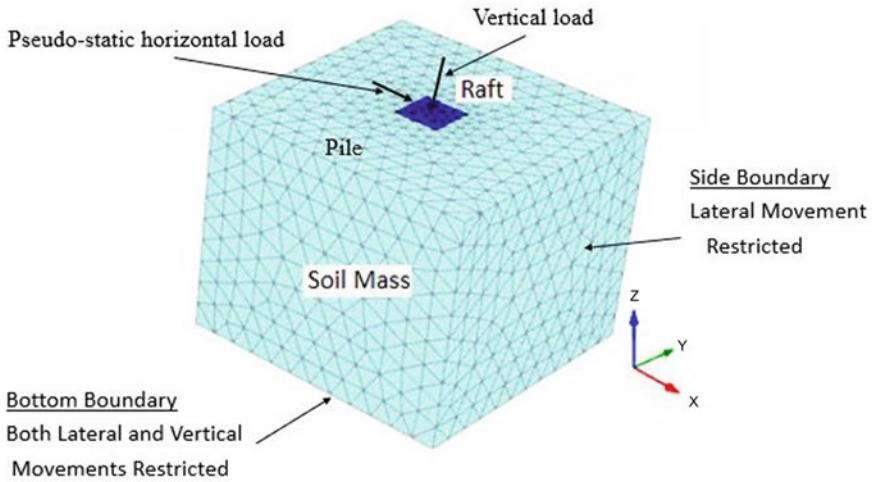


**Fig. 1** Finite element model of the piled raft system

**Table 1** Properties of soil, pile and raft used for analysis

Properties	Soil	Pile	Raft
Elastic modulus, $E$ (kN/m <sup>2</sup> )	$40 \times 10^3$	$42 \times 10^6$	$70 \times 10^6$
Friction angle, $\phi$ (Degree)	31	–	–
Poisson's ratio, $\nu$	0.3	0.2	0.35
Unit weight, $\gamma$ (kN/m <sup>3</sup> )	16.3	24	24
Cohesion, $c$ (kN/m <sup>2</sup> )	1	–	–

of 5880 kN is applied on the model. The properties of sand, pile and raft used for the analysis are taken from Kumar et al. [8] and presented in Table 1.

## 2.2 Validation of the FE Model

The three-dimensional piled raft model is validated using the results presented in Kumar et al. [8]. The results obtained in terms of pile load proportion, and total vertical settlement of piled raft is compared with the reported values. Table 2 shows the comparison between the present FE analysis and the reported value in literature.

**Table 2** Comparison between FE result and reported values by Kumar et al. [8]

Parameters	Settlement (mm)	Pile load proportion (%)
FE analysis	22.56	45.3
Kumar et al. [8]	21	47

Here, the pile load proportion is calculated as the percentage of total applied vertical load carried by the piles only in a piled raft. From Table 2, it can be seen that the obtained results of the current FE analysis are in close agreement with that of the literature. The settlement of piled raft is over predicted by only 7.4%, whereas the pile load proportion is under predicted by only 3.6% in comparison with the reported values. Therefore, this validated 3D FE model is used to investigate the response of piled raft foundation under pseudo-static loading condition.

### 2.3 Pseudo-Static Loading Condition

In this paper, an attempt is made to investigate the response of piled raft system under the action of seismic load using the popular pseudo-static approach. According to this approach, the earthquake induced load is replaced with equivalent static horizontal load to be acted at the level of the raft along with the vertical load on the raft [11]. This specific horizontal load is popularly termed as pseudo-static load. This load is calculated by multiplying the applied vertical load with the seismic coefficient of a particular earthquake. Figure 2 shows the details of the earthquake input motions, i.e. Sikkim (2011) with peak ground acceleration (PGA) value of 0.202 g and Uttarkashi (1991) having PGA value of 0.38 g used for the pseudo-static analysis. The equivalent static horizontal loads for Sikkim (2011) and Uttarkashi (1991) earthquakes are calculated as 1187.1 kN and 2234.4 kN, respectively, and applied at the level of the raft.

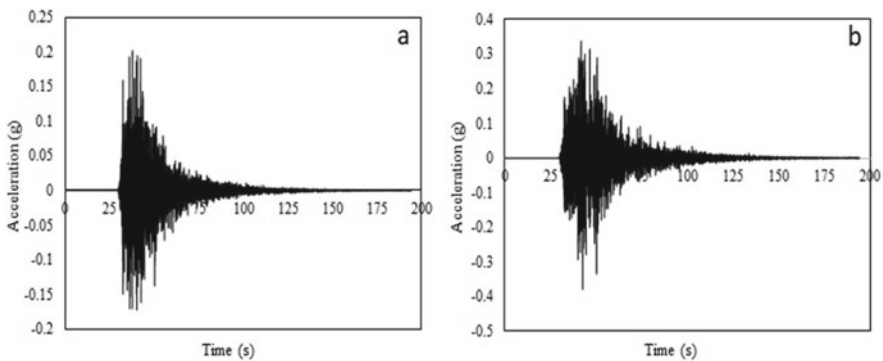


**Fig. 2** Time-acceleration history: **a** Sikkim Eq. (2011), **b** Uttarkashi Eq. (1991)

**Table 3** Proportion of load shared between piles and raft

Pseudo-static load	Pile load proportion (%)	Raft load proportion (%)
Sikkim Eq. (2011)	51.3	48.7
Uttarkashi Eq. (1991)	56.8	43.2

### 3 Results and Discussion

This section highlights the results obtained from the finite element analysis. Emphasis is given on the load sharing between piles and raft as well as on the structural behaviour of piles in a piled raft system.

#### 3.1 Load Sharing Between Piles and Raft

The proportion of load sharing between the piles and raft as found from the FE analysis is presented in Table 3. From Table 3, it is evident that piles carry majority of the applied pseudo-static load as compared to the raft component in a piled raft system.

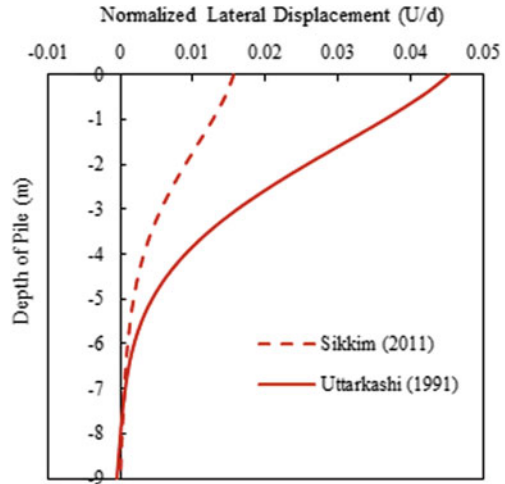
Such phenomenon is unlike the case of vertically loaded piled raft, where the raft takes more load than the piles. It is noteworthy that with the increase of the horizontal pseudo-static load, the piles share more load than the raft in a piled raft system.

#### 3.2 Horizontal Displacement of Pile

Figure 3 shows the normalized horizontal displacement ( $U/d$ ) profile along the length of the pile. Here,  $U$  is horizontal displacement and  $d$  is diameter of pile.

Figure 3 depicts that the lateral displacement is maximum at the pile head and becomes almost zero at the pile tip. The normalized lateral displacements ( $U/d$ ) are found 0.016 and 0.045 for Sikkim (2011) and Uttarkashi (1991) earthquakes, respectively. With higher magnitude of pseudo-static force, the lateral displacement also becomes larger.

**Fig. 3** Variation of lateral displacement of pile along the length

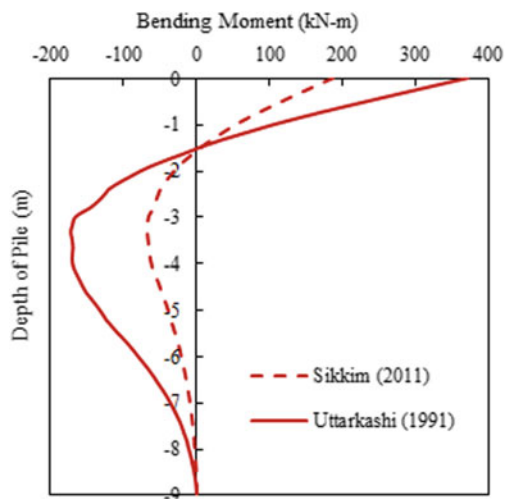


### 3.3 Bending Moment of Pile

Figure 4 shows the bending moment distribution along the length of the pile.

From Fig. 4, it can be observed that the maximum bending moment occurs at the pile head due to fixed connection with the raft. It can also be noted that bending moment gets transformed from positive to negative along the pile length and finally comes to zero at pile tip. The maximum bending moments, as found from Fig. 4, are 192 kN m and 380 kN m for Sikkim (2011) and Uttarkashi (1991) earthquakes, respectively. Here also the bending moment increases with the increase of PGA of the earthquake motion.

**Fig. 4** Variation of bending moment of pile along the length



## 4 Conclusions

In the present study, three-dimensional analyses are performed using geotechnical FE software PLAXIS 3D to investigate the seismic response of piled raft foundations embedded in sand under pseudo-static loading condition. Two earthquake motions having different PGAs are used here for estimating the pseudo-static loads on the piled raft. From the work presented in this paper, the following significant conclusions can be drawn:

- The mesh convergence study is useful for selecting the appropriate meshing scheme for any FE model and getting realistic responses.
- The piles in a piled raft system are found to carry maximum percentage of the externally applied pseudo-static load ranging from 51.3 to 56.8% for the two earthquakes considered in this present study.
- The proportion of pile load is found to increase with increase of pseudo-static load.
- Both the lateral displacement and the bending moment of pile are observed to have the maximum values at the pile head portion due to fixity with the raft.
- The bending moment gets transformed from positive to negative along the pile length and finally comes to zero at pile tip.
- With higher magnitude of pseudo-static force, i.e. higher PGA of the earthquake motion, both the lateral displacement and bending moment become higher in magnitude as well.

## References

1. Burland JB, Broms BB, De Mello VFB (1977) Behavior of foundations and structures. In: 9th International conference on soil mechanics, vol 2, pp 495–546, Tokyo
2. Horikoshi K, Randolph MF (1998) A contribution to optimum design of piled rafts. *Geotechnique* 48(3):301–317
3. Poulos HG (2001) Piled raft foundations: design and applications. *Geotechnique* 51(2):95–113
4. Horikoshi K, Matsumoto T, Hashizume Y, Watanabe T, Fukuyama H (2003) Performance of piled raft foundations subjected to static horizontal loads. *Int J Phys Modell Geotech* 3(2):37–50
5. Horikoshi K, Matsumoto T, Hashizume Y, Watanabe T, Fukuyama H (2003) Performance of piled raft foundations subjected to dynamic loading. *Int J Phys Modelling Geotech* 3(2):51–62
6. Zheng C, Ding X, Sun Y (2015) Vertical vibration of a pipe pile in viscoelastic soil considering the three-dimensional wave effect of soil. *Int J Geomech* 16(1):04015037
7. Plaxis AE (2015) Netherland user manual, PLAXIS 3D
8. Kumar A, Choudhury D, Katzenbach R (2016) Effect of earthquake on combined pile-raft foundation. *Int J Geomech* 16(5):04016013
9. Alnuaim AM, El Naggar MH, El Naggar H (2016) Numerical investigation of the performance of micro piled rafts in sand. *Comput Geotech* 77:91–105
10. Elwakil AZ, Azzam WR (2016) Experimental and numerical study on piled raft system. *Alexandria Eng J* 55:547–560
11. Liyanapathirana S, Poulos H (2005) Pseudo-static approach for seismic analysis of piles in liquefying soil. *J Geotech Geoenviron Eng* 131(12):1480–1487

# **Engineering Properties and Characteristics of Soil**

# Effect of Salt Solution on Engineering Behaviour of Soil



Swagatika Senapati, Subhadeep Banerjee, and T. Thyagaraj

**Abstract** The response of any soil structure depends on the interaction of clay flakes, water and variety of minerals mixed in the water. Soil containing various minerals may change its geotechnical properties when undergoes both static and cyclic loading. Distilled water is generally not used at the field for any kind of construction works. This paper discusses the compressibility characteristics of marine clay by varying pore medium chemistry. This paper also articulates the change in static and cyclic behaviour of clayey soil mixed with sodium chloride solution. To examine this behaviour, a set of unconfined compressive strength and cyclic triaxial tests were conducted on slurry consolidated samples. Three different strain amplitudes (0.3, 0.7 and 1%) and a constant effective confining pressure of 150 kPa were used in the study for determining cyclic properties. A consistent trend was observed for the set of data which shows an increment in secant modulus values with the increase in pore fluid concentration. The change in electrolyte concentration makes a substantial contribution for enhancing the stiffness properties of the soils.

**Keywords** Compressibility · Unconfined compressive strength · Cyclic triaxial test · Slurry consolidated sample · Secant modulus

## 1 Introduction

The variation in geotechnical characteristics of fine grained soils owing to change in pore fluid chemistry is of major concern in case of geotechnical structures. The variation in pore fluid composition of natural clay may occur at any time which may affect the foundation of structure when subjected to different static and cyclic loading conditions. The dissimilarities in pore fluid composition may involve increase or decrease in pore fluid concentration which may result in change in soil properties such as strength, compressibility and hydraulic conductivity. The physico-chemical effects on compressibility characteristics of clayey soil is well established in literature

---

S. Senapati (✉) · S. Banerjee · T. Thyagaraj  
Indian Institute of Technology Madras, Chennai 600036, India

© Springer Nature Singapore Pte Ltd. 2022  
A. K. Dey et al. (eds.), *Proceedings of the 7th Indian Young Geotechnical Engineers Conference*, Lecture Notes in Civil Engineering 195,  
[https://doi.org/10.1007/978-981-16-6456-4\\_51](https://doi.org/10.1007/978-981-16-6456-4_51)



[1–5]. They have also reported that the compressibility and swelling characteristics are strongly influenced by the mechanism of double-layer repulsive force. The pore fluid concentration and cation valency and the soil properties including base exchange capacity and surface area are the convoluted factors in the double-layer theory. The cyclic properties of cohesive soil using distilled water or tap water as pore fluid are well studied in literature [6–9]. The effect of clay mineralogy is significant on the cyclic properties of fine grained soil [10]. The cyclic behaviour of cohesive soil with varying pore fluid concentration are not well understood, and the studies are limited [11]. The present study comprises the pore fluid influence on compressibility characteristics, unconfined compressive strength, and cyclic properties of reconstituted marine clay samples.

## 2 Materials Used for Testing

The marine clay used for experimental purpose is taken from Ennore coast of Tamil Nadu. The Atterberg limits and particle size distribution of soil were obtained following the guidelines of Indian standards (IS), and the values are presented in Table 1. The free swell tests were conducted as per the procedure defined in IS 2720-Part 40, 1977 [12]. The free swell ratio of marine clay is 1.65. Prakash and Sridharan [13] asserted that free swell ratio ranging from 1.5 to 2 indicates moderate swelling type clay. From XRD analysis, it is confirmed that the tested clay consists of mixed clay minerals (i.e. kaolinite and illite). Tests were employed to determine both physical and engineering properties of marine clay.

**Table 1** Basic properties of marine clay

Property	Value
pH	6.7
Specific gravity	2.71
Atterberg limits (%)	
Liquid limit	59
Plastic limit	30
Plasticity index	29
Free swell index (%)	65
Particle size distribution (%)	
Fine sand (0.075–4.75 mm)	5
Silt fraction (0.002–0.075 mm)	25
Clay fines (<0.002 mm)	70
IS soil classification	CH
Organic matter (%)	3.3

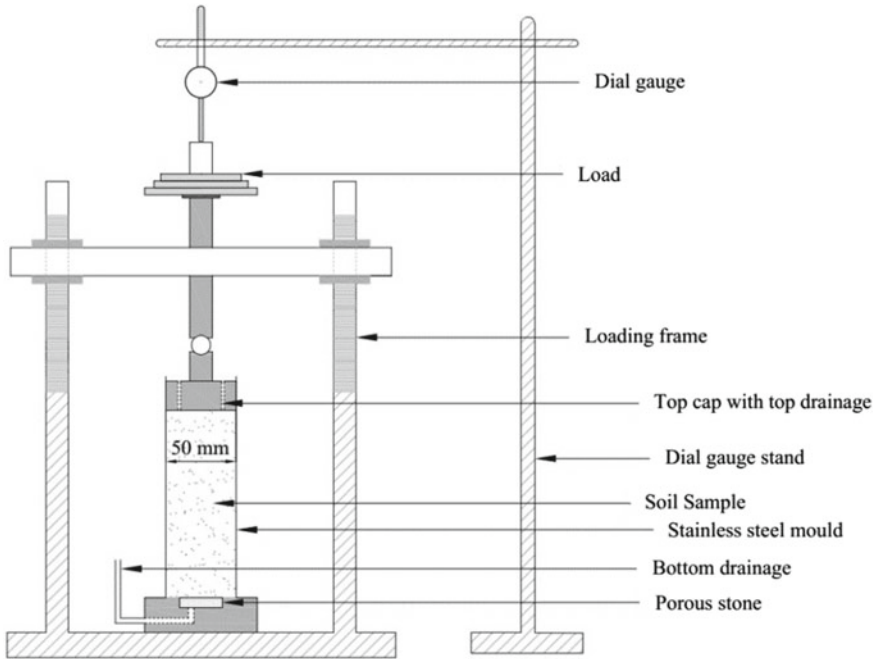


Fig. 1 Schematic test arrangement for slurry consolidation [14]

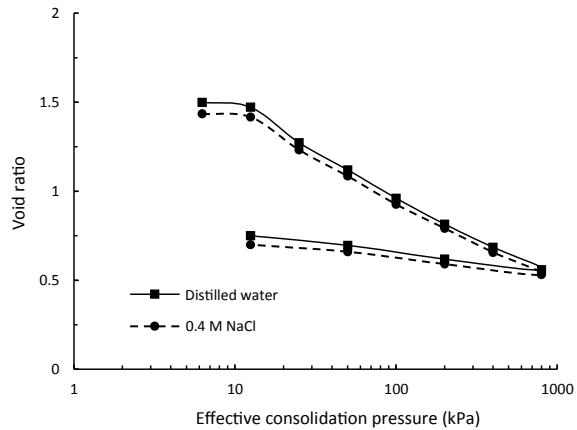
One-dimensional slurry consolidated samples with pore fluid as distilled water and 0.4 M sodium chloride salt solution were prepared separately as per the procedure defined in Swagatika et al. [14]. Samples were processed at 1.5 times the liquid limit (LL) of marine clay. The schematic diagram of arrangement for slurry consolidated samples is shown in Fig. 1. The reconstituted slurry consolidated samples of 50 mm (5 cm) diameter and 100 mm (10 cm) height with varying pore fluids were subjected to static and cyclic load conditions.

### 3 Experimental Results

#### 3.1 Oedometer Test Results

Soil passing 2 mm sieve was mixed with water content of 1.3 times LL to prepare the soil slurry for measuring the compressibility characteristics. The slurry was allowed to consolidate in oedometer set up following a load increment ratio of 1:1. Void ratio ( $e$ ) and effective pressure ( $p$ ) relationship for reconstituted marine soil mixed with distilled water (DW) and sodium chloride solution of 0.4 M concentration is depicted in Fig. 2. The figure illustrates, variation in compression curve for both distilled water

**Fig. 2** One-dimensional consolidation curve of reconstituted samples saturated with DW and salt solution

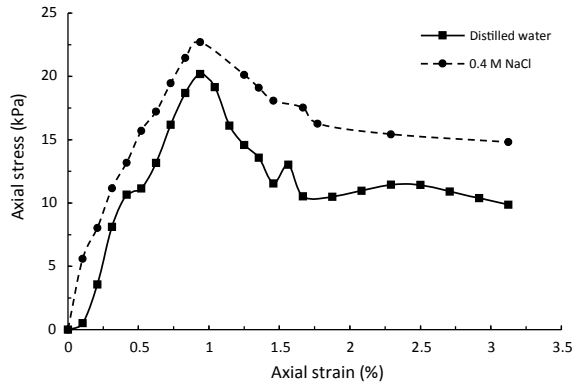


and salt solution samples is relatively small. The variation of void ratio with pressure indicates the importance of electrolyte concentration influencing compression curve. The experimental results are in accordance with Bolt [1] and Mesri and Olson [15]. Change in void ratio with a load increment from 6.25 to 800 kPa is found to be 0.94 and 0.9 for samples mixed with DW, and 0.4 M sodium chloride salt solution, respectively. The void ratio under any loading varies inversely with the valency of exchangeable cation present in the clayey soil [4]. The compressibility decreases with increase in electrolyte concentration. The slope of  $e$ - $\log p$  curve gives the compression index value. Compression index ( $C_c$ ) is 0.30 and 0.29 for the samples mixed with distilled water and 0.4 M NaCl solution, respectively. The compression index ( $C_c$ ) directly depends on surface area and clay type and is independent of the void ratio for higher concentration ( $>0.1$  M) of pore fluid [4].

### 3.2 Unconfined Compressive Strength (UCS)

The UCS tests carried out on slurry consolidated samples mixed with DW and 0.4 M sodium chloride salt solution are presented in Fig. 3. The tests were conducted as per the procedure given in IS 2720 (Part 10)-1991 [16]. The water content of reconstituted samples saturated with DW and 0.4 M sodium chloride solution was found to be 64% and 59%, respectively. The cylindrical samples were subjected to axial strain at a rate of 0.625 mm per minute for both samples. The electrolyte solution enhanced the compressive strength from 20.2 (for distilled water samples) to 22.7 kPa (samples mixed with salt solution). Abood et al. [17] stated that the unconfined compressive strength (UCS) of compacted samples increases with increase in salt solution.

**Fig. 3** Axial stress—axial strain plots of reconstituted marine clay samples saturated with DW and salt solution

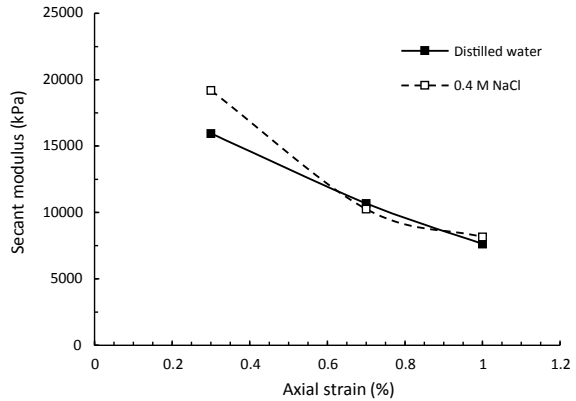


### 3.3 Cyclic Properties

The undrained cyclic triaxial tests were performed on reconstituted marine clay samples as per the procedure detailed in ASTM D3999-91. The samples prepared with two different pore fluid (DW and 0.4 M sodium chloride solution) were saturated with same fluid as that of the pore water. After ensuring *B*-value of 0.95, the samples were consolidated isotopically at effective confining pressure of 150 kPa. Then, the reconstituted samples were subjected to strain controlled cyclic loading conditions at different strain range of 0.3–1% and a frequency of 1 Hz at 100 number of loading cycles. The stress strain relationship obtained from cyclic triaxial tests was plotted as hysteresis loop by considering deviatoric stress in *Y*-axis and axial strain in *X*-axis. The slope of the hysteresis loop is known as secant modulus (*E*<sub>sec</sub>). Figure 3 interprets the effect of pore fluid variation on secant modulus of reconstituted samples at different strain amplitude. Lower secant modulus values are observed with increase in strain amplitude irrespective of pore fluid variation, based on the trend as depicted in Fig. 3. A close observation of this figure elucidates that the increment in pore fluid salt concentration leads to higher secant modulus values.

The damping ratio values presented in author’s previous literature [14, 18] reported that irrespective of pore fluid of the reconstituted samples, the damping ratio values increases with increase in strain amplitude. These conclusion was obtained by conducting cyclic triaxial tests on reconstituted marine clay with varying pore fluid concentration such as DW and 0.4 M sodium chloride solution. There is also an increase in damping values from 15.7 to 16.9 at 1% strain amplitude with increment in concentration of the pore fluid. This increase in stiffness properties under cyclic loading may be reasoned as the reduced diffuse double-layer thickness due to the addition of salt solution in the samples (Fig. 4).

**Fig. 4** Relationship between secant modulus and axial strain



## 4 Conclusion

The variation noticed in the engineering behaviour of cohesive soil can be due to the variation in pore fluid chemistry. The change in pore water electrolyte concentration slightly influence the  $e$ -log  $p$  relationship as the double-layer effects were smaller due to presence of both illite and kaolinite minerals in the clay. The unconfined compressive strength is observed to increase with increment in pore fluid concentration. The results provided clearly demonstrates the increment in cyclic properties of reconstituted marine clay with increase in salt concentration in pore water which can be reasoned as the reduced diffuse double layer due to addition of 0.4 M sodium chloride salt solution.

## References

1. Bolt GH (1956) Physico-chemical analysis of compressibility of pure clays. *Géotechnique* 6(2):86–93
2. Mitchell JK (1973) Influence of mineralogy and pore solution chemistry on the swelling and stability of clays. In: *Proceedings of 3rd international conference expansive soils*, vol 2. Haifa, pp 11–25
3. Olson RE, Mesri G (1970) Mechanisms controlling compressibility of clays. *J Soil Mech Found Div* 96(6):1863–1877 (ASCE)
4. Sridharan A, Jayadeva MS (1982) Double layer theory and compressibility of clays. *Geotechnique* 32(2):133–144
5. Sridharan A, Rao GV (1973) Mechanisms controlling volume change of saturated clays and the role of the effective stress concept. *Geotechnique* 23(3):359–382
6. Hardin BO, Drnevich VP (1972) Shear modulus and damping in soils: measurement and parameter effects. *J Soil Mech Found Div Proc ASCE* 98(6):603–624
7. Hu L, Ding J, Liu H (2010) Mechanical behaviour of marine clay under wave loading. *Int J Offshore Polar Eng* 20(1):1–8
8. Kagawa T (1992) Modulus and damping factors of soft marine clays. *J Geotech Eng ASCE* 118(9):1360–1375

9. Vucetic M, Dobry R (1988) Degradation of marine clays under cyclic loading. *J Geotech Eng* 114(2):133–149 (ASCE)
10. Gratchev IB, Sassa K (2009) The cyclic behavior of fine grained soils at different pH values. *J Geotech Geoenviron Eng* 135:271–279
11. Gratchev IB, Sassa K (2013) Cyclic shear strength of soil with different pore fluids. *J Geotech Geoenviron Eng* 139(10):1817–1821
12. IS: 2720 (1977) Indian standard methods of test for soils: Part 40. Determination of free swell index of soils. BSI, New Delhi
13. Prakash K, Sridharan A (2004) Free swell ratio and clay mineralogy of fine-grained soils. *Geotech Testing J* 27(2):220–225 (ASTM)
14. Swagatika S, Banerjee S, Thyagaraj T (2018) Effect of pore fluid on cyclic behavior of re-constituted marine clay. *Geotech Earthquake Eng Soil Dyn V:219–226 (GSP 293, ASCE)*
15. Mesri G, Olson RE (1971) Consolidation characteristics of montmorillonite. *Géotechnique* 21(4):341–352
16. IS: 2720 (1991) Indian standard methods of test for soils: Part 10. Determination of unconfined compressive strength. BSI, New Delhi
17. Abood T, Anuar B, Chik Z (2007) Stabilisation of silty clay soil using chloride compounds. *J Eng Sci Technol* 2(1):102–110
18. American Society for Testing and Materials D3999-91 (2003) Standard test methods for the determination of the modulus and damping properties of soils using the cyclic triaxial apparatus

# Application of X-Ray Computed Tomography for Capturing the Desiccation Cracks of Soils



M. Julina and T. Thyagaraj

**Abstract** The inherent nature of compacted clay soils is to shrink and crack during drying. The development of cracks in compacted clay soils is complex as it is three dimensional with vertical and horizontal cracks. In laboratory testing, the surface cracks pattern of desiccated clays can be visualized and quantified using digital camera images. For capturing the interior cracks pattern of desiccated clays, the X-ray computed tomography (XCT) serves as a valuable tool. This paper highlights the significance of non-destructive imaging experiments using XCT for visualizing the interior cracks and capturing the cracks pattern of desiccated clay soils accurately. The XCT imaging experiments, vernier caliper measurements and binary image analysis of XCT images using *ImageJ* software were used for capturing the cracks pattern of desiccated clay soils in terms of cracks area and volume. The variation of cracks pattern and void ratio of compacted clay soil inundated with distilled water and  $\text{CaCl}_2$  solution at the desiccated state is brought out.

**Keywords** Clay · Cracks pattern · X-ray computed tomography

## 1 Introduction

The shrinkage and desiccation cracks influence the hydraulic performance of low hydraulic conductivity barriers like compacted clay liners (CCLs) and geosynthetic clay liners [1–3]. Both shrinkage and desiccation cracks are formed in these barriers due to post construction moisture loss during construction, rise in temperatures caused by the degrading waste and seasonal moisture fluctuations during the life span of landfill [1, 4–6]. In laboratory testing, the surface visible desiccation cracks development in thin clay soils was monitored and quantified using digital camera images (DCIs) and binary image processing technique [3, 7]. Recent advancement in imaging techniques utilizing non-destructive imaging experiments like non-contact

---

M. Julina (✉) · T. Thyagaraj

Department of Civil Engineering, Indian Institute of Technology Madras, Chennai 600036, India

© Springer Nature Singapore Pte Ltd. 2022

A. K. Dey et al. (eds.), *Proceedings of the 7th Indian Young Geotechnical Engineers*

*Conference*, Lecture Notes in Civil Engineering 195,

[https://doi.org/10.1007/978-981-16-6456-4\\_52](https://doi.org/10.1007/978-981-16-6456-4_52)

2D laser scanner and X-ray computed tomography (XCT) have assisted in visualizing and quantifying the non-visible desiccation cracks developed in the interior surface of clay soils [2, 8].

It is well studied in the literature that the physico-chemical interactions between the clay and salt solutions alter the swelling behaviour of clay soils due to osmotic consolidation and osmotic induced consolidation [9, 10]. Few studies have also showed that these physico-chemical interactions also influence the shrinkage and desiccation cracks development in clay soils [10–12].

This paper highlights the significance of XCT imaging experiments for visualizing the desiccation cracks in the interior surfaces and quantifying the cracks pattern (cracks area and volume) of desiccated clay soils accurately. In addition, the effect of concentration of interacting fluid using distilled water (DW) and Calcium Chloride ( $\text{CaCl}_2$ ) salt solutions on the volume change behaviour of compacted clay soil subjected to one wet-dry cycle is studied. And the variation of cracks pattern and void ratio of compacted clay soil at the desiccated state is brought out.

## 2 Experimental Program

### 2.1 Materials

Basic properties of clay soil used in the present study are tabulated in Table 1. Clay soil passing through 2 mm sieve was prewetted with required quantity of DW for attaining the optimum moisture content (28%). After 3 days of moisture equilibrium, the compacted clay specimens (diameter:  $7.54 \times 10^{-2}$  m, height:  $2 \times 10^{-2}$  m) were prepared by compacting the prewetted soil in oedometer rings to standard Proctor maximum dry density ( $1.34 \text{ Mg/m}^3$ ). Oedometer wet-dry test [2, 3] were carried out by inundating identical compacted clay specimens with different interacting fluids

**Table 1** Basic properties of clay soil

Property of soil	Value
Specific gravity	2.71
<i>Atterberg limits</i>	
Liquid limit (%)	78
Plastic limit (%)	27
Shrinkage limit (%)	9
<i>Grain size distribution (%)</i>	
Clay	82
Silt	15
Sand	3
Unified soil classification symbol	CH



(DW, 0.4 M (Molar) and 4 M  $\text{CaCl}_2$  solutions) in separate oedometer setups. After swell equilibrium, the swollen specimens were allowed to desiccate to water content less than the shrinkage limit water content of the soil.

## 2.2 *Imaging Experiments and Methods for Quantification of Desiccation Cracks*

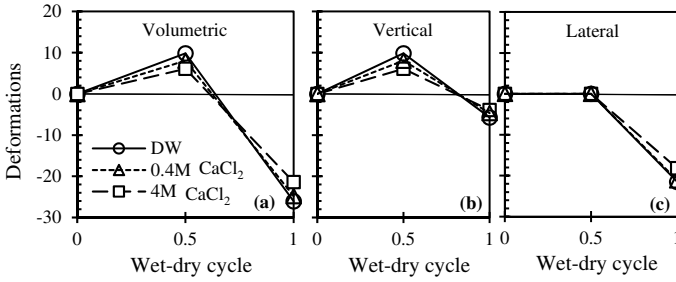
The surface DCIs and horizontal sectional 2D (dimensional) XCT images of desiccated clay specimens were captured using a digital camera and General Electric Phoenix Vtomex S 240 kV micro-focus XCT equipment, respectively [2, 3]. Binary image processing technique was employed on these images using *ImageJ* software [13] for calculating the cracks area (void space in XCT images are not considered as cracks). Two methods were employed for the quantification of average cracks area. First method includes the determination of cracks area from top, bottom and assumed mid-depth DCI images as proposed by Julina and Thyagaraj [3]. Second method includes determination of cracks area from fifty horizontal sectional XCT images as proposed by Julina and Thyagaraj [2]. The area of damaged edges is also considered as cracks in this study. For localized selection of cracks in either binary or raw images, “wand (tracing)” selection tool in *ImageJ* software was also used. The cracks volume of desiccated clay specimens in both the methods was calculated by multiplying the average cracks area with average vernier caliper height measurement. The cracks volume was reduced from the overall volume of the desiccated clay specimen to determine the void ratio accurately.

## 3 Results and Discussion

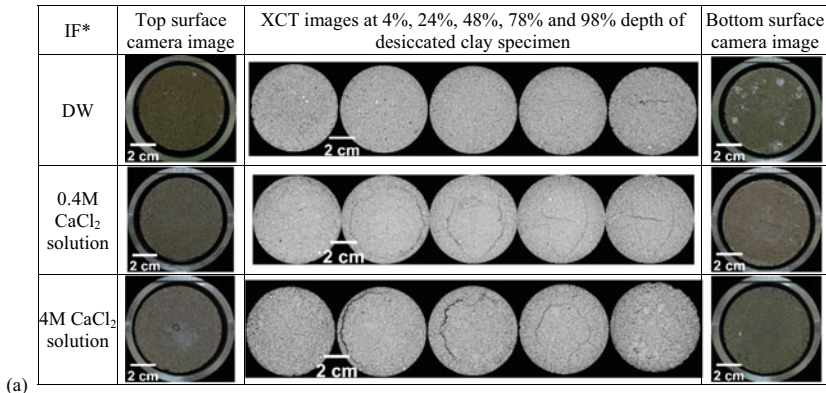
### 3.1 *Volume Change*

Figure 1 brings out the effect of interaction fluid concentration using DW and  $\text{CaCl}_2$  solutions on the volume change behaviour of compacted clay specimen subjected to one wet-dry cycle. And Fig. 2a, b present the corresponding surface DCI images and horizontal sectional XCT images along the depth, and lateral surface DCI images of desiccated clay specimen at the desiccated state, respectively. The increase in interacting fluid concentration resulted in decrease in the volumetric and vertical deformations during wetting of compacted clay specimens (Fig. 1a, b) due to osmotic consolidation and osmotic induced consolidation [9, 10].

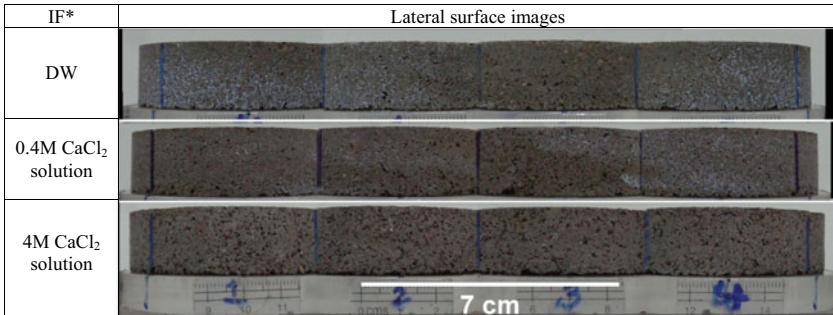
During subsequent drying, the shrinkage occurs in both vertical and lateral directions (Figs. 1b, c and 2). Table 2 presents the variation of void ratio (calculated using vernier measurements) of desiccated clay specimens due to effect of interacting fluid concentration. The volumetric, vertical and lateral deformations decreased and the



**Fig. 1** Effect of interacting fluid on: **a** volumetric, **b** vertical and **c** lateral deformations of compacted clay specimens subjected to one wet-dry cycle



(a)



(b)

\*IF: Interacting fluid used for wetting

**Fig. 2** **a** Surface digital camera and XCT images, and **b** lateral surface digital camera images of desiccated clay specimens

**Table 2** Effect of interacting fluid on cracks area, cracks volume and void ratio of desiccated clay specimens

IF for wetting cycle	Average cracks area ( $\times 10^{-4} \text{ m}^2$ )			Cracks volume ( $\times 10^{-6} \text{ m}^3$ )			Void ratio		
	Vernier	XCT and vernier	XCT and vernier	Vernier	DCI and vernier	XCT and vernier	Vernier	DCI and vernier	XCT and vernier
DW	NA	0.008	0.062	NA	0.015	0.117	0.512	0.511	0.509
0.4 M CaCl <sub>2</sub> solution	NA	0.025	0.327	NA	0.049	0.629	0.535	0.533	0.520
4 M CaCl <sub>2</sub> solution	NA	0.000	0.397	NA	0.000	0.862	0.606	0.606	0.588

\*IF: Interacting fluid used for wetting; NA: not applicable

void ratio increased with the increase in concentration of interacting fluid during drying (Fig. 1 and Table 2).

### 3.2 Cracks Pattern

The cracks pattern of desiccated clay specimens is analysed in terms of cracks area and volume. It can be observed from Fig. 2 that in addition to vertical and lateral shrinkage, fewer non-propagating cracks (surface cracks that do not extend throughout the depth of soil specimen) were present on the bottom surface DCIs of desiccated clay specimens interacted with DW and 0.4 M  $\text{CaCl}_2$  solution. Horizontal cracks were not present on the lateral surface of all the desiccated soil specimens (Fig. 2b). However, the XCT images captured at different depths show the presence of desiccation cracks on the interior of desiccated clay specimens interacted with both 0.4 M and 4 M  $\text{CaCl}_2$  solutions. Figure 3 presents the reconstructed 3D and 3D sectional views of desiccated clay specimens using 2D XCT images and *ImageJ* software.

From Figs. 2a and 3, it can be said that the formation of interior cracks was very similar in desiccated clay specimen interacted with both 0.4 M and 4 M  $\text{CaCl}_2$  solutions. However, the intensity of interior desiccation cracks varied with the concentration of interacting fluid. Figure 4 compares the variation of cracks area with depth (from top) after first drying of compacted clay specimens inundated with DW, and 0.4 M and 4 M  $\text{CaCl}_2$  solutions. Julina and Thyagaraj [2] reported that the presence of both propagating (surface cracks extend throughout the depth of soil specimen) and non-propagating cracks increased the cracks area at the top and bottom surfaces of soil specimen throughout the drying process. Similar variation in cracks area with depth of desiccated clay specimens can be observed in Fig. 4. However, greater cracks area near the top and bottom surfaces of desiccated clay specimens is attributed to the damaged edges rather than the presence of surface cracks (Figs. 2–4). The cracks area in desiccated state of compacted clay specimen interacted with DW was less compared to clay specimens interacted with 0.4 M and 4 M  $\text{CaCl}_2$  solutions throughout the depth of soil specimen (Fig. 4). This variation is due to the presence of comparatively large desiccation cracks on interior surfaces of compacted clay specimens interacted with 0.4 M and 4 M  $\text{CaCl}_2$  solutions (Figs. 2–4). And the cracks area in desiccated state of compacted clay specimen interacted with 4 M  $\text{CaCl}_2$  solution is predominantly higher throughout the depth than the specimen interacted with 0.4 M  $\text{CaCl}_2$  solution.

Table 2 also compares the variation of average cracks area, cracks volume and void ratio in desiccated state of compacted clay specimens inundated with DW and  $\text{CaCl}_2$  solutions. The variation in cracks area is calculated using DCI and XCT images along with vernier caliper height measurements. It is evident from Table 2 and Fig. 4 that the average cracks area and the corresponding cracks volume calculated from both DCI and XCT methods increased with the increase in concentration of interacting fluid. However, the cracks area and volume calculated from DCI method

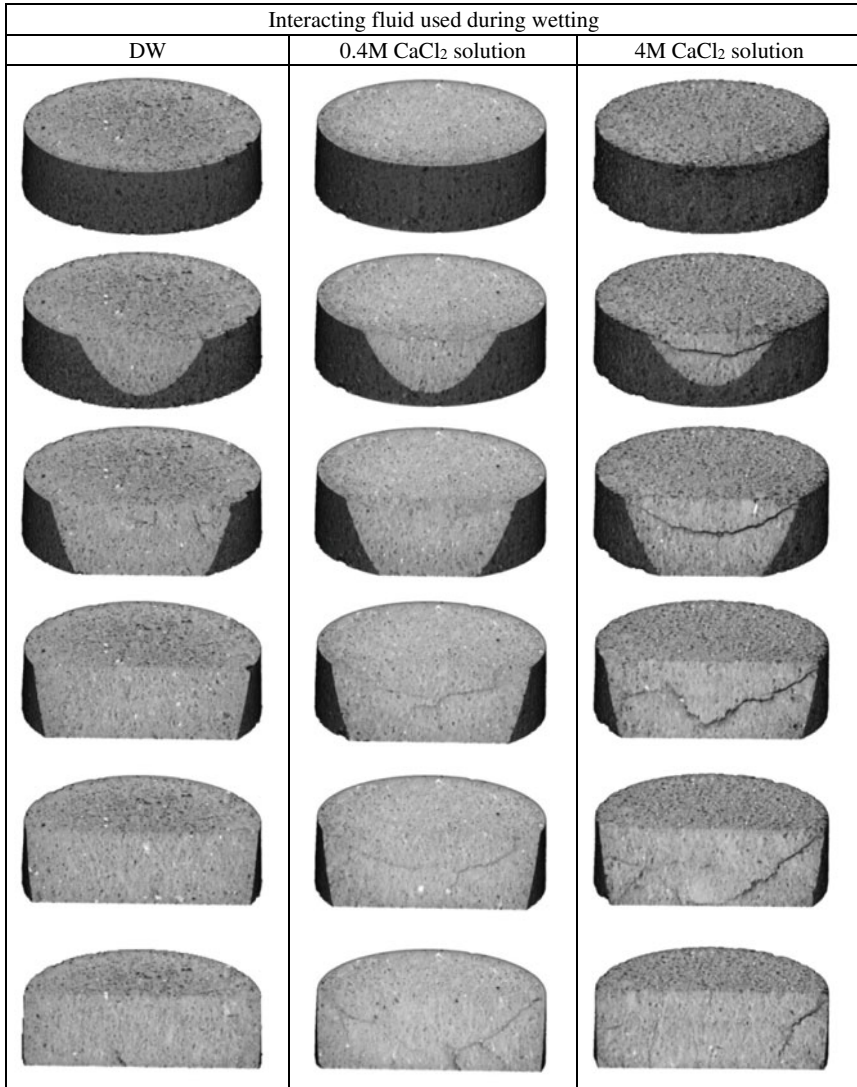
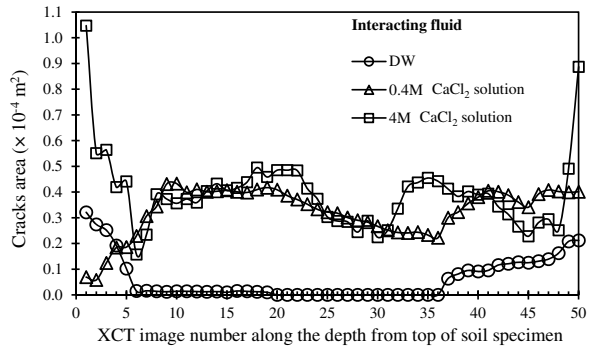


**Fig. 3** 3D view and 3D sectional view of desiccated clay specimens constructed using XCT images (not to scale)

are comparatively lower than that calculated using XCT method for the compacted clay specimens interacted with 0.4 M and 4 M CaCl<sub>2</sub> solutions due to the presence of interior desiccation cracks which are not captured in digital camera images.

The variation in void ratio of desiccated clay specimen interacted with DW calculated from average vernier caliper measurement and DCI and XCT methods was less due to presence of only few non-propagating cracks at the bottom surface (Table 2).

**Fig. 4** Variation of cracks area with XCT image number of desiccated clay specimens



Similar to the vernier caliper measurements, the void ratio of desiccated clay specimens, interacted with DW, 0.4 M and 4 M  $\text{CaCl}_2$  solutions, calculated from DCI and XCT methods increased with the increase in concentration of interacting fluid. However, marked reduction in void ratio was observed when void ratios were calculated from XCT method than the vernier caliper measurements due to the presence of desiccation cracks in the interior surface of desiccated clay specimens interacted with 0.4 M and 4 M  $\text{CaCl}_2$  solutions. When comparing the void ratio determined from DCI and XCT methods for desiccated clay specimens interacted with 0.4 M and 4 M  $\text{CaCl}_2$  solutions, it is observed that the void ratio calculated from DCI method were comparatively higher than void ratio calculated from XCT method. This is due to the presence of desiccation cracks in the interior surface of desiccated clay specimens which cannot be visualized using DCIs and quantified using DCI method (Figs. 2 and 3). Such type of investigation and accurate determination of void ratio of compacted clay specimens using XCT images are essential for the understanding of water retention and hydraulic behaviour during wet-dry cycles.

## 4 Summary and Conclusions

The presence of desiccation cracks in the interior surfaces of desiccated clay specimens interacted with salt solutions is visualized and captured using XCT images. Then the captured XCT images were used to quantify the cracks pattern and determine the void ratio of desiccated clay specimens accurately. The conclusions of the present study are as follows:

- Interaction of salt solutions has significant influence on the shrinkage and desiccation cracking behaviour similar to its influence on swelling behaviour of clays soils.
- The cracks area, cracks volume and void ratio of desiccated clay specimens increased with the increase in concentration of interacting fluid.

- In the present study, the cracks pattern in the desiccated state of compacted soil specimens were captured more accurately using XCT imaging experiments than with the vernier and DCI methods due to the presence of interior cracks.

## References

1. Yesiller N, Hanson JL, Oettle KN, Liu WL (2008) Thermal analysis of cover systems in municipal solid waste landfills. *J Geotech Geoenviron Eng* 131(11):1655–1664
2. Julina M, Thyagaraj T (2019) Quantification of desiccation cracks using X-ray tomography for tracing shrinkage path of compacted expansive soil. *Acta Geotech* 14(1):35–56
3. Julina M, Thyagaraj T (2018) Determination of volumetric shrinkage of an expansive soil using digital camera images. *Int J Geotech Eng*. <https://doi.org/10.1080/19386362.2018.1460961>
4. Yoshida H, Rowe RK (2003) Consideration of landfill liner temperature. In: Proceedings Sardinia 2003, ninth international waste management and landfill symposium, S. Margherita di Pula, Cagliari, Italy
5. Rowe RK (2005) Long-term performance of contaminant barrier systems. *Geotechnique* 55(9):631–678
6. Rowe RK (2012) Short-and long-term leakage through composite liners. The 7th Arthur Casagrande Lecture 11. This lecture was presented at the 14th Pan-American conference on soil mechanics and geotechnical engineering, Toronto, Ont., October 2011, and a pre-print appeared in the conference proceedings. *Can Geotech J* 49(2):141–169
7. Lakshmikantha MR, Prat PC, Ledesma A (2009) Image analysis for the quantification of a developing crack network on a drying soil. *Geotech Test J* 32(6):1–11
8. Sanchez M, Atique A, Kim S, Romero E, Zielinski M (2013) Exploring desiccation cracks in soils using a 2D profile laser device. *Acta Geotech* 8:583–596
9. Rao SM, Thyagaraj T, Thomas HR (2006) Swelling of compacted clay under osmotic gradients. *Géotechnique* 56(10):707–713
10. Thyagaraj T, Thomas SR, Das AP (2016) Physico-chemical effects on shrinkage behavior of compacted expansive clay. *Int J Geomech* 06016013
11. Gebrenegus T, Ghezzehei TA, Tuller M (2011) Physicochemical controls on initiation and evolution of desiccation cracks in sand–bentonite mixtures: X-ray CT imaging and stochastic modeling. *J Contam Hydrol* 126(1–2):100–112
12. Shin H, Santamarina JC (2011) Desiccation cracks in saturated fine-grained soils: particle-level phenomena and effective-stress analysis. *Géotechnique* 61(11):961–972
13. Rasband WS (2006) “*ImageJ*” National Institutes of Health, Bethesda, Maryland, USA. <https://imagej.nih.gov/ij/> (1997–2016)

# A Study on the Improvement of Engineering Properties of Locally Available Soil of Kokrajhar by Using Burnt Brick Dust



Shafi Kamal Rahman, Mantu Kumar Das, and Joutish Deka

**Abstract** Soil stabilization is the process by which the engineering properties of poor soil is improved by means of changing the physical and chemical properties. Improving the bearing capacity, compressibility, soil permeability are some of the main objectives of soil stabilization. Due to high activity and unstable property of soil it is very difficult to construct any type of civil engineering structure on such type of soil. Soil stabilization is recommended to improve the engineering properties of such soil. This study deals with the complete analysis of the improvement of soil properties and its stabilization using burnt brick dust. Several experiments are conducted to determine the engineering properties of local soil (which are collected from TINALI area nearby CIT Kokrajhar campus) such as specific gravity, sieve analysis, plastic limit, liquid limit, proctor test, CBR by mixing burnt brick dust in different proportions (25%, 50%, 75% etc.) by volume. The objective of this study is to represent the variation of engineering properties of local soil when admixed with burnt brick dust.

**Keywords** Soil stabilization · Burnt brick dust · California bearing ratio (CBR)

## 1 Introduction

Kokrajhar is a fast growing city of BTAD (Assam). The soil in many areas of Kokrajhar has poor bearing capacity and ground water level is just near to the ground. To improve the engineering properties of the soil it's necessary to stabilize the soil by some stabilizers. The burnt brick dust as stabilizing additive to silty soil is evaluated for improving the engineering properties of soil. Kunal et al. [1] had conducted experimental investigation for stabilization of black cotton soil by using burnt brick dust. Kumar et al. [2] conducted experiments to stabilizing various properties of black cotton soil by mixing brick dust and lime as admixture. Neha and Trivedi [3] studied about the improvement of permanent soil subgrade by using burnt brick dust.

---

S. K. Rahman (✉) · M. K. Das · J. Deka  
Central Institute of Technology, Kokrajhar, India  
e-mail: [sk.rahman@cit.ac.in](mailto:sk.rahman@cit.ac.in)

© Springer Nature Singapore Pte Ltd. 2022  
A. K. Dey et al. (eds.), *Proceedings of the 7th Indian Young Geotechnical Engineers Conference*, Lecture Notes in Civil Engineering 195,  
[https://doi.org/10.1007/978-981-16-6456-4\\_53](https://doi.org/10.1007/978-981-16-6456-4_53)

515



**Table 1** List of samples with proportions

Sl. No.	Composition	Abbreviation
1.	100% soil	S100B0
2.	75% soil + 25% burnt brick dust	S75B25
3.	50% soil + 50% burnt brick dust	S75B25
4.	25% soil + 75% burnt brick dust	S75B25

Sikha and Kumar [4] studied about the improvement of engineering properties of cohesive soil using brick dust as admixture. Sudharani et al. [5] studied the stabilization of black cotton soil using brick dust and bagasse ash. Razvi et al. [6] studied on stabilization of the locally available dump yard site soil using burnt brick ash.

## 2 Materials Used and Testing Methods

Soil was collected from local site of tinali near CIT, Kokrajhar campus and burnt brick were collected from local market. All the experiments were conducted as per relevant IS code. In this study, soil was replaced by burnt brick dust at 25, 50 and 75% by volume of soil. By taking this three standard number of percentages the different laboratory tests were performed.

### 2.1 Preparation of Samples

See Table 1.

## 3 Result and Discussions

### 3.1 Determination of Field Density of Soil

See Table 2.

**Table 2** Experimental results for core cutter method of soil

Sl. No.	Property	Result
1.	Bulk density in $\text{g/cm}^3$	1.895
2.	Water content in (W) percentage	17.714
3.	Dry density in $\text{g/cm}^3$	1.61

**Table 3** Experimental results for specific gravity

Sl. No.	Composition	Result
1.	S100B0	2.41
2.	S25B75	2.453
3.	S50B50	2.58
4.	S75B25	2.66

### 3.2 Determination of Specific Gravity

See Table 3.

### 3.3 Sieve Analysis

See Fig. 1 and Table 4.

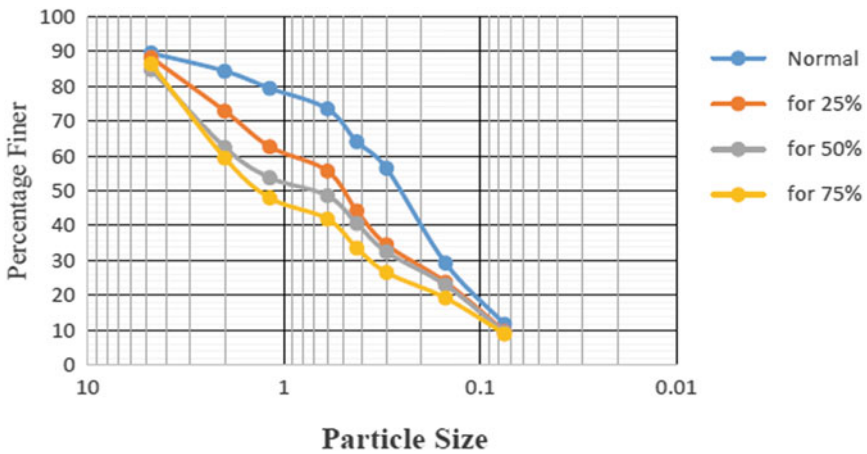


**Fig. 1** Grain size distribution comparisons

**Table 4** Experimental results of sieve analysis

Sl. No.	Composition	$C_U$	$C_c$
1.	S100B0	4.47	0.87
2.	S25B75	10.48	0.68
3.	S50B50	46.15	0.82
4.	S75B25	23.33	0.648

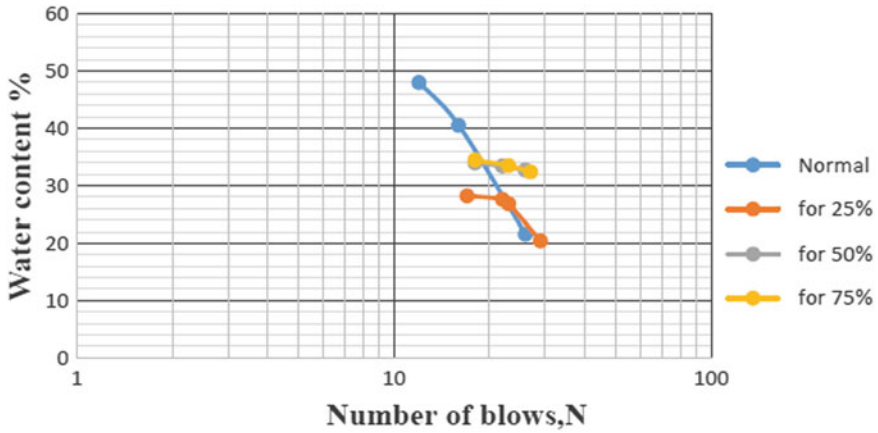


Fig. 2 Liquid limit comparisons

Table 5 Experimental results of liquid limit and plastic limit

Sl. No.	Composition	LL (%)	PL (%)
1.	S100B0	23	21
2.	S25B75	27	23
3.	S50B50	32	24
4.	S75B25	33	31

### 3.4 Liquid Limit and Plastic Limit

See Fig. 2 and Table 5.

### 3.5 Proctor Test

See Fig. 3 and Table 6.

### 3.6 California Bearing Ratio (CBR) Test

See Fig. 4 and Table 7.

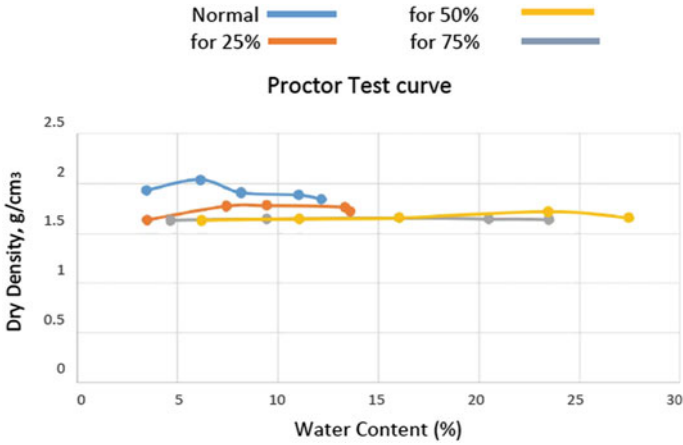


Fig. 3 Proctor test comparisons

Table 6 Experimental results of proctor test

Sl. No.	Composition	Optimum moisture content (OMC)
1.	S100B0	6.14
2.	S25B75	7.43
3.	S50B50	16.04
4.	S75B25	27.46

Fig. 4 CBR test comparisons

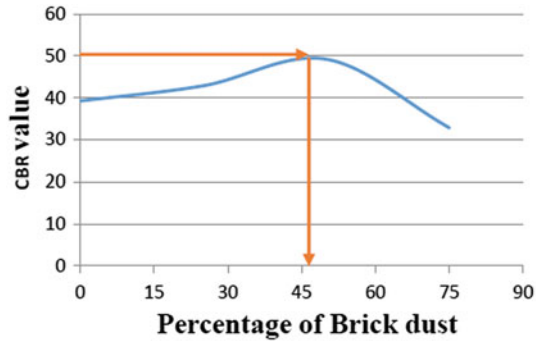


Table 7 Experimental results of CBR test

Sl. No.	Composition	California bearing ratio (CBR) (%)
1.	S100B0	39.26
2.	S25B75	42.89
3.	S50B50	49.29
4.	S75B25	32.82

## 4 Conclusions

In this study, the locally available soil of Kokrajhar was replaced by brick dust of 25, 50 and 75% by volume. By taking this three standard number of percentage the tests were performed. For samples S100B0, S75B25, S50B50 and S25B75 we got liquid limit value as 23%, 27%, 32% and 33%, Plastic limit value as 21%, 23%, 24%, 31%, Standard Proctor test value as 6.41%, 7.43%, 16.04%, 27.46%, CBR value as 39.26%, 42.895%, 49.253% and 32.82% respectively. It has been observed that CBR value increased with the addition of brick dust in the proportion of 25% up to 45% but after the addition of 50% and 75%, the value decreased. So, from the graph we can summarized that CBR value at 50% gives the highest strength of CBR value as comparing with others value. On increasing the percentage of brick dust, the optimum moisture content also increased. Liquid limit and plastic limit is also increased due to increase of brick dust proportion. So, the major conclusion is that due to addition of burnt brick dust the compressive strength of the local soil of Kokrajhar increased but up to a certain percentage. So, analyzing the all results and graph, it is found that at 45% of admixture of brick dust to the soil signify the standard admixture for the higher strength for the test denote as S55B45.

## References

1. Kunal RP, Yogesh RB, Rahul RJ (2015) Stabilization of black cotton soil by using burnt-brick dust. *Int Res J Eng Technol (IRJET)* 02(05)
2. Kumar A, Kumar A, Prakash V (2016) Improve by stabilizing various properties of black cotton soil by mixing brick dust and lime as admixture. *Int J All Res Educ Sci Methods (IJARESM)* 4(9). ISSN: 2455-6211
3. Neha N, Trivedi MK (2017) Improvement of permanent soil subgrade by using burnt brick dust. *Int J Res Appl Sci Eng Technol (IJRASET)* 5(V)
4. Sikha S, Kumar P (2017) Cohesive soil mixed with brick dust is suitable for stabilizing the subgrade of the road and embankment construction. In: *Indian geotechnical conference 2017 GeoNEst*, 14–16 Dec 2017
5. Sudharani K, Abhishek SK, Adarsh N, Harish T, Manjunath (2017) Stabilization of black cotton soil using brick dust and Bagasse ash. *IJSRD Int J Sci Res Dev* 5(05)
6. Razvi SS, Nannaware D, Bankar S, Yadav A, Shaikh H, Bade S (2018) Study on stabilization of soil using burnt brick. *Int J Adv Res Sci Eng* 07(03)

# Geotechnical Properties of Sand-Bentonite Liner Material Permeated with Calcium Chloride Solution



Debtanu Seth , Suryaleen Rout , and Suresh Prasad Singh 

**Abstract** Sand-bentonite mixture is conventionally used as the liner material for waste disposal facilities. Depending upon the nature of waste, a host of chemicals is generated as leachate. The present study focuses on the effect of  $\text{CaCl}_2$  solutions on an optimised sand-bentonite mixture, which simulates the effect of leachates on geotechnical characteristics of sand-bentonite liner material. The selection of  $\text{CaCl}_2$  solution as a permeating liquid for sand-bentonite mixture is based on the abundant ions in leachate and by referring works of previous researchers. Sand-bentonite mixtures compacted at OMC and MDD are permeated with 0.1, 0.3 and 0.6 M of solutions of  $\text{CaCl}_2$  for 7, 14 and 21 days. The geotechnical properties of optimised sand-bentonite mixture permeated with distilled water and 0.1, 0.3 and 0.6 M of solutions of  $\text{CaCl}_2$  were evaluated. It is observed that liquid limit and plasticity index decrease with increasing permeating time and concentration of chemical. Coefficient of consolidation increases with increasing concentration of solution and permeating time. However, the unconfined compressive strength of the sample decrease with increase in the concentration of chemical and permeating time. Similarly, swelling index is found to be decreased with increasing permeating time and concentration of  $\text{CaCl}_2$  solution. XRD is performed to identify the composition of the sand-bentonite mixture. The observed chemical changes are correlated to engineering behaviour. The engineering properties of sand-bentonite liner material permeated through  $\text{CaCl}_2$  solutions of different concentration is attributed to the changes in thickness of diffused double layer due to permeation of the  $\text{CaCl}_2$  solution.

**Keywords** Compacted clay liner · High concentration chemical solutions · Geotechnical properties

---

D. Seth · S. Rout · S. P. Singh (✉)  
National Institute of Technology, Rourkela, Odisha, India  
e-mail: [spsingh@nitrrkl.ac.in](mailto:spsingh@nitrrkl.ac.in)

D. Seth  
e-mail: [217ce1033@nitrrkl.ac.in](mailto:217ce1033@nitrrkl.ac.in)

S. Rout  
e-mail: [514ce1017@nitrrkl.ac.in](mailto:514ce1017@nitrrkl.ac.in)

## 1 Introduction

Liner is a crucial part of a landfill. Liner retards the movement of leachates to the surroundings of the landfill or groundwater. As liner material, optimised sand-bentonite mixture is widely used. From various testing, it is found that sand-bentonite mixture containing 85% of sand and 15% bentonite and compacted in modified Proctor at OMC to MDD fulfilling the requirements of a liner material as suggested by the United States Environment Protection Agency.

While passing through a liner, leachates affect the soil structure and cause changes in various index properties and engineering properties of liner material. To simulate field conditions and to define different geotechnical properties using distilled water is far from being correct. From the leachate analysis performed by several researchers, it is found that the mostly found ions in MSW leachate are Chloride, Sodium, Calcium, Potassium, Iron [1, 2]. In this study, sand-bentonite mixture is permeated with different concentration of  $\text{CaCl}_2$  solutions, as it is known to have more effect than other salt solutions used for chemical compatibility test on the compacted clay liner [2–8].

## 2 Materials

### 2.1 Soil

Naturally occurring Sand and commercially available Sodium-Bentonite are used in this study. The sand is excavated from Koelriver, at Rourkela, by open excavation. Later the sand is oven-dried and sieved through 2 mm sieve. The passing portion of the sand is collected. The  $C_u$  and  $C_c$  value of sand is calculated as 2.8 and 1.23 respectively from which the sand is classified as SP (poorly graded sand) as per IS classification system. Bentonite is commercially procured from Nilkantha Mine Chem, Jodhpur. From X-Ray diffraction, it is found that the sand-bentonite mixture contains Montmorillonite, Quartz, Feldspar and Aluminium Silicate. The properties of sand and bentonite are given in Table 1.

Mixture is prepared by adding 15% bentonite with 85% sand, and it is found out that the mixture fulfils the requirements of a liner material as referred by USEPA. Both the materials are oven-dried before mixing. Before every test, sand-bentonite mixture is to be mixed with desired water and kept at least 24 h for homogeneous mixing of water. The tests, which are performed on sand-Bentonite mixture follows the Indian Standard code.

**Table 1** Properties of individual materials and sand-bentonite mixture

Properties	Bentonite	Sand	Sand-bentonite
Specific gravity	2.77	2.60	2.68
Fine contents (%)	97.07	3	17.11
Liquid limit (%)	330	–	55
Plastic limit (%)	32.89	–	24.88
Shrinkage limit	6.28	–	–
Plasticity index (%)	292.11	–	30.12
Swelling index (%)	624.14	–	–

## 2.2 Permeating Liquid

The permeating liquids used in the experiments are deionised water and different concentration solutions of  $\text{CaCl}_2$ . The solutions are prepared by dissolving  $\text{CaCl}_2$  in distilled water to yield solutions of  $\text{CaCl}_2$  concentrations of 0.1, 0.3 and 0.6 M. This range of concentrations is selected to obtain a broad range of hydraulic conductivities.

## 3 Methodology

### 3.1 Permeability

Specimens are compacted in a rigid wall permeameter following IS 2720 (Part 17) 1986 [9] and permeated with deionised water and  $\text{CaCl}_2$  solutions of different concentration for different permeating time. Three specimens are permeated with  $\text{CaCl}_2$  for 7, 14 and 21 days. Due to the low permeability of sand-bentonite mixture, the permeability test is performed under hydraulic gradient of 10 m. During each permeability test, soil samples are collected at 7th, 14th and 21st day and various tests are performed on them.

### 3.2 Consistency Index

The samples are taken out from the mould on 7th, 14th and 21st day and oven-dried. The oven-dried sample is then sieved through 425-micron sieve, and the portion which is passing is mixed with water and kept for 24 h so that the water homogeneously mixes with sand-bentonite mixture. After 24 h, the mixture is used to determine the consistency index and swelling index following the respective IS codes.

Liquid limit, plastic limit and shrinkage limit are executed following IS 2720 (Part 5) 1985 [10] and (Part 6) [11] respectively.



### 3.3 Swelling Index

Swelling Index test is performed following IS 2720 (Part 40) 1977 [12]. The material is sieved through 425-micron sieve and from the passing portion, 10 g of soil is collected in each of two 100 ml measuring cylinder. One of the two measuring cylinders is filled with water, and another one is with kerosene. The percentage difference of soil volume in the kerosene and the water is reported as swelling index.

### 3.4 Unconfined Compressive Strength

Specimens are compacted at optimum moisture content to maximum dry density in a compaction mould. UCS samples of diameter 38 mm and height 76 mm are extracted from the compaction mould or permeability mould at 7th, 14th and 21st day, using two coring tools. Then the cored sample is tested following IS 2720 (Part-10) 1973 [13].

## 4 Result and Analyses

### 4.1 Atterberg's Limit

Liquid limit of sample is determined periodically from the permeated sample, and it is found that the liquid limit decreases with increasing permeating time and also the plots become steeper with increasing concentration of  $\text{CaCl}_2$  solution, which matches with the trend of Petrov and Rowe [14]. Also, from Fig. 3 it is evident that for a constant permeating time with increasing concentration of chemical, liquid limit decreases. After permeating 0.1 M  $\text{CaCl}_2$  for 21 days, the liquid limit of the sample is found out to be 25%, i.e. decrease in liquid limit by 54% from the liquid limit value of the sample permeated with distilled water which is 55. Again, for seven days permeating with 0.1 M  $\text{CaCl}_2$  solution, liquid limit of a sample is found out to be 45% and for 0.3 molarity  $\text{CaCl}_2$  solution liquid limit of the sample is 25% which means liquid limit decreases by 44% under the effect of higher concentration  $\text{CaCl}_2$  solution. Such behaviour can be attributed to the decrease in adsorbed water or diffused double layer in soil. Bowders and Daniel [15] proposed that inorganic salt solutions tended to reduce the thickness of the Diffuse Double Layer (DDL), causing the soil particles to flocculate. It is observed that the plasticity index is also decreasing with increasing time. Initially, the sample permeated with distilled water has a plasticity index of 30.12%, which decreased by 66% and become 10.24% when permeated with 0.1 M  $\text{CaCl}_2$  for 21 days. The variation of liquid limit and plasticity index is shown in Figs. 1 and 2 respectively.

**Fig. 1** Variation of liquid limit ratio with permeating time

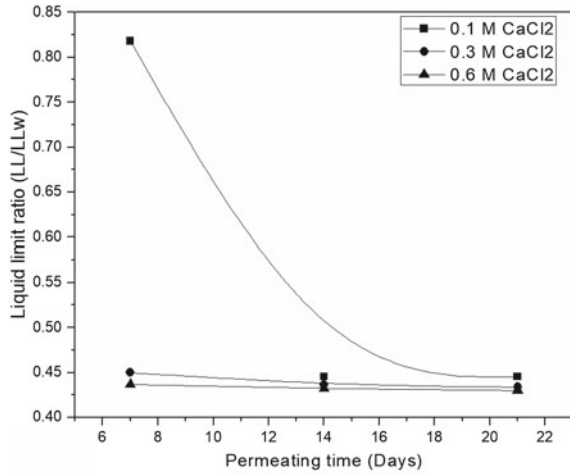
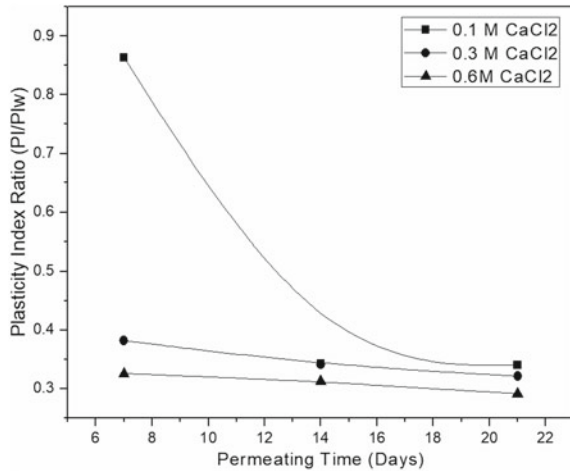


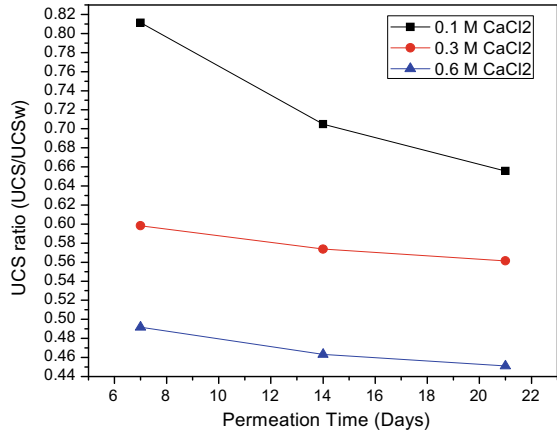
**Fig. 2** Variation of plasticity index ratio with permeating time



### 4.2 Unconfined Compressive Strength (UCS)

From Fig. 3 it is clear that UCS of the samples decreases with increasing days of permeation. Failure strength decreases from 244 to 160 kPa when permeated with 0.1 M CaCl<sub>2</sub> for 21 days. Similarly, with increasing concentration of solution, the unconfined compressive strength decreases. For example, for permeation time 21 days the sample which is permeated with 0.1 M CaCl<sub>2</sub> solution has UCS 160 kPa whereas the sample permeated with 0.3 M CaCl<sub>2</sub> has UCS value 137 kPa, i.e. decrease in 14.38%. Sivapullaiah and Lakshmikantha [16] indicate that the lower strength of

**Fig. 3** Variation of UCS ratio with permeating time



the soil exposed to an electrolyte solution is due to reduction in soil cohesion by stabilisation of surface charge after interaction of the sand-bentonite mixture with leachate ions.

### 4.3 Swelling Index

From Fig. 4 it is evident that swelling index decreases with increasing number of days. Initially, it decreases rapidly, and later rate of decrease stabilises. It is also observed that with increasing concentration of CaCl<sub>2</sub> the slopes of the curves increase, i.e. the rate of decrease in swelling index increases. The above phenomena can be described

**Fig. 4** Variation of swelling index ratio with permeating time

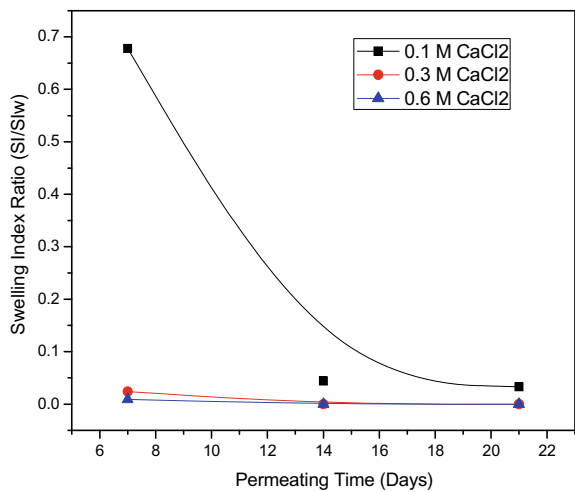
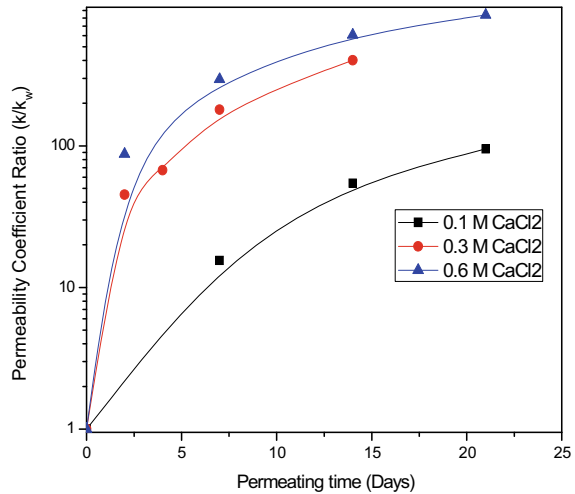


**Fig. 5** Variation of  $k/k_w$  ratio with permeating time



as the cation from the permeating liquid replace the lower electronegative cations at the soil surface, causing the particle surface charge stabilisation. Thus the capacity of soil to ad-sorb water decreases and thickness of DDL decreases, causing a reduction in swelling index of the soil.

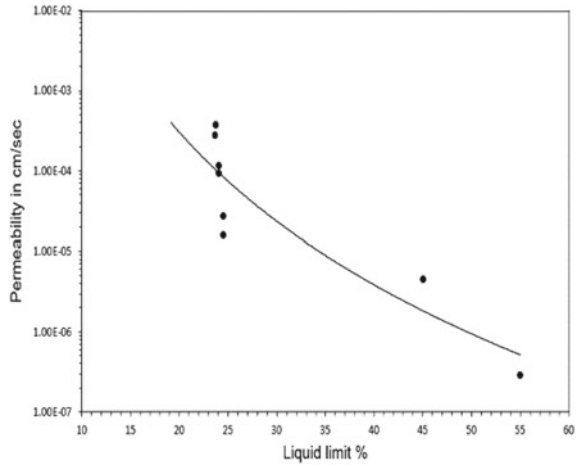
#### 4.4 Permeability

From Fig. 5, it is obvious that the permeability of soil increases with increasing permeating time. The increase in permeability is due to the flocculation of the soil structure after interaction between sand-bentonite mixture and CaCl<sub>2</sub> solution.

#### 4.5 Relationship Between Liquid Limit and Permeability

It is observed that with decreasing liquid limit, the permeability of sand-bentonite mixture increases. The decrease of liquid limit indicates the decrease in thickness of diffused double layer around soil particles which helps the soil particles to come closer and flocculate, which in turn increases the permeability. Figure 6 supports the above statement.

**Fig. 6** Variation of permeability with liquid limit



## 5 Conclusion

The aim of the study is to gain knowledge about the effect of interaction between leachate and sand-bentonite liner and to assess the change in different geotechnical properties of sand-bentonite liner material when permeated with  $\text{CaCl}_2$  solution of different concentration. The samples are permeated for 7, 14 and 21 days. From the result, it is obvious that with increasing permeating time and concentration of permeating liquid the liquid limit and plasticity of the sand-bentonite mixture decreases and the unconfined compressive strength of the sand-bentonite mixture decreases too. It is also observed that with increasing permeating time and concentration of  $\text{CaCl}_2$  solution the swelling index decreases. However, the permeability increases when the permeating time and concentration of the  $\text{CaCl}_2$  solution increase. It is noticeable that the permeability increases with increasing liquid limit. The rate of consolidation increases with increasing permeating time and concentration of permeating liquid. Again, with increasing concentration of  $\text{CaCl}_2$  in the solution the pH of the solution slightly increases which in turn should decrease the permeability, but as the effect of cation exchange between permeating liquid and sand-bentonite mixture mask the effect of pH increase, the permeability, in fact, increases. The changes in the geotechnical properties are due to the changes in the thickness of the diffused double layer. The cation exchange between soil particles and permeating liquid causes the diffused double layer to shrink and the soil structure to be flocculated which in turn changes the geotechnical properties of the sand-bentonite mixture.

## References

1. Kayabali K, Mollamahmutoglu M (2000) The influence of hazardous liquid waste on the permeability of earthen liners. *Environ Geol* 39(3-4):201–210
2. Lin LC, Benson CH (2000) Effect of wet-dry cycling on swelling and hydraulic conductivity of GCLs. *J Geotech Geoenvironmental Eng* 126(1):40–49
3. Daniel DE (1993) Clay Liners. In: *Geotechnical practice for waste disposal*, Chapter 7, pp 137–163
4. Das BM (2006) *Principles of geotechnical engineering*. Thomson, India
5. James AN, Fullerton D, Drake R (1997) Field performance of GCL under ion exchange conditions. *J Geotech Geoenvironmental Eng* 123(10):897–901
6. Ruhl JL, Daniel DE (1997) Geosynthetic clay liners permeated with chemical solutions and leachates. *J Geotech Geoenvironmental Eng* 123(4):369–381
7. Shackelford CD (1994) Waste-soil interactions that alter hydraulic conductivity. In: *Hydraulic conductivity and waste contaminant transport in soil*. ASTM International
8. Shackelford CD, Benson CH, Katsumi T, Edil TB, Lin L (2000) Evaluating the hydraulic conductivity of GCLs permeated with non-standard liquids. *Geotext Geomembr* 18(2-4):133–161
9. IS 2720 (Part-17)-1986 Methods of test for soils, Laboratory determination of permeability. Bureau of Indian Standards. New Delhi
10. IS 2720 (Part-5)-1985 Methods of test for soils, Determination of liquid and plastic limit. Bureau of Indian Standards. New Delhi
11. IS 2720 (Part- 6)-1985 Methods of test for soils, Part 6: Determination of shrinkage factors. Bureau of Indian Standards, New Delhi
12. IS 2720 (Part-40)-1977 Methods of test for soils, Determination of free swell index of soil. Bureau of Indian Standards, New Delhi
13. IS 2720 (Part-10)-1991 Methods of test for soils, Determination of unconfined compressive strength. Bureau of Indian Standards, New Delhi
14. Petrov RR, Rowe RK (1997) Geosynthetic clay liner (GCL) - Chemical compatibility by hydraulic conductivity testing and factors impacting its performance. *Can Geotech J* 34(6):863–885
15. Bowders Jr JJ, Daniel DE (1987) Hydraulic conductivity of compacted clay to dilute organic chemicals. *J Geotech Eng* 113(12):1432–1448
16. Sivapullaiah PV, Lakshmikantha H (2004) Properties of fly ash as hydraulic barrier. *Soil Sediment Contam* 13(5):391–406